The computational power of many-body systems

by

Zak Webb

A thesis
presented to the University of Waterloo
in fulfillment of the
thesis requirement for the degree of
Doctor of Philosophy
in
Physics and Astronomy (Quantum Information)

Waterloo, Ontario, Canada, 2016

Author's Declaration

I hereby declare that I am the sole author of this thesis. This is a true copy of the thesis, including any required final revisions, as accepted by my examiners.

I understand that my thesis may be made electronically available to the public.

Abstract

Many-body systems are well known throughout physics to be hard problems to exactly solve, but much of this is folklore resulting from the lack of an analytic solution to these systems. This thesis attempts to classify the complexity inherent in many of these systems, and give quantitative results for why the problems are hard. In particular, we analyze the many-particle system corresponding to a multi-particle quantum walk, showing that the time evolution of such systems on a polynomial sized graph is universal for quantum computation, and thus determining how a particular state evolves is as hard as an arbitrary quantum computation. We then analyze the ground energy properties of related systems, showing that for bosons, bounding the ground energy of the same Hamiltonian with a fixed number of particles is **QMA**-complete. Similar techniques also show that the single-particle case has related computational power. Finally, a nice relation between spin systems and hard-core bosons can be used to show that bounding the smallest eigenvalue of the XY-model is **QMA**-complete.

Acknowledgements

I would like to thank my advisor, Andrew Childs, for his great help and support during my graduate studies at the University of Waterloo. His research guidance and support during hard times was very helpful, and this thesis would not be written without his support.

I would also like to thank David Gosset, who acted as a sounding board, and guided much of my research. He was a fountain of useful ideas, with an ability to conceive of complex solutions to difficult problems. His work ethic made many of the results in this thesis possible.

I'd like to thank Norbert Lütkenhaus, who helped get me back on my feet during troubled times, as well as Chris Pugh, who got me started and kept me going. To all of my friends at the Institute for Quantum Computing, from the optics groups of my early years to the eclectic bunch now eating cookies at 4, thank you.

Dedication

This is dedicated to the ones I love, my family and friends.

Table of Contents

List of Figures

Chapter 1

Introduction

The first thing I would like to mention is that this thesis is not complete. I ran out of time and was unable to complete the thesis. I had to submit something to the graduate office, and this is it. I do apologize, and I expect to have major revisions required. At this point, I do not believe that any one chapter is actually completed, and in fact many of the state results have not been completely written up. Basically, I recognize that this thesis is defensible as is, and am planning major revisions.

When examining the physics literature, the three-body problem is extremely well known, as is its usual impossibility to solve. In these cases, people generally mean that there does not exist a closed form solution in general, but can we quantify exactly how hard the problem is?

In particular, if one is working with some particular many body system, how hard is it to compute various attributes about the system. I'd really like to know the answer.

While such questions have not generally been asked in physics, classifying the computation power of a problem in terms of the necessary resources in order to solve it is a foundational idea in computer science. The entire field of computational complexity arose in the attempt to classify these problems. This thesis will attempt to use tools founded in this field and apply them to the various physical systems.

1.1 Quantum walk

Over the years, randomness proved itself as a useful tool, allowing access to physical systems that are too large to accurately simulate. By assuming the dynamics of such systems can be modelled as independent events, Markov chains provide insight to the structure of the dynamics. These ideas can then be cast into the framework of random walk, where the generating Markov matrix describes the weighted, directed graph on which the walk takes place.

Using the principle of "put quantum in front," one can then analyze what happens when the random dynamics are replaced by unitary dynamics. This actually poses a little difficulty, as there is no obvious way to make a random walk have unitary dynamics. In particular, there are many ways that the particle can arrive at one particular vertex in the underlying graph, and thus after arriving at the vertex there is no way to reverse the dynamics.

There are (at least) two ways to get around this. One continues with the discrete-time structure of a random walk, and keeps track of a "direction" in addition to the position of the particle. Each step of the walk is then a movement in the chosen direction followed by a unitary update to the direction register. These Szegedy walks are extremely common in the literature, and go by the name of "discrete-time quantum walk."

Another way to get around the reversibility problem is to generalize the continuous-time model of random walks. In particular, assuming that the underlying graph is symmetric, we look at the unitary generated by taking the adjacency matrix of the graph as a Hamiltonian. This is a one-parameter family of unitaries, and thus easily reversible. The "continuous-time quantum walk" model is the one we'll be focussing on in this thesis.

1.2 Many-body systems

Everything in nature has many particles, and the reason that physicists are so interested in smaller dynamics is the relatively understandable fact that many-body systems are extremely complicated. The entire branch of statistical physics was created in an attempt to make a coherent understanding of these large systems, since writing down the dynamics of every particle is impossible in general.

Along these lines, many models of simple interactions between particles exist in the literature. As an example, on can consider a lattice of occupation sites, where bosons can sit at any point in the lattice. Without interactions between the particles, the dynamics are easily understood as decoupled plane waves. However, by including even a simple energy penalty when multiple particles occupy the same location (i.e. particles don't like to bunch), we no longer have a closed form solution and are required to look at things such as the Bethe ansatz.

1.3 Computational complexity

While this is a physics thesis, much of my work is focused on understanding the computational power of these physical systems, and as such an understanding of the classification framework is in order. I should explain some of the motivation behind this area of research, giving a bit of background for the physicist.

These classifications are generally described by languages, or subsets of all possible 0-1 strings. In particular, given some string x, the requisite power in order to determine whether the string belongs to a language or not describes the complexity of the language.

1.4 Layout of thesis

With all of this background in mind, we'd like to give a basic understanding of what this thesis is going to entail. The underlying theme of this thesis is to understand the computational power of quantum walk, when restricted to various questions. As such, we will look both at the single and multi-particle cases. Note that most of this thesis is based on the papers [16], [**?**], [17], and [**?**]. While I am an author on all four papers, Andrew Childs and David Gosset are co-authors on all four papers, while Daniel Nagaj and Mouktik Raha are co-authors on [**?**].

However, in Chapter 2, we will at first define various terms related to computational complexity that will be of use to us, as well as some lemmas that might be of independent interest.

In Chapter **??** we will describe single-particle scattering on graphs. In particular, we will give some simple motivations and understanding of what is going on in a simple case. This chapter will also describe some basic algorithmic uses for the single particle case. This paper will include some review of previous papers [**TO DO:** *Cite quantum walk papers*] that I have not written, as well as a broad overview of techniques used in [16] and [**?**].

At this point, we will transition into understanding the computational power of time evolving according to single- and multi-particle quantum walks. In particular, Chapter **??** will include a novel proof that quantum walk of a single particle on an exponentially sized graph for polynomial time

is universal quantum computing, using techniques slightly different than that of [**?**][**TO DO:** *Find correct citation*] . While this proof has not been submitted as a paper in any journal, it makes use of many of the techniques of [16]. In Chapter **??**, we extend this result to show that a multi-particle quantum walk with almost any finite-range interaction is universal for quantum computing, the main result of [16].

With the computational power of time evolved quantum walk, we will want to understand the ground energy problem of the quantum walk. In particular, Chapter **??** shows that determining whether the ground energy of a sparse, row-computable graph is above or below some threshold is **QMA**-complete, which is work is found in an appendix of the [17] paper. As this corresponds exactly to the ground energy problem of a single particle quantum walk on an exponentially large, but specifiable, graph, this shows that the ground energy problem for single-particle quantum walk is **QMA**-complete. Chapter **??** then expands on this result, and shows that the ground energy problem for multi-particle quantum walk with bosons on simple graphs is **QMA**complete. While this result follows the proof techniques of [16] and [**?**], the extension to arbitrary finite-range interactions for bosons is novel.

With the quantum walk interactions out of the way, Chapter **??** makes use of these results on the multi-particle ground energy problem to study the ground energy problem of various spin systems.

Finally, Chapter **??** concludes with some discussion of these results, along with some avenues for future research.

Chapter 2

Mathematical Preliminaries

Several topics in this thesis require a background that not all researcher will have experience in. Especially as this thesis is multi-disciplinary, I would like to include at least some basic introduction to various physical and computer science topics. Additionally, several lemmas used in this manuscript might be of independent interest, as their applicability is not restricted to the various models studied in this thesis.

2.1 Mathematical notation

Perhaps the most simple point that I would like to raise before the thesis begins in ernest is the notation that I will use throughout the paper. Much of the paper uses notation not necessarily standard in every area of physics or computer science, and I want to make sure that no confusion occurs. I will assume that various notations that are common do not need to be described, such at $\mathcal{H}$ describing a Hilbert space, or that $\mathbb{I}$ describes a the identity operator on a particular Hilbert space.

The first such notation will be for the shorthand definition of sets of particular size. Namely,

$$[k] := \{0, 1, \cdots, k-1\}. \tag{2.1}$$

This is a set of size k, with the elements ordered and labeled by the integers from 0 to $k-1$. We will often think of these as elements from $\mathbb{Z}_k$, with addition and multiplication defined over the integers modulo k.

Often this paper will want to investigate systems with many particles, and we will want an operator to only act nontrivially on one particle. In particular, if we have a Hilbert space $\mathcal{H}_{\text{total}} = \mathcal{H}_{\text{single}}^{\otimes N}$ that consists of N copies of some single Hilbert space, and if we have an operator M that acts on $\mathcal{H}_{\text{single}}$, we can define an operator $M^{(w)}$ that acts nontrivially only on the w-th copy of $\mathcal{H}_{\text{single}}$, namely

$$M^{(w)} = \mathbb{I}^{\otimes w-1} \otimes M \otimes \mathbb{I}^{N-w}. \tag{2.2}$$

In this manner, only the w-th copy of $\mathcal{H}_{\text{single}}$ is effected.

As we will also be working with graphs, we will want to note that the letter G usually denotes a particular graph. Further, $A(G)$ describes the adjacency matrix of the graph G. $V(G)$ then describes the vertex set of G, and $E(G)$ describes the edge set of G. Note that this thesis will always deal with undirected graphs, with at most a single edge between vertices. As such, the adjacency matrix $A(G)$ will be a symmetric 0-1 matrix. We will at times want to work with a

simple graph, in which self-loops do not occur, but unless otherwise specified a graph G might contain self-loops.

Much of the work in this thesis, especially when describing the ground energy of particular Hamiltonian, deals only with positive semi-definite operators. As such, if A is a positive semi-definite matrix, then $\gamma(A)$ is the smallest non-zero eigenvalue. Note that if A has a 0-eigenvalue, then this corresponds to the energy gap between the ground state and the first excited state, but if A does not have a 0-eigenvalue then this is simply the smallest eigenvalue of A.

Finally, let us assume that A acts on a Hilbert space $\mathcal{H}$, and that $\mathcal{S}$ is a subspace of $\mathcal{H}$. We will then write the restriction of A to the subspace $\mathcal{S}$ as $A\big|_{\mathcal{S}}$.

Big O notation.

Overloading of notation; in particular, when adding $z \in \mathbb{F}_2$ to $j \in \mathbb{N}$, the result is in $\mathbb{N}$.

Permutation operators.

2.2 Quantum information

As this thesis is about quantum information, I will assume a familiarity with the basics

2.3 Complexity Theory

While this thesis is for the physics department, many of the results require some basic quantum complexity theory. In particular, the computer science idea for classification of computational problems in terms of the requisite resources gives a particularly nice interpretation of why certain physical systems don't equilibrate, and give a simple explanation on why certain systems do not have a known closed form solution.

This is a simple introduction, with a focus designed to make the rest of this thesis comprehensible to those without a background in complexity theory. For a more formal introduction to Complexity Theory, I would recommend [37], with a more in depth review found in [3]. For a focus on complexity as found in quantum information, I would recommend [39].

2.3.1 Languages and promise problems

The main foundation of computational complexity is in the classification of languages based on the requisited resources to determine whether some string is in a language. Unfortunately, this requires the definition of many of these terms.

In particular, what exactly is a string? Any person who has taken a basic programming class knows that a string is simply a word, but the mathematical definition is slightly more complicated. In particular, we first need to define an alphabet, and then define a string over a particular alphabet.

Definition 1 (Alphabet)**.** An alphabet is a finite collection of symbols.

Usually, an arbitrary alphabet is denoted by Γ, while the binary alphabet is denoted by $\Sigma = \{0, 1\}$. The chosen alphabet has no impact on a particular complexity result, as any finite alphabet can be represented via the binary alphabet with overhead that is logarithmic in the size of the original alphabet (essentially, just use a binary encoding of the new alphabet).

With this definition of an alphabet, a string is simply a finite sequence of elements from the alphabet. In particular, we define Γ^n to be all length n sequences of elements from Γ, and then

define

$$\Gamma^* = \bigcup_{n=0}^{\infty} \Gamma^n. \tag{2.3}$$

With this, Γ^* is the set of all strings over Γ.

Computational complexity then deals with understanding subsets of these strings. In particular, let Π_{yes} be a subset of Γ^*. The language problem related to Π_{yes} is to determine whether a given string $x \in \Gamma^*$ is contained within Π_{yes} or not. This can be trivial, such as for the case of $\Pi_{\text{yes}} = \Gamma^*$, or it can be impossible, such as in the case of the famous Halting Problem.

Related to these language problems are promise problems, in which there are two subsets of Γ^*, namely Π_{yes} and Π_{no}, such that $\Pi_{\text{yes}} \cap \Pi_{\text{no}} = \emptyset$. We are then *promised* that the $x \in \Gamma^*$ that we need to sort is contained either $\Pi_{\text{yes}} \cup \Pi_{\text{no}}$. This generally opens up some more interesting problems, as without this restriction certain complexity classes do not make sense.

[**TO DO:** *revise and revisit*]

2.3.2 Turing machines

Up to this point, we have only discussed classifications of strings, and stated that we will want to understand the various resources required to sort a given string into one of two different sets, but we have not explained how these resources are defined. There are various ways to do this, depending on the various computational model one is interested in, but to give the most intuition we will need to define a Turing Machine. These machines are a mathematical construction that allow for the explicit definition of algorithms.

At their most basic level, a Turing machine is simply a finite program along with a (countably) infinite tape that allows the machine to store information. The input to the algorithm is initially written on the tape, and the machine starts in some initial configuration. The machine can only access it's internal memory along with a single character at a time from the infinite tape, and the program progresses by changing the internal state of the machine, changing one character on the tape, and moving along the tape. While extremely limited, these machines have so far captured our ideas of computation.

Formally, a Turing-machine is M is described by a tuple (Γ, Q, δ), where Γ is a finite set of symbol's that can be written on the infinite tape, Q is a set of possible internal states that M can store as internal memory, and δ is a function $Q \times \Gamma \to Q \times \Gamma \times \{L, S, R\}$ describing the required action of the machine M. Included in Q are two special "halting" states generally labeled `accept` and `reject`, such that the machine stops operating if it ever enters these two states, and the machine either accepts or rejects the current string. Note that we always assume that the alphabet contains a special character $\llcorner$that is not used for the input but denotes empty space along the infinite tape after the input string.

During an actual computation, a Turing Machine always starts with its internal state in a specified position, with the string used for input on the initial segment of the infinite tape and the special character $\llcorner$on every character after the input. Additionally, the pointer of the machine is located at the beginning of the tape, so that the machine is able to start reading the input (if needed). At each time step the machine then applies the transition function, updating its internal state, the character located at the current position of the tape, along with the current position of the tape until the machine reaches one of its halting states.

Note that there are several variations on these Turing Machines, such as those that have multiple infinite tapes instead of just one, and one that can move to an arbitrary position along the tape. These variations do not change the overall computational power of the model, just make it slightly more efficient. This definition is perhaps the most simple, and will suffice for now.

[**TO DO:** *get a picture of a TM here*]

One slight modification that will be useful for us is machines that compute a particular function. In particular, for a given function $f : \Gamma^* \to \Gamma^*$, we say that a Turing Machine M computes the function f if for all inputs x, the machine eventually halts and after it halts the tape will have $f(x)$ on the output tape (and nothing else).

2.3.2.1 Resources

With an explicit definition of Turing Machines, we also want to have some way to quantify the amount of resources used by a computation. Since each machine is expected to work on strings of arbitrary length, we somehow need to quantify the resources in terms of the input to a given string. So far, the important quantity in these resource problems has been the length of an input string x. Basically, the number of characters has been the interesting aspect to measure, since any machine will at least need to read the string.

With this n as the yardstick for any of our measurements, we then need to measure the length of the actual computation. In general, there are two ways to measure this length: the number of transitions that the computation used before it halted (as a measure of time), or else the number of elements of the tape that the machine visited during its computation (as a measure of space). It is important to realize that the exact value of these resources depend on the definitions used for the machine, such as the alphabet size or the number of internal states. As such, we will generally not be interested in the exact value for a given input, but will be more interested in the asymptotic scaling of the resources.

These requisite resources will generally be something of the form $\mathcal{O}(f(n))$ for some easily computable function f such as a polynomial or an exponential in n. These various scalings will give us a nice method of classifying the difficulty of computational problems. In general, we will say that a specific Turing Machine M runs in time $f(n)$ if for all inputs it halts in time $t(x)$ and $t(x) \in \mathcal{O}(f(n))$.

2.3.2.2 Uniform circuit families

While Turing Machines are sufficient for classical computation, when we want to describe some quantum complexity classes it will be useful to instead discuss quantum circuits. However, an important aspect of Turing Machines is that they are defined independently of the size of the input, while circuits need to have unique definitions for all different input sizes.

One might be tempted to simply define a computation via circuits by whether or not there exists a circuit of a given length, but this ends up giving an unreasonable amount of power to the computational model. In particular, the algorithm can hide computation in the definition of the circuit, as opposed to the actual running of the circuit itself.

To get around this, we will need to compute the circuit for the computation given the length. Namely, we will have a Turing Machine take as input the string length in unary, and the machine will output a description of the circuit. I won't go into the details here, but the

Definition 2 (Uniform family of circuits)**.** A collection $\{C_x : x \in S \subseteq \Sigma^*\}$ of circuits is a (polynomial-time) *uniform family of circuits* if there exists a deterministic Turing Machine M such that

- M runs in polynomial time.
- For all $x \in S$, M outputs a description of C_x.

Note that this definition makes no reference to the type of circuit, although we will generally assume that the circuit comes from some specific gate set.

[**TO DO:** *completely update this*]

2.3.3 Useful complexity classes

Once we have an understanding of what defines a relation, and how these are related, we can attempt to classify those languages that require different resources in order to solve.

2.3.3.1 Classical complexity classes

Perhaps the most well known question in computational complexity is the **P**vs **NP**problem. However, what exactly are these classes. At a most basic level, one can think of **P**as those classification problems that have an efficient classical solution, while **NP**are those that can be checked in an efficient manner.

Definition 3 (**P**)**.** A promise problem $\mathcal{A} = (\mathcal{A}_{\text{yes}}, \mathcal{A}_{\text{no}})$ is in the class **P**if there exists a polynomial-time Turing Machine M such that $M(x)$ accepts x if and only if $x \in \mathcal{A}_{\text{yes}}$.

Note that the Turing Machine M is required to halt on all inputs, and thus this is exactly what we mean by a polynomial-computation. Some simple examples of languages in ¶are

[**TO DO:** *find* **P***languages*]

Definition 4 (**NP**)**.** A promise problem $\mathcal{A} = (\mathcal{A}_{\text{yes}}, \mathcal{A}_{\text{no}})$ is in the class **NP**if there exists a polynomial q and a polynomial-time Turing Machine M such that

- if $x \in \mathcal{A}_{\text{yes}}$, then there exists a string $y \in \Sigma^{q(|x|)}$ such that $M(x, y)$ accepts.
- if $x \in \mathcal{A}_{\text{no}}$, then for all strings $y \in \Sigma^{(q(|x|)}$, $M(x, y)$ rejects.

Essentially, a language is in **NP**if a given string can be proven to be in the language. This includes useful problems such as whether a given graph has a 3-coloring, whether an integer p has at least k prime factors, and all problems in ¶.

2.3.3.2 Bounded-Error Quantum Polynomial Time

With these classical problems now defined, we will want to understand what happens when we include quantum mechanics. There is a way to define a quantum Turing machine, in an analog to the classical case, but the current state of the art has instead gone toward using quantum circuits instead.

Intuitively, the idea behind Bounded-Error Quantum Polynomial Time (**BQP**) consists of those problems that can be solved by a quantum computer efficiently. However, we need to somehow encode the circuit

Definition 5 (**BQP**)**.** A promise problem $\mathcal{A} = (\mathcal{A}_{\text{yes}}, \mathcal{A}_{\text{no}})$ if there exist a uniform family of quantum circuits $Q = \{Q_n : n \in \mathbb{N}\}$ such that

- If $x \in \mathcal{A}_{\text{yes}}$, then $Q_{|x|}(|\,x\rangle) \geq \frac{2}{3}$.
- If $x \in \mathcal{A}_{\text{no}}$, then $Q_{|x|}(|\,x\rangle) \leq \frac{1}{3}$.

Note that these t

2.3.3.3 Quantum Merlin-Arthur

In addition to having an understanding of when a quantum computer can solve a particular problem, we will also want an understanding of those problems that most likely cannot be

Definition 6 (**QMA**)**.** A promise problem $\mathcal{A} = (\mathcal{A}_{\text{yes}}, \mathcal{A}_{\text{no}})$ if there exists a uniform family of quantum circuits $Q = \{Q_n : n \in \mathbb{N}\}$ such that

- If $x \in \mathcal{A}_{\text{yes}}$, then there exists a state $|\psi\rangle \in \mathbb{C}^{p(|x|)}$ such that $Q_{|x|}(|x\rangle, |\psi\rangle) \geq \frac{2}{3}$.
- If $x \in \mathcal{A}_{\text{no}}$, then for all states $|\psi\rangle \in \mathbb{C}^{p(|x|)}$, $Q_{|x|}(|x\rangle, |\psi\rangle) \leq \frac{1}{3}$.

Intuitively, this is like the class **NP**in that the circuit only accepts if there exists a proof that the input is in the language. This proof might be extremely difficult to construct, but it still exists.

2.3.3.4 Reductions and Complete Problems

While we are interested in these complexity classes, it is often difficult to work with the exact definitions used. As an example, in the definition of **NP**, to show something for all of the class we would somehow need to encode the entire computation of the Turing machine in our proof. One way to get around this is via reductions.

Essentially a reduction is a polynomial-time computable function from one computational problem to another. Because this reduction is easy to compute, if we can solve the second problem, then we can also solve the first problem. More concretely, let $\mathcal{A} = (\mathcal{A}_{\text{yes}}, \mathcal{A}_{\text{no}}$ and $\mathcal{B} = (\mathcal{B}_{\text{yes}}, \mathcal{B}_{\text{no}})$ be two promise problems. We say that there

2.4 Hamiltonian simulation

[**TO DO:** *Give a high level overview of the simulation algorithm?*]

With the definitions of the various complexity classes, and in particular defining complete problems for these classes, we will find that we often need to reduce one problem to another, in order to show that a given problem is contained within a complexity class. Of particular interest to us will be the simulation of Hamiltonian dynamics, as all of the problems in this thesis are defined in terms of Hamiltonians.

In particular, we will need to show how to simulate the evolution of a sparse, row-computable Hamiltonian on a given state $|\phi\rangle$. The state $|\phi\rangle$ might be a en efficiently computable state, or it might be a provided to us in a **QMA**-style procedure, but we are really only interested in understanding the dynamics.

The problem of simulating Hamiltonian dynamics has been featured rather heavily in the literature, as it was the original motivation that Feynman gave for quantum computers [22, 23]. In particular, Lloyd showed how to simulate sums of local operators [26], and this idea was generalized by Aharanov and Ta-Shma to (efficiently computable) sparse Hamiltonians [1]. Since then, various schemes have improved the requirements on time [4, 40, 5], as well as the dependence on the precision [6, 7] and various other avenues of research [11, 32], have managed to greatly improve our ability to simulate quantum dynamics.

While Hamiltonians that are a sum of local operations are relatively easy to understand, d-sparse Hamiltonians are relatively more complex. The reason that much of the literature has focused on local Hamiltonians is that they are easy to specify, as we need only write down each of the local Hamiltonians. In particular, they are succinct representations for Hamiltonians on an exponential-sized Hilbert space, such that each non-zero term of the Hamiltonian corresponding

to a specific basis vector can be determined efficiently. Additionally, these local-Hamiltonians are further restricted to only have non-zero transition amplitudes for states that satisfy some locality conditions, but for the purposes of simulation the succinctness property is what we care about.

Namely, the fact that a local Hamiltonian is succinctly representable is all that is used in the algorithms for simulating Hamiltonian dynamics. As such, if we can generalize these properties, we can generalize the Hamiltonians that we can simulate. A row-computable, d-spare matrix is such a generalization, in which each row of a given Hamiltonian has at most d non-zero entries, and there exists some efficiently computable function $f_i(x)$ that outputs the value (and position) of the ith nonzero entry of the xth row. Note that k-local Hamiltonians are d-sparse (for some d depending on the local dimension and connectivity), and easily row-computable; this is the natural generalization.

The basic idea behind most simulation algorithms is to color each non-zero matrix element of the Hamiltonian H so that the matrix corresponding to each color satisfies some technical property, show how to simulate each color individually for a short period of time, and then show how to combine the individual simulations into a simulation of the entire Hamiltonian. The current state of the art [8] uses several techniques, including quantum walk algorithms, simulations of linear combinations of unitaries, and Bessel functions, but their main result is the following

Theorem 1 (Theorem 1 of [8])**.** *A d-sparse Hamiltonian H acting on n qubits can be simulated for time t within error ϵ with*

$$\mathcal{O}\Big(\tau \frac{\log(\tau/\epsilon)}{\log\log(\tau/\epsilon)}\Big) \tag{2.4}$$

queries and

$$\mathcal{O}\Big(\tau\big[n + \log^{5/2}(\tau/\epsilon)\big] \frac{\log(\tau/\epsilon)}{\log\log(\tau/\epsilon)}\Big) \tag{2.5}$$

additional 2-qubit gates, where $\tau := d\|H\|_{\max} t$.

Note that the theorem was proved in the black box model, where the function f was provided via black box. Assume that f is superlinear in both n and $\log^{5/2}(\tau/\epsilon)$, the time-complexity for simulating such a Hamiltonian is simply the product of the complexity of f with (2.4). Note that if f is efficient to compute, this is an efficient simulation of the Hamiltonian dynamics.

2.5 Various Mathematical Lemmas

In addition to these various complexity results, it will also be useful to have a list of certain mathematical lemmas that will be used several times in the thesis. These lemmas might also be of independent interest.

2.5.1 Truncation Lemma

Perhaps the first such lemma we called the truncation lemma. The idea behind this lemma is to approximate the evolution of a state under some particular Hamiltonian with another, where the differences between the two Hamiltonians only occur far from the support of the given state. One would expect that since the state must evolve "far" in order to reach the differs between the two Hamiltonians, the evolution between the two will be close. This lemma makes this intuition precise.

Lemma 1 (Truncation Lemma)**.** *Let H be a Hamiltonian acting on a Hilbertspace $\mathcal{H}$ and let $|\Phi\rangle \in \mathcal{H}$ be a normalized state. Let $\mathcal{K}$ be a subspace of $\mathcal{H}$, let P be the projector onto $\mathcal{K}$, and let $\tilde{H} = PHP$ be the Hamiltonian within this subspace. Suppose that, for some $T > 0$, $W \in \{H, \tilde{H}\}$, $N_0 \in \natural$, and $\delta > 0$, we have, for all $0 \leq t \leq T$,*

$$e^{-iWt}|\Phi\rangle = |\gamma(t)\rangle + |\epsilon(t)\rangle \text{ with } \||\epsilon(t)\rangle\| \leq \delta$$

and

$$(1-P)H^r|\gamma(t)\rangle = 0 \text{ for all } r \in \{0, 1, \ldots, N_0 - 1\}.$$

Then, for all $0 \leq t \leq T$,

$$\left\| \left(e^{-iHt} - e^{-i\tilde{H}t} \right) |\Phi\rangle \right\| \leq \left(\frac{4e\|H\|t}{N_0} + 2 \right) \left(\delta + 2^{-N_0}(1+\delta) \right).$$

This lemma actually combines two different methods. The first assumes that the

Proposition 1. *Let H be a Hamiltonian acting on a Hilbert space $\mathcal{H}$, and let $|\Phi\rangle \in \mathcal{H}$ be a normalized state. Let $\mathcal{K}$ be a subspace of $\mathcal{H}$ such that there exists an $N_0 \in \natural$ so that for all $|\alpha\rangle \in \mathcal{K}^\perp$ and for all $n \in \{0, 1, 2, \ldots, N_0 - 1\}$, $\langle \alpha | H^n | \Phi \rangle = 0$. Let P be the projector onto $\mathcal{K}$ and let $\tilde{H} = PHP$ be the Hamiltonian within this subspace. Then*

$$\|e^{-it\tilde{H}}|\Phi\rangle - e^{-itH}|\Phi\rangle\| \leq 2 \left(\frac{e\|H\|t}{N_0} \right)^{N_0}.$$

Proof. Define $|\Phi(t)\rangle$ and $|\tilde{\Phi}(t)\rangle$ as

$$|\Phi(t)\rangle = e^{-itH}|\Phi\rangle = \sum_{k=0}^{\infty} \frac{(-it)^k}{k!} H^k |\Phi\rangle \qquad |\tilde{\Phi}(t)\rangle = e^{-it\tilde{H}}|\Phi\rangle = \sum_{k=0}^{\infty} \frac{(-it)^k}{k!} \tilde{H}^k |\Phi\rangle.$$

Note that by assumption, $\tilde{H}^k|\Phi\rangle = H^k|\Phi\rangle$ for all $k < N_0$, and thus the first N_0 terms in the two above sums are equal. Looking at the difference between these two states, we have

$$\begin{aligned}
\||\Phi(t)\rangle - |\tilde{\Phi}(t)\rangle\| &= \left\| \sum_{k=0}^{\infty} \frac{(-it)^k}{k!} \left(H^k - \tilde{H}^k \right) |\Phi\rangle \right\| \\
&= \left\| \sum_{k=0}^{N_0-1} \frac{(-it)^k}{k!} \left(H^k - \tilde{H}^k \right) |\Phi\rangle - \sum_{k=N_0}^{\infty} \frac{(-it)^k}{k!} \left(H^k - \tilde{H}^k \right) |\Phi\rangle \right\| \\
&\leq \sum_{k=N_0}^{\infty} \frac{t^k}{k!} \left(\|H\|^k + \|\tilde{H}\|^k \right) \\
&\leq 2 \sum_{k=N_0}^{\infty} \frac{t^k}{k!} \|H\|^k
\end{aligned}$$

where the last step uses the fact that $\|\tilde{H}\| \leq \|P\|\|H\|\|P\| = \|H\|$. Thus for any $c \geq 1$, we have

$$\begin{aligned}
\||\Phi(t)\rangle - |\tilde{\Phi}(t)\rangle\| &\leq \frac{2}{c^{N_0}} \sum_{k=N_0}^{\infty} \frac{(ct)^k}{k!} \|H\|^k \\
&\leq \frac{2}{c^{N_0}} \exp(ct\|H\|).
\end{aligned}$$

We obtain the best bound by choosing $c = N_0/\|Ht\|$, which gives

$$\| |\Phi(t)\rangle - |\tilde{\Phi}(t)\rangle \| \leq 2 \left(\frac{e\|H\|t}{N_0} \right)^{N_0}$$

as claimed. (If $c < 1$ then the bound is trivial.) □

Proposition 2. *Let $U_1, \ldots, U_n$ and $V_1, \ldots, V_n$ be unitary operators. Then for any $|\psi\rangle$,*

$$\left\| \left(\prod_{i=n}^{1} U_i - \prod_{i=n}^{1} V_i \right) |\psi\rangle \right\| \leq \sum_{j=1}^{n} \left\| (U_j - V_j) \prod_{i=j-1}^{1} U_i |\psi\rangle \right\|. \tag{2.6}$$

Proof. The proof is by induction on n. The case $n = 1$ is obvious. For the induction step, we have

$$\left\| \left(\prod_{i=n}^{1} U_i - \prod_{i=n}^{1} V_i \right) |\psi\rangle \right\| = \left\| \left(\prod_{i=n}^{1} U_i - V_n \prod_{i=n-1}^{1} U_i + V_n \prod_{i=n-1}^{1} U_i - \prod_{i=n}^{1} V_i \right) |\psi\rangle \right\| \tag{2.7}$$

$$\leq \left\| (U_n - V_n) \prod_{i=n-1}^{1} U_i |\psi\rangle \right\| + \left\| \left(\prod_{i=n-1}^{1} U_i - \prod_{i=n-1}^{1} V_i \right) |\psi\rangle \right\| \tag{2.8}$$

$$\leq \sum_{j=1}^{n} \left\| (U_j - V_j) \prod_{i=j-1}^{1} U_i |\psi\rangle \right\| \tag{2.9}$$

where the last step uses the induction hypothesis. □

Proof of Lemma **??**. For $M \in \natural$ write

$$\begin{aligned}
\|(e^{-iHt} - e^{-i\tilde{H}t})|\Phi\rangle\| &= \left\| \left(\left(e^{-iH\frac{t}{M}} \right)^M - \left(e^{-i\tilde{H}\frac{t}{M}} \right)^M \right) |\Phi\rangle \right\| \\
&\leq \sum_{j=1}^{M} \left\| \left(e^{-iH\frac{t}{M}} - e^{-i\tilde{H}\frac{t}{M}} \right) e^{-iW(j-1)\frac{t}{M}} |\Phi\rangle \right\| \\
&\leq \sum_{j=1}^{M} \left\| \left(e^{-iH\frac{t}{M}} - e^{-i\tilde{H}\frac{t}{M}} \right) \left(|\gamma(\tfrac{(j-1)t}{M})\rangle + |\epsilon(\tfrac{(j-1)t}{M})\rangle \right) \right\| \\
&\leq 2M\delta + \sum_{j=1}^{M} \left\| \left(e^{-iH\frac{t}{M}} - e^{-i\tilde{H}\frac{t}{M}} \right) \frac{|\gamma(\frac{(j-1)t}{M})\rangle}{\left\| |\gamma(\frac{(j-1)t}{M})\rangle \right\|} \right\| \left\| |\gamma(\tfrac{(j-1)t}{M})\rangle \right\| \\
&\leq 2M\delta + 2M \left(\frac{e\|H\|t}{MN_0} \right)^{N_0} (1+\delta)
\end{aligned}$$

where in the second line we have used Proposition **??** and in the last step we have used Proposition **??** and the fact that $\||\gamma(t)\rangle\| \leq 1 + \delta$. Now, for some $\eta > 1$, choose

$$M = \left\lceil \frac{\eta e\|H\|t}{N_0} \right\rceil$$

for $0 < t \leq T$ to get

$$\begin{aligned}
\|(e^{-iHt} - e^{-i\tilde{H}t})|\Phi\rangle\| &\leq 2M \left(\delta + \eta^{-N_0}(1+\delta) \right) \\
&\leq 2 \left(\frac{\eta e\|H\|t}{N_0} + 1 \right) \left(\delta + \eta^{-N_0}(1+\delta) \right).
\end{aligned}$$

The choice $\eta = 2$ gives the stated conclusion. □

Note that it would be slightly better to take a smaller value of η. However, this does not significantly improve the final result; the above bound is simpler and sufficient for our purposes.

2.5.2 Nullspace Projection Lemma

When we discuss the ground spaces and ground energies of various Hamiltonians, we will often want to know what happens to the ground spaces and ground energies when two such Hamiltonians are added together (such as adding penalties enforcing particular initial states). As such, the Nullspace Projection Lemma exactly discusses how such systems add together. As far as I am aware this lemma was initially used (implicitly) by Mizel et. al. [**TO DO:** *find correct reference*] We then used this in our proof of the **QMA**-completeness for the Bose-Hubbard model. We then found an additional place that used a similar lemma, with slightly better bounds. While the improvement is minor, here is a proof of the improved bound (and note that the improvement was left as a proof for the reader in the newer result).

Lemma 2 (Nullspace Projection Lemma)**.** *Let H_A and H_B be positive semi-definite matrices. Suppose that the nullspace, S, of H_A is nonempty, and that*

$$\gamma\big(H_B|_S\big) \geq c > 0 \qquad \textit{and} \qquad \gamma(H_A) \geq d > 0. \tag{2.10}$$

Then,

$$\gamma(H_A + H_B) \geq \frac{cd}{d + \|H_B\|}. \tag{2.11}$$

Proof. Let $|\psi\rangle$ be a normalized state satisfying

$$\langle\psi|H_A + H_B|\psi\rangle = \gamma(H_A + H_B). \tag{2.12}$$

Let Π_S be the projector onto the nullspace of H_A. First suppose that $\Pi_S|\psi\rangle = 0$, in which case

$$\langle\psi|H_A + H_B|\psi\rangle \geq \langle\psi|H_A|\psi\rangle \geq \gamma(H_A) \tag{2.13}$$

and the result follows. On the other hand, if $\Pi_S|\psi\rangle \neq 0$ then we can write

$$|\psi\rangle = \alpha|a\rangle + \beta|a^\perp\rangle \tag{2.14}$$

with $|\alpha|^2+|\beta|^2 = 1$, $\alpha \neq 0$, and two normalized states $|a\rangle$ and $|a^\perp\rangle$ such that $|a\rangle \in S$ and $|a^\perp\rangle \in S^\perp$. (If $\beta = 0$ then we may choose $|a^\perp\rangle$ to be an arbitrary state in $S^\perp$ but in the following we fix one specific choice for concreteness.) Note that any state $|\phi\rangle$ in the nullspace of $H_A + H_B$ satisfies $H_A|\phi\rangle = 0$ and hence $\langle\phi|a^\perp\rangle = 0$. Since $\langle\phi|\psi\rangle = 0$ and $\alpha \neq 0$ we also see that $\langle\phi|a\rangle = 0$. Hence any state

$$|f(q, r)\rangle = q|a\rangle + r|a^\perp\rangle \tag{2.15}$$

is orthogonal to the nullspace of $H_A + H_B$, and

$$\gamma(H_A + H_B) = \min_{|q|^2+|r|^2=1} \langle f(q, r)|H_A + H_B|f(q, r)\rangle. \tag{2.16}$$

Within the subspace Q spanned by $|a\rangle$ and $|a^\perp\rangle$, note that

$$H_A|_Q = \begin{pmatrix} w & v^* \\ v & z \end{pmatrix} \qquad H_B|_Q = \begin{pmatrix} 0 & 0 \\ 0 & y \end{pmatrix} \tag{2.17}$$

where $w = \langle a|H_B|a\rangle$, $v = \langle a^\perp|H_B|a\rangle$, $y = \langle a^\perp|H_A|a^\perp\rangle$, and $z = \langle a^\perp|H_B|a^\perp\rangle$, and that we are interested in the smaller eigenvalue of

$$M = H_A|_Q + H_B|_Q = \begin{pmatrix} w & v^* \\ v & y+z \end{pmatrix}. \tag{2.18}$$

Letting ϵ_+ and ϵ_- be the two eigenvalues of M with $\epsilon_+ \geq \epsilon_-$, note that

$$\epsilon_+ = \|M\| \leq \|H_A|_Q\| + \|H_B|_Q\| \leq y + \|H_B|_Q\| \leq y + \|H_B\|, \tag{2.19}$$

where we have used the Cauchy interlacing theorem to note that $\|H_B|_Q\| \leq \|H_B\|$. Additionally, we have that

$$\epsilon_+\epsilon_- = \det(M) = w(y+z) - |v|^2 \geq wy \tag{2.20}$$

where we used the fact that $H_B|_Q$ is positive-semidefinite. Putting this together, we have that

$$\gamma(H_A + H_B) = \min_{|q|^2+|r|^2=1} \langle f(q,r)|H_A + H_B|f(q,r)\rangle = \epsilon_- \geq \frac{wy}{y + \|H_B\|}. \tag{2.21}$$

As the right hand side increased monotonically with both w and y, and as $w \geq \gamma(H_B|_S) \geq c$ and $y \geq \gamma(H_A) \geq d$, we have

$$\gamma(H_A + H_B) \geq \frac{cd}{d + \|H_B\|} \tag{2.22}$$

as required. □

Chapter 3

Scattering on graphs

[**TO DO:** *write a better introduction, including more citations*]

Scattering is one of the more basic ideas of physics, with a surprisingly large usefulness. The old joke about physicists throwing two frogs at each other [**TO DO:** *cite*] in order to understand their internal components has a grain of truth; particle accelerators [**TO DO:** *cite*] , gravitational lensing [**TO DO:** *cite*] , and x-ray crystallography [**TO DO:** *cite*] are just some examples out of many in which scattering plays a key role in physicists probing of the universe.

Along these lines, we would wonder at the usefulness of scattering in quantum information. High energy physics uses scattering to probe atoms and molecules [**TO DO:** *cite multiple*] , but we would want to discretize the system for use in quantum information [**TO DO:** *should I include some bit about discretized quantum field theories? Probably not*] . In this manner, we would replace the continuum by a discrete set of positions, and understand the evolution in such a model.

With this discretization, we are analyzing a system propagating on an infinite graph, and thus we can also think of this as the limit of a continuous time quantum walk to infinite graphs. We know that quantum walks are useful algorithmic devices [**TO DO:** *cite QW algorithms*] , and one might wonder whether these infinite systems can allow for intuitive algorithms. It turns out that this answer is yes, and the original motivation for graph scattering was an algorithm using graph scattering to solve a problem on boolean formulas faster than any randomized classical computation [21]. This algorithm was easily understood using the intuition from scattering, and thus graph scattering became a useful tool for understanding quantum walk algorithms.

This chapter should serve as a broad introduction to graph scattering. In particular, the notations of scattering matrices, bound states, and wavepackets have all been used in previous works. This chapter attempts to standardize notations, while also explaining how everything works. While there is some original work in this chapter, we also utilize and state several of the results from [21, 11, 18, 14] in which the author did not contribute.

3.1 Free particles in the continuum

Let us first take a look at one of the most simple quantum systems seen in any quantum mechanics text (e.g., [24] or [34]): a free particle in one dimension. Without any potential or interactions, we have that the time independent Schrödinger equation reads

$$\frac{\partial^2}{\partial x^2}\psi(x) = -\frac{2m}{\hbar^2}E\psi(x) = -k^2\psi(x), \tag{3.1}$$

which requires the (unnormalizable) solutions,

$$\psi(x) = A\exp(-ikx) + B\exp(ikx) \tag{3.2}$$

for real k and for arbitrary constant A and B. These *momentum states* correspond to particles travelling with momentum k along the real line, and form a basis for the entire Hilbert space.

While these momentum states are useful for understanding the propagation of particles in the quantum setting, if we want to understand more complicated behavior we need to change the potential energy of the system. In particular, we will now include some finite-range potential V that is non-zero only for $|x| < d$ for some constant d, so that outside this range the eigenstates remain unchanged. The only difference is that we will deal with a superposition of states for each energy instead of the pure momentum states, forcing some relation between the A and B of equation (3.2). Namely, the eigenstates of this system become

$$\psi(x) = \begin{cases} \exp(-ikx) + R(k)\exp(ikx) & x \leq -d \\ T(k)\exp(-ikx) & x \geq d \\ \phi(x,k) & |x| \leq d \end{cases} \tag{3.3}$$

for some functions $R(k)$, $T(k)$, and $\phi(x,k)$ that depends on the interaction V. As intuition, these states can be seen as a particle with momentum k coming in from the left, hitting the potential, and then scattering (which motivates the T and R labels).

In addition to these scattering states, it is also possible for bound states to exist. These are normalizable states that have most (or all) of their amplitude near the non-zero potential, so that they do not affect scattering states that originate far from the interaction. They simply exist as additional states in the Hilbert space.

[**TO DO:** *possibly include a δ-function potential scattering problem in the thesis*]

3.1.1 Free particles on an infinite path

With the simple free-particle example in mind, let us now examine the discretized system. Namely, instead of allowing arbitrary real positions, let us restrict attention to some regular 1-D lattice, such as the natural numbers. Further, much as there is a natural linear ordering on the positions in the continuum, and in order for a particle to move between a and b it must travel over all positions between a and b, in the discretized system we only allow particles to move between adjacent integers. Explicitly, the position basis for this discretized Hilbert space will be labeled by $n \in \mathbb{N}$, with transport only allowed between integers that differ by one.

If we then want to understand how this discretized system works, it will be useful to discretize the entire Schrödinger equation. Along those lines, remember that the second derivative of a function f at x can be written as

$$\frac{d^2}{dx^2}f(x) = \lim_{h\to 0}\frac{f(x+h) - 2f(x) - f(x-h)}{h^2}. \tag{3.4}$$

Since we were originally working in the continuum, we could let h go to zero without any problems. In our discretize world, however, there exists some smallest difference in x, namely 1. As such, we have that in our discretized space, the operator corresponding to the second position derivative can be written as

$$\Delta^2 = \sum_{x=-\infty}^{\infty} |x\rangle\big(\langle x-1| - 2\langle x| + \langle x+1|\big) = \sum_{x=-\infty}^{\infty}\big(|x\rangle\langle x-1| + |x\rangle\langle x+1|\big) - 2\mathbb{I}. \tag{3.5}$$

If we then rescale the energy levels, we have that the identity term in the right hand side of (3.5) can be removed, so that Δ^2 on this discretized one-dimensional system is proportional to the adjacency matrix of an infinite path.

With this representation of the second derivative operator, we can see that when discretized, the time-independent Schrödinger equation for a free particle becomes

$$\Delta^2|\psi\rangle = \Big(\sum_{x=-\infty}^{\infty} \big(|x+1\rangle\langle x| + |x-1\rangle\langle x|\big) - 2\mathbb{I}\Big)|\psi\rangle = E'_\psi|\psi\rangle. \tag{3.6}$$

If we rescale the energy term, and then break the vector equation into its components, we find that

$$\langle x+1\,|\,\psi\rangle + \langle x-1\,|\,\psi\rangle = E_\psi\langle x\,|\,\psi\rangle \tag{3.7}$$

for all $x \in \mathbb{Z}$. Taking motivation from the continuous case, we then make the ansatz that $\langle x\,|\,\psi\rangle = e^{ikx}$ for some k, and find

$$\langle x+1\,|\,\psi\rangle + \langle x-1\,|\,\psi\rangle = e^{ik}e^{ikx} + e^{-ik}e^{ikx} = E_\psi e^{ikx} = E_\psi\langle x\,|\,\psi\rangle \qquad \Rightarrow \tag{3.8}$$

$$E_\psi = e^{ik} + e^{-ik} = 2\cos(k). \tag{3.9}$$

If we then use the fact that E_ψ must be real, and that the amplitudes should not diverge to infinity as $x \to \pm\infty$, we find that the only possible values of k are between $[-\pi, \pi)$. Hence, in analogy with the continuous case, the eigenbasis of the Hamiltonian corresponds to momentum states, but where the possible momenta only range over $[-\pi, \pi)$. We represent this momentum state with momenta k as $|\tilde{k}\rangle$.

Additionally, we can discuss the "speed" of these eigenstates, which is given by the derivative of the energy with respect to momentum. We con then see that

$$s = \left|\frac{dE_k}{dk}\right| = 2\sin(|k|), \tag{3.10}$$

which is to be compared with $s \propto |k|$ for in the continuum case. While the discretization does change the relationship between momentum, energy, and speed, if we restrict ourselves to small k (so that the discretization is not noticeable), we recover the linear relationship. In this way, as the distance between vertices grows smaller, we recover the continuum case.

One slight problem with this discussion is that these momentum states are not normalizable, and thus technically are not states in the Hilbert space. This problem is identical to that of the continuum, and thus we shall not worry about these states of the extended Hilbert space. However, one problem that is unique to our discretized system is that there are an uncountable number of momentum states, while the position basis contains only a countable number of basis states. It turns out that the resolution to this conundrum is that the two bases have different orthogonality conditions: the position basis elements are Kronecker delta orthogonal, while the momentum basis elements are Dirac δ-function orthogonal. Namely,

$$\langle\tilde{k}\,|\,\tilde{p}\rangle = \sum_{x=-\infty}^{\infty} e^{-ikx}e^{ikp} = \sum_{x=-\infty}^{\infty} e^{i(p-k)x} = 2\pi\delta(p-k), \tag{3.11}$$

so that we can decompose the identity on this space as

$$\mathbb{I} = \sum_{x=-\infty}^{\infty} |x\rangle\langle x| = \frac{1}{2\pi}\int_{-\pi}^{\pi} dk|\tilde{k}\rangle\langle\tilde{k}|. \tag{3.12}$$

3.2 Graph scattering

Essentially, at this point we have recovered many of the results of the continuous free particle, but with a discretized position space. The main idea behind the discretization was the change in the second derivative operator, and noting that it became proportional to the adjacency matrix of a simple graph. This seems very similar to the case of continuous time quantum walks, in which the Hamiltonian is explicitly taken to be the adjacency matrix of a (finite sized) graph.

As such, let us assume that the Hamiltonian of the entire system is proportional to the adjacency matrix for these graph scattering problems. If we now want to add some finite potential to the system, in an attempt to discretize the scattering formalism, we could add a potential function, with explicit potential energies at various vertices of the infinite path. However, if we wish to examine scattering only on unweighted graphs, we need to be a little more clever.

To solve this problem, we will connect graphs in such a way that far from our connections the graphs will look identical to that of an infinite path, but near our changes the graph can differ drastically from an infinite path. In particular, we will use an arbitrary (finite) graph as a base, and connect semi-infinite (infinite in one direction) paths to this base graph.

With this construction, the eigenvalue equation must still be satisfied along the semi-infinite paths, and thus the form of the eigenstates along the paths must still be of the form e^{ikx} for some k and x. However, we can no longer assume that k is real, as the fact that the attached semi-infinite paths are only infinite in one direction allow for an exponentially decaying amplitudes along the paths. Additionally, we can have nontrivial correlations between the amplitudes among the different paths, similar to the correlated reflection and transmission coefficients in the continuous case.

Note that the topic of graph scattering is widely used in the literature. Most of this section is not original work, and should be taken as background material. In particular, these results are taken from [21, 11, 18, 14]

[**TO DO:** *Find more accurate citations*]

3.2.1 Infinite path and a Graph

In the most simple example, let us attached a graph $\widetilde{G}$ to an infinite path. In particular, we assume that $\widetilde{G}$ is attached to a single vertex of the infinite path, and that the graph is attached by adding an edge from each vertex in $S \subset V(\widetilde{G})$ to one specific vertex of the infinite path, which we label 0, as seen in Figure 3.1. Calling this new graph G, the adjacency matrix of G, and thus the Hamiltonian for this scattering problem, can be seen to be

$$A(G) = A(\widetilde{G}) + \sum_{v \in S \subset V(\widetilde{G})} |v\rangle\langle 0| + |0\rangle\langle v| + \sum_{x=-\infty}^{\infty} |x\rangle\langle x+1| + |x+1\rangle\langle x|. \tag{3.13}$$

If we then want to inspect the eigenvectors of this Hamiltonian, we find that the eigenvalue equation on the infinite path is identical to that of an infinite path without the graph attached. Hence, we can see that any eigenstate of the Hamiltonian must take the form $Ae^{ikx} + Be^{-ikx}$ for some k along the infinite paths.

With this assumption, we can see that there are three distinct cases for the form of the eigenstates. In particular, the eigenstate could have no amplitude along the infinite paths, being confined to the finite graph $\widehat{G}$. It could also be a normalizable state not confined to the finite graph $\widehat{G}$, in that the amplitude along the infinite paths decays exponentially. Finally, the eigenstate could be an unnormalizable state, in which case we will call it a scattering state.

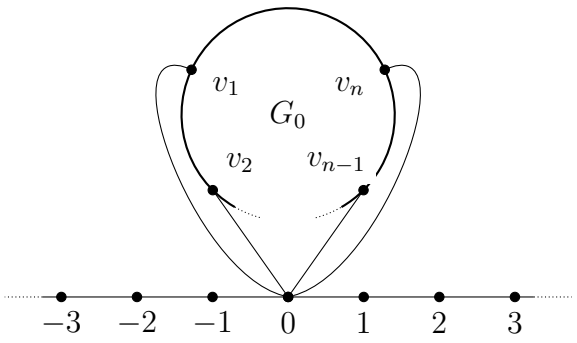

Figure 3.1: A simple example for graph scattering. A graph $\widetilde{G}$ is attached to an infinite path.

In the first case, where the state is confined to the graph $\widetilde{G}$, we have the major restriction that the state $|\psi\rangle$ satisfies

$$\langle x|\psi\rangle = 0 \tag{3.14}$$

for all $x \in \mathbb{N}$. Additionally, if $|\phi\rangle$ is the restriction of $|\phi\rangle$ to the finite graph $\widetilde{G}$, we have that

$$A(\widetilde{G})|\phi\rangle = E|\phi\rangle \tag{3.15}$$

so that $|\phi\rangle$ is an eigenstate of the graph $\widetilde{G}$, that also satisfies

$$\sum_{v\in S}\langle v|\phi\rangle = 0. \tag{3.16}$$

These restrictions together show that these completely bound states have an extremely restricted form as eigenstates of $A(\widetilde{G})$, but the infinite path does not really affect them. In particular, their energies are not restricted by anything other than the graph itself, but we are guaranteed to have at most $|V(\widetilde{G})|$ of these confined bound states.

In the second case, we could have that the eigenstate is normalizable, but is not confined to the graph $\widetilde{G}$. In this case, we have that the amplitudes along the infinite paths must go to zero, but they must still be a sum of exponentials. As such, we have that $|\psi\rangle$ must be of the form

$$\langle x|\psi\rangle = Az^x \tag{3.17}$$

for some $z \in (-1,1)\setminus\{0\}$ for all $x \in \mathbb{N}$, so that the energy must be $z + z^{-1}$ (the case for $z = 0$ forces $A = 0$, and we are in the first case). Additionally, we can see that if $|\phi\rangle$ is the restriction of $|\psi\rangle$ to those vertices inside the graph $A(\widetilde{G})$, they must satisfy

$$A(\widetilde{G}) + A\sum_{v\in S}|v\rangle\langle v|\phi\rangle = 2\cos(k)|\phi\rangle, \tag{3.18}$$

a modified version of the eigenvalue equation for the graph $A(\widetilde{G})$.

Let us finally assume that the state is a scattering state. Note that the eigenvalue of the state must be in the range $[-2,2]$, and that the form of the eigenstate along the paths must be scalar multiples of e^{ikx} and e^{-ikx}, for some $k \in [-\pi,\pi]$. Explicitly, the state must be of the form

$$\langle x|\psi\rangle = \begin{cases} Ae^{ikx} + Be^{ikx} & x \le 0 \\ Ce^{ikx} + De^{ikx} & x \ge 0 \end{cases} \tag{3.19}$$

where we note that the amplitude can change at $x = 0$, since we have attached the graph $\widetilde{G}$. However, we do have that $A + B = C + D$, since the amplitude at 0 is single valued, and that the eigenvalue of this state is given by $2\cos(k)$. Note that we have not yet determined the form of the eigenstate inside the graph $\widetilde{G}$, but if we define $|\phi\rangle$ to be the restriction of $|\psi\rangle$ to the finite graph $\widetilde{G}$, then $|\phi\rangle$ must satisfy the equation

$$A(G)|\phi\rangle + (A+B)\sum_{v\in S}|v\rangle\langle v|\phi\rangle = 2\cos(k)|\phi\rangle, \tag{3.20}$$

where the additional term arises from the fact that the vertices in S are connected to the vertex 0. Finally, we have that

$$2\cos(k)\langle 0|\psi\rangle = Ae^{-ik} + Be^{ik} + Ce^{ik} + De^{-ik} + \sum_{v\in S}\langle v|\phi\rangle, \tag{3.21}$$

since the eigenvalue equation must be satisfied at 0.

In the first two cases, we have that the state is highly localized to the area surrounding the graph $\widetilde{G}$, and thus they do not have a large effect on wavefunctions that originate far from the graph. However, the aptly named scattering states can be used to determine the time evolution of these wave functions. In particular, if we look at the case where $A = 1$ and $D = 0$, we can see that

$$\langle x|\psi\rangle = \begin{cases} e^{-ikx} + Be^{ikx} & x \le 0 \\ Ce^{-ikx} & x \ge 0 \end{cases} \tag{3.22}$$

so that $1 + B = C$. Note that this is reminiscent of a scattering state, with reflection amplitude B and transmission amplitude C. We can then take as intuition that these scattering states represent a wavepacket with momentum exactly k traveling towards the graph G, and then scattering with these amplitudes. We will use this intuition for our definitions of scattering on more general graphs.

3.2.2 General graphs

Let us now turn our attention to scattering on more general graphs. In particular, let $\widehat{G}$ be any finite graph, with $N + m$ vertices and an adjacency matrix given by the block matrix

$$A(\widehat{G}) = \begin{pmatrix} A & B^\dagger \\ B & D \end{pmatrix}, \tag{3.23}$$

where A is an $N \times N$ matrix, B is an $m \times N$ matrix, and D is an $m \times m$ matrix. When examining graph scattering, we will be interested in the graph G given by the graph-join of $\widehat{G}$ and N semi-infinite paths, with an additional edge between each of the first N vertices of $\widehat{G}$ and the first vertex of one semi-infinite path. A schematic example can be seen in Figure 3.2.

We shall label call the first N vertices of the graph *terminal vertices*, as they connect the semi-infinite paths to the finite graph $\widehat{G}$, and we shall label them as $(1, i)$, where $i \in [N]$. Analogously, we will refer to the vertices on the N semi-infinite paths as (x, i) for $x \in \mathbb{N}^+$ and $i \in [N]$, with the i label referring to the particular semi-infinite path on which the vertex is labeled, while the label x denotes the location along the path. We also refer to the remaining m vertices of $\widehat{G}$ as the *internal vertices* of $\widehat{G}$, and label them as $w \in [m]$. With this labeling of the vertices of G, the adjacency matrix of G is then given by

$$A(G) = A(\widehat{G}) + \sum_{j=1}^{N}\sum_{x=1}^{\infty}\big(|x, j\rangle\langle x+1, j| + |x+1, j\rangle\langle x, j|\big). \tag{3.24}$$

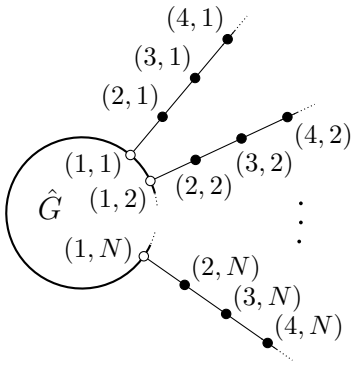

Figure 3.2: An infinite graph G obtained from a finite graph $\widehat{G}$ by attaching n semi-infinite paths. The open circles are *terminals*, vertices of $\widehat{G}$ to which semi-infinite paths are attached. The internal vertices of $\widehat{G}$ are not shown.

At this point, we want to examine the possible eigenstates of the matrix $A(G)$. It turns out that there are 3 different kinds of eigenstates, corresponding to the different qualitative properties of the eigenstate along the semi-infinite paths, exactly as in the case studied in Section 3.2.1.

While we will mostly be interested in the third such type, corresponding to scattering off of the graph, the other two kinds remain important for a decomposition of the identity. In particular, we will be guaranteed that these three kinds of eigenstates will form an orthogonal basis for the Hilbert space, and thus we will be able to use this decomposition to guarantee particular behavior of time evolved states.

3.2.2.1 Confined bound states

The easiest states to analyze are the confined bound states, which are eigenstates in which the only nonzero amplitudes are on vertices inside the finite graph $\widehat{G}$. If any vertex on the semi-infinite paths has nonzero amplitude for some eigenstate of the Hamiltonian, then the form of the Hamiltonian forces all vertices on that path to have nonzero amplitude, and thus these confined bound states are exactly those states that have finite support in the basis of vertex states.

To find these confined bound states, we restrict our Hilbert space to the space spanned by the internal vertices of $\widehat{G}$. The states of interest then correspond to the eigenstates of D (the induced adjacency matrix of $A(G)$ when restricted to the internal vertices of $\widehat{G}$) with the additional restriction that the state lies in the nullspace of $B^\dagger$, so that we can extend this state to the full Hilbert space by simply assuming all other amplitudes are zero.

As we originally assumed that there are only m internal vertices of $\widehat{G}$, there are at most m such confined bound states. Additionally, note that there are no restrictions on the eigenvalues of these states, other than those that are inherited from any restrictions placed on it by D (such as the energy being bounded by the maximum degree of $\widehat{D}$).

3.2.2.2 Unconfined bound states

The next possible type of eigenstates are those that are not confined to the finite graph $\widehat{G}$ but are still normalizable. Since these states still have amplitude along the semi-infinite paths, we know that they must be of the form Ae^{ikx}, for some A and k. However, when k is not real (corresponding to a decaying amplitude along the paths), we have that

$$2\cos(k) = 2\cos(k_r + ik_i) = 2\cos(k_r)\cosh(k_i) - i\sin(k_r)\sinh(k_i). \tag{3.25}$$

Hence, if we assume that the state is normalizable, then $k_i \neq 0$, and as the adjacency matrix is Hermitian, we must have that the eigenvalue is real, forcing $k_r = \pi n$ for some $n \in \mathbb{N}$. Note that this then implies that $e^{ik} = z$, for some $z \in (-1, 1) \setminus \{0\}$ (where 0 corresponds to the confined bound states).

As the eigenvalue equation for these states are guaranteed to be satisfied along the paths, we need to construct the form of the eigenstates inside the graph $\widehat{G}$. We can then see that the eigenvalue equation for these vertices is given by

$$\left[\begin{pmatrix} A & B^\dagger \\ B & D \end{pmatrix} + \begin{pmatrix} z \\ 0 \end{pmatrix} \right] \begin{pmatrix} \vec{\alpha} \\ \vec{\beta} \end{pmatrix} = \left(z + \frac{1}{z} \right) \begin{pmatrix} \vec{\alpha} \\ \vec{\beta} \end{pmatrix} \tag{3.26}$$

where $\vec{\alpha} \in \mathbb{C}^N$ and $\vec{\beta} \in \mathbb{C}^m$. Note that the amplitudes for a vertex (x, i) is given by $\vec{\alpha}_i z^{x-1}$. Note that we are implicitly assuming that $\vec{\alpha} \neq \vec{0}$, for in that case we are working with a confined bound state.

While there is no immediate reason to guess that the total number of bound states is finite, it has been shown that this number is indeed finite (see [14] for a more thorough explanation, using Levinson's theorem for graphs).

[**TO DO:** *I know that they are finite from the Levinson's theorem, but is there any other reason to guarantee that they are finite?*]

3.2.2.3 Scattering states

We finally reach the point of scattering states, or those unnormalizable eigenstates of the Hamiltonian. We first assume that these states are orthogonal to all bound states, and in particular that we are orthogonal to all confined bound states, as this allows us to uniquely construct the scattering states (without this assumption, if there existed a confined bound state at the appropriate energy, then we could simply add any multiple of the confined bound state to get a different scattering state).

Taking some intuition from the classical case, we will construct a set of states that correspond to sending a particle in towards the graph $\widehat{G}$ along one of the semi-infinite paths and understanding how it scatters off of the graph. Namely, for each $i \in [N]$ we will assume that there exists a state with amplitude along the i-th path of the form $e^{ikx} + S_{i,i}(k)e^{-ikx}$ for $k \in (-\pi, 0)$, and that the rest of the paths have amplitudes given by $S_{i,q}(k)e^{ikx}$. More concretely, we assume that the form of the states is given on the infinite paths by

$$\langle x, q \,|\, \mathrm{sc}_j(k) \rangle = \delta_{j,q} e^{-ikx} + S_{qj} e^{ikx}. \tag{3.27}$$

We then need to see whether such an eigenstate exists. In this case, note that S_{qj} corresponds to the transmitted amplitude along the q-th path if the particle was incident along the j-th path. In the continuous case, S forms a unitary matrix, which essentially means that any incoming particle must also leave, and be distinguishable from a particle incident from a different direction. This intuition will also hold in the discrete case, but we will show this later.

[**TO DO:** *this seems a little clunkly; try to go over and rewrite*]

If we continue to make the assumption that these states exist, we can also write the amplitudes of the m interval vertices as a column vector, as $\vec{\psi}_i(k)$, in which $\vec{\psi}_i(k)$ is the projection of $|\mathrm{sc}_j(k)\rangle$ onto the internal vertices of $\widehat{G}$. We can then collect these vectors into an $m \times N$ matrix, namely

$$\Psi(k) := \begin{pmatrix} \vec{\psi}_1(k) & \vec{\psi}_2(k) & \cdots & \vec{\psi}_N(k) \end{pmatrix} \tag{3.28}$$

Noting that the amplitudes for $|\mathrm{sc}_j(k)\rangle$ on the terminal vertices is given by $e^{-ik}\delta_{j,q} + S_{qj}(k)e^{ik}$, we can then collect all of the eigenvalue equations for the vertices in $\widehat{G}$ (both internal and termal) as

$$\begin{pmatrix} A & B^\dagger \\ B & D \end{pmatrix} \begin{pmatrix} e^{-ik}\mathbb{I} + S(k)e^{ik} \\ \Psi(k) \end{pmatrix} + \begin{pmatrix} e^{-2ik}\mathbb{I} + e^{2ik}S(k) \\ 0 \end{pmatrix} = 2\cos(k) \begin{pmatrix} e^{-ik}\mathbb{I} + S(k)e^{ik} \\ \Psi(k) \end{pmatrix}, \tag{3.29}$$

where we have constructed the scattering matrix $S(k)$ using the scattering amplitudes $S_{qj}(k)$.

By examining the lower half of this matrix equation, we can see that

$$\Psi(z) = \frac{1}{2\cos(k)\mathbb{I} - D}\big(e^{-ik}B + e^{ik}BS(z)\big), \tag{3.30}$$

which gives the amplitudes of the internal vertices in terms of the scattering matrix. Note that we have assumed that the matrix D does not have an eigenvalue equal to $2\cos(k)$, but this assumption will not be critical, as the eventual matrix $|\Psi\rangle(z)$ will be defined by analytic continuation.

Let us now examine the upper half of the matrix equation, to find

$$A\big(e^{-ik}\mathbb{I} + e^{ik}S(k)\big) + B^\dagger\Psi(k) + \big(e^{-2ik}\mathbb{I} + e^{2ik}S(z)\big) = 2\cos(k)\big(e^{-ik}\mathbb{I} + e^{ik}S(k)\big) \tag{3.31}$$

$$-\left(\mathbb{I} - e^{ik}\Big(A + B^\dagger\frac{1}{2\cos(k) - D}B\Big)\right)S(k) = \mathbb{I} - e^{-ik}\Big(A + B^\dagger\frac{1}{2\cos(k) - D}B\Big). \tag{3.32}$$

Hence, if we define

$$Q(k) = \mathbb{I} - e^{ik}\Big(A + B^\dagger\frac{1}{2\cos(k) - D}B\Big), \tag{3.33}$$

we find that

$$S(k) = -Q(k)^{-1}Q(-k), \tag{3.34}$$

if we assume that the matrix $Q(k)$ can be inverted. Note that for all $k \in (-\pi, 0)$, this might only be impossible for k in which D has a $2\cos(k)$ eigenvalue, in which case we have already run into a problem with the definition of $\Psi(k)$.

Putting this all together, we then have that the states $|\mathrm{sc}_j(k)\rangle$ exist for all $k \in (-\pi, 0)$ for which D does not have a $2\cos(k)$ eigenvalue. We will see in Section 3.2.2.5 that this restriction is an artifact of our construction of $S(k)$, and thus the scattering states will be well defined for all $k \in (-\pi, 0)$.

3.2.2.4 Half-bound states

As a limiting case for both the scattering states and the unconfined bound states, we have those states with $k = 0$ or $k = \pi$ (or equivalently with $z = \pm 1$). In either case, the two momenta correspond to particles that don't move, but the states themselves are not normalizable. They won't play much of a role in this paper, but I did want to mention them.

3.2.2.5 Scattering states for all k

While the above construction is a useful definition of the scattering states for most $k \in (-\pi, 0)$, unfortunately there are specific values of k (namely those for which D has eigenvalue $2\cos(k)$) in which the above analysis doesn't hold, due to the singularity of particular matrices. If we want to show that these scattering states exist for all $k \in (-\pi, 0)$, we need to somehow show that these singularities are just a problem of the analysis and are not intrinsic barriers to existence. Note that this construction closely follows that of [14].

Along these lines, let us extend our analysis to complex z, instead of only focusing on amplitudes of the form e^{ik}. We will define the matrix

$$\gamma(z) := \begin{pmatrix} zA - \mathbb{I} & zB^\dagger \\ zB & zD - (1+z^2)\mathbb{I} \end{pmatrix}. \tag{3.35}$$

This matrix is closely related to the eigenvalue equation for vertices of the graph $\widehat{G}$, but with e^{ik} replaced with z.

With this definition, it will be useful to note the following matrix equalities. In particular, assuming that z is a complex number such that the following matrices are not singular, we have:

$$\begin{pmatrix} \mathbb{I} & zB^\dagger \\ 0 & zD - (1+z^2)\mathbb{I} \end{pmatrix} \begin{pmatrix} -Q(z) & 0 \\ \frac{z}{zD-(1+z^2)\mathbb{I}} B & \mathbb{I} \end{pmatrix} = \begin{pmatrix} -Q(z) + zB^\dagger \frac{1}{D-(z+z^{-1})} B & zB^\dagger \\ zB & zD - (1+z^2)\mathbb{I} \end{pmatrix} \tag{3.36}$$

$$= \gamma(z) \tag{3.37}$$

Additionally, if we note that the inverse of a block diagonal matrix can be written as

$$\begin{pmatrix} X & Y \\ Z & W \end{pmatrix}^{-1} = \begin{pmatrix} \big(X - YW^{-1}Z\big)^{-1} & -X^{-1}Y\big(W - ZX^{-1}Y\big)^{-1} \\ -W^{-1}Z\big(X - YW^{-1}Z\big)^{-1} & \big(W - ZX^{-1}Y\big)^{-1} \end{pmatrix}, \tag{3.38}$$

we can then invert this equation for $\gamma(z)$ as

$$\gamma(z)^{-1} = \begin{pmatrix} -Q(z) & 0 \\ \frac{z}{zD-(1+z^2)\mathbb{I}} B & \mathbb{I} \end{pmatrix}^{-1} \begin{pmatrix} \mathbb{I} & zB^\dagger \\ 0 & zD - (1+z^2)\mathbb{I} \end{pmatrix}^{-1} \tag{3.39}$$

$$= \begin{pmatrix} -Q(z)^{-1} & 0 \\ \frac{z}{zD-(1+z^2)\mathbb{I}} BQ(z)^{-1} & \mathbb{I} \end{pmatrix} \begin{pmatrix} \mathbb{I} & -B^\dagger \frac{z}{zD-(1+z^2)\mathbb{I}} \\ 0 & \frac{1}{zD-(1+z^2)\mathbb{I}} \end{pmatrix}. \tag{3.40}$$

Combining these two matrix equations, we can then find that

$$\gamma(z)^{-1}\gamma(z^{-1}) = \begin{pmatrix} -Q(z)^{-1} & 0 \\ \frac{z}{zD-(1+z^2)\mathbb{I}} BQ(z)^{-1} & \mathbb{I} \end{pmatrix} \begin{pmatrix} \mathbb{I} & -B^\dagger \frac{z}{zD-(1+z^2)\mathbb{I}} \\ 0 & \frac{1}{zD-(1+z^2)\mathbb{I}} \end{pmatrix}$$
$$\times \begin{pmatrix} \mathbb{I} & z^{-1}B^\dagger \\ 0 & z^{-1}D - (1+z^{-2})\mathbb{I} \end{pmatrix} \begin{pmatrix} -Q\big(z^{-1}\big) & 0 \\ \frac{z^{-1}}{z^{-1}D-(1+z^{-2})\mathbb{I}} B & \mathbb{I} \end{pmatrix} \tag{3.41}$$

$$= \begin{pmatrix} -Q(z)^{-1} & 0 \\ \frac{z}{zD-(1+z^2)\mathbb{I}} BQ(z)^{-1} & \mathbb{I} \end{pmatrix} \begin{pmatrix} \mathbb{I} & 0 \\ 0 & z^{-2}\mathbb{I} \end{pmatrix} \begin{pmatrix} -Q\big(z^{-1}\big) & 0 \\ \frac{z^{-1}}{z^{-1}D-(1+z^{-2})\mathbb{I}} B & \mathbb{I} \end{pmatrix} \tag{3.42}$$

$$= \begin{pmatrix} -Q(z)^{-1} & 0 \\ \frac{z}{zD-(1+z^2)\mathbb{I}} BQ(z)^{-1} & z^{-2}\mathbb{I} \end{pmatrix} \begin{pmatrix} -Q\big(z^{-1}\big) & 0 \\ \frac{z^{-1}}{z^{-1}D-(1+z^{-2})\mathbb{I}} B & \mathbb{I} \end{pmatrix} \tag{3.43}$$

$$= \begin{pmatrix} Q(z)^{-1}Q(z^{-1}) & 0 \\ \frac{1}{D-(z+z^{-1})\mathbb{I}} B\big(z^{-2}\mathbb{I} - Q(z)^{-1}Q(z^{-1})\big) & z^{-2}\mathbb{I} \end{pmatrix} \tag{3.44}$$

$$= -\begin{pmatrix} S(z) & 0 \\ z^{-1}\Psi(s) & -z^{-2}\mathbb{I} \end{pmatrix}, \tag{3.45}$$

where we have extended the definition of S and Ψ to all complex z instead of just e^{ik}

With these matrix equations, we have a representation of the scattering matrix and the interior amplitudes in terms of the matrix γ. If we then note that

$$\gamma(z)^{-1} = \frac{1}{\det \gamma(z)} \operatorname{adj} \gamma(z) \tag{3.46}$$

where $\operatorname{adj}\gamma(z)$ is the adjugate matrix of $\gamma(z)$, then by (3.45) we can then see that the entries of $\gamma(z)$, and thus the entries of $S(z)$ and $\Psi(z)$, are rational functions of z.

With this fact, to show that the problems defining the states $|\mathrm{sc}_j(k)\rangle$ are a result of our analysis rather than intrinsic difficulties, we need only show that there are no poles in the matrix elements for $S(z)$ or $\Psi(z)$ for z on the unit circle. We actually have that for all such z, there is an upper bound on the norm of the scattering amplitudes, which might depend on the graph $\widehat{G}$.

Lemma 3. *Given $\widehat{G}$, there exists a constant $\lambda \in \mathbb{R}$ such that $|\langle v|sc_j(k)\rangle| < \lambda$ for all $k \in [-\pi, \pi)$, $j \in \{1, \ldots, N\}$, and $v \in \widehat{G}$.*

Proof. Note that

$$\gamma\left(\frac{1}{z}\right) = \frac{1}{z^2}\gamma(z) + \left(\frac{1}{z^2} - 1\right)\widehat{P} \tag{3.47}$$

where

$$\widehat{P} = \begin{pmatrix} 1 & 0 \\ 0 & 0 \end{pmatrix} \tag{3.48}$$

projects onto the N vertices of $\widehat{G}$ attached to semi-infinite paths. Hence

$$-\gamma(z)^{-1}\gamma\left(\frac{1}{z}\right) = -\frac{1}{z^2} + \left(1 - \frac{1}{z^2}\right)\gamma(z)^{-1}\widehat{P}. \tag{3.49}$$

Let $\{|\psi_c\rangle : c \in \{1, \ldots, n_c\}\}$ be eigenstates of $\widehat{H}$ satisfying $\widehat{P}|\psi_c\rangle = 0$, and let this set be an orthonormal basis for the span of all such states. Then

$$\left(1 - \frac{1}{z^2}\right)\gamma(z)^{-1}\widehat{P} = \left(1 - \frac{1}{z^2}\right)\left(1 - \sum_{j=1}^{n_c} |\psi_c\rangle\langle\psi_c|\right)\gamma(z)^{-1}\left(1 - \sum_{j=1}^{n_c} |\psi_c\rangle\langle\psi_c|\right)\widehat{P} \tag{3.50}$$

since each $|\psi_c\rangle$ is an eigenvector of $\gamma(z)$ and $\widehat{P}|\psi_c\rangle = 0$. Reference [14] shows (in Part 2 of the proof of Theorem 1) that

$$\det\left(\frac{1}{1 - z^2}\right) M(z) \neq 0 \text{ for } |z| = 1, \tag{3.51}$$

where $M(z)$ is the $(N + m - n_c) \times (N + m - n_c)$ matrix of $\gamma(z)$ in the subspace of states orthogonal to the span of $\{|\psi_c\rangle : c \in \{1, \ldots, n_c\}\}$. Therefore

$$\begin{aligned} \frac{1}{z}\langle v|\mathrm{sc}_j(k)\rangle &= -\langle v|\gamma(z)^{-1}\gamma\left(\frac{1}{z}\right)|j\rangle \\ &= \langle v|\left(1 - \frac{1}{z^2}\right)\left(1 - \sum_{j=1}^{n_c} |\psi_c\rangle\langle\psi_c|\right)\gamma(z)^{-1}\left(1 - \sum_{j=1}^{n_c} |\psi_c\rangle\langle\psi_c|\right)|j\rangle \end{aligned}$$

has no poles on the unit circle, and the result follows.

□

As such, we have that the scattering states are well defined for all $k \in (-\pi, 0)$.

3.2.3 Scattering matrix properties

While the use of the γ matrix gives an explicit construction of the form of the eigenstates on the internal vertices, the alternate definition in terms o the Q matrix can be used to easily show several properties of the scattering matrix. In particular, remember that

$$S(k) = -Q(z)^{-1}Q(z^{-1}), \tag{3.52}$$

where $z = e^{ik}$, and the matrices $Q(z)$ are given by

$$Q(z) = \mathbb{I} - z\Big(A + B^\dagger \frac{1}{\frac{1}{z} + z - D} B\Big). \tag{3.53}$$

Note that $Q(z)$ and $Q(z^{-1})$ commute for all $z \in \mathbb{C}$, as they can both be written as $\mathbb{I} + zH(z + z^{-1})$.

Using this expression for the scattering matrix, it is easy to see that $S(k)$ is a unitary matrix, as

$$S(k)^\dagger = -Q(z^{-1})^\dagger (Q(z)^{-1})^\dagger \tag{3.54}$$

and that

$$Q(z)^\dagger = \mathbb{I}^\dagger - z^\dagger\Big(A^\dagger + B^\dagger\Big(\frac{1}{\frac{1}{z} + z - D}\Big)^\dagger (B^\dagger)^\dagger\Big) = \mathbb{I} - z^\dagger\Big(A + B^\dagger \frac{1}{\frac{1}{z^\dagger} + z^\dagger - D} B\Big) = Q(z^\dagger) \tag{3.55}$$

and thus

$$S(k)^\dagger = -Q(z^{-1})^\dagger (Q(z)^{-1})^\dagger = -Q(z)Q(z^{-1})^{-1} = Q(z^{-1})^{-1}Q(z) = S(k)^{-1} \tag{3.56}$$

where we used the fact that $z = e^{ik}$ so that $z^\dagger = z^{-1}$, and the fact that $Q(z)$ and $Q(z^{-1})$ commute.

Additionally, we can make use of the fact that S is derived from an unweighted graph to show that the scattering matrices are symmetric. In particular, note that $Q(z)$ is symmetric for all z, since D is symmetric, symmetric matrices are closed under inversion, A is symmetric and B is a 0-1 matrix. As such, we have that

$$S(k)^T = -\big(Q(z)^{-1}Q(z^{-1})\big)^T = -Q(z^{-1})^T (Q(z)^{-1})^T \tag{3.57}$$

$$= -Q(z^{-1})Q(z)^{-1} = -Q(z)^{-1}Q(z^{-1}) = S(k) \tag{3.58}$$

where we used the fact that $Q(z)$ and $Q(z^{-1})$ commute.

Putting this together, we have that $S(k)$ is a symmetric, unitary matrix for all k.

3.2.4 Orthonormality of the scattering states

We now have some basic ideas behind the scattering behavior. In particular, we have that the scattering states exist for all k, and that the scattering matrices are symmetric and unitary. However, one of the most important behaviors we need is that the scattering states are orthonormal, and that they form a basis for the Hilbert space corresponding to the graph.

We will first show that two scattering states are orthonormal.

Lemma 4. *Let $k, p \in (-\pi, 0)$, and let $i, j \in [N]$. We then have that*

$$\langle\, sc_i(p) \,|\, sc_j(k) \,\rangle = \frac{1}{2\pi}\delta_{i,j}\delta(p - k), \tag{3.59}$$

where the two sides are equal as functionals against integration.

Proof. Let

$$\Pi_1 = \sum_{x=1}^{\infty}\sum_{q=1}^{N} |x,q\rangle\langle x,q| \qquad \Pi_2 = \mathbb{I} - \sum_{x=2}^{\infty}\sum_{q=1}^{N} |x,q\rangle\langle x,q| \qquad \Pi_3 = \sum_{q=1}^{N} |1,q\rangle\langle 1,q|. \tag{3.60}$$

First write

$$\begin{aligned}
\langle \mathrm{sc}_i(p)|\Pi_1|\mathrm{sc}_j(k)\rangle &= \sum_{x=1}^{\infty}\sum_{q=1}^{N}(\delta_{iq}e^{ipx} + S^*_{qi}(p)e^{-ipx})(\delta_{jq}e^{-ikx} + S_{qj}(k)e^{ikx}) \\
&= \frac{1}{2}\left(\delta_{ij} + \sum_{q=1}^{N} S^*_{qi}(p)S_{qj}(k)\right)\left(\sum_{x=1}^{\infty} e^{i(p-k)x} + \sum_{x=1}^{\infty} e^{-i(p-k)x}\right) \\
&\quad + \frac{1}{2}\left(\delta_{ij} - \sum_{q=1}^{N} S^*_{qi}(p)S_{qj}(k)\right)\left(\sum_{x=1}^{\infty} e^{i(p-k)x} - \sum_{x=1}^{\infty} e^{-i(p-k)x}\right) \\
&\quad + \frac{1}{2}(S^*_{ji}(p) + S_{ij}(k))\left(\sum_{x=1}^{\infty} e^{-i(p+k)x} + \sum_{x=1}^{\infty} e^{i(p+k)x}\right) \\
&\quad + \frac{1}{2}(S^*_{ji}(p) - S_{ij}(k))\left(\sum_{x=1}^{\infty} e^{-i(p+k)x} - \sum_{x=1}^{\infty} e^{i(p+k)x}\right).
\end{aligned}$$

We use the following identities for $p, k \in (-\pi, 0)$:

$$\begin{aligned}
\sum_{x=1}^{\infty} e^{i(p-k)x} + \sum_{x=1}^{\infty} e^{-i(p-k)x} &= 2\pi\delta(p-k) - 1 \\
\sum_{x=1}^{\infty} e^{i(p+k)x} + \sum_{x=1}^{\infty} e^{-i(p+k)x} &= -1 \\
\sum_{x=1}^{\infty} e^{i(p-k)x} - \sum_{x=1}^{\infty} e^{-i(p-k)x} &= i\cot\left(\frac{p-k}{2}\right) \\
\sum_{x=1}^{\infty} e^{i(p+k)x} - \sum_{x=1}^{\infty} e^{-i(p+k)x} &= i\cot\left(\frac{p+k}{2}\right).
\end{aligned}$$

These identities hold when both sides are integrated against a smooth function of p and k. Substituting, we get

$$\begin{aligned}
\langle \mathrm{sc}_i(p)|\Pi_1|\mathrm{sc}_j(k)\rangle &= 2\pi\delta_{ij}\delta(p-k) + \delta_{ij}\left(\frac{i}{2}\cot\left(\frac{p-k}{2}\right) - \frac{1}{2}\right) \\
&\quad + \sum_{q=1}^{N} S^*_{qi}(p)S_{qj}(k)\left(-\frac{i}{2}\cot\left(\frac{p-k}{2}\right) - \frac{1}{2}\right) \\
&\quad + S^*_{ji}(p)\left(-\frac{1}{2} - \frac{i}{2}\cot\left(\frac{p+k}{2}\right)\right) \\
&\quad + S_{ij}(k)\left(-\frac{1}{2} + \frac{i}{2}\cot\left(\frac{p+k}{2}\right)\right)
\end{aligned} \tag{3.61}$$

where we used unitarity of the S-matrix to simplify the first term. Now turning to Π_2 we have

$$\langle \mathrm{sc}_i(p)|H\Pi_2|\mathrm{sc}_j(k)\rangle = 2\cos(p)\langle \mathrm{sc}_i(p)|\Pi_2|\mathrm{sc}_j(k)\rangle \tag{3.62}$$

and

$$\begin{aligned}\langle \mathrm{sc}_i(p)|H\Pi_2|\mathrm{sc}_j(k)\rangle = \langle \mathrm{sc}_i(p)|\Bigg(&2\cos(k)\Pi_2|\mathrm{sc}_j(k)\rangle + \sum_{q=1}^{N}(e^{-ik}\delta_{qj} + S_{qj}(k)e^{ik})|2,q\rangle \\ &- \sum_{q=1}^{N}(e^{-2ik}\delta_{qj} + S_{qj}(k)e^{2ik})|1,q\rangle\Bigg).\end{aligned}$$

Using these two equations we get

$$\begin{aligned}(2\cos(p) - 2\cos(k))\langle \mathrm{sc}_i(p)|\Pi_2|\mathrm{sc}_j(k)\rangle = {}& \delta_{ij}(e^{2ip-ik} - e^{-2ik+ip}) + S^*_{ji}(p)(e^{-2ip-ik} - e^{-2ik-ip}) \\ &+ S_{ij}(k)(e^{2ip+ik} - e^{2ik+ip}) \\ &+ \sum_{q=1}^{N} S^*_{qi}(p)S_{qj}(k)(e^{-2ip+ik} - e^{2ik-ip}).\end{aligned}$$

Noting that

$$\langle \mathrm{sc}_i(p)|\Pi_3|\mathrm{sc}_j(k)\rangle = \sum_{q=1}^{N}(\delta_{iq}e^{ip} + S^*_{qi}(p)e^{-ip})(\delta_{jq}e^{-ik} + S_{qj}(k)e^{ik}), \tag{3.63}$$

we have

$$\begin{aligned}\langle \mathrm{sc}_i(p)|\Pi_2 - \Pi_3|\mathrm{sc}_j(k)\rangle = {}& \delta_{ij}\left(\frac{e^{2ip-ik} - e^{-2ik+ip}}{2\cos(p) - 2\cos(k)} - e^{ip-ik}\right) \\ &+ S^*_{ji}(p)\left(\frac{e^{-2ip-ik} - e^{-2ik-ip}}{2\cos(p) - 2\cos(k)} - e^{-ip-ik}\right) \\ &+ S_{ij}(k)\left(\frac{e^{2ip+ik} - e^{2ik+ip}}{2\cos(p) - 2\cos(k)} - e^{ip+ik}\right) \\ &+ \sum_{q=1}^{N} S^*_{qi}(p)S_{qj}(k)\left(\frac{e^{-2ip+ik} - e^{2ik-ip}}{2\cos(p) - 2\cos(k)} - e^{-ip+ik}\right) \\ = {}& \delta_{ij}\left(\frac{1}{2} - \frac{i}{2}\cot\left(\frac{p-k}{2}\right)\right) + S^*_{ji}(p)\left(\frac{1}{2} + \frac{i}{2}\cot\left(\frac{p+k}{2}\right)\right) \\ &+ S_{ij}(k)\left(\frac{1}{2} - \frac{i}{2}\cot\left(\frac{p+k}{2}\right)\right) \\ &+ \sum_{q=1}^{N} S^*_{qi}(p)S_{qj}(k)\left(\frac{1}{2} + \frac{i}{2}\cot\left(\frac{p-k}{2}\right)\right).\end{aligned} \tag{3.64}$$

Adding equation (3.61) to equation (3.64) gives equation (3.59). □

With the fact that the scattering states are orthogonal, it will also be useful to see that they form an orthonormal basis for the Hilbert space. In particular, Childs and Gosset showed in [14] that this holds. Assuming that the confined bound states were spanned by the orthonormal states $\{|\psi_c\rangle : c \in [n_c]\}$ and that the orthogonal bound states are spanned by the orthonormal basis $\{|\phi_b\rangle : b \in [n_b]\}$, they showed the following theorem:

Theorem 2 (Theorem 1 of [14]). *Let v and w be any two vertices of the graph G. Then*

$$\langle v | \left[\int_{-\pi}^{0} \frac{dk}{2\pi} | sc_j(k) \rangle\langle sc_j(k) | + \sum_{b=1}^{n_b} | \phi_b \rangle\langle \phi_b | + \sum_{c=1}^{n_c} | \psi_c \rangle\langle \psi_c | \right] | w \rangle = \delta_{v,w}. \tag{3.65}$$

[**TO DO:** *Should I include a proof of this theorem? It's not mine, but I will use.*]

Most of our results will be in regards to the scattering states, but having this decomposition of the identity will allow us to show better bounds. In particular, we will be able to guarantee that certain states have almost no support on states other than scattering states.

3.3 Applications of graph scattering

While graph scattering is a relatively new area of study, it has found several applications. As the behavior of a scattered particle is heavily dependent on both the momentum and the graph used for scattering, we can use the scattering behavior as a probe of properties about the graph, as well as a kind of probe for the momentum of the incoming particle. In particular, if we know the momentum of a wavepacket, we can determine the scattering amplitudes to gain information about the graph, such as whether it has eigenstates at particular momentum. If we know a graphs scattering behavior, we can then use the scattering to check whether a wavepacket has a desired momentum, and then do something to the particular wavepacket.

3.3.1 NAND Trees

The original motivating idea for understanding graph scattering was an oracular separation between quantum and classical computation, for a problem involving NAND trees. In particular, Edward Fahri, Jeffrey Goldstone, and Sam Gutmann gave a scattering algorithm [21] for this problem that was provably faster than any classical algorithm.

A NAND tree is a function on N variables, where N is a power of two, such that the value of the leaves are given by the input to the function, while each parent node's value is given by the NAND of its children's values. The NAND tree problem is then to evaluate the root.

Now for any oracular problem, we are given black-box access to the input, and want to minimize the total number of queries to the input. In particular, the actual runtime of an algorithm generally is not measured, and instead we simply count the number of bits of the input the algorithm accesses. While this might not always give a realistic gauge for the time a particular problem takes to solve, it does allow for information theoretic bounds on the number of queries. In particular, oracular problems often allow us to guarantee that any algorithm will require a certain number of queries in order to solve the problem.

If we perform an analysis on the NAND tree problem, any deterministic algorithm will require N queries in order to evaluate the root, as in the worst case we will need to examine every bit of the input. However, if we instead work with probabilistic computation, there is a randomized algorithm [33] that can solve this problem in $\mathcal{O}(N^\alpha)$ time, where $\alpha = \log_2(1 + \sqrt{33}) - 2 \approx 0.753$. Additionally, any randomized algorithm will require this many queries [36]. Fahri, Goldstone, and Gutmann were able to construct a quantum algorithm that solves the NAND tree using only $\mathcal{O}(\sqrt{N})$ queries, which is provably better than in the classical case.

The reason that we are interested in this is that the original algorithm uses graph scattering explicitly. In particular, a binary tree is attached to an infinite path at the root, and then additional vertices are attached to the leaves depending on whether the binary value is 0 or 1. It turns out

that at energy 0 (i.e., momentum $-\pi/2$), such a tree has perfect transmission from one path to the other if the tree evaluates to 1, and perfect reflection if the tree evaluates to 0. Hence, if a wave packet with momentum centered around $-\pi/2$ is scattered off of such a graph, by determining the location of the particle after it has scattered we evaluate the tree.

In this case, the requisite size of the wavepacket turns out to be $\mathcal{O}(\sqrt{N})$, and thus this amount of time is required in order for the scattering to occur. The total evolution time is closely related to the number of queries that the algorithm uses during the computation, and thus this is a quantum algorithm that has a provable advantage over classical computing.

3.4 Wavepacket scattering

Up until this point, we have taken as intuition that the scattering states correspond to an incoming wave packet at some momentum, and then scatterings with a corresponding S-matrix. However, this is somewhat weird, in that the scattering states are eigenstates of the Hamiltonian, and thus do not change over time, while scattering states explicitly move.

In this section, we will show that our intuitive naming is useful. In particular, we will show that preparing a wave packet centered at some momenta will scatter as the S-matrix of the corresponding scattering state. Further, the shape of the wave packet will remain approximately the same.

In [16], Childs, Gosset, and W. proved a nice bound on the time-evolution of square wave packets. These approximations were useful as the necessary mathematics involved in proving the related bounds only involved unweighted sums of amplitudes that were identical to the eigenstates of the corresponding Hamiltonians. In particular, they were able to prove the following bound:

Theorem 3 (Childs, Gosset, W.[16])**.** *Let $\widehat{G}$ be an $(N+m)$-vertex graph. Let G be a graph obtained from $\widehat{G}$ by attaching semi-infinite paths to N of its vertices, and let S be the corresponding S-matrix. Let $k \in (-\pi, 0)$, $M, L \in \natural$, $j \in \{1, \ldots, N\}$, and*

$$|\psi^j(0)\rangle = \frac{1}{\sqrt{L}} \sum_{x=M+1}^{M+L} e^{-ikx} |x, j\rangle. \tag{3.66}$$

Let c_0 be a constant independent of L. Then, for all $0 \leq t \leq c_0 L$,

$$\left\| e^{-iA(G)t} |\psi^j(0)\rangle - |\alpha^j(t)\rangle \right\| = \mathcal{O}(L^{-1/4}) \tag{3.67}$$

where

$$|\alpha^j(t)\rangle = \frac{1}{\sqrt{L}} e^{-2it\cos k} \sum_{x=1}^{\infty} \sum_{q=1}^{N} \left(\delta_{qj} e^{-ikx} R(x - \lfloor 2t \sin k \rfloor) + S_{qj}(k) e^{ikx} R(-x - \lfloor 2t \sin k \rfloor) \right) |x, q\rangle \tag{3.68}$$

with

$$R(l) = \begin{cases} 1 & \text{if } l \in \{M+1, M+2, \ldots, M+L\} \\ 0 & \text{otherwise.} \end{cases} \tag{3.69}$$

While these bounds were sufficient for the purposes of their paper, as they only required polynomial versus exponential overhead, the bounds they proved where not the best possible. Their use of square approximations was most likely not optimal in terms of the resulting errors.

As such, this section is devoted to proving a corresponding bound on the scattering behavior of a Gaussian wave packet, instead of square wave packets. We prove near quadratically better bounds than those of [16] in regards to the single-particle scattering, as the Guassian wave packets have nice dispersion properties, but unfortunately the proof becomes a little more complicated. In particular, we prove the following lemma:

Theorem 4. *Let $\widehat{G}$ be an $(N+m)$-vertex graph, let G be the graph obtained from $\widehat{G}$ by attaching N semi-infinite paths to the first N of its vertices, and let S be the corresponding S-matrix. Let $|\psi_j(0)\rangle$ be a cut-off Gaussian distribution with momentum k and standard deviation σ centered at μ, with the cut-off at a distance L from the center. Namely, let*

$$|\psi^j(0)\rangle = \gamma \sum_{x=\mu-L}^{\mu+L} e^{-ikx} e^{-(x-\mu)^2/2\sigma^2} |x,j\rangle, \tag{3.70}$$

where γ is the normalization of $|\psi^j(0)\rangle$. Then let us define the state

$$\begin{aligned} |\alpha^j(t)\rangle = \gamma e^{-2it\cos k} \Bigg[&\sum_{x=\max\{\mu(t)-L,1\}}^{\max\{\mu(t)+L,0\}} e^{-ikx} e^{-(x-\mu(t))^2/2\sigma^2} |x,j\rangle \\ &+ \sum_{x=\max\{-\mu(t)-L,1\}}^{\max\{-\mu(t)+L,0\}} \sum_{q=1}^{N} S_{qj}(k) e^{ikx} e^{-(x+\mu(t))^2/2\sigma^2} |x,q\rangle \Bigg] \end{aligned} \tag{3.71}$$

where

$$\mu(t) = \mu - \lceil 2t\sin(k) \rceil. \tag{3.72}$$

If $\sigma = c_1 \frac{L}{\sqrt{\log L}}$ for some constant $c_1 < \frac{1}{\sqrt{2}}$, we then have that for $0 < t < c_2 L$,

$$\| e^{-iA(G)t} |\psi^j(0)\rangle - |\alpha^j(t)\rangle \| \in \mathcal{O}\left(\sqrt{\frac{\log L}{L}} \right)., \tag{3.73}$$

Note that this bound is extremely similar to that of [16], albeit with a slightly more complicated definition for the approximate state. However, when the wave packet is far from the

3.4.1 Jacobi Θ-function

Before we delve into the proof of the wavepacket scattering, it will be useful to define a kind of discrete approximation to a Gaussian. In particular, let us define the function

$$h_L^\sigma(\phi) = \sum_{n=-L}^{L} e^{i\phi n} e^{-\frac{x^2}{2\sigma^2}}. \tag{3.74}$$

This is closely related to the amplitude of the original wavepacket in Theorem 4, and will be used extensively in our proof.

Additionally, this function is closely related to the Jacobi theta function, for which we refer the reader to Chapter 10 of [38] for a broad overview. This function, $\Theta(z,q)$ is defined for all complex z and all q with positive imaginary part as

$$\Theta(z,q) = \sum_{n=-\infty}^{\infty} e^{\pi i n^2 \tau} e^{2\pi i n z} \tag{3.75}$$

and is related to our h as

$$h_\infty^\sigma(\phi) = \sum_{n=-\infty}^{\infty} e^{i\phi n} e^{-\frac{n^2}{2\sigma^2}} = \Theta\left(\frac{\phi}{2\pi}, \frac{i}{2\pi\sigma^2}\right). \tag{3.76}$$

The Jacobi theta function has several symmetries, such as the fact that $\Theta(z,q) = \Theta(-z,q)$, and one that is similar to the Fourier transform. In particular, using our language and Theorem 1.6 from Chapter 10 of [38], we have

$$h_\infty^\sigma(\phi) = \Theta\left(\frac{\phi}{2\pi}, \frac{i}{2\pi\sigma^2}\right) = \sqrt{2\pi}\sigma e^{-\frac{\sigma^2\phi^2}{2}} \Theta\big(i\phi\sigma^2, 2\pi i\sigma^2\big) = \sqrt{2\pi}\sigma e^{-\frac{\sigma^2\phi^2}{2}} h_\infty^{1/(2\pi\sigma)}\big(2\pi i\phi\sigma^2\big). \tag{3.77}$$

This can be viewed as a discrete version of a Fourier transform, as the summand goes from a Gaussian distribution with standard deviation σ to one that has standard deviation proportional to σ^{-1} along with an exponential suppression term. Additionally, note that the argument to the h function is now complex, but we will only use such terms when dealing with the full infinite sum.

Let us now give some bounds on the various norms of h_L^σ, where some of our bounds where found in [19]. These will assist us greatly in our proof of the theorem. Assuming that $L > 0$, and that ϕ is real, we have that

$$\begin{aligned}
\big|h_\infty^\sigma(\phi) - h_L^\sigma(\phi)\big| &= \Big| \sum_{n=L+1}^{\infty} 2\cos(n\phi) e^{-\frac{n^2}{2\sigma^2}} \Big| && (3.78)\\
&\leq 2 \sum_{n=L+1}^{\infty} e^{-\frac{n^2}{2\sigma^2}} && (3.79)\\
&\leq 2 \int_L^\infty e^{-\frac{x^2}{2\sigma^2}} dx && (3.80)\\
&= 2\sigma \int_{L/\sigma}^\infty e^{-\frac{u^2}{2}} du && (3.81)\\
&< 2\sigma \int_{L/\sigma}^\infty \frac{\sigma u}{L} e^{-\frac{u^2}{2}} du && (3.82)\\
&= \frac{2\sigma^2}{L} e^{-\frac{L^2}{2\sigma^2}}, && (3.83)
\end{aligned}$$

while if $L = 0$ we instead have

$$\begin{aligned}
\big|h_\infty^\sigma(\phi) - 1\big| &= \Big| \sum_{n=1}^{\infty} 2\cos(n\phi) e^{-\frac{n^2}{2\sigma^2}} \Big| && (3.84)\\
&\leq 2e^{-\frac{1}{2\sigma^2}} + \sum_{n=2}^{\infty} e^{-\frac{n^2}{2\sigma^2}} && (3.85)\\
&\leq 2e^{-\frac{1}{2\sigma^2}} + 2\int_1^\infty e^{-\frac{x^2}{2\sigma^2}} dx && (3.86)\\
&< 2e^{-\frac{1}{2\sigma^2}} + 2\sigma^2 e^{-\frac{1}{2\sigma^2}} && (3.87)\\
&= 2(1+\sigma^2) e^{-\frac{1}{2\sigma^2}}. && (3.88)
\end{aligned}$$

In addition, if ϕ is complex, We will now try to bound the size of $h_\infty^\sigma(\phi)$, for small (but real) σ and imaginary ϕ (so as to use the discrete Fourier transform). In particular, if we assume that

$\phi = \phi_r + i\phi_i$ and that $1 > \sigma^2|\phi_i|$, we will have

$$\left|h^\sigma_\infty(\phi) - 1\right| = \left|\sum_{n=1}^{\infty} 2\cos(n\phi)e^{-\frac{n^2}{2\sigma^2}}\right| \tag{3.89}$$

$$\leq 4e^{-\frac{1}{2\sigma^2}+|\phi_i|} + 4e^{\frac{\sigma^2|\phi_i|^2}{2}}\sum_{n=2}^{\infty}\exp\Big[-\frac{1}{2}\Big(\frac{n}{\sigma} - \sigma|\phi_i|\Big)^2\Big] \tag{3.90}$$

$$< 4e^{-\frac{1}{2\sigma^2}+|\phi_i|} + 4e^{\frac{\sigma^2|\phi_i|^2}{2}}\int_1^{\infty}\exp\Big[-\frac{1}{2}\Big(\frac{x}{\sigma} - \sigma|\phi_i|\Big)^2\Big]dx \tag{3.91}$$

$$< 4e^{-\frac{1}{2\sigma^2}+|\phi_i|} + \frac{4\sigma e^{\frac{\sigma^2|\phi_i|^2}{2}}}{\frac{1}{\sigma} - \sigma|\phi_i|}\int_{\frac{1}{\sigma}-\sigma|\phi_i|}^{\infty} ue^{-\frac{u^2}{2}}du \tag{3.92}$$

$$= 4e^{-\frac{1}{2\sigma^2}+|\phi_i|} + \frac{4\sigma}{\frac{1}{\sigma} - \sigma|\phi_i|}e^{-\frac{1}{2\sigma^2}+|\phi_i|} \tag{3.93}$$

$$= 4\Big[1 + \frac{\sigma^2}{1-\sigma^2|\phi_i|}\Big]e^{-\frac{1}{2\sigma^2}+|\phi_i|}. \tag{3.94}$$

We can then collect these bounds into a lemma, which we will reference several times in the thesis.

Lemma 5. *Let $h^\sigma_L(\phi)$ be defined as above. For any real ϕ, and $L > 0$, we have that*

$$\left|h^\sigma_\infty(\phi) - h^\sigma_L(\phi)\right| < \frac{2\sigma^2}{L}e^{-\frac{L^2}{2\sigma^2}} \tag{3.95}$$

and

$$\left|h^\sigma_\infty(\phi) - 1\right| < 2(1+\sigma^2)e^{-\frac{1}{2\sigma^2}}. \tag{3.96}$$

Additionally, for complex $\phi = \phi_r + i\phi_i$ with $|\phi_i|\sigma^2 < 1$, we have that

$$\left|h^\sigma_\infty(\phi) - 1\right| < 4\left[1 + \frac{\sigma^2}{1-\sigma^2|\phi_i|}\right]e^{-\frac{1}{2\sigma^2}+|\phi_i|}. \tag{3.97}$$

In most of the cases we will use, the value of the h function can be approximated by the equivalent value if we use a Guassian distribution over the continuum, plus some small error term that is exponential in either the standard deviation σ or its inverse. As such, we will generally take as intuition that these h functions are Gaussians, which will allow us to construct approximations that are easier to work with.

In addition to this h function, when the particle is incident on the scattering gadget, we will need to bound half of the sum involved in the h function, corresponding to the portion of the wave packet that has support on the same vertices. In particular, let us define

$$V^\sigma_{v,L}(\phi) = \sum_{x=v}^{L} e^{i\phi x}e^{-x^2/2\sigma^2}, \tag{3.98}$$

where v, L are integers larger than zero, and let us assume that $\phi \in (-\pi, -\delta) \cup (\delta, \pi)$, for some constant $\delta > 0$. As the finite sums are often difficult to work with, we will try to approximate the sum via an integral over the points of interest.

Lemma 6. *Let v, L, σ, and ϕ be as above, where we also assume that $\sigma^2\phi > L+1$. There then exists some constant χ such that*

$$V^{\sigma}_{v,L}(\phi) < \chi. \tag{3.99}$$

Proof. We then have that

$$\sum_{x=v}^{L} e^{-\frac{x^2}{2\sigma^2}} \int_x^{x+1} e^{i\phi y} dy = \frac{i}{\phi}\big(1-e^{i\phi}\big)V^{\sigma}_{v,L}(\phi), \tag{3.100}$$

and thus

$$\frac{i}{\phi}\big(1-e^{i\phi}\big)V^{\sigma}_{v,L}(\phi) = \int_v^{L+1} e^{-\frac{x^2}{2\sigma^2}} e^{i\phi x} dx + \sum_{x=v}^{L} \int_{y=x}^{x+1} e^{i\phi y}\big(e^{-\frac{x^2}{2\sigma^2}} - e^{-\frac{y^2}{2\sigma^2}}\big) dy. \tag{3.101}$$

While this doesn't look much better in terms of the integrals, we have that

$$\int_v^{L+1} e^{-\frac{x^2}{2\sigma^2}} e^{i\phi x} dx = e^{-\frac{\phi^2\sigma^2}{2}} \int_v^{L+1} e^{\left(\frac{\phi\sigma}{\sqrt{2}} - \frac{ix}{\sqrt{2}\sigma}\right)^2} dx \tag{3.102}$$

$$= e^{-\frac{\phi^2\sigma^2}{2}} \int_0^{L+1} e^{\left(\frac{\phi\sigma}{\sqrt{2}} - \frac{ix}{\sqrt{2}\sigma}\right)^2} dx - e^{-\frac{\phi^2\sigma^2}{2}} \int_0^{v} e^{\left(\frac{\phi\sigma}{\sqrt{2}} - \frac{ix}{\sqrt{2}\sigma}\right)^2} dx. \tag{3.103}$$

While this expansion isn't particularly different, these integrals are almost exactly of the form of the imaginary error function, erfi. In fact, as both integrals have the same real part in the exponent, after a change of variables we have that

$$\int_v^{L+1} e^{-\frac{x^2}{2\sigma^2}} e^{i\phi x} dx = ie^{-\frac{\phi^2\sigma^2}{2}} \sqrt{\frac{\pi}{2}}\sigma \left[\operatorname{erfi}\left(\frac{\phi\sigma}{\sqrt{2}} - i\frac{L+1}{\sqrt{2}\sigma}\right) - \operatorname{erfi}\left(\frac{\phi\sigma}{\sqrt{2}} - i\frac{v}{\sqrt{2}\sigma}\right)\right]. \tag{3.104}$$

While erfi diverges for arguments with large real part, when multiplied by e^{-z^2} the resulting function is called the Dawson function. The Dawson function has nice properties, and in fact converges to zero like z^{-1} for large z. We then have that

$$\int_v^{L+1} e^{-\frac{x^2}{2\sigma^2}} e^{i\phi x} dx = ie^{-\frac{\phi^2\sigma^2}{2}} \sqrt{\frac{\pi}{2}}\sigma \left[\operatorname{erfi}\left(\frac{\phi\sigma}{\sqrt{2}} - i\frac{L+1}{\sqrt{2}\sigma}\right) - \operatorname{erfi}\left(\frac{\phi\sigma}{\sqrt{2}} - i\frac{v}{\sqrt{2}\sigma}\right)\right] \tag{3.105}$$

$$= i\sigma\sqrt{\frac{\pi}{2}}\Bigg[e^{-\left(\frac{\phi\sigma}{\sqrt{2}} - i\frac{L+1}{\sqrt{2}\sigma}\right)^2} e^{-i\phi(L+1)} e^{-\frac{(L+1)^2}{2\sigma^2}} \operatorname{erfi}\left(\frac{\phi\sigma}{\sqrt{2}} - i\frac{L+1}{\sqrt{2}\sigma}\right)$$

$$- e^{-\left(\frac{\phi\sigma}{\sqrt{2}} - i\frac{v}{\sqrt{2}\sigma}\right)^2} e^{-i\phi v} e^{-\frac{v^2}{2\sigma^2}} \operatorname{erfi}\left(\frac{\phi\sigma}{\sqrt{2}} - i\frac{v}{\sqrt{2}\sigma}\right)\Bigg] \tag{3.106}$$

$$= i\sigma\sqrt{2}\Bigg[e^{-i\phi(L+1)} e^{-\frac{(L+1)^2}{2\sigma^2}} D\left(\frac{\phi\sigma}{\sqrt{2}} - i\frac{L+1}{\sqrt{2}\sigma}\right)$$

$$- e^{-i\phi v} e^{-\frac{v^2}{2\sigma^2}} D\left(\frac{\phi\sigma}{\sqrt{2}} - i\frac{v}{\sqrt{2}\sigma}\right)\Bigg], \tag{3.107}$$

where $D(z)$ is the Dawson function, defined over the entire complex plane as

$$D(z) = \frac{\sqrt{\pi}}{2} e^{-z^2} \operatorname{erfi}(z). \tag{3.108}$$

Additionally, there exists a continued fractioned expansion of Dawson's function, which when restricted to the first value gives an approximation of

$$D(z) \approx \frac{z}{1+2z^2}. \tag{3.109}$$

Putting all of this together, we then have that

$$\frac{i}{\phi}(1-e^{i\phi})V^{\sigma}_{v,L}(\phi) = \sum_{x=v}^{L}\int_{y=x}^{x+1} e^{i\phi x}\big(e^{-\frac{x^2}{2\sigma^2}}dx - e^{-\frac{y^2}{2\sigma^2}}\big) + i\sigma\sqrt{2}\Bigg[e^{-i\phi(L+1)}e^{-\frac{(L+1)^2}{2\sigma^2}}D\bigg(\frac{\phi\sigma}{\sqrt{2}} - i\frac{L+1}{\sqrt{2}\sigma}\bigg)$$
$$- e^{-i\phi v}e^{-\frac{v^2}{2\sigma^2}}D\bigg(\frac{\phi\sigma}{\sqrt{2}} - i\frac{v}{\sqrt{2}\sigma}\bigg)\Bigg]. \tag{3.110}$$

If we then take the absolute value of both sides, we find that

$$\big|V^{\sigma}_{v,L}(\phi)\big| \leq \frac{|\phi|}{|1-e^{i\phi}|}\Bigg[\sum_{x=v}^{L}\int_{y=x}^{x+1}\big(e^{-\frac{x^2}{2\sigma^2}} - e^{-\frac{y^2}{2\sigma^2}}\big)dx + \sqrt{2}\sigma e^{-\frac{L^2}{2\sigma^2}}\bigg|D\bigg(\frac{\phi\sigma}{\sqrt{2}} - i\frac{L+1}{\sqrt{2}\sigma}\bigg)\bigg|$$
$$+ \sqrt{2}\sigma e^{-\frac{v^2}{2\sigma^2}}\bigg|D\bigg(\frac{\phi\sigma}{\sqrt{2}} - i\frac{v}{\sqrt{2}\sigma}\bigg)\bigg|\Bigg]. \tag{3.111}$$

If we then attempt to bound the norm of each term on the right, we can find that

$$\int_{x}^{x+1}\big(e^{-\frac{x^2}{2\sigma^2}} - e^{-\frac{y^2}{2\sigma^2}}\big)dy \leq \int_0^1 t \max_{y\in(x,x+1)}\big\{-e^{-\frac{y^2}{2\sigma^2}}\big\}dt = \begin{cases} \frac{x+1}{2\sigma^2}e^{-\frac{(x+1)^2}{2\sigma^2}} & x+1<\sigma \\ \frac{x}{2\sigma^2}e^{-\frac{x^2}{2\sigma^2}} & x>\sigma \\ \frac{1}{2e\sigma} & 0\leq\sigma-x\leq 1, \end{cases} \tag{3.112}$$

we can then bound the first term in the bound of $V^{\sigma}_{v,L}(\phi)$ as (assuming first that $v<\sigma$)

$$\sum_{x=v}^{L}\int_{x}^{x+1}\big(e^{-\frac{x^2}{2\sigma^2}} - e^{-\frac{y^2}{2\sigma^2}}\big)dy \leq \frac{1}{2e\sigma} + \sum_{x=v+1}^{L}\frac{x}{2\sigma^2}e^{-\frac{x^2}{2\sigma^2}} \tag{3.113}$$
$$\leq \frac{1}{e\sigma} + \int_{v+1}^{L}\frac{x}{2\sigma^2}e^{-\frac{x^2}{2\sigma^2}}dx \tag{3.114}$$
$$\leq \frac{1}{e\sigma} + \frac{e^{-\frac{(v+1)^2}{2\sigma^2}} - e^{-\frac{L^2}{2\sigma^2}}}{2}, \tag{3.115}$$

whereas if $v>\sigma$ we can bound the first term as

$$\sum_{x=v}^{L}\int_{x}^{x+1}\big(e^{-\frac{x^2}{2\sigma^2}} - e^{-\frac{y^2}{2\sigma^2}}\big)dy \leq \sum_{x=v}^{L}\frac{x}{2\sigma^2}e^{-\frac{x^2}{2\sigma^2}} \tag{3.116}$$
$$\leq \frac{v}{2\sigma^2}e^{-\frac{v^2}{2\sigma^2}} + \int_{v}^{L}\frac{x}{2\sigma^2}e^{-\frac{x^2}{2\sigma^2}}dx \tag{3.117}$$
$$\leq \frac{v}{2\sigma^2}e^{-\frac{v^2}{2\sigma^2}} + \frac{e^{-\frac{v^2}{2\sigma^2}} - e^{-\frac{L^2}{2\sigma^2}}}{2}. \tag{3.118}$$

Combining these bounds, we then have that for any $0<v<L$, we have that

$$\sum_{x=v}^{L}\int_{x}^{x+1}\big(e^{-\frac{x^2}{2\sigma^2}} - e^{-\frac{y^2}{2\sigma^2}}\big)dy \leq \frac{1}{e\sigma} + \frac{e^{-\frac{v^2}{2\sigma^2}}}{2}. \tag{3.119}$$

For the two terms involving the Dawson's function, we will refer to a paper dealing explicitly with Dawson's function, namely [28]. In this paper, McCabe shows that

$$D(z) - \frac{z}{1+2z^2} = \frac{4e^{-2z^2}z^3}{3}, \tag{3.120}$$

and thus

$$\left|D(x+iy)\right| \leq \frac{4e^{-2(x^2-y^2)}(x^2+y^2)^{3/2}}{3} + \frac{\sqrt{x^2+y^2}}{1+2x^2-2y^2}. \tag{3.121}$$

For the two points of interest, we then have that

$$\left|D\left(\frac{\phi\sigma}{\sqrt{2}} - i\frac{L+1}{\sqrt{2}\sigma}\right)\right| \leq \frac{4e^{-\phi^2\sigma^2+(L+1)^2/\sigma^2}}{3}\left(\frac{\phi^2\sigma^2}{2} + \frac{(L+1)^2}{2\sigma^2}\right)^{3/2} + \frac{\sqrt{\phi^2\sigma^2 + \frac{(L+1)^2}{\sigma^2}}}{2(1+2\phi^2\sigma^2-2(L+1)^2/\sigma^2)} \tag{3.122}$$

$$\leq \frac{4}{3}e^{-\frac{\phi^2\sigma^2}{2}}|\phi|^3\sigma^3 + \frac{\sqrt{2\phi^2\sigma^2}}{2\phi^2\sigma^2}, \tag{3.123}$$

where we used the assumption that $|\phi| > \delta$, along with the fact that $(L+1)/\sigma < \phi\sigma$. Additionally, we have that

$$\left|D\left(\frac{\phi\sigma}{\sqrt{2}} - i\frac{L+1}{\sqrt{2}\sigma}\right)\right| \leq \frac{4e^{-\phi^2\sigma^2+v^2/\sigma^2}}{3}\left(\frac{\phi^2\sigma^2}{2} + \frac{v^2}{2\sigma^2}\right)^{3/2} + \frac{\sqrt{\phi^2\sigma^2 + \frac{v^2}{\sigma^2}}}{2(1+2\phi^2\sigma^2-2v^2/\sigma^2)} \tag{3.124}$$

$$\leq \frac{4}{3}e^{-\frac{\phi^2\sigma^2}{2}}|\phi|^3\sigma^3 + \frac{\sqrt{2\phi^2\sigma^2}}{2\phi^2\sigma^2}. \tag{3.125}$$

If we now put all of these bounds together, and assume that σ is large enough that $e^{-\frac{\phi^2\sigma^2}{2}}|\phi|^3\sigma^4 < 1$, we have

$$\left|V^{\sigma}_{v,L}(\phi)\right| \leq \frac{|\phi|}{|1-e^{i\phi}|}\left[\sum_{x=v}^{L}\int_{y=x}^{x+1}\left(e^{-\frac{x^2}{2\sigma^2}} - e^{-\frac{y^2}{2\sigma^2}}\right)dx + \sqrt{2}\sigma e^{-\frac{L^2}{2\sigma^2}}\left|D\left(\frac{\phi\sigma}{\sqrt{2}} - i\frac{L+1}{\sqrt{2}\sigma}\right)\right|\right.$$
$$\left. + \sqrt{2}\sigma e^{-\frac{v^2}{2\sigma^2}}\left|D\left(\frac{\phi\sigma}{\sqrt{2}} - i\frac{v}{\sqrt{2}\sigma}\right)\right|\right] \tag{3.126}$$

$$\leq \frac{|\phi|}{|1-e^{i\phi|}|}\left[\frac{1}{e\sigma} + \frac{e^{-\frac{v^2}{2\sigma^2}}}{2} + \sqrt{2}\sigma\left(\frac{4}{3}e^{-\frac{\phi^2\sigma^2}{2}}|\phi|^3\sigma^3 + \frac{\sqrt{2\phi^2\sigma^2}}{2\phi^2\sigma^2}\right)\left(e^{-\frac{L^2}{2\sigma^2}} + e^{-\frac{v^2}{2\sigma^2}}\right)\right] \tag{3.127}$$

$$\leq \frac{|\phi|}{|1-e^{i\phi|}|}\left[\frac{1}{e\sigma} + \frac{1}{2} + 2\sqrt{2}\left(\frac{4}{3} + \frac{1}{\sqrt{2}|\phi|}\right)\right]. \tag{3.128}$$

As $\sigma > 1$ and as $|\phi| > \delta$, we then have that $|V^{\sigma}_{v,L}(\phi)|$ is bounded by a constant, as required. □

Note that this proof most likely is not the most clean of proofs, but it will suffice for our purposes.

3.4.2 Propagated approximation bounds

Now that we have some grasp on the mathematics surrounding the definition of the $|\alpha_j(t)\rangle$ states, it will be useful in our proof to show that these states are approximately normalized for all times t.

As such, let us simply calculate the inner product:

$$\begin{aligned}\langle \alpha_j(t)|\alpha_j(t)\rangle &= \gamma^2\Bigg[\sum_{x=\max\{\mu(t)-L,1\}}^{\mu(t)+L} e^{-\frac{(x-\mu(t))^2}{\sigma^2}} + \sum_{x=\max\{-\mu(t)-L,1\}}^{-\mu(t)+L} e^{-\frac{(x+\mu(t))^2}{\sigma^2}} \sum_{q=1}^{N} S_{qj}(k)S_{qj}^*(k) \\ &\quad + \sum_{x=1}^{\min\{\mu(t)+L,-\mu(t)+L\}} e^{-\frac{x^2+\mu(t)^2}{\sigma^2}}\Big(e^{2ikx}S_qj(k) + e^{-2ikx}S_{qj}^*(k)\Big)\Bigg] \qquad (3.129)\\ &= \gamma^2\Bigg[\sum_{x=-L}^{L} e^{-\frac{x^2}{\sigma^2}} - \delta_{|\mu(t)|\leq L}e^{-\frac{\mu(t)^2}{\sigma^2}} + 2e^{-\frac{\mu(t)^2}{\sigma^2}}\Re\Big[S_{qj}(k)V^{\sigma/\sqrt{2}}_{1,\min\{\mu(t)+L,-\mu(t)+L\}}(2k)\Big]\Bigg] \qquad (3.130)\\ &= 1-\gamma^2 e^{-\frac{\mu(t)^2}{\sigma^2}}\Bigg[\delta_{|\mu(t)|\leq L} - 2\Re\Big[S_{qj}(k)V^{\sigma/\sqrt{2}}_{1,\min\{\mu(t)+L,-\mu(t)+L\}}(2k)\Big]\Bigg]. \qquad (3.131)\end{aligned}$$

We used in the second equality that $S(k)$ is a unitary matrix, and then combined the first and second sums into one sum. Note that the second term in (3.131) is zero for $\mu(t)$ larger than L, and thus for these times the state $|\alpha_j(t)\rangle$ is exactly normalized. Further, we have from Lemma 6 that the last term in (3.131) is bounded in norm by a constant, and thus the norm of α is bonuded away from 1 by some constant times γ^2.

Additionally, it will be helpful to actually have bounds on γ^{-2}. In particular, we have from Lemma 5 that

$$\gamma^{-2} = h_L^{\sigma/\sqrt{2}}(0) < h_\infty^{\sigma/\sqrt{2}}(0) = \sqrt{\pi}\sigma h_\infty^{1/(\pi\sigma\sqrt{2})}(0) \leq \sqrt{\pi}\sigma\Big[1+2\Big(1+\frac{1}{2\pi^2\sigma^2}\Big)e^{-\pi^2\sigma^2}\Big] \qquad (3.132)$$

works as an upper bound, while

$$\begin{aligned}\gamma^{-2} &= h_L^{\sigma/\sqrt{2}}(0) = h_\infty^{\sigma/\sqrt{2}}(0) - \big(h_L^{\sigma/\sqrt{2}}(0) - h_\infty^{\sigma/\sqrt{2}}(0)\big) \geq \sqrt{\pi}\sigma - \frac{\sigma^2}{L}e^{-\frac{L^2}{\sigma^2}} \qquad (3.133)\\ &= \sqrt{\pi}\sigma\Big(1-\frac{\sigma}{L\sqrt{\pi}}e^{-\frac{L^2}{\sigma^2}}\Big) \qquad (3.134)\end{aligned}$$

can be used as a lower bound. However, these bounds are not particular nice to use and thus we will use the slightly weaker bounds of

$$\gamma^{-2} \leq \sqrt{\pi}\sigma\big[1+3e^{-\pi^2\sigma^2}\big] \qquad (3.135)$$

and

$$\gamma^{-2} \geq \sqrt{\pi}\sigma\big[1-e^{-\frac{L^2}{\sigma^2}}\big], \qquad (3.136)$$

where we assume that $L > \sigma > 1$.

From this, we have that the norm of $|\alpha_j(t)\rangle$ is within some constant times σ^{-1} of 1 for all times t.

3.4.3 Proof of Theorem 4

Now that we have the requisite bounds on the mathematical quantities used to define our approximations, we can prove Theorem 4.

Proof. The main idea behind this proof will be to show that $|\psi_j(0)\rangle$ and $|\alpha_j(t)\rangle$ are both well approximated by a Gaussian distribution over momentum states near k, and then show that the time evolved Gaussian approximation of $|\psi_j(0)\rangle$ is well approximated by the Gaussian approximation for $|\alpha_j(t)\rangle$.

In particular, let us examine the inner product between a scattering state $|\mathrm{sc}_j(k+\phi)\rangle$ and $|\alpha_j(t)\rangle$. We can see that

$$\begin{aligned}
&\langle \mathrm{sc}_j(k+\phi)\,|\,\alpha_j(t)\rangle \\
&\quad= \gamma e^{-2it\cos(k)}\Bigg[\sum_{x=\max\{\mu(t)-L,1\}}^{\mu(t)+L} e^{-\frac{(x-\mu(t))^2}{2\sigma^2}}\left(e^{i\phi x}+S^*_{jj}(k+\phi)e^{-i(2k+\phi)x}\right) \\
&\qquad+\sum_{x=\max\{-\mu(t)-L,1\}}^{-\mu(t)+L} e^{-\frac{(x+\mu(t))^2}{2\sigma^2}}\left[S_{jj}(k)e^{i(2k+\phi)x}+e^{-i\phi x}\sum_{q=1}^{N}S^*_{qj}(k+\phi)S_{qj}(k)\right]\Bigg] \qquad (3.137)\\
&\quad= \gamma e^{-2it\cos(k)}\Bigg[\sum_{x=\mu(t)-L}^{\mu(t)+L} e^{-\frac{(x-\mu(t))^2}{2\sigma^2}}e^{i\phi x} \\
&\qquad+\sum_{x=\max\{\mu(t)-L,1\}}^{-\mu(t)+L} e^{-i\phi x}e^{-\frac{(x+\mu(t))^2}{2\sigma^2}}\sum_{q=1}^{N}\Big(S^*_{qj}(k+\phi)-S^*_{qj}(k)\Big)S_{qj}(k) \\
&\qquad+\Big[\delta_{\mu(t)\geq 0}S^*_{jj}(k+\phi)+\delta_{\mu(t)<0}S_{jj}(k)\Big]\sum_{x=-\mu(t)-L}^{\mu(t)+L} e^{-i(2k+\phi)x}e^{-\frac{(x-\mu(t))^2}{2\sigma^2}} \\
&\qquad+\big(S_{jj}(k)-S^*_{jj}(k+\phi)\big)\big(1-2\delta_{\mu(t)<0}\big)\sum_{x=1}^{-|\mu(t)|+L} e^{-\frac{(x+|\mu(t)|)^2}{2\sigma^2}}e^{-i(2k+\phi)x} \\
&\qquad-\delta_{|\mu(t)|\leq L}\Big(1+S^*_{jj}(k+\phi)\delta_{\mu(t)\geq 0}+S_{jj}(k)\delta_{\mu(t)<0}\Big)e^{-\frac{\mu(t)^2}{2\sigma^2}}\Bigg]. \qquad (3.138)
\end{aligned}$$

Note that we gained this expression by collecting terms corresponding to the same Gaussian expressions, along with adding and subtracting some terms to make the sums more easily understood. In fact, we can then restructure the above expression into the form:

$$\begin{aligned}
&\langle \mathrm{sc}_j(k+\phi)\,|\,\alpha_j(t)\rangle \\
&\quad= \gamma e^{-2it\cos(k)}\Bigg[e^{i\phi\mu(t)}h^\sigma_L(\phi)+e^{-i(2k+\phi)\mu(t)}h^\sigma_L(2k+\phi)\Big[\delta_{\mu(t)\geq 0}S^*_{jj}(k+\phi)+\delta_{\mu(t)<0}S_{jj}(k)\Big] \\
&\qquad+\sum_{x=\max\{-\mu(t)-L,1\}}^{-\mu(t)+L} e^{-i\phi x}e^{-\frac{(x+\mu(t))^2}{2\sigma^2}}\sum_{q=1}^{N}\Big(S^*_{qj}(k+\phi)-S^*_{qj}(k)\Big)S_{qj}(k) \\
&\qquad+\big(S_{jj}(k)-S^*_{jj}(k+\phi)\big)\big(1-2\delta_{\mu(t)<0}\big)e^{i(2k+\phi)|\mu(t)|}V^\sigma_{|\mu(t)|+1,L}(-2k-\phi) \\
&\qquad-\delta_{|\mu(t)|\leq L}\Big(1+S^*_{jj}(k+\phi)\delta_{\mu(t)\geq 0}+S_{jj}(k)\delta_{\mu(t)<0}\Big)e^{-\frac{\mu(t)^2}{2\sigma^2}}\Bigg]. \qquad (3.139)
\end{aligned}$$

While this is a rather complicated expression, most of the amplitude is contained in the $h_L^\sigma(\phi)$ term, as the rest of the terms are relatively small. Using this, and noting that $h_\infty^\sigma(\phi) \propto e^{-\frac{\sigma^2\phi^2}{2}}$ for constant σ, let us define

$$|\, w_j(t)\rangle = \eta e^{-2it\cos k}\int_{-\delta}^{\delta}\frac{d\phi}{2\pi}e^{i\phi\mu(t)}e^{-\frac{\sigma^2\phi^2}{2}}|\,\mathrm{sc}_j(k+\phi)\rangle \tag{3.140}$$

where δ is a constant that we will define later, and where η is an approximate normalization factor defined as

$$\eta^{-2} = \int_{-\infty}^{\infty}\frac{d\phi}{2\pi}e^{-\sigma^2\phi^2} = \frac{1}{2\sqrt{\pi}\sigma} \tag{3.141}$$

The state $|\, w_j(t)\rangle$ will be our Gaussian approximation to the state $|\,\alpha_j(t)\rangle$.

Note that the states $|\, w_j(t)\rangle$ are not exactly normalized, but that

$$\langle\, w_j(t)\,|\, w_j(t)\,\rangle = \eta^2\int_{-\delta}^{\delta}\frac{d\phi}{2\pi}e^{-\sigma^2\phi^2} = \eta^2\int_{-\infty}^{\infty}\frac{d\phi}{2\pi}e^{-\sigma^2\phi^2} - 2\eta^2\int_{\delta}^{\infty}\frac{d\phi}{2\pi}e^{-\sigma^2\phi^2} \tag{3.142}$$

$$= 1 - \frac{2\sigma}{\sqrt{\pi}}\int_{\delta}^{\infty}d\phi e^{-\sigma^2\phi^2}. \tag{3.143}$$

Hence, we have that

$$\langle\, w_j(t)\,|\, w_j(t)\,\rangle \geq 1 - \frac{1}{\delta\sigma\sqrt{\pi}}e^{-\sigma^2\delta^2} \tag{3.144}$$

and

$$\langle\, w_j(t)\,|\, w_j(t)\,\rangle \leq 1 - \frac{2\sigma\delta}{\sqrt{\pi}(2\sigma^2\delta^2+1)}e^{-\sigma^2\delta^2}. \tag{3.145}$$

Now that understand the overlap of $|\,\alpha_j(t)\rangle$ with each scattering state, and also have our approximations $|\, w_j(t)\rangle$ defined, we will want to approximate the overlap between the two states. Namely, we will want to understand:

$$\langle\, w_j(t)\,|\,\alpha_j(t)\,\rangle = \eta e^{2it\cos k}\int_{-\delta}^{\delta}\frac{d\phi}{2\pi}\langle\,\mathrm{sc}_j(k+\phi)\,|\,\alpha_j(t)\rangle e^{-\frac{\sigma^2\phi^2}{2}}e^{-i\phi\mu(t)} \tag{3.146}$$

$$\begin{aligned}
&= \eta\gamma\int_{-\delta}^{\delta}\frac{d\phi}{2\pi}e^{-\frac{\sigma^2\phi^2}{2}}e^{-i\phi\mu(t)}\Bigg[e^{i\phi\mu(t)}h_L^\sigma(\phi)\\
&\quad + e^{-i(2k+\phi)\mu(t)}h_L^\sigma(2k+\phi)\Big[\delta_{\mu(t)\geq 0}S_{jj}^*(k+\phi) + \delta_{\mu(t)<0}S_{jj}(k)\Big]\\
&\quad + \sum_{x=\max\{-\mu(t)-L,1\}}^{-\mu(t)+L}e^{-i\phi x}e^{-\frac{(x+\mu(t))^2}{2\sigma^2}}\sum_{q=1}^{N}\Big(S_{qj}^*(k+\phi) - S_{qj}^*(k)\Big)S_{qj}(k)\\
&\quad + \big(S_{jj}(k) - S_{jj}^*(k+\phi)\big)\big(1-2\delta_{\mu(t)<0}\big)e^{i(2k+\phi)|\mu(t)|}V^\sigma_{|\mu(t)|+1,L}(-2k-\phi)\\
&\quad - \delta_{|\mu(t)|\leq L}\Big(1 + S_{jj}^*(k+\phi)\delta_{\mu(t)\geq 0} + S_{jj}(k)\delta_{\mu(t)<0}\Big)e^{-\frac{\mu(t)^2}{2\sigma^2}}\Bigg]
\end{aligned} \tag{3.147}$$

We will show that most of the overlap between $|\, w_j(t)\rangle$ and $|\,\alpha_j(t)\rangle$ comes from the first term on the right hand side of the above equation. To do so, we will approximate each of the $h_L^\sigma(\theta)$ terms

by the corresponding $h^{\sigma}_{\infty}(\theta)$ terms, and bound the difference in norms. We will then also show that the remaining integrals are bounded some small number.

As a first step forward in our proof, note that

$$\int_{-\delta}^{\delta} \frac{d\phi}{2\pi} e^{-\frac{\sigma^2\phi^2}{2}} h^{\sigma}_{L}(\phi) = \int_{-\delta}^{\delta} \frac{d\phi}{2\pi} e^{-\frac{\sigma^2\phi^2}{2}} h^{\sigma}_{\infty}(\phi) + \int_{-\delta}^{\delta} \frac{d\phi}{2\pi} e^{-\frac{\sigma^2\phi^2}{2}} \big(h^{\sigma}_{L}(\phi) - h^{\sigma}_{\infty}(\phi)\big). \tag{3.148}$$

If we can bound the first integral from above and below, and also show that the norm of the rest of the terms are relatively small, we will have the first tool to prove our theorem. In particular, we we can bound the first integral from above as

$$\begin{aligned}
\int_{-\delta}^{\delta} \frac{d\phi}{2\pi} e^{-\frac{\sigma^2\phi^2}{2}} h^{\sigma}_{\infty}(\phi) &= \frac{\sigma}{\sqrt{2\pi}} \int_{-\delta}^{\delta} d\phi e^{-\sigma^2\phi^2} h^{1/(2\pi\sigma)}_{\infty}(2\pi i\sigma^2\phi) && (3.149)\\
&\leq \frac{2\sigma}{\sqrt{2\pi}} \int_{0}^{\delta} d\phi e^{-\sigma^2\phi^2} \Big[1 + 2\Big(1 + \frac{1}{4\pi^2\sigma^2}\frac{1}{2\pi-\phi}\Big) e^{-2\pi\sigma^2(\pi-\phi)}\Big] && (3.150)\\
&\leq \frac{2\sigma}{\sqrt{2\pi}} \Big[1 + 2\Big(1 + \frac{1}{2\pi\sigma^2}\frac{1}{2\pi-\delta}\Big) e^{-2\pi\sigma^2(\pi-\delta)}\Big] \int_{0}^{\delta} d\phi e^{-\sigma^2\phi^2} && (3.151)\\
&\leq \frac{1}{\sqrt{2}} \Big[1 + 3e^{-\pi^2\sigma^2}\Big] && (3.152)
\end{aligned}$$

where we assumed that $\delta < \frac{\pi}{2}$. If we also note that $h^{\sigma}_{L}(i\phi) \geq 1$ for all L and all real ϕ, we have

$$\begin{aligned}
\int_{-\delta}^{\delta} \frac{d\phi}{2\pi} e^{-\frac{\sigma^2\phi^2}{2}} h^{\sigma}_{\infty}(\phi) &= \frac{\sigma}{\sqrt{2\pi}} \int_{-\delta}^{\delta} d\phi e^{-\sigma^2\phi^2} h^{1/(2\pi\sigma)}_{\infty}(2\pi i\sigma^2\phi) && (3.153)\\
&\geq \frac{\sigma}{\sqrt{2\pi}} \int_{-\delta}^{\delta} d\phi e^{-\sigma^2\phi^2} && (3.154)\\
&= \sigma\sqrt{2\pi}\eta^{-2} \langle w_j(t) \,|\, w_j(t)\rangle && (3.155)\\
&\geq \frac{1}{\sqrt{2}} \Big(1 - \frac{1}{\delta\sigma\sqrt{\pi}} e^{-\sigma^2\delta^2}\Big). && (3.156)
\end{aligned}$$

We can then use the bound of (3.95) from Lemma 5 to see that

$$\begin{aligned}
\Big| \int_{-\delta}^{\delta} \frac{d\phi}{2\pi} e^{-\frac{\sigma^2\phi^2}{2}} \big(h^{\sigma}_{L}(\phi) - h^{\sigma}_{\infty}(\phi)\big)\Big| &\leq \int_{-\delta}^{\delta} \frac{d\phi}{2\pi} e^{-\frac{\sigma^2\phi^2}{2}} \big|h^{\sigma}_{L}(\phi) - h^{\sigma}_{\infty}(\phi)\big| && (3.157)\\
&\leq \int_{-\delta}^{\delta} \frac{d\phi}{2\pi} \frac{2\sigma^2}{L} e^{-\frac{L^2}{2\sigma^2}} e^{-\frac{\sigma^2\phi^2}{2}} && (3.158)\\
&\leq \frac{\sigma^2}{\pi L} e^{-\frac{L^2}{2\sigma^2}} \int_{-\infty}^{\infty} d\phi e^{-\frac{\sigma^2\phi^2}{2}} && (3.159)\\
&= \sqrt{\frac{2}{\pi}} \frac{\sigma}{L} e^{-\frac{L^2}{2\sigma^2}}. && (3.160)
\end{aligned}$$

At this point, we then want to bound the norm of each individual term in (3.147). The next term

in particular can be bounded in a similar manner to the first, where we approximate h_L by h_∞:

$$\left| \int_{-\delta}^{\delta} \frac{d\phi}{2\pi} e^{-\frac{\sigma^2\phi^2}{2}} e^{-2i(k+\phi)\mu(t)} h_L^\sigma(2k+\phi)) \left[\delta_{\mu(t)\geq 0} S_{jj}^*(k+\phi) + \delta_{\mu(t)<0} S_{jj}(k) \right] \right| \tag{3.161}$$

$$\leq \int_{-\delta}^{\delta} \frac{d\phi}{2\pi} e^{-\frac{\sigma^2\phi^2}{2}} \left| h_L^\sigma(2k+\phi) \right| \tag{3.162}$$

$$\leq \int_{-\delta}^{\delta} \frac{d\phi}{2\pi} e^{-\frac{\sigma^2\phi^2}{2}} \left| h_\infty^\sigma(2k+\phi) \right| + \int_{-\delta}^{\delta} \frac{d\phi}{2\pi} e^{-\frac{\sigma^2\phi^2}{2}} \left| h_L^\sigma(2k+\phi) - h_\infty^\sigma(2k+\phi) \right|. \tag{3.163}$$

Note that the second term can be bounded exactly as in (3.160), while the first term can be bound as

$$\int_{-\delta}^{\delta} \frac{d\phi}{2\pi} e^{-\frac{\sigma^2\phi^2}{2}} \left| h_\infty^\sigma(2k+\phi) \right| \tag{3.164}$$

$$= \int_{-\delta}^{\delta} \frac{d\phi}{\sqrt{2\pi}} \sigma e^{-\frac{\sigma^2}{2}\left((2k+\phi)^2+\phi^2\right)} h_\infty^{1/(2\pi\sigma)}(2\pi i(2k+\phi)\sigma^2) \tag{3.165}$$

$$\leq \frac{\sigma}{\sqrt{2\pi}} \int_{-\delta}^{\delta} d\phi e^{-\frac{\sigma^2}{2}\left((2k+\phi)^2+\phi^2\right)} \left(1 + 2\left[1 + \frac{1}{2\pi\sigma^2} \frac{1}{2\pi - |2k+\phi|} \right] e^{-2\pi\sigma^2(\pi - |2k+\phi|)} \right) \tag{3.166}$$

where we used equation (3.97) from Lemma 5 in the third step. If $2|k|+\delta < \pi$, then $h_\infty^{1/(2\pi\sigma)}(2k+\phi)$ can be bounded by 2 for $\sigma > (\pi - 2|k| - \delta)^{-1}$. We then have

$$\int_{-\delta}^{\delta} \frac{d\phi}{2\pi} \left| h_\infty^\sigma(2k+\phi) e^{-\frac{\sigma^2\phi^2}{2}} \right| \leq \sqrt{\frac{2}{\pi}} \sigma \int_{-\delta}^{\delta} d\phi e^{-\frac{\sigma^2}{2}\left((2k+\phi)^2+\phi^2\right)} \tag{3.167}$$

$$= \sqrt{\frac{2}{\pi}} \sigma \int_{-\delta}^{\delta} d\phi e^{-\sigma^2 k^2 - \sigma^2(k+\phi)^2} \tag{3.168}$$

$$\leq \sqrt{\frac{2}{\pi}} \sigma e^{-\sigma^2 k^2} \int_{-\infty}^{\infty} d\phi e^{-\sigma^2\phi^2} \tag{3.169}$$

$$= \sqrt{2} e^{-\sigma^2 k^2}. \tag{3.170}$$

However, if we instead have that $2|k| + \delta > \pi$, then we can instead bound equation (3.166) as

$$\int_{-\delta}^{\delta} \frac{d\phi}{2\pi} \left| h_\infty^\sigma(2k+\phi) e^{-\frac{\sigma^2\phi^2}{2}} \right|$$

$$\leq \sqrt{\frac{2}{\pi}} \sigma \int_{-\delta}^{\delta} d\phi e^{-\frac{\sigma^2}{2}\left((2k+\phi)^2+\phi^2\right)} \left(1 + 2\left[1 + \frac{1}{2\pi\sigma^2} \frac{1}{2\pi - |2k+\phi|} \right] e^{-2\pi\sigma^2(\pi - |2k+\phi|)} \right) \tag{3.171}$$

$$\leq 4\sqrt{\frac{2}{\pi}} \sigma \int_{-\delta}^{\delta} d\phi e^{-\frac{\sigma^2}{2}\left((2k+\phi)^2+\phi^2\right)} e^{2\pi\sigma^2(2|k|+\delta-\pi)} \tag{3.172}$$

$$= 4\sqrt{\frac{2}{\pi}} \sigma \int_{-\delta}^{\delta} d\phi e^{2\sigma^2\left(-k^2+2\pi|k|-\pi^2+\pi\delta-k\phi-\frac{\phi^2}{2}\right)} \tag{3.173}$$

$$= 4\sqrt{\frac{2}{\pi}} \sigma e^{2\sigma^2[-(\pi-|k|)^2+\pi\delta]} \int_{-\delta}^{\delta} d\phi e^{-\sigma^2(\phi^2+2k\phi)} \tag{3.174}$$

$$\leq 4\sqrt{\frac{2}{\pi}} \sigma e^{2\sigma^2[-(\pi-|k|)^2+(\pi+|k|)\delta]} \int_{-\delta}^{\delta} d\phi e^{-\sigma^2\phi^2} \tag{3.175}$$

$$\leq 4\sqrt{2} e^{-\sigma^2(\pi-|k|)^2} \tag{3.176}$$

where we assumed that $\delta < \frac{(\pi-|k|)^2}{\pi+|k|}$. In either case, we have that

$$\int_{-\delta}^{\delta} \frac{d\phi}{2\pi} \left| h_\infty^\sigma(2k+\phi) e^{-\frac{\sigma^2\phi^2}{2}} \right| \leq 4\sqrt{2} e^{-\sigma^2\delta}. \tag{3.177}$$

For the third term in (3.147), we have

$$\begin{aligned}
&\left| \int_{-\delta}^{\delta} \frac{d\phi}{2\pi} e^{-\frac{\sigma^2\phi^2}{2}} e^{-i\phi\mu(t)} \sum_{x=\max\{-\mu(t)-L,1\}}^{-\mu(t)+L} e^{i\phi x} e^{-\frac{(x+\mu(t))^2}{2\sigma^2}} \sum_{q=1}^{N} \big(S_{qj}^*(k+\phi) - S_{qj}^*(k)\big) S_{qj}(k) \right| \\
&\quad \leq \int_{-\delta}^{\delta} \frac{d\phi}{2\pi} e^{-\frac{\sigma^2\phi^2}{2}} N|\phi|\Gamma \sum_{x=\max\{-\mu(t)-L,1}^{-\mu(t)+L} e^{-\frac{(x+\mu(t))^2}{2\sigma^2}} && (3.178) \\
&\quad \leq \int_{-\delta}^{\delta} \frac{d\phi}{2\pi} e^{-\frac{\sigma^2\phi^2}{2}} N|\phi|\Gamma h_\infty^\sigma(0) && (3.179) \\
&\quad \leq \frac{N\Gamma h_\infty^\sigma(0)}{\pi} \int_0^\infty \phi e^{-\frac{\sigma^2\phi^2}{2}} d\phi && (3.180) \\
&\quad \leq \frac{N\Gamma h_\infty^\sigma(0)}{\pi\sigma^2} && (3.181) \\
&\quad \leq \frac{3\sqrt{2}N\Gamma}{\sigma} && (3.182)
\end{aligned}$$

where we used (3.77) to relate the $h_\infty^\sigma(0)$, and then (**??**) from Lemma 5. Additionally, we used the fact that S is a matrix of bounded rational functions, so that the Lipschitz constant

$$\Gamma = \max_{q,j\in[N]} \max_{p\in[-\pi,\pi]} \left| \frac{d}{dk'} S_{qj}(k') \Big|_{k'=p} \right| \tag{3.183}$$

is well defined.

For the fourth and fifth terms in (3.147), we can use Lemma 6 and the fact that each of these terms in the integrand are constant. In particular we have

$$\begin{aligned}
&\left| \int_{-\delta}^{\delta} \frac{d\phi}{2\pi} e^{-\frac{\sigma^2\phi^2}{2}} e^{-i\phi\mu(t)} \big(S_{jj}(k) - S_{jj}^*(k+\phi)\big)\big(1 - 2\delta_{\mu(t)<0}\big) e^{i(2k+\phi)|\mu(t)|} V_{|\mu(t)|+1,L}^\sigma(-2k-\phi) \right. \\
&\qquad \left. - \delta_{|\mu(t)|\leq L}\Big(1 + S_{jj}^*(k+\phi)\delta_{\mu(t)\geq 0} + S_{jj}(k)\delta_{\mu(t)<0}\Big) e^{-\frac{\mu(t)^2}{2\sigma^2}} \right| && (3.184) \\
&\quad \leq \int_{-\delta}^{\delta} \frac{d\phi}{2\pi} e^{-\frac{\sigma^2\phi^2}{2}} \left(2\big|V_{|\mu(t)|+1,L}^\sigma(-2k-\phi)\big| + 2e^{-\frac{-\mu(t)^2}{2\sigma^2}}\right) && (3.185) \\
&\quad \leq \frac{\chi+1}{\pi} \int_{-\infty}^{\infty} e^{-\frac{\sigma^2\phi^2}{2}} d\phi && (3.186) \\
&\quad \leq \sqrt{\frac{2}{\pi}} \frac{\chi+1}{\pi\sigma}. && (3.187)
\end{aligned}$$

With these bounds, we can then guarantee that $|\alpha_j(t)\rangle$ and $|w_j(t)\rangle$ approximate each other

well. In particular, we have

$$\begin{aligned}
&\| |\alpha_j(t)\rangle - |w_j(t)\rangle \|^2 \\
&\quad = \langle \alpha_j(t) | \alpha_j(t)\rangle + \langle w_j(t) | w_j(t)\rangle - 2\Re\big[\langle \alpha_j(t) | w_j(t)\rangle\big] && (3.188)\\
&\quad \leq 2 + \gamma^2 e^{-\frac{\mu(t)^2}{\sigma^2}}(1+2\chi) + \frac{2\sigma\delta}{\sqrt{\pi}(2\sigma^2\delta^2+1)} e^{-\sigma^2\delta^2} - \sqrt{2}\eta\gamma\left(1 - \frac{1}{\delta\sigma\sqrt{\pi}} e^{-\sigma^2\delta^2}\right) \\
&\qquad + \sqrt{\frac{8}{\pi}}\frac{\eta\gamma\sigma}{L} e^{-\frac{L^2}{2\sigma^2}} + 8\sqrt{2}\eta\gamma e^{-\sigma^2\delta} + \frac{6\sqrt{2}N\Gamma\eta\gamma}{\sigma} + \sqrt{\frac{8}{\pi}}\frac{(\chi+1)\eta\gamma}{\pi\sigma} && (3.189)
\end{aligned}$$

We can then use our bounds on γ from equations (3.135) and (3.136) to see that

$$\begin{aligned}
&\| |\alpha_j(t)\rangle - |w_j(t)\rangle \|^2 \\
&\quad \leq 2 + \frac{1}{\sqrt{\pi}\sigma} e^{-\frac{\mu(t)^2}{\sigma^2}}(1+2\chi)\big(1 + e^{-\frac{L^2}{2\sigma^2}}\big) + \frac{10}{\delta\sigma} e^{-\sigma^2\delta^2} - 2\left(1 + \frac{3}{2}e^{-\pi^2\sigma^2}\right)\left(1 - \frac{1}{\delta\sigma\sqrt{\pi}} e^{-\sigma^2\delta^2}\right) \\
&\qquad + \left(1 + \frac{1}{2}e^{-\frac{L^2}{2\sigma^2}}\right)\left(\frac{4\sigma}{L}e^{-\frac{L^2}{2\sigma^2}} + 16e^{-\sigma^2\delta} + \frac{12N\Gamma}{\sigma} + \frac{4(\chi+1)}{\sqrt{\pi^3}\sigma}\right) && (3.190)\\
&\quad \leq \frac{1+2\chi}{\sigma} + \frac{1}{\sigma} + \frac{8\sigma}{L}e^{-\frac{L^2}{2\sigma^2}} + \frac{4}{\delta\sqrt{\pi}\sigma} + 32e^{-\sigma^2\delta} + \frac{24N\Gamma}{\sigma} + \frac{8(\chi+1)}{\sigma} && (3.191)\\
&\quad \leq \frac{10(\chi+1) + 24N\Gamma + \delta^{-1}}{\sigma} + \frac{8\sigma}{L}e^{-\frac{L^2}{2\sigma^2}} + 32e^{-\sigma^2\delta}. && (3.192)
\end{aligned}$$

Hence, we have a bound on the difference in norm between these two states that is independent of the time at which we compare them.

At this point, we can now bound the error that arises when approximating $|\alpha_j(t)\rangle$ by a Gaussian for any time t. However, we don't yet know how well $|\alpha_j(t)\rangle$ approximates $|\psi_j(t)\rangle$. Note, however, that $|\alpha_j(0)\rangle = |\psi_j(0)\rangle$, and thus we already have an approximation to the initial state. We can then time-evolve this approximation, and compare it to the Gaussian approximation for $|\alpha_j(t)\rangle$.

Along these lines, let us define

$$|v_j(0)\rangle = |w_j(0)\rangle = \eta \int_{-\delta}^{\delta} \frac{d\phi}{2\pi} e^{i\phi\mu} e^{-\frac{\sigma^2\phi^2}{2}} |\mathrm{sc}_j(k+\phi)\rangle \tag{3.193}$$

and then define

$$|v_j(t)\rangle = e^{-iHt}|v_j(0)\rangle = \eta \int_{-\delta}^{\delta} \frac{d\phi}{2\pi} e^{i\phi\mu - 2it\cos(k+\phi)} e^{-\frac{\sigma^2\phi^2}{2}} |\mathrm{sc}_j(k+\phi)\rangle. \tag{3.194}$$

We then want to compare this time evolved state with our approximation to $|\alpha_j(t)\rangle$. We can see

$$\begin{aligned}
\langle v_j(t) | w_j(t)\rangle &= \eta^2 \int_{-\delta}^{\delta} \frac{d\phi}{2\pi} e^{2it\cos(k+\phi) - 2it\cos(k)} e^{i\phi\mu - i\phi\mu - i\phi\lceil 2t\sin k\rceil} e^{-\sigma^2\phi^2} && (3.195)\\
&= \eta^2 \int_{-\delta}^{\delta} \frac{d\phi}{2\pi} e^{-\sigma^2\phi^2} - \eta^2 \int_{-\delta}^{\delta} \frac{d\phi}{2\pi} \big(1 - e^{2it\cos(k+\phi) - 2it\cos(k) + i\phi\lceil 2t\sin k\rceil}\big) e^{-\sigma^2\phi^2}. && (3.196)
\end{aligned}$$

The first term is simply the norm of both $|v_j(t)\rangle$ and $|w_j(t)\rangle$, while the third term can be bounded

as

$$\left| \int_{-\delta}^{\delta} \frac{d\phi}{2\pi} \big(1 - e^{2it\cos(k+\phi) - 2it\cos(k) + i\phi\lceil 2t\sin k\rceil}\big) e^{-\sigma^2\phi^2} \right| \tag{3.197}$$

$$\leq \int_{-\delta}^{\delta} \frac{d\phi}{2\pi} \big|1 - e^{2it\cos(k+\phi) - 2it\cos(k) + i\phi\lceil 2t\sin k\rceil}\big| e^{-\sigma^2\phi^2} \tag{3.198}$$

$$\leq \int_{-\delta}^{\delta} \frac{d\phi}{2\pi} \big|2t\cos(k+\phi) - 2t\cos(k) + \phi\lceil 2t\sin k\rceil\big| e^{-\sigma^2\phi^2} \tag{3.199}$$

$$\leq \int_{-\delta}^{\delta} \frac{d\phi}{2\pi} \Big(2t\big|\cos(k)\cos(\phi) - \sin(k)\sin(\phi) - \cos(k) + \phi\sin(k)\big| + |\phi|\Big) e^{-\sigma^2\phi^2} \tag{3.200}$$

$$\leq \int_{-\delta}^{\delta} \frac{d\phi}{2\pi} \Big(t\big|\cos(k)\phi^2 + \sin(k)|\phi|^3\big| + |\phi|\Big) e^{-\sigma^2\phi^2} \tag{3.201}$$

$$\leq 2\int_{0}^{\delta} \frac{d\phi}{2\pi} \big(2t\phi^2 + \phi\big) e^{-\sigma^2\phi^2} \tag{3.202}$$

$$\leq \frac{1}{2\pi\sigma^2} + \frac{t}{2\sqrt{\pi}\sigma^3}. \tag{3.203}$$

Noting that the norm of $\langle v_j(t) | v_j(t) \rangle$ doesn't change with time (and is in fact exactly normalized, assuming that $\mu(t) > L$), we have that

$$\| |v_j(t)\rangle - |w_j(t)\rangle \|^2 = \langle v_j(t) | v_j(t) \rangle + \langle w_j(t) | w_j(t) \rangle - \langle v_j(t) | w_j(t) \rangle - \langle w_j(t) | v_j(t) \rangle \tag{3.204}$$

$$\leq 2\eta^2 \int_{\delta}^{\delta} \frac{d\phi}{2\pi} e^{-\sigma^2\phi^2} - 2\eta^2 \int_{\delta}^{\delta} \frac{d\phi}{2\pi} e^{-\sigma^2\phi^2} + \frac{2\eta^2}{2\pi\sigma^2} + \frac{2\eta^2 t}{2\sqrt{\pi}\sigma^3} \tag{3.205}$$

$$= 2\frac{\sqrt{\pi}}{\sigma} + \frac{2t}{\sigma^2}. \tag{3.206}$$

Finally, we can combine these bounds, remembering that $|\psi_j(0)\rangle = |\alpha_j(0)\rangle$. In particular, we have that

$$\| |\psi_j(t)\rangle - |\alpha_j(t)\rangle \|$$

$$\leq \| |\psi_j\rangle(t) - |v_j(t)\rangle \| + \| |v_j(t)\rangle - |w_j(t)\rangle \| + \| |w_j(t)\rangle - |\alpha_j(t)\rangle \| \tag{3.207}$$

$$\leq 2\left[\frac{10(\chi+1) + 24N\Gamma + \delta^{-1}}{\sigma} + \frac{8\sigma}{L} e^{-\frac{L^2}{2\sigma^2}} + 32e^{-\sigma^2\delta} \right]^{1/2} + \left[\frac{2\sqrt{\pi}}{\sigma} + \frac{2t}{\sigma^2} \right]^{1/2}. \tag{3.208}$$

If we then assume that $\sigma = \frac{c_1 L}{\sqrt{\log L}}$ for some constant $c_1 < \frac{1}{\sqrt{2}}$, and that $t < c_2 L$ for some constant c_2, we have that for L large enough

$$\| |\psi_j(t)\rangle - |\alpha_j(t)\rangle \|$$

$$\leq 2\left[\frac{10(\chi+1) + 24N\Gamma + \delta^{-1}}{c_1} \frac{\sqrt{\log L}}{L} + \frac{8c_1}{\sqrt{\log L}} e^{-\frac{\log L}{2c_1^2}} + 32e^{-L\delta} \right]^{1/2}$$

$$+ \left[\frac{2\sqrt{\pi}}{c_1} \frac{\sqrt{\log L}}{L} + \frac{2c_2 \log L}{c_1^2 L} \right]^{1/2}. \tag{3.209}$$

$$\in \mathcal{O}\left(\sqrt{\frac{\log L}{L}} \right) \tag{3.210}$$

and we have the requisite growth properties. □

3.5 Conclusions and extensions

[**TO DO:** *I still don't like this conclusions section, but something is better than nothing*]

At this point, we have a general understanding of graph scattering off of a single graph. The idea of a wavepacket moving along an infinite path makes sense, as does its scattering behavior off of some given graph. We know how to calculate this scattering behavior for a given graph at a particular momenta, and we have bounds on the error arising from such a scattering event.

Additionally, we know how to construct graphs with simple scattering behaviors. While these behaviors depend on the eigenstates of arbitrary graphs, we have given examples that might be of use as building blocks for some scattering algorithm.

Finally, we have also shown that some scattering behavior cannot exist. While this means that certain schemes cannot be simplified, this is of theoretical interest. Further, it also allows us to stop searching for graphs with these behaviors.

While these form a nice foundation, more research can always be done in these fields. Ideally, giving an explicit algorithm that constructs a graph with a particular scattering behavior, or says that such a graph doesn't exist, would be of great interest. Even if such an algorithm took an exponential amount of time, this would be a theoretical achievement since we don't know whether this problem is currently decidable.

Less ambitiously, if we could give such an algorithm for a restricted set of graphs, such as that given for type 1 and type 2 R/T gadgets, but generalized to multiple input and outputs.

Along different lines, improving the bounds on our scattering behavior, or showing that they cannot be improved by more than a constant, would give better bounds on results later in the thesis. This scattering behavior is foundational to the idea of computation via scattering, and thus improved bounds result in smaller guaranteed errors.

[**TO DO:** *talk about how this can't really be improved without changing our approximation*] One area in which improvement can be made is in our analysis on the error of propagating Guassian wave packets. While our results in this chapter are an improvement over [16], much of the error in the analysis arises from the approximation of our approximate wave packets with exponentials over the scattering states. Far from the graph gadget, our approximations could

Essentially, graph scattering seems to be a new subfield in the study of graphs, with several areas of research opening up.

Chapter 4

Scattering gadgets

[**TO DO:** *fix everything!*]

4.0.1 Momentum dependent actions

While the NAND tree algorithm gives a good example of how graph scattering can work as an algorithmic tool, in that the scattering evaluates a binary function, the scattering behavior was relatively simple: a particle transmits or reflects. However, we can use similar ideas in order to have nontrivial scattering behavior, by creating graphs that have different behaviors at different momenta, or that perfectly transmits to some subset of the attached paths (i.e., a generalization of perfect transmission to multiple semi-infinite paths).

[**TO DO:** *Should I include schematic pictures of these gadgets? I'm not sure if that would improve readability*]

4.0.1.1 R/T gadgets

The easiest thing we could hope for is the same behavior as in the NAND tree algorithm, with two attached paths and at some fixed momenta the wavepacket either completely transmits, or it completely reflects. However, we will utilize a single graph with several different momenta.

In particular, these reflection/transmission (R/T) gadgets will have two sets of momenta. One set will have perfect transmission, while the other will have perfect reflection. While these gadgets have relatively simple scattering behavior, they can be used to filter particular momenta, or as building blocks in more complicated gadgets. Additionally, the simple behavior will allow us to show that certain scattering behaviors are not possible.

4.0.1.2 Momentum Switches

We can generalize the idea of R/T gadgets to multiple semi-infinite paths, so that the gadget has a kind of routing behavior. In particular, we can attempt to construct graphs with three attached semi-infinite paths, in which when a wavepacket is incident along one particular path, it either perfectly transmits to the second path, or it perfectly transmits to the third path, depending on the incident momenta. In this way, we construct something like a momentum dependent railroad switch, sending different wavepackets to different locations.

These momentum switches are extremely useful, as they will allow us to construct much more interesting momentum dependent behavior. By using two of these gadgets in series (with the paths 2 and 3 connected to each other), we can then place a single obstacle along only one of the paths.

Since only those momenta that travel along that particular path are incident on the additional obstacle, we can use this to do something like applying a momentum dependent phase.

4.0.2 Encoded unitary

While the above two gadgets can be thought to have one input but two output paths, we can generalize this idea to having multiple input paths. In particular, if we have two input and two output paths, we can encode a logical qubit in a dual-rail encoding (i.e., one path corresponds to a state $|0\rangle$, while the other corresponds to a state $|1\rangle$). If we can ensure that wavepackets incident along the input paths always transmit to the output paths, we can think of this as applying a unitary gate to the encoded qubit.

In particular, by constructing a gadget whose S-matrix at a particular momentum is block diagonal, with two zero blocks along the diagonal, we have that a wavepacket at that momenta always transmits from the input to the output vertices. Additionally, as the S-matrix is itself unitary, we have that the 2×2 block matrix that corresponds to the transmitted amplitudes is also unitary, and thus we have applied a unitary operation to the encoded qubit.

4.1 Constructing graphs with particular scattering behavior

While we have shown that the scattering behavior of some given graph is easy to compute, finding graphs with a given behavior is much more difficult. We don't even know whether such an operation is decidable, and thus finding an algorithm to construct a graph with a given S-matrix seems unlikely. However, there are specific behaviors at particular momenta in which constructions are known, and exhaustive searches of small sized graphs have yielded graphs with nice scattering properties.

In particular, Andrew Childs found several gadgets in his paper proving the universality of quantum walks [11]. After this result, Blumer, Underwood and Feder [9] performed an exhaustive search over all graphs with at most 9 vertices, finding those graphs that implement an encoded unitary at several momenta of interest. Childs, Gosset, and Webb then constructed several gadgets in [16]. This section is mainly based on [15], a paper by Chlids, Gosset, Nagaj, Raha, and Webb, as it gives explicit constructions for gadgets with particular behavior.

4.1.1 R/T gadgets

Perhaps the most simple behavior, and the one that will for which we will have the easiest time finding a solution, are two-terminal gadgets that either perfectly reflect at some particular momenta, or perfectly transmit. These R/T gadgets can be thought of as a proof-of-principle for constructing gadgets, but they also have uses of their own.

This problem is still rather complicated when we work with arbirtary graphs with two terminal vertices, things become much simpler if we work with a graph attached to an infinite path via a single vertex. In this case, we can determine exactly when the gadget will lead to perfect reflection, and when it will lead to perfect transmission.

Along these lines, we will investigate the scattering behavior of graphs where $\widehat{G}$ is of the form found in Figure 4.1. While we still have that $\widehat{G}$ is of the form described in Section 3.2.2, the graph G with the semi-infinite paths is that of a infinite path, with the graph G_0 attached to the vertex a. As such, the graph that will be of more interest is the graph G_0 consisting of those vertices other than those along the infinite path. We will label those vertices $p_i \in V(G_0)$ connected to the vertex a as *periphery* vertices, and we will label the set of periphery vertices as P. In the special

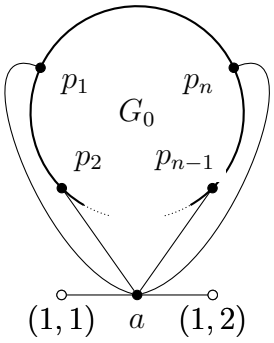

Figure 4.1: A type 1 R/T gadget. Vertices of G_0 that are not part of the periphery $P = \{p_1, \ldots, p_n\}$ are not shown.

case that $|P| = 1$, or that a single vertex of G_0 is connected to a, we will call the gadget a type 2 R/T gadget (see Figure 4.2 for an example of a type 2 R/T gadget).

For a given R/T gadget $\widehat{G}$, those momenta for which perfect reflection occurs shall be collected in the *reflection set* which shall be denoted $\mathcal{R}$. Similarly, those momenta for which perfect transmission occurs shall be collected in the *transmission set* which shall be label $\mathcal{T}$. Note that these two sets have empty intersection, and that there isn't any nice relationship between them.

Let us now examine the scattering eigenstates for the graph $\widehat{G}$. For any scattering state $|\mathrm{sc}_1(k)\rangle$, by examining the eigenvalue equation at vertices $(1,1)$ and $(1,2)$ we see that the amplitude at vertex a satisfies

$$\langle a|\mathrm{sc}_1(k)\rangle = 1 + R(k) = T(k). \tag{4.1}$$

Thus perfect reflection at momentum k occurs if and only if $R(k) = -1$ and $\langle a|\mathrm{sc}_1(k)\rangle = 0$, while perfect transmission occurs if and only if $T(k) = 1$ and $\langle a|\mathrm{sc}_1(k)\rangle = 1$. Using this fact, we now derive conditions on the graph G_0 that determine when perfect transmission and reflection occur.

For any type 1 R/T gadget, we have necessary and sufficient conditions for momentum k to be in the reflection set: G_0 should have an eigenvector for which the sum of amplitudes on the periphery is nonzero.

Lemma 7. *Let $\widehat{G}$ be a type 1 R/T gadget. A momentum $k \in (-\pi, 0)$ is in the reflection set $\mathcal{R}$ if and only if G_0 has an eigenvector $|\chi_k\rangle$ with eigenvalue $2\cos(k)$ satisfying*

$$\sum_{i=1}^{n} \langle p_i|\chi_k\rangle \neq 0. \tag{4.2}$$

Proof. Let us first suppose that $\widehat{G}$ has perfect reflection at momentum k, i.e., $R(k) = -1$ and $\langle a|\mathrm{sc}_1(k)\rangle = 0$. As $\langle (1,1)|\mathrm{sc}_1(k)\rangle = e^{-ik} - e^{ik} \neq 0$ and $\langle (1,2)|\mathrm{sc}_1(k)\rangle = 0$, to satisfy the eigenvalue equation at vertex a, we have

$$\sum_{j=1}^{n} \langle p_j|\mathrm{sc}_1(k)\rangle = e^{ik} - e^{-ik} \neq 0. \tag{4.3}$$

Further, since G_0 only connects to vertex a and the amplitude at this vertex is zero, the restriction of $|\mathrm{sc}_1(k)\rangle$ to G_0 must be an eigenvector of G_0 with eigenvalue $2\cos(k)$. Hence the condition is necessary for perfect reflection.

Next suppose that G_0 has an eigenvector $|\chi_k\rangle$ with eigenvalue $2\cos(k)$ satisfying (4.2), with the sum equal to some nonzero constant c. Define a scattering state $|\psi_k\rangle$ on the Hilbert space of the full graph G with amplitudes

$$\langle v|\psi_k\rangle = \frac{e^{ik} - e^{-ik}}{c}\langle v|\chi_k\rangle \tag{4.4}$$

for all $v \in V(G_0)$, $\langle a|\psi_k\rangle = 0$, and

$$\langle (x,j)|\psi_k\rangle = \begin{cases} e^{-ikx} - e^{ikx} & j = 1 \\ 0 & j = 2 \end{cases} \tag{4.5}$$

for all $x \in \mathbb{Z}^+$.

We claim that $|\psi_k\rangle$ is an eigenvector of G with eigenvalue $2\cos(k)$. The state clearly satisfies the eigenvalue equation on the semi-infinite paths since it is a linear combination of states with momentum $\pm k$. At vertices of G_0, the state is proportional to an eigenvector of G_0, and since the state has no amplitude at a, the eigenvalue equation is also satisfied at these vertices. It remains to see that the eigenvalue equation is satisfied at a, but this follows immediately by a simple calculation.

Since $|\psi_k\rangle$ has the form of a scattering state with perfect reflection, we see that $R(k) = -1$ and $T(k) = 0$ as claimed. □

In a similar manner, the following lemma gives a sufficient condition for a momentum k to be in the transmission set (which is also necessary for type 2 gadgets). Let g_0 denote the induced subgraph on $V(G_0) \setminus P$ where $P = \{p_i : i \in [n]\}$ is the periphery.

Lemma 8. *Let $\widehat{G}$ be a type 1 R/T gadget and let $k \in (-\pi, 0)$. Suppose $|\xi_k\rangle$ is an eigenvector of g_0 with eigenvalue $2\cos k$ and with the additional property that, for all $i \in [n]$,*

$$\sum_{\substack{v \in V(g_0): \\ (v,p_i) \in E(G_0)}} \langle v|\xi_k\rangle = c \neq 0 \tag{4.6}$$

for some constant c that does not depend on i. Then k is in the transmission set $\mathcal{T}$. If $\hat{G}$ is a type 2 R/T gadget, then this condition is also necessary.

Proof. If g_0 has a suitable eigenvector $|\xi_k\rangle$ satisfying (4.6), define a scattering state $|\psi_k\rangle$ on the full graph G, with amplitudes $\langle a|\psi_k\rangle = 1$,

$$\langle v|\psi_k\rangle = \begin{cases} -\frac{1}{c}\langle v|\xi_k\rangle & v \in V(g_0) \\ 0 & v \in P \end{cases} \tag{4.7}$$

in the graph G_0, and

$$\langle (x,j)|\psi_k\rangle = \begin{cases} e^{-ikx} & j = 1 \\ e^{ikx} & j = 2 \end{cases} \tag{4.8}$$

for $x \in \mathbb{Z}^+$. As in the proof of Lemma 7, the state $|\psi_k\rangle$ is clearly satisfies the eigenvalue equation (with eigenvalue $2\cos(k)$) at vertices on the semi-infinite paths and vertices of g_0. The factor of $-\frac{1}{c}$ in (4.7) is chosen so that the eigenvalue condition is satisfied at vertices in P. It is easy to see that the eigenvalue condition is also satisfied at a.

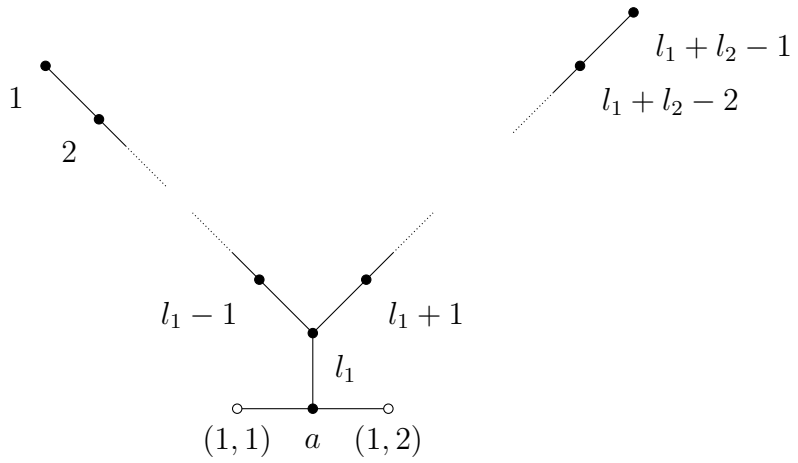

Figure 4.2: An R/T gadget built from a path of length $l_1 + l_2 - 2$.

Since $|\psi_k\rangle$ is a scattering eigenvector of G with eigenvalue $2\cos(k)$ and perfect transmission, we have $T(k) = 1$.

Now suppose $\widehat{G}$ is a type 2 R/T gadget, with $P = \{p\}$. Perfect transmission along with the eigenvalue equation at vertex a implies

$$\langle p | \mathrm{sc}_1(k) \rangle = 0, \tag{4.9}$$

so the restriction of $|\mathrm{sc}_1(k)\rangle$ to g_0 must be an eigenvector (since p is the only vertex connected to g_0). The eigenvalue equation at p gives

$$\langle a | \mathrm{sc}_1(k) \rangle + \sum_{w\colon (w,p)\in E(G_0)} \langle w | \mathrm{sc}_1(k) \rangle = 0 \quad \Longrightarrow \quad \sum_{w\colon (w,p)\in E(G_0)} \langle w | \mathrm{sc}_1(k) \rangle = -1. \tag{4.10}$$

Hence the restriction of $|\mathrm{sc}_1(k)\rangle$ to $V(g_0)$ is an eigenvector of the induced subgraph, with the additional property that the sum of the amplitudes at vertices connected to p is nonzero. □

With these two lemmas, if we can guarantee the form of the eigenstates for the graph G_0, we can guarantee certain momenta to be in either the reflection or the transmission set.

4.1.1.1 Explicit constructions

While the two lemmas do give a nice abstract explanation for the construction of R/T gadgets, it doesn't provide us with a concrete example. As such, let us look at two simple graphs and examine when they satisfy the conditions of the lemmas.

As a first example, suppose G_0 is a finite path of length $l_1 + l_2 - 2$ connected to a at the l_1th vertex, as shown in Figure 4.2. As this is a type 2 R/T gadget, we can then determine the reflection and transmission sets as a function of l_1 and l_2.

Using Lemma 7, we see that perfect reflection occurs at momentum $k \in (-\pi, 0)$ if and only if the path has an eigenvector with eigenvalue $2\cos(k)$ with non-zero amplitude on vertex l_1. Recall that the path of length L (where the length of a path is its number of edges) has eigenvectors $|\psi_j\rangle$ for $j \in [L+1]$ given by

$$\langle x | \psi_j \rangle = \sin\left(\frac{\pi j x}{L+2}\right) \tag{4.11}$$

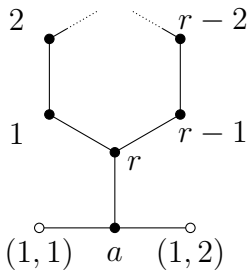

Figure 4.3: An R/T gadget built from an r-cycle.

with eigenvalues $\lambda_j = 2\cos(\pi j/(L+2))$. Hence

$$\mathcal{R}_{\text{path}} = \left\{ -\frac{\pi j}{l_1 + l_2} : j \in [l_1 + l_2 - 1] \text{ and } \frac{j l_1}{l_1 + l_2} \notin \mathbb{Z} \right\}. \tag{4.12}$$

To characterize the momenta at which perfect transmission occurs, consider the induced subgraph obtained by removing the l_1th vertex from the path of length $l_1 + l_2 - 2$ (a path of length $l_1 - 2$ and a path of length $l_2 - 2$). We can choose bases for the eigenspaces of this induced subgraph so that each eigenvector has all of its support on one of the two paths, and has nonzero amplitude on only one of the vertices $l_1 - 1$ or $l_1 + 1$. Thus Lemma 8 implies that $\widehat{G}$ perfectly transmits for all momenta in the set

$$\mathcal{T}_{\text{path}} = \left\{ -\frac{\pi j}{l_1} : j \in [l_1 - 1] \right\} \cup \left\{ -\frac{\pi j}{l_2} : j \in [l_2 - 1] \right\}. \tag{4.13}$$

As an explicit example, if we set $l_1 = l_2 = 2$, we get $\mathcal{T}_{\text{path}} = \{-\frac{\pi}{2}\}$ and $\mathcal{R}_{\text{path}} = \{-\frac{\pi}{4}, -\frac{3\pi}{4}\}$.

Now let us suppose G_0 is a cycle of length r. Labeling the vertices by $x \in [r]$, where $x = r$ is the vertex attached to the path (as shown in Figure 4.3), the eigenvectors of the r-cycle are

$$\langle x | \phi_m \rangle = e^{2\pi i x m / r} \tag{4.14}$$

with eigenvalue $2\cos(2\pi m/r)$, where $m \in [r]$. For each momentum $k = -2\pi m/r \in (-\pi, 0)$, there is an eigenvector with nonzero amplitude on the vertex r (i.e., $\langle r | \phi_m \rangle \neq 0$), so Lemma 7 implies that perfect reflection occurs at each momentum in the set

$$\mathcal{R}_{\text{cycle}} = \left\{ -\frac{\pi j}{r} : j \text{ is even and } j \in [r - 1] \right\}. \tag{4.15}$$

To see which momenta perfectly transmit, we use Lemma 8. Consider the induced subgraph obtained by removing vertex r. This subgraph is a path of length $r - 2$ and has eigenvalues $2\cos(\pi m/r)$ for $m \in [r - 1]$ as discussed in the previous section. Using the expression (4.11) for the eigenvectors, we see that the sum of the amplitudes on the two ends is nonzero for odd values of m. Perfect transmission occurs for each of the corresponding momenta:

$$\mathcal{T}_{\text{cycle}} = \left\{ -\frac{\pi j}{r} : j \text{ is odd and } j \in [r - 1] \right\}. \tag{4.16}$$

For example, the 4-cycle (i.e., square) has $\mathcal{T}_{\text{cycle}} = \{-\frac{\pi}{4}, -\frac{3\pi}{4}\}$ and $\mathcal{R}_{\text{cycle}} = \{-\frac{\pi}{2}\}$.

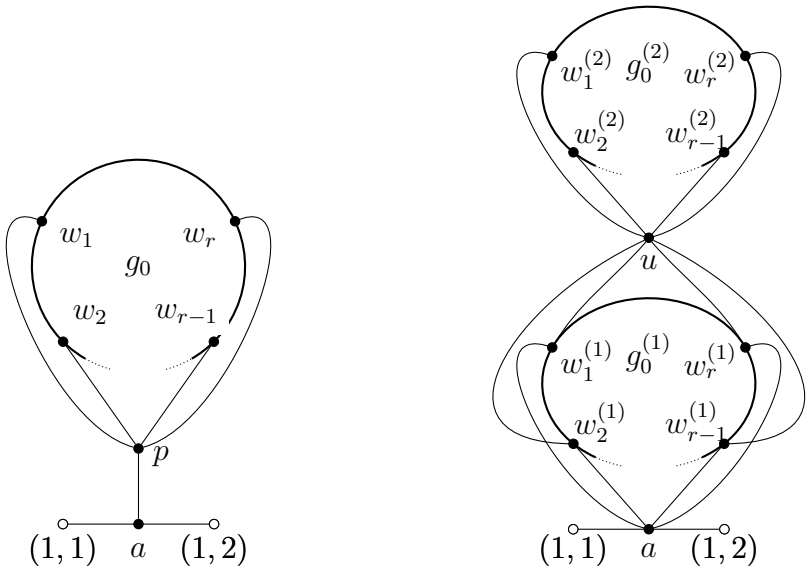

Figure 4.4: (a) A type 2 R/T gadget, (i.e., a type 1 gadget with $|P| = 1$). (b) The R/T gadget $\widehat{G}^{\leftrightarrow}$ reversing the reflection and transmission sets of (a).

4.1.1.2 Reversing reflection and transmission sets

With these explicit examples of R/T gadgets, it will be useful to know how to interchange the reflection and transmission set. Namely, if we have one gadget that transmits all momenta in $\mathcal{T}$ and reflects all momenta in $\mathcal{R}$, it will be useful to also have a gadget that reflects all momenta in $\mathcal{T}$ and transmits all momenta in $\mathcal{R}$. Basically, we will be able to use these two gadgets together to construct gadgets with more interesting scattering behavior.

In particular, let $\widehat{G}$ be a type 2 R/T gadget, as seen in Figure 4.4a, and assume that it has a reflection set $\mathcal{R}$ and a transmission set $\mathcal{T}$. We will construct a type 1 R/T gadget $\widehat{G}^{\leftrightarrow}$ with reflection set $\mathcal{R}' \supset \mathcal{T}$ and transmission set $\mathcal{T}' \supset \mathcal{R}$. The graph $\widehat{G}^{\leftrightarrow}$ is depicted pictorially in Figure 4.4b.

Explicitly, the R/T gadget $\widehat{G}^{\leftrightarrow}$ is obtained by taking two copies of the subgraph g_0 from the type 2 R/T gadget in Figure 4.4a, connecting both to a single additional vertex u, and connecting one copy of g_0 to the infinite path at a. More concretely, for each vertex $w_j \in V(g_0)$, the graph $\widehat{G}^{\leftrightarrow}$ has two vertices $w_j^{(1)}$ and $w_j^{(2)}$, and the graph $\widehat{G}^{\leftrightarrow}$ inherits the edge set of g_0. Additionally, for each $w_j \in V(g_0)$ connected to the periphery vertex p, we have that $w_j^{(i)}$ is connected to u, and $w_j^{(1)}$ is connected to a.

With this definition, we now prove that the graph $\widehat{G}^{\leftrightarrow}$ reverses the reflection and transmission sets of $\widehat{G}$.

Lemma 9. *Let $\widehat{G}$ be a type 2 R/T gadget with transmission set $\mathcal{T}$ and reflection set $\mathcal{R}$. The type 1 R/T gadget $\widehat{G}^{\leftrightarrow}$ defined above has transmission set $\mathcal{T}' \supseteq \mathcal{R}$ and reflection set $\mathcal{R}' \supseteq \mathcal{T}$.*

Proof. First consider a momentum $k \in \mathcal{T}$. Using the condition derived in Lemma 8, we see that g_0 has an eigenvector $|\xi_k\rangle$ with eigenvalue $2\cos(k)$ where the sum of the amplitudes on vertices $w_1, \ldots, w_r$ is nonzero. Now consider the induced subgraph $G_0^{\leftrightarrow}$ of Figure 4.4b obtained by removing vertices $(1,1)$, $(1,2)$, and a. This subgraph has an eigenvector $|\chi_k^{\leftrightarrow}\rangle$ with eigenvalue $2\cos(k)$ given

by

$$\langle v^{(i)}|\,\chi_k^{\leftrightarrow}\,\rangle = (-1)^i\langle v|\,\xi_k\,\rangle \quad \text{and} \quad \langle u|\,\chi_k^{\leftrightarrow}\,\rangle = 0 \tag{4.17}$$

for all vertices $v \in V(g_0)$ and for $i \in \{1,2\}$. The fact that $|\,\chi_k^{\leftrightarrow}\,\rangle$ is an eigenvector follows from the fact that $|\,\xi_k\,\rangle$ is an eigenvector of g_0. Additionally, we have that

$$\sum_{j=1}^{r}\langle w_j^{(1)}|\,\chi_k^{\leftrightarrow}\,\rangle = -\sum_{j=1}^{r}\langle w_j|\,\xi_k\,\rangle \neq 0. \tag{4.18}$$

Using Lemma 7, we see that perfect reflection occurs at momentum k, and thus $\mathcal{T} \subseteq \mathcal{R}'$.

Next suppose $k \in \mathcal{R}$. Lemma 7 states that G_0 has an eigenvector $|\chi_k\rangle$ with eigenvalue $2\cos(k)$ such that $\langle p|\,\chi_k\,\rangle \neq 0$. Now consider the induced subgraph $g_0^{\leftrightarrow}$ of Figure 4.4b obtained by removing vertices $(1,1)$, $(1,2)$, a, and $w_1^{(1)},\ldots,w_r^{(1)}$. This graph has an eigenvector $|\,\xi_k^{\leftrightarrow}\,\rangle$ with eigenvalue $2\cos(k)$ defined by

$$\langle v|\,\xi_k^{\leftrightarrow}\,\rangle = \begin{cases} \langle v|\,\chi_k\,\rangle & \text{for } v \in V(g_0^{(2)}) \\ \langle p|\,\chi_k\,\rangle & v = u \\ 0 & \text{otherwise.} \end{cases} \tag{4.19}$$

To see that this is an eigenvector, observe that $g_0^{\leftrightarrow}$ is a disconnected graph and $|\,\chi_k\,\rangle$ is an eigenvector of one of its components. Using this and Lemma 8 (since u is the only vertex adjacent to the periphery of $\hat{G}^{\leftrightarrow}$ with non-zero amplitude), we see that $k \in \mathcal{T}'$, so $\mathcal{R} \subseteq \mathcal{T}'$. □

4.1.2 Momentum switches

To construct a momentum switch between a given pair of momenta, it will be worthwhile to first construct two R/T gadgets between the momenta, with the two gadgets having swapped reflection and transmission sets. We can then construct something like a railroad switch, by placing the two gadgets immediately after a 3-claw. With this design, the incident wavepacket will only see one of the two outgoing paths, and the resulting S-matrix will be exactly what we want.

In particular, we can construct a momentum switch between the reflection and transmission sets $\mathcal{R}$ and $\mathcal{T}$ of a type 2 R/T gadget. We attach the gadget and its reversal (defined in Section 4.1.1.2) to the leaves of a claw, as shown in Figure 4.5. Specifically, given a type 2 R/T gadget $\widehat{G}$, the corresponding momentum switch $\widehat{G}^{\prec}$ consists of a copy of G_0, a copy of $G_0^{\leftrightarrow}$, and a claw, with the three leaves of the claw acting as the terminal vertices. Vertex p of G_0 is connected to leaf 2 of the claw, and vertices $w_1^{(1)},\ldots,w_r^{(1)}$ of $G_0^{\leftrightarrow}$ are each connected to leaf 3 of the claw.

Intuitively, the momentum switch acts the same as a railroad switch. For momenta in the transmission set, the gadget perfectly transmits while its reversal perfectly reflects, so the claw is effectively a path connecting terminals 1 and 2. For momenta in the reflection set, the roles of transmission and reflection are reversed, so the claw is effectively a path connecting terminals 1 and 3.

We can now prove that this gadget acts as a momentum switch, by constructing the desired scattering eigenstates.

Lemma 10. *Let $\widehat{G}$ be a type 2 R/T gadget with reflection set $\mathcal{R}$ and transmission set $\mathcal{T}$. The gadget $\hat{G}^{\prec}$ described above is a momentum switch between the sets $\mathcal{R}$ and $\mathcal{T}$.*

Proof. We construct a scattering eigenstate for each momentum $k \in \mathcal{T}$ with perfect transmission from path 1 to path 2, and similarly construct a scattering eigenstate for each momentum $k' \in \mathcal{R}$ with perfect transmission from 1 to 3. These eigenstates show that $S_{2,1}(k) = 1$ and $S_{3,1}(k') = 1$.

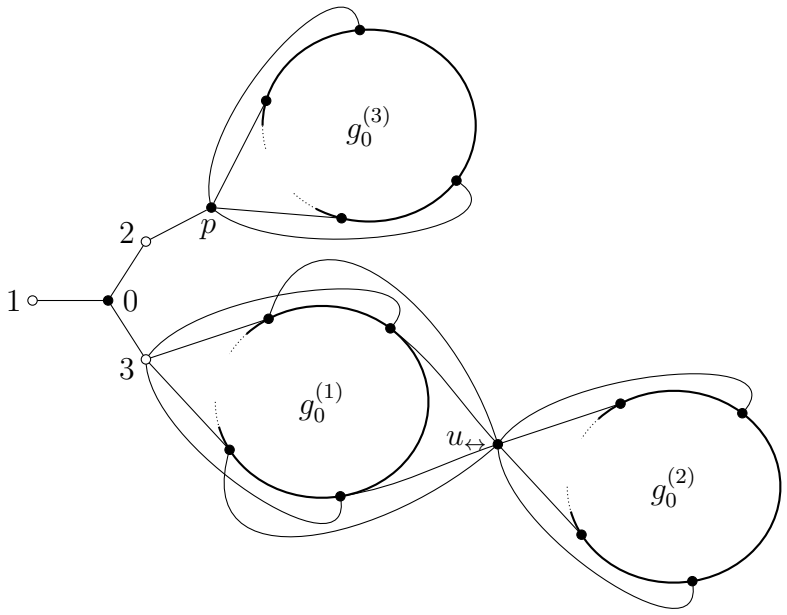

Figure 4.5: A momentum switch $\hat{G}^{\prec}$ built from a type 2 R/T gadget and its reversal.

Since the S-matrix is symmetric and unitary, this gives the complete form of the S-matrix for all momenta in $\mathcal{R} \cup \mathcal{T}$. In particular, this shows that $\hat{G}^{\prec}$ is a momentum switch between $\mathcal{R}$ and $\mathcal{T}$.

We first construct the scattering states for momenta $k \in \mathcal{T}$. Lemma 8 shows that the graph g_0 has a $2\cos(k)$-eigenvector $|\,\xi_k\,\rangle$ satisfying equation (4.6) with some nonzero constant c. We define a state $|\,\mu_k\,\rangle$ on $G^{\prec}$ and we show that it is a scattering eigenstate with perfect transmission between paths 1 and 2. The amplitudes of $|\,\mu_k\,\rangle$ on the semi-infinite paths and the claw are

$$\langle (x,1)|\mu_k\rangle = e^{-ikx} \qquad \langle 0|\mu_k\rangle = 1 \qquad \langle (x,2)|\mu_k\rangle = e^{ikx} \qquad \langle (x,3)|\mu_k\rangle = 0. \tag{4.20}$$

The rest of the graph consists of the three copies of the subgraph g_0 and the vertices p and $u_{\leftrightarrow}$. The corresponding amplitudes are

$$\langle\, v\,|\,\mu_k\,\rangle = \begin{cases} -\frac{1}{c}\langle\, v\,|\,\xi_k\,\rangle & v \in V(g_0^{(1)}) \\ \frac{1}{c}\langle\, v\,|\,\xi_k\,\rangle & v \in V(g_0^{(2)}) \\ -\frac{e^{ik}}{c}\langle\, v\,|\,\xi_k\,\rangle & v \in V(g_0^{(3)}) \\ 0 & v = p \text{ or } v = u_{\leftrightarrow}. \end{cases} \tag{4.21}$$

We claim that $|\,\mu_k\,\rangle$ is an eigenstate of the Hamiltonian with eigenvalue $2\cos(k)$. As in previous proofs, the state clearly satisfies the eigenvalue condition on the semi-infinite paths and at the vertices of G_0 and $G_0^{\leftrightarrow}$, and the factors of $\frac{1}{c}$ in the above equation are chosen so that the state also satisfies the eigenvalue condition at vertices p and $u_{\leftrightarrow}$. Since $|\,\mu_k\,\rangle$ is a scattering state with perfect transmission from path 1 to path 2, we see that $S_{2,1}(k) = 1$.

We now construct an eigenstate $|\,\nu_{k'}\,\rangle$ with perfect transmission from path 1 to path 3 for each momentum $k' \in \mathcal{R}$. This state has the form

$$\langle (x,1)|\nu_{k'}\rangle = e^{-ik'x} \qquad \langle 0|\nu_{k'}\rangle = 1 \qquad \langle (x,2)|\nu_{k'}\rangle = 0 \qquad \langle (x,3)|\nu_{k'}\rangle = e^{ik'x} \tag{4.22}$$

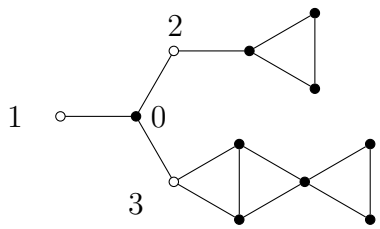

Figure 4.6: A momentum switch between $-\frac{\pi}{3}$ and $-\frac{2\pi}{3}$.

on the semi-infinite paths and the claw. Lemma 7 shows that G_0 has a $2\cos(k')$-eigenstate $|\chi_{k'}\rangle$ with $\langle p|\chi_{k'}\rangle \neq 0$, which determines the form of $|\nu_{k'}\rangle$ on the remaining vertices:

$$\langle v|\nu_{k'}\rangle = \begin{cases} -\frac{1}{\langle p|\chi_{k'}\rangle}\langle v|\chi_{k'}\rangle & v \in V(G_0) \\ -\frac{e^{ik'}}{\langle p|\chi_{k'}\rangle}\langle v|\chi_{k'}\rangle & v \in V(g_0^{(2)}) \\ -e^{ik'} & v = u^{\leftrightarrow} \\ 0 & \text{otherwise.} \end{cases} \tag{4.23}$$

As before, it is easy to check that this a momentum-k' scattering state with perfect transmission from path 1 to path 3, so $S_{3,1}(k') = 1$.

Thus the gadget from Figure 4.5 is a momentum switch between $\mathcal{R}$ and $\mathcal{T}$. □

4.1.2.1 Explicit example

Using this construction for momentum switches, we can obtain a momentum switch from any of the examples discussed in Section 4.1.1.1. Explicitly, using the R/T gadget built from the 3-cycle, we get a momentum switch between $-\frac{\pi}{3}$ and $-\frac{2\pi}{3}$, as shown in Figure 4.6. More generally, using an r-cycle, we obtain a switch between momenta of the form $-\frac{\pi j}{r}$ with odd or even values of j. As another example, using a path of length 4 connected at the center vertex, we obtain a switch between $-\frac{\pi}{4}$ and $-\frac{\pi}{2}$.

4.1.3 Encoded unitaries

While there is no known efficient method to find graphs that fixed scattering behavior, it is possible to search over all small graphs in order to find gadgets with some particular scattering behavior. This was the manner in which the gadgets for most known scattering results were found, such as in Childs' original universality proof for graph scattering [11] and Childs, Gosset, and Webb's universality result [16]. Additionally, Blumer, Underwood, and Feder have a paper [9] in which they searched over all graphs with up to 9 vertices for scattering behavior at particular momentum.

Essentially, the main idea behind this method is a brute force search. Since we can easily compute the scattering matrix for a particular graph at a particular momentum, if we want to find a graph that has some prescribed scattering behavior, we simply assume that such a graph exists and search for it over all graphs, starting with those having a small number of vertices. While this exhaustive search is not guaranteed to find such a graph, a surprising number of systems can be found with this structure. In particular, if we restrict ourselves to momenta that are simple multiples of π, such as $-\frac{\pi}{2}$ or $-\frac{\pi}{4}$, then most simple scattering behaviors can be found.

Of particular interest to us will be gadgets with four terminal vertices, such that the scattering

matrix at some particular momenta takes the form

$$S(k) = \begin{pmatrix} 0 & U^T \\ U & 0 \end{pmatrix}. \tag{4.24}$$

Namely, if we use a dual-rail encoding for a qubit, and think of one pair of semi-infinite paths as the input rails and the other pair as the output rails, then after scattering this gadget will have applied the unitary U to the encoded qubit.

While the general problem is difficult, we might be able to guide our search for specific unitaries. As a particular example, any one-qubit unitary with a zero-entry will allow us to work with disconnected graphs, and focus on finding a two-terminal gadgets with perfect transmission coefficients. If we find two such gadgets such that the ratio between their transmission coefficients are the same as the ratio of the entries in the unitary, we can thus implement the unitary.

[**TO DO:** *maybe make a picture of this?*]

In the most trivial non-trivial example, we can use this idea to implement an X gate at all momentum by using two length-two paths, where the input terminal for logical z connects to the output terminal of logical $1 + z$. For a slightly less trivial example, note that for any momentum k we can always implement an encoded $\mathrm{diag}\{1, e^{ik}\}$ by using as our graph gadget $\widehat{G}$ a path of length 3. Both unitaries are essentially just a relabeling of the vertices, but they are still useful computationally.

[**TO DO:** *make e^{ik} gadget*]

Later in this thesis we will describe a scheme for arbitrary quantum computation using scattering theory as the basic computational tool. While the scheme makes no reference to a particular momenta, it does require that there are a set of graph gadgets at the correct momenta implementing a universal gate set. As such, we will want to show that the set of momenta satisfying this assumption is non-empty.

4.1.3.1 Universal gate set for $-\frac{\pi}{2}$

Since the energy corresponding to momentum $-\frac{\pi}{2}$ is zero, the eigenvalue equations for this gadget are slightly easier than average to manipulate. Additionally, this was the momentum used in [**?**] in their algorithm for the AND-OR tree.

Note that the the graph in Figure 4.7a and Figure 4.7b both implement a Hadamard gate for a qubit encoded at momentum $-\frac{\pi}{2}$, but that the graph in Figure 4.7b is planar. In particular, Figure 4.7a has a scattering matrix of the form (4.24), with

$$U = -\frac{e^{i\frac{\pi}{4}}}{\sqrt{2}} \begin{pmatrix} 1 & 1 \\ 1 & -1 \end{pmatrix}, \tag{4.25}$$

while Figure 4.7b implements

If we then combine this unitary with the $\mathrm{diag}\{e^{-i\pi/2}\}$ gate that works for all unitaries, we then have that we can implement all single-qubit Clifford gates. Thus in order to have a universal set of single-qubit gates we simply need to find a single unitary not contained within the Clifford group.

As such an example, we can use the diagonal graph depicted in Figure 4.8. This is related to the V-basis often used for fault-tolerant computations, where the implemented unitary is

$$U = \begin{pmatrix} 1 & 0 \\ 0 & \frac{4-3i}{5} \end{pmatrix}. \tag{4.26}$$

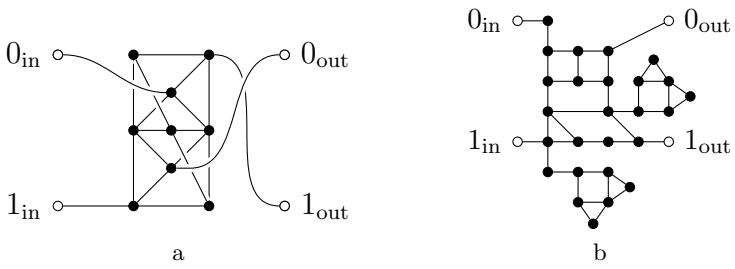

Figure 4.7: Two gates that implement an encoded Hadamard at $-\frac{\pi}{4}$. (a) A simple gate. (b) More complicated but planar gate.

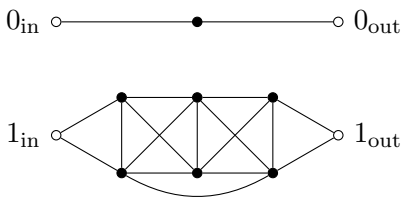

Figure 4.8: Graph implementing a non-Clifford gate at $k = -\frac{\pi}{2}$.

4.1.3.2 Universal gate set for $-\frac{\pi}{4}$

Historically [11, 16], momentum $-\frac{\pi}{4}$ has been used to show universality results. I'm unsure why, except that the graph gadgets that implement a universal gate set are rather simple at this momenta.

In particular, Childs found that the two gadgets in Figure 4.9 implement a universal gate set. His original proof required some additional attributes on the graph gadgets, which is the reason for the slightly more complicated T-gate, but this is sufficient for our purposes.

In particular, we have that the graph in Figure 4.9a has a scattering matrix of the form of equation (4.24) at momentum $k = -\frac{\pi}{4}$, with

$$U = \begin{pmatrix} e^{-i\frac{\pi}{4}} & 0 \\ 0 & 1 \end{pmatrix}, \tag{4.27}$$

while the gadget in Figure 4.9b also has a scattering matrix of the form (4.24) at momentum $k = -\frac{\pi}{4}$, where

$$U = -\frac{i}{\sqrt{2}} \begin{pmatrix} 1 & -i \\ -i & 1 \end{pmatrix}. \tag{4.28}$$

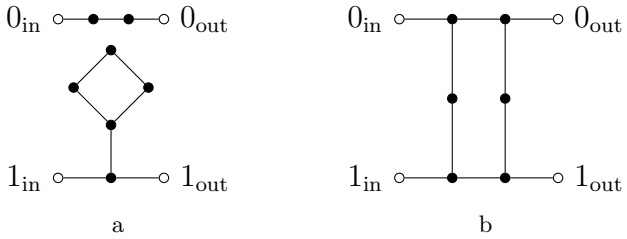

Figure 4.9: Encoded one-qubit gates at $k = -\frac{\pi}{4}$. (a) A phase gate. (b) Basis-changing gate.

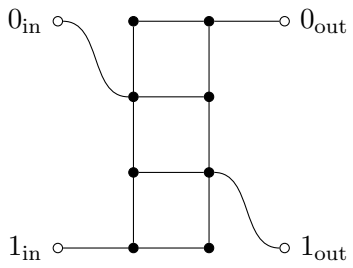

Figure 4.10: A non-clifford gate used for universal computation at $-\frac{\pi}{3}$ and $-\frac{2\pi}{3}$.

With these examples, we then have a universal gate set for single-qubit unitaries at $-\frac{\pi}{4}$, which will be sufficient for our eventual purposes.

4.1.3.3 Universal gate set at $-\frac{\pi}{3}$ and $-\frac{2\pi}{3}$

While the previous two momenta are relevant for historical reasons, we would also like to show a universal gate set at other momentum. By looking forward in the thesis, where we will be interested in two momenta moving along adjacent paths, it will be useful to have the two wave-functions move at the same speed, and thus will be interesting to study k and $-\pi - k$ for some $k \in (-\pi, 0)$. A natural choice would be then to understand $-\frac{\pi}{3}$ and $-\frac{2\pi}{3}$, since they are nicely separated, and further we have an explicit momentum switch between the two momenta.

Unfortunately, most gadgets in the Blumer, et. al., database for these two momenta are related to $e^{-i\pi/3}$, whereas most Clifford gates are related to $e^{i\pi/4}$, and thus we unfortunately don't know of a set of gadgets implementing a Clifford+T-gate set. However, there are sufficient graphs in order to have a universal set, but it is one note widely used.

In particular, note that the simple shifted diagonal gadget described in the beginning of this section allows us to implement a $\text{diag}\{1, e^{2i\pi/3}\}$ gate for both momenta of interest. In addition to this single gadget, the graph in Figure 4.10 implements another gate, corresponding to a rotation along a different axis on the Bloch sphere.

The graph in Figure 4.10 has an S-matrix with perfect transmission at both momenta of interest, with the corresponding unitary given by

$$U(-\frac{\pi}{3}) = \frac{e^{5i\pi/6}}{2}\begin{pmatrix}\sqrt{3} & e^{i\pi/6}\\ e^{-i\pi/6} & \sqrt{3}\end{pmatrix} \qquad U(-\frac{2\pi}{3}) = \frac{e^{-5i\pi/6}}{2}\begin{pmatrix}\sqrt{3} & e^{-i\pi/6}\\ e^{i\pi/6} & \sqrt{3}\end{pmatrix} \tag{4.29}$$

4.1.4 Other momenta

While the previous sections have given us nice

4.2 Various facts about scattering

While the previous constructions yield graphs with particular behavior which will be useful when attempting to construct scattering algorithms, we will also want to understand some simple relations between graphs and their respective scattering matrices. In particular, understanding what properties are necessary in order to have a given scattering matrix, and understanding the relation between various the scattering matrices of various momenta will be useful in constructing additional scattering graphs.

4.2.1 Degree-3 graphs are sufficient

One of the most simple assumptions that could be made is that certain scattering behaviors require high degree graphs. In particular, having many connections might allow for additional correlations between outputs on larger graphs.

If we restrict our attention to a finite number of rational momenta, however, this does not turn out to be the case. We can show that any graph can be replaced by a degree-three graph with a identical scattering behavior at some fixed momenta. In particular, we will show that a single vertex can be replaced by a finite path while still satisfying the eigenvalue equation at the fixed momenta, where the length of the path is dependent on the fixed momenta.

As degree two graphs are the graph joins of cycles and paths, degree three graphs are the smallest graphs to have nontrivial scattering behaviors. This lemma shows that, in a certain sense, they are also all that are required.

Lemma 11. *Let $\widehat{G}$ be a finite graph, and let M be a finite set of rational multiples of π. If $v \in V(G)$ is a degree d vertex, there exists a graph H that extends G with the vertex v being replaced by a degree-$(\lceil \frac{d}{2} \rceil + 1)$ subgraph such that the scattering matrices at the momenta $k \in M$ are preserved.*

Proof. The main idea behind this proof is to partition the vertices adjacent to v into two sets, and then replace v by a finite path, with the two sets connected to opposites ends of the finite path. By choosing the length of the path correctly, we can show that the amplitudes at either end of the path are the same as the amplitude on v at each momenta in M, and thus the eigenvalue equation remains satisfied without changing the scattering behavior.

In particular, let v be the degree d vertex in G, and let $S = \{w \in V(G) : w \sim v\}$ be the set of vertices adjacent to v. Additionally, let us arbitrarily partition S into two sets, S_1 and S_2, such that $\big||S_1| - |S_2|\big| \leq 1$.

As each $k \in M$ is a rational multiple of π, there exists some $m \in \mathbb{N}^+$ such that $\frac{mk}{2\pi} \in \mathbb{N}$ for all $k \in M$. Let us then examine the graph H where v is replaced by a path of length m, and where S_1 is attached to one end of the path while S_2 is attached to the other end. Explicitly:

$$V(H) = \big(V(G) \setminus \{v\}\big) \cup \{(v, j) : j \in [m+1]\} \tag{4.30}$$

$$E(H) = \big\{e \in E(G) : v \notin e\big\} \cup \big\{\{(v, j), (v, j+1)\} : j \in [m]\big\} \cup \big\{\{s, (v, 0)\} : s \in S_1\big\} \cup \big\{\{s, (v, m)\} : s \in S_2\big\}. \tag{4.31}$$

Now, for any $k \in M$, let $|\phi\rangle$ be an eigenstate of $A(G)$ with eigenvalue $2\cos(k)$. We will show that there exists an eigenstate $|\psi\rangle$ of $A(H)$ with energy $2\cos(k)$ such that for any $w \in V(G) \setminus \{v\}$, $\langle w|\phi\rangle = \langle w|\psi\rangle$.

Concretely, for any vertex other than v, let us define $|\psi\rangle$ in this manner, and note that by assumption, $|\psi\rangle$ satisfies the eigenvalue equation with energy $2\cos(k)$ for all vertices other than those in S or those replacing v. Additionally, let

$$\alpha = \sum_{w \in S_1} \langle w|\phi\rangle, \qquad \beta = \langle v|\phi\rangle, \qquad \text{and} \qquad \gamma = \sum_{w \in S_2} \langle w|\phi\rangle. \tag{4.32}$$

We will then defined the amplitude along the path replacing the vertex v as

$$\langle (v, j)|\psi\rangle = \beta\cos(kj) + \frac{\gamma - \beta\cos(k)}{\sin(k)}\sin(kj). \tag{4.33}$$

Note that $\langle (v, 0)|\psi\rangle = \langle (v, m)|\psi\rangle = \beta = \langle v|\phi\rangle$, and thus the eigenvalue equation is satisfied at all vertices in S. As the eigenstates along a path with energy $2\cos(k)$ are scalar multiples of $\sin(kx)$

and $\cos(kj)$, we can also see that the eigenvalue equation is necessarily satisfied for all (v, j) with $j \neq 0$ and $j \neq m$.

If we then examine the eigenvalue equation at $(v, 0)$, we can see that

$$\sum_{s \in S_1} \langle s \,|\, \psi \rangle + \langle (v,1) \,|\, \psi \rangle = \alpha + \beta \cos(k) + \frac{\gamma - \beta \cos(k)}{\sin(k)} \sin(k) \tag{4.34}$$

$$= \alpha + \gamma \tag{4.35}$$

$$= 2\cos(k)\beta = 2\cos(k) \langle (v,0) \,|\, \psi \rangle \tag{4.36}$$

where the third equality follows from the fact that $|\phi\rangle$ satisfies the eigenvalue equation at v with eigenvalue $2\cos(k)$, and thus we have that the eigenvalue equation for H is satisfied at $(v, 0)$.

Let us finally examine the eigenvalue equation at (v, m), noting that

$$\sum_{s \in S_2} \langle s \,|\, \psi \rangle + \langle (v,m-1) \,|\, \psi \rangle = \gamma + \beta \cos(k(m-1)) + \frac{\gamma - \beta \cos(k)}{\sin(k)} \sin(k(m-1)) \tag{4.37}$$

$$= \gamma + \beta \cos(k) - \big(\gamma - \beta \cos(k)\big) \tag{4.38}$$

$$= 2\cos(k)\beta = 2\cos(k) \langle (v,0) \,|\, \psi \rangle \tag{4.39}$$

where the second equality follows from some trigonometric identities. We can then see that $|\psi\rangle$ satisfies the eigenvalue equation at (v, m) with energy $2\cos(k)$.

Putting this together, we have that $|\psi\rangle$ is an eigenvector of $A(H)$ with energy $2\cos(k)$ such that $|\psi\rangle$ and $|\phi\rangle$ are identical on those vertices contained in both G and H. As this result holds for any energy $2\cos(k)$ eigenvector of $A(G)$, and as the two graphs are identical along the semi-inifinite paths, we have that the scattering states for these two graphs are identical, and thus the scattering matrices are preserved under this degree reduction procedure. □

By repeated use of this lemma, we can then reduce any graph used as a scattering gadget down to a degree-3 graph without changing the scattering matrix at some fixed momentum.

4.2.2 Some behavior impossible

So far, all of our constructions have generally assumed that the scattering behavior that we want does exist. Hence, if we simply search over large enough graphs, we will eventually find a graph that implements our desired scattering behavior.

However, it turns out that in some cases this is not a valid assumption. In particular, there exist pairs of momenta for which no R/T gadget can be constructed. The main idea is that for specific momentum, there exists a basis for the scattering states in which all amplitudes are taken from a field extension of the rationals. If two momenta are related by a Galois conjugation over this field, then perfect reflection at one momenta implies perfect reflection at the second.

As an illuminating example, we will use those states with momenta $k = -\frac{\pi}{4}$ and $p = -\frac{3\pi}{4}$. For the two momenta, the corresponding energy is $2\sqrt{2}$ or $-2\sqrt{2}$, and in this case the Galois conjugation is simply replacing $\sqrt{2}$ by $-\sqrt{2}$.

4.2.2.1 Basis vectors with entries in $\mathbb{Q}(\sin(k), \cos(k))$

Recall the general setup shown in Figure 3.2: N semi-infinite paths are attached to a finite graph $\widehat{G}$, resulting in an infinite graph G. Additionally, we have that the adjacency matrix for $\widehat{G}$ can be

written in block diagonal form

$$A(\widehat{G}) = \begin{pmatrix} A & B^\dagger \\ B & D \end{pmatrix}, \tag{4.40}$$

where A is an $N \times N$ matrix, B is an $m \times N$ matrix, and D is an $m \times m$ matrix. We have that the N semi-infinite paths are attached, in order, to the first N vertices of $\widehat{G}$.

Let us now consider an eigenvector $|\tau_k\rangle$ of the adjacency matrix of G with eigenvalue $2\cos(k)$ for $k \in (-\pi, 0)$. We have from Theorem 2 that this eigenspace is spanned by incoming scattering states with momentum k and confined bound states (which have zero amplitude on the semi-infinite paths) . We can thus write the amplitudes of $|\tau_k\rangle$ on the semi-infinite paths as

$$\langle (x,j) | \tau_k \rangle = \kappa_j \cos(k(x-1)) + \sigma_j \sin(k(x-1)) \tag{4.41}$$

for $x \in \mathbb{Z}^+$, $j \in [N]$, and $\kappa_j, \sigma_j \in \mathbb{C}$, and the amplitudes on the internal vertices as

$$\langle w | \tau_k \rangle = \iota_w \tag{4.42}$$

for $\iota_w \in \mathbb{C}$, where w indexes the internal vertices. Since the state $|\tau_k\rangle$ satisfies the eigenvalue equation on the semi-infinite paths, it remains to satisfy the conditions specified by the block matrix equation

$$\begin{pmatrix} A & B^\dagger \\ B & D \end{pmatrix} \begin{pmatrix} \kappa \\ \iota \end{pmatrix} + \cos(k) \begin{pmatrix} \kappa \\ 0 \end{pmatrix} + \sin(k) \begin{pmatrix} \sigma \\ 0 \end{pmatrix} = 2\cos(k) \begin{pmatrix} \kappa \\ \iota \end{pmatrix}.$$

Hence, the nullspace of the matrix

$$M = \begin{pmatrix} A - \cos(k)\mathbb{I} & \sin(k)\mathbb{I} & B^\dagger \\ 0 & 0 & 0 \\ B & 0 & D - 2\cos(k)\mathbb{I} \end{pmatrix} \tag{4.43}$$

is in one-to-one correspondence with the $2\cos(k)$-eigenspace of the infinite matrix (here the first block corresponds to κ, the second to σ, and the third to ι). Further, M only has entries in $\mathbb{Q}(\cos(k), \sin(k))$, so its nullspace has a basis with amplitudes in $\mathbb{Q}(\cos(k), \sin(k))$, as can be seen using Gaussian elimination.

We can then use this, along with the form of the eigenstates along the semi-infinite paths, to see that all of the amplitudes can be written as elements over the rationals extended by $\sin(nk)$ and $\cos(nk)$ for all $n \in \mathbb{N}^+$. While this is not particularly useful in general, if k is a rational multiple of π, this is a finite extension. Further, there exist special cases in which this field extension is a quadratic extension, such that all of the amplitudes can be taken from $\mathbb{Q}[\sqrt{d}]$ for some d.

As a slight caveat noted above, the spectrum of G may include confined bound states (Theorem 2) with eigenvalues at $2\cos(k)$. However, any such state is also in the nullspace of the matrix M, while also satisfying the rational constraints that both κ and σ are zero. As such, these states can always be written with amplitudes over the field $\mathbb{Q}[\sin(k), \cos(k)]$. Thus forcing the scattering eigenstates to be orthogonal to these confined bound states only involves constraints over the same field, and we still have that the scattering eigenstates can be written with all of their amplitudes over the field $\mathbb{Q}$ extended by $\sin(nk)$ and $\cos(nk)$.

As an explicit example, let us examine the case where $2\cos(k) = \pm\sqrt{2}$ corresponding to $k = -\frac{\pi}{4}$ or $k = -\frac{3\pi}{4}$. In these cases $\mathbb{Q}(\cos(k), \sin(k)) = \mathbb{Q}(\sqrt{2})$, and we may choose a basis for the nullspace of M with amplitudes from $\mathbb{Q}(\sqrt{2})$. Furthermore, $\cos(kx), \sin(kx) \in \mathbb{Q}(\sqrt{2})$ for all $x \in \mathbb{Z}^+$, so with such a choice of basis, each amplitude of $|\tau_k\rangle$ is also an element of $\mathbb{Q}(\sqrt{2})$.

We can then use the fact that $\mathbb{Q}[\sqrt{2}]$ can be thought of as a two-dimensional vectorspace over $\mathbb{Q}$ to see that any member of this extended rational basis can be written as

$$|\tau_k\rangle = |u_k\rangle + \sqrt{2}|w_k\rangle, \tag{4.44}$$

for rational vectors $|u_k\rangle$ and $|w_k\rangle$. Further, as $H^2|\tau_k\rangle = 2|\tau_k\rangle$, we can see that $H|u_k\rangle = \pm 2|w_k\rangle$ and $H|w_k\rangle = \pm|u_k\rangle$, so

$$|\tau_k\rangle = (H \pm \sqrt{2}\mathbb{I})|w_k\rangle, \tag{4.45}$$

where the $\pm$ depends on whether we are working with $k = -\frac{\pi}{4}$ or $-\frac{3\pi}{4}$.

While this expression does not easily generalize to most pairs of momenta, we do have a similar equation whenever the extended field is a quadratic extension, where 2 replaced with d.

4.2.2.2 Impossibility of R/T gadgets

With the above rational basis for scattering states, we will be able to transform an eigenstate at one energy into an eigenstate at another energy via a Galois conjugation. However, the existence of particular eigenstates will not immediately give us the results that we want.

Along these lines, we will use the following basic fact about two-terminal gadgets several times:

Fact 1. *If a two-terminal gadget has a momentum-k scattering state $|\phi\rangle$ with zero amplitude along path 2, then the gadget perfectly reflects at momentum k.*

Proof. Without loss of generality, we may assume that $|\phi\rangle$ is orthogonal to all confined bound states. If $|\phi\rangle$ has zero amplitude along path 2, then there exist some $\mu, \nu \in \mathbb{C}$ such that

$$\langle(x,2)|\phi\rangle = \mu\langle(x,2)|\mathrm{sc}_2(k)\rangle + \nu\langle(x,2)|\mathrm{sc}_1(k)\rangle = \mu e^{-ikx} + \mu R e^{ikx} + \nu T e^{ikx} = 0 \tag{4.46}$$

for all $x \in \mathbb{Z}^+$. Since this holds for all x, we have $\mu = \mu R + \nu T = 0$. Since μ and ν cannot both be zero, we have $T = 0$. □

For an R/T gadget, the scattering states (at some fixed momentum) that are orthogonal to the confined bound states span a two-dimensional space. As shown in Section 4.2.2.1, we can expand each scattering eigenstate over an extension to the field $\mathbb{Q}$. Let us restrict our attention to the case where this extension is quadratic, with discriminant d.

In particular, let us assume that the scattering state at k has energy $\sqrt{d}$ (with d nonsquare) and can be written in a basis with entries over $\mathbb{Q}(\sqrt{d})$, where each basis vector takes the form (4.45). This gives

$$|\mathrm{sc}_1(k)\rangle = (H + \sqrt{d}\mathbb{I})(\alpha|a\rangle + \beta|b\rangle)$$

where $\alpha, \beta \in \mathbb{C}$, $\alpha \neq 0$, and $|a\rangle$ and $|b\rangle$ are rational d-eigenvectors of H^2.

If $T(k) = 0$, then for all $x \geq 0$,

$$\langle x,2|\mathrm{sc}_1(k)\rangle = 0 = \langle x,2|(H + \sqrt{d}\mathbb{I})(\alpha|a\rangle + \beta|b\rangle). \tag{4.47}$$

Dividing through by α and rearranging, we get that for all $x \geq 0$,

$$\frac{\beta}{\alpha}(\langle x,2|H|b\rangle + \sqrt{d}\langle x,2|b\rangle) = -\langle x,2|H|a\rangle - \sqrt{d}\langle x,2|a\rangle.$$

If the left-hand side is not zero, then $\beta/\alpha \in \mathbb{Q}(\sqrt{d})$ since H, $|a\rangle$, and $|b\rangle$ are rational. If the left-hand side is zero, then $(H + \sqrt{d}\mathbb{I})|a\rangle$ is an eigenstate at energy $2\cos(k)$ with no amplitude along path 2, so $\beta = 0$ (using Fact 1), and again $\beta/\alpha \in \mathbb{Q}(\sqrt{d})$.

Now write $\beta/\alpha = r + s\sqrt{d}$ with $r, s \in \mathbb{Q}$, and consider the rational d-eigenvector of H^2

$$|c\rangle := |a\rangle + (r + sH)|b\rangle. \tag{4.48}$$

Note that

$$\alpha(H + \sqrt{d}\mathbb{I})|c\rangle = \alpha(H + \sqrt{d}\mathbb{I})|a\rangle + \alpha(rH + r\sqrt{d} + sH^2 + sH\sqrt{d})|b\rangle. \tag{4.49}$$

Since $|b\rangle$ is a d-eigenvector of H^2 and $\beta/\alpha = r + s\sqrt{d}$, this simplifies to

$$\alpha(H + \sqrt{d}\mathbb{I})|c\rangle = \alpha(H + \sqrt{d}\mathbb{I})|a\rangle + \beta(H + \sqrt{d}\mathbb{I})|b\rangle = |\mathrm{sc}_1(k)\rangle, \tag{4.50}$$

so $|\mathrm{sc}_1(k)\rangle$ can be written as $\alpha(H + \sqrt{d}\mathbb{I})$ times a rational d-eigenvector of H^2.

Since $\langle x, 2|\mathrm{sc}_1(k)\rangle = 0$ for all $x \geq 1$ (and $\alpha \neq 0$), we have

$$\langle x, 2|(H + \sqrt{d}\mathbb{I})|c\rangle = \langle x, 2|H|c\rangle + \sqrt{d}\langle x, 2|c\rangle = 0. \tag{4.51}$$

As H is a rational matrix and $|c\rangle$ is a rational vector, the rational and irrational components must both be zero, implying $\langle x, 2|c\rangle = \langle x, 2|H|c\rangle = 0$ for all $x \geq 1$. Furthermore, since $|\mathrm{sc}_1(k)\rangle$ is a scattering state with zero amplitude on path 2, it must have some nonzero amplitude on path 1 and thus there is some $x_0 \in \mathbb{Z}^+$ for which $\langle x_0, 1|c\rangle \neq 0$ or $\langle x_0, 1|H|c\rangle \neq 0$.

Now consider the state obtained by replacing $\sqrt{d}$ with $-\sqrt{d}$, or in other words after performing a Galois conjugation:

$$|\overline{\mathrm{sc}}_1(k)\rangle := \alpha(H - \sqrt{d}\mathbb{I})|c\rangle. \tag{4.52}$$

This is a $-\sqrt{d}$-eigenvector of H, which can be confirmed using the fact that $|c\rangle$ is a d-eigenvector of H^2. As $\langle x, 2|H|c\rangle = \langle x, 2|c\rangle = 0$ for all $x \geq 1$, $\langle x, 2|\overline{\mathrm{sc}}_1(k)\rangle = 0$ for all $x \geq 1$. Furthermore the amplitude at vertex $(x_0, 1)$ is nonzero, i.e., $\langle x_0, 1|\overline{\mathrm{sc}}_1(k)\rangle \neq 0$, and hence $|\overline{\mathrm{sc}}_1(k)\rangle$ has a component orthogonal to the space of confined bound states (which have zero amplitude on both semi-infinite paths). Hence, there exists a scattering state with eigenvalue $-\sqrt{d}$ with no amplitude on path 2. By Fact 1, the gadget perfectly reflects at momentum p, where $p = -\pi - k$ corresponds to this energy. It follows that no perfect R/T gadget (and hence no perfect momentum switch) exists between these momenta.

As particular cases, we can take $k = -\frac{\pi}{4}$, where $d = 2$. In this case, we have that there does not exist an R/T gadget splitting k and $-\frac{3\pi}{4}$. Similarly, it is possible to show that $k = -\frac{\pi}{6}$ can be written in a basis with entries over $\mathbb{Q}[\sqrt{3}]$, and thus there does not exist a R/T gadget between k and $-\frac{5\pi}{6}$.

4.2.2.3 Approximate R/T gadget

[**TO DO:** *I never particularly liked this bit, and I'll think I'll include it later if I have the time*]

4.2.3 Laplacians vs adjacency matrix

[**TO DO:** *If I have time, write this section. The basic idea is similar to proof removing self-loops from the graph for the BH model. In particular, in order to turn a degree 3 graph into a 3-regular graph, we use three copies of the original graph. For each degree-2 vertex u in the original graph, we add another vertex u_0 to the overall graph, and add edges from all three u_i for $i \in [3]$ to u_0. For each degree-1 vertex, we do this twice. Note that for each eigenstate of the original graph, there are two with nearly the same amplitudes. We can then use these for our scattering eigenstates*]

4.3 Conclusions and extensions

Chapter 5

Universality of Quantum Walk

Quantum walk is an intuitive framework for developing quantum algorithms, inspired by the classical model of random walk. This framework has lead to examples of exponential speedups over classical computation [13], as well as optimal algorithms for element distinctness [2] and formula evaluation [21]. We have also seen examples of this in Chapter 3 and Chapter 4, as graph scattering can be seen as a restricted form of quantum walk.

With all of these algorithmic uses (and thinking of the title to this thesis), we would then wonder at the computational power of quantum walk. We already know that this model is contained in **BQP**from Chapter 3, and thus can only be as powerful as a quantum computer, but we would also like to give a lower bound on its power. Using the ideas of graph scattering, Childs [11] was able to show that the model of continuous-time quantum walk is universal for quantum computation. (Childs later showed that the discrete-time model was also universal by giving a method to simulate a continuous-time quantum walk via a discrete-time quantum walk in [12], but this universality was shown directly by Lovett, et.al. soon after in [27].) In this chapter, we will again show the universality of quantum walk, using the tools of Chapter 3 and Chapter 4.

In particular, we have from Chapter 4 several scattering gadgets whose scattering behavior can be viewed as an encoded single qubit gate. Using our results on the scattering behavior of finite-length wave-packets from Theorem 4 and our finite truncation of Hamiltonians from Lemma 1, we will show how to implement single-qubit gates using finite graphs. We will then show how to combine these single-qubit gates to have multiple scattering events to encode an entire computation.

This chapter can be thought of as a primer for Chapter 7, as many of the proof techniques and ideas from this chapter will be used for the multi-particle case as well. However, there will be some additional difficulties in Chapter 7, so having an intuitive understanding of the proof idea will be helpful. Additionally, this is a novel use of our results on graphs scattering, which might lead to some more uses for the techniques. Note that the encoding and global scheme for this chapter is similar to that of Childs original universality result [11], using the proof techniques of Childs, Gosset, and Webb's universality result for multiple particles [16]. However, this particular proof is new to this thesis.

The eventual goal of this chapter is to simulate a given circuit $\mathcal{C}_X = U_M U_{M-1} \cdots U_1$ acting on some initial state $|x\rangle$, where each gate U_i comes from some universal gate set and the simulation accepts the state with high probability if and only if the circuit accepts with high probability. We will first show how to do this for single-qubit computations in Section 5.1. We will then extend this technique to multi-qubit computations in Section 5.2.

[**TO DO:** *Make many figures (after writeup of other chapters)*] [**TO DO:** *Explict encodings for different momenta*]

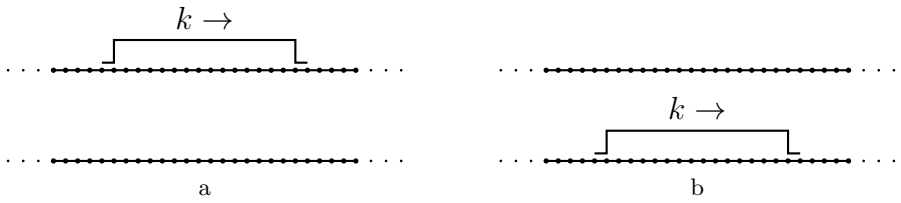

Figure 5.1: A qubit is encoded using single-particle wave packets at momentum k. (a) An encoded $|0\rangle$. (b) An encoded $|1\rangle$.

5.1 Single qubit simulation

With our eventual goal of simulating an entire circuit via graph scattering, we will first need to understand how to perform single-qubit computations. We will use many of the results of Chapter 3 and gadgets from Chapter 4, and show that specific scattering behavior can be used as a computational tool. This section will first encode the qubit, then show how to have a simulate a single gate, and finally show how to simulate multiple single-qubit gates. These results will then be generalized for multiple-qubits in Section **??**. This section will be used nearly in Chapter 7.

5.1.1 Single qubit encoding

In our endeavour to simulate a circuit, we will first need to encode the logical state of the circuit into a state on some simple graph. Taking motivation from the literature, we will encode our logical system in a dual-rail encoding on two long paths. In particular, a single qubit will correspond to two infinite paths, with a single wave-packet at some specified momentum k traveling along one of the two paths. If the particle is located on the first (top) path, then the encoded qubit is in the logical state $|0\rangle$, while if the particle is on the second (bottom) path then the encoded qubit is in the logical state $|1\rangle$. Schematically, this can be seen in Figure 5.1.

[**TO DO:** *change figure to Gaussian as opposed to square?*]

If we could use an infinite Hilbert space to encode our qubits, we could then actually use the eigenstates of the two paths to correspond to the two logical states. However, since we will eventually want to measure the encoded states, we will want to assume that the encodings have a well-defined position in space to ensure that we need only measure a (relatively) small number of vertices in order to determine the encoded logical state with high probability. To ensure this localization in space (and to use some of our error bounds on the time evolution), we will assume that the logical states are encoded using a truncated Gaussian wave-packet, with four attributes that specify the state: the momentum k, the standard deviation σ, the center of mass μ, and the cutoff range L (which will be closely related to σ). With these four values, and assuming that the vertices of the two infinite paths are labeled as (x, z) for $x \in \mathbb{Z}$ and $z \in \mathbb{F}_2$, we will have that the logical qubit for our system will be encoded into the states

$$|z\rangle_{\log} = \gamma \sum_{x=\mu-L}^{\mu+L} e^{ikx} e^{-\frac{(x-\mu)^2}{2\sigma^2}} |x, z\rangle. \tag{5.1}$$

It is important to realize that none of these four values depend on the value of the encoded qubit; this will allow us to interfere the wave-packets arising from different paths to the same computational basis, as there will be no extraneous information about the logical state.

This encoding is specifically chosen so that we can use Theorem 4, and guarantee various attributes about the time evolution of such systems.

5.1.2 One single-qubit unitary

With an actual encoding of a logical qubit, the next step will be to apply an encoded unitary to the logical state. However, our current encoding is on two (disconnected) paths, and as such if we want to apply any unitary that mixes amplitudes among the two basis states we somehow need to connect the two paths. (Unitaries diagonal in the computational basis will use the same formalism, but they have additional constraints that might make them easier to apply.)

Note that Chapter 4 was all about connecting (semi-) infinite paths, where the amplitudes move from one path to another. As hinted in the chapter, we can implement encoded unitaries in this manner, if we restrict ourselves to specific momenta and specific scattering gadgets. Namely, we will examine graphs $\widehat{G}$ with four terminal vertices such that at the momentum k encoding the qubits, the scattering matrices take the form

$$S(k) = \begin{pmatrix} 0 & U^T \\ U & 0 \end{pmatrix}, \tag{5.2}$$

where U is a specific 2×2 unitary matrix. Note that if we label the four basis states as 0_{in}, 1_{in}, 0_{out}, and 1_{out} (in order), we have that the scattering has perfect transfer from input to output vertices. We will be able to use scattering gadgets of this form to apply the unitary U to the encoded qubit. Note that there are several explicit examples of these gadgets in Section 4.1.3.

More explicitly, we will have four semi-infinite paths, and we will label the four paths by 0_{in}, 1_{in}, 0_{out}, and 1_{out} (where this labeling of the paths is the same as in equation (5.2)). (This graph is similar to that of Figure 5.2, except with semi-infinite paths.) We assume that the wave-packet encoding a qubit travels toward the graph $\widehat{G}$ along the two paths 0_{in} and 1_{in}. Far from the graph the evolution of this wavepacket is nearly identical to that of an infinite path, and thus our encoded qubit is well defined. As the wavepacket scatters through the graph $\widehat{G}$, the state of the qubit is not well defined, but after scattering, most of the amplitude is on the 0_{out} and 1_{out} paths, and is in the form of an encoded qubit.

For specific μ, L, σ, and t, we the have from Theorem 4 that the outgoing wave-packet for the two computational basis states is well approximated by the wave-packet corresponding to the state $U|z\rangle$. If we remember that the form of the wave-packet doesn't depend on the value of the initial encoded qubit, we can see that the evolution of the two basis states interfere, and thus for any encoded state $|\phi\rangle$, the outgoing wavepacket is well approximated by the encoded $U|\phi\rangle$. This is exactly what we were looking for.

[**TO DO:** *make graph?*]

5.1.3 Evolution on a finite graph

Unfortunately, a single unitary will not be sufficient for our purposes; while we could probably find a four-terminal graph that computes whether a given circuit accepts or rejects its input, most of the computation would be found in the construction of the underlying graph, as opposed to the evolution itself. To ensure that the computational power arises from the time evolution of the system, we will need to place multiple graphs as scattering obstacles for the computation. This causes problems, though, in that we extensively utilize the semi-infinite paths in our analysis; we somehow need to truncate the graph while maintaining our results about the time-evolution.

To do this, we will apply our truncation lemma (Lemma 1), as it was designed specifically for this reason. Assuming that two Hamiltonians are identical on some set of basis states, and assuming that the support of the initial state is far (in some specified sense) from the difference, then the evolution of the state is the same for the two Hamiltonians, up to a small error term.

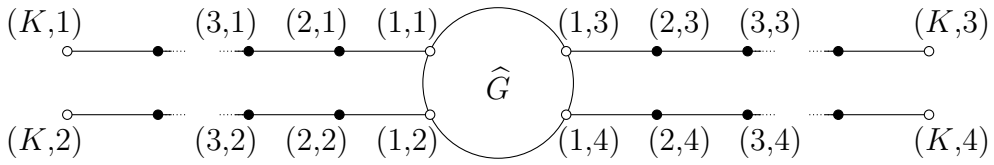

Figure 5.2: A graph $G(K)$ used to perform a single-qubit gate on an encoded qubit.

By using this lemma on the scattering graph with semi-infinite paths, we can then see that if the paths are long enough (as compared to the location of the initial state), then the evolution of an initial wave-packet is relatively unchanged by the removal of the far vertices. Basically, Lemma 1 will allow us to prove an analog of Theorem 4 for finite graphs.

More concretely, let $H = A(G)$ be the Hamiltonian for a single particle scattering off of a finite graph $\widehat{G}$ with N paths. Let $G(K)$ be the finite graph obtained from G by truncating each of the paths to have a total length K (so that the endpoints of the paths are labeled (K, j) for $j \in [N]$), and choose $\widetilde{H} = A(G(K))$ (see Figure 5.2 in the special case for $N = 4$). Let the subspace $\mathcal{K}$ be spanned by basis states corresponding to vertices in $G(K)$. Choose a momentum $k \in (-\pi, 0)$, a position μ, and a cutoff length L, and let $|\Phi\rangle = |\psi^j(0)\rangle$ be the same initial state as in Theorem **??**. We will choose the evolution time T so that for $0 \leq t \leq T$, the time-evolved state remains far from the vertices labeled (K, j) (for each $j \in \{1, \ldots, N\}$), and thus far from the effect of truncating the paths. Note that this requires $K > \mu + L$. More precisely, we will choose $T = \mathcal{O}(L)$ and $K = \mathcal{O}(L)$ so that, for times $0 \leq t \leq T$, the state $|\alpha^j(t)\rangle$ from Theorem 4 has no amplitude on vertices within a distance $N_0 = \Omega(L)$ from the endpoints of the paths. For such times t we have

$$(1 - P)\, H^r |\alpha^j\,(t)\rangle = 0 \text{ for all } 0 \leq r < N_0, \tag{5.3}$$

where P is the projector onto $\mathcal{K}$. With these values, we can apply Lemma 1 where $W = H = A(G)$, $|\gamma(t)\rangle = |\alpha^j(t)\rangle$, and the bound $\delta = \mathcal{O}(\sqrt{\log L / L})$ from Theorem 4. The lemma then says that, for times t such that $0 \leq t \leq T$,

$$\left\| \left(e^{-iA(G)t} - e^{-iA(G(K))t} \right) |\psi^j(0)\rangle \right\| = \mathcal{O}\left(\sqrt{\frac{\log L}{L}} \right) \tag{5.4}$$

so, for $0 \leq t \leq T$, when combined with Theorem 4, we can see

$$\left\| e^{-iA(G(K))t} |\psi^j(0)\rangle - |\alpha^j(t)\rangle \right\| = \mathcal{O}\left(\sqrt{\frac{\log L}{L}} \right). \tag{5.5}$$

In other words, for small enough evolution times, the conclusion of Theorem 4 still holds if we replace the full Hamiltonian $A(G)$ with the truncated Hamiltonian $A(G(K))$ (albeit with a larger constant). Note that this analysis is rather informal, and is more to give an intuition for the more exact analysis.

With the guaranteed bounds on the scattering behavior for finite graphs, we can give explicit bounds on the time-evolution of encoded qubits. In particular, let us assume that $\widehat{G}$ is a four-terminal gadget used to implement a unitary U at momentum k, and let us assume that our initial states are encoded as Gaussian wave-packets a distance μ from the graph, with a cutoff distance L. We will give explicit values of K, along with μ and L, so that the scattering event will cause the unitary U to be applied to the encoded qubits, along with bounds on the error term.

Explicitly, assuming that the four paths are labeled as in Figure 5.2, where 0_{in}, 1_{in}, 0_{out} and 1_{out} are labeled as 1, 2, 3, and 4, respectively, we have that our input logical basis states are

$$|z\rangle_{\text{log,in}} = \gamma \sum_{x=\mu-L}^{\mu+L} e^{ikx} e^{-\frac{(x-\mu)^2}{2\sigma^2}} |x, z+1\rangle, \tag{5.6}$$

where we assume that $\sigma = \frac{L}{2\sqrt{\log L}}$, as in Theorem 4. Further, we can make us of the theorem, noting that $|z\rangle_{\text{log,in}}$ are of the form $|\alpha^{z+1}(0)\rangle$, to define output logical states as well:

$$|z\rangle_{\text{log,out}} = \gamma e^{-2iT\cos k} \sum_{x=\mu-L}^{\mu+L} e^{-ikx} e^{-\frac{(x-\mu)^2}{2\sigma^2}} |x, z+3\rangle, \tag{5.7}$$

where $T = \frac{\mu}{\sin|k|}$. Note that the momentum k for the output logical states implies that the particles are moving away from the graph $\widehat{G}$. In addition to these logical basis states, we can define logical superpositions for a state $|\psi\rangle = \alpha|0\rangle + \beta|1\rangle$ as

$$|\psi\rangle_{\text{log,in}} = \alpha|0\rangle_{\text{log,in}} + \beta|1\rangle_{\text{log,in}} \tag{5.8}$$

and

$$|U\psi\rangle_{\text{log,out}} = \big(\alpha U_{00} + \beta U_{01}\big)|0\rangle_{\text{log,out}} + \big(\alpha U_{10} + \beta U_{11}\big)|1\rangle_{\text{log,out}}. \tag{5.9}$$

With these definitions, we will want to show that the input states evolve to the corresponding output states, in a manner similar to Theorem 4. Working through the math, we then find:

Lemma 12. *Let $k \in (-\pi, 0)$, and let $\widehat{G}$ be a four-terminal gate gadget, such that its scattering matrix at momentum k is of the form (5.2). Letting the logical states $|z\rangle_{log,in}$ and $|z\rangle_{log,out}$ be defined as in (5.6) and (5.7), where $\mu \geq L$, $\mu \in \mathcal{O}(L)$, $K \geq \frac{5\mu}{3}$, and $T = \frac{\mu}{\sin|k|}$, we have that there exists some constant ξ such that for all $0 \leq t \leq T$*

$$\left\| e^{-iA(G(K))t} |\phi(0)\rangle - |\phi(t)\rangle \right\| \leq \xi \sqrt{\frac{\log L}{L}}, \tag{5.10}$$

where

$$|\phi(t)\rangle = \alpha|\alpha^1(t)\rangle + \beta|\alpha^2(t)\rangle, \tag{5.11}$$

and the $|\alpha^j(t)\rangle$ are as defined in Theorem 4. In particular, we have

$$\left\| e^{-iA(G(K))T} |\psi\rangle_{log,in} - |U\psi\rangle_{log,out} \right\| \leq \xi \sqrt{\frac{\log L}{L}}. \tag{5.12}$$

Proof. Note that

$$\begin{aligned} &\left\| e^{-iA(G(K))t} |\phi(0)\rangle - |\phi(t)\rangle \right\| \\ &\quad \leq |\alpha| \left\| e^{-iA(G(K))t} |\alpha^1(0)\rangle - |\alpha^1(t)\rangle \right\| + |\beta| \left\| e^{-iA(G(K))t} |\alpha^2(0)\rangle - |\alpha^2(t)\rangle \right\|. \end{aligned} \tag{5.13}$$

We now have nearly have the form of the bound in Theorem 4, but where we use truncated paths.

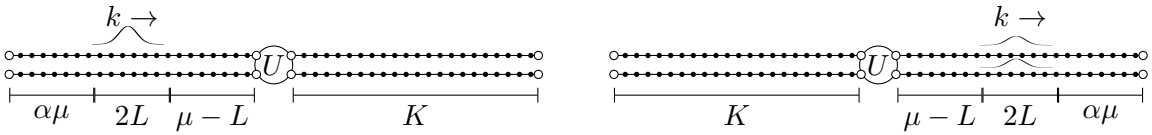

Figure 5.3: A single-qubit gate U acts on an encoded qubit. The wave packet starts on the paths on the left-hand side of the figure, a distance $\alpha\mu$ from the ends of the paths (for some constant α). After time $\frac{\mu}{\sin|k|}$ the logical gate has been applied and the wave packet has traveled a distance 2μ.

We will use Lemma 1, with $H = A(G)$, $\tilde{H} = A(G(K))$, and $N_0 = K - \mu - L \geq \frac{\mu}{6}$, and where the error bound $\delta = \chi\sqrt{\frac{\log L}{L}}$ comes from Theorem 4. Assuming that L is taken large enough so that $\delta < 1$, the lemma then gives us that for all $0 \leq t \leq T$,

$$\left\| \left(e^{-iA(G)t} - e^{-iA(G(K))t}\right) |\alpha^j(0)\rangle \right\| \leq \left(\frac{4e\|A(G)\|t}{N_0} + 2\right)\left[\chi\sqrt{\frac{\log L}{L}} + 2^{-N_0}\left(1 - \chi\sqrt{\frac{\log L}{L}}\right)\right]. \tag{5.14}$$

If we then note that $\|A(G)\|$ is bounded by the maximum degree of the graph G which is given by d (a constant), and our bounds on N_0, we then have

$$\left\| \left(e^{-iA(G)t} - e^{-iA(G(K))t}\right) |\alpha^j(0)\rangle \right\| \leq \left(\frac{12ed}{\mu}\frac{\mu}{\sin|k|} + 2\right)(\chi+1)\sqrt{\frac{\log L}{L}} \leq \zeta\sqrt{\frac{\log L}{L}}, \tag{5.15}$$

where ζ is a constant (but does depend on k and the graph $\widehat{G}$).

We can then combine these results, as

$$\begin{aligned} &\left\| e^{-iA(G(K))t} |\alpha^j(0)\rangle - |\alpha^j(t)\rangle \right\| \\ &\quad \leq \left\| \left(e^{-iA(G(K))t} - e^{-iA(G)t}\right) |\alpha^j(0)\rangle \right\| + \left\| e^{-iA(G)t} |\alpha^j(0)\rangle - |\alpha^j(t)\rangle \right\| \leq (\chi + \zeta)\sqrt{\frac{\log L}{L}}. \end{aligned} \tag{5.16}$$

From this, we can then see that

$$\begin{aligned} &\left\| e^{-iA(G(K))t} |\phi(0)\rangle - |\phi(t)\rangle \right\| \\ &\quad \leq |\alpha| \left\| e^{-iA(G(K))t} |\alpha^1(0)\rangle - |\alpha^1(t)\rangle \right\| + |\beta| \left\| e^{-iA(G(K))t} |\alpha^2(0)\rangle - |\alpha^2(t)\rangle \right\| \qquad (5.17) \\ &\quad \leq (|\alpha| + |\beta|)(\chi + \zeta)\sqrt{\frac{\log L}{L}}, \qquad (5.18) \end{aligned}$$

and by setting $\xi = \sqrt{2}(\chi + \zeta)$ we have the requisite bound (for large enough L).

If we then note that $\phi(0) = |\psi\rangle_{\log,\text{in}}$ and $\phi(T) = |U\psi\rangle_{\log,\text{out}}$, we also have the particular bound we were looking for. □

Essentially, Lemma 12 tells us that even when truncated to finite length paths, the scattering events on our graphs apply an encoded unitary to the logical states. This is represented pictorially in Figure 5.3.

5.1.4 Multi-gate computations

Now that we have a good approximation for the time evolution of a scattering event on a finite-sized graph, we can expand our results to multiple scattering events. In particular, if we can guarantee that the eventual graph corresponding to a given circuit locally looks like $G(K)$ for each unitary in the circuit, we will be able to use the results of Lemma 12 iteratively. Essentially, if the graph is two semi-infinite paths with regularly spaced scattering obstacles, our previous results will still apply.

[**TO DO:** *make a figure*]

Along these lines, let us assume that a single-qubit circuit $\mathcal{C}$ is composed of g unitaries, where the ith unitary applied is given by U_i. Moreover, let us assume that at a momentum k, the graphs $\widehat{G}_i$ have scattering matrices of the form (5.2) corresponding to the unitary U_i (i.e., at momentum k, the graph $\widehat{G}_i$ implements an encoded U_i). We can then construct a graph $G_{\mathcal{C}}$ which we will use to compute the circuit $\mathcal{C}$ using wave-packets at momentum k.

The graph $G_{\mathcal{C}}$ is constructed by combining the $G_i(K)$ into a single graph (where $G_i(K)$ is defined in Section 5.1.2) by associating the output paths of $G_i(K)$ with the input paths of $G_{i+1}(K)$. Assuming that the vertices of $G_i(K)$ are labeled as (u, i), this essentially means that most of the vertices along the long paths have two labels, $(x, 3, i)$ and $(K+1-x, i+1)$ or $(x, 4, i)$ and $(K+1-x, 2, i+1)$. Equivalently, the graph $G_{\mathcal{C}}$ can be constructed by removing the input paths (paths 1 and 2) for all the $G_i(K)$ (except for $G_1(K)$), shortening each of the terminal paths by 1 (except for $G_g(K)$), and then connect the end of the paths for $G_i(K)$ to the input terminals of $G_{i+1}(K)$.

[**TO DO:** *make a simple figure*]

With this construction of $G_{\mathcal{C}}$, note that if we look only at the vertices supported within a distance of $K-2$ of $\widetilde{G_i}$, we actually have the graph $G_i(K-1)$. As such, we will be able to use Lemma 1 and Lemma 12 to determine the evolution while a Gaussian wave-packet is located near the graph $\widehat{G}_i$. If we assume that the initial wave-packet is located in the correct position near $\widehat{G}_i$, we can iteratively apply this idea, where the "input" logical state for the $(i+1)$th scattering event is simply the "output" from the ith scattering event. As such, the logical state after the gth scattering event will correspond to the logical state after the circuit $\mathcal{C}$ has been applied.

Concretely, let us choose some cutoff length L, set $\sigma = \frac{L}{2\sqrt{\log L}}$, chose $\mu = 2L$, $K = 2\mu - 1$ and $T = \frac{\mu}{\sin|k|}$. With these choices, our initial logical state will be nearly identical to (5.6), but where the basis states also have a label corresponding to fact that there are multiple long paths:

$$|\,z\,\rangle_{\log,\text{in}} = \gamma \sum_{x=\mu-L}^{\mu+L} e^{ikx} e^{-\frac{(x-\mu)^2}{2\sigma^2}} |\,x, z+1, 1\,\rangle. \tag{5.19}$$

In a similar manner, the final state of the qubit will be defined as

$$|\,z\,\rangle_{\log,\text{out}} = \gamma e^{-2iTg\cos k - 2ik(g-1)\mu} \sum_{x=\mu-L}^{\mu+L} e^{-ikx} e^{-\frac{(x-\mu)^2}{2\sigma^2}} |\,x, z+3, g\,\rangle, \tag{5.20}$$

where the additional global phase arises from the change in bases between the various scattering events. We will also need to define logical states at several times throughout the computation, corresponding to the states after each applied unitary. We will thus define the logical state after

the jth scattering event (and before the $(j+1)$th scattering event) as

$$|z\rangle_{\log,j} = \gamma e^{-2iTj\cos k - 2ik\mu(j-1)} \sum_{x=\mu-L}^{\mu+L} e^{-ikx} e^{-\frac{(x-\mu)^2}{2\sigma^2}} |x, z+3, j\rangle \tag{5.21}$$

$$= \gamma e^{-2iTj\cos k - 2ijk\mu} \sum_{x=\mu-L}^{\mu+L} e^{ikx} e^{-\frac{(x-\mu)^2}{2\sigma^2}} |x, z+1, j+1\rangle. \tag{5.22}$$

Except for the additional (global) phase arising from the change of basis, these are exactly the logical states necessary for Lemma 12.

We can now bound the error in approximating the time evolution of an initial state with the output state corresponding to the logical application of the circuit:

$$\left\| e^{-iA(G_{\mathcal{C}})gT} |\psi\rangle_{\log,\text{in}} - |U_{\mathcal{C}}\psi\rangle_{\log,\text{out}} \right\|$$

$$\leq \sum_{j=0}^{g-1} \left\| e^{-iA(G_{\mathcal{C}})T} |U_j U_{j-1} \cdots U_1 \psi\rangle_{\log,j} - |U_{j+1} U_j \cdots U_1 \psi\rangle_{\log,j+1} \right\| \tag{5.23}$$

Note that each individual term is close to that in Lemma 12, but where the Hamiltonian is given by $A(G_{\mathcal{C}})$ as opposed to $A(G(K))$. However, we can use Lemma 1, with $H = A(G_{\mathcal{C}})$, $\tilde{H} = G(K-1)$, $N_0 = \frac{\mu}{4}$, and the error δ from Lemma 12, we have that for all logical states $|\phi\rangle$,

$$\left\| e^{-iA(G_{\mathcal{C}})T} |\phi\rangle_{\log,j} - |U_{j+1}\phi\rangle_{\log,j+1} \right\|$$

$$\leq \left(\frac{16e\|A(G_{\mathcal{C}})\|T}{\mu} + 2 \right) \left[\xi \sqrt{\frac{\log L}{L}} + 2^{-\mu+L+2} \left(1 - \chi \sqrt{\frac{\log L}{L}} \right) \right] \tag{5.24}$$

$$\leq \kappa \sqrt{\frac{\log L}{L}}, \tag{5.25}$$

where κ depends on k and the maximum degree of $G_{\mathcal{C}}$ (which we assume to be constant). We can then see that

$$\left\| e^{-iA(G_{\mathcal{C}})gT} |\psi\rangle_{\log,\text{in}} - |U_{\mathcal{C}}\psi\rangle_{\log,\text{out}} \right\|$$

$$\leq \sum_{j=0}^{g-1} \left\| e^{-iA(G_{\mathcal{C}})T} |U_j U_{j-1} \cdots U_1 \psi\rangle_{\log,j} - |U_{j+1} U_j \cdots U_1 \psi\rangle_{\log,j+1} \right\| \tag{5.26}$$

$$\leq g\kappa \sqrt{\frac{\log L}{L}}. \tag{5.27}$$

As such, if we take L larger than $g^2\kappa^2 \log^2(g\kappa)$ we find that the error can be made arbitrarily small, and thus we were able to simulate the circuit $\mathcal{C}$ via scattering on a constant-degree graph with $\mathcal{O}(g^3 \log^2 g)$ vertices.

5.2 Multi-qubit computations

Now that we understand how to simulate a single-qubit circuit via scattering, we can try to apply our results to multi-qubit circuits. The intuitive construction remains the same, but the requisite

number of vertices will become rather large. In particular, our construction will require an exponential number of long paths, corresponding to the exponential size of the Hilbert space we want to simulate.

To begin, let us give the encoding of n qubits in our scattering framework. As in Section 5.1.1, we will encode the state as a wave-packet traveling along an infinite path, where the value of the qubit is encoded in the path on which the particle is located. For a single qubit, this meant that we had two infinite paths, corresponding to logical 0 and 1. For n qubits, however, this means that we need 2^n infinite paths, one path corresponding to each logical basis state.

We will still have four important quantities that are independent of the state of the qubit, namely the momentum of the wave-packet k, the position of the center of the wave-packet μ (which depends on t), the cutoff distance L, and the standard deviation of the approximating Gaussian σ. As such, if we label the 2^n infinite paths by the strings $\mathbf{z} \in \mathbb{F}_2^n$, and the vertices as $(x, \mathbf{s})$ for $x \in \mathbb{Z}$ and $\mathbf{z} \in \mathbb{F}_2^n$, we have that the logical states are encoded in the wave-packets

$$|\mathbf{z}\rangle_{\log} = \gamma \sum_{x=\mu-L}^{\mu+L} e^{ikx} e^{-\frac{(x-\mu)^2}{2\sigma^2}} |x, \mathbf{z}\rangle. \tag{5.28}$$

Note that we again use this encoded form so that we will be able to analyze the dynamics via Theorem 4.

5.2.1 One multi-qubit unitary

Now that we have an encoding of our qubits, we will need to somehow apply encoded unitary gates. We have already done most of the work in Section 5.1, and we just need to show how to use the single-qubit results in our larger encoding, and how to perform multi-qubit entangling gates.

Our implementation of single-qubit unitaries for multi-qubit computations is to use many copies of the single-qubit implementation. In particular, since a single qubit unitary U acting on qubit $w \in [n]$ can be written as

$$\mathbb{I}_{2^{w-1}} \otimes U \otimes \mathbb{I}_{2^{n-w}} = \sum_{x \in \mathbb{F}_2^{w-1}, y \in \mathbb{F}_2^{n-w}} |x\rangle\langle x| \otimes U \otimes |y\rangle\langle y|, \tag{5.29}$$

we can apply the unitary U on the encoded w qubit by ensuring that the scattering occurs for each computational basis state of the other qubits. This means that by placing 2^{n-1} copies of the graph $\widehat{G}$ as obstacles in the paths, one for each computational basis state of the qubits not used in the unitary, the scattering behavior is exactly as expected. We will call the infinite graph corresponding to the unitary U acting on n qubits G_U^n.

For multi-qubit entangling unitaries, the solution is even more simple; we simply relabel the output paths. Noting that many multi-qubit gates, such as the controlled-NOT gate or the Toffoli gate, simply permute the computational basis states, along with the fact that the particular path a particle travels along corresponds to its logical state, by relabeling the paths, or equivalently by permuting the paths, we apply an encoded entangling gate. Note that this method of applying a multi-qubit gate is independent of the encoding momenta, and thus can be used for all momenta (so that we don't need to find additional graphs with scattering matrices at the encoding momentum).

Assuming that a given two-qubit unitary V occurs after some single-qubit unitary U, we construct the graph G_{VU}^n implementing VU by taking a copy of G_U^n, and then permuting its output paths. Note that this means that for a given copy of $\widehat{G}_j$, the logical states corresponding to the input paths might be different from the logical states corresponding to the output paths. However,

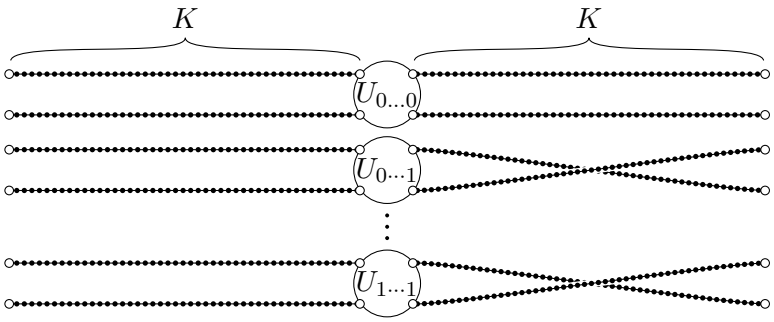

Figure 5.4: The intuitive idea for the graph simulating a single unitary. Each U_x for $x \in \mathbb{F}_2^{n-1}$ is the same, and note that the output paths are flipped if the last bit is 1.

since V is only a two-qubit permutation, the output paths can be efficiently determined for a given copy of $\widehat{G}_j$. An example of such a graph can be seen in Figure 5.4, except with semi-infinite paths.

As in Section 5.1.3, we can then define $G_{VU}^n(K)$ as the graph that that remains after truncating each of the infinite paths of G_{VU}^n to length K.

With all of this, and assuming that the 2^{n+1} paths are labeled with the path corresponding to $\mathbf{z}_{\text{in}}$ for $\mathbf{z} \in \mathbb{F}_2^n$ is labeled as $z+1$ while the $\mathbf{z}_{\text{out}}$ are labeled as $z+2^n+1$, we have that our input logical basis states are

$$|\mathbf{z}\rangle_{\text{log,in}} = \gamma \sum_{x=\mu-L}^{\mu+L} e^{ikx} e^{-\frac{(x-\mu)^2}{2\sigma^2}} |x, z+1\rangle, \tag{5.30}$$

where we assume that $\sigma = \frac{L}{2\sqrt{\log L}}$, as in Theorem 4. Note that this generalizes the single particle case (5.6) to more input and output paths. We can then take inspiration from the single qubit case, and define the output logical states as well:

$$|\mathbf{z}\rangle_{\text{log,out}} = \gamma e^{-2iT\cos k} \sum_{x=\mu-L}^{\mu+L} e^{-ikx} e^{-\frac{(x-\mu)^2}{2\sigma^2}} |x, z+2^n+1\rangle, \tag{5.31}$$

where $T = \frac{\mu}{\sin|k|}$. In addition to these logical basis states, for an arbitrary state $|\psi\rangle = \sum_{\mathbf{z}\in\mathbb{F}_2^N} \alpha_{\mathbf{z}} |\mathbf{z}\rangle$ in $\mathbb{C}^{\mathbb{F}_2^n}$

$$|\psi\rangle_{\text{log,in}} = \sum_{\mathbf{z}\in\mathbb{F}_2^n} \alpha_{\mathbf{z}} |\mathbf{z}\rangle_{\text{log,in}} \tag{5.32}$$

and

$$|U\psi\rangle_{\text{log,out}} = \sum_{\mathbf{y},\mathbf{z}\in\mathbb{F}_2^N} U_{\mathbf{z},\mathbf{y}} \alpha_{\mathbf{y}} |\mathbf{z}\rangle_{\text{log,out}}, \tag{5.33}$$

where U is thought of as a unitary on n qubits. With these definitions, we will want to show that the input states evolve to the corresponding output states. This nearly follows from Lemma 12, but we need to do some small work showing that the errors don't grow like the number of paths.

Corollary 1. *Let $k \in (-\pi, 0)$, let $\widehat{G}$ be a four-terminal gate gate, such that its scattering matrix at momentum k is of the form (5.2) for a given unitary U, and let V be a permutation of the*

underlying basis states. Letting the logical states $|\mathbf{z}\rangle_{log,in}$ *and* $|\mathbf{z}\rangle_{log,out}$ *be as in (5.30) and (5.31), where* $\mu \geq 2L$ *and* $K \geq \frac{5\mu}{3}$ *and* $T = \frac{\mu}{\sin|k|}$*, we have that there exists some constant* ξ *such that for all* $0 \leq t \leq T$*,*

$$\left\| e^{-iA(G^n_{VU}(K))t} |\phi(0)\rangle - |\phi(t)\rangle \right\| \leq \xi \sqrt{\frac{\log L}{L}}, \tag{5.34}$$

where

$$|\phi(t)\rangle = \sum_{\mathbf{z}\in\mathbb{F}_2^n} \beta_{\mathbf{z}} |\alpha^{z+1}(t)\rangle, \tag{5.35}$$

and the $|\alpha^j(t)\rangle$ *are as defined in Theorem 4. In particular, we have for any* $|\psi\rangle \in \mathbb{C}^{\mathbb{F}_2^n}$*,*

$$\left\| e^{-iA(G^n_V(K))T} |\psi\rangle_{log,in} - |U\psi\rangle_{log,out} \right\| \leq \xi \sqrt{\frac{\log L}{L}}. \tag{5.36}$$

Proof. Note that $G^n_{VU}(K)$ is a disconnected graph, with 2^{n-1} components. As such, we have that $e^{-iA(G^n_{VU}(K)t}$ decomposes into the product of 2^{n-1} commuting operators, all acting on disjoint Hilbert spaces. Because of this, error cannot interfere between the various disconnected paths, and thus the total error is bounded by the maximum error on any individual component.

In each component, however, we can use Lemma 12 to see that the first part of the corollary holds, with the appropriate error (and with a constant equal to that of Lemma 12). Hence, the total error is bounded by $\xi\sqrt{\frac{\log L}{L}}$.

For the second part of the corollary, we can use Lemma 12 to see that the result holds on each component of $G^n_{VU}(K)$, and thus holds in general. □

5.2.2 Multi-gate computations

At this point, we have most of the requirements to simulate a multi-qubit circuit. We know from Section 5.2.1 how to apply a single encoded unitary on multiple qubits via scattering on a finite graph, and we know from Section 5.1.4 how to apply multiple single-qubit gates. We need only to combine these two results.

We will make use of the same block structure as in Section 5.1.4, where the graph corresponding to a single unitary is shown in Figure 5.4. Additionally, we will assume that the circuit we want to simulate only consists of a single-qubit gates followed by a two-qubit gate. This assumption isn't difficult to enforce, as these gates can simply consist of identity operations. The circuit that we want to simulate is then given by

$$U_{\mathcal{C}} = V_g U_g V_{g-1} U_{g-1} \cdots V_1 U_1, \tag{5.37}$$

where each V_j is a two-qubit gate, and each U_1 is a one-qubit gate.

As in Section 5.1.4, we will construct a graph for this circuit, $G_{\mathcal{C}}$, by examining the graphs $G^n_{V_jU_j}$ for each $j \in [g]$, and then combining them by associating the output paths of $G^n_{V_jU_jj}(K)$ with the input paths of $G^n_{V_{j+1}U_{j+1}}(K)$. Explicitly, the vertices along the output paths of $G^n_{V_jU_j}(K)$ labeled as $(x, 2^n + 1 + z, j)$ for $\mathbf{z} \in \mathbb{F}_2^n$ are defined to be the same vertices on the input paths of $G^n_{V_{j+1}U_{j+1}}(K)$ labeled as $(K + 1 - x, z + 1, j + 1)$. This can be seen pictorially in Figure 5.4 for one of these blocks.

With this construction, we will use exactly the same idea as in the Section 5.1.4 to analyze the time-evolution of a particular initial logical state, with the analysis proceeding accordingly. Using

Lemma 1 to focus on the vertices close to a the wavepacket (and in particular the nearest copy of $G^n_{V_jU_j}(K)$) we can the use Corollary 1 to approximate the evolution.

Concretely, let us choose some cutoff length L, set $\sigma = \frac{L}{2\sqrt{\log L}}$, chose $\mu = 2L$ and $K = 2\mu - 1$ and $T = \frac{\mu}{\sin|k|}$. With these choices, our initial logical state will be nearly identical to (5.6), but where the labels for the basis states also have a label corresponding to fact that there are multiple long paths:

$$|\mathbf{z}\rangle_{\log,\text{in}} = \gamma \sum_{x=\mu-L}^{\mu+L} e^{ikx} e^{-\frac{(x-\mu)^2}{2\sigma^2}} |x, z+1, 1\rangle. \tag{5.38}$$

In a similar manner, the final state of the qubit will be defined as

$$|\mathbf{z}\rangle_{\log,\text{out}} = \gamma e^{-2iTg\cos k - 2i(g-1)\mu} \sum_{x=\mu-L}^{\mu+L} e^{-ikx} e^{-\frac{(x-\mu)^2}{2\sigma^2}} |x, z+2^n+1, g\rangle, \tag{5.39}$$

Additionally, we will need to define logical states at several times throughout the computation, corresponding to the states after each applied unitary. As such, we will define the logical state after the jth scattering event (and before the $(j+1)$th scattering event) as

$$|\mathbf{z}\rangle_{\log,j} = \gamma e^{-2iTj\cos k - 2ik\mu(j-1)} \sum_{x=\mu-L}^{\mu+L} e^{-ikx} e^{-\frac{(x-\mu)^2}{2\sigma^2}} |x, z+2^n+1, j\rangle \tag{5.40}$$

$$= \gamma e^{-2iTj\cos k - 2ijk\mu} \sum_{x=\mu-L}^{\mu+L} e^{ikx} e^{-\frac{(x-\mu)^2}{2\sigma^2}} |x, z+1, j+1\rangle, \tag{5.41}$$

where as in the single-qubit case, the additional phase arises from the change of labeling of the vertices.

From here, we can now bound the error in approximating the time evolution of $|\mathbf{z}\rangle_{\log,\text{in}}$ for a time Tg by the output logical state corresponding to an application of the circuit, by breaking the evolution into blocks of length T. Explicitly:

$$\begin{aligned}
&\left\| e^{iA(G_\mathcal{C})gT} |\psi\rangle_{\log,\text{in}} - |U_\mathcal{C}\psi\rangle_{\log,\text{out}} \right\| \\
&\quad \le \sum_{j=0}^{g-1} \left\| e^{iA(G_\mathcal{C})T} |U_jU_{j-1}\cdots U_1\psi\rangle_{\log,j} - |U_{j+1}U_j\cdots U_1\psi\rangle_{\log,j+1} \right\|
\end{aligned} \tag{5.42}$$

Note that each individual term is close to that in Corollary 1, but where the Hamiltonian is given by $A(G_\mathcal{C})$ as opposed to $A(G_{V_jU_j}(K))$. However, using Lemma 1 with $H = A(G_\mathcal{C})$, $\tilde{H} = G_{V_jU_j}(K-1)$, $N_0 = \frac{\mu}{4}$, and the error δ from Corollary 1, we have that for all logical states $|\phi\rangle$,

$$\begin{aligned}
&\left\| e^{iA(G_\mathcal{C})T} |\phi\rangle_{\log,j} - |U_{j+1}\phi\rangle_{\log,j+1} \right\| \\
&\quad \le \left(\frac{16e\|A(G_\mathcal{C})\|T}{\mu} + 2 \right) \left[\xi \sqrt{\frac{\log L}{L}} + 2^{-\mu+L+2} \left(1 - \chi\sqrt{\frac{\log L}{L}} \right) \right] &(5.43)\\
&\quad \le \kappa \sqrt{\frac{\log L}{L}}, &(5.44)
\end{aligned}$$

where κ is depends on k and the maximum degree of $G_{\mathcal{C}}$ (which we assume to be constant). We can then see that

$$\begin{aligned}
&\left\| e^{iA(G_{\mathcal{C}})gT} |\psi\rangle_{\log,\text{in}} - |U_{\mathcal{C}}\psi\rangle_{\log,\text{out}} \right\| \\
&\quad \leq \sum_{j=0}^{g-1} \left\| e^{iA(G_{\mathcal{C}})T} |U_j U_{j-1} \cdots U_1 \psi\rangle_{\log,j} - |U_{j+1} U_j \cdots U_1 \psi\rangle_{\log,j+1} \right\| \qquad (5.45) \\
&\quad \leq g\kappa \sqrt{\frac{\log L}{L}}, \qquad (5.46)
\end{aligned}$$

exactly as in Section 5.1.4 and our error bound does not explicitly depend on n. As such, if we take L larger than $g^2\kappa^2 \log^2(g\kappa)$ we find that the error can be made arbitrarily small, and thus we can simulate a particular n-qubit g-gate circuit with constant error via graph scattering on a graph of $\mathcal{O}(2^n g^3 \log^2 g)$ vertices for a time $\mathcal{O}(g^3 \log^2 g)$.

5.2.3 Explicit examples

[**TO DO:** *include explicit mention of momenta for which this works*]

5.3 Discussion and extensions

At this point, we have shown that single-particle graph scattering can be used to simulate an arbitrary quantum computation. In particular, we were able to use a dual-rail encoding, and simulate each unitary from a universal gate set via scattering. By combining these scattering events (and bounding the resulting error), we were able to simulate the computation. It is important to realize that most of the technical results for this universality proof are contained in our understanding of single-particle scattering from Chapter 3, along with a technical truncation lemma (Lemma 1), and the portion of the proof in this chapter are simply applications of those results.

While this is a novel proof of the universality of quantum walk, both the result and the proof strategy are not new. In particular, Childs gave a similar result using scattering theory [11], but where his time evolution arose from the theory of stationary phases, while the proof strategy is nearly identical to that of Childs, Gosset, and Webb in their proof of universality for multi-particle quantum walk [16]. However, the point of this chapter was not to prove anything novel, but to give an intuitive understanding for the proof strategy.

Additionally, the discussion in this chapter has essentially been plug-and-play for the momentum k, assuming that a set of universal scattering gadgets are known for the momentum in question. However, we have only found these gadgets for a small set of momenta, described in Section 4.1.3. One might be able to extend this proof to work for all momenta, if we could find a set of gadgets that work for all momenta. It might also be possible to show that this construction does not work for some momentum, although I think that unlikely.

As a possible extension of this work, the permutation of the underlying paths corresponding to a two-qubit unitary plays a key part in our encoded gates. However, these permutations are intrinsically non-planar (assuming that there are more than three non-identity 2-qubit gates). One might ask whether any planar graph could be used to encode a computation, or whether non-planarity is required to capture the entire power of quantum walk. In a similar manner, one might ask what other properties of the underlying graph are needed to maintain the same computational power. While this is not necessary for any physical reason (since the exponential size of the graph is

infeasible to construct in reality), there might be some relation between different graph properties and their use as a computational tool.

Additionally, our current construction assumes no errors, and error-correction cannot trivially be implemented in our scheme. We are unsure how error correction could be implemented using this construction, since both non-local measurements and measurements in the middle of the computation seem rather difficult. Further, one of the inherent properties of quantum walk is the lack of a time-dependent Hamiltonian; most current error correction methods seem contrary to the spirit of quantum walk. As such, including some kind of error correction naturally in our graph scattering (or quantum walk in general) would be of great help in the applications toward universality. This might also help us in Chapter 7, as we use similar methods to show the universality of multi-qubit quantum walk.

Chapter 6

Multi-particle quantum walk

[**TO DO:** *rewrite entire intro, find more MPQW stuff*]

So far, we have only focused on the case of a single walker moving on a graph. These systems exhibit all the hallmarks of quantum systems, with superpositions of states, entanglement, and the like, but neccessity forces the corresponding graphs to be unphysical; as each vertex corresponds to a computational basis state, in order to get nontrivial computational power we are forced to work on graphs that are not practical to implement in the real world.

From a computational point of view, this does not matter. Chapter 5 showed that quantum walk is universal for quantum computation, and thus we wouldn't expect it to be easier to implement than a universal quantum computer. However, several experimental implementations of quantum walk have been carried out [20, 25, 30], where the encoding has been done in a non-scalable manner.

Continuing in this manner, experimentalists have also examined what happens when multiple particles interact on the same graph. Explicitly, they have analyzed what happens when two bosons walk on a graph [10, 31, 35], what happens when multiple bosons move along a long path, and various other simple experiments.

[**TO DO:** *find more recent MPQW stuff*]

While these experimental realizations of multi-particle quantum walk have flourished, the theoretical side has only seen some small development. In particular, there have been attempts to use these MPQW as tools for analyzing graph properties, in the hope that they might be useful for the graph isomorphism problem, but many of these avenues have been proven impossible. Additionally, there are some continuous space analysis on the eigenstates of some interaction Hamiltonians, but in most cases no closed form solution exists.

In this chapter, we will define our model of multi-particle quantum walk, and analyze the dynamics of such a model on some simple systems. While this will not improve drastically our previous knowledge this does give us a better understanding of simple interactions.

[**TO DO:** *a lot more citations*]

6.1 Multi-particle quantum walk

In Chapter 3, we analyzed a single-particle quantum walk, and in particular we found that the evolution proceeds with a Hamiltonian given by the adjacency matrix of the graph. If we want to generalize this framework to multiple particles, we will want to ensure that each individual particle in our framework evolves as in the single-particle case.

Namely, we had that the Hilbert space for the single-particle quantum walk on a graph G was given by $\mathbb{C}^{|V(G)|}$, with the computational basis given by the states labeled by the vertices of the

graph:

$$\big\{|\, v\,\rangle : v \in V(G)\big\}. \tag{6.1}$$

If we want to extend this to multiple particles, we shall take multiple copies of this Hilbert space. As such, we will assume that Hilbert space for the N-particle quantum walk on a graph G is $\mathbb{C}^{|V(G)|^N}$, with the computational basis given by

$$\big\{|\, v_1, v_2, \cdots, v_N\,\rangle : \forall i \in [N], v_i \in V(G)\big\}. \tag{6.2}$$

Note that for the moment we assume that the N particles are distinguishable.

Now that we have a Hilbert space for the N-particle quantum walk, we still need the Hamiltonian to understand the time-evolution. As the Hamiltonian for a single particle is simply the adjacency matrix of the graph G, we will take as our definition of the N-particle quantum walk (without interaction) as a sum of Hamiltonians that each generate the correct single-particle evolution for a given particle. Namely, we have that the N particle quantum walk with no interaction takes the form

$$H^N_{\text{mov}} = \sum_{w\in[N]} A(G)^{(w)} \tag{6.3}$$

where $B^{(w)}$ is the operator that acts on N particles as B on the wth particle and $\mathbb{I}$ on the rest. With such a Hamiltonian, the evolution operator decomposes into a product of commuting terms, where each term acts as the single particle evolution for a different particle, exactly as we want.

While this definition of an N-particle quantum walk does nicely generalize that of a single-particle quantum walk, it is not any more interesting than the original single-particle walk. In particular, the eigenstates of (6.3) easily decompose into product states, where each of the individual particles are in an eigenstate of $A(G)$. Such a system is only as computationally powerful as that of a single-particle system, since we can simulate the N-particle system via N single-particle evolutions. To get around this, we will thus want to force some interaction between the particles. We will also want to ensure that we capture the intuitive structure of particle interactions from the continuum, so that our model makes sense as a quantum walk. Note that in the continuum, the interaction between particles only depends on the distance between the particles. This translation invariance can have several different abstractions to a general graph, but on a one dimensional lattice we would expect the interaction to only depend on the distance between the particles, as measured by the shortest path between vertices.

We will take this requirement on the infinite path and use it for all vertices. Further, we will assume some finite range of interaction, so that particles with large physical separation don't interact. Namely, let us choose some $d_{\max} \in \mathbb{N}$ to be the finite range of the interaction, and then choose $d+1$ symmetric polynomials in two variables, U_d, for $0 \le d \le d_{\max}$. Additionally, assuming that we know that there are a total of N particles, let $\hat{n}_v$ for $v \in V(G)$ be the operator that counts the number of particles at vertex v, explicitly given by

$$\hat{n}_v = \sum_{w\in[N]} |\, v\rangle\langle v\,|^{(w)}. \tag{6.4}$$

With these values, and if $d(u,v)$ is the distance function on the graph G given by the length of the shortest path between u and v, we can define the interaction

$$H_{\text{int}} = \sum_{d=0}^{d_{\max}} \sum_{\substack{u,v\in V(G)\\ d(u,v)=d}} U_d(\hat{n}_u, \hat{n}_v). \tag{6.5}$$

Note that on the infinite path (and in fact on any lattice), this interaction has the form we require.

With such a chosen interaction, (i.e., with $d_{\max}$ and the U_d well defined), we can then define the N-particle quantum walk on G with this interaction. Namely, we let

$$H_G^N = H_{\text{mov}}^N + H_{\text{int}}^N = \sum_{w\in[N]} A(G)^{(w)} + \sum_{d=0}^{d_{\max}} \sum_{\substack{u,v\in V(G)\\ d(u,v)=d}} U_d(\hat{n}_u, \hat{n}_v). \tag{6.6}$$

Hamiltonians of this form will be the study of this thesis. Note that we call the component of (6.6) corresponding to the sum of adjacency matrices (6.3) the movement term of the Hamiltonian, while the part corresponding to the interaction (6.5) is called the interaction term.

Several times in the thesis, we will need to reference particular values that the interaction Hamiltonian takes. As such, we will use as shorthand

$$\mathcal{U}_d^{a,b} = \mathcal{U}_d(a,b). \tag{6.7}$$

6.1.1 Indistinguishable particles

Note that in our definition of MPQW, we assume that the particles are all distinguishable, and thus we can locate each of the N particles. In many cases of interest, though, we will actually not have this ability, as the particles will be indistinguishable. One might then think that we would need to change our definition in order to characterize these indistinguishable walks.

This turns out to not be the case, however, as Hamiltonian (6.6) is permutation invariant. In other words, we have that for any permutation of the underlying particle particles (given by V_π for a given permutation $\pi \in S_N$),

$$V_\pi H_G^N V_\pi^\dagger = H_G^N. \tag{6.8}$$

Using this, we can then see that the Hamiltonian preserves the symmetric and anti-symmetric subspaces, corresponding to either fermions or bosons.

As such, if we want to restrict our attention to bosonic multi-particle quantum walk, we simply have that the relevant Hilbert space is

$$\Big\{ \text{Sym}\left(|\, v_1, v_2, \cdots, v_N \,\rangle\right) : \forall i \in [N], v_i \in V(G) \Big\}, \tag{6.9}$$

where

$$\text{Sym}\left(|\, \phi \,\rangle\right) = \frac{1}{N!} \sum_{\pi\in S_n} V_\pi |\, \phi \,\rangle, \tag{6.10}$$

but where the Hamiltonian for the walk is still given by (6.6). Similarly, we have that fermionic MPQW, the Hilbert space is given by

$$\Big\{ \text{Asym}\left(|\, v_1, v_2, \cdots, v_N \,\rangle\right) : \forall i \in [N], v_i \in V(G) \Big\}, \tag{6.11}$$

where

$$\text{Sym}\left(|\, \phi \,\rangle\right) = \frac{1}{N!} \sum_{\pi\in S_n} \text{sign}(\pi) V_\pi |\, \phi \,\rangle, \tag{6.12}$$

and we again use the same Hamiltonian.

6.1.2 Examples

While (6.6) is a well defined mathematical object for a given graph G, interaction range $d_{\max}$, symmetric polynomials $\mathcal{U}_d$, and a number of particles, N, as of yet we haven't given any well-known models that fall into this class of interactions. However, the idea of translation invariant interactions, in which the interaction does not depend on the particular location of a given particle, is abundant in physics, and thus there are several well-know models that relate to our MPQW.

6.1.2.1 Bose-Hubbard model

The Bose-Hubbard model on a graph, where the particles are taken to be bosons, and there is a given onsite interaction between the particles in probably the first interaction that falls into our class of interactions. In particular, we have that in the second quantized basis, the Hamiltonian for the Bose-Hubbard model on a graph G is usually given by

$$H_G^{\mathrm{BH}} = t_{\mathrm{hop}} \sum_{i,j \in V(G)} A(G)_{ij} a_i^\dagger a_j + J_{\mathrm{int}} \sum_{k \in V(G)} n_k(n_k - 1), \tag{6.13}$$

where $a_i^\dagger$ creates a boson at vertex i, and $n_i = a_i a_i^\dagger$ counts the number of particles at vertex i. Note that this form of the Hamiltonian does not require knowledge of the number of particles, as it works in the Fock space which allows for an arbitrary number of particles. Additionally, we have that (6.13) preserves the number of particles, and thus decomposes into blocks for each particle number.

While this form of (6.13) is not quite that of (6.6), if we assume that there are N particles, we can rewrite the Hamiltonian in the first quantized basis (after restricting to the symmetric subspace) as

$$H_G^{\mathrm{BH},N} = t_{\mathrm{hop}} \sum_{w \in [N]} \sum_{i,j \in V(G)} A_{i,j} \big(|\, i \rangle\langle j \,| \big)^{(w)} + J_{\mathrm{int}} \sum_{v \in V(G)} \hat{n}_v \big(\hat{n}_v - 1 \big). \tag{6.14}$$

This is simply a rescaling by t_{hop} of a Hamiltonian the form (6.6), where $d_{\max} = 0$ and

$$\mathcal{U}_0(x, y) = \frac{J_{\mathrm{int}}}{4 t_{\mathrm{hop}}} (x + y)(x + y - 2) \tag{6.15}$$

6.1.2.2 Nearest-neighbor interactions

While the Bose-Hubbard model (and onsite-interactions in general) are a well studied phenomenon, they unfortunately do not affect anti-symmetric states at all. As such, if we want an interaction that will change the structure of the entire Hilbert space, we will need to increase our $d_{\max}$ to at least 1, arriving at the nearest neighbor interactions.

While there are many different interactions with $d_{\max} = 1$, probably the most simple is given by $\mathcal{U}_0 = 0$ and

$$\mathcal{U}_1(x, y) = \gamma x y. \tag{6.16}$$

With this interaction, we then have that the corresponding MPQW Hamiltonian is given by

$$H_G^{\mathrm{NN},N} = \sum_{w \in [N]} A(G)^{(w)} + \gamma \sum_{\{u,v\} \in E(G)} \hat{n}_u, \hat{n}_v \tag{6.17}$$

6.1.3 Evolution on disconnected graphs

While a general result about the eigenstates of an N-particle quantum walk on a given graph G might be difficult, we can reason about some properties of the eigenstates and time-evolved states without needing to explicitly calculate the overall form of the eigenstates. In particular, if a given graph on which the particles walk has some property, then so too might the time-evolved states.

Perhaps the most obvious such property is the connectivity of the graph itself. In particular, our MPQW Hamiltonian (6.6) only allows particles to move between vertices that have a path between them; if two vertices are not connected in G, then the corresponding off-diagonal element of the time evolution unitary will always be zero.

We can use this to decompose the time-evolution unitary into a product of commuting unitaries, each corresponding to a specific component of G. If each of the N particles in a state $|\phi\rangle$ have support only on one component of the graph G, then the evolution operator is simply a product of n_c-particle MPQW evolutions for each component G_c of G, where n_c particles are on the c-th component. Explicitly, we have the following lemma:

Lemma 13. *Let G be a disconnected graph with M components, and let us examine the N-particle MPQW on G. If $|\psi\rangle$ is an N-particle state such that each particle j only has support on the G_{c_j}th component of G, then*

$$e^{-iH_G^N t}|\phi\rangle = \prod_{c=1}^{M} W_c^\dagger \left(e^{-iH_{G_c}^{n_c} t}\right)^{(1,2,\cdots,n_c)} W_c|\phi\rangle \tag{6.18}$$

where n_c is the number of particles with support on G_c, and W_c is a permutation operator that takes the particles with support on G_c to the first n_c particles. In the special case where $n_c \leq 1$ for all c, this then reduces to

$$e^{-iH_G^N t}|\phi\rangle = \prod_{j=1}^{n} \left(e^{-iA(G_{k_j})t}\right)^{(j)}|\phi\rangle. \tag{6.19}$$

Proof. Let us assume an arbitrary ordering on the components of G, and let $|\phi\rangle = |v_1, v_2, \cdots, v_N\rangle$ be any N-particle basis state on G, with n_c particles on the c-th component of G, and where that the first n_1 vertices are in G_1, then next n_2 vertices are in G_2, and continuing for all components of G. Note that for all times $t \in \mathbb{R}$, $e^{-iA(G)t}|v_i\rangle$ only has support on the component of G to which v_i belongs, and thus $e^{-iA(G)t}|v_i\rangle = e^{-iA(G_{c_j})t}|v_i\rangle$ (with the natural identification between basis vectors in the smaller Hilbert space).

As the interaction term of (6.6) is diagonal in the computational basis, we have that for all times t, $e^{-iH_G^N t}|\phi\rangle$ only has support on states

$$\left\{|w_1, \cdots, w_N\rangle : \forall i \in [N], w_i \in V(G_{c_i})\right\}. \tag{6.20}$$

Further, as the interaction in (6.6) is finite range (and vertices in different components have infinite distance), this implies that only particles on the same component can interact, and the interaction is restricted to $H(G_c, n_c)$ for each component.

Combining these two results, we then have that, when restricted to states of the form $|\phi\rangle$, we have that the evolution according to H_G^N is equal to that of

$$e^{-iH_G^N t}|\phi\rangle = \prod_{c=1}^{M} \left(e^{-iH_{G_c}^{n_c} t}\right)^{(m_c+1, m_c+2, \cdots, m_c+n_c)}|\phi\rangle, \tag{6.21}$$

where $m_c = \sum_{j=1}^{c-1} n_c$. If we then use the fact that H_G^N commutes with all permutations of the underlying particles, and that states of the form $|\phi\rangle$ (and their permutations) span the relevant space, we then have (6.18). If we restrict ourselves to the case where each particle is on a separate component, the second equation follows immediately. □

Note that if we combine this lemma with the truncation lemma (Lemma 1), we have that when particles are separated from each other they almost evolve independently, as one might expect. We will use this intuition several times in the remainder of the thesis.

6.2 Two-particle scattering on an infinite path

After choosing a given interaction, equation (6.6) provides us with a well defined MPQW Hamiltonian for N-particles. With this, we can explicitly evolve a given state, and hopefully use such systems for algorithmic advantages. However, this requires an understanding of the eigenstates of a multi-particle interacting system, for which we have few examples of analytic solutions. On the other hand, we *can* analyze some highly symmetric systems, when we restrict ourselves to a small number of particles. Our understanding of these small systems can then be leveraged to gain some information about MPQW with many particles on some given graphs.

In particular, we already know from Chapter 3 the basic properties of a single particle moving on a long path. One might expect that that next step would be to understand two particles interacting on a similar scattering graph, but unfortunately even this is a little too complicated for this thesis. However, we can analyze two particles interacting on an infinite path.

Namely, let us assume that the interaction Hamiltonian has been chosen, such that there is a $d_{\max}$ and a set of $d+1$ symmetric functions U_d. We can then write the Hamiltonian (6.6) in the basis $|x, y\rangle$, where $x, y \in \mathbb{Z}$ are the positions of the first and second particles, as

$$H^2 = H^1 \otimes \mathbb{I}_y + \mathbb{I}_x \otimes H^1 + \sum_{x\in\mathbb{Z}} \sum_{d=0}^{d_{\max}} U_d(\hat{n}_x, \hat{n}_{x+d}), \tag{6.22}$$

where the single-particle Hamiltonian H^1 is simply the adjacency matrix for the infinite path, namely

$$H^1 = \sum_{x\in\mathbb{Z}} |x+1\rangle\langle x| + |x\rangle\langle x+1|. \tag{6.23}$$

Without the interaction term, the eigenstates for this Hamiltonian would simply by two independent scattering eigenstates, with amplitudes of the form $e^{ik_1x+ik_2y}$. However, the interaction causes there to be correlations between the two particles, and these correlations will be similar to the single particle interactions scattering off of a graph with two attached semi-infinite paths.

While our given Hamiltonian (6.22) is simple to define, in order to understand dynamics we will want to diagonalize it. Further, while the current basis does have a permutation invariance between the two particles, it does not make use of the translation invariance of the interaction. To make use of this symmetry, we will need to change to a different basis.

In particular, let us look at the new basis $|s; r\rangle$, where $s = x + y$ and $r = x - y$, and where the allowed values of (s, r) range over those values where s and r are either both even or both odd (i.e., $s + r$ must be even). If we then expand (6.22) in this basis, we find

$$H^{(1)} \otimes H^{(1)} + \mathbb{I} \otimes \sum_{r\in\mathbb{Z}} \mathcal{V}(|r|)\,|r\rangle\langle r|, \tag{6.24}$$

where $V(0) = U_0(2,2)$ and $V(r) = U_r(1,1)$ for $r > 0$.

Note that (6.24) looks to be much nicer to analyze than (6.22), as we nearly have a separable decomposition of the Hamiltonian. We do have a decomposition such that the eigenstates corresponding to s don't rely on the current state of r, and we will see that once we chose a particular eigenstate for the s, the corresponding eigenvalue equation for r will look exactly as a scaled single-particle scattering equation as in Chapter 3.

6.2.1 Eigenstates on the path

With the decomposition of (6.22) that nicely decouples the center of mass movement from the relative movement of two particles (i.e., the physical meaning of r and s), we can determine the eigenvalues and eigenvectors of the Hamiltonian.

Namely, let us make the ansatz that the eigenstates of (6.24) take the form

$$\langle s; r \,|\, \psi \rangle = e^{-ip_1 s/2} \langle r \,|\, \phi_{p_1} \rangle \tag{6.25}$$

where $p_1 \in (-\pi, \pi)$. With this assumption, we then have that the effective Hamiltonian for $|\, \phi_{p_1} \,\rangle$ takes the form

$$2\cos\left(\frac{p_1}{2}\right) H_r^{(1)} + \sum_{r \in \mathbb{Z}} \mathcal{V}(|r|) \,|\, r \rangle\langle\, r \,|. \tag{6.26}$$

Note that this is simply a rescaled single-particle scattering problem, as in Chapter 3, except where the weights of the graph gadget need not be normalized, and with a slight relabeling of the semi-infinite paths (i.e., the paths do not start from 1). We can then use the intuition from the chapter to see that for each $p_2 \in (0, \pi)$ there is a scattering eigenstate of the form

$$\langle r | \psi(p_1; p_2) \rangle = \begin{cases} e^{-ip_2 r} + R(p_1, p_2) e^{ip_2 r} & \text{if } r \leq -d_{\max} \\ f(p_1, p_2, r) & \text{if } |r| < d_{\max} \\ T(p_1, p_2) e^{-ip_2 r} & \text{if } r \geq d_{\max}. \end{cases} \tag{6.27}$$

for $p_2 \in (0, \pi)$. Here the reflection and transmission coefficients R and T and the amplitudes of the scattering state for $|r| < d_{\max}$ (described by the function f) depend on both momenta as well as the interaction $\mathcal{V}$. With R, T, and f chosen appropriately, the state $|\mathrm{sc}(p_1; p_2)\rangle$ is an eigenstate of $H^{(2)}$ with eigenvalue $4\cos(p_1/2)\cos(p_2)$. While it is not possible to give an explicit closed-form solution for all interactions, the form of (6.27) will be sufficient for most of our purposes.

Additionally, we can use the fact that $\mathcal{V}(|r|)$ is an even function of r to also define scattering states for $p_2 \in (-\pi, 0)$ by

$$\langle s; r | \mathrm{sc}(p_1; p_2) \rangle = \langle s; -r | \mathrm{sc}(p_1; -p_2) \rangle. \tag{6.28}$$

These other states are obtained by swapping x and y, corresponding to interchanging the two particles.

While we will not need a complete basis for for this Hamiltonian, note that if there are any bound states of (6.26), then there will be corresponding traveling states where the two particles move together. These are the well known dimer states, and while they are important to find a basis for the entire Hilbert space they will play a role similar to the bound states of single-particle scattering; only exponentially small amplitude of the states of interest will be on these states, and thus we will neglect their study.

The construction of the symmetric and anti-symmetric scattering states follows as one would expect. For $p_1 \in (-\pi, \pi)$ and $p_2 \in (0, \pi)$, we define

$$|\mathrm{sc}(p_1; p_2)\rangle_\pm = \frac{1}{\sqrt{2}}\big(|\mathrm{sc}(p_1; p_2)\rangle \pm |\mathrm{sc}(p_1; -p_2)\rangle\big). \tag{6.29}$$

If we note that the unitarity of the underlying scattering matrix S and the fact that $V(|r|)$ being even in r forces $R(p_1, p_2) = R(p_1, -p_2)$ and $T(p_1, p_2) = T(p_1, -p_2)$ we can then see that the combinations

$$|T(p_1, p_2) \pm R(p_1, p_2)| = 1. \tag{6.30}$$

With this, we can then see that the symmeterized scattering states can be expanded as

$$\langle s; r\,|\mathrm{sc}(p_1; p_2)\rangle_\pm = \frac{1}{\sqrt{2}} e^{-ip_1 s/2} \begin{cases} e^{-ip_2 r} \pm e^{i\theta_\pm(p_1,p_2)} e^{ip_2 r} & \text{if } r \le -C \\ f(p_1, p_2, r) \pm f(p_1, -p_2, -r) & \text{if } |r| < C \\ e^{i\theta_\pm(p_1,p_2)} e^{-ip_2 r} \pm e^{ip_2 r} & \text{if } r \ge C, \end{cases} \tag{6.31}$$

where $\theta_\pm(p_1; p_2)$ is a real function defined through

$$e^{i\theta_\pm(p_1;p_2)} = T(p_1; p_2) \pm R(p_1; p_2). \tag{6.32}$$

These eigenstates allow us to understand what happens when two particles with momenta $k_1 \in (-\pi, 0)$ and $k_2 \in (0, \pi)$ move toward each other. Here $p_1 = -k_1 - k_2$ and $p_2 = (k_2 - k_1)/2$. Similar to the scattering states of Chapter 3, we have that for $|r| \ge C$ the scattering state is a sum of two terms, one corresponding to the two particles moving toward each other and one corresponding to the two particles moving apart after scattering, but where the outgoing term has a phase of $T \pm R$ relative to the incoming term (as depicted in Figure 6.1). This phase arises from the interaction between the two particles.

In particular, we can transform (6.31) to the (x, y) basis as

$$\begin{aligned} &\langle x, y\,|\mathrm{sc}(k_1, k_2)\rangle_\pm \\ &\quad = \frac{1}{\sqrt{2}} e^{i(k_1+k_2)\frac{x+y}{2}} \begin{cases} e^{i(k_1-k_1)\frac{x-y}{2}} \pm e^{i\theta_\pm(k_1,k_2)} e^{i(k_2-k_2)\frac{x-y}{2}} & \text{if } x - y \le -C \\ f\Big(-k_1 - k_2, \frac{k_2-k_1}{2}, x - y\Big) \pm f(-k_1 - k_2, \frac{k_1-k_2}{2}, y - x) & \text{if } |x - y| < C \\ e^{i\theta_\pm(k_1,k_2)} e^{i(k_1-k_2)\frac{x-y}{2}} \pm e^{i(k_2-k_1)\frac{x-y}{2}} & \text{if } x - y \ge C, \end{cases} \end{aligned} \tag{6.33}$$

where we defined $\theta_\pm(k_1, k_2) = \theta_\pm(-k_1 - k_2; (k_2 - k_1)/2)$.

6.2.2 Examples

While our understanding of two-particle scattering for arbitrary interactions is useful, as we know that for almost any interaction the form of the eigenstates are scattering states, it will be useful to instantiate our claims and have explicit examples for the functions $\theta_\pm$.

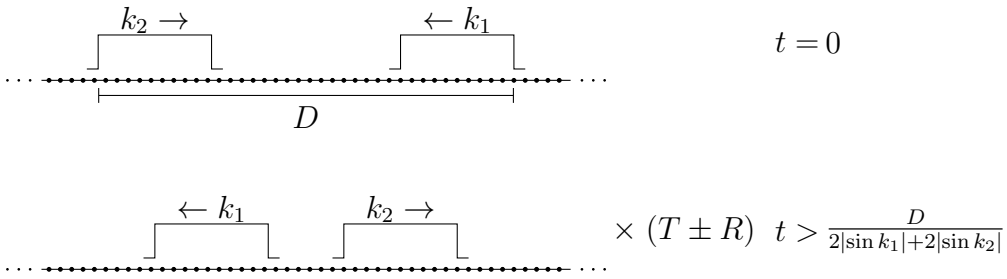

Figure 6.1: Scattering of two particles on an infinite path.

6.2.2.1 Bose-Hubbard model

If we consider the Bose-Hubbard model for two particles, we have $\mathcal{V}(|r|) = \mathcal{U}_0^{2,2}\delta_{r,0}$. Here $C = 0$ and $T = 1 + R$. In this case the scattering state $|\mathrm{sc}(p_1; p_2)\rangle_+$ is

$$\langle x, y|\mathrm{sc}(p_1; p_2)\rangle_+ = \frac{1}{\sqrt{2}} e^{-ip_1\left(\frac{x+y}{2}\right)} \left(e^{ip_2|x-y|} + e^{i\theta_+(p_1,p_2)} e^{-ip_2|x-y|}\right). \tag{6.34}$$

The first term describes the two particles moving toward each other and the second term describes them moving away from each other. To solve for the applied phase $e^{i\theta_+(p_1,p_2)}$ we look at the eigenvalue equation for $|\psi(p_1; p_2)\rangle$ at $r = 0$. This gives

$$R(p_1, p_2) = -\frac{\mathcal{U}_0^{2,2}}{\mathcal{U}_0^{2,2} - 4i\cos(p_1/2)\sin(p_2)}. \tag{6.35}$$

So for the Bose-Hubbard model,

$$e^{i\theta_+(p_1,p_2)} = T(p_1, p_2) + R(p_1, p_2) = -\frac{\mathcal{U}_0^{2,2} + 4i\cos(p_1/2)\sin(p_2)}{\mathcal{U}_0^{2,2} - 4i\cos(p_1/2)\sin(p_2)} = \frac{2\left(\sin(k_2) - \sin(k_1)\right) - i\mathcal{U}_0^{2,2}}{2\left(\sin(k_2) - \sin(k_1)\right) + i\mathcal{U}_0^{2,2}}. \tag{6.36}$$

For example, if $\mathcal{U}_0^{2,2} = 2 + \sqrt{2}$ then two particles with momenta $k_1 = -\pi/2$ and $k_2 = \pi/4$ acquire a phase of $e^{-i\pi/2} = -i$ after scattering.

6.2.2.2 Nearest-neighbor interaction

[**TO DO:** *if time, find perfect reflection with good momenta*]

For a multi-particle quantum walk with nearest-neighbor interactions, $\mathcal{V}(|r|) = \mathcal{U}_1^{1,1}\delta_{|r|,1}$ and $C = 1$. In this case the eigenvalue equations for $|\psi(p_1; p_2)\rangle$ at $r = -1$, $r = 1$, and $r = 0$ are

$$4\cos\left(\frac{p_1}{2}\right)\cos(p_2)(e^{ip_2} + R(p_1, p_2)e^{-ip_2}) = U_1^{1,1}(e^{ip_2} + R(p_1, p_2)e^{-ip_2}) \tag{6.37}$$

$$+ 2\cos\left(\frac{p_1}{2}\right)\left(e^{2ip_2} + R(p_1, p_2)e^{-2ip_2} + f(p_1, p_2, 0)\right) \tag{6.38}$$

$$4\cos\left(\frac{p_1}{2}\right)\cos(p_2)T(p_1, p_2)e^{-ip_2} = U_1^{1,1}T(p_1, p_2)e^{-ip_2} \tag{6.39}$$

$$+ 2\cos\left(\frac{p_1}{2}\right)\left(f(p_1, p_2, 0) + T(p_1, p_2)e^{-2ip_2}\right) \tag{6.40}$$

$$2\cos(p_2)f(p_1, p_2, 0) = T(p_1, p_2)e^{-ip_2} + e^{ip_2} + R(p_1, p_2)e^{-ip_2}, \tag{6.41}$$

respectively.

Solving these equations for R, T, and $f(p_1, p_2, 0)$, we can construct the corresponding scattering states for bosons, fermions, or distinguishable particles. Unlike the case of the Bose-Hubbard model, we may not have $1 + R = T$. For example, when $U_1^{1,1} = -2 - \sqrt{2}$, $p_1 = \pi/4$, and $p_2 = 3\pi/8$, we get $R = 0$ and $T = i$.

Additionally, in the special case of $k_1 = \frac{2\pi}{3}$ and $k_2 = -\frac{\pi}{3}$, we have that

$$R = \frac{U_1^{1,1}}{U_1^{1,1} - i\sqrt{3}} \qquad T = 1 - R = \frac{\sqrt{3}}{\sqrt{3} + iU_1^{1,1}}, \tag{6.42}$$

and thus $\theta_+(k_1, k_2) = 0$, while

$$e^{i\theta_-(k_1,k_2)} = -\frac{U_1^{1,1} + i\sqrt{3}}{U_1^{1,1} - i\sqrt{3}}. \tag{6.43}$$

In this way, we have that the symmetric subspace has no acquired phase, while the anti-symmetric does acquire a phase.

6.2.3 Two-particle orthonormality

While the states $|\mathrm{sc}(p_1; p_2)\rangle$ do not necessarily span the entire Hilbert space, they will span the portion of the space that will be needed for this thesis. However, we will need that they satisfy some orthogonality constraints, and in particular that they are (delta-function) orthonormal. As such, we have that the states $\{|\mathrm{sc}(p_1; p_2)\rangle \colon p_1 \in (-\pi, \pi),\ p_2 \in (-\pi, 0) \cup (0, \pi)\}$ have the following inner product:

$$\begin{aligned}
\langle \mathrm{sc}(p_1'; p_2') | \mathrm{sc}(p_1; p_2)\rangle &= \langle \mathrm{sc}(p_1'; p_2')| \left(\sum_{r,\, s \text{ even}} |r\rangle\langle r| \otimes |s\rangle\langle s| \right) |\mathrm{sc}(p_1; p_2)\rangle \\
&\quad + \langle \mathrm{sc}(p_1'; p_2')| \left(\sum_{r,\, s \text{ odd}} |r\rangle\langle r| \otimes |s\rangle\langle s| \right) |\mathrm{sc}(p_1; p_2)\rangle \qquad (6.44) \\
&= \sum_{s \text{ even}} e^{-i(p_1 - p_1')s/2} \sum_{r \text{ even}} \langle \psi(p_1'; p_2')|r\rangle\langle r|\psi(p_1; p_2)\rangle \\
&\quad + \sum_{s \text{ odd}} e^{-i(p_1 - p_1')s/2} \sum_{r \text{ odd}} \langle \psi(p_1'; p_2')|r\rangle\langle r|\psi(p_1; p_2)\rangle \qquad (6.45) \\
&= 2\pi\delta(p_1 - p_1') \sum_{r=-\infty}^{\infty} \langle \psi(p_1; p_2')|r\rangle\langle r|\psi(p_1; p_2)\rangle \qquad (6.46) \\
&= 4\pi^2 \delta(p_1 - p_1')\delta(p_2 - p_2') \qquad (6.47)
\end{aligned}$$

where in the last step we used the fact that $\langle \psi(p_1; p_2')|\psi(p_1; p_2)\rangle = 2\pi\delta(p_2 - p_2')$, which can be derived from Lemma 4.

6.3 Wave-packet scattering

Now that we have an understanding of the two-particle scattering eigenstates on an infinite path, we will want to understand the time-evolution of wave-packets on the infinite path. In particular,

if we initially have a product state corresponding to two Gaussian wave-packets traveling towards each other, how does the time-evolved state look?

We would expect that the two wave-packets would simply evolve forward in time, where the center of the wave-packets each move with a speed $2\sin k_i$, possibly acquiring a phase if they move past each other. It turns out that this is exactly what happens, but proving the fact is a little complicated.

[**TO DO:** *put everything inside margins!*]

Along these lines, this section is focused on proving the following lemma discussing wave-packet propagation:

Theorem 5. *Let $H^{(2)}$ be a two-particle Hamiltonian of the form (6.6) with interaction range at most d. Let $\theta_\pm(p_1;p_2)$ be given by equation (6.32) (with associated $\theta_\pm(k_1,k_2)$). Let $k_1 \in (-\pi, 0)$ and let $k_2 \in (0,\pi)$, let $L, \mu, \nu \in \mathbb{N}$ with $L > 0$ and and let $\sigma > 0$. Let us then define the states*

$$|\alpha(t)\rangle_\pm = \frac{\gamma}{\sqrt{2}} e^{-2it(\cos k_1 + \cos k_2)} \sum_{x=\mu(t)-L}^{\mu(t)+L} \sum_{y=\nu(t)-L}^{\nu(t)+L} e^{-\frac{(x-\mu(t))^2}{2\sigma^2} - \frac{(y-\nu(t))^2}{2\sigma^2}} e^{ik_1 x + ik_2 y} \alpha_{xy} \big(|x,y\rangle \pm |y,x\rangle \big), \tag{6.48}$$

where

$$\mu(t) = \mu - \lceil 2t \sin k_1 \rceil, \quad \nu(t) = \nu - \lceil 2t \sin k_2 \rceil, \qquad \alpha_{xy} = \begin{cases} 1 & y - x > r \\ e^{i\theta_\pm(k_1,k_2)} & x - y > r \\ 0 & \text{otherwise,} \end{cases} \tag{6.49}$$

and

$$\gamma^{-2} = \sum_{x,y=-L}^{L} e^{-\frac{1}{\sigma^2}(x^2+y^2)} = \left(h_L^{\sigma/\sqrt{2}}(0) \right)^2. \tag{6.50}$$

Additionally, let us define the initial state

$$|\psi(0)\rangle_\pm = |\alpha(0)\rangle_\pm. \tag{6.51}$$

If $\sigma = \frac{L}{2\sqrt{\log L}}$, and if $0 \le t < cL$ for some constant c, then

$$\| e^{-iH^2 t} |\psi(0)\rangle_\pm - |\alpha(t)\rangle \|_\pm \le 4 \sqrt{\frac{c \log L}{L}}. \tag{6.52}$$

Note that we will use many of the tools used in the proof of Theorem **??**, and in particular we use the function $h_L^\sigma(\phi)$ several times.

Proof. We will first want to show that our approximation to the time-evolved state is a nearly

normalized state. In particular, we have that

$$
\begin{aligned}
&{}_{\pm}\langle \alpha(t) \,|\, \alpha(t) \rangle_{\pm} \\
&\quad = \gamma^2 \Bigg[\sum_{x=\mu(t)-L}^{\mu(t)+L} \sum_{y=\nu(t)-L}^{\nu(t)+L} e^{-\frac{(x-\mu(t))^2}{\sigma^2} - \frac{(y-\nu(t))^2}{\sigma^2}} \\
&\qquad \pm \sum_{x,y=\max\{\mu(t),\nu(t)\}-L}^{\min\{\mu(t),\nu(t)\}+L} e^{-\frac{(x-\mu(t))^2+(x-\nu(t))^2+(y-\mu(t))^2+(y-\nu(t))^2}{2\sigma^2}} e^{i(k_1-k_2)x} e^{i(k_2-k_1)y} \alpha_{xy} \alpha_{yx}^* \\
&\qquad - \sum_{x=\max\{\mu(t),\nu(t)\}-L}^{\min\{\mu(t),\nu(t)\}+L} \sum_{y=\max\{x-d,\mu(t)-L,\nu(t)-L\}}^{\min\{x+d,\mu(t)+L,\nu(t)+L\}} e^{-\frac{(x-\mu(t))^2}{\sigma^2} - \frac{(y-\nu(t))^2}{\sigma^2}} \Bigg].
\end{aligned} \tag{6.53}
$$

While this is a rather complicated expression when $|\mu(t) - \nu(t)| \leq 2L$, for times outside this range only the first term is nonzero, and is in fact exactly γ^{-2}. Hence, for times when the two wave-packets do not overlap, our approximation $|\alpha(t)\rangle_{\pm}$ is exactly normalized. If we can show that the latter two terms are small for all times t, we will then have that our approximation is almost normalized, as we need.

Let us first inspect the second term in (6.53), corresponding to the cross terms between the two wave-packets. We can expand the sum as

$$
\begin{aligned}
&\sum_{x,y=\max\{\mu(t),\nu(t)\}-L}^{\min\{\mu(t),\nu(t)\}+L} e^{-\frac{(x-\mu(t))^2+(x-\nu(t))^2+(y-\mu(t))^2+(y-\nu(t))^2}{2\sigma^2}} e^{i(k_1-k_2)x} e^{i(k_2-k_1)y} \alpha_{xy} \alpha_{yx}^* \\
&\quad = e^{-i\theta_{\pm}} \sum_{\substack{x,y=\max\{\mu(t),\nu(t)\}-L \\ y-x>d}}^{\min\{\mu(t),\nu(t)\}+L} e^{-\frac{(x-\mu(t))^2+(x-\nu(t))^2+(y-\mu(t))^2+(y-\nu(t))^2}{2\sigma^2}} e^{i(k_1-k_2)x} e^{i(k_2-k_1)y} \\
&\qquad + e^{i\theta_{\pm}} \sum_{\substack{x,y=\max\{\mu(t),\nu(t)\}-L \\ x-y>d}}^{\min\{\mu(t),\nu(t)\}+L} e^{-\frac{(x-\mu(t))^2+(x-\nu(t))^2+(y-\mu(t))^2+(y-\nu(t))^2}{2\sigma^2}} e^{i(k_1-k_2)x} e^{i(k_2-k_1)y},
\end{aligned} \tag{6.54}
$$

and then inspect each of these two terms individually. We can then see

$$
\begin{aligned}
&\sum_{\substack{x,y=\max\{\mu(t),\nu(t)\}-L \\ y-x>d}}^{\min\{\mu(t),\nu(t)\}+L} e^{-\frac{(x-\mu(t))^2+(x-\nu(t))^2+(y-\mu(t))^2+(y-\nu(t))^2}{2\sigma^2}} e^{i(k_1-k_2)x} e^{i(k_2-k_1)y} \\
&\quad = \sum_{x=\max\{\mu(t),\nu(t)\}-L}^{\min\{\mu(t),\nu(t)\}+L} e^{-\frac{(x-\mu(t))^2+(x-\nu(t))^2}{2\sigma^2}} e^{i(k_1-k_2)x} \sum_{y=x+d+1}^{\min\{\mu(t),\nu(t)\}+L} e^{-\frac{(y-\mu(t))^2+(y-\nu(t))^2}{2\sigma^2}} e^{i(k_2-k_1)y}
\end{aligned} \tag{6.55}
$$

$$
\begin{aligned}
&\quad = \sum_{x=\max\{\mu(t),\nu(t)\}-L}^{\min\{\mu(t),\nu(t)\}+L} e^{-\frac{(x-\mu(t))^2+(x-\nu(t))^2}{2\sigma^2}} e^{i(k_1-k_2)x} e^{-\frac{(\mu(t)-\nu(t))^2}{4\sigma^2}} \sum_{y=x+d+1}^{\min\{\mu(t),\nu(t)\}+L} e^{-\frac{(y-\frac{\mu(t)+\nu(t)}{2})^2}{\sigma^2}} e^{i(k_2-k_1)y}.
\end{aligned} \tag{6.56}
$$

Now, this second sum is simply a finite Gaussian approximation related to the h function from

Chapter 3, with an offset from the center. From this, we have

$$\sum_{y=x+d+1}^{\min\{\mu(t),\nu(t)\}+L} e^{-\frac{(y-\frac{\mu(t)+\nu(t)}{2})^2}{\sigma^2}} e^{i(k_2-k_1)y} = e^{i(k_2-k_1)\frac{\mu(t)+\nu(t)}{2}} \sum_{y=x+d+1-\frac{\mu(t)+\nu(t)}{2}}^{\min\{\mu(t),\nu(t)\}+L-\frac{\mu(t)+\nu(t)}{2}} e^{-\frac{y^2}{\sigma^2}} e^{i(k_2-k_1)y}. \tag{6.57}$$

Assuming that $\mu(t)+\nu(t)$ is even, this is simply

$$\begin{aligned} &e^{i(k_1-k_2)\frac{\mu(t)+\nu(t)}{2}} \sum_{y=x+d+1}^{\min\{\mu(t),\nu(t)\}+L} e^{-\frac{(y-\frac{\mu(t)+\nu(t)}{2})^2}{\sigma^2}} e^{i(k_2-k_1)y} \\ &= \begin{cases} V^{\frac{\sigma}{\sqrt{2}}}_{1,\frac{\mu(t)+\nu(t)}{2}-x-d-1}(k_1-k_2)+1+V^{\frac{\sigma}{\sqrt{2}}}_{1,L-\frac{|\mu(t)-\nu(t)|}{2}}(k_2-k_1) & \mu(t)+\nu(t)>2(x+d+1) \\ V^{\frac{\sigma}{\sqrt{2}}}_{x+d+1-\frac{\nu(t)+\mu(t)}{2},L-\frac{|\nu(t)-\mu(t)|}{2}}(k_2-k_1) & \text{otherwise.} \end{cases} \end{aligned} \tag{6.58}$$

For both cases, we have that this is bounded by some constant value in norm by Lemma 6 from Chapter 3. If $\mu(t)+\nu(t)$ is odd, we can simply note that

$$\sum_{y=a}^{b} e^{-\frac{1}{\sigma^2}(y+\frac{1}{2})^2} e^{i\phi y} = e^{-i\frac{\phi}{2}} \sum_{y=a}^{b} e^{-\frac{(2y+1)^2}{4\sigma^2}} e^{i\frac{\phi}{2}(2y+1)} \tag{6.59}$$

$$= e^{-i\frac{\phi}{2}} \left[\sum_{z=2a+1}^{2b+1} e^{-\frac{z^2}{4\sigma^2}} e^{i\frac{\phi}{2}z} - \sum_{z=a}^{b} e^{-\frac{z^2}{\sigma^2}} e^{i\phi z} \right], \tag{6.60}$$

where both of the sums can be bounded by constants in norm in a manner similar to (6.58). As such, we have that for all times t,

$$\left| \sum_{y=x+d+1}^{\min\{\mu(t),\nu(t)\}+L} e^{-\frac{(y-\frac{\mu(t)+\nu(t)}{2})^2}{\sigma^2}} e^{i(k_2-k_1)y} \right| < \kappa \tag{6.61}$$

for some constant κ that might depend on L, σ, and k_2-k_1. We can then use this to bound the norm of (6.56) as

$$\begin{aligned} &\left| \sum_{\substack{x,y=\max\{\mu(t),\nu(t)\}-L \\ y-x>d}}^{\min\{\mu(t),\nu(t)\}+L} e^{-\frac{(x-\mu(t))^2+(x-\nu(t))^2+(y-\mu(t))^2+(y-\nu(t))^2}{2\sigma^2}} e^{i(k_1-k_2)x} e^{i(k_2-k_1)y} \right| \\ &\leq \kappa e^{-\frac{(\mu(t)-\nu(t))^2}{2\sigma^2}} \sum_{x=\max\{\mu(t),\nu(t)\}-L}^{\min\{\mu(t),\nu(t)\}+L} e^{-\frac{\left(x-\frac{\mu(t)+\nu(t)}{2}\right)^2}{\sigma^2}} \qquad (6.62) \\ &\leq \kappa e^{-\frac{(\mu(t)-\nu(t))^2}{2\sigma^2}} h^{\sqrt{2}\sigma}_{\infty}(0) \qquad (6.63) \\ &\leq 6\sqrt{\pi}\sigma\kappa e^{-\frac{(\mu(t)-\nu(t))^2}{2\sigma^2}}, \qquad (6.64) \end{aligned}$$

where the second inequality arose since we didn't know whether $\mu(t)+\nu(t)$ was even or odd, and the third from our bounds on $h^{\sigma}_{\infty}(0)$. A similar argument gives the same bound for the sum with $x-y>d$.

For the third term in (6.53), we again use a rather simple approximation. Namely, we have

$$\sum_{x=\max\{\mu(t),\nu(t)\}-L}^{\min\{\mu(t),\nu(t)\}+L} \sum_{y=\max\{x-d,\mu(t)-L,\nu(t)-L\}}^{\min\{x+d,\mu(t)+L,\nu(t)+L\}} e^{-\frac{(x-\mu(t))^2}{\sigma^2}-\frac{(y-\nu(t))^2}{\sigma^2}} < (2d+1)h_\infty^{\sigma/\sqrt{2}}(0) \tag{6.65}$$

$$< (2d+1)2\sqrt{\pi}\sigma, \tag{6.66}$$

where we again used our bounds on $h_\infty^\sigma(0)$ from Lemma 5 from Chapter 3.

Putting these bounds together, we then have that

$$\begin{aligned}
&\Big|{}_\pm\langle \alpha(t)\,|\,\alpha(t)\rangle_\pm - 1\Big| \\
&\quad\leq \gamma^2\Bigg[\Bigg|\sum_{x,y=\max\{\mu(t),\nu(t)\}-L}^{\min\{\mu(t),\nu(t)\}+L} e^{-\frac{(x-\mu(t))^2+(x-\nu(t))^2+(y-\mu(t))^2+(y-\nu(t))^2}{2\sigma^2}} e^{i(k_1-k_2)x} e^{i(k_2-k_1)y}\alpha_{xy}\alpha^*_{yx}\Bigg| \\
&\qquad + \Bigg|\sum_{x=\max\{\mu(t),\nu(t)\}-L}^{\min\{\mu(t),\nu(t)\}+L} \sum_{y=\max\{x-d,\mu(t)-L,\nu(t)-L\}}^{\min\{x+d,\mu(t)+L,\nu(t)+L\}} e^{-\frac{(x-\mu(t))^2}{\sigma^2}-\frac{(y-\nu(t))^2}{\sigma^2}}\Bigg|\Bigg] \qquad (6.67)\\
&\quad\leq \gamma^2\left[2\left(6\sqrt{\pi}\sigma\kappa e^{-\frac{(\mu(t)-\nu(t))^2}{2\sigma^2}}\right) + 2(2d+1)\sqrt{\pi}\sigma\right] \qquad (6.68)\\
&\quad\leq 2\sqrt{\pi}\sigma\gamma^2\big(\kappa+2d+1\big). \qquad (6.69)
\end{aligned}$$

Since $\gamma^2 \propto \sigma^{-2}$, we then have that our normalization is then off by something bounded by $\mathcal{O}(\sigma^{-1})$, which will be sufficient for our purposes.

With the above bounds on the normalization, we can now analyze our approximations to the time-evolved states. We find that

$$\begin{aligned}
&{}_\pm\langle \mathrm{sc}(p_1;p_2)\,|\,\alpha(t)\rangle_\pm \\
&\quad= \frac{\gamma e^{-2it(\cos(k_1)+\cos(k_2))}}{\sqrt{2}} \sum_{x=\mu(t)-L}^{\mu(t)+L}\sum_{y=\nu(t)-L}^{\nu(t)+L} e^{ik_1x}e^{ik_2y}e^{-\frac{(x-\mu(t))^2}{2\sigma^2}}e^{-\frac{(y-\nu(t))^2}{2\sigma^2}}\beta_{x,y} \\
&\qquad\times\Big({}_\pm\langle \mathrm{sc}(p_1;p_2)\,|\,x,y\rangle \pm {}_\pm\langle \mathrm{sc}(p_1;p_2)\,|\,y,x\rangle\Big) \qquad (6.70)\\
&\quad= \gamma e^{-2it(\cos(k_1)+\cos(k_2))} \sum_{x=\mu(t)-L}^{\mu(t)+L}\sum_{\substack{y=\nu(t)-L\\ y>x+r}}^{\nu(t)+L} e^{ik_1x}e^{ik_2y}e^{-\frac{(x-\mu(t))^2}{2\sigma^2}}e^{-\frac{(y-\nu(t))^2}{2\sigma^2}} \\
&\qquad\times e^{i\frac{p_1}{2}(x+y)}\Big(e^{ip_2(x-y)} \pm e^{-i\theta_\pm(p_1;p_2)}e^{-ip_2(x-y)}\Big) \\
&\qquad+ \gamma e^{-2it(\cos(k_1)+\cos(k_2))} \sum_{x=\mu(t)-L}^{\mu(t)+L}\sum_{\substack{y=\nu(t)-L\\ y<x-r}}^{\nu(t)+L} e^{ik_1x}e^{ik_2y}e^{-\frac{(x-\mu(t))^2}{2\sigma^2}}e^{-\frac{(y-\nu(t))^2}{2\sigma^2}}e^{i\theta_\pm(k_1,k_2)} \\
&\qquad\times e^{i\frac{p_1}{2}(x+y)}\Big(e^{-i\theta_\pm(p_1;p_2)}e^{ip_2(x-y)} \pm e^{-ip_2(x-y)}\Big). \qquad (6.71)
\end{aligned}$$

While this is a rather complicated expression, if we break the terms into smaller pieces, we find

that

$$
\begin{aligned}
&{}_{\pm}\langle \mathrm{sc}(p_1;p_2)\,|\,\alpha(t)\rangle_{\pm} \\
&\quad= \gamma e^{-2it(\cos(k_1)+\cos(k_2))}\Bigg[\sum_{x=\mu(t)-L}^{\mu(t)+L}\sum_{\substack{y=\nu(t)-L\\ y>x+r}}^{\nu(t)+L} e^{-\frac{(x-\mu(t))^2}{2\sigma}-\frac{(y-\nu(t))^2}{2\sigma^2}} e^{i\left(\frac{k_1+k_2}{2}+\frac{p_1}{2}\right)(x+y)} \\
&\qquad\times\left(e^{i\left(\frac{k_1-k_2}{2}+p_2\right)(x-y)} \pm e^{-i\theta_{\pm}(p_1;p_2)} e^{i\left(\frac{k_1-k_2}{2}-p_2\right)(x-y)}\right) \\
&\qquad+\sum_{x=\mu(t)-L}^{\mu(t)+L}\sum_{\substack{y=\nu(t)-L\\ y<x-r}}^{\nu(t)+L} e^{-\frac{(x-\mu(t))^2}{2\sigma}-\frac{(y-\nu(t))^2}{2\sigma^2}} e^{i\left(\frac{k_1+k_2}{2}+\frac{p_1}{2}\right)(x+y)} \\
&\qquad\times\left(e^{i\left(\theta_{\pm}(k_1,k_2)-\theta_{\pm}(p_1;p_2)\right)} e^{i\left(\frac{k_1-k_2}{2}+p_2\right)(x-y)} \pm e^{i\theta_{\pm}(k_1,k_2)} e^{i(\frac{k_1-k_2}{2}-p_2)(x-y)}\right)\Bigg] \qquad (6.72)
\end{aligned}
$$

$$
\begin{aligned}
&= \gamma e^{-2it(\cos(k_1)+\cos(k_2))}\Bigg[\sum_{x=\mu(t)-L}^{\mu(t)+L}\sum_{y=\nu(t)-L}^{\nu(t)+L} e^{-\frac{(x-\mu(t))^2}{2\sigma^2}-\frac{(y-\nu(t))^2}{2\sigma^2}} e^{i(k_1+\frac{p_1}{2}+p_2)x} e^{i(k_2+\frac{p_1}{2}-p_2)y} \\
&\quad+\left(e^{i(\theta_{\pm}(k_1,k_2)-\theta_{\pm}(p_1;p_2))}-1\right)\sum_{x=\mu(t)-L}^{\mu(t)+L}\sum_{\substack{y=\nu(t)-L\\ y>x+r}}^{\nu(t)+L} e^{-\frac{(x-\mu(t))^2}{2\sigma^2}-\frac{(y-\nu(t))^2}{2\sigma^2}} e^{i(k_1+\frac{p_1}{2}+p_2)x} e^{i(k_2+\frac{p_1}{2}-p_2)y} \\
&\quad\pm\left(e^{-i\theta_{\pm}(p_1;p_2)}\delta_{\mu(t)\le\nu(t)}+e^{i\theta_{\pm}(k_1,k_2)}\delta_{\mu(t)>\nu(t)}\right)\sum_{x=\mu(t)-L}^{\mu(t)+L}\sum_{y=\nu(t)-L}^{\nu(t)+L} e^{-\frac{(x-\mu(t))^2}{2\sigma^2}-\frac{(y-\nu(t))^2}{2\sigma^2}} e^{i(k_1+\frac{p_1}{2}-p_2)x} e^{i(k_2+\frac{p_1}{2}+p \\
&\quad\pm\delta_{\mu(t)\le\nu(t)}\left(e^{i\theta_{\pm}(k_1,k_2)}-e^{-i\theta_{\pm}(p_1;p_2)}\right)\sum_{x=\mu(t)-L}^{\mu(t)+L}\sum_{\substack{y=\nu(t)-L\\ y<x-r}}^{\nu(t)+L} e^{-\frac{(x-\mu(t))^2}{2\sigma}-\frac{(y-\nu(t))^2}{2\sigma^2}} e^{i(k_1+\frac{p_1}{2}-p_2)x} e^{i(k_2+\frac{p_1}{2}+p_2)y} \\
&\quad\pm\delta_{\mu(t)>\nu(t)}\left(e^{-i\theta_{\pm}(p_1;p_2)}-e^{i\theta_{\pm}(k_1,k_2)}\right)\sum_{x=\mu(t)-L}^{\mu(t)+L}\sum_{\substack{y=\nu(t)-L\\ y>x+r}}^{\nu(t)+L} e^{-\frac{(x-\mu(t))^2}{2\sigma}-\frac{(y-\nu(t))^2}{2\sigma^2}} e^{i(k_1+\frac{p_1}{2}-p_2)x} e^{i(k_2+\frac{p_1}{2}+p_2)y} \\
&\quad-\sum_{x=\mu(t)-L}^{\mu(t)+L}\sum_{\substack{y=\nu(t)-L\\ |x-y|\le r}}^{\nu(t)+L} e^{-\frac{(x-\mu(t))^2}{2\sigma}-\frac{(y-\nu(t))^2}{2\sigma^2}}\Bigg(e^{i(k_1+\frac{p_1}{2}+p_2)x} e^{i(k_2+\frac{p_1}{2}-p_2)y} \\
&\quad\pm\left(e^{-i\theta_{\pm}(p_1;p_2)}\delta_{\mu(t)\le\nu(t)}+e^{i\theta_{\pm}(k_1,k_2)}\delta_{\mu(t)>\nu(t)}\right)e^{i(k_1+\frac{p_1}{2}-p_2)x} e^{i(k_2+\frac{p_1}{2}+p_2)y}\Bigg)\Bigg]. \qquad (6.73)
\end{aligned}
$$

While this expansion takes up much more room than before, it nicely organizes each of the terms in the inner product. Depending on the value of p_1 and p_2, most of the norm in (6.73) is on either the first or the third terms, with the rest small corrections. In fact, the first of these terms is proportional to $h_L^{\sigma}(k_1+p_1/2+p_2)h_L^{\sigma}(k_2+p_1/2-p_2)$, while the second is similar but with $p_2 \mapsto -p_2$.

With a decent understanding of these inner products, we can now define a Gaussian approximation to our assumed approximation of the time-evolved states. In particular, since most of the norm is contained on terms proportional to a product of $h_L^{\sigma}(\theta)$, our approximated time-evolved states will be centered about those p_1 and p_2 such that the $\theta \approx 0$. Explicitly, let us then define the

states

$$|w(t)\rangle = \eta e^{-2it(\cos k_1+\cos k_2)} \int_{-\delta}^{\delta}\int_{-\delta}^{\delta} \frac{d\phi_1 d\phi_2}{4\pi^2} e^{i\phi_1\left(\frac{\mu(t)+\nu(t)}{2}\right)} e^{i\phi_2(\mu(t)-\nu(t))} e^{-\frac{\sigma^2\phi_1^2}{4}} e^{-\sigma^2\phi_2^2} |\mathrm{sc}(p_1+\phi_1; p_2+\phi_2)\rangle_{\pm} \tag{6.74}$$

where

$$p_1 = -k_1 - k_2 \qquad p_2 = \frac{k_2-k_1}{2} \qquad \eta^{-2} = \int_{-\infty}^{\infty}\int_{-\infty}^{\infty} \frac{d\phi_1 d\phi_2}{4\pi^2} e^{-\sigma^2\left(\frac{\phi_1^2}{2}+2\phi_2^2\right)} = \frac{1}{4\pi\sigma^2}, \tag{6.75}$$

and δ is a constant that we will define later. While the states $|w(t)\rangle$ are not exactly normalized, we have that

$$\langle w(t)|w(t)\rangle = \eta^2 \iint_{-\delta}^{\delta}\int_{-\delta}^{\delta} \frac{d\phi_1 d\phi_2}{4\pi^2} e^{-\sigma^2\left(\frac{\phi_1^2}{2}+2\phi_2^2\right)} = 1 - \frac{\eta^2}{\pi^2}\int_{\delta}^{\infty}\int_{\delta}^{\infty} d\phi_1 d\phi_2 e^{-\sigma^2\left(\frac{\phi_1^2}{2}+2\phi_2^2\right)} \tag{6.76}$$

$$\geq 1 - \frac{1}{\pi\delta^2\sigma^2} e^{-\frac{5\sigma^2\delta^2}{2}}, \tag{6.77}$$

and as the second term on the right hand side of (6.76) is non-negative, we have that $\langle w(t)|w(t)\rangle \leq 1$.

We will now want to understand the relationship between the $|\alpha(t)\rangle$ and $|w(t)\rangle$, as we did in the proof of Theorem **??**. We then have

$$\begin{aligned}\langle w(t)|\alpha(t)\rangle_{\pm} &= \eta e^{2it(\cos k_1+\cos k_2)} \int_{-\delta}^{\delta} \frac{d\phi_1 d\phi_2}{4\pi^2} e^{-i\phi_1\frac{\mu(t)+\nu(t)}{2}} e^{i\phi_1(\nu(t)-\mu(t))} e^{-\frac{\sigma^2\phi_1^2}{4}-\sigma^2\phi_2^2} \\ &\quad {}_{\pm}\langle \mathrm{sc}(p_1+\phi_1; p_2+\phi_2)|\alpha(t)\rangle_{\pm}.\end{aligned} \tag{6.78}$$

It will then be worthwhile to expand ${}_{\pm}\langle \mathrm{sc}(p_1+\phi_2; p_2+\phi_2)|\alpha(t)\rangle_{\pm}$ as in (6.73), and bound the norm for each term individually. By contracting terms and by a slight relabelling of the dummy variable used for the sums, we then have the first term in the integrand for (6.78) is exactly

$$\iint_{-\delta}^{\delta} \frac{d\phi_1 d\phi_2}{4\pi^2} e^{-\frac{\sigma^2\phi_1^2}{2}-\sigma^2\phi_2^2} h_L^{\sigma}\left(\frac{\phi_1}{2}+\phi_2\right) h_L^{\sigma}\left(\frac{\phi_1}{2}-\phi_2\right) \tag{6.79}$$

$$\begin{aligned}&= \iint_{-\delta}^{\delta} \frac{d\phi_1 d\phi_2}{4\pi^2} e^{-\frac{\sigma^2\phi_1^2}{2}-\sigma^2\phi_2^2} \Bigg[h_{\infty}^{\sigma}\left(\frac{\phi_1}{2}+\phi_2\right) h_{\infty}^{\sigma}\left(\frac{\phi_1}{2}-\phi_2\right) \\ &\quad + h_{\infty}^{\sigma}\left(\frac{\phi_1}{2}+\phi_2\right)\left[h_L^{\sigma}\left(\frac{\phi_1}{2}-\phi_2\right) - h_{\infty}^{\sigma}\left(\frac{\phi_1}{2}-\phi_2\right)\right] \\ &\quad + \left[h_L^{\sigma}\left(\frac{\phi_1}{2}+\phi_2\right) - h_{\infty}^{\sigma}\left(\frac{\phi_1}{2}+\phi_2\right)\right] h_L^{\sigma}\left(\frac{\phi_1}{2}-\phi_2\right)\Bigg].\end{aligned} \tag{6.80}$$

Again, there are several integrals, but most of the amplitude is contained on the first. For the first

term, we can actually show that the integral is at least

$$\int_{-\delta}^{\delta}\int_{-\delta}^{\delta}\frac{d\phi_1 d\phi_2}{4\pi^2}e^{-\frac{\sigma^2\phi_1^2}{4}-\sigma^2\phi_2^2}h_\infty^\sigma\Big(\frac{\phi_1}{2}-\phi_2\Big)h_\infty^\sigma\Big(\frac{\phi_1}{2}+\phi_2\Big)$$

$$=\frac{\sigma^2}{2\pi}\int_{-\delta}^{\delta}\int_{-\delta}^{\delta}d\phi_1 d\phi_2 e^{-\frac{\sigma^2\phi_1^2}{2}-2\sigma^2\phi_2^2}h_\infty^{1/(2\pi\sigma)}\Big[2\pi i\sigma^2\Big(\frac{\phi_1}{2}-\phi_2\Big)\Big]h_\infty^{1/(2\pi\sigma)}\Big[2\pi i\sigma^2\Big(\frac{\phi_1}{2}+\phi_2\Big)\Big] \tag{6.81}$$

$$\geq\frac{\sigma^2}{2\pi}\int_{-\delta}^{\delta}\int_{-\delta}^{\delta}d\phi_1 d\phi_2 e^{-\frac{\sigma^2\phi_1^2}{2}-2\sigma^2\phi_2^2} \tag{6.82}$$

$$=\frac{1}{2}\langle w(t)\,|\,w(t)\rangle \tag{6.83}$$

where we used the fact that $h_\infty^\sigma(i\phi)\geq 1$ for real ϕ. Using the upper bounds on h from Lemma 5, we also have that

$$\int_{-\delta}^{\delta}\int_{-\delta}^{\delta}\frac{d\phi_1 d\phi_2}{4\pi^2}e^{-\frac{\sigma^2\phi_1^2}{4}-\sigma^2\phi_2^2}h_\infty^\sigma\Big(\frac{\phi_1}{2}-\phi_2\Big)h_\infty^\sigma\Big(\frac{\phi_1}{2}+\phi_2\Big)$$

$$\leq\frac{\sigma^2}{2\pi}\int_{-\delta}^{\delta}\int_{-\delta}^{\delta}d\phi_1 d\phi_2 e^{-\frac{\sigma^2\phi_1^2}{2}-2\sigma^2\phi_2^2}\left[1+2\Big(1+\frac{1}{\pi\sigma^2}\frac{1}{4\pi-|\phi_1-2\phi_2|}\Big)e^{-2\pi^2\sigma^2+\pi\sigma^2(\phi_1-2\phi_2)}\right]$$

$$\times\left[1+2\Big(1+\frac{1}{\pi\sigma^2}\frac{1}{4\pi-|\phi_1+2\phi_2|}\Big)e^{-2\pi^2\sigma^2+\pi\sigma^2(\phi_1+2\phi_2)}\right] \tag{6.84}$$

$$\leq\frac{1}{2}\Big[1+3e^{-\pi^2\sigma^2(2\pi-3\delta)}\Big]^2\langle w(t)\,|\,w(t)\rangle \tag{6.85}$$

where we assumed that $2\pi>3\delta$, and that $\sigma\geq 1$.

For the second and third terms of (6.80), note that for any real φ_1, φ_2, and for any $L_1, L_2>\sigma\geq 1$, we have that

$$\Big|h_{L_1}^\sigma(\varphi_1)\big(h_{L_2}^\sigma(\varphi_2)-h_\infty^\sigma(\varphi_2)\big)\Big|$$

$$\leq\big|h_\infty^\sigma(0)\big|\frac{2\sigma^2}{L_2}e^{-\frac{L_2^2}{2\sigma^2}} \tag{6.86}$$

$$\leq\frac{2\sigma^2}{L}e^{-\frac{L^2}{2\sigma^2}}\Big[1+2(1+\sigma^2)e^{-\frac{1}{2\sigma^2}}\Big] \tag{6.87}$$

$$\leq\frac{6\sigma^4}{L}e^{-\frac{L^2}{2\sigma^2}}. \tag{6.88}$$

If we then use this bound for both of the integrands, we have

$$\begin{aligned}
&\left| \int_{-\delta}^{\delta}\int_{-\delta}^{\delta} \frac{d\phi_1 d\phi_2}{4\pi^2} e^{-\frac{\sigma^2\phi_1^2}{4}} e^{-\sigma^2\phi_2^2} \left[h_\infty^\sigma\Big(\frac{\phi_1}{2}+\phi_2\Big)\left[h_L^\sigma\Big(\frac{\phi_1}{2}-\phi_2\Big) - h_\infty^\sigma\Big(\frac{\phi_1}{2}-\phi_2\Big)\right]\right.\right. \\
&\qquad \left.\left. + \left[h_L^\sigma\Big(\frac{\phi_1}{2}+\phi_2\Big) - h_\infty^\sigma\Big(\frac{\phi_1}{2}+\phi_2\Big)\right] h_L^\sigma\Big(\frac{\phi_1}{2}-\phi_2\Big)\right]\right| \\
&\qquad \le 2\int_{-\delta}^{\delta}\int_{-\delta}^{\delta} \frac{d\phi_1 d\phi_2}{4\pi^2} e^{-\frac{\sigma^2\phi_1^2}{4}} e^{-\sigma^2\phi_2^2} \frac{6\sigma^4}{L} e^{-\frac{L^2}{2\sigma^2}} && (6.89)\\
&\qquad < \frac{3\sigma^4}{\pi^2 L} e^{-\frac{L^2}{2\sigma^2}} \int_{-\infty}^{\infty}\int_{-\infty}^{\infty} d\phi_1 d\phi_2 e^{-\frac{\sigma^2\phi_1^2}{4}} e^{-\sigma^2\phi_2^2} && (6.90)\\
&\qquad = \frac{6\sigma^2}{\pi L} e^{-\frac{L^2}{2\sigma^2}}. && (6.91)
\end{aligned}$$

From this, we then approximately know the norm of the first term in (6.78).

For the second term in (6.78), we will show that it can be bounded in norm, using the fact that the angle $\theta_\pm(p_1,p_2)$ is a bounded rational function of the momentum. From this, we know that it is differentiable as a function of both ϕ_1 and ϕ_2 on some neighborhood U of (p_1,p_2). Let us assume that δ is chosen so that $[-\delta,\delta]\times[-\delta,\delta]\subset U$, and now let

$$\Gamma = \max_{[-\delta,\delta]\times[-\delta,\delta]} \left|\nabla e^{i\theta_\pm(p_1+\phi_1,p_2+\phi_2)}\right|. \tag{6.92}$$

We then have that

$$\begin{aligned}
&\left| \iint_{-\delta}^{\delta} \frac{d\phi_1 d\phi_2}{4\pi^2} e^{-i\phi_1\frac{\mu(t)+\nu(t)}{2}} e^{i\phi_1(\nu(t)-\mu(t))} e^{-\frac{\sigma^2\phi_1^2}{4}-\sigma^2\phi_2^2} \right. \\
&\qquad \left. \times \left(e^{i(\theta_\pm(k_1,k_2)-\theta_\pm(p_1;p_2))}-1\right) \sum_{x=\mu(t)-L}^{\mu(t)+L} \sum_{\substack{y=\nu(t)-L \\ y>x+r}}^{\nu(t)+L} e^{-\frac{(x-\mu(t))^2}{2\sigma^2}-\frac{(y-\nu(t))^2}{2\sigma^2}} e^{i(k_1+\frac{p_1}{2}+p_2)x} e^{i(k_2+\frac{p_1}{2}-p_2)y} \right| \\
&\qquad < \iint_{-\delta}^{\delta} \frac{d\phi_1 d\phi_2}{4\pi^2} \Gamma\sqrt{\phi_1^2+\phi_2^2} e^{-\frac{\sigma^2\phi_1^2}{4}-\sigma^2\phi_2^2} h_L^\sigma(0) h_L^\sigma(0) && (6.93)\\
&\qquad < \frac{\Gamma\sigma^2}{2\pi} \iint_{-\infty}^{\infty} d\phi_1 d\phi_2 \sqrt{\phi_1^2+\phi_2^2} e^{-\frac{\sigma^2}{4}(\phi_1^2+\phi_2^2)} && (6.94)\\
&\qquad = \Gamma\sigma^2 \int_0^\infty r^2 e^{-\frac{\sigma^2}{4}r^2} dr && (6.95)\\
&\qquad = \frac{2\sqrt{\pi}\Gamma}{\sigma} && (6.96)
\end{aligned}$$

and we have a bound on the norm of the second term in (6.78).

The third term in (6.78) is bound in a manner very similar to the first term. In particular, can rearrange the sums, so that the term is proportional to the product of two $h_L^\sigma(\theta)$, where the θ is bounded away from 0. If we take the absolute value, so as to get rid of the extraneous phases, we

find that

$$\left| \int_{-\delta}^{\delta} \int_{-\delta}^{\delta} \frac{d\phi_1 d\phi_2}{4\pi^2} e^{-\frac{\sigma^2\phi_1^2}{4} - \sigma^2\phi_2^2} \left(e^{-i\theta_{\pm}(p_1;p_2)} \delta_{\mu(t)\leq\nu(t)} + e^{i\theta_{\pm}(k_1,k_2)} \delta_{\mu(t)>\nu(t)} \right) \right.$$
$$\left. e^{i(k_1-k_2-2\phi_2)\mu(t)} e^{i(k_2-k_1+2\phi_2)\nu(t)} h_L^{\sigma}\Big(k_1 - k_2 + \frac{\phi_1}{2} - \phi_2\Big) h_L^{\sigma}\Big(k_2 - k_1 + \frac{\phi_1}{2} + \phi_2\Big) \right|$$
$$\leq \iint_{-\delta}^{\delta} \frac{d\phi_1 d\phi_2}{4\pi^2} e^{-\frac{\sigma^2\phi_1^2}{4} - \sigma^2\phi_2^2} \left| h_L^{\sigma}\Big(k_1 - k_2 + \frac{\phi_1}{2} - \phi_2\Big) h_L^{\sigma}\Big(k_2 - k_1 + \frac{\phi_1}{2} + \phi_2\Big) \right|. \quad (6.97)$$

If we then approximate the h_L by h_σ, as we did for the first term, we can use the exact same bound for the difference, as there was no reliance on the arguments to the h functions, other than that they were purely real. As such, we need only bound the above integral for infinite h's.

$$\iint_{-\delta}^{\delta} \frac{d\phi_1 d\phi_2}{4\pi^2} e^{-\frac{\sigma^2\phi_1^2}{4} - \sigma^2\phi_2^2} \left| h_{\infty}^{\sigma}\Big(k_1 - k_2 + \frac{\phi_1}{2} - \phi_2\Big) h_{\infty}^{\sigma}\Big(k_2 - k_1 + \frac{\phi_1}{2} + \phi_2\Big) \right|$$
$$\leq \frac{\sigma^2}{2\pi} \iint_{-\delta}^{\delta} e^{-\sigma^2\left(\frac{\phi_1^2}{2} + \phi_2^2 + \left(\phi_2 + k_1 - k_2\right)^2\right)}$$
$$\times h_{\infty}^{1/(2\pi\sigma)} \left[2\pi i\sigma^2 \Big(k_2 - k_1 + \frac{\phi_1}{2} + \phi_2\Big) \right] h_{\infty}^{1/(2\pi\sigma)} \left[2\pi i\sigma^2 \Big(k_1 - k_2 + \frac{\phi_1}{2} - \phi_2\Big) \right] \quad (6.98)$$
$$\leq \frac{\sigma^2}{2\pi} \int_{-\delta}^{\delta} \int_{-\delta}^{\delta} d\phi_1 d\phi_2 e^{-\frac{\sigma^2\phi_1^2}{2}} e^{-\sigma^2(\phi_2^2 + (2p_2+\phi_2)^2)}$$
$$\times \left(1 + 3e^{-2\pi\sigma^2(\pi - |2p_2 + \phi_2 - \frac{\phi_1}{2}|)}\right)\left(1 + 3e^{-2\pi\sigma^2(\pi - |2p_2 + \phi_2 + \frac{\phi_1}{2}|)}\right) \quad (6.99)$$

At this point, if $\pi > |k_1 - k_2|$, we can choose δ so that $\pi > |k_1 - k_2| + 2\delta$ and thus

$$\iint_{-\delta}^{\delta} \frac{d\phi_1 d\phi_2}{4\pi^2} e^{-\frac{\sigma^2\phi_1^2}{4} - \sigma^2\phi_2^2} \left| h_{\infty}^{\sigma}\Big(k_1 - k_2 + \frac{\phi_1}{2} - \phi_2\Big) h_{\infty}^{\sigma}\Big(k_2 - k_1 + \frac{\phi_1}{2} + \phi_2\Big) \right|$$
$$\leq \frac{2\sigma^2}{\pi} \int_{-\delta}^{\delta} \int_{-\delta}^{\delta} d\phi_1 d\phi_2 e^{-\sigma^2\phi_1^2} e^{-\sigma^2(\phi_2^2 + (2p_2+\phi_2)^2)} \quad (6.100)$$
$$\leq \frac{2\sigma}{\sqrt{\pi}} \int_{-\delta}^{\delta} d\phi_2 e^{-2\sigma^2(p_2^2 + (p_2+\phi_2)^2)} \quad (6.101)$$
$$\leq 4\sqrt{2} e^{-2\sigma^2 p_2^2} = 4\sqrt{2} e^{-\frac{\sigma^2}{2}(k_2 - k_1)^2}. \quad (6.102)$$

However, if $\pi \leq |k_1 - k_2|$, we can instead bound the functions approximating h by their largest

value, which is attained when $2\phi_2 \pm \phi_1 = 3\delta$. In particular, we have

$$\begin{aligned}
&\iint_{-\delta}^{\delta} \frac{d\phi_1 d\phi_2}{4\pi^2} e^{-\frac{\sigma^2\phi_1^2}{4}-\sigma^2\phi_2^2} \left| h_\infty^\sigma\Big(k_1-k_2+\frac{\phi_1}{2}-\phi_2\Big) h_\infty^\sigma\Big(k_2-k_1+\frac{\phi_1}{2}+\phi_2\Big)\right| \\
&\quad \leq \frac{8\sigma^2}{\pi}\int_{-\delta}^{\delta}\int_{-\delta}^{\delta} d\phi_1 d\phi_2 e^{-\sigma^2\phi_1^2} e^{-\sigma^2(\phi_2^2+(2p_2+\phi_2)^2)} e^{4\pi\sigma^2(2|p_2|+\frac{3\delta}{2}-\pi)} && (6.103)\\
&\quad \leq \frac{8\sigma}{\sqrt{\pi}} e^{4\pi\sigma^2(2|p_2|+\frac{3}{2}\delta-\pi)-2\sigma^2p_2^2}\int_{-\delta}^{\delta} d\phi_2 e^{-2\sigma^2(p_2+2p_2\phi_2+\phi_2^2)} && (6.104)\\
&\quad \leq \frac{16\delta}{\sqrt{\pi}} e^{-\sigma^2(4\pi^2-8\pi|p_2|+4\sigma^2p_2^2-6\pi\delta+2\delta^2-4\delta|p_2|)} && (6.105)\\
&\quad \leq \frac{16\delta}{\sqrt{\pi}} e^{-\sigma^2(4[\pi-|p_2|]^2-(4|p_2|+6\pi)\delta)} && (6.106)\\
&\quad \leq \frac{16\delta}{\sqrt{\pi}} e^{-3\sigma^2\delta} && (6.107)
\end{aligned}$$

where we assume that $\delta < \frac{(\pi-|p_2|)^2}{4|p_2|+6\pi}$ (and note that $|p_2| < \pi$ by assumption). We can then put these two bounds together, if we assume that $\delta < \frac{|\pi-2|p_2||}{2}$ for $2|p_2| < \pi$ or that $\delta < \frac{(\pi-|p_2|)^2}{4|p_2|+6\pi}$ for $2|p_2| \geq \pi$, and thus

$$\begin{aligned}
&\iint_{-\delta}^{\delta} \frac{d\phi_1 d\phi_2}{4\pi^2} e^{-\frac{\sigma^2\phi_1^2}{4}-\sigma^2\phi_2^2} \left| h_\infty^\sigma\Big(k_1-k_2+\frac{\phi_1}{2}-\phi_2\Big) h_\infty^\sigma\Big(k_2-k_1+\frac{\phi_1}{2}+\phi_2\Big)\right| \\
&\quad \leq \frac{16}{\sqrt{\pi}} e^{-2\sigma^2\delta}. && (6.108)
\end{aligned}$$

For the fourth term in (6.78), we will use Lemma 6 from Chapter 3, as this is nearly the same system as used in that lemma. In particular, we have that

$$\begin{aligned}
&\left| \sum_{x=\mu(t)-L}^{\mu(t)+L} \sum_{\substack{y=\nu(t)-L \\ y<x-r}}^{\nu(t)+L} e^{-\frac{(x-\mu(t))^2}{2\sigma}-\frac{(y-\nu(t))^2}{2\sigma^2}} e^{i(k_1+\frac{p_1}{2}-p_2)x} e^{i(k_2+\frac{p_1}{2}+p_2)y}\right| \\
&\quad \leq \left| \sum_{x=\nu(t)-L+r+1}^{\mu(t)+L} e^{-\frac{(x-\mu(t))^2}{2\sigma^2}} e^{i(k_1+\frac{p_1}{2}-p_2)x} V^\sigma_{x-r-1-\nu(t),L}\Big(k_2-k_1+\frac{\phi_1}{2}+\phi_2\Big)\right| && (6.109)\\
&\quad \leq \chi h_\infty^\sigma(0) \leq \sqrt{8\pi}\chi\sigma. && (6.110)
\end{aligned}$$

As such, the corresponding integral can be bounded as

$$\begin{aligned}
&\left| \int_{-\delta}^{\delta}\int_{-\delta}^{\delta} \frac{d\phi_1 d\phi_2}{4\pi^2} e^{-\frac{\sigma^2\phi_1^2}{4}-\sigma^2\phi_2^2} e^{-i(\frac{\phi_1}{2}+\phi_2)\mu(t)} e^{-i(\frac{\phi_1}{2}-\phi_2)\nu(t)} \delta_{\mu(t)\leq\nu(t)} \left(e^{i\theta_\pm(k_1,k_2)} - e^{-i\theta_\pm(p_1;p_2)}\right)\right. \\
&\qquad \left. \times \sum_{x=\mu(t)-L}^{\mu(t)+L} \sum_{\substack{y=\nu(t)-L \\ y<x-r}}^{\nu(t)+L} e^{-\frac{(x-\mu(t))^2}{2\sigma}-\frac{(y-\nu(t))^2}{2\sigma^2}} e^{i(k_1+\frac{p_1}{2}-p_2)x} e^{i(k_2+\frac{p_1}{2}+p_2)y}\right| \\
&\quad \leq 2\iint_{-\delta}^{\delta} \frac{d\phi_1 d\phi_2}{4\pi^2} e^{-\frac{\sigma^2\phi_1^2}{4}-\sigma^2\phi_2^2}\sqrt{8\pi}\chi\sigma && (6.111)\\
&\quad \leq \sqrt{\frac{8}{\pi}}\frac{\chi}{\sigma}. && (6.112)
\end{aligned}$$

We can use a near exact method to bound the fifth term in (6.78), except where we interchange the place of x and y.

Finally, we can also bound the sixth term in (6.78) in a manner similar to the fourth term. Basically, this term is a sum along the diagonal, and the second sum only includes a constant number of terms. Hence, we will bound this by a constant, and have a result similar to the fourth. Explicitly, we have that the sum can be bounded as

$$\begin{aligned}
&\Bigg| \sum_{x=\mu(t)-L}^{\mu(t)+L} \sum_{\substack{y=\nu(t)-L \\ |x-y|\leq r}}^{\nu(t)+L} e^{-\frac{(x-\mu(t))^2}{2\sigma}-\frac{(y-\nu(t))^2}{2\sigma^2}} \Bigg(e^{i(k_1+\frac{p_1}{2}+p_2)x} e^{i(k_2+\frac{p_1}{2}-p_2)y} \\
&\qquad \pm \left(e^{-i\theta_\pm(p_1;p_2)} \delta_{\mu(t)\leq\nu(t)} + e^{i\theta_\pm(k_1,k_2)} \delta_{\mu(t)>\nu(t)} \right) e^{i(k_1+\frac{p_1}{2}-p_2)x} e^{i(k_2+\frac{p_1}{2}+p_2)y} \Bigg) \Bigg| \\
&\qquad\qquad \leq \sum_{x=-L}^{L} e^{-\frac{x^2}{2\sigma^2}} \sum_{y=-r}^{r} 2e^{-\frac{y^2}{2\sigma^2}} \qquad (6.113) \\
&\qquad\qquad \leq 2(2r+1)h_\infty^\sigma(0) \leq 4(2r+1)\sqrt{2\pi}\sigma. \qquad (6.114)
\end{aligned}$$

Hence, the integral can be bounded as

$$\begin{aligned}
&\Bigg| \iint_{-\delta}^{\delta} \frac{d\phi_1 d\phi_2}{4\pi^2} e^{-\frac{\sigma^2\phi_1^2}{4}-\sigma^2\phi_2^2} e^{-i(\frac{\phi_1}{2}+\phi_2)\mu(t)} e^{-i(\frac{\phi_1}{2}-\phi_2)\nu(t)} \\
&\qquad \times \sum_{x=\mu(t)-L}^{\mu(t)+L} \sum_{\substack{y=\nu(t)-L \\ |x-y|\leq r}}^{\nu(t)+L} e^{-\frac{(x-\mu(t))^2}{2\sigma}-\frac{(y-\nu(t))^2}{2\sigma^2}} \Bigg(e^{i(k_1+\frac{p_1}{2}+p_2)x} e^{i(k_2+\frac{p_1}{2}-p_2)y} \\
&\qquad \pm \left(e^{-i\theta_\pm(p_1;p_2)} \delta_{\mu(t)\leq\nu(t)} + e^{i\theta_\pm(k_1,k_2)} \delta_{\mu(t)>\nu(t)} \right) e^{i(k_1+\frac{p_1}{2}-p_2)x} e^{i(k_2+\frac{p_1}{2}+p_2)y} \Bigg) \Bigg| \qquad (6.115) \\
&\qquad\qquad \leq (2r+1)\sigma\sqrt{\frac{2}{\pi^3}} \iint_{-\delta}^{\delta} d\phi_1 d\phi_2 e^{-\frac{\sigma^2\phi_1^2}{4}-\sigma^2\phi_2^2} \qquad (6.116) \\
&\qquad\qquad \leq \frac{2(2r+1)}{\sigma}\sqrt{\frac{2}{\pi}}. \qquad (6.117)
\end{aligned}$$

At this point, we can then bound the norm in distance between $|\, w(t)\,\rangle$ and $|\, \alpha(t)\,\rangle_\pm$. Explicitly, we have

$$\begin{aligned}
&\| |\, \alpha(t)\,\rangle_\pm - |\, w(t)\,\rangle \|^2 \\
&\qquad \leq {}_\pm\langle \alpha(t)\,|\,\alpha(t)\,\rangle_\pm + \langle\, w(t)\,|\,w(t)\,\rangle - \langle\, w(t)\,|\,\alpha(t)\,\rangle_\pm - {}_\pm\langle \alpha(t)\,|\,w(t)\,\rangle \qquad (6.118) \\
&\qquad \leq 2 + 4\sqrt{\pi}\sigma\gamma^2(\kappa+2d+1) - 2\eta\gamma \Bigg[\left(\frac{1}{2} - \frac{7}{2} e^{-\pi^2\sigma^2(2\pi-3\delta)} \right) \left(1 - \frac{1}{\pi\delta^2\sigma^2} e^{-\frac{5\sigma^2\delta^2}{2}} \right) \\
&\qquad\qquad - \frac{6\sigma^2}{\pi L} e^{-\frac{L^2}{2\sigma^2}} - \frac{2\sqrt{\pi}\Gamma}{\sigma} - \frac{16}{\sqrt{\pi}} e^{-2\sigma^2\delta} - 2\sqrt{\frac{8}{\pi}}\frac{\chi}{\sigma} + \frac{2(2d+1)}{\sigma}\sqrt{\frac{2}{\pi}} \Bigg]. \qquad (6.119)
\end{aligned}$$

By consolidating terms, using our bounds on $\langle\, w(t)\,|\,w(t)\,\rangle$, γ, and the definition of η, we then have

the following bound:

$$
\begin{aligned}
&\| |\alpha(t)\rangle_{\pm} - |w(t)\rangle \|^2 \\
&\quad \leq 2 + \frac{\kappa + 2d + 1}{\sqrt{\pi}\sigma}\left(1 + 3e^{-\pi^2\sigma^2} + \frac{\sigma^2}{L}e^{-\frac{L^2}{\sigma^2}}\right) \\
&\qquad - \frac{2\sqrt{\pi}\sigma}{\sqrt{\pi}\sigma}\left(1 - \frac{1}{2}\left[3e^{-\pi^2\sigma^2} + \frac{\sigma^2}{L}e^{-\frac{L^2}{\sigma^2}}\right]\right)\left(1 - 7e^{-\pi^2\sigma^2(2\pi - 3\delta)}\right) \\
&\qquad + \frac{2\sqrt{\pi}\sigma}{\sqrt{\pi}\sigma}\left(1 + \frac{1}{2}\left[3e^{-\pi^2\sigma^2} + \frac{\sigma^2}{L}e^{-\frac{L^2}{\sigma^2}}\right]\right) \\
&\qquad\quad \times \left[\frac{6\sigma^2}{\pi L}e^{-\frac{L^2}{2\sigma^2}} + \left(2\sqrt{\pi}\Gamma + 2\sqrt{\frac{8}{\pi}}\chi + 2(2d+1)\sqrt{\frac{2}{\pi}}\right)\frac{1}{\sigma} + \frac{16}{\sqrt{\pi}}e^{-2\sigma^2\delta}\right] \qquad (6.120) \\
&\quad \leq \frac{2\kappa + 8\pi\Gamma + 16\sqrt{2}\chi + 24(2d+1)}{\sqrt{\pi}}\frac{1}{\sigma} + 21e^{-2\sigma^2\delta} + \frac{9\sigma^2}{L}e^{-\frac{L^2}{2\sigma^2}}. \qquad (6.121)
\end{aligned}
$$

Note that in the last step we rounded some constants, and used the assumption that $\delta < \pi/2$. We then have our bounds on the difference between the assumed time-evolved states and our Gaussian approximations.

At this point, we will want to actually bound something to do with the time-evolved state. In particular, if we remember that $|\alpha(0)\rangle_{\pm} = |\psi(0)\rangle_{\pm}$, and thus that $|w(0)\rangle$ is a good approximation to the initial state, if we can analyze the dynamics of $|w(0)\rangle$ we will also have a good approximation to the state $|\psi(t)\rangle_{\pm}$. Along these lines, if we define the state

$$
\begin{aligned}
|v(t)\rangle &= e^{-iH^{(2)}t}|w(0)\rangle \qquad (6.122) \\
&= \eta \iint_{-\delta}^{\delta} \frac{d\phi_1 d\phi_2}{4\pi^2} e^{i\phi_1\left(\frac{\mu+\nu}{2}\right)} e^{i\phi_2(\nu-\mu)} e^{-\frac{\sigma^2\phi_1^2}{4}} e^{-\sigma^2\phi_2^2} \\
&\qquad\qquad \times e^{-4it\cos\left(\frac{p_1+\phi_1}{2}\right)\cos(p_2+\phi_2)} |\mathrm{sc}(p_1+\phi_1; p_2+\phi_2)\rangle_{\pm} \qquad (6.123)
\end{aligned}
$$

we will have that this state does not change its overlap with $|\psi(t)\rangle$ over time since they both change by the same unitary. If we can show that $|v(t)\rangle$ and $|w(t)\rangle$ are close in norm, we will have our bound on the time evolution of $|\psi(t)\rangle$. As expected, one can see

$$
\begin{aligned}
&\langle v(t)|w(t)\rangle \\
&\quad = \eta^2 \int_{-\delta}^{\delta}\int_{-\delta}^{\delta} \frac{d\phi_1 d\phi_2}{4\pi^2} e^{i\phi_1\left(\frac{\mu(t)+\nu(t)}{2} - \frac{\mu+\nu}{2}\right)} e^{i\phi_2(\nu(t)-\mu(t)-\nu+\mu)} \\
&\qquad \times e^{-\frac{\sigma^2\phi_1^2}{2}} e^{-2\sigma^2\phi_2^2} e^{2it\left(2\cos\left(\frac{p_1+\phi_1}{2}\right)\cos(p_2+\phi_2) - \cos(k_1) - \cos(k_2)\right)} \qquad (6.124) \\
&\quad = \langle w(t)|w(t)\rangle - \eta^2 \int_{-\delta}^{\delta}\int_{-\delta}^{\delta} \frac{d\phi_1 d\phi_2}{4\pi^2} e^{-\frac{\sigma^2\phi_1^2}{2}} e^{-2\sigma^2\phi_2^2} \\
&\qquad \times \left[1 - e^{i\phi_1\left(\frac{\mu(t)+\nu(t)}{2} - \frac{\mu+\nu}{2}\right)} e^{i\phi_2(\nu(t)-\mu(t)-\nu+\mu)} e^{2it\left(2\cos\left(\frac{p_1+\phi_1}{2}\right)\cos(p_2+\phi_2) - \cos(k_1) - \cos(k_2)\right)}\right]. \qquad (6.125)
\end{aligned}
$$

We can then bound the value of the integrand, using the fact that $|1 - e^{i\theta}| \leq |\theta|$:

$$\begin{aligned}
&\left|1 - e^{i\phi_1\left(\frac{\mu(t)+\nu(t)}{2} - \frac{\mu+\nu}{2}\right)} e^{i\phi_2(\nu(t)-\mu(t)-\nu+\mu)} e^{2it\left(2\cos\left(\frac{p_1+\phi_1}{2}\right)\cos(p_2+\phi_2)-\cos(k_1)-\cos(k_2)\right)}\right| \\
&\quad\leq \Big| -\frac{\phi_1}{2}\big[\lceil 2t\sin k_1\rceil + \lceil 2t\sin k_2\rceil\big] - \phi_2\big[\lceil 2t\sin k_2\rceil - \lceil 2t\sin k_1\rceil\big] \\
&\qquad + 2t\Big[2\cos\Big(\frac{p_1+\phi_1}{2}\Big)\cos(p_2+\phi_2) - \cos(k_1) - \cos(k_2)\Big]\Big| && (6.126) \\
&\quad\leq |\phi_1| + 2|\phi_2| + 2t\Big|2\cos\Big(\frac{p_1+\phi_1}{2}\Big)\cos(p_2+\phi_2) - \cos(k_1) - \cos(k_2) \\
&\qquad - \frac{\phi_1}{2}\big[\sin k_1 + \sin k_2\big] - \phi_2\big[\sin k_2 - \sin k_1\big]\Big| && (6.127) \\
&\quad\leq |\phi_1| + 2|\phi_2| + 2t\Big|\cos\Big(-k_2 + \frac{\phi_1}{2} + \phi_2\Big) + \cos\Big(-k_1 + \frac{\phi_1}{2} - \phi_2\Big) - \cos(k_1) - \cos(k_2) \\
&\qquad - \Big(\frac{\phi_1}{2} + \phi_2\Big)\sin k_2 - \Big(\frac{\phi_1}{2} - \phi_2\Big)\sin k_1\Big| && (6.128) \\
&\quad\leq |\phi_1| + 2|\phi_2| + 2t\Big|\cos(k_2)\big[\cos\big(\tfrac{\phi_1}{2} + \phi_2\big) - 1\big] - \sin(k_2)\big[\big(\tfrac{\phi_1}{2} + \phi_2\big) - \sin\big(\tfrac{\phi_1}{2} + \phi_2\big)\big]\Big| \\
&\qquad + 2t\Big|\cos(k_1)\Big[\cos\Big(\frac{\phi_1}{2} - \phi_2\Big) - 1\Big] - \sin(k_1)\Big[\frac{\phi_1}{2} - \phi_2 - \sin\Big(\frac{\phi_1}{2} - \phi_2\Big)\Big]\Big| && (6.129) \\
&\quad\leq |\phi_1| + 2|\phi_2| + 2t\Big(\frac{\phi_1}{2} + \phi_2\Big)^2 + 2t\Big(\frac{\phi_1}{2} - \phi_2\Big)^2 && (6.130) \\
&\quad\leq |\phi_1| + \frac{t}{2}\phi_1^2 + 2|\phi_2| + 4t\phi_2^2. && (6.131)
\end{aligned}$$

We can then use this in the bound, so that

$$\begin{aligned}
&\Big|\int_{-\delta}^{\delta}\int_{-\delta}^{\delta}\frac{d\phi_1 d\phi_2}{4\pi^2} e^{-\frac{\sigma^2\phi_1^2}{2}} e^{-2\sigma^2\phi_2^2}\Big[1 - e^{i\phi_1\left(\frac{\mu(t)+\nu(t)}{2} - \frac{\mu+\nu}{2}\right)} e^{i\phi_2(\nu(t)-\mu(t)-\nu+\mu)} \\
&\qquad\qquad \times e^{2it\left(2\cos\left(\frac{p_1+\phi_1}{2}\right)\cos(p_2+\phi_2)-\cos(k_1)-\cos(k_2)\right)}\Big]\Big| \\
&\quad\leq \int_{-\delta}^{\delta}\int_{-\delta}^{\delta}\frac{d\phi_1 d\phi_2}{4\pi^2} e^{-\frac{\sigma^2\phi_1^2}{2}} e^{-2\sigma^2\phi_2^2}\Big[|\phi_1| + \frac{t}{2}\phi_1^2 + 2|\phi_2| + 4t\phi_2^2\Big] && (6.132) \\
&\quad\leq \int_0^{\infty}\int_0^{\infty}\frac{d\phi_1 d\phi_2}{\pi^2} e^{-\frac{\sigma^2\phi_1^2}{2}} e^{-2\sigma^2\phi_2^2}\Big[\phi_1 + \frac{t}{2}\phi_1^2 + 2\phi_2 + 4t\phi_2^2\Big] && (6.133) \\
&\quad= \frac{3t}{8\pi\sigma^4} + \frac{\sqrt{2\pi}}{2\pi^2\sigma^3}. && (6.134)
\end{aligned}$$

With this, we can then bound the difference between $|\,v(t)\rangle$ and $|\,w(t)\rangle$. In particular, we have

$$\begin{aligned}
\big\||\,v(t)\rangle - |\,w(t)\rangle\big\|^2 &= \langle\,v(t)\,|\,v(t)\,\rangle + \langle\,w(t)\,|\,w(t)\,\rangle - \langle\,v(t)\,|\,w(t)\,\rangle - \langle\,w(t)\,|\,v(t)\,\rangle && (6.135) \\
&\leq 2\langle\,w(t)\,|\,w(t)\,\rangle - 2\Big[\langle\,w(t)\,|\,w(t)\,\rangle - \eta^2\frac{3t}{8\pi\sigma^4} - \eta^2\frac{\sqrt{2\pi}}{2\pi^2\sigma^3}\Big] && (6.136) \\
&= \frac{3t}{\sigma^2} + \frac{4\sqrt{2}}{\sqrt{\pi}\sigma}. && (6.137)
\end{aligned}$$

We now have the requisite bounds in order to prove the statement of the theorem, namely bounding the norm of the difference between the time evolved initial state $|\psi(t)\rangle_\pm$ and our approximation $|\alpha(t)\rangle_\pm$. In particular, if we once again note that $|\alpha(0)\rangle_\pm = |\psi(0)\rangle_\pm$, and remember that $|v(t)\rangle = e^{-iH^{(2)}t}|w(0)\rangle$, we have

$$\begin{aligned}
&\| |\psi(t)\rangle_\pm - |\alpha(t)\rangle_\pm \| \\
&\quad \leq \| |\alpha(0)_\pm\rangle - |w(0)\rangle \| + \| |\alpha(t)\rangle_\pm - |w(t)\rangle \| + \| |v(t)\rangle - |w(t)\rangle \| \qquad (6.138) \\
&\quad \leq 2\left[\frac{2\kappa + 8\pi\Gamma + 16\sqrt{2}\chi + 24(2d+1)}{\sqrt{\pi}} \frac{1}{\sigma} + 21 e^{-2\sigma^2\delta} + \frac{9\sigma^2}{L} e^{-\frac{L^2}{2\sigma^2}} \right]^{1/2} + \left(\frac{3t}{\sigma^2} + \frac{4\sqrt{2}}{\sqrt{\pi}\sigma} \right)^{1/2}. \qquad (6.139)
\end{aligned}$$

If we chose $\sigma = \frac{L}{2\sqrt{\log(L)}}$, we then have that for L large enough and for $0 < t < cL$,

$$\begin{aligned}
&\| |\psi(t)\rangle_\pm - |\alpha(t)\rangle_\pm \| \\
&\quad \leq 4\left[\frac{\kappa + 4\pi\Gamma + 8\sqrt{2}\chi + 12(2d+1)}{\sqrt{\pi}+1} \right]^{1/2} \frac{(\log L)^{1/4}}{\sqrt{L}} + \sqrt{13c}\sqrt{\frac{\log L}{L}} \qquad (6.140) \\
&\quad \leq 4\sqrt{\frac{c \log L}{L}} \qquad (6.141)
\end{aligned}$$

Note that the constant in our bound only arises from the term corresponding to our approximate time evolution, as the other terms use a slightly smaller power of $\log L$. □

6.4 MPQW with positive-semidefinite interactions

Up to this point, we have studied MPQW with near-arbitrary finite-range interactions. In particular, while the exact phase $\theta_\pm(k_1, k_2)$ from Section 6.2 depends on the particular interaction, the overall framework for the scattering does not rely on the interaction. If we want to relate the eigenvalues of a MPQW with N particles to that of the same walk with $N+1$ particles, we will need to have some additional restrictions on the interaction.

In particular, in order to easily relate the low-energy eigenvalues of the quantum walks, we will restrict our attention to non-negative interactions. Namely, we want to restrict our attention to interactions such that for all $x, y \in \mathbb{N}^+$, and all $0 \leq d \leq d_{\max}$,

$$0 \leq \mathcal{U}_{d_{\max}}(x, y) \leq \mathcal{U}_{d_{\max}}(x+1, y). \qquad (6.142)$$

With such a restriction, we then have that the interaction Hamiltonian is a positive-semidefinite matrix that can only increase its energy when particles are added. We can then use several properties of positive-semidefinite matrices to relate the eigenvalues between MPQW on a graph G with differing number of particles.

While the interaction term of the MPQW is now guaranteed to be positive-semidefinite, it is possible that the movement term is negative. However, if we let $\mu(G)$ be the smallest eigenvalue of $A(G)$, and define the Hamiltonian

$$H_{\mathcal{U}}(G, N) = H^n_{\mathcal{U},G} - N\mu(G). \qquad (6.143)$$

Since $A(G) - \mu(G)\mathbb{I} \geq 0$ (by the definition of $\mu(G)$), and since $H_{\text{int}} \geq 0$, we then have that $H_{\mathcal{U}}(G, N)$ is positive-semidefinite.

With a particular choice of interaction, we shall write

$$0 \leq \lambda_N^1(G) \leq \lambda_N^2(G) \leq \cdots \leq \lambda_N^{|V(G)|^N}(G) \tag{6.144}$$

for the eigenvalues of $H_{\mathcal{U}}(G,N)$ and $\{|\,\lambda_N^j(G)\rangle\}$ for the associated eigenvectors.

Note that when $\lambda_N^1(G) = 0$, the ground energy of the N-particle MPQW Hamiltonian $H_{\mathcal{U},G}^N$ is equal to N times the single-particle ground energy $\mu(G)$. In this case, we say that the N-particle MPQW Hamiltonian is frustration free, as the ground state minimizes both the movement term and the interaction term (this terminology arises from spin systems). With this idea, we can then define N-particle frustration-free states:

Definition 7 (Frustration-free state)**.** If $|\,\psi\rangle \in \mathbb{C}^{|V(G)|^N}$ satisfies $H_{\mathcal{U}}(G,N)|\,\psi\rangle = 0$, then we say that $|\,\psi\rangle$ is an N-particle frustration-free state for $\mathcal{U}$ on G.

These frustration-free states will be very useful to us in Chapter 9, as we can use them to iteratively construct the ground states of larger and larger graphs.

6.4.1 Basic properties of $H(G,N)$

We now give some basic properties of $H_{\mathcal{U}}(G,N)$. In particular we will want to understand how the eigenvalues of the Hamiltonian change when we increase the number of particles, as well as understand such a system when looking at many disconnected copies of graphs.

Lemma 14. *For all $N > 1$, $\lambda_{N+1}^1(G) \geq \lambda_N^1(G)$.*

Proof. Let $\widehat{n}_i^N$ be the number operator (6.4) defined in the N-particle space and let $\widehat{n}_i^{N+1}$ be the corresponding operator in the $(N+1)$-particle space. Noting that

$$\widehat{n}_i^{N+1} = \widehat{n}_i^N \otimes \mathbb{I} + |i\rangle\langle i|^{(N+1)} \geq \widehat{n}_i^N \otimes \mathbb{I}, \tag{6.145}$$

we can use this, the fact that $A(G) \geq \mu(G)$, and our assumptions on the interaction $\mathcal{U}$, to see

$$H_G^{N+1} - (N+1)\,\mu(G) = \sum_{w\in[N+1]} \big(A(G) - \mu(G)\mathbb{I}\big)^{(w)} + \sum_{d=0}^{d_{\max}} \sum_{\substack{u,v\in V(G)\\ d(u,v)=d}} \mathcal{U}_d(\hat{n}_v^{N+1}, \hat{n}_u^{N+1}) \tag{6.146}$$

$$\geq \sum_{w\in[N]} \big(A(G) - \mu(G)\mathbb{I}\big)^{(w)} + \sum_{d=0}^{d_{\max}} \sum_{\substack{u,v\in V(G)\\ d(u,v)=d}} \mathcal{U}_d(\hat{n}_v^N \otimes \mathbb{I}, \hat{n}_u^N \otimes \mathbb{I}) \tag{6.147}$$

$$= \big(H_G^N - N\mu(G)\big) \otimes \mathbb{I}. \tag{6.148}$$

Hence

$$\lambda_{N+1}^1(G) = \min_{|\psi\rangle\in\mathbb{C}^{|V(G)|^{N+1}}\,:\,\langle\psi|\psi\rangle=1} \langle\psi|H_G^{N+1} - (N+1)\,\mu(G)|\psi\rangle \tag{6.149}$$

$$\geq \min_{|\psi\rangle\in\mathbb{C}^{|V(G)|^{N+1}}\,:\,\langle\psi|\psi\rangle=1} \langle\psi|\left(H_G^N - N\mu(G)\right)\otimes\mathbb{I}|\psi\rangle \tag{6.150}$$

$$= \lambda_N^1(G) \qquad \square$$

Note that this theorem remains true if we restrict ourselves to the symmetric (or anti-symmetric) subspaces, as the only part that would change is the minimization in (6.149). However, the inequality still holds true if we restrict ourselves to the symmetric (anti-symmetric) subspace for the $n+1$-particle subspace and n-particle subspace.

Additionally, we will often encounter graphs G with more than one component and, in the cases of interest, the smallest eigenvalue of the adjacency matrix for each component is the same. The following Lemma shows that the eigenvalues of $H(G,N)$ on such a graph can be written as sums of eigenvalues for the components. Note that this lemma is similar in flavor to Lemma 13.

Lemma 15. *Suppose $G = \bigcup_{i=1}^{k} G_i$ with $\mu(G_1) = \mu(G_2) = \cdots = \mu(G_k)$. The eigenvalues of $H(G,N)$ are*

$$\sum_{i\in[k]\colon N_i\neq 0} \lambda_{N_i}^{y_i}(G_i) \tag{6.151}$$

where $N_1,\ldots,N_k \in \{0,1,2,\ldots\}$ with $\sum_i N_i = N$ and $y_i \in [V(G)^{N_i}]$. The corresponding eigenvectors are (possibly including repeats)

$$V_\pi\left(\bigotimes_{i\in[k]\colon N_i\neq 0} |\lambda_{N_i}^{y_i}(G_i)\rangle\right), \tag{6.152}$$

for each $\pi \in S_n$.

Proof. To prove this lemma, we will show that each state of the form (6.152) is an eigenvector of $H(G,N)$ with the corresponding eigenvalue, and that these states span the entire Hilbert space.

Let us first note that since $H(G,N)$ is permutation invariant, we have that

$$H(G,N)V_\pi\left(\bigotimes_{i\in[k]\colon N_i\neq 0} |\lambda_{N_i}^{y_i}(G_i)\rangle\right) = V_\pi H(G,N)\left(\bigotimes_{i\in[k]\colon N_i\neq 0} |\lambda_{N_i}^{y_i}(G_i)\rangle\right), \tag{6.153}$$

and thus we need only determine whether

$$H(G,N)\left(\bigotimes_{i\in[k]\colon N_i\neq 0} |\lambda_{N_i}^{y_i}(G_i)\rangle\right) = \sum_{i\in[k]\colon N_i\neq 0} \lambda_{N_i}^{y_i}(G_i)\left(\bigotimes_{i\in[k]\colon N_i\neq 0} |\lambda_{N_i}^{y_i}(G_i)\rangle\right). \tag{6.154}$$

However, note that the interaction Hamiltonian H_{int} is zero between different components, and thus

$$H(G,N) = \sum_{w\in[N]}\sum_{i=1}^{k} A(G_i)^{(w)} + \sum_{i=1}^{k}\sum_{d=0}^{d_{\max}} \sum_{\substack{u,v\in V(G_i)\\ d(u,v)=d}} \mathcal{U}_d(\hat{n}_u,\hat{n}_v) - N\mu(G) \tag{6.155}$$

$$\sum_{i=1}^{k}\left[\sum_{w\in[N]} A(G_i)^{(w)} + \sum_{d=0}^{d_{\max}} \sum_{\substack{u,v\in V(G_i)\\ d(u,v)=d}} \mathcal{U}_d(\hat{n}_u,\hat{n}_v)\right] - N\mu(G). \tag{6.156}$$

Using this expansion of $H(G,N)$, we then have that for each component G_i, only the eigenvector supported on G_i is not annihilated by the sum:

$$\left[\sum_{w\in[N]} A(G_i)^{(w)} + \sum_{d=0}^{d_{\max}} \sum_{\substack{u,v\in V(G_i)\\ d(u,v)=d}} \mathcal{U}_d(\hat{n}_u,\hat{n}_v)\right]\left(\bigotimes_{i\in[k]\colon N_i\neq 0} |\lambda_{N_i}^{y_i}(G_i)\rangle\right)$$

$$= \left(\lambda_{N_i}^{y_i}(G_i) + N_i\mu(G)\right) \bigotimes_{i\in[k]\colon N_i\neq 0} |\lambda_{N_i}^{y_i}(G_i)\rangle. \tag{6.157}$$

If we then sum over each component, we have the requisite eigenvalue.

We now show that these states span the relevant Hilbert space. First of all, note that for two states $|\phi\rangle$ and $|\psi\rangle$, if the number of particles in each component for the two states is not equal (i.e., $(N_1, \cdots, N_k) \neq (M_1, \cdots, M_k)$), then the states $|\phi\rangle$ and $|\psi\rangle$ are orthogonal, since they are supported on orthogonal states. Additionally, if the number of particles is the same, but the two permutations π and σ don't satisfy the condition that $\pi^{-1}\sigma$ is contained in $S_{N_1} \times S_{N_2} \times \cdots \times S_{N_k}$ (i.e., it permutes the support of the particles), then $|\phi\rangle$ and $|\psi\rangle$ are still orthogonal. The only time that the two states might overlap is when the permutation between the two states $(\sigma^{-1}\pi)$ only permutes the particles within a given component. As such, we have that the space spanned by the vectors (6.152) is at least dimension

$$\sum_{\substack{0 \leq N_1, \cdots N_k \\ N_1 + \cdots + N_k = N}} \frac{N!}{N_1! N_2! \cdots N_k!} |V(G_1)|^{N_1} \cdots |V(G_k)|^{N_k}. \tag{6.158}$$

However, this combinatoric problem can be simplified if we use the binomial theorem:

$$(A+B)^C = \sum_{x=0}^{C} \binom{C}{x} A^x B^{C-x}. \tag{6.159}$$

Namely, we have

$$\begin{aligned}
&\sum_{\substack{0 \leq N_1, \cdots N_k \\ N_1 + \cdots + N_k = N}} \frac{N!}{N_1! N_2! \cdots N_k!} |V(G_1)|^{N_1} \cdots |V(G_k)|^{N_k} \\
&\quad = \sum_{\substack{0 \leq N_1, \cdots N_{k-1} \\ N_1 + \cdots + N_{k-1} = N}} \frac{N!}{N_1! N_2! \cdots N_{k-1}!} |V(G_1)|^{N_1} \cdots |V(G_{k-2})|^{N_{k-2}} \big(|V(G_{k-1})| + |V(G_k)|\big)^{N_{k-1}} \qquad (6.160) \\
&\quad = \Big(|V(G_1)| + \cdots |V(G_k)|\Big)^N = |V(G)|^N, \qquad (6.161)
\end{aligned}$$

which is the dimension of the entire Hilbert space. As such, we have that the vectors (6.152) span the entire Hilbert space. □

Note that this theorem remains true if we restrict ourselves to the symmetric or antisymmetric subspaces, but note that the dimension of the relevant Hilbert spaces becomes much smaller.

6.5 Simulation of MPQW on a quantum computer

As this thesis is about the computational power of various many-body systems, we would like to place an upper bound on the computational resources necessary in order to compute various problems related to the walk. This can be done by showing how to simulate the interaction on a given initial state to high probability.

As one might expect, we will show that a universal quantum computer can simulate an N-particle quantum walk. The main idea will be to note that our Hamiltonians are sparse, and thus can be simulated using standard techniques.

6.6 Conclusions and extensions

It might be informative to think about other models for a MPQW. Namely, what happens if instead of the movement term of the Hamiltonian being a sum of terms that only act nontrivially on a single particle, it is a tensor product of the single-particle Hamiltonian. While I don't expect this to drastically change the eventual scattering form, especially as in the two-particle case our change of variables does this for us, there might be some nontrivial interactions that occur independent of an actual interaction Hamiltonian.

Chapter 7

Universality of multi-particle quantum walk

So far in this thesis, we have managed to show several basic results for single-particle scattering on graphs in Chapter 3 and Chapter 4, which we then combined in Chapter 5 to show that quantum walk is universal for quantum computing. We then proved many analogous results for multi-particle quantum walk in Chapter 6, and we might then question whether this system is also universal. As MPQW is a generalization of quantum walk, we have that this model is already universal for quantum computing from, but this reduction requires the same exponential sized graph as in Chapter 5. The interesting question for MPQW is then whether the model remains universal when we restrict ourselves to polynomially sized graphs.

Without surprising anyone, this chapter is dedicated to proving this universality result. The proof strategy is very similar to that of Chapter 5, in that we encode the computational state in a traveling wave-packet, using the ideas of graph scattering in order to implement single-qubit gates. The difference, however, for the multi-particle case is that we encode each qubit via a different particle, thus allowing for much smaller graphs at the expense of more complicated multi-gate behavior. In particular, we will implement two-qubit gates using gadgets from Chapter 4 to route two particles toward each other, and then us our results on two-particle scattering from Theorem 5 to understand the resulting dynamics.

Note that the proof strategy used in this chapter is identical to that of Childs, Gosset, and Webb's [16]. In particular, the encoding of individual qubits using distinct particles, the simulation of single-qubit gates via scattering, and the form of the two-qubit gates are all as in their paper. The difference in results between this chapter and their paper arises from improved technical theorems (namely Theorem **??** and Theorem 5), along with some additional scattering gadgets found in Chapter 4.

The eventual goal of this chapter is to simulate a given circuit $\mathcal{C}_X = U_M U_{M-1} \cdots U_1$ acting on some initial state $|x\rangle$, where each gate U_i comes from some universal gate set and the simulation accepts the state with high probability if and only if the circuit accepts with high probability. We will first show how to do this for single-qubit computations in Section **??**. We will then extend this technique to multi-qubit computations in Section **??**.

7.1 Qubit Encoding

As is Chapter 5, the first step for simulating a given quantum circuit will be to encode the Hilbert space that we want to simulate. In Chapter 5, we were able to do this by having a number of

infinite paths equal to the dimension of the Hilbert space, where the encoded state corresponded to the path on which the particle was located. While this construction works, the fact that the number of paths grows exponentially in the number of encoded qubits makes this impractical for constructing a physical system with a quantum walker.

However, for a bounded number of basis states this construction is simple and technically feasible. The problem of exponential growth arises from the necessary growth of the Hilbert space when having an unbounded number of qubits, since having a larger number of paths was the only means of adding states to the scattering space. When we analyze the multi-particle quantum walk, adding additional particles then becomes an avenue for increasing the size of the Hilbert space, and we can avoid this exponential increase in the size of the graph.

As such, our encoding of a single-qubit will be identical to that of Chapter 5; with some specific momenta chosen k, we encoded the value of the qubit in a dual-rail encoding. The value of the encoded qubit will be $|0\rangle$ if the particle is located along the first (top) path, while the value of the encoded qubit will be $|1\rangle$ if the particle is located along the second (bottom) path.

To expand our encoding to multiple qubits, we then add additional paths, but we also add additional particles. Namely, for each additional qubit, we add two paths and a single particle with some momentum k_i. Again, for that qubit, the value of the encoded qubit is $|0\rangle$ if the particle is located along the top path, wile the value of the qubit will be $|1\rangle$ if the particle moves along the bottom path.

Note that each qubit has its own momentum: while we could require each particle to be encoded at the same momentum, our eventual construction of a multi-qubit entangling gate requires at least two different momenta. Because of this, we will label each qubits momentum k_i, but we will eventually have that most will be equal to some particular value. One problem that this will lead to is a possible difference in speeds; given the fact that the momenta is explicitly related to the speed of propagation for a given wave-packet, we will need to ensure that the wave-packets move together through the graph.

With the general idea for the encodings out of the way, we will need to explicitly define our states. In particular, for each qubit we want to simulate, let us assume that there are two infinite paths, where the vertices are labeled as (x, z, i), for $x \in \mathbb{Z}$, $z \in \mathbb{F}_2$ and $i \in [n]$. Note that the infinite assumption won't be necessary

Recall from Chapter **??** and Chapter 6 that for a given σ, cutoff length L, and momentum k, that we used states of the form

$$|\phi_{\mu}^{L,\sigma}(k)\rangle = \gamma \sum_{\mu-L}^{\mu+L} e^{ikx} e^{-\frac{(x-\mu)^2}{2\sigma^2}} |x\rangle \tag{7.1}$$

as our assumed wave-packets. We will use similar states for our encoded qubits, where σ and L will depend on the overall length of the computation. Moreover, we will use the same L and σ for all of the qubits.

In particular, we will have that a logically encoded basis state $|\mathbf{z}\rangle$ for $\mathbf{z} \in \mathbb{F}_2^n$ will be encoded in the state

$$|\mathbf{z}\rangle_{\log} = \gamma^n \bigotimes_{j\in[n]} \sum_{\mu_j-L}^{\mu_j+L} e^{ik_j x} e^{-\frac{(x-\mu_j)^2}{2\sigma^2}} |x, z_j, j\rangle, \tag{7.2}$$

with the rest of the Hilbert space defined in a linear manner. Note that each individual qubit has its own momentum k_i and position μ_i, and is supported on disjoint sets of vertices. Further, we have that the j-th particle corresponds to the j-th qubit.

If we want to restrict our attention to indistinguishable particles, we can easily change our definition of the logical states. In particular, we have that in the case of bosonic particles,

$$|\mathbf{z}\rangle_{\log}^{\mathrm{Sym}} = \frac{\gamma^n}{\sqrt{n!}} \sum_{\pi \in S_n} V_\pi \left[\bigotimes_{j \in [n]} \sum_{\mu_j - L}^{\mu_j + L} e^{ik_j x} e^{-\frac{(x-\mu_j)^2}{2\sigma^2}} |x, z_j, j\rangle \right], \tag{7.3}$$

while in the case of fermionic particles,

$$|\mathbf{z}\rangle_{\log}^{\mathrm{Asym}} = \frac{\gamma^n}{\sqrt{n!}} \sum_{\pi \in S_n} (-1)^{\mathrm{sign}(\pi)} V_\pi \left[\bigotimes_{j \in [n]} \sum_{\mu_j - L}^{\mu_j + L} e^{ik_j x} e^{-\frac{(x-\mu_j)^2}{2\sigma^2}} |x, z_j, j\rangle \right]. \tag{7.4}$$

For the purposes of this chapter, we will usually not care about the symmetries of the particles, as the only time we will use them is in the analysis of the two-particle gadget. Namely, the phase acquired when two particles move past each other on a long path depends on the symmetries between the particle, and thus the resulting two-qubit unitary will depend on the type of particles. However, since this chapter is a general construction, the particular two-qubit gate applied does not greatly affect our proof.

7.2 Single-qubit gate simulation

With our encoding of the relevant Hilbert space, the next step in our attempt to simulate a given circuit will be to encode the simulation of a single-qubit gate. If we restrict ourselves to a single qubit, this will be done exactly as in Section 5.1.2, as our encoded systems are exactly the same. Namely, for a given qubit with momentum k, if we want to apply the unitary U, we will place a graph $\widehat{G}$ as an obstacle along the pair of infinite paths, where the scattering matrix at k of $\widehat{G}$ takes the form

$$S(k) = \begin{pmatrix} 0 & U^T \\ U & 0 \end{pmatrix}, \tag{7.5}$$

and where we assume that the labeling of the four terminal vertices proceeds as 0_{in}, 1_{in}, 0_{out}, and 1_{out}, as in Figure 5.2.

When we add additional qubits, however, things differ from the single-particle case. In Chapter 5, our simulation of a single-qubit unitary on n qubits required 2^{n-1} copies of the graph gadget $\widehat{G}$ in order to implement the logical gate, corresponding to the computational basis states of all the qubits that the particular unitary does not effect. For our multi-particle encoding, only a single copy of the graph is used, and it is placed as an obstacle on the pair of paths corresponding to the qubit on which the gate is to be applied, while the rest of the qubits simply remain unimpeded.

Assuming that the graph G we use to simulate is of this form, and if the qubits are encoded as in Section 7.1 with momenta traveling towards the gadget $\widehat{G}$, we can use Lemma 13 and Theorem **??** to see that the time-evolved state corresponds to the encoded logical state after the unitary U is applied to the appropriate question (modulo some error and details about the encoded logical state at different times). The intuitive idea behind this scattering behavior is represented schematically in [**TO DO:** *find fig*] .

7.2.1 Finite graphs for single-qubit gates

While an understanding of the scattering behavior for infinite graphs is useful to give a broad overview of the dynamics, we will eventually need to restrict ourselves to finite sized graphs. In

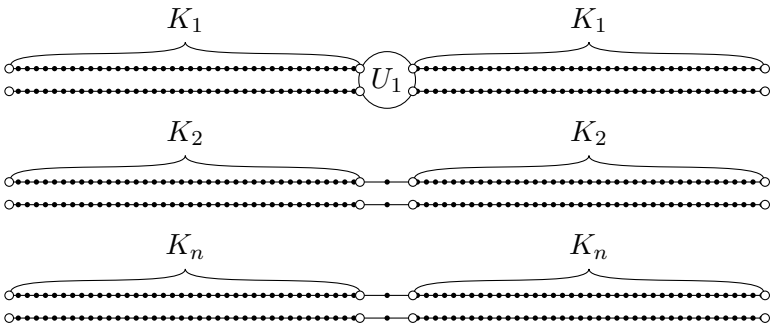

Figure 7.1: A finite graph applying a single-qubit unitary to the first qubit.

particular, we will restrict ourselves exactly as in the case for single-particle scattering in Chapter 5. Moreover, we will actually be able to use Lemma 12, as our encoded logical states satisfy the assumptions of Lemma 13. More exactly, we will be able to use Lemma 13 to evolve each particle independently of the others using the approximations of Lemma 12, and see that the errors add linearly.

Along these lines, let us assume that we want to apply a single-qubit gate U to qubit j, where there exists a gadget $\widehat{G}$ that implements this unitary at momentum k_j. We then let $H = A(G)$, where G is the infinite graph corresponding to single-particle scattering off of $\widehat{G}$ along with $2(n-1)$ infinite paths. Let $G(\vec{K})$ then be the finite graph obtained from G, where we truncate each semi-infinite path attached to $\widehat{G}$ to total length K_j, and we truncate the infinite paths so that there are two length-$(2K_\ell + 2)$ paths for each $\ell \in [n]$ with $\ell \neq j$. We have that the vertices on the long paths are labeled by (ℓ, z, x) for $j \neq \ell \in [n]$ $z \in \mathbb{F}_2$ and $x \in \mathbb{Z}$ with $|x| \leq K_\ell$, while the vertices on the paths connected to $\widehat{G}$ are labeled (j, x, i) for $1 \leq x \leq K_j$, $i \in [4]$ (as in Section 5.1.3). Let the subspace $\mathcal{K}$ be spanned by basis states corresponding to vertices in $G(K)$. Graphs of this form will be used to simulate the application of U to qubit j.

We show that for specific μ_ℓ, σ, L, and $\vec{K}$, initial logical states evolve to output logical states. In particular, let us assume that the j-th particle is in the state

$$|\, z\rangle_{\text{log,in},j} = \gamma \sum_{x=\mu_j - L}^{\mu_j + L} e^{ik_j x} e^{-\frac{(x-\mu_j)^2}{2\sigma^2}} |\, j, x, z\rangle, \tag{7.6}$$

while each of the other particles are in the state

$$|\, z\rangle_{\text{log,in},\ell} = \gamma \sum_{x=-\mu_\ell - L}^{-\mu_\ell + L} e^{-ik_\ell x} e^{-\frac{(x-\mu_\ell)^2}{2\sigma^2}} |\, \ell, x, z+1\rangle. \tag{7.7}$$

Further, let us assume that each $\mu_\ell = T \sin|k_\ell|$, so that each particle travels a distance $2\mu_\ell$ in time T. We then have that after a time T, we will want the output logical states to be given by

$$|\, z\rangle_{\text{log,out},j} = \gamma e^{-2iT\cos(k_j)} \sum_{x=\mu_j - L}^{\mu_j + L} e^{-ik_j x} e^{-\frac{(x-\mu_j)^2}{2\sigma^2}} |\, j, x, z+3\rangle, \tag{7.8}$$

for the j-th particle, while each of the other particles are in the state

$$|\, z\rangle_{\text{log,out},\ell} = \gamma e^{-2iT\cos(k_\ell)} \sum_{x=\mu_\ell - L}^{\mu_\ell + L} e^{-ik_\ell x} e^{-\frac{(x-\mu_\ell)^2}{2\sigma^2}} |\, \ell, x, z\rangle. \tag{7.9}$$

As in the case for single-particle universality, for a give state $|\phi\rangle = \sum_{x\in\mathbb{F}_2^n} \alpha_x |x\rangle$, we define the encoded state

$$|\phi\rangle_{\text{log,in}} = \sum_{x\in\mathbb{F}_2^n} \alpha_x \bigotimes_{i=1}^{n} |x_i\rangle_{\text{log,in,i}} \tag{7.10}$$

and for a given unitary U,

$$|U\phi\rangle_{\text{log,out}} = \sum_{x,y\in\mathbb{F}_2^n} U_{xy}\alpha_y \bigotimes_{i=1}^{n} |x_i\rangle_{\text{log,in,i}}. \tag{7.11}$$

With these definitions, we can give an analogous result to Lemma 12.

Lemma 16. *Let $k_j \in (-\pi, 0)$ for all $j \in [n]$, and let $\widehat{G}$ be a four-terminal gate gadget, such that its scattering matrix at momentum k_j is of the form (7.5). Letting the logical states $|z\rangle_{log,in}$ and $|z\rangle_{log,out}$ be defined as in (7.10) and (7.11), and let $G(K)$ be defined as above, where each $\mu_\ell \geq L$, $K_\ell \geq \frac{5\mu_\ell}{3}$, and $T = \frac{\mu_\ell}{\sin|k_\ell|}$, we have that there exists some constant ξ such that for all $0 \leq t \leq T$ and any interaction $\mathcal{U}$,*

$$\left\| e^{-iH_G^N t}|\phi(0)\rangle - |\phi(t)\rangle \right\| \leq \xi n \sqrt{\frac{\log L}{L}}, \tag{7.12}$$

where

$$|\phi(t)\rangle = \sum_{x\in\mathbb{F}_2^n} \alpha_x \bigotimes_{\ell=1}^{n} |\alpha_\ell^{x_\ell}(t)\rangle, \tag{7.13}$$

the $|\alpha_j^{x_j}(t)\rangle$ are equal to $|\alpha^1(t)\rangle$ and $|\alpha^2(t)\rangle$ as defined in Theorem 4, and for the rest of the particles we have

$$|\alpha_\ell^z(t)\rangle = \gamma e^{-2it\cos(k_\ell)} \sum_{x=\mu_\ell(t)-L}^{\mu_\ell(t)+L} e^{-ik_\ell x} e^{-\frac{(x-\mu_\ell(t))^2}{2\sigma^2}} |\ell, x, z\rangle, \tag{7.14}$$

with

$$\mu_\ell(t) = -\mu_\ell + 2t\sin|k_\ell|. \tag{7.15}$$

In particular, we have

$$\left\| e^{-iH_G^N T}|\psi\rangle_{log,in} - |U\psi\rangle_{log,out} \right\| \leq \xi n \sqrt{\frac{\log L}{L}}. \tag{7.16}$$

Proof. Note that the states $|\phi(t)\rangle$ all have the particles supported on different components of G, and thus by Lemma 13 we have that

$$e^{-iH_G^N t}|\phi(0)\rangle = \prod_{\ell=1}^{n} \left(e^{-iA(G_\ell)t}\right)^{(\ell)} |phi(0)\rangle, \tag{7.17}$$

where G_ℓ is the component on which the ℓ-th particle is located. However, we have that each of these unitaries commute, and

$$\left(e^{-iA(G_\ell)t}\right)^{(\ell)}|\,\phi(0)\,\rangle = \sum_{x\in\mathbb{F}_2^n} \alpha_x \bigotimes_{i=1}^{n} e^{-i\delta_{i,\ell}A(G_\ell)t}|\,\alpha_i^{x_i}(0)\,\rangle \tag{7.18}$$

$$= \sum_{x\in\mathbb{F}_2^n} \alpha_x \left[\bigotimes_{i=1}^{n} \left(|\,\alpha_i^{x_i}(\delta_{\ell,i}t)\,\rangle + \delta_{\ell,i}|\,\epsilon_{\alpha_x,\ell}(t)\,\rangle\right)\right], \tag{7.19}$$

by Lemma 12, with $\||\,\epsilon_{\alpha_x,\ell}(t)\,\rangle\| \leq \xi\sqrt{\log L/L}$ for some constant ξ. (We can use the theorem to understand the scattering on the paths, with $\widehat{G}$ the four-terminal gadget composed of two length-2 paths in the middle of the length $2K_i + 2$ length paths.)

Combining these results, we then have that

$$e^{-iH_G^N t}|\,\phi(0)\,\rangle = \sum_{x\in\mathbb{F}_2^n} \alpha_x \left[\bigotimes_{i=1}^{n} \left(|\,\alpha_i^{x_i}(t)\,\rangle + |\,\epsilon_{\alpha_x,\ell}(t)\,\rangle\right)\right] \tag{7.20}$$

$$= |\,\phi(t)\,\rangle + |\,\varepsilon(t)\,\rangle, \tag{7.21}$$

where $\||\,\varepsilon(t)\,\rangle\| \leq n\xi\sqrt{\log L/L}$.

□

Note that most of the analysis up until this point is essentially a rehashing of results from Chapter 5, as we have kept the particles far apart.

7.3 Entangling gate

Now that we have encoded qubits and, at specific momenta, a universal set of single-qubit gates, we need to construct some kind of entangling gate between our encoded qubits. In the single-particle encoding, this gate was trivial, as a controlled-not gate (and in fact any permutation gate) simply corresponded to a relabelling of the encoding paths. For our multi-particle encoding, however, the entanglement procedure is rather more involved. Our gate will necessarily involve a two-particle Hamiltonian, but we will arrange the graph (and the encoded states) in such a manner that the two-particles will only ever interact on a (long) path. As such, we can use Theorem **??** to see that the result of such scattering is simply an applied phase (at least when particles are indistinguishable).

Explicitly, our entangling gate will be a controlled-θ gate, for some θ that depends on the interaction and the momenta used to encode the qubits. Further, our entangling gate will only exist between qubits that are encoded with particles for which a momentum switch (see Section 4.1.2) exists, which necessitates the use of at least two different momenta. The main idea behind the gate is to place two momentum switches (represented schematically as Figure 7.2a) on the 1-paths of the qubits as obstacles, where the two switches are connected by a long path for their third terminals. If either particle is in the logical state 1, it will be routed along the long connecting path between the two paths, and then routed along 1_{out} for the opposite qubit. By arranging the lengths of the various paths correctly, we can ensure that if at most a single encoded qubit is in the logical 1 state, then the corresponding single-particle scattering events encode identity operations. However, if both encoded qubits are logically 1, then the two particles move past each other along the long connecting path, acquiring an additional phase that depends on their momenta and the interaction. As such, the graph in Figure 7.2b applies an encoded Cθ gate (along two single-qubit gates arising from the phase acquired during the momentum switches).

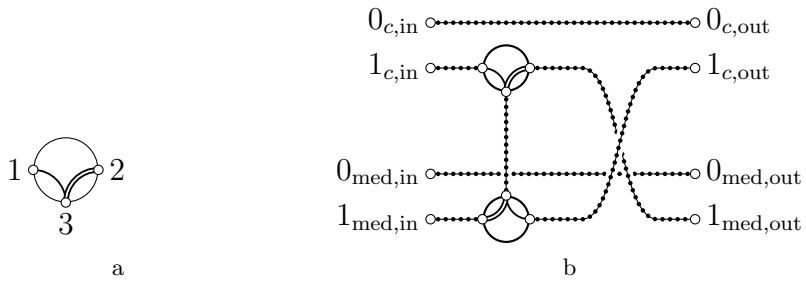

Figure 7.2: (a) Momentum switch schematic. (b) Cθ gate.

Note that the graph and analysis described here only works for two particles. However, we will use a lemma similar to Lemma 16 in order to analyze the related n-particle Hamiltonian.

7.3.0.1 Momentum switch

Remember from Section 4.1.2 that momentum switches are three-terminal scattering gadgets that act like railroad switches, where at specific momenta the gadget has perfect transmission from terminal 3 to terminal 1, while at other momenta there is perfect transmission from terminal 3 to terminal 2. We will represent gadgets with this behavior schematically as in Figure 7.2a, where one set of momenta follow the single line while the other specified set follows the double line.

For our purposes, we will assume that the momentum switch splits the two momenta used to encode the different qubits k_1 and k_2. Explicitly, we will assume that the S-matrix for the given momentum switch at k_1 and k_2 are given by

$$S_{\text{switch}}(k_1) = \begin{pmatrix} 0 & 0 & T_1 \\ 0 & R_1 & 0 \\ T_1 & 0 & 0 \end{pmatrix} \qquad S_{\text{switch}}(k_2) = \begin{pmatrix} R_2 & 0 & 0 \\ 0 & 0 & T_2 \\ 0 & T_2 & 0 \end{pmatrix}. \tag{7.22}$$

In other words, we will assume that the momentum switch has perfect transmission between terminals 1 and 3 at momentum k_1, and perfect transmission between terminals 2 and 3 at momentum k_2, possibly with an additional phase. With this, we have that a particle with momentum k_1 follows the single line of the schematic representation of Figure 7.2a, while a particle with momentum k_2 follows the double line.

7.3.1 Constructing the graph

We will now construct the entangling graph, where we will assume that we know the encoded initial states. Note that this construction depends on the momenta of the encoded qubits in more than just the form of the momentum switch; the fact that the timing of the wave-packets is important forces us to change the length of the connecting paths depending on the initial momentum so that they arrive on the infinite path at the same time, while the requirement that the particles only interact along the path forces us to change the lengths depending on the size of the wave-packets.

The Cθ gate is implemented using the graph shown in Figure 7.3. In this section we specify the logical input states, the logical output states, the distances X, Z, and W appearing in the figure, and the total evolution time as functions of the momentum k_1 and k_2. With these choices, we show that a Cθ gate is applied to the logical states at the end of the time evolution under the quantum

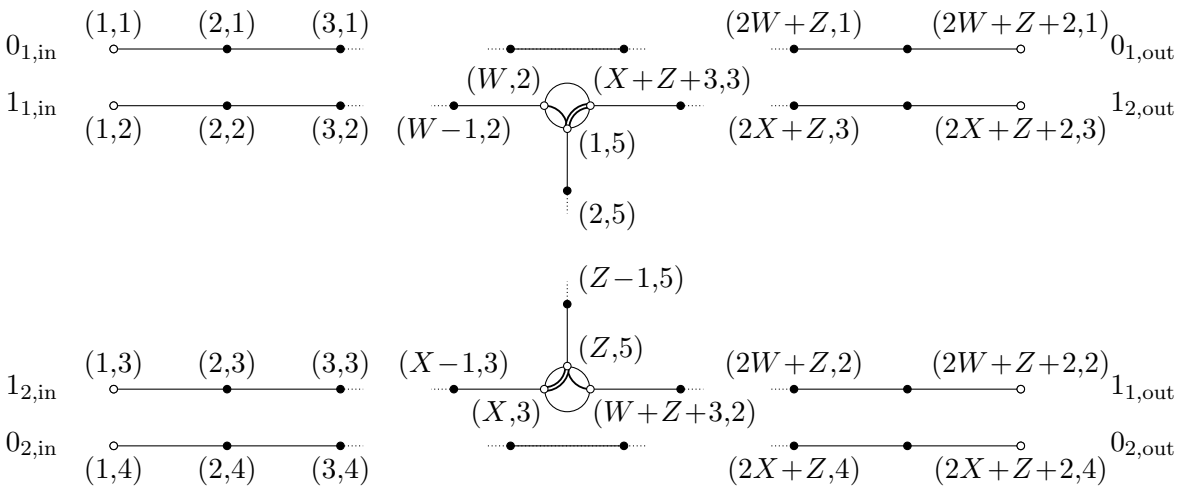

Figure 7.3: Graph G' used to implement the Cθ gate. The integers Z, X, and W are specified in equations (7.25), (7.26), and (7.27), respectively.

walk Hamiltonian (up to error terms that are $\tilde{\mathcal{O}}(L^{-1/2})$). The results of this section pertain to the two-particle Hamiltonian $H_{G'}^{(2)}$ for the graph G' shown in Figure 7.3.

We first need to construct the assumed encoded initial states. Note that the important feature about these encodings are the momenta k_i and the cutoff distance L. While the distance from the ends and the distance from the scattering widgets are important, they won't affect the overall qualitative action of the wave-packets. With the labelling scheme for the vertices as in Figure 7.3, we can then assume that our initial logical states are

$$|0_{\text{in}}\rangle^1 = \gamma \sum_{x=\mu_1-L}^{\mu_1+L} e^{ik_1 x} e^{-\frac{(x-\mu_1)^2}{2\sigma^2}} |x,1\rangle \qquad |1_{\text{in}}\rangle^1 = \gamma \sum_{x=\mu_1-L}^{\mu_1+L} e^{ik_1 x} e^{-\frac{(x-\mu_1)^2}{2\sigma^2}} |x,2\rangle \tag{7.23}$$

for the qubit with momentum k_1 and

$$|0_{\text{in}}\rangle^2 = \gamma \sum_{x=\mu_2-L}^{\mu_2+L} e^{ik_2 x} e^{-\frac{(x-\mu_2)^2}{2\sigma^2}} |x,4\rangle \qquad |1_{\text{in}}\rangle^2 = \gamma \sum_{x=\mu_2-L}^{\mu_2+L} e^{ik_2 x} e^{-\frac{(x-\mu_2)^2}{2\sigma^2}} |x,3\rangle \tag{7.24}$$

for the qubit with momentum k_2. Additionally, let us assume that $|\sin k_1| \leq |\sin k_2|$, so that the wave-packet with momentum k_1 travels no faster than the wave-packet with momentum k_2 (this assumption is without loss of generality as we can simply relabel k_1 and k_2).

Note that the two computational basis states for each qubit are centered at the same distance from the ends, but that the distances are different for the two qubits. The reason for this is that while the wave-packets for each individual qubit travel at the same speed, the fact that $k_1 \neq k_2$ (which is implied by the existence of the momentum switch) allows the two wave-packets to travel at differing speeds. This difference in the distance allows us to ensure that this difference in speed is taken care of when we combine these gadgets.

With these initial logical states chosen, note that there are seven path lengths that we will need to determine before we can analyze the propagation. Explicitly, there is the distance on path 2 corresponding to the initial distance the wave-packet with momentum k_1 travels before hitting the first momentum switch, the same for path 3 and the wave-packet with momentum k_2, the distance between the two momentum switches where the two-particles will interact, the lengths of the two

output paths after the second momentum switches, and finally the two paths corresponding to the logical states 0. Note that these final two path lengths (corresponding to the logical 0 states) will be determined by the total distance traveled by the logical 1 states, and that we can assume that the distances after the momentum switch are the same as the distances before the momentum switches. As such, there are three distances that we care about.

Putting this together, we will need to chose the three distances Z, X, and W from Figure 7.3 to ensure that we can analyze the wave-packet propagation, while also ensuring that the output approximated wave-packets are in agreeing positions. While these choices are somewhat arbitrary, we will make the choice

$$Z = \lceil (7+\alpha)L \rceil \tag{7.25}$$
$$X = \lceil 2L + D + M(k_2) \rceil \tag{7.26}$$
$$W = \lceil 2L + M(k_1) \rceil \tag{7.27}$$

where

$$\alpha = 3\frac{\sin|k_2| - \sin|k_1|}{\sin|k_1| + \sin|k_2|} \tag{7.28}$$
$$D = \left(\frac{7\sin|k_2|}{\sin|k_1|} + \frac{6\sin|k_1|}{\sin|k_1| + \sin|k_2|} - 9\right)L \tag{7.29}$$
$$M(k_i) = 2t_0 \sin|k_i| = \mu_i. \tag{7.30}$$

With these choices, a wave-packet moving with speed $\sin|k_1|$ travels a distance $Z+4L \approx (11+\alpha)L$ in approximately the same time that a wave-packet moving with speed k_2 takes to travel a distance $Z + 2D + 2L \approx (9+\alpha)L + 2D$, since

$$t_{C\theta} = \frac{(11+\alpha)L}{2\sin|k_1|} \approx \frac{(9+\alpha)L + 2D}{2\sin|k_2|}. \tag{7.31}$$

Additionally, these distances are chosen so that at time $t_1 = (4+\alpha)L/2\sin|k_1|$, the two particles are both located on the center path, with the wave-packet with momentum k_1 a distance $(1+\alpha)L$ from the first momentum switch, the other a distance L from the second momentum switch, and the two wave-packets a distance L apart, and so that at a time $t_2 = t_1 + 6L/(\sin|k_1| + \sin|k_2|)$, the wave-packets have passed each other, but are now the same distance from the other momentum switch. This is represented pictorially in Figure 7.4.

One point to notice is that the distances $M(k_i) = \mu_i$ are chosen to be the distance traveled by each particle over some time t_0. As such, if at time $-t_0$ the two particles were both centered along the endpoints of the paths, they would . This isn't particularly important, except to allow us to nicely combine this result with other scattering events.

7.3.2 Time evolution analysis

With the graph G well defined for two momenta k_1 and k_2 and cut-off distance L, we now want to actually analyze the dynamics of the system. We want to claim that the initial states evolve into encoded logical output states, where the acquired phases correspond to an entangling gate. In particular, we will want that the evolution of an encoded state on this graph corresponds to some unitary diagonal in the computational basis, in which an additional phase is acquired for the state $|11\rangle$. While in an ideal case, this will simply be a controlled-θ gate, in which the applied unitary is the identity for the other three basis states, our graph will also have additional phases

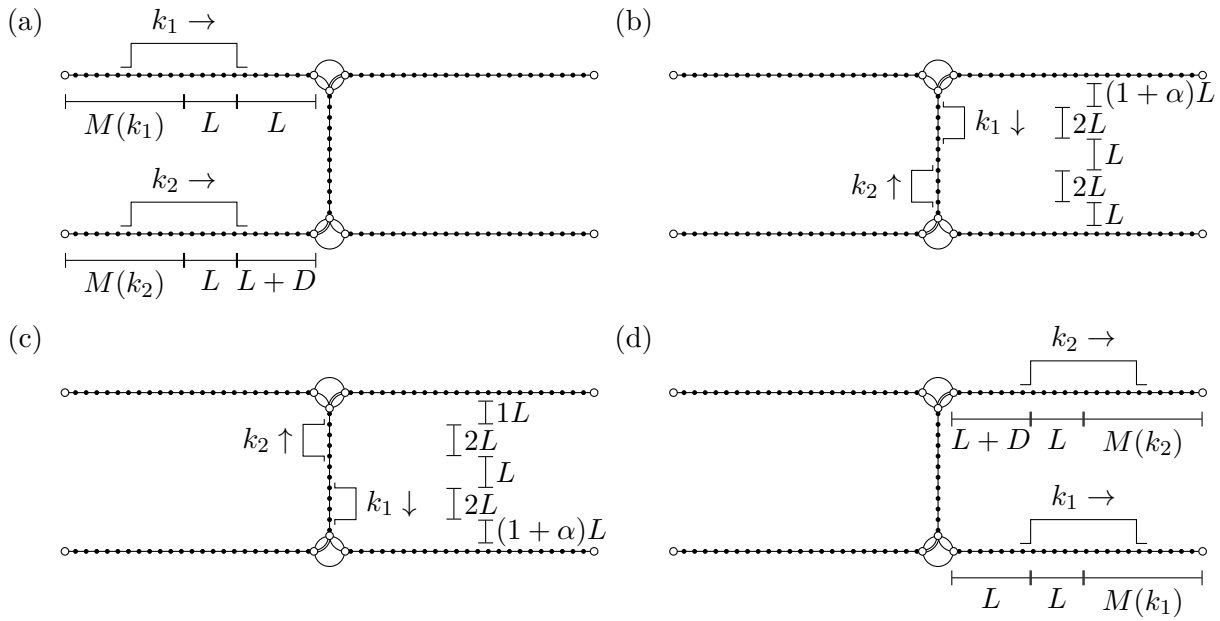

Figure 7.4: This picture illustrates the scattering process for two wave-packets that are incident on the input paths as shown in figure (a) at time $t = 0$. Figure (b) shows the location of the two wave-packets after a time t_1 and figure (c) shows the wave-packets after a time t_2. After the particles pass one another they acquire an overall phase of $e^{i\theta_\pm}$. Figure (d) shows the final configuration of the wave-packets after a total evolution time $t_{C\theta}$.

corresponding to a product of single-qubit unitaries, arising from the transmission coefficients of the two momentum switches.

However, in order to apply an encoded unitary, we will need to have an encoding of the logical output states. Letting $t_{C\theta}$ be as defined in (7.31), we will have that the encoded output states for each qubit will be

$$|0_{\text{out}}\rangle^1 = \gamma e^{-2it_{C\theta}\cos(k_1)} \sum_{x=\nu_1-L}^{\nu_1+L} e^{ik_1x} e^{-\frac{(x-\nu_1)^2}{2\sigma^2}} |x,1\rangle \tag{7.32}$$

$$|1_{\text{out}}\rangle^1 = \gamma e^{-2it_{C\theta}\cos(k_1)} \sum_{x=\nu_1-L}^{\nu_1+L} e^{ik_1x} e^{-\frac{(x-\nu_1)^2}{2\sigma^2}} |x,2\rangle \tag{7.33}$$

$$|0_{\text{out}}\rangle^2 = \gamma e^{-2it_{C\theta}\cos(k_2)} \sum_{x=\nu_2-L}^{\nu_2+L} e^{ik_2x} e^{-\frac{(x-\nu_2)^2}{2\sigma^2}} |x,4\rangle \tag{7.34}$$

$$|1_{\text{out}}\rangle^2 = \gamma e^{-2it_{C\theta}\cos(k_2)} \sum_{x=\nu_2-L}^{\nu_2+L} e^{ik_2x} e^{-\frac{(x-\nu_2)^2}{2\sigma^2}} |x,3\rangle \tag{7.35}$$

where $\nu_1 = \mu_1 + \lceil 2t_{C\theta}\sin|k_1|\rceil$ and $\nu_2 = \mu_2 + \lceil 2t_{C\theta}\sin|k_2|\rceil$. Intuitively, these are simply the expected positions of the wave-packets corresponding to the initial logical states after a time $t_{C\theta}$, along with the phases acquired from their energies.

Additionally, note that the eigenstates of H_G^2 decompose into a symmetric and an antisymmetric subspace. While it is intuitively more clean to work with distinguishable particles, the phases

acquired during the evolution on G will depend on the symmetry of the underlying particles. As such, let us define the eight states

$$|(z_1z_2)_{\text{in/out}}\rangle_\pm = \frac{1}{\sqrt{2}}\Big(|(z_1)_{\text{in/out}}\rangle^1|(z_2)_{\text{in/out}}\rangle^2 \pm |(z_2)_{\text{in/out}}\rangle^2|(z_1)_{\text{in/out}}\rangle^1\Big). \tag{7.36}$$

Our analysis will be for these states.

If we note that the input states don't particularly rely on the initial distance from the graph, and that the output states similarly don't rely on the distance from the end, we will be able to easily combine the time evolution on these graphs with the time evolution on other graphs. Just so long as the initial wave-packets start a distance proportional to L away from the ends, and similarly end a distance proportional to L from the ends, we can us Lemma 1 in order to determine the overall time evolution.

In particular, we have the following lemma:

Lemma 17. *Let G' be the graph given in Figure 7.3 with distances given by (7.25)–(7.27), and where we assume that the initial and final states as defined in (7.23), (7.24), and (7.32)-(7.35) only have support on vertices a distance at least $L/3$ from the ends of the truncated paths. If the momentum switch has transmission coefficient T_1 for momentum k_1 and transmission coefficient T_2 for momentum k_2, and if the phase acquired for two particle scattering between momentum k_1 and k_2 is given by $\theta_\pm$ for symmetric and antisymmetric states, then we have the following approximations for the time-evolved states:*

$$\left\|e^{-iH^{(2)}_{G'}t_{\text{II}}}|00_{in}\rangle_\pm - |00_{out}\rangle_\pm\right\| \leq \chi\sqrt{\frac{\log L}{L}} \tag{7.37}$$

$$\left\|e^{-iH^{(2)}_{G'}t_{\text{II}}}|01_{in}\rangle_\pm - T_2^2|01_{out}\rangle_\pm\right\| \leq \chi\sqrt{\frac{\log L}{L}} \tag{7.38}$$

$$\left\|e^{-iH^{(2)}_{G'}t_{\text{II}}}|10_{in}\rangle_\pm - T_1^2|10_{out}\rangle_\pm\right\| \leq \chi\sqrt{\frac{\log L}{L}} \tag{7.39}$$

$$\left\|e^{-iH^{(2)}_{G'}t_{\text{II}}}|11_{in}\rangle_\pm - e^{i\theta_\pm}T_1^2T_2^2|11_{out}\rangle_\pm\right\| \leq \chi\sqrt{\frac{\log L}{L}}. \tag{7.40}$$

Proof. The first three bounds (7.37), (7.38), and (7.39) are similar to the proofs of Chapter 5, since in each case the two particles are supported on disconnected subgraphs and thus we can use Lemma 13. For each of the single-particle scattering events, we can use a strategy similar to Lemma 12 to bound the error in our time-evolution for the unsymmetrized two-particle states. To get the bound of (7.40), the proof strategy will be similar, but we will also need an application of Theorem 5 during the times at which both particles are located on the long path.

Let us first understand the single-particle evolutions on the long paths. Note that $t_{C\theta} \leq cL$ for some constant c, and thus according to Theorem **??**, on an infinite path P we have that

$$\left\|\gamma e^{-iPt}\sum_{\mu-L}^{\mu+L} e^{ikx}e^{-\frac{(x-\mu)^2}{2\sigma}}|\,x\,\rangle - \gamma e^{-2it\cos(k)}\sum_{\mu(t)-L}^{\mu(t)+L} e^{ikx}e^{-\frac{(x-\mu(t))^2}{2\sigma^2}}|\,x\,\rangle\right\| \leq \xi\sqrt{\frac{\log L}{L}} \tag{7.41}$$

for some constant ξ and where $\mu(t) = \mu + \lceil 2t\sin(k)\rceil$. While Theorem **??** doesn't exactly give us this, if we apply the theorem to a graph gadget $\widehat{G}$ that results in the final graph being a long path, and assume that the initial location is far from the scattering event, the result follows after

a relabeling of the basis states. If we then note that the corresponding approximation involving $\mu(t)$ on the finite path always remains a distance at least $L/3$ away from the ends of the finite approximation, Lemma 1 with $H = A(P)$, $\tilde{H} = A(G')$, and $N_0 = \frac{L}{3}$, and the error bound of $\delta = \xi\sqrt{\log L/L}$ gives us

$$\left\|e^{-iA(G')t_{C\theta}}|0_{\text{in}}\rangle^i - |0_{\text{out}}\rangle^i\right\| \leq \left(\frac{8et_{C\theta}}{N_0} + 2\right)\left[\xi\sqrt{\frac{\log L}{L}} + 2^{-N_0}\left(1 - \xi\sqrt{\frac{\log L}{L}}\right)\right] \tag{7.42}$$

$$\leq \zeta\sqrt{\frac{\log L}{L}} \tag{7.43}$$

for some constant χ that is independent of the momentum k. Hence, we have that this approximation holds for both long paths.

Now let us analyze the single-particle evolution on the subgraph that connects the two particles. For both particles, we will define approximations to the time-evolved wave-packets that will equal both the initial state and the corresponding final states. Namely, if we also label the vertices of the path 5 (the one of length Z which are currently labeled $(x, 5)$) as $(W+1+x, 2)$ and $(X+Z-x+2, 3)$, then we can define the states

$$|\alpha_1^1(t)\rangle = \gamma e^{-2it\cos(k_1)} \sum_{x=\mu(t)-L}^{\mu(t)+L} e^{ik_1x} e^{-\frac{(x-\mu(t))^2}{2\sigma^2}} |x, 2\rangle \tag{7.44}$$

$$|\alpha_2^1(t)\rangle = \gamma e^{-2it\cos(k_2)} \sum_{x=\nu(t)-L}^{\nu(t)+L} e^{ik_2x} e^{-\frac{(x-\nu(t))^2}{2\sigma^2}} |x, 3\rangle \tag{7.45}$$

where $\mu(t) = \mu + \lceil 2t\sin(k_1)\rceil$ and $\nu(t) = \nu + \lceil 2t\sin(k_2)\rceil$. Note that these are (almost) the same approximations as used for the long paths, where we assume that the momentum switches essentially act as connections between the correct long paths.

With these approximations, we will then want to show that the time evolution of the initial states approximately follow these output states, possibly with some additional phases. In particular, note that there are three times (not including $t = 0$) that are important for our evolution,

$$t_1 = \frac{(4+\alpha)L}{2\sin|k_1|} \tag{7.46}$$

$$t_2 = t_1 + \frac{6L}{\sin|k_1| + \sin|k_2|} \tag{7.47}$$

$$t_{C\theta} = \frac{(11+\alpha)L}{2\sin|k_1|}. \tag{7.48}$$

If we can show that the time-evolved approximation at one time is close to the approximation at the next time for each of these times, we then have that our final approximation and the time-evolved initial state are close as well. To do so, we will use the same procedure for combining our time-evolution on graphs as was done in Chapter 5.

Namely, we can use Lemma 1 and Lemma **??** to analyze the evolution of these states. Note that Lemma **??** gives us an approximation for the evolution of $|\alpha_j^1(t)\rangle$ via the momentum switch on the infinite path, and two applications of Lemma 1 allows us to then analyze the evolution of the state for times $0 \leq t \leq t_1$ (after a suitable relabeling of the vertices). In particular, we have that

$$\left\|e^{-iH_{G'}^{(1)}t_1}|\alpha_j^1(0)\rangle - T_j|\alpha_j^1(t_1)\rangle\right\| \leq \zeta_j^1\sqrt{\frac{\log L}{L}}, \tag{7.49}$$

where the dependence of the constant on j is only there in terms of the initial distance of the wave-packet from the ends of the finite paths.

We can then use the same trick, namely two applications of Lemma 1 and a single application of Lemma **??** to understand the evolution on the path of length Z between times t_1 and t_2. Literally the same analysis as in the previous paragraph again gives us that

$$\left\| e^{-iH^{(1)}_{G'}(t_2-t_1)} |\alpha^1_j(t_1)\rangle - |\alpha^1_j(t_2)\rangle \right\| \leq \zeta^2_j \sqrt{\frac{\log L}{L}} \tag{7.50}$$

where again the constant only depends on the distance between the support of the approximation and the truncated ends, but in both cases is a constant.

Finally, a third application of this trick around the second momentum switch gives us

$$\left\| e^{-iH^{(1)}_{G'}(t_{C\theta}-t_2)} |\alpha^1_j(t_2)\rangle - T_j |\alpha^1_j(t_C\theta)\rangle \right\| \leq \zeta^3_j \sqrt{\frac{\log L}{L}}, \tag{7.51}$$

where we again have used a necessary relabeling of the vertices.

Combining the three bounds (7.49)–(7.51), we then have that

$$\left\| e^{-iH^{(1)}_{G'}(t_{C\theta})} |\alpha^1_j(0)\rangle - T^2_j |\alpha^1_j(t_C\theta)\rangle \right\| \leq (\zeta^1_j + \zeta^2_j + \zeta^3_j) \sqrt{\frac{\log L}{L}}, \tag{7.52}$$

and thus we have approximations to the single-particle evolutions.

From this, if we use Lemma 13 along with these three bounds on the evolution for times $t_{C\theta}$, we have bounds similar (7.37), (7.38), and (7.39) for the unsymmetrized states. However, since the bounds (and approximations) don't depend on the symmetrization of the underlying states, we also have the symmetrized and antisymmetrized bounds as well.

Finally, we need to show the bound (7.40). Unfortunately, this bound is slightly more difficult to prove, as we cannot naively use Lemma 13. However, a more nuanced application of Lemma 1 will allow us to approximate the evolution of both particles on G' by the evolution on a disconnected graph for times less that t_1 and larger than t_2. We will then only need to work with the two-particle interactions for times between t_1 and t_2, and here we will be able to use Lemma 1 to approximate the analysis by that on an infinite path for both the symmetric and anti-symmetric states. Putting everything together, we have a good approximations for all times $0 < t < t_{C\theta}$, and thus we also have a good approximation for the final state.

To do this, let us define the graph G^{sep}_1 to be the G' with the vertex labeled $(\lceil (3+\alpha+1/2)L \rceil, 5)$ removed and let G^{sep}_2 be G' with the vertex labeled $(\lceil (3+1/2)L \rceil, 5)$ removed. Note that both G^{sep}_i have four components, whereas G' had three, but importantly that the two particles only have amplitude on separate components. As such, we can then use Lemma 13 and Lemma 1 as in the case for any of the other logical computational basis states, at least for times in which the single-particle wave-packets remain far from the removed graph. In particular, for all times $0 < t < t_1$, the approximation arising from the corresponding two-particle evolution on disconnected graphs (i.e., both the single-particle evolutions) remain a distance at least $L/3$ from the removed vertex. Hence, using Lemma 13 and the same single-particle evolutions as above, we have that

$$\left\| e^{-iH^{(2)}_{G'}t_1} |11_{\text{in}}\rangle - T_1 T_2 |\alpha^1_1(t_1)\rangle |\alpha^2_1(t_1)\rangle \right\| \leq \xi_3 \sqrt{\frac{\log L}{L}} \tag{7.53}$$

for some constant ξ_3. In particular, we have that each of the individual single-particle evolutions an the finite-sized graphs have errors bounded by ξ_1 and ξ_2 times $\sqrt{\log L/L}$ (as in the above examples),

and thus the two-particle evolution on G^{sep} has an error bound with constant $\xi_1 + \xi_2$. Another application of Lemma 1, using the fact that we are dealing with two-particles and thus the norm of $H^{(2)}_{G'}$ is bounded, the approximations are far from the removed vertex, and our bound on the error when evolving on G^{sep}, then gives the error as claimed.

At this point, our approximations to the time-evolved wave function are only supported on the long path far from the ends of the path, and thus we can use two applications of Lemma 1 to look at the time-evolution on an infinite path. This is exactly the reason for Theorem 5, and we can thus use it's bounds. It is at this point that we discover different evolutions for symmetric and anti-symmetric particles, as the relevant phase acquired during the overlap is dependent on the symmetry between the particles.

In particular, if P is the infinite path with vertices corresponding to the finite path of length Z, we have that Theorem 5 gives us that

$$\begin{aligned}
&\Big\| e^{-iH_P^2(t_2-t_1)} \Big(|\, \phi^{L,\sigma}_{\lceil (2+\alpha)L \rceil}(-k_1)\rangle |\, \phi^{L,\sigma}_{\lceil (7+\alpha)L \rceil}(k_2)\rangle \pm |\, \phi^{L,\sigma}_{\lceil (7+\alpha)L \rceil}(k_2)\rangle |\, \phi^{L,\sigma}_{\lceil (2+\alpha)L \rceil}(-k_1)\rangle \Big) \\
&\quad - e^{i\theta_\pm} e^{-2i(t_2-t_2)(\cos k_1 + \cos k_2)} \Big(|\, \phi^{L,\sigma}_{4L}(-k_1)\rangle |\, \phi^{L,\sigma}_{2L}(k_2)\rangle \pm |\, \phi^{L,\sigma}_{2L}(k_2)\rangle |\, \phi^{L,\sigma}_{4L}(-k_1)\rangle \Big) \Big\| \\
&\qquad \leq \xi_4 \sqrt{\frac{L}{L}}, \qquad (7.54)
\end{aligned}$$

with an approximation for all intermediate times that has a similar bound. With two applications of Lemma 1, along with a relabelling of vertices, we can see

$$\Big\| e^{-iH'^{(2)}_G (t_2-t_1)} |\, \alpha^1_1(t_1), \alpha^1_2(t_1)\rangle_\pm - e^{i\theta_\pm} |\, \alpha^1_1(t_2), \alpha^1_2(t_2)\rangle_\pm \Big\| \leq \zeta_4 \sqrt{\frac{\log L}{L}}. \qquad (7.55)$$

After the two particles have moved passed each other and we have reach time t_2, we can use the same trick to approximate the time evolution for $t_2 < t < t_{C\theta}$ as for the early times, except on the graph G^{sep}_2. We find that the error in our approximation for these times is bounded by the same value as for the early times, as the analysis is nearly identical.

If we then put together these three bounds, we have:

$$\begin{aligned}
&\Big\| e^{-iH'^{(2)}_G t_{C\theta}} |\, 11_{\text{in}}\rangle^{1,2}_\pm - e^{i\theta_\pm} T_1^2 T_2^2 |\, 11_{\text{out}}\rangle^{1,2}_\pm \Big\| \qquad (7.56) \\
&\quad \leq \Big\| e^{-iH'^{(2)}_G t_1} |\, \alpha^1_1(0), \alpha^1_2(0)\rangle_\pm - T_1 T_2 |\, \alpha^1_1(t_1), \alpha^1_2(t_1)\rangle_\pm \Big\| \\
&\qquad + \Big\| e^{-iH'^{(2)}_G (t_2-t_1)} |\, \alpha^1_1(t_1), \alpha^1_2(t_1)\rangle_\pm - e^{i\theta_\pm} |\, \alpha^1_1(t_2), \alpha^1_2(t_2)\rangle_\pm \Big\| \\
&\qquad + \Big\| e^{-iH'^{(2)}_G (t_{C\theta}-t_2)} |\, \alpha^1_1(t_2), \alpha^1_2(t_2)\rangle_\pm - T_1 T_2 |\, \alpha^1_1(t_C\theta), \alpha^1_2(t_C\theta)\rangle_\pm \Big\| \qquad (7.57) \\
&\quad \leq \xi_5 \sqrt{\frac{\log L}{L}} \qquad (7.58)
\end{aligned}$$

and we have (7.40).

If we then take χ to be the maximum constant for our four bounds, we have proven the theorem. □

At this point, we now understand how our assumed initial state propagates for single- and two-particle states, and we have the necessary building blocks for our universality result.

Note that if $\theta_+(k_1, k_2) = \theta_-(k_1, k_2)$, then our results from above hold for distinguishable particles as well, since the applied unitary is then the same for all linear combinations of the two states.

7.3.3 n-qubit evolution

With our analysis of Lemma 17, we can apply an encoded Cθ-gate between two qubits, assuming the appropriate gadgets exist. However, we are actually interested in the n-particle evolution, and before we turn our attention to combining several gates we need to extend our analysis to the case of n-qubits.

This will actually be very similar to that of Lemma 16, in that we will assume that our encoded initial state has each particle on separate components of a graph, except for the two particles on the graph G that will be used to implement the encoded Cθ-gate. In particular, let G' be the infinite graph with $2(n-2)$ infinite paths, and the infinite version of Figure 7.3 (i.e., $X = W = \infty$). Assuming that we want to apply the encoded Cθ gate between qubits j_1 and j_2, and that we want the wave packet for qubit ℓ to be centered a distance μ_ℓ from the first edge of the path, we then let $G(\vec{K})$ be the finite restriction of G. In particular, we have that for the two qubits we want to interact, we have a copy of Figure 7.3 where (7.25)–(7.27) define the lengths, and for each qubit not involved in the applied unitary, there are two paths of length $2\mu_\ell + \lceil 2t_{C\theta} \sin |k_\ell| \rceil$. We then have that the labelling scheme for the vertices in the copy of Figure 7.3 are as in the previous section, while the remaining vertices are labelled as (ℓ, z, x) for $\ell \in [n]$ with $\ell \neq j_1, j_2$, $x \in [2\mu_\ell + \lceil 2t_{C\theta} \sin |k_\ell| \rceil]$ and $z \in \mathbb{F}_2$.

With this labelling scheme for the vertices, we have that our initial logical states for qubits not affected by the unitary are given by

$$|\, z \,\rangle_{\log,\mathrm{in},\ell} = \gamma \sum_{x=-\mu_\ell-L}^{-\mu_\ell+L} e^{-ik_\ell x} e^{-\frac{(x-\mu_\ell)^2}{2\sigma^2}} |\, \ell, x, z \,\rangle, \tag{7.59}$$

(exactly as in Lemma 16) with output encoded states given by

$$|\, z \,\rangle_{\log,\mathrm{out},\ell} = \gamma e^{-2iT\cos(k_\ell)} \sum_{x=\mu_\ell-L}^{\mu_\ell+L} e^{-ik_\ell x} e^{-\frac{(x-\mu_\ell)^2}{2\sigma^2}} |\, \ell, x, z+1 \,\rangle. \tag{7.60}$$

For the two qubits affected by the Cθ-gate, we have that the input encoded logical states are given by (7.23) and (7.24), while the encoded logical output is given by (7.32)–(7.35). We then have that the n-qubit state $|\phi\rangle = \sum_{x\in\mathbb{F}_2^n} \alpha_x |x\rangle$ is represented by

$$|\, \phi \,\rangle_{\log,\mathrm{in}} = \sum_{x\in\mathbb{F}_2^n} \alpha_x \bigotimes_{i=1}^{n} |\, x_i \,\rangle_{\log,\mathrm{in,i}} \tag{7.61}$$

and for a given unitary U,

$$|\, U\phi \,\rangle_{\log,\mathrm{out}} = \sum_{x,y\in\mathbb{F}_2^n} U_{xy}\alpha_y \bigotimes_{i=1}^{n} |\, x_i \,\rangle_{\log,\mathrm{in,i}}. \tag{7.62}$$

Note that these logical encodings assume that the i-th particle is used to represent the i-th qubit. The fact that these particles are distinguishable will make our theorem difficult, so we will work with the states

$$|\, \phi \,\rangle^{\pm}_{\log,\mathrm{in/out}} = \frac{1}{\sqrt{2}} \big(|\, \phi_{\log,\mathrm{in/out}} \,\rangle \pm V_{(j_1 j_2)} |\, \phi_{\log,\mathrm{in/out}} \,\rangle \big). \tag{7.63}$$

Note that these states are symmetric (antisymmetric) between the two particles that interact, which will be sufficient for our purposes. Further, since the Hamiltonian H_G^N is permutation invariant, we will have the same result for any $V_\pi |\, \phi \,\rangle_{\log,\mathrm{in/out}}$.

We then have the following theorem on the evolution of a given logical state.

Lemma 18. *Let $k_j \in (-\pi, 0)$ for all $j \in [n]$, and let us assume that there exists a momentum switch between k_{j_1} and k_{j_2}. Let the logical states $|z\rangle^{\pm}_{log,in}$ and $|z\rangle^{\pm}_{log,out}$ be defined as in (7.10) and (7.11), and let $G(\vec{K})$ be defined as above, where each $\mu_\ell \geq (1+\beta)L$. We then have that there exists some constant ξ such that for all $0 \leq t \leq t_{C\theta}$ and any interaction $\mathcal{U}$,*

$$\left\| e^{-iH_G^N t} |\phi(0)\rangle^{\pm} - |\phi(t)\rangle^{\pm} \right\| \leq \xi n \sqrt{\frac{\log L}{L}}, \tag{7.64}$$

where

$$|\phi(t)\rangle^{\pm} = \sum_{x \in \mathbb{F}_2^n} \alpha_x W_\pi \left[|\beta_{x_{j_1} x_{j_2}}(t)\rangle^{\pm} \otimes \bigotimes_{\substack{\ell=1 \\ \ell \neq j_1, j_2}}^{n} |\alpha_\ell^{x_\ell}(t)\rangle \right], \tag{7.65}$$

the $|\beta_{x_{j_1} x_{j_2}}(t)\rangle$ are the approximations used in Lemma 17 for the logical input $x_{j_1} x_{j_2}$, W_π is the permutation that takes the j_1-st particle to the first location, the j_2-nd particle to the second equation, and orders the rest of the particles, and

$$|\alpha_\ell^z(t)\rangle = \gamma e^{-2it\cos(k_\ell)} \sum_{x=\mu_\ell(t)-L}^{\mu_\ell(t)+L} e^{-ik_\ell x} e^{-\frac{(x-\mu_\ell(t))^2}{2\sigma^2}} |\ell, x, z\rangle, \tag{7.66}$$

with

$$\mu_\ell(t) = \mu_\ell + 2t \sin|k_\ell|. \tag{7.67}$$

In particular, we have

$$\left\| e^{-iH_G^N T} |\psi\rangle^{\pm}_{log,in} - |U\psi\rangle^{\pm}_{log,out} \right\| \leq \xi n \sqrt{\frac{\log L}{L}}. \tag{7.68}$$

where U is a diagonal two-qubit unitary given by $\mathrm{diag}\{1, T_2^2, T_1^2, T_1^2 T_2^2 e^{i\theta_\pm}\}$, where T_j is the transmission coefficient for the momentum switch at momentum k_j, and $\theta_\pm$ is as in Lemma 17.

Proof. The proof of this theorem follows nearly identically to that of Lemma 16, in that we use Lemma 13 to break the analysis into the components of the graph, and then use our results on each component.

Using the fact that the states $|\phi(t)\rangle$ all have the particles supported on different components of G (except for j_1 and j_2), we have by Lemma 13 that

$$e^{-iH_G^N t} |\phi(0)\rangle^{\pm} = \left(e^{-iH_G'^2 t}\right)^{(j_1, j_2)} \prod_{\substack{\ell=1 \\ \ell \neq j_1 j_2}}^{n} \left(e^{-iA(G_\ell)t}\right)^{(\ell)} |\phi(0)\rangle, \tag{7.69}$$

where G_ℓ is the component on which the ℓ-th particle is located. However, we have that each of these unitaries commute, and

$$\left(e^{-iA(G_\ell)t}\right)^{(\ell)} |\phi(0)\rangle = \sum_{x \in \mathbb{F}_2^n} \alpha_x \bigotimes_{i=1}^{n} e^{-i\delta_{i,\ell} A(G_\ell) t} |\alpha_i^{x_i}(0)\rangle \tag{7.70}$$

$$= \sum_{x \in \mathbb{F}_2^n} \alpha_x \left[\bigotimes_{i=1}^{n} \left(|\alpha_i^{x_i}(\delta_{\ell,i} t)\rangle + \delta_{\ell,i} |\epsilon_{\alpha_x,\ell}(t)\rangle \right) \right], \tag{7.71}$$

by Lemma 12, with $\| |\epsilon_{\alpha_x,\ell}(t)\rangle \| \leq \xi\sqrt{\log L/L}$ for some constant ξ.

Additionally, we have from Lemma 17 that

$$e^{-iH_{G'}^2 t}|\beta_{x_{j_1}x_{j_2}}(0)\rangle = |\beta_{x_{j_1}x_{j_2}}(t)\rangle + |\xi_{x_{j_1},x_{j_2}}(t)\rangle, \tag{7.72}$$

where $\| |\xi_{x_{j_1},x_{j_2}}(t)\rangle \| \leq \xi\sqrt{\log L/L}$

Combining these results, we then have that

$$e^{-iH_G^N t}|\phi(0)\rangle = \sum_{x\in\mathbb{F}_2^n} \alpha_x \left[\bigotimes_{i=1}^{n} \left(|\alpha_i^{x_i}(t)\rangle + |\epsilon_{\alpha_x,\ell}(t)\rangle\right)\right] \tag{7.73}$$

$$= |\phi(t)\rangle + |\varepsilon(t)\rangle, \tag{7.74}$$

where $\| |\varepsilon(t)\rangle \| \leq n\xi\sqrt{\log L/L}$. □

From this, we then have the relevant bounds on the multi-qubit evolution.

7.4 Multi-gate simulation

At this point, we know how to encode n qubits into the MPQW of n-particles, we can simulate a single-qubit unitary on one of the qubits, assuming an appropriate gadget exists, and we can perform an entangling gate between two qubits, assuming the existence of a particular momentum switch and nontrivial phase in the two-particle scattering. As such, if we can show how to combine these results without a large increase in the error, we will have our universality result.

Note that there are several arbitrary choices in this construction, as a proof of universality only requires the existence of a simulating graph; we expect that other choices would also provide universal simulation. Additionally, our choice depends on the particular interaction Hamiltonian used in the MPQW, as the phase of the entangling gate Cθ depends on the interaction between the particles.

Along those lines, let us fix some interaction $\mathcal{U}$ between the particles, and let us assume that $\|H_{\text{int}}^n\| \leq \gamma n^\nu$, for some constant γ and ν. We will show almost all such interactions can be used for universal quantum computation.

We will assume that we want to simulate a circuit $\mathcal{C}_X = U_m U_{m_1} \cdots U_1$, where each U_i is from some finite gate set. After making our choices for our encoding, we will place some restrictions on this gate set related to the existence of certain scattering gadgets and the phase $\theta_\pm$ for two-particle interactions arising from H_{int}.

7.4.1 Encoded qubits

The first step in our construction will be to choose how to encode our qubits. As in Section 7.1, we will encode each qubit via a particle in a dual-rail encoding, where the logical states are given by (7.2). At this point, however, we need only choose the values of k_i for each qubit and the initial location of the center of the particles, μ_i.

From our results in Section 7.3, our construction will require at least two different momenta in order to simulate an entangling gate. We will make the choice to only use two momenta, k_1 and k_2, where $\sin|k_1| \leq \sin|k_2|$ and where there exists a momentum switch between the two particles. We also assume that for k_1 and k_2, there are scattering gadgets that implement a universal set of single-qubit unitaries. Note that several such pairs of momentum are known from Chapter 4.

Additionally, for our most simple scheme, we will assume that the particles indistinguishable. All of our results from this chapter will hold with this assumption, and in addition we will easily be able to use Lemma 18. Assuming that $\theta_+(k_1, k_2) \neq 0$, we will assume that our particles are bosons, but if $\theta_+(k_1, k_2) = 0$ we will assume the particles are fermions. If both $\theta_\pm(k_1, k_2) = 0$, note that our entangling gate cannot be constructed at this pair of momenta.

With these choices, we will choose for the n-th qubit to have momentum k_2, while the remaining $n-1$ qubits will have momentum k_1. With this choice, we will require that all two-qubit gates affect the n-th qubit, and thus it will act as a mediator qubit. Further, we assume that each Gaussian wave-packet has a cut-off length L, with standard deviation $\sigma = \frac{L}{2\sqrt{\log L}}$.

7.4.2 Constructing the simulating graph

At this point, we have chosen our logical states, and we now want to construct the graph for our simulation. Note that the idea behind this is almost the same as in Chapter 5, in that we build the simulating graph by concatenating scattering events. In particular, for each unitary U_i, we will include a single-gate circuit of the form described in Section 7.2 or Section 7.3. We then combine these graphs by removing the output paths from the graph U_i, and connecting the corresponding trailing edges to the input paths of U_{i+1}. An example of such combinations is given in Figure 7.5.

More concretely, for single-qubit unitary U_i, we will include a graph of the form described in Section 7.2 with the scattering event corresponding to the unitary U_i on the correct qubit. We will assume that each K_j for $j < n$ is equal to $4L - 1$, and that

$$K_n = \left\lceil 4L \frac{\sin|k_2|}{\sin|k_1|} \right\rceil - 1. \tag{7.75}$$

The reason for these choices is that we want a particle (with momentum k_1) to travel from a position centered at $-2L$ to a position centered about $2L$ during each single-qubit gate, and $K_n + 1$ is the corresponding distance a particle with momentum k_2 travels. Further, we want that the this centered position to be equidistant from the endpoints of the long paths and the corresponding locations where the graph gadgets are attached. In this way, if we combine multiple scattering events implement a single-qubit unitary to the same qubit, when the wave-packet is centered it is a distance $2L - 1$ from both gadgets.

Additionally, for each two-qubit unitary U_i, we will include a graph of the form described in Section 7.3, with the choice of $M(k_1) = 2L - 1$ and $M(k_2) = \lceil 2L \sin|k_2| / \sin|k_1| \rceil - 1$. This choice of $M(k_i)$ is done to facilitate the attachment between graphs at neighboring times.

To combing the graphs for the unitaries U_i, for each $i < m$, we remove the rightmost $2L - 1$ vertices from each outgoing path from U_i, and remove the leftmost vertex from each input path for U_{i+1}. For each qubit $j \in [n]$ and each logical state $z \in \mathbb{F}_2$, we then add an additional edge from the rightmost outgoing vertex from the modified graph for U_i on the path corresponding to logical z_j to the corresponding leftmost vertex of the modified graph of U_{i+1}.

We can think of this in another manner, in that instead of removing the vertices, we simply identify the vertex (i, x, j, z) (where i identifies which unitary the vertex belongs to) with the vertex $(i + 1, x - 4L, j, z)$ if $j \neq n$ (where we assume that the unitary U_i and U_{i+1} are both single-qubit unitaries that do not affect qubit j). We have a similar results for $j = n$, except that (i, x, n, z) is identified with $(i + 1, 1 - 2M(k_2) + x, z)$. In the case where U_i is a two-qubit unitary, we have a similar result.

Let the resulting graph be called G_X

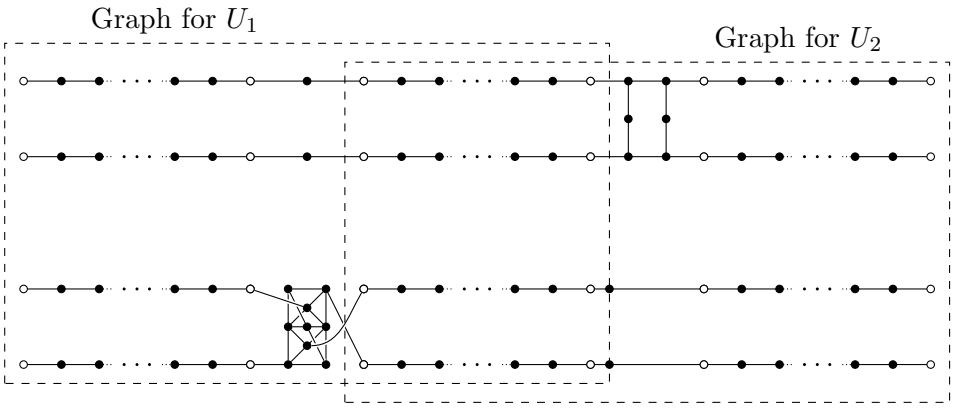

Figure 7.5: An example of concatenating two single-gate graphs. The particular gadgets are between momenta $k_1 = -\frac{\pi}{4}$ and $k_2 = -\frac{\pi}{2}$.

7.4.3 Evolution analysis

Now that we have our defined graph, we will want to show that the n-particle quantum walk on G_X simulates the circuit $\mathcal{C}_X$. We will do this by repeated application of the truncation lemma, so that we can analyze the evolution of the state iteratively. In particular, if the particle is moving toward the graph gadget for the i-th unitary (and is sufficiently far from the graph gadget implementing the $(i-1)$-st unitary), we can use the truncation lemma to approximate the analysis using our results on the scattering behavior for the i-th graph (and only the i-th graph). After the particles have proceeded with the appropriate scattering events and are leaving the i-th graph, we then repeat the process. If we can show that each such gate implements a logical U_i on the encoded space without leaving much error, we will have that the simulation is a success.

Along these lines, we will need to define encoded logical states for both input and output, as well as the logical states between unitaries. If we let

$$t_{\text{single}} = \frac{2L}{\sin|k_1|}, \tag{7.76}$$

and remember the definition for $t_{C\theta}$ in (7.48), we have that these are the two times required to implement a single-qubit gate (t_{single}) and to implement a two-qubit gate ($t_{C\theta}$). Additionally, let us define $m+1$ times, where $t_0 = 0$ and

$$t_{i+1} = \begin{cases} t_i + t_{\text{single}} & U_i \text{ is a single-qubit gate} \\ t_i + t_{C\theta} & U \text{ is a two-qubit gate.} \end{cases} \tag{7.77}$$

In this manner, each time t_i is after the i-th scattering event and before the $i+1$-th scattering event. We will also have that at these times, the wave-packets for each qubit should be centered between scattering events.

Let us now define our logical input and output states for each qubit at time t_i. The most simple case is given at $t = 0$, as the input logical states are exactly the symmetrized states from (7.10) if the first unitary is a single-qubit gate or the symmetrized states (7.61) if the first unitary is a two-qubit unitary (additionally, let us label this basis by 1, since it correspond to the first logical basis). Assuming that the initial state is the logical 0 state, we then have that at time t_1, the state is of the form

$$e^{-iH^N_{G_X} t_1}|0\rangle_{\text{log,in,1}}. \tag{7.78}$$

If we then use Lemma 1 for the vertices of the graph G_X that arose from the graph implementing U_1, along with our approximation to the evolution according to G_1 given by either Lemma 16 or Lemma 18, we can see that for all times $0 \leq t \leq t_1$, the support of our approximation to evolution according to the truncated Hamiltonian remains a distance $\frac{L}{2}$ from the removed vertices. Using the error bounds from the appropriate lemma, we then have that

$$e^{-iH_{G_X}^N t_1}|0\rangle_{\text{log,in},1} = |U_1 0\rangle_{\text{log,out},1} + |\epsilon\rangle \tag{7.79}$$

where

$$\big\||\epsilon\rangle\big\| \leq \xi n \|H_{G_X}^n\| \sqrt{\frac{\log L}{L}}, \tag{7.80}$$

for some constant ξ.

Additionally, note that the output logical states for the first unitary have the exact form as the input logical states to the second unitary (by construction), except for a global phase resulting from a change of vertex labelling between the two graphs computing the unitaries and the acquired phase from the energy. As such, we repeat the above process with the truncation lemma to evolve $|U_1 0\rangle_{\text{log,out},1}$ according to G_2 for times $t_1 \leq t \leq t_2$, while only acquiring an additional error of (7.80).

We can repeat this process for each unitary U_i, until we get that

$$\left\| e^{-iH_{G_X}^N t_1}|0\rangle_{\text{log,in},1} - e^{i\phi}|U_m U_{m-1} \cdots U_1 0\rangle_{\text{log,out},m} \right\| \leq \xi mn \|H_{G_X}^n\| \sqrt{\frac{\log L}{L}}, \tag{7.81}$$

where ϕ is a global phase that doesn't affect the logical state.

From this, if we then choose

$$L = \Theta\Big(m^2 n^2 \|H_{G_X}^n\|^2 \log(mn)\Big), \tag{7.82}$$

we can make the error in the evolution constant. (Note that we used our bound on $\|H_(G_X)^n\|$ in the logarithm.) From this, we then have that the total number of vertices of our graph will be $\mathcal{O}(m^3 n^3 \|H_{G_X}^n\|^2 \log(mn))$ and the total evolution time will be $\mathcal{O}(m^3 n^2 \|H_{G_X}^n\|^2 \log(mn))$. In the case of the Bose-Hubbard model and the most simple nearest-neighbor interactions, we have that $\|H_{G_X}^n\| \leq \gamma n^2$, and these bounds become $\mathcal{O}(m^3 n^7 \log(mn))$ and $\mathcal{O}(m^3 n^6 \log(mn))$.

I would like to point out that this is a near quadratic improvement over the results of Childs, Gosset, and Webb [16]. This occurred by the novel analysis using Gaussian states.

7.4.4 Universality

At this point, we have only shown how to simulate a circuit of a particular form. Namely, our construction requires that each unitary U in the circuit comes from a gate set where

$$U \in \begin{cases} S_{k_2} & \text{if } U \text{ is a single-qubit gate and acts on qubit } n \\ S_{k_1} & \text{if } U \text{ is a single-qubit gate otherwise} \\ \mathrm{C}\theta_{i,n} & \text{otherwise,} \end{cases} \tag{7.83}$$

and where S_{k_i} requires the existence of a particular scattering gadget and $\mathrm{C}\theta_{i,j}$ is a single gate. However, if we assume that each S_{k_i} is a universal set of single-qubit gates, and if we assume that the phase acquired between k_1 and k_2 when they interact on a long path is $\alpha\pi$, for some irrational

α, then we can approximate a $\text{CNOT}_{i,n}$ gate and a $\text{CNOT}_{n,i}$ gate. We can then use these CNOT gates to implement swap gates, and thus we have approximate $\text{CNOT}_{i,j}$ gates between all pairs of qubits. Combining this with the universal single-qubit gate set for all qubits, we then have that we can approximate an arbitrary circuit with circuits of the form required for our construction.

Note that the acquired phase is a ration function of e^{ik_1}, e^{ik_2}, and the interaction strength, and thus for almost all values of the interaction strength we have that the acquired phase is an irrational multiple of π. From this, we have that MPQW with almost any interaction is universal for quantum computing.

7.4.4.1 $k_1 = -\frac{\pi}{4}$ and $k_2 = -\frac{\pi}{2}$

Note from Section 4.1.3, we have a universal gate set for both k_1 and k_2. Further, we have from Chapter 6 that for onsite interactions with strength $\mathcal{U}_0^{2,2}$ that the phase acquired between these two momenta in the symmetric subspace is

$$\frac{2\left(\sin(k_2)-\sin(k_1)\right)-i\mathcal{U}_0^{2,2}}{2\left(\sin(k_2)-\sin(k_1)\right)+i\mathcal{U}_0^{2,2}}. \tag{7.84}$$

In the special case of $\mathcal{U}_0^{2,2} = 2+\sqrt{2}$, this results in a C$\theta$ gate equal to $\text{diag}\{1, i, -1, -1\}$. Using some additional single qubit gates from our gate set, we then have that we can implement the two-qubit unitary $\text{diag}\{1, 1, 1, i\}$.

This gives an explicit example of a set of momenta that can be used in our construction for universality.

7.4.4.2 $k_1 = -\frac{\pi}{3}$ and $k_2 = -\frac{2\pi}{3}$

We also have from Section 4.1.3 that k_1 and k_2 have (the same) universal gate set. Further, from Chapter 6 we have that in the case of nearest-neighbor interactions with interaction strength $\mathcal{U}_1^{1,1}$, the phase acquired between these two momenta in the antisymmetric subspace is

$$-\frac{\mathcal{U}_1^{1,1}+i\sqrt{3}}{\mathcal{U}_1^{1,1}-i\sqrt{3}}. \tag{7.85}$$

And we thus have a universal set of gates at this pair of momenta.

We also have that this set of momenta travel at the same speed, which might be of interest to an experimentalist.

7.5 Extensions

At this point, we have shown the universality of MPQW for almost all interactions. However, some further considerations might be important if this is ever used experimentally. One of the original motivations for this construction was to build a physically realizable graph instead of the exponential graph used in the universality result for quantum walk, and we have succeeded, but any further constraints we can place on the evolution are useful.

7.5.1 Planar graphs

Perhaps the most physically relevant constraint we could place on the graph is to make it planar. If the graph G_X were planar, an experimentalist could lay the graph on a 2D surface, and actually have particles move on the graph.

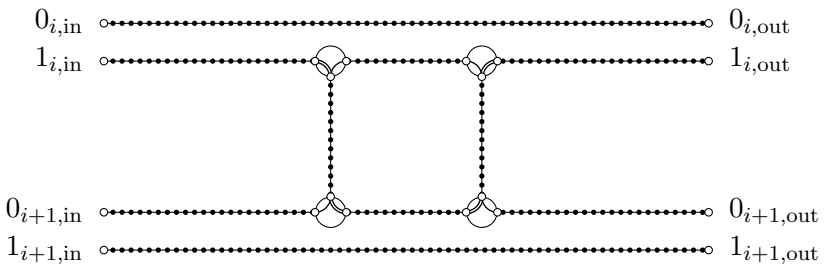

Figure 7.6: The planar entangling gate between adjacent encoded qubits i and $i+1$. This graph implements the unitary $\mathrm{X}_{i+1}(\mathrm{C}\theta)^2_{i,i+1}\mathrm{X}_{i+1}$.

Unfortunately, our current construction cannot be made planar, as we require each two-qubit unitary to involve the n-th qubit, since it has the distinct momentum. However, we can get around this by making every odd qubit have momentum k_1 and every even qubit have momentum k_2. We then only interact adjacent qubits. Note that this is still not planar, as each two-qubit gate affects the bottom path for each qubit, and after the interaction we cross the paths to ensure that the particles remain in the correct locations.

To implement two-qubit gates in a planar manner, we use the graph shown in Figure 7.6. This graph is obtained by concatenating two Cθ graphs and uncrossing paths to make the drawing planar. We only use this gate between adjacent encoded qubits, one of which is a mediator qubit and one of which is a computational qubit. Note that this graph involves two adjacent paths (path 1 of the top encoded qubit and path 0 of the bottom encoded qubit) as opposed to the two 1 paths in the Cθ gate in Figure 7.2. The resulting logical gate is $(\mathrm{C}\theta)^2$ conjugated by an X gate on the bottom qubit.

If we can then also guarantee that the scattering gadgets used to implement the universal gate set and the momentum switch are are planar, then we have that the resulting construction leads to a planar graph. Thankfully, we have that $k_1 = -\frac{\pi}{4}$ and $k_2 = -\frac{\pi}{2}$ both have planar single-particle gadgets, and the momentum switch splitting them is planar as well. If we then look at the symmetric subspace of the onsite interaction with strength $2+\sqrt{2}$, we have a planar construction for universality.

7.5.2 Distinguishable particles

So far we have focused on the case of indistinguishable particles. However, we can also perform universal quantum computation with distinguishable particles, provided the interaction has an appropriate form.

For distinguishable particles we will use use the same encoding of qubits as before, except that now each qubit is associated with a specific particle (e.g., computational qubit 1 is associated with particle 1). We have from Lemma 16 that the single particle evolutions do not depend on the symmetries of the particles, and thus we need only examine the implementation of the Cθ gate to see how our construction must be modified. In this section we show that with a simple nearest-neighbor interaction we can make our scheme work for distinguishable particles by carefully choosing the strength of the interaction term in the Hamiltonian, but with no other modifications.

When two indistinguishable particles of momenta k_1 and k_2 scatter on an infinite path, there is no distinction between the final state where the particles reflect off of each other (exchanging momenta) and where the particles transmit through one another. Thus, after scattering, the global phase of the wave function is multiplied by a factor $T \pm R$, the sum of the amplitude to transmit

and the amplitude to reflect (or the difference if the particles are fermions). For any interaction potential, $|T \pm R| = 1$, and in most cases the applied phase is nontrivial and can be used for universal computation within our scheme.

In contrast, when two *distinguishable* particles of momenta k_1 and k_2 scatter on an infinite path, there are two distinct outgoing states: one corresponding to the case where the two particles reflect and one where the particles transmit. We circumvent this potential problem by choosing the interaction strength so that the transmission probability for two-particle scattering at momenta k_1 and k_1 is 1 (forcing $R = 0$), yet $T \neq 1$ (so that T is a nontrivial phase). With such a choice, the graph implementing the Cθ gates preserves our encoding of qubits. In other words, if encoded qubit 1 is associated with particle 1 before applying the gate, then it is still associated with particle 1 after applying the gate (and similarly for the second qubit involved in the gate). We can then use the same graph as before to implement the controlled phase gate between encoded qubits.

Consider the nearest-neighbor Hamiltonian with $\mathcal{U}1(x, y) = \mathcal{U}_1 xy$. For two particles on an infinite path, this is (**??**) with $\mathcal{V}(|r|) = U\delta_{|r|,1}$. The reflection coefficient $R(k_1, k_2)$ for $k_1 = -\frac{\pi}{4}$ and $p_2 = \frac{\pi}{2}$ is

$$R\left(-\frac{\pi}{4}, \frac{\pi}{2}\right) = \frac{-2U_1^{1,1}\left(\sqrt{2} + (\sqrt{2}-1)\mathcal{U}_1^{1,1}\right)}{(\sqrt{2}-2)(1+i)(\mathcal{U}_1^{1,1})^2 - 4\mathcal{U}_1^{1,1} + 2i(\sqrt{2}+2)}.$$

Our goal is to choose $\mathcal{U}_1^{1,1}$ so that $R = 0$ and T is a nontrivial phase. The values of $\mathcal{U}_1^{1,1}$ that set $R = 0$ are $\mathcal{U}_1^{1,1} = 0$ or $\mathcal{U}_1^{1,1} = -2 - \sqrt{2}$. The solution $\mathcal{U}_1^{1,1} = 0$ corresponds to no interaction and the trivial phase $T = 1$ which is not sufficient for universal computation within our scheme. Choosing $\mathcal{U}_1^{1,1} = -2 - \sqrt{2}$ sets $T = i$ which allows us to perform a CP gate.

We expect that other types of multi-particle quantum walk with distinguishable particles can also be used for universal computation. However, unlike in the case of indistinguishable particles, the interaction term may have to be tuned to satisfy the conditions $R = 0$ and $T \neq 1$ as was the case here. For some interactions, it may not be possible to satisfy these two requirements. For example, for a model where interactions only occur when particles occupy the same site (such as in the Bose-Hubbard model) we have $1 + R = T$ for all momenta, so the transmission amplitude is trivial whenever $R = 0$.

Note that it may be possible to implement an entangling two-qubit gate in other ways. For example, some interactions may allow two-particle scattering with $T = 0$ and $R = i$, in which case the graph shown in Figure 7.6 preserves the encoding of qubits and implements such a gate.

7.6 Conclusions and open problems

What about long-range interactions, but where the interactions die off? Additionally, what about error correction?

smaller constants

Chapter 8

Ground energy of quantum walk

To get some flavor for **QMA**-completeness results.

Now that we have shown the universality of these Quantum Walk Hamiltonians via time evolution, we might want to ask related computational questions about these systems. In particular, once the computational universality of a system is shown, people often ask about the related ground energy problem. The reason for this is that many of these systems that allow for universal computation via time evolution also allow for the encoding of a computation in the ground space, which along with some energy penalties, allow one to show that the ground energy problem is **QMA**-hard.

The point of this chapter is to give a decent introduction to the flavor of **QMA**-hardness proofs, as well as providing a **QMA**-complete problem that might be more accessible to classical computer scientists.

8.1 The ground-energy problem

Essentially, we know that the single-particle quantum walk is governed by the adjacency matrix of the underlying graph. In particular, the Hamiltonian is exactly equal to the adjacency matrix, and thus asking questions about the ground energy of a single-particle quantum walk is simply asking a question about the smallest eigenvalue of a particular adjacency matrix.

However, the Hilbert space on which the quantum walk acts is necessarily exponential in size, with efficiently computable matrix entries. As such, this is a question about very specific types of matrices.

Problem 1 (d-sparse graph eigenvalue problem)**.** Given a d-sparse, row-computable graph G, and two constants $a < b$, is the smallest eigenvalue of $A(G)$ below a or above b, with the guarantee that one of these cases occur.

While this problem is definitely inspired from quantum walks, it actually makes no reference to quantum mechanics.

8.1.1 Containment in QMA

The proof that this problem is in **QMA**follows many other such Hamiltonian problems. In particular, this proof strategy works for any system in which we can evolve according to a particular Hamiltonian.

The main idea is to be given a particular state, and use phase estimation to determine the energy of the given state, up to some error. In the case that the smallest eigenvalue of the system

is below a, the prover can provide the corresponding eigenvector encoded in a quantum state. The phase estimation algorithm will then (with high probability) find this eigenvalue, and the system will accept. If the smallest eigenvalue is above b, then no matter what state the prover provides, the phase estimation algorithm will project onto one of the eigenstates and determine the corresponding eigenvalue, which will necessarily be above b.

More concretely, we have

8.2 QMA-hardness

The main way that this works is that we will use the well known Kitaev Hamiltonian, with some particular changes so that we get taken to a Hamiltonian of a particular form. Once we have that form, we can easily see that the result we want.

8.2.1 Kitaev Hamiltonian

With the definition of the class **QMA**, the requirement is that for each input there exists some quantum circuit and some particular input state that the circuit either accepts or rejects. When attempting to prove that a particular Hamiltonian has a similar computational power, we need to construct a "circuit-to-Hamiltionian" map. The predominant (and really only) such map is the so-called Kitaev-Hamiltonian.

In this mapping, we attempt to encode the computation into the ground space of the Hamiltonian, in a similar manner to how the proof that 3-SAT is NP-Hard encodes the entire computation of a nondeterministic Turing Machine. [**TO DO:** *NP-hardness of 3-Sat reference*] However, we run into a problem on how to insure that neighboring time steps are only seperated by a single local unitary. In the classical case we can write down the entire state of the system at each timestep, or else only write down the changes that occur at each time step. In the first case we run into a problem in that information is copied between time steps, which is impossible for a general state by the no-cloning theorem [**TO DO:** *reference no-cloning*] while the second case quickly becomes infeasible as the changes to the quantum state might effect many basis states.

Kitaev worked around this problem by enlarging the Hilbert space on which the circuit acts, by having both a clock and a state register. The computation of the system was then encoded as an entangled state between these two registers. In this way, by having a projection into those states that evolve correctly for a particular time step, we can have a local check for the correctness of evolution.

In particular, if a given circuit $\mathcal{C}$ acts on $\mathbb{C}^{2^m}$ and can be written as $\mathcal{C} = U_T U_{T-1} \cdots U_1$, then the Kitaev Hamiltonian $H_\mathcal{C}$ acts on the Hilbert space $\mathbb{C}^{2^m} \otimes \mathbb{C}^{T+1}$, and can be written as

$$H_\mathcal{C} = \sum_{t=0}^{T-1} \left(\mathbb{I}_{\mathbb{C}^{2^m}} \otimes |t\rangle - U_{t+1} \otimes |t+1\rangle\right)\left(\mathbb{I}_{\mathbb{C}^{2^m}} \otimes \langle t| - U_{t+1}^\dagger \otimes \langle t+1|\right) = \sum_{t=0}^{T-1} H_t \tag{8.1}$$

Note that each term H_t is a projector off those states of the form

$$|\psi\rangle \otimes |t\rangle + U_{t+1}|\psi\rangle \otimes |t+1\rangle. \tag{8.2}$$

Hence, we have that the ground state of H_C corresponds to the history states:

$$|\psi_{\text{hist}}\rangle = \sum_{t=0}^{T} U_t U_{t-1} \cdots U_1 |\psi\rangle \otimes |t\rangle. \tag{8.3}$$

These states encode the computation, as for a given initial state $|\psi\rangle$, the projection onto the time register gives the state of the computation at time t. Note that the energy gap for this Hamiltonian is exactly $1 - \cos(\pi/T)$, as the Hamiltonian is unitarily equivalent to a quantum walk on a line of length T.

With this mapping corresponding to a particular circuit, we can then force the initial state to have a particular form by adding in projectors tensored with a projection onto the $|t = 0\rangle$ state, with a similar projection for the requisite form of the final state. Putting everything together we then have a log-local Hamiltonian that will have a polynomial gap depending on whether the initial circuit accepted or rejected.

One can then show that this Hamiltonian will have a low energy eigenvector if and only if the corresponding circuit $\mathcal{C}$ has an accepting input.

8.2.2 Transformation to Adjacency Matrix

While the above prescription works well for the conversion to local-Hamiltonians in the general case, in the situation we are interested in we want all of the non-zero matrix elements to be the same value. As the matrix elements of $H_{\mathcal{C}}$ are related to the matrix values of the unitaries involved in the circuit $\mathcal{C}$, we thus want to force the matrix values of $\mathcal{C}$ to all be of the same form.

To enforce this, we suppose $\mathcal{C}$ implements a unitary

$$U_{\mathcal{C}_x} = U_M \dots U_2 U_1 \tag{8.4}$$

where each U_i acts as

$$\mathcal{G} = \{H, HT, (HT)^\dagger, (H \otimes \mathbb{I})\,\mathrm{CNOT}\} \tag{8.5}$$

on some qubits, and the identity on the rest.

Note that this gate set is universal, as we can easily simulate the gate set $\{H, T, \mathrm{CNOT}\}$ with gates from $\mathcal{G}$ since $H^2 = \mathbb{I}$ and we can thus cancel the H terms before the interesting portion of the gates. Further, each non-zero matrix element of these unitaries has norm $2^{-1/2}$, as we wanted.

However, when we look at one of the local terms in the Hamiltonian, we find that not all of the matrix elements have the same norm. In particular, we find that

$$\begin{aligned} H_t &= \left(\mathbb{I}_{\mathbb{C}^{2^m}} \otimes |t\rangle - U_{t+1} \otimes |t+1\rangle\right)\left(\mathbb{I}_{\mathbb{C}^{2^m}} \otimes \langle t| - U_{t+1}^\dagger \otimes \langle t+1|\right) && (8.6)\\ &= \mathbb{I}_{\mathbb{C}^{2^m}} \otimes \left(|t\rangle\langle t| + |t+1\rangle\langle t+1|\right) - \left(U_{t+1} \otimes |t+1\rangle\langle t| + U_{t+1}^\dagger \otimes |t\rangle\langle t+1|\right). && (8.7)\end{aligned}$$

While each off-diagonal term is either zero or has norm $2^{-1/2}$ in (8.7), the diagonal terms have norm 1. When each term is summed, we almost have that the sum of the diagonal terms are proportional to the identity, but unfortunately the boundary terms (with $t = 0$ or $t = T$) are only involved in one unitary. However, this problem can be avoided by having circular time, in which we both compute and uncompute the comptutation. With this, each timestep is involved in exactly two local terms, and thus the diagonal term is proportional to the identity.

With this, it will be convenient to consider

$$U_{\mathcal{C}}^\dagger U_{\mathcal{C}} = W_{2M} \dots W_2 W_1 \tag{8.8}$$

where

$$W_t = \begin{cases} U_t & 1 \le t \le M \\ U_{2M+1-t}^\dagger & M+1 \le t \le 2M. \end{cases} \tag{8.9}$$

As in Section 8.2.1 we start with a version of the Feynman-Kitaev Hamiltonian (with a different norm) [23, ?] acting on the Hilbert space $\mathcal{H}_{\mathrm{comp}} \otimes \mathcal{H}_{\mathrm{clock}}$ where $\mathcal{H}_{\mathrm{comp}} = \left(\mathbb{C}^2\right)^{\otimes m}$ is an m-qubit

computational register and $\mathcal{H}_{\text{clock}} = \mathbb{C}^{2M}$ is a $2M$-level register with periodic boundary conditions (i.e., we let $|2M+1\rangle = |1\rangle$). However, we then subtract a term proportional to the identity, which yields the Hamiltonian

$$H_{\mathcal{C}} = -\sqrt{2}\sum_{t=1}^{2M}\left(W_t^\dagger \otimes |t\rangle\langle t+1| + W_t \otimes |t+1\rangle\langle t|\right). \tag{8.10}$$

Note that

$$V^\dagger H_{\mathcal{C}} V = -\sqrt{2}\sum_{t=1}^{2M}\left(\mathbb{I}\otimes|t\rangle\langle t+1| + \mathbb{I}\otimes|t+1\rangle\langle t|\right) \tag{8.11}$$

where

$$V = \sum_{t=1}^{2M}\left(\prod_{j=t-1}^{1} W_j\right)\otimes|t\rangle\langle t| \tag{8.12}$$

and $W_0 = 1$. Since V is unitary, the eigenvalues of H_x are the same as the eigenvalues of (8.11), namely

$$-2\sqrt{2}\cos\left(\frac{\pi\ell}{M}\right) \tag{8.13}$$

for $\ell = 0,\ldots,2M-1$. The ground energy of (8.11) is $-2\sqrt{2}$ and its ground space is spanned by

$$|\phi\rangle\frac{1}{\sqrt{2M}}\sum_{j=1}^{2M}|t\rangle, \quad |\phi\rangle \in \Lambda \tag{8.14}$$

where Λ is any orthonormal basis for $\mathcal{H}_{\text{comp}}$. A basis for the ground space of H_x is therefore

$$V\left(|\phi\rangle\frac{1}{\sqrt{2M}}\sum_{j=1}^{2M}|t\rangle\right) = \frac{1}{\sqrt{2M}}\sum_{t=1}^{2M}W_{t-1}W_{t-2}\ldots W_1|\phi\rangle|t\rangle \tag{8.15}$$

where $|\phi\rangle \in \Lambda$. The first excited energy of H_x is

$$\eta = -2\sqrt{2}\cos\left(\frac{\pi}{M}\right) \tag{8.16}$$

and the gap between ground and first excited energies is lower bounded as

$$\eta + 2\sqrt{2} \geq \sqrt{2}\frac{\pi^2}{M^2} \tag{8.17}$$

(using the fact that $1-\cos(x) \leq \frac{x^2}{2}$).

The universal set $\mathcal{G}$ is chosen so that each gate has nonzero entries that are integer powers of $\omega = e^{i\frac{\pi}{4}}$. Correspondingly, the nonzero standard basis matrix elements of $H_{\mathcal{C}}$ are also integer powers of $\omega = e^{i\frac{\pi}{4}}$. We consider the 8×8 shift operator

$$S = \sum_{j=0}^{7}|j+1 \bmod 8\rangle\langle j| \tag{8.18}$$

and note that ω is an eigenvalue of S with eigenvector

$$|\omega\rangle = \frac{1}{\sqrt{8}}\sum_{j=0}^{7}\omega^{-j}|j\rangle. \tag{8.19}$$

We modify $H_{\mathcal{C}}$ as follows. For each operator $-\sqrt{2}H$, $-\sqrt{2}HT$, $-\sqrt{2}(HT)^\dagger$, or $-\sqrt{2}\,(H \otimes \mathbb{I})\,\mathrm{CNOT}$ appearing in equation (8.10), define another operator that acts on $\mathbb{C}^2 \otimes \mathbb{C}^8$ or $\mathbb{C}^4 \otimes \mathbb{C}^8$ (as appropriate) by replacing nonzero matrix elements with powers of the operator S:

$$\omega^k \mapsto S^k.$$

Matrix elements that are zero are mapped to the 8×8 all-zeroes matrix. Write $B(W)$ for the operators obtained by making this replacement, e.g.,

$$-\sqrt{2}HT = \begin{pmatrix} \omega^4 & \omega^5 \\ \omega^4 & \omega \end{pmatrix} \mapsto B(HT) = \begin{pmatrix} S^4 & S^5 \\ S^4 & S \end{pmatrix}.$$

Adjoining an 8-level ancilla as a third register and making this replacement in equation (**??**) gives

$$H_{\mathrm{prop}} = \sum_{t=1}^{2M} \Big(B(W_t)^\dagger_{13} \otimes |t\rangle\langle t+1|_2 + B(W_t)_{13} \otimes |t+1\rangle\langle t|_2 \Big) \tag{8.20}$$

which is a symmetric 0-1 matrix (the subscripts indicate which registers the operators act on). Note that H_{prop} commutes with S (acting on the 8-level ancilla) and therefore is block diagonal with eight sectors. In the sector where S has eigenvalue ω, H_{prop} is identical to the Hamiltonian $H_{\mathcal{C}}$ that we started with (see equation (8.10)). There is also a sector (where S has eigenvalue ω^*) where the Hamiltonian is the element-wise complex conjugate of $H_{\mathcal{C}}$. We will add a term to H_{prop} that introduces an energy penalty for states in any of the other six sectors, ensuring that none of these states lie in the ground space.

To see what kind of energy penalty is needed, we lower bound the eigenvalues of H_{prop}. Note that for each $W \in \mathcal{G}$, $B(W)$ contains at most 2 ones in each row or column. Looking at equation (8.20) and using this fact, we see that each row and each column of H_{prop} contains at most four ones (with the remaining entries all zero). Therefore $\|H_{\mathrm{prop}}\| \leq 4$, so every eigenvalue of H_{prop} is at least -4.

The matrix A_x associated with the circuit $\mathcal{C}_x$ acts on the Hilbert space

$$\mathcal{H}_{\mathrm{comp}} \otimes \mathcal{H}_{\mathrm{clock}} \otimes \mathcal{H}_{\mathrm{anc}} \tag{8.21}$$

where $\mathcal{H}_{\mathrm{anc}} = \mathbb{C}^8$ holds the 8-level ancilla. We define

$$A_x = H_{\mathrm{prop}} + H_{\mathrm{penalty}} + H_{\mathrm{input}} + H_{\mathrm{output}} \tag{8.22}$$

where

$$H_{\mathrm{penalty}} = \mathbb{I} \otimes \mathbb{I} \otimes \left(S^3 + S^4 + S^5\right) \tag{8.23}$$

is the penalty ensuring that the ancilla register holds either $|\omega\rangle$ or $|\omega^*\rangle$ and the terms

$$H_{\mathrm{input}} = \sum_{j=n_{\mathrm{input}}+1}^{n} |1\rangle\langle 1|_j \otimes |1\rangle\langle 1| \otimes \mathbb{I}$$
$$H_{\mathrm{output}} = |0\rangle\langle 0|_{\mathrm{output}} \otimes |M+1\rangle\langle M+1| \otimes \mathbb{I}$$

ensure that the ancilla qubits are initialized in the state $|0\rangle$ when $t = 1$ and that the output qubit is in the state $|1\rangle\langle 1|$ when the circuit $\mathcal{C}_x$ has been applied (i.e., at time $t = M + 1$). Observe that A_x is a symmetric 0-1 matrix.

Now consider the ground space of the first two terms $H_{\text{prop}} + H_{\text{penalty}}$ in (8.22). Note that $[H_{\text{prop}}, H_{\text{penalty}}] = 0$, so these operators can be simultaneously diagonalized. Furthermore, H_{penalty} has smallest eigenvalue $-1 - \sqrt{2}$, with eigenspace spanned by $|\omega\rangle$ and $|\omega^*\rangle$. One can also easily confirm that the first excited energy of H_{penalty} is -1.

The ground space of $H_{\text{prop}} + H_{\text{penalty}}$ lives in the sector where H_{penalty} has minimal eigenvalue $-1 - \sqrt{2}$. To see this, note that within this sector H_{prop} has the same eigenvalues as H_x, and therefore has lowest eigenvalue $-2\sqrt{2}$. The minimum eigenvalue e_1 of $H_{\text{prop}} + H_{\text{penalty}}$ in this sector is

$$e_1 = -2\sqrt{2} + \left(-1 - \sqrt{2}\right) = -1 - 3\sqrt{2} = -5.24\ldots, \tag{8.24}$$

whereas in any other sector H_{penalty} has eigenvalue at least -1 and (using the fact that $H_{\text{prop}} \geq -4$) the minimum eigenvalue of $H_{\text{prop}} + H_{\text{penalty}}$ is at least -5. Thus, an orthonormal basis for the ground space of $H_{\text{prop}} + H_{\text{penalty}}$ is furnished by the states

$$\frac{1}{\sqrt{2M}} \sum_{t=1}^{2M} W_{t-1} W_{t-2} \ldots W_1 |\phi\rangle |t\rangle |\omega\rangle \tag{8.25}$$

$$\frac{1}{\sqrt{2M}} \sum_{t=1}^{2M} (W_{t-1} W_{t-2} \ldots W_1)^* |\phi^*\rangle |t\rangle |\omega^*\rangle \tag{8.26}$$

where $|\phi\rangle$ ranges over the basis Λ for $\mathcal{H}_{\text{comp}}$ and $*$ denotes (elementwise) complex conjugation.

At this point, we then have a symmetric 0-1 matrix whose ground-space is spanned by history states. While we have not yet shown that determining the ground energy of this matrix is **QMA**-hard, this graph is the result of our circuit-to-graph mapping.

8.2.3 Upper bound on the smallest eigenvalue for yes instances

Suppose x is a yes instance; then there exists some n_{input}-qubit state $|\psi_{\text{input}}\rangle$ satisfying $\text{AP}\left(\mathcal{C}_x, |\psi_{\text{input}}\rangle\right) \geq 1 - \frac{1}{2^{|x|}}$. Let

$$|\text{wit}\rangle = \frac{1}{\sqrt{2M}} \sum_{t=1}^{2M} W_{t-1} W_{t-2} \ldots W_1 \left(|\psi_{\text{input}}\rangle |0\rangle^{\otimes n - n_{\text{input}}}\right) |t\rangle |\omega\rangle \tag{8.27}$$

and note that this state is in the e_1-energy ground space of $H_{\text{prop}} + H_{\text{penalty}}$ (since it has the form (8.25)). One can also directly verify that $|\text{wit}\rangle$ has zero energy for H_{input}. Thus

$$\begin{aligned}
\langle \text{wit}| A_x |\text{wit}\rangle &= e_1 + \langle \text{wit}| H_{\text{output}} |\text{wit}\rangle \\
&= e_1 + \frac{1}{2M} \langle \psi_{\text{input}}| \langle 0|^{\otimes n - n_{\text{input}}} U_{\mathcal{C}_x}^\dagger |0\rangle \langle 0|_{\text{output}} U_{\mathcal{C}_x} |\psi_{\text{input}}\rangle |0\rangle^{\otimes n - n_{\text{input}}} \\
&= e_1 + \frac{1}{2M} \left(1 - \text{AP}(\mathcal{C}_x, |\psi_{\text{input}}\rangle)\right) \\
&\leq e_1 + \frac{1}{2M} \frac{1}{2^{|x|}}.
\end{aligned}$$

8.2.4 Lower bound on the smallest eigenvalue for no instances

Now suppose x is a no instance. Then the verification circuit $\mathcal{C}_x$ has acceptance probability $\text{AP}\left(\mathcal{C}_x, |\psi\rangle\right) \leq \frac{1}{3}$ for all n_{input}-qubit input states $|\psi\rangle$.

We backtrack slightly to obtain bounds on the eigenvalue gaps of the Hamiltonians $H_{\text{prop}} + H_{\text{penalty}}$ and $H_{\text{prop}} + H_{\text{penalty}} + H_{\text{input}}$. We begin by showing that the energy gap of $H_{\text{prop}} + H_{\text{penalty}}$

is at least an inverse polynomial function of M. Subtracting a constant equal to the ground energy times the identity matrix sets the smallest eigenvalue to zero, and the smallest nonzero eigenvalue satisfies

$$\gamma(H_{\text{prop}} + H_{\text{penalty}} - e_1 \cdot \mathbb{I}) \geq \min\left\{\sqrt{2}\frac{\pi^2}{M^2}, -5 - e_1\right\} \geq \frac{1}{5M^2}. \tag{8.28}$$

since $-5 - e_1 \approx 0.24\ldots > \frac{1}{5}$. The first inequality above follows from the fact that every eigenvalue of H_{prop} in the range $[e_1, -5)$ is also an eigenvalue of H_x (as discussed above) and the bound (8.17) on the energy gap of H_x.

Now use the Nullspace Projection Lemma (Lemma **??**) with

$$H_A = H_{\text{prop}} + H_{\text{penalty}} - e_1 \cdot \mathbb{I} \qquad H_B = H_{\text{input}}. \tag{8.29}$$

Note that H_A and H_B are positive semidefinite. Let S_A be the ground space of H_A and consider the restriction $H_B|_{S_A}$. Here it is convenient to use the basis for S_A given by (8.25) and (8.26) with $|\phi\rangle$ ranging over the computational basis states of n qubits. In this basis, $H_B|_{S_A}$ is diagonal with all diagonal entries equal to $\frac{1}{2M}$ times an integer, so $\gamma(H_B|_{S_A}) \geq \frac{1}{2M}$. We also have $\gamma(H_A) \geq \frac{1}{5M^2}$ from equation (8.28), and clearly $\|H_B\| \leq n$. Thus Lemma **??** gives

$$\gamma(H_{\text{prop}} + H_{\text{penalty}} + H_{\text{input}} - e_1 \cdot \mathbb{I}) \geq \frac{\left(\frac{1}{5M^2}\right)\left(\frac{1}{2M}\right)}{\frac{1}{5M^2} + \frac{1}{2M} + n} \geq \frac{1}{10M^3\,(1+n)} \geq \frac{1}{20M^3 n}. \tag{8.30}$$

Now consider adding the final term H_{output}. We use Lemma **??** again, now setting

$$H_A = H_{\text{prop}} + H_{\text{penalty}} + H_{\text{input}} - e_1 \cdot \mathbb{I} \qquad H_B = H_{\text{output}}. \tag{8.31}$$

Let S_A be the ground space of H_A. Note that it is spanned by states of the form (8.25) and (8.26) where $|\phi\rangle = |\psi\rangle|0\rangle^{\otimes n - n_{\text{input}}}$ and $|\psi\rangle$ ranges over any orthonormal basis of the n_{input}-qubit input register. The restriction $H_B|_{S_A}$ is block diagonal, with one block for states of the form

$$\frac{1}{\sqrt{2M}} \sum_{t=1}^{2M} W_{t-1} W_{t-2} \ldots W_1 \left(|\psi\rangle|0\rangle^{\otimes n - n_{\text{input}}}\right) |t\rangle|\omega\rangle \tag{8.32}$$

and another block for states of the form

$$\frac{1}{\sqrt{2M}} \sum_{t=1}^{2M} (W_{t-1} W_{t-2} \ldots W_1)^* \left(|\psi\rangle^*|0\rangle^{\otimes n - n_{\text{input}}}\right) |t\rangle|\omega^*\rangle. \tag{8.33}$$

We now show that the minimum eigenvalue of $H_B|_{S_A}$ is nonzero, and we lower bound it. We consider the two blocks separately. By linearity, every state in the first block can be written in the form (8.32) for some state $|\psi\rangle$. Thus the minimum eigenvalue within this block is the minimum expectation of H_{output} in a state (8.32), where the minimum is taken over all n_{input}-qubit states $|\psi\rangle$. This is equal to

$$\min_{|\psi\rangle} \frac{1}{2M}\left(1 - \text{AP}(\mathcal{C}_x, |\psi\rangle)\right) \geq \frac{1}{3M} \tag{8.34}$$

where we used the fact that $\text{AP}\left(\mathcal{C}_x, |\psi\rangle\right) \leq \frac{1}{3}$ for all $|\psi\rangle$. Likewise, every state in the second block can be written as (8.33) for some state $|\psi\rangle$, and the minimum eigenvalue within this block is

$$\min_{|\psi\rangle} \frac{1}{2M}\left(1 - \text{AP}(\mathcal{C}_x, |\psi\rangle)^*\right) \geq \frac{1}{3M} \tag{8.35}$$

(since $\mathrm{AP}(\mathcal{C}_x, |\psi\rangle)^* = \mathrm{AP}(\mathcal{C}_x, |\psi\rangle) \leq \frac{1}{3}$). Thus we see that $H_B|_{S_A}$ has an empty nullspace, so its smallest eigenvalue is equal to its smallest nonzero eigenvalue, namely

$$\gamma(H_B|_{S_A}) \geq \frac{1}{3M}. \tag{8.36}$$

Now applying Lemma **??** using this bound, the fact that $\|H_B\| = 1$, and the fact that $\gamma(H_A) \geq \frac{1}{20M^3n}$ (from equation (8.30)), we get

$$\gamma(A_x - e_1 \cdot \mathbb{I}) \geq \frac{\frac{1}{60M^4n}}{\frac{1}{20M^3n} + \frac{1}{3M} + 1} \geq \frac{1}{120M^4n}. \tag{8.37}$$

Since $H_B|_{S_A}$ has an empty nullspace, $A_x - e_1 \cdot \mathbb{I}$ has an empty nullspace, and this is a lower bound on its smallest eigenvalue.

8.3 Extensions and Discussion

While this result is interesting in its own right, as it shows that finding the ground energy of a sparse, row-computable matrix is **QMA**-complete, perhaps the most interesting result is that nothing particularly quantum is involved in the definition of the problem. In particular, the only condition we have on the matrix is that it is sparse, and row-computable. This condition might allow for a more natural understanding for more classically-minded computer scientists, as a **QMA**-complete problem could be stated without having to delve into any quantum computing.

As an additional problem, since the circuit-to-Hamiltonian map creates a 7-regular, simple graph, one might wonder if the removal of these conditions are necessary when the boundary terms are added. This is obviously going to be necessary, as otherwise we would have that determining the lowest eigenvalue of a Laplacian is **QMA**-complete, but it is a well known fact that the smallest eigenvalue of a Laplacian is zero.

[**TO DO:** *can I use the same techniques as the self-loop removal to remove self-loops from this system?*]

[**TO DO:** *Write more*]

Chapter 9

Ground energy of multi-particle quantum walk

With our proof that the ground state problem for a single-particle quantum walk is **QMA**-complete, we would now like to examine the corresponding problem for the multi-particle quantum walk. The similarities between the two systems make us expect that very similar results will hold for the multi-particle case, but we will again need to examine the problem in a lot of detail.

In particular, the **QMA**-completeness for the single particle walk was relatively straightforward, in that there is really only one particle to deal with. Because of this, we understand the dynamics and can exactly analyze the system on which things interact, leading to exact solutions for the energies of the resulting Hamiltonian. With the MPQW, a full analysis is currently beyond our knowledge, and our universality construction relied on a reduction to the cases with at most two interacting particles. In order to show that finding the ground energy of a MPQW is **QMA**-complete using our techniques, we'd need to again reduce to the case of a small number of particles.

To make this reduction, we will show that the problem is **QMA**-hard when restricted to the problem where the interaction term adds (almost) no energy to the ground state, so that the ground state is contained within the span of single-particle states that don't overlap. With this restriction, we will still have correlations between many particles, but we will be able to analyze the correlations and determine the corresponding ground energy.

Our proof strategy, using repeated applications of the Nullspace Projection Lemma, is analogous to that of reference [**?**], where the so-called Projection Lemma was used similarly. Our technique has the advantage of not requiring the terms we add to our Hamiltonian to have "unphysical" problem-size dependent coefficients (it also has this advantage over the method of perturbative gadgets [**?**, **?**]). This allows us to prove results about the "physically realistic" Bose-Hubbard Hamiltonian. A similar technique based on Kitaev's Geometric Lemma was used recently in reference [**?**] (however, that method is slightly more computation intensive, requiring a lower bound on $\gamma(H_B)$ as well as bounds on $\gamma(H_A)$ and $\gamma(H_B|_S)$).

9.1 MPQW Hamiltonian ground-energy problem

In order to make things precise, we will fix a particular finite-range interaction, and show that with this fixed interaction, the resulting question is **QMA**-complete to solve. In particular let $\mathcal{U}$ be an interaction with finite support and no negative coefficients. For a particular graph G, we can then

define a Hamiltonian on such a graph as [**TO DO:** *find a correct way to define* $\mathcal{U}$]

$$H_{f,G} = \sum_{(i,j)\in E(G)} a_i a_j + a_j a_i + \sum_{i,j\in V(G)} U_{d(i,j)}(n_i, n_j) = H_{G,\text{move}} + H_{G,\text{int}}. \tag{9.1}$$

Note that because of the positivity restrictions placed on $\mathcal{U}$, we have that $H_{G,\text{int}}$ is positive semi-definite, and thus the ground energy of $H_{f,G}$ is at least the ground energy of $H_{G,\text{move}}$.

With this particular interaction, we can then construct the corresponding problem.

Note that these Hamiltonians actually act on an infinite dimensional Hilbert space, in that the number of particles is unbounded. In order to reduce the complexity of these problems to a reasonable amount, we restrict our attention to a particular number of particles. Once again, as each term in the Hamiltonian preserves the number of particles, we have that $H_{\mathcal{U},G}$ decomposes into blocks with a particular particle number, and we represent these blocks as $\overline{H}^N_{\mathcal{U},G}$.

Problem 2 ($\mathcal{U}$-interaction MPQW Hamiltonion)**.** Given as input a K-vertex graph G, a number of particles N, a real number c, and a precision parameter $\epsilon = 1/T$, where the positive integers N and T are given in unary, and the graph G is given as its adjacency matrix (a $K \times K$ symmetric 0-1 matrix), the $\mathcal{U}$-interaction MPQW Hamiltonian problem is to determine whether the smallest eigenvalue of $\overline{H}^N_{\mathcal{U},G}$ is at most c or is at least $c+\epsilon$, with a promise that one of these two cases hold.

9.1.1 MPQW Hamiltonian is contained in QMA

To prove that $\mathcal{U}$-interaction MPQW Hamiltonian problem is contained in **QMA**, we provide a verification algorithm satisfying the requirements of Definition **??**. In the Definition this algorithm is specified by a circuit involving only one measurement of the output qubit at the end of the computation. The procedure we describe below, which contains intermediate measurements in the computational basis, can be converted into a verification circuit of the desired form by standard techniques.

We are given an instance specified by G, N, c, and ϵ. We are also given an input state $|\phi\rangle$ of n_{input} qubits, where $n_{\text{input}} = \lceil \log_2 D_N \rceil$ and D_N is the dimension of $\mathcal{Z}_N(G)$ as given in equation (**??**). Note, using the inequality $\binom{a}{b} \leq a^b$ in equation (**??**), that $n_{\text{input}} = \mathcal{O}(K \log(N+K))$, where $K = |V|$ is the number of vertices in the graph G. We embed $\mathcal{Z}_N(G)$ into the space of n_{input} qubits straightforwardly as the subspace spanned by the first D_N standard basis vectors (with lexicographic ordering, say). The first step of the verification procedure is to measure the projector onto this space $\mathcal{Z}_N(G)$. If the measurement outcome is 1 then the resulting state $|\phi'\rangle$ is in $\mathcal{Z}_N(G)$ and we continue; otherwise we reject.

In the second step of the verification procedure, the goal is to measure $\bar{H}^N_G$ in the state $|\phi'\rangle$. The Hamiltonian $\bar{H}^N_G$ is sparse and efficiently row-computable, with norm

$$\left\|\bar{H}^N_G\right\| \leq \left\|H^N_G\right\| \leq N \left\|A(G)\right\| + \left\|\sum_{k\in V} \hat{n}_k \left(\hat{n}_k - 1\right)\right\| \leq NK + N^2. \tag{9.2}$$

We use phase estimation (see for example [**?**]) to estimate the energy of $|\phi'\rangle$, using sparse Hamiltonian simulation [1] to approximate evolution according to $\bar{H}^N_G$. We choose the parameters of the phase estimation so that, with probability at least $\frac{2}{3}$, it produces an approximation E of the energy with error at most $\frac{\epsilon}{4}$. This can be done in time $\text{poly}(N, K, \frac{1}{\epsilon})$. If $E \leq c + \frac{\epsilon}{2}$ then we accept; otherwise we reject.

We now show that this verification procedure satisfies the completeness and soundness requirements of Definition **??**. For a yes instance, an eigenvector of $\bar{H}^N_G$ with eigenvalue $e \leq c$ is accepted

by this procedure as long as the energy E computed in the phase estimation step has the desired precision. To see this, note that we measure $|E - e| \leq \frac{\epsilon}{4}$, and hence $E \leq c + \frac{\epsilon}{4}$, with probability at least $\frac{2}{3}$. For a no instance, write $|\phi'\rangle \in \mathcal{Z}_N(G)$ for a state obtained after passing the first step. The value E computed by the subsequent phase estimation step satisfies $E \geq c + \frac{3\epsilon}{4}$ with probability at least $\frac{2}{3}$, in which case the state is rejected. From this we see that the probability of accepting a no instance is at most $\frac{1}{3}$.

9.1.1.1 QMA-hard problem

With all of these definitions floating around, it will then be useful to actually define the basic problem that we will show is **QMA**-hard. In particular, we have that for any positive integer α, the following problem:

Problem 3 (α-frustration-free$\mathcal{U}$-interaction MPQW Hamiltonian)**.** We are given as input a K-vertex simple graph G, a number of particles $N \leq K$, and a precision parameter $\epsilon = 1/T$, where the positive integers N and $T \geq 4K$ are given in unary, and the graph G is given as its adjacency matrix (a $K \times K$ symmetric 0-1 matrix). We arp promised that either $\lambda_N^1(G) \leq \epsilon^\alpha$ (a yes instance), or else that $\lambda_N^1(G) \geq \epsilon + \epsilon^\alpha$ (a no instance) and we are asked to decide which is the case.

Note that for each interaction type, this is an infinite family of problems. The positive integer α parameterizes how much the yes cases can deviate from a true frustration-free case. The reason that we define the problem in such a way is that it will facilitate the reduction found in Chapter **??**.

Note that this is a special case of the $\mathcal{U}$-interaction MPQW Hamiltonian, with $c = N\mu(G) + \epsilon^\alpha$. As such, if we show that the α-frustration free $\mathcal{U}$-interaction MPQW Hamiltonian problem is **QMA**-hard, we will also show that the non-frustration-free problem is **QMA**-complete.

9.2 Useful graph primitives

At this point, we will want to construct a graph for which our **QMA**-hardness result will hold. As such, we will at this point restrict our attention to a particular interaction, $\mathcal{U}$. While the idea behind the construction of these graphs will not change, the exact graph will depend on both the largest distance for which there is a non-zero interaction. We will want to construct a foundational graph that does not have a two-particle ground state, and also we will want to ensure that our connections between these building blocks will not have multiple particles interacting except on specially chosen building blocks.

As such, let us assume that the minimum distance that the interaction $\mathcal{U}$ has non-zero interactions is $d_{\min}$, while the maximum distance is $d_{\max}$. Our graph will only depend on $d_{\max}$, but it will be useful to also know $d_{\min}$. We will also assume that $\mathcal{U}_{d_{\min}}^{(1,1)} > 0$, so that there is some energy penalty if two particles are at a distance $d_{\min}$ (assuming that $d_{\min} > 0$ — otherwise we will assume that $\mathcal{U}_0^2 > 0$).

Additionally, we will want the eventual graph to be a simple graph, so that there is always at most a single edge between two vertices and no self-loops. Unfortunately, our proof strategy will involve adding many positive semi-definite terms to the adjacency matrix, which correspond to adding in edges and self-loops. As such, we will instead force every vertex in the graph to contain a self-loop, so that by removing all of the self loops we only shift the energy levels by a constant amount. Keep this in mind, as the eventual graph is defined.

With all of this said, however, this section will only define some useful foundational graphs that will be used in the final construction of the graph. All of these graphs will be constant sized, and we

will show a spanning set for their single-particle and two-particle ground states. By construction, they will not have any three-particle frustration-free states.

9.2.1 Gate graphs

[**TO DO:** *rewrite this introduction*] In this section we define a class of graphs (*gate graphs*) and a diagrammatic notation for them (*gate diagrams*) that will allow us to more easily construct the graphs that will be used in our proofs. Additionally, we will also discuss the MPQW Hamiltonian acting on these graphs, with a particular emphasis on the low-energy states. We will eventually use this characterization of the low energy states on these small graphs to analyze and give bounds on the low energy states of the more complicated graphs corresponding to particular gate diagrams.

Every gate graph is constructed using a specific, finite-sized graph g_0 as a building block that only depends on the interaction range of the interaction Hamiltonian for the MPQW. This building block is shown in Figure 9.1 (in the specific instance of for graphs with $d_{\min} <= 1$ and discussed in Section 9.2.1.1). These graphs are designed so that in the low energy sector, each copy of g_0 can only contain a single particle at a time, so that we can force particles to occupy certain states. Additionally, the low energy states correspond to the history states of a simple single-qubit circuits, as described in Chapter 5.

[**TO DO:** *fix this part*] In Section **??** we discuss the ground states of the Bose-Hubbard model on gate graphs. For any gate graph G, the smallest eigenvalue $\mu(G)$ of the adjacency matrix $A(G)$ satisfies $\mu(G) \geq -1 - 3\sqrt{2}$. It is convenient to define the constant

$$e_1 = -1 - 3\sqrt{2}. \tag{9.3}$$

When $\mu(G) = e_1$ we say G is an e_1-gate graph. We focus on the frustration-free states of e_1-gate graphs (recall from Definition **??** that $|\phi\rangle \in \mathcal{Z}_N(G)$ is frustration free iff $H(G,N)|\phi\rangle = 0$). We show that all such states live in a convenient subspace (called $\mathcal{I}(G,N)$) of the N-particle Hilbert space. This subspace has the property that no two (or more) particles ever occupy vertices of the same copy of g_0. The restriction to this subspace makes it easier to analyze the ground space.

In Section **??** we consider a class of subspaces that, like $\mathcal{I}(G,N)$, are defined by a set of constraints on the locations of N particles in an e_1-gate graph G. We state an "Occupancy Constraints Lemma" (proven in Appendix **??**) that relates a subspace of this form to the ground space of the Bose-Hubbard model on a graph derived from G.

9.2.1.1 The graph g_0

The graph g_0 shown in Figure 9.1 is constructed using the method of Chapter 8, with the single qubit circuit corresponding to a sequence of H and HT gates. The intuition behind this graph is to force the ground state to correspond to the history state of these simple computations, thus allowing us to reference the computational value of the corresponding qubit in several disparate locations. We will eventually combine several of these g_0 graphs using projectors, which will remove certain states from the ground space depending on the value of the corresponding qubits.

As such, let $k = 4 + 2\lfloor \frac{d_{\max}}{2} \rfloor$, and then let us look at the single-qubit circuit $\mathcal{C}_0$ with k gates U_j, for $j \in [k]$, where

$$U_1 = HT \qquad U_2 = (HT)^\dagger \tag{9.4}$$

and the rest of the $U_j = H$. We will use the second, third, and fourth of these time steps as computations in the eventual gadgets, while the remaining time steps act as padding to ensure that

the computational time steps used in the eventual graph occur at a distance at least $d_{\max}$ from each other. As the circuit $\mathcal{C}_0$ implements an identity operation, we can easily concatenate several of these circuits and examine the graph corresponding to the circuit using circular time, as in the construction used in Chapter 8. For our purposes, we will want to use 8 copies of $\mathcal{C}_0$ in series, as the eventual gadgets used in our proof have 8 possible locations for interactions with other copies of g_0.

In particular, we will have that the 0-1 Hamiltonian corresponding to the eventual adjacency matrix of g_0 acts on the Hilbert space $\mathcal{H}(g_0) = \mathbb{C}^2 \otimes \mathbb{C}^{8k} \otimes \mathbb{C}^8$. If we then remember that $B(U)$ is the operator that takes $\omega \mapsto S$, where $\omega = e^{i\pi/4}$ and S is the shift operator acting on $\mathbb{C}^8$, we have that the component of the Hamiltonian corresponding to the circuit is

$$H_{\text{prop}} = -\sqrt{2} \sum_{t=0}^{8k-1} B(V_t)_{13} \otimes |t+1\rangle\langle t| + B(V_t^\dagger)_{13} \otimes |t\rangle\langle t+1|, \tag{9.5}$$

where the $B(U)_{13}$ act on the Hilbert spaces $\mathbb{C}^2 \otimes \mathbb{C}^8$ while the clock acts on the $\mathbb{C}^{8k}$ Hilbert space, and where

$$V_t = \begin{cases} HT & t = 0 \mod 8 \\ (HT)^\dagger & t = 1 \mod 8 \\ H & \text{otherwise.} \end{cases} \tag{9.6}$$

This term, along a penalty to the $\mathbb{C}^8$ Hilbert space given by

$$H_{\text{pen}} = \mathbb{I}_{\mathbb{C}^2} \otimes \mathbb{I}_{\mathbb{C}^{8k}} \otimes \left(S^3 + S^4 + S^3\right), \tag{9.7}$$

which forces the third register into a particularly useful state, allows us to guarantee that the ground state is a history state. Altogether, we then have that the adjacency matrix of $g(0)$ is given by

$$A(g_0) = H_{\text{prop}} + H_{\text{pen}}, \tag{9.8}$$

where each vertex is labeled by a computational basis state in the Hilbert space, namely (z, t, j) with $z \in \mathbb{F}_2$, $t \in [8k]$, and $j \in [8]$. The graph g_0 in the special case that $d_{\max} = 0$ is shown in Figure 9.1.

We can then use the results of Chapter 8 to calculate the smallest eigenvalue of $A(g_0)$, the corresponding eigenvectors, and the eigenvalue gap. In particular, we have that the smallest eigenvalue is

$$e_1 = -1 - 3\sqrt{2} = -5.24\ldots,, \tag{9.9}$$

corresponding to a four dimensional ground space spanned by the states

$$|\psi_{z,0}\rangle = \frac{1}{\sqrt{8k}} \sum_{t=0}^{8k-1} \left(V_t V_{t-1} \cdots V_1\right) |z\rangle|t\rangle|\omega\rangle = \frac{1}{\sqrt{8k}} \sum_{t'=0}^{4k-1} |z\rangle|2t'\rangle|\omega\rangle + V_{2t'+1}|z\rangle|2t'+1\rangle|\omega\rangle \tag{9.10}$$

$$|\psi_{z,1}\rangle = \frac{1}{\sqrt{8k}} \sum_{t'=0}^{4k-1} |z\rangle|2t'\rangle|\overline{\omega}\rangle + V_{2t'+1} * |z\rangle|2t'+1\rangle|\overline{\omega}\rangle, \tag{9.11}$$

where

$$|\omega\rangle = \frac{1}{\sqrt{8}} \sum_{j=0}^{7} e^{i\pi j/4} |j\rangle \qquad \text{and} \qquad |\overline{\omega}\rangle = \frac{1}{\sqrt{8}} \sum_{j=0}^{7} e^{-i\pi j/4} |j\rangle. \tag{9.12}$$

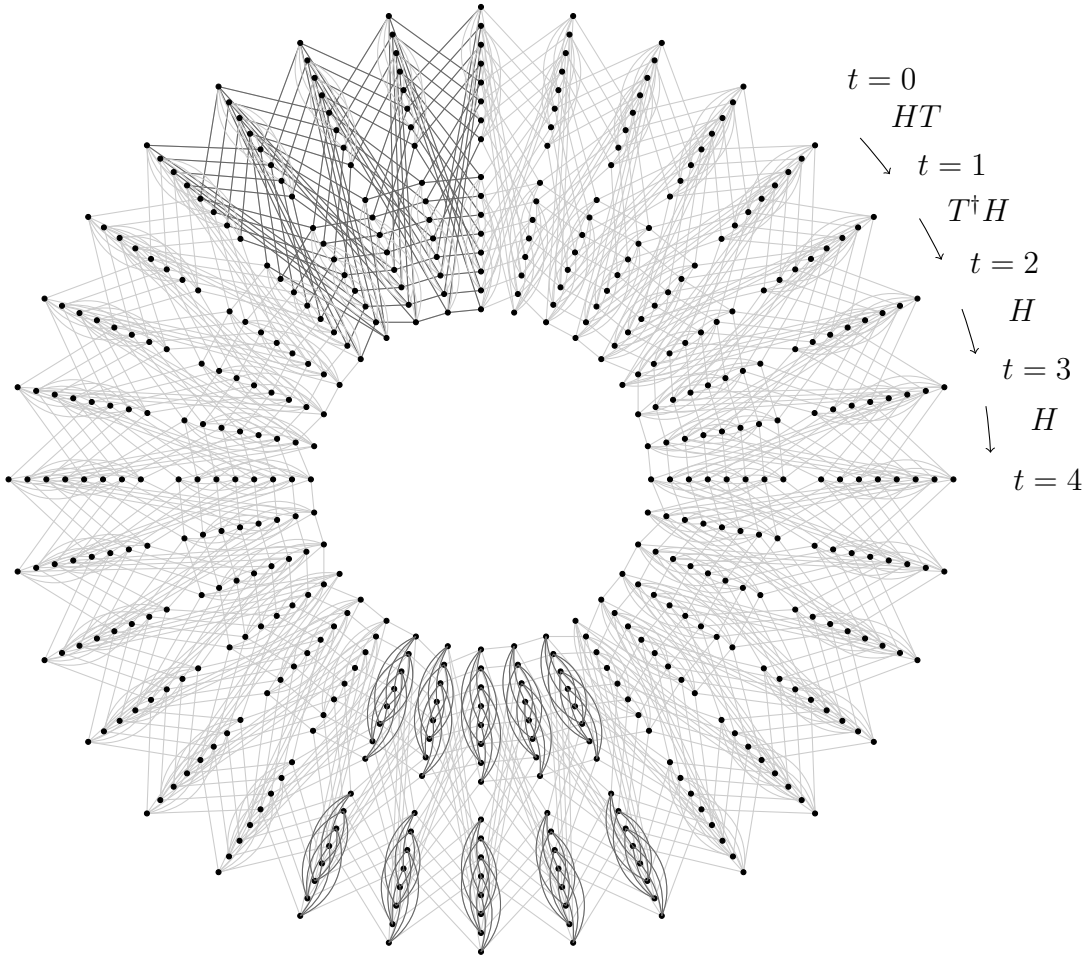

Figure 9.1: The graph g_0 for the case $d_{\max} \leq 1$. Vertices are arranged with each ray corresponding to a specific time t proceeding clockwise, with the outer 8 vertices corresponding to logical 0 and the inner 8 corresponding to logical 1, with the further breakdown into 8 vertices corresponding to the ancillary register. The difference in color for some edges is an attempt to highlight those edges corresponding to the penalty term (bottom of the figure) and the circuit (top left of the figure).

Additionally, we have that the energy gap is at least

$$\lambda_1^2(g_0) \geq \sqrt{2}\cos\left(\frac{\pi}{4k}\right) \geq \frac{\pi\sqrt{2}}{16k^2} = c_k, \tag{9.13}$$

which is constant for all interactions with a given $d_{\max}$.

Note that the amplitudes of $|\psi_{z,0}\rangle$ in the above basis contain the result of computing either the identity, Hadamard, or HT gate acting on the "input" state $|z\rangle$, while the amplitudes $|\psi_{z,1}\rangle$ corresponds to the result of the identity, Hadamard or $\overline{HT}$ gate acting on the "input" state. Additionally, this information is repeated at least 8 times, once for each copy of $\mathcal{C}_0$.

With these bounds on the single particle eigenvalues and their corresponding eigenstates, we can now show that the graph g_0 has no two-particle frustration-free states. By Lemma **??**, it follows that g_0 has no N-particle frustration-free states for $N \geq 2$. While we would like this to be true for all interactions, in the case of only onsite interactions ($d_{\max} = 0$) no anti-symmetric state is penalized and thus there is a 4-particle frustration-free state. However, we show that this is the only case for which this is true, and further that if we restrict ourselves to the symmetric subspace, we again have that there are no frustration-free two-particle states.

Lemma 19. *If $d_{max} > 0$, then $\lambda_2^1(g_0) > 0$ for all states. If $d_{max} = 0$, then when restricted to symmetric states, $\lambda_2^1(g_0) > 0$.*

Proof. Suppose (for a contradiction) that $|Q\rangle \in \mathcal{H}(g_0)^{\otimes 2}$ is a nonzero vector in the nullspace of $H(g_0, 2)$, so

$$H_{g_0}^2|Q\rangle = \left(A(g_0)\otimes\mathbb{I} + \mathbb{I}\otimes A(g_0) + \sum_{i,j\in g_0}\mathcal{U}_{d(i,j)}(\hat{n}_i,\hat{n}_j)\right)|Q\rangle = 2e_1|Q\rangle. \tag{9.14}$$

This implies

$$A(g_0)\otimes\mathbb{I}|Q\rangle = \mathbb{I}\otimes A(g_0)|Q\rangle = e_1|Q\rangle \tag{9.15}$$

since $A(g_0)$ has smallest eigenvalue e_1 and the interaction term is positive semidefinite. We can therefore write

$$|Q\rangle = \sum_{z,a,x,y\in\mathbb{F}_2} Q_{za,xy}|\psi_{z,a}\rangle|\psi_{x,y}\rangle \tag{9.16}$$

and

$$\mathcal{U}_{d(u,v)}(\hat{n}_u,\hat{n}_v)|Q\rangle = 0 \tag{9.17}$$

for all vertices $u, v \in g_0$.

We then have by assumption that $\mathcal{U}_{d_{\max}}^{(1,1)} > 0$ if $d_{\max} > 0$ or $\mathcal{U}_0^2 > 0$ if $d_{\max} = 0$, and thus for all vertices u, v of distance $d_{\max}$,

$$\langle u, v\,|\,Q\rangle = 0. \tag{9.18}$$

We will use this equation to show a contradiction, so that $|Q\rangle$ cannot exist.

Note that vertices of the form (x, T, j) and $(z, T+t, k)$ are at least a distance t apart for all times $t < 4k$, since edges only connect vertices with corresponding times that differ by at most 1. Further, note that the portion of the Hamiltonian that connect adjacent times only arise from the terms corresponding to the circuit. Since each unitary for $k > t \geq 2$ corresponds to a Hadamard, and the corresponding term in the Hamiltonian only connects vertices with the same j or j's that differ by 4, we have that only vertices of the form $(x, 2, j)$ and $(z, 2+t, j)$ or $(x, 2, j)$ and $(z, 2+t, j+4)$ can be a distance t apart; all other pairs of vertices with these two times must be at a distance of at least $t+1$.

With all of this in mind, let us assume that $d_{\max}$ is an even integer greater than zero. We then have that the vertices $(0,2,j)$ and $(0,1+d_{\max},j+4)$ are a distance $d_{\max}-1$ apart. Further, we have that $(0,1+d_{\max},j+4)$ is also connected to the vertices $(0,1+d_{\max},j+1)$ and $(0,1+d_{\max},j-1)$ (from the penalty term of the Hamiltonian), and thus we have that the vertices $u=(0,2,j)$ and $v=(0,1+d_{\max},j+\ell)$ are a distance $d_{\max}$ apart for all $j\in[8]$ and for $\ell=\pm1$. Using (9.18) with these pairs of vertices we then have that

$$\begin{aligned}
\langle u,v\,|\,Q\rangle &= \sum_{x,a,z,b\in\mathbb{F}_2} Q_{xa,zb}\langle 0,2,j\,|\,\psi_{x,a}\rangle\langle 0,1+d_{\max},j+\ell\,|\,\psi_{zb}\rangle && (9.19)\\
&= \frac{1}{64k}\sum_{x,a,z,b\in\mathbb{F}_2} Q_{xa,zb}\langle 0\,|\,x\rangle\langle 0\,|H|\,z\rangle\omega^{(-1)^a j+(-1)^b(j+\ell)} && (9.20)\\
&= \frac{1}{64\sqrt{2}k}\big((Q_{00,00}+Q_{00,10})\omega^{2j+\ell}+(Q_{00,01}+Q_{00,11})\omega^{-\ell}\\
&\qquad +(Q_{01,00}+Q_{01,10})\omega^{\ell}+(Q_{01,01}+Q_{01,11})\omega^{-2j-\ell}\big), && (9.21)
\end{aligned}$$

and thus we have that $Q_{0a,0b}=-Q_{0a,1b}$ for all $a,b\in\mathbb{F}_2$. Using the same reasoning with vertices $u=(0,2,j)$ and $v=(1,1+d_{\max},j+\ell)$ with $\ell=\pm1$ then gives us

$$\begin{aligned}
\langle u,v\,|\,Q\rangle &= \sum_{x,a,z,b\in\mathbb{F}_2} Q_{xa,zb}\langle 0,2,j\,|\,\psi_{x,a}\rangle\langle 1,d_{\max},j+\ell\,|\,\psi_{zb}\rangle && (9.22)\\
&= \frac{1}{64k}\sum_{x,a,z,b\in\mathbb{F}_2} Q_{xa,zb}\langle 0\,|\,x\rangle\langle 1\,|H|\,z\rangle\omega^{(-1)^a j+(-1)^b(j+\ell)} && (9.23)\\
&= \frac{1}{64\sqrt{2}k}\big((Q_{00,00}-Q_{00,10})\omega^{2j+\ell}+(Q_{00,01}-Q_{00,11})\omega^{-\ell}\\
&\qquad +(Q_{01,00}-Q_{01,10})\omega^{\ell}+(Q_{01,01}-Q_{01,11})\omega^{-2j-\ell}\big), && (9.24)
\end{aligned}$$

which combined with our previous results show that $Q_{0a,zb}=0$ for all $a,b,z\in\mathbb{F}_2$. Again using the same reasoning with $u=(1,2,j)$ and $v=(1,1+d_{\max},j+\ell)$ for $\ell=3$ or $\ell=5$ gives us

$$\begin{aligned}
\langle u,v\,|\,Q\rangle &= \sum_{x,a,z,b\in\mathbb{F}_2} Q_{xa,zb}\langle 1,2,j\,|\,\psi_{x,a}\rangle\langle 1,1+d_{\max},j+\ell\,|\,\psi_{zb}\rangle && (9.25)\\
&= \frac{1}{64k}\sum_{x,a,z,b\in\mathbb{F}_2} Q_{xa,zb}\langle 1\,|\,x\rangle\langle 1\,|H|\,z\rangle\omega^{(-1)^a j+(-1)^b(j+\ell)} && (9.26)\\
&= \frac{1}{64\sqrt{2}k}\big((Q_{10,00}-Q_{10,10}\omega^{2j+\ell}+(Q_{10,01}-Q_{10,11})\omega^{-\ell}\\
&\qquad +(Q_{11,00}-Q_{11,10})\omega^{\ell}+(Q_{11,01}-Q_{11,11})\omega^{-2j-\ell}\big), && (9.27)
\end{aligned}$$

which forces $Q_{1a,0b}=Q_{1a,1b}$ for all $a,b\in\mathbb{F}_2$. Finally, using this same technique for $u=(1,2,j)$ and $v=(0,1+d_{\max},j+\ell)$ with $\ell=\pm1$ gives us

$$\begin{aligned}
\langle u,v\,|\,Q\rangle &= \sum_{x,a,z,b\in\mathbb{F}_2} Q_{xa,zb}\langle 1,2,j\,|\,\psi_{x,a}\rangle\langle 0,1+d_{\max},j+\ell\,|\,\psi_{zb}\rangle && (9.28)\\
&= \frac{1}{64k}\sum_{x,a,z,b\in\mathbb{F}_2} Q_{xa,zb}\langle 1\,|\,x\rangle\langle 0\,|H|\,z\rangle\omega^{(-1)^a j+(-1)^b(j+\ell)} && (9.29)\\
&= \frac{1}{64\sqrt{2}k}\big((Q_{10,00}+Q_{10,10}\omega^{2j+\ell}+(Q_{10,01}+Q_{10,11})\omega^{-\ell}\\
&\qquad +(Q_{11,00}+Q_{11,10})\omega^{\ell}+(Q_{11,01}+Q_{11,11})\omega^{-2j-\ell}\big), && (9.30)
\end{aligned}$$

which combined with our previous results implies that $Q_{1a,zb} = 0$ for all $a, b, z \in \mathbb{F}_2$. Putting this together, we then have each $Q_{xa,zb} = 0$, and thus $|Q\rangle$ does not exist; in other words, if $d_{\max} > 0$ is even, then the nullspace of $H(g_0, 2)$ is empty.

Now let us assume that $d_{\max}$ is a positive odd integer. For all such $d_{\max}$, we can then use equation (9.18) with vertices $u = (y, 2, j)$ and $v = (y, 1 + d_{\max}, j + \ell)$ for $y \in \mathbb{F}_2$, $j \in [8]$, and $\ell = \pm 1$ to see

$$\langle u, v | Q \rangle = \sum_{x,a,z,b \in \mathbb{F}_2} Q_{xa,zb} \langle y, 2, j | \psi_{x,a} \rangle \langle y, 1 + d_{\max}, j + \ell | \psi_{zb} \rangle \tag{9.31}$$

$$= \frac{1}{64k} \sum_{x,a,z,b \in \mathbb{F}_2} Q_{xa,zb} \langle y | x \rangle \langle y | z \rangle \omega^{(-1)^a j + (-1)^b (j+\ell)} \tag{9.32}$$

$$= \frac{1}{64k} \big(Q_{y0,y0} \omega^{2j+\ell} + Q_{y0,y1} \omega^{-\ell} + Q_{y1,y0} \omega^{\ell} + Q_{y1,y1} \omega^{-2j-\ell} \big), \tag{9.33}$$

to see that $Q_{ya,yb} = 0$ for all $a, b, y \in \mathbb{F}_2$. With this result, let us now examine vertices at times that differ by $d_{\max}$. Using equation (9.18) with $u = (0, 2, j)$ and $v = (0, 2 + d_{\max}, j + 4)$ gives us

$$\langle u, v | Q \rangle = \sum_{x,a,z,b \in \mathbb{F}_2} Q_{xa,zb} \langle 0, 2, j | \psi_{x,a} \rangle \langle 0, 2 + d_{\max}, j + 4 | \psi_{zb} \rangle \tag{9.34}$$

$$= \frac{1}{64k} \sum_{x,a,z,b \in \mathbb{F}_2} Q_{xa,zb} \langle 0 | x \rangle \langle 0 | H | z \rangle \omega^{(-1)^a j + (-1)^b (j+4)} \tag{9.35}$$

$$= -\frac{1}{64k\sqrt{2}} \big((Q_{00,00} + Q_{00,10}) \omega^{2j} + (Q_{01,01} + Q_{01,11}) \omega^{-2j} + (Q_{01,00} + Q_{01,10} + Q_{00,01} + Q_{00,11}) \big) \tag{9.36}$$

$$= -\frac{1}{64k\sqrt{2}} \big(Q_{00,10} \omega^{2j} + Q_{01,11} \omega^{-2j} + (Q_{01,10} + Q_{00,11}) \big) \tag{9.37}$$

where in the last line we used the fact that $Q_{za,zb} = 0$. A similar result with $u = (0, 2, j)$ and $v = (1, 2 + d_{\max}, j + 4)$ then gives us that $Q_{0a,zb} = 0$. Finally, repeating this same procedure with $u = (1, 2, j)$ and $v = (1, 2 + d_{\max}, j)$ and with $u = (1, 2, j)$ and $v = (0, 2 + d_{\max}, j + 4)$ gives us that $Q_{1a,zb} = 0$. Putting this all together, we have that each $Q_{xa,zb} = 0$ and thus $|Q\rangle$ does not exist if $d_{\max}$ is an odd integer.

Finally, let us assume that $d_{\max} = 0$, and that the state $|Q\rangle$ is symmetric (so that $Q_{xa,zb} = Q_{zb,xa}$). With these assumptions, let us examine equation (9.18) with $u = v = (y, 0, j)$ for $y \in \mathbb{F}_2$ and $j \in [8]$:

$$\langle u, v | Q \rangle = \sum_{x,a,z,b \in \mathbb{F}_2} Q_{xa,zb} \langle y, 0, j | \psi_{x,a} \rangle \langle y, 0, j | \psi_{zb} \rangle \tag{9.38}$$

$$= \frac{1}{64k} \sum_{x,a,z,b \in \mathbb{F}_2} Q_{xa,zb} \langle y | x \rangle \langle y | z \rangle \omega^{(-1)^a j + (-1)^b j} \tag{9.39}$$

$$= \frac{1}{64k} \big(Q_{y0,y0} \omega^{2j} + Q_{y1,y1} \omega^{-2j} + 2 Q_{y1,y0} \big). \tag{9.40}$$

Evaluating these equations together then gives us that $Q_{xa,xb} = 0$ for all $a, b, x \in \mathbb{F}_2$. If we now use

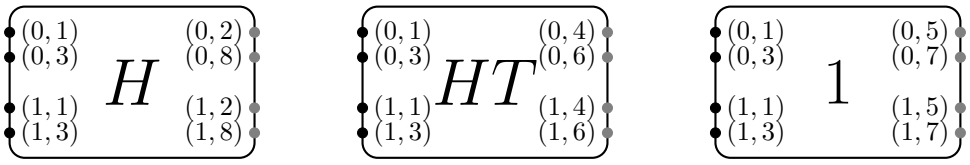

Figure 9.2: Diagram elements from which a gate diagram is constructed. Each diagram element is a schematic representation of the graph g_0 shown in Figure 9.1.

equation (9.18) with $u = v = (0, 3, j)$ for all $j \in [8]$, we find that

$$\langle u, v \,|\, Q \rangle = \sum_{x,a,z,b \in \mathbb{F}_2} Q_{xa,zb} \langle 0, 3, j \,|\, \psi_{x,a} \rangle \langle 0, 3, j \,|\, \psi_{zb} \rangle \tag{9.41}$$

$$= \frac{1}{64k} \sum_{x,a,z,b \in \mathbb{F}_2} Q_{xa,zb} \langle 0|H|x\rangle \langle 0|H|z\rangle \omega^{(-1)^a j + (-1)^b j} \tag{9.42}$$

$$= \frac{1}{128k} \big(2Q_{00,10}\omega^{2j} + 2Q_{01,11}\omega^{-2j} + (2Q_{01,10} + 2Q_{00,11}) \big). \tag{9.43}$$

and thus $Q_{00,10} = Q_{01,11} = 0$ and $Q_{01,10} = -Q_{00,11}$. If we now use (9.18) with the only remaining vertices leading to novel restrictions, namely $u = v = (0, 1, 0)$, we find

$$\langle u, v \,|\, Q \rangle = \sum_{x,a,z,b \in \mathbb{F}_2} Q_{xa,zb} \langle 0, 1, j \,|\, \psi_{x,a} \rangle \langle 0, 1, j \,|\, \psi_{zb} \rangle \tag{9.44}$$

$$= \frac{1}{64k} \big(2Q_{01,10} \langle 0|\overline{HT}|0\rangle \langle 0|HT|1\rangle + 2Q_{00,11} \langle 0|HT|0\rangle \langle 0|\overline{HT}|1\rangle \big) \tag{9.45}$$

$$= \frac{1}{64k} \big(Q_{01,10}\omega + Q_{00,11}\omega^{-1} \big) \tag{9.46}$$

$$= \frac{Q_{01,10}}{64k} (\omega - \omega^{-1}) \tag{9.47}$$

must be zero, and thus each $Q_{xa,zb} = 0$. Hence, if $d_{\max} = 0$ no symmetric state $|Q\rangle$ is in the nullspace of $H(g_0, 2)$.

Combining all of this together, we have that if $d_{\max} > 0$, then the nullspace of $H(g_0, 2)$ is empty and $\lambda_2^1(g_0) > 0$, while if $d_{\max} = 0$ then no symmetric state is in the nullspace of $H(g_0, 2)$, and thus when restricted to symmetric states, $\lambda_2^1(g_0) > 0$. □

9.2.1.2 Diagram elements

We use several different graphs closely related to the graph g_0, with some depicted in Figure 9.2. We call these figures *diagram elements*, which are also the simplest examples of *gate diagram*, which we will define shortly. The idea behind these graphs is to encode a single qubit computation, complete with inputs and outputs.

[**TO DO:** *fix diagram element graphs*]

Each diagram element corresponds to two copies of the graph g_0, along with self-loops and edges between the two copies. The idea of these elements is to ensure that the ground state of the diagram element is closely related to that of the g_0 graph, but where almost all of the vertices of the diagram element has a self-loop. The only vertices without such a self-loop are those corresponding

to input and outputs of the diagram element, which will have a self-loop added to them in the final gate diagram.

Along these lines, each diagram element will be labeled by the unitary it computes, along with four numbers between zero and two, corresponding to the number of inputs "nodes" and output "nodes" for each logical state of the diagram. Each such node will correspond to 16 vertices of the underlying graph representing one logical state and time of the two g_0 graphs. These nodes are placed so that the minimal distance between two vertices in separate nodes will be at least $d_{\max}$.

Explicitly, each diagram element will be labeled by a unitary $U \in \{\mathbb{I}, H, HT\}$, along with four integers $n_{0,\text{in}}$, $n_{0,\text{out}}$, $n_{1,\text{in}}$, and $n_{1,\text{out}}$, each between 0 and 2. These numbers correspond to the number of nodes for each particular input or output. We shall label such a diagram element a $U^{(n_{0,\text{in}},n_{1,\text{in}})}_{(n_{0,\text{out}},n_{1,\text{out}})}$ element. The vertex set for the corresponding diagram element corresponds to two copies of g_0 (namely, $2 \times 8k \times 8 \times 2$ vertices, labeled as (z, t, j, d) for $z, d \in \mathbb{F}_2$, $t \in [8k]$, and $j \in [8]$).

For each node of the gate diagram, we will associate a time for which the underlying history state has computed the correct unitary. Further, we will have these times each be a distance of at least $d_{\max}$ apart, to ensure that each node is at least a distance $d_{\max}$ apart. Namely, for each logical input and output, we will associate two times:

- 0-input: $t^{\text{in}}_{0,1} = 2$ and $t^{\text{in}}_{0,2} = k + 2$,
- 1-input: $t^{\text{in}}_{1,1} = 2k + 2$ and $t^{\text{in}}_{1,2} = 3k + 2$,
- 0-output: $t^{\text{out}}_{0,1} = 4k + \ell$ and $t^{\text{out}}_{0,2} = 5k + \ell$,
- 1-output: $t^{\text{out}}_{1,1} = 4k + \ell$ and $t^{\text{out}}_{1,2} = 5k + \ell$,

where ℓ is 1, 2, or 3, depending on whether the labeled unitary is HT, $\mathbb{I}$, or H, respectively.

For a given diagram element $U^{(n_{0,\text{in}},n_{1,\text{in}})}_{(n_{0,\text{out}},n_{1,\text{out}})}$, it will be useful to have defined the set of logical states and corresponding times explicitly used as input and output in the diagram element. As such, let $T \subset \mathbb{F}_2 \times [8k]$ be defined as

$$T = \bigcup_{z \in \mathbb{F}_2} \{(z, t^{\text{in}}_{z,j}) : j \leq n_{z,\text{in}}\} \cup \{(z, t^{\text{out}}_{z,j}) : j \leq n_{z,\text{out}}\}, \tag{9.48}$$

and note that T contains those nodes (i.e., the sets of times and logical states) used as input and output for the given gate diagram, and that $|T|$ corresponds to the number of nodes in the diagram element.

With T defined, the adjacency matrix for the corresponding diagram element $U^{(a,b)}_{(c,d)}$ will be

$$A\left(G_U^{(a,b),(c,d)}\right) = A(g_0) \otimes \mathbb{I}_2 + \sum_{(z,t) \notin T, j \in [8]} |\, z, t, j \,\rangle\langle\, z, t, j \,| \otimes \sum_{a,b \in \mathbb{F}_2} |\, a \,\rangle\langle\, b \,| \tag{9.49}$$

$$= A(g_0) \otimes \mathbb{I}_2 + 2\Pi_{\neg T} \otimes \mathbb{I}_8 \otimes |+\rangle\langle+| \tag{9.50}$$

In particular, the graph for $G_U^{(a,b),(c,d)}$ will simply correspond to two copies of g_0, along with a projector onto the equal superposition between the two graphs for each vertex not used in a node of the diagram.

Because of the very similar form between $G_U^{(a,b),(c,d)}$ and g_0, their ground spaces and ground energies are closely related. As the second term in (9.50) is positive semi-definite, we have that the ground energy of $A(G_U^{(a,b),(c,d)})$ is at least that of $A(g_0)$. With more exact results, we have the following lemma:

Lemma 20. *Let $G_U^{(a,b),(c,d)}$ be the graph corresponding to a diagram element. The ground space of $A(G_U^{(a,b),(c,d)})$ is*

$$S = \text{span}\{|\,\psi_{z,a}, -\rangle : z, a \in \mathbb{F}_2\}. \tag{9.51}$$

Proof. Note that $A(G_U^{(a,b),(c,d)})$ commutes with $\mathbb{I}_2 \otimes \mathbb{I}_{8k} \otimes \mathbb{I}_8 \otimes |+\rangle\langle+|$, and thus there exists an eigenbasis for the adjacency matrix in which each vector is of the form $|\phi\rangle|+\rangle$ or $|\phi\rangle|-\rangle$. For states of this latter form, the second term in (9.50) vanishes, so $|\psi, -\rangle$ is in the ground space of $A(g_U^{(a,b),(c,d)})$ if and only if $|\psi\rangle$ is in the ground space of $A(g_0)$, and thus we have that S is a subspace of the nullspace.

Now let us examine $|\alpha, +\rangle$ for any state $|\alpha\rangle$. Since the second term of (9.50) is positive semi-definite, we have that the ground energy of $A(G_U^{(a,b),(c,d)})$ is at least e_1. Hence, if $|\alpha, +\rangle$ is in the ground space, then

$$\langle \alpha, + | A\big(G_U^{(a,b),(c,d)}\big) | \alpha, + \rangle = e_1 = \langle \alpha | A(g_0) | \alpha \rangle \tag{9.52}$$

and thus

$$\langle \alpha | \Pi_{\neg S} \otimes \mathbb{I}_8 | \alpha \rangle = 0, \tag{9.53}$$

with $|\alpha\rangle$ in the ground space of $A(g_0)$.

However, note that for all diagram elements (and all $d_{\max}$), $(z, 0)$ is not in T. We then have that

$$\Pi_{\neg S} \geq \mathbb{I}_2 \otimes |0\rangle\langle 0| \otimes \mathbb{I}_8. \tag{9.54}$$

As this operator is strictly positive when restricted to the ground space of $A(g_0)$,

$$\langle \psi_{x,\gamma} | \mathbb{I}_2 \otimes |0\rangle\langle 0| \otimes \mathbb{I}_8 | \psi_{z,\delta} \rangle = \frac{1}{8k} \delta_{\gamma,\delta} \delta_{x,z}, \tag{9.55}$$

we also have that $\Pi_{\neg S}$ is strictly positive when restricted to the ground space of $A(g_0)$, and thus $|\alpha, +\rangle$ is not in the ground space of $A(G_U^{(a,b),(c,d)})$.

Putting this together, we have that the ground space of $A(G_U^{(a,b),(c,d)})$ is S, as claimed □

With this bound on the form of the ground space of $A(G_U^{(a,b),(c,d)})$, we can then use our knowledge of the two-particle interaction Hamiltonian on g_0 to relate this to the two-particle interaction Hamiltonian on $G_U^{(a,b),(c,d)}$. Namely, we show that since there does not exist a two-particle frustration-free state on g_0, there also does not exists a two-particle frustration-free state on $G_U^{(a,b),(c,d)}$.

Lemma 21. *If $d_{max} > 0$, then $\lambda_2^1(G_U^{(a,b),(c,d)}) > 0$ for all states. If $d_{max} = 0$, then when restricted to symmetric states, $\lambda_2^1(G_U^{(a,b),(c,d)}) > 0$.*

Proof. Note that using Lemma 20, the ground space of $A(G_U^{(a,b),(c,d)})$ is in one-to-one correspondence with the ground space of $A(g_0)$, by the transformation

$$|\,\phi_{x,a}, -\rangle \leftrightarrow |\,\phi_{x,a}\rangle. \tag{9.56}$$

Namely, by attaching (or removing) a second register in the $|-\rangle$ state, corresponding to having equal and opposite amplitudes between the two copies of g_0 present in $G_U^{(a,b),(c,d)}$, we can transform between these two single-particle ground spaces.

We will use this relation, along with the fact that $\lambda_2^1(g_0) > 0$ from Lemma 19, to show that $\lambda_2^1(G_U^{(a,b),(c,d)}) > 0$ with the same assumptions.

Let us then look at any two-particle state that minimizes the movement term. In particular, it takes the form

$$|\overline{\phi}\rangle = \sum_{\alpha,\beta,x,z\in\mathbb{F}_2} Q^{x,z}_{\alpha,\beta} |\psi_{x,\alpha},-\rangle|\psi_{z,\beta},-\rangle. \tag{9.57}$$

Additionally, let us define the related two-particle state on g_0 as

$$|\phi\rangle = \sum_{\alpha,\beta,x,z\in\mathbb{F}_2} Q^{x,z}_{\alpha,\beta} |\psi_{x,\alpha}\rangle|\psi_{z,\beta}\rangle. \tag{9.58}$$

We can then see what the expectation of the interaction term of the Hamiltonian is under the state $|\overline{\phi}\rangle$:

$$\begin{aligned}
\langle\overline{\phi}|H_{\text{int}}|\overline{\phi}\rangle &= \sum_{u,v\in V(G_U^{(a,b),(c,d)})} \langle\overline{\phi}|U_{d(u,v)}(\hat{n}_u,\hat{n}_v)|\overline{\phi}\rangle &(9.59)\\
&= \sum_{u,v\in V(g_0),d_1,d_2\in\mathbb{F}_2} \langle\overline{\phi}|U_{d((u,d_1),(v,d_2))}(\hat{n}_{(u,d_1)},\hat{n}_{(v,d_2)})|\overline{\phi}\rangle &(9.60)\\
&\geq \sum_{u,v\in V(g_0),d_1\in\mathbb{F}_2} \langle\overline{\phi}|U_{d(u,v)}(\hat{n}_{(u,d_1)},\hat{n}_{(v,d_1)})|\overline{\phi}\rangle &(9.61)
\end{aligned}$$

where in the third line we only count the contributions to the interaction when both particles are in the same copy of g_0. As the interaction is positive-semidefinite, this can only decrease the expectation.

Now, from the form of $|\overline{\phi}\rangle$, we have that for any two $u,v\in V(g_0)$ and either copy of g_0,

$$\begin{aligned}
&\langle\overline{\phi}|U_{d(u,v)}(\hat{n}_{(u,d_1)},\hat{n}_{(v,d_1)})|\overline{\phi}\rangle\\
&= \sum_{\substack{x_1,x_2,z_1,z_2\in\mathbb{F}_2\\ \alpha_1,\alpha_2,\beta_1,\beta_2\in\mathbb{F}_2}} (Q^{x_1,z_1}_{\alpha_1,\beta_1})^* Q^{x_2,z_2}_{\alpha_2,\beta_2} \langle\overline{\psi_{x_1,\alpha_1}}|\langle\overline{\psi_{z_1,\beta_1}}|U_{d(u,v)}(\hat{n}_{(u,d_1)},\hat{n}_{(v,d_1)})|\overline{\psi_{x_2,\alpha_2}}\rangle|\overline{\psi_{z_2,\beta_2}}\rangle &(9.62)\\
&\geq \left|\langle d_1|-\rangle\right|^4 \sum_{\substack{x_1,x_2,z_1,z_2\in\mathbb{F}_2\\ \alpha_1,\alpha_2,\beta_1,\beta_2\in\mathbb{F}_2}} (Q^{x_1,z_1}_{\alpha_1,\beta_1})^* Q^{x_2,z_2}_{\alpha_2,\beta_2} \langle\psi_{x_1,\alpha_1}|\langle\psi_{z_1,\beta_2}|U_{d(u,v)}(\hat{n}_u,\hat{n}_v)|\psi_{x_2,\alpha_2}\rangle|\psi_{z_2,\beta_2}\rangle &(9.63)\\
&= \frac{1}{4}\langle\phi|U_{d(u,v)}(\hat{n}_u,\hat{n}_v)|\phi\rangle. &(9.64)
\end{aligned}$$

Hence, we have that

$$\begin{aligned}
\langle\overline{\phi}|H_{\text{int}}|\overline{\phi}\rangle &\geq \sum_{u,v\in V(g_0),d_1\in\mathbb{F}_2} \langle\overline{\phi}|U_{d(u,v)}(\hat{n}_{(u,d_1)},\hat{n}_{(v,d_1)})|\overline{\phi}\rangle &(9.65)\\
&\geq \frac{1}{4}\sum_{u,v\in V(g_0),d_1\in\mathbb{F}_2} \langle\phi|U_{d(u,v)}(\hat{n}_u,\hat{n}_v)|\phi\rangle &(9.66)\\
&= \frac{1}{4}\sum_{d_1\in\mathbb{F}_2} \langle\phi|H_{\text{int}}|\phi\rangle &(9.67)\\
&= \frac{1}{2}\langle\phi|H_{\text{int}}|\phi\rangle. &(9.68)
\end{aligned}$$

Using Lemma 19, we have that (9.68) is larger than zero for all states and interactions that satisfy the conditions of Lemma 19, and thus $\langle\overline{\phi}|H_{\text{int}}|\overline{\phi}\rangle > 0$. As such, there does not exist a two-particle frustration-free state on the graph $G_U^{(a,b),(c,d)}$ under the same assumptions as for g_0.

□

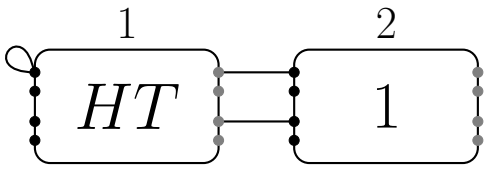

Figure 9.3: A gate diagram with two diagram elements labeled $q = 1$ (left) and $q = 2$ (right).

9.2.1.3 Gate diagrams

While the diagram elements do have nice properties, we will eventually want to construct larger graphs using the diagram elements as basic elements. Further, as the diagram elements themselves are rather complicated graphs, it will be useful to have a diagrammatic construction for these graphs: these shall be the gate diagrams.

The rules for constructing gate diagrams are simple. A gate diagram consists of some number $R \in \{1, 2, \ldots\}$ of diagram elements, with self-loops attached to a subset $\mathcal{S}$ of the nodes and edges connecting a set $\mathcal{E}$ of pairs of nodes. A node may have a single edge or a single self-loop attached to it, but never more than one edge or self-loop and never both an edge and a self-loop. Each node in a gate diagram has a label (q, z, t) where $q \in [R]$ indicates the diagram element it belongs to. An example is shown in Figure 9.3.

Sometimes it is convenient to draw the input nodes on the right-hand side of a diagram element; e.g., in Figure 9.4 the node closest to the top left corner is labeled $(q, z, t) = (3, 2, 4k + 3)$.

To every gate diagram we associate a *gate graph* G with vertex set

$$\{(q, z, t, j, d) \colon q \in [R],\ z, d \in \mathbb{F}_2,\ t \in [8k],\ j \in [8]\} \tag{9.69}$$

and adjacency matrix

$$A(G) = \sum_{q \in [R]} |\,q\rangle\langle q\,| \otimes A(G_q) + h_{\mathcal{S}} + h_{\mathcal{E}} \tag{9.70}$$

$$A(G_q) = A(G_{U_q}^{(a_q,b_q),(c_q,d_q)}) \tag{9.71}$$

$$h_{\mathcal{S}} = \sum_{\mathcal{S}} |q, z, t\rangle\langle q, z, t| \otimes \mathbb{I}_8 \otimes \mathbb{I}_2 \tag{9.72}$$

$$h_{\mathcal{E}} = \sum_{\mathcal{E}} \big(|q, z, t\rangle + |q', z', t'\rangle\big)\big(\langle q, z, t| + \langle q', z', t'|\big) \otimes \mathbb{I}_8 \otimes \mathbb{I}_2. \tag{9.73}$$

The sums in equations (9.72) and (9.73) run over the set of nodes with self-loops $(q, z, t) \in \mathcal{S}$ and the set of pairs of nodes connected by edges $\{(q, z, t), (q', z', t')\} \in \mathcal{E}$, respectively. We see from the above expression that each self-loop in the gate diagram corresponds to 16 self-loops in the graph G, and an edge in the gate diagram corresponds to 16 edges and 32 self-loops in G. Note that we can determine the type of each diagram element from the gate diagram, as the implemented unitary and number of nodes is encoded in the diagram.

As a node in a gate graph never has more than one edge or self-loop attached to it, equations (9.72) and (9.73) are sums of orthogonal Hermitian operators. Therefore

$$\|h_{\mathcal{S}}\| = \max_{\mathcal{S}} \||q, z, t\rangle\langle q, z, t| \otimes \mathbb{I}_j\| = 1 \quad \text{if } \mathcal{S} \neq \emptyset \tag{9.74}$$

$$\|h_{\mathcal{E}}\| = \max_{\mathcal{E}} \big\|\big(|q, z, t\rangle + |q', z', t'\rangle\big)\big(\langle q, z, t| + \langle q', z', t'|\big) \otimes \mathbb{I}_j\big\| = 2 \quad \text{if } \mathcal{E} \neq \emptyset \tag{9.75}$$

for any gate graph. (Of course, this also shows that $\|h_{\mathcal{S}'}\| = 1$ and $\|h_{\mathcal{E}'}\| = 2$ for any nonempty subsets $\mathcal{S}' \subseteq \mathcal{S}$ and $\mathcal{E}' \subseteq \mathcal{E}$.)

Consider the adjacency matrix $A(G)$ of a gate graph G, and note (from equation (9.70) that its smallest eigenvalue $\mu(G)$ satisfies

$$\mu(G) \geq e_1 \tag{9.76}$$

since $h_{\mathcal{S}}$ and $h_{\mathcal{E}}$ are positive semidefinite and $A(G_U^{(a,b),(c,d)})$ has smallest eigenvalue e_1. In the special case where $\mu(G) = e_1$, we say G is an e_1-gate graph.

Definition 8. An e_1-gate graph is a gate graph G such that the smallest eigenvalue of its adjacency matrix is $e_1 = -1 - 3\sqrt{2}$.

When G is an e_1-gate graph, a single-particle ground state $|\Gamma\rangle$ of $A(G)$ satisfies

$$\left(\sum_{q \in [R]} |\, q \rangle\langle q \,| \otimes A(G_q) \right) |\Gamma\rangle = e_1 |\Gamma\rangle \tag{9.77}$$

$$h_{\mathcal{S}} |\Gamma\rangle = 0 \tag{9.78}$$

$$h_{\mathcal{E}} |\Gamma\rangle = 0. \tag{9.79}$$

Indeed, to show that a given gate graph G is an e_1-gate graph, it suffices to find a state $|\Gamma\rangle$ satisfying these conditions. Note that equation (9.77) implies that $|\Gamma\rangle$ can be written as a superposition of the states

$$|\overline{\psi^q_{z,a}}\rangle = |q\rangle |\overline{\psi_{z,a}}\rangle, \quad z, a \in \mathbb{F}_2, q \in [R] \tag{9.80}$$

where $|\overline{\psi_{z,a}}\rangle$ is given by equations (9.10) and (9.11) under the transform of (9.56). The coefficients in the superposition are then constrained by equations (9.78) and (9.79).

[**TO DO:** *fix frustration free stuff*]

9.2.2 Gadgets

[**TO DO:** *rewrite this, removing the examples stuff*]

In Example **??** we saw how a single-particle ground state can encode a single-qubit computation. In this Section we see how a two-particle frustration-free state on a suitably designed e_1-gate graph can encode a two-qubit computation. We design specific e_1-gate graphs (called *gadgets*) that we use in Section **??** to prove that these ground state problems for the MPQW are QMA-hard. For each gate graph we discuss, we show that the smallest eigenvalue of its adjacency matrix is e_1 and we solve for all of the frustration-free states.

We first design a gate graph where, in any two-particle frustration-free state, the locations of the particles are synchronized. We then design gadgets for two-qubit gates using four move-together gadgets, one for each two-qubit computational basis state. Finally, we describe a small modification of a two-qubit gate gadget called the "boundary gadget."

In important piece of these gadgets will be the inclusion of $\mathbb{I}^{(1,0)}_{(1,0)}$ diagram elements to separate the locations of particles. With these separations, we will only ever need to analyze the case when particles occupy the same diagram element, as these identity elements ensure that for the states that we care about, particles are always located at a distance more than $d_{\max}$.

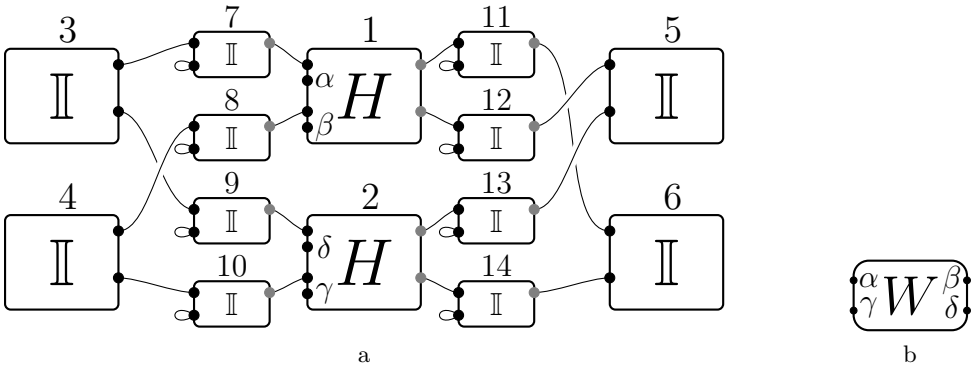

Figure 9.4: (a) The gate diagram for the move-together gadget. Note the four labeled nodes, α, β, γ, and δ, which have no attached edges. (b) A schematic representation for a move-together gadget, with the four labeled nodes corresponding to the four labeled nodes of (a).

9.2.2.1 The move-together gadget

The gate diagram for the *move-together gadget* is shown in Figure 9.4. Using equation (9.70), we write the adjacency matrix of the corresponding gate graph G_W as

$$A(G_W) = \sum_{q=1}^{14} |q\rangle\langle q| \otimes A(G_q) + h_{\mathcal{E}} \tag{9.81}$$

where

$$G_q = \begin{cases} G_H^{(2,2),(1,1)} & q \in \{1,2\} \\ G_{\mathbb{I}}^{(1,1),(0,0)} & q \in \{3,4,5,6\} \\ G_{\mathbb{I}}^{(1,0),(1,0)} & q > 6, \end{cases} \tag{9.82}$$

$h_{\mathcal{E}}$ is given by (9.73), $h_{\mathcal{S}}$ is given by (9.72), $\mathcal{E}$ is the set of edges in the gate diagram, and $\mathcal{S}$ is the set of self-loops in the diagram.

We begin by solving for the single-particle ground states, i.e., the eigenvectors of (9.81) with eigenvalue $e_1 = -1 - 3\sqrt{2}$. Note that we can solve for the states with $a = 0$ and $a = 1$ separately, since

$$\langle \psi_{x,1}^j | h_{\mathcal{E}} | \psi_{z,0}^i \rangle = 0 \tag{9.83}$$

for all $i, j \in [14]$ and $x, z \in \mathbb{F}_2$. We write a single-particle ground state as

$$\sum_{i=1}^{14} \left(\tau_i |\psi_{0,a}^i\rangle + \nu_i |\psi_{1,a}^i\rangle \right) \tag{9.84}$$

and solve for the coefficients τ_i and ν_i using equation (9.79). Enforcing (9.78) gives us that $\nu_i = 0$

for all $i > 6$. Enforcing (9.79) gives sixteen equations, one for each edge in the gate diagram:

$$\tau_3 = -\tau_7 \qquad \tau_7 = -\tau_1 \qquad \frac{1}{\sqrt{2}}(\tau_1 + \nu_1) = -\tau_{11} \qquad \tau_{11} = -\tau_6 \tag{9.85}$$

$$\nu_3 = -\tau_9 \qquad \tau_9 = -\tau_2 \qquad \frac{1}{\sqrt{2}}(\tau_2 + \nu_2) = -\tau_{13} \qquad \tau_{13} = -\nu_5 \tag{9.86}$$

$$\tau_4 = -\tau_8 \qquad \tau_8 = -\nu_1 \qquad \frac{1}{\sqrt{2}}(\tau_1 - \nu_1) = -\tau_{12} \qquad \tau_{12} = -\tau_5 \tag{9.87}$$

$$\nu_3 = -\tau_{10} \qquad \tau_{10} = -\nu_2 \qquad \frac{1}{\sqrt{2}}(\tau_2 - \nu_2) = -\tau_{14} \qquad \tau_{14} = -\nu_6. \tag{9.88}$$

Similarly, enforcing (9.78) gives eight equations, namely that $\nu_q = 0$ for $q > 6$. There are four linearly independent solutions to this set of equations, given by

$$\textit{Solution 1:} \quad \tau_1 = \tau_3 = -\tau_7 = 1 \quad \tau_5 = \tau_6 = -\tau_{11} = -\tau_{12} = \frac{1}{\sqrt{2}} \quad \text{all other coefficients } 0 \tag{9.89}$$

$$\textit{Solution 2:} \quad \nu_1 = \tau_4 = -\tau_8 = 1 \quad -\tau_5 = \tau_6 = -\tau_{11} = \tau_{12} = \frac{1}{\sqrt{2}} \quad \text{all other coefficients } 0 \tag{9.90}$$

$$\textit{Solution 3:} \quad \nu_2 = \nu_4 = -\tau_{10} = 1 \quad \nu_5 = -\nu_6 = -\tau_{13} = \tau_{14} = \frac{1}{\sqrt{2}} \quad \text{all other coefficients } 0 \tag{9.91}$$

$$\textit{Solution 4:} \quad \tau_2 = \nu_3 = -\tau_9 = 1 \quad \nu_5 = \nu_6 = -\tau_{13} = -\tau_{14} = \frac{1}{\sqrt{2}} \quad \text{all other coefficients } 0. \tag{9.92}$$

For each of these solutions, and for each $a \in \{0, 1\}$, we find a single-particle state with energy e_1. This result is summarized in the following Lemma.

Lemma 22. *G_W is an e_1-gate graph. A basis for the eigenspace of $A(G_W)$ with eigenvalue e_1 is*

$$|\chi_{1,a}\rangle = \frac{1}{\sqrt{5}}\big(|\psi^1_{0,a}\rangle + |\psi^3_{0,a}\rangle - |\psi^7_{0,a}\rangle\big) + \frac{1}{\sqrt{10}}\big(|\psi^5_{0,a}\rangle + |\psi^6_{0,a}\rangle - |\psi^{11}_{0,a}\rangle - |\psi^{12}_{0,a}\rangle\big) \tag{9.93}$$

$$|\chi_{2,a}\rangle = \frac{1}{\sqrt{5}}\big(|\psi^1_{1,a}\rangle + |\psi^4_{0,a}\rangle - |\psi^8_{0,a}\rangle\big) + \frac{1}{\sqrt{10}}\big(-|\psi^5_{0,a}\rangle + |\psi^6_{0,a}\rangle - |\psi^{11}_{0,a}\rangle + |\psi^{12}_{0,a}\rangle\big) \tag{9.94}$$

$$|\chi_{3,a}\rangle = \frac{1}{\sqrt{5}}\big(|\psi^2_{1,a}\rangle + |\psi^4_{1,a}\rangle - |\psi^{10}_{0,a}\rangle\big) + \frac{1}{\sqrt{10}}\big(|\psi^5_{1,a}\rangle - |\psi^6_{1,a}\rangle - |\psi^{13}_{0,a}\rangle + |\psi^{14}_{0,a}\rangle\big) \tag{9.95}$$

$$|\chi_{4,a}\rangle = \frac{1}{\sqrt{5}}\big(|\psi^2_{0,a}\rangle + |\psi^3_{1,a}\rangle - |\psi^9_{0,a}\rangle\big) + \frac{1}{\sqrt{10}}\big(|\psi^5_{1,a}\rangle + |\psi^6_{1,a}\rangle - |\psi^{13}_{0,a}\rangle - |\psi^{14}_{0,a}\rangle\big) \tag{9.96}$$

where $a \in \mathbb{F}_2$.

In Figure 9.4 we have used a shorthand $\alpha, \beta, \gamma, \delta$ to identify four nodes of the move-together gadget; these are the nodes with labels $(q, z, t) = (1, 0, 2), (1, 1, 3k + 2), (2, 1, 3k + 2), (2, 0, 2)$, respectively. We view α and γ as "input" nodes and β and δ as "output" nodes for this gate diagram. It is natural to associate each single-particle state $|\chi_{i,a}\rangle$ with one of these four nodes. We will also associate the set of 16 vertices represented by the node with the corresponding node, e.g.,

$$S_\alpha = \{(1, 0, 2, j, d) \colon j \in [8], d \in \mathbb{F}_2\}. \tag{9.97}$$

Looking at equation (9.93) (and perhaps referring back to equation (9.10)) we see that $|\chi_{1,a}\rangle$ has support on vertices in S_α but has no support on vertices in S_β, S_γ, or S_δ. Looking at the picture on the right-hand side of the equality sign in Figure 9.4, we think of $|\chi_{1,a}\rangle$ as localized at the node

α, with no support on the other three nodes. The states $|\chi_{2,a}\rangle, |\chi_{3,a}\rangle, |\chi_{4,a}\rangle$ are similarly localized at nodes β, γ, δ. We view $|\chi_{1,a}\rangle$ and $|\chi_{3,a}\rangle$ as input states and $|\chi_{2,a}\rangle$ and $|\chi_{4,a}\rangle$ as output states for the move-together gadget.

Now we turn our attention to the two-particle frustration-free states of the move-together gadget, i.e., the states $|\Phi\rangle \in \mathcal{H}(G_W)^{\otimes 2}$ in the nullspace of $H(G_W, 2)$ (with the additional restriction to symmetric states if $d_{\max} = 0$). As $\lambda_2^1(G_U) > 0$ for all U from Lemma 21, we have that any such state must take the form

$$|\Phi\rangle = \sum_{a,b\in\{0,1\},\, I,J\in[4]} C_{(I,a),(J,b)} |\chi_{I,a}\rangle |\chi_{J,b}\rangle \tag{9.98}$$

where

$$\langle\psi^q_{z,a}|\langle\psi^q_{x,b}|\Phi\rangle = 0 \tag{9.99}$$

for all $z, a, x, b \in \mathbb{F}_2$ and $q \in [14]$, and where the coefficients are symmetric if $d_{\max} = 0$, i.e.,

$$C_{(I,a),(J,b)} = C_{(J,b),(I,a)},. \tag{9.100}$$

Note that these conditions are only necessary, and not sufficient, for the state to be frustration free. These conditions do not take into account the fact that the addition of edges might cause the distance of vertices to fall below $d_{\max}$, and thus add an interaction term between two occupied vertices.

However, in our construction of the G_W gadget we placed the $H^{(1,1)}_{(1,0)}$ elements specifically to ensure that the two-particle states were separated by a distance of at least $2 + d_{\max}$. Since each input/output node of a given diagram element is separated by a distance at least $d_{\max}$, if we can ensure that the state $|\Phi\rangle$ has no support on adjacent diagram elements, in addition to the other conditions in (9.99), then we can guarantee that $|\Phi\rangle$ is frustration-free.

The move-together gadget is designed so that each solution $|\Phi\rangle$ to these equations is a superposition of a term where both particles are in input states and a term where both particles are in output states, with the intuition that particles move from input nodes to output nodes together. We now solve equations (9.98)–(9.99) and prove the following.

Lemma 23. *A basis for the nullspace of $H(G_W, 2)$ is*

$$|\Phi^{\pm}_{a,b}\rangle = \frac{1}{2}\big(|\chi_{1,a}\rangle|\chi_{3,b}\rangle \pm |\chi_{3,b}\rangle|\chi_{1,a}\rangle + |\chi_{2,a}\rangle|\chi_{4,b}\rangle \pm |\chi_{4,b}\rangle|\chi_{2,a}\rangle\big), \quad a, b \in \mathbb{F}_2 \tag{9.101}$$

for $d_{max} > 0$, and if $d_{max} = 0$ a basis for the nullspace of $H(G_W, 2)$ when restricted to symmetric states is $|\Phi^+_{a,b}\rangle$ for $a, b \in \mathbb{F}_2$.

There are no N-particle frustration-free states on G_W for $N \geq 3$ for any d_{max} (with a restriction to symmetric states for $d_{max} = 0$), i.e.,

$$\lambda^1_N(G_W) > 0 \quad \textit{for } N \geq 3. \tag{9.102}$$

Proof. The states $|\Phi^{\pm}_{a,b}\rangle$ manifestly satisfy equations (9.98), and one can directly verify that they also satisfy (9.99) (the nontrivial cases to check are for $q = 5$, $q = 6$, and $q > 10$). Additionally, one can also directly verify that $|\Phi^{\pm}_{a,b}\rangle$ has no support on states for which the two particles are located on adjacent diagram elements, and thus the state is in the ground space of the interaction Hamiltonian.

To complete the proof that (9.101) is a basis for the nullspace of $H(G_W, 2)$, we will show that any state satisfying the conditions (9.98) and (9.99) must be a linear combination of these four

states. Assuming that the state satisfies (9.98), applying equation (9.99) to the first 4 diagram elements gives

$$\langle\psi^1_{0,a}|\langle\psi^1_{0,b}|\Phi\rangle = \frac{1}{5}C_{(1,a),(1,b)} = 0 \qquad \langle\psi^1_{1,a}|\langle\psi^1_{1,b}|\Phi\rangle = \frac{1}{5}C_{(2,a),(2,b)} = 0 \tag{9.103}$$

$$\langle\psi^2_{1,a}|\langle\psi^2_{1,b}|\Phi\rangle = \frac{1}{5}C_{(3,a),(3,b)} = 0 \qquad \langle\psi^2_{0,a}|\langle\psi^2_{0,b}|\Phi\rangle = \frac{1}{5}C_{(4,a),(4,b)} = 0 \tag{9.104}$$

$$\langle\psi^1_{0,a}|\langle\psi^1_{1,b}|\Phi\rangle = \frac{1}{5}C_{(1,a),(2,b)} = 0 \qquad \langle\psi^2_{0,a}|\langle\psi^2_{1,b}|\Phi\rangle = \frac{1}{5}C_{(4,a),(3,b)} = 0 \tag{9.105}$$

$$\langle\psi^1_{1,a}|\langle\psi^1_{0,b}|\Phi\rangle = \frac{1}{5}C_{(2,a),(1,b)} = 0 \qquad \langle\psi^2_{1,a}|\langle\psi^2_{0,b}|\Phi\rangle = \frac{1}{5}C_{(3,a),(4,b)} = 0 \tag{9.106}$$

$$\langle\psi^3_{0,a}|\langle\psi^3_{1,b}|\Phi\rangle = \frac{1}{5}C_{(1,a),(4,b)} = 0 \qquad \langle\psi^4_{0,a}|\langle\psi^4_{1,b}|\Phi\rangle = \frac{1}{5}C_{(2,a),(3,b)} = 0 \tag{9.107}$$

$$\langle\psi^3_{1,a}|\langle\psi^3_{0,b}|\Phi\rangle = \frac{1}{5}C_{(4,a),(1,b)} = 0 \qquad \langle\psi^4_{1,a}|\langle\psi^4_{0,b}|\Phi\rangle = \frac{1}{5}C_{(3,a),(2,b)} = 0 \tag{9.108}$$

for all $a, b \in \{0, 1\}$. Using the fact that all of these coefficients are zero, we can then see that

$$|\Phi\rangle = \sum_{\substack{a,b\in\mathbb{F}_2\\ j\in[4]}} C_{(j,a),(j+2,b)}|\chi_{j,a}\rangle|\chi_{j+2,b}\rangle. \tag{9.109}$$

Finally, applying equation (9.99) to diagram 6 gives

$$\langle\psi^6_{0,a}|\langle\psi^6_{1,b}|\Phi\rangle = \frac{1}{6}C_{(2,a),(4,b)} - \frac{1}{6}C_{(1,a),(3,b)} = 0 \tag{9.110}$$

$$\langle\psi^6_{1,a}|\langle\psi^6_{0,b}|\Phi\rangle = \frac{1}{6}C_{(4,a),(2,b)} - \frac{1}{6}C_{(3,a),(1,b)} = 0. \tag{9.111}$$

Hence

$$|\Phi\rangle = \sum_{\substack{a,b\in\mathbb{F}_2\\ j\in[4]}} C_{(j,a),(j+2,b)}\big(|\chi_{j,a}\rangle|\chi_{j+2,b}\rangle + |\chi_{j+1,a}\rangle|\chi_{j+3,b}\rangle\big), \tag{9.112}$$

which is a superposition of the states $|\Phi^{\pm}_{a,b}\rangle$.

Note that the above analysis holds completely if we restrict ourselves to symmetric states, and thus if $d_{\max} = 0$, we end up with the same results except that we only care about the states $|\Phi^{+}_{a,b}\rangle$, as they span the symmetric nullspace.

Finally, we prove that there are no frustration-free ground states of the Bose-Hubbard model on G_W with more than two particles. By Lemma **??**, it suffices to prove that there are no frustration-free three-particle states.

Suppose (for a contradiction) that $|\Gamma\rangle \in \mathcal{H}(G_W)^{\otimes 3}$ is a normalized three-particle frustration-free state. Write

$$|\Gamma\rangle = \sum D_{(i,a),(j,b),(k,c)}|\chi_{i,a}\rangle|\chi_{j,b}\rangle|\chi_{k,c}\rangle. \tag{9.113}$$

Note that each reduced density matrix of $|\Gamma\rangle$ on two of the three subsystems must have all of its support on two-particle frustration-free states (see the remark following Lemma **??**), i.e., on the states $|\Phi_{a,b}\rangle$. Using this fact for the subsystem consisting of the first two particles, we see in particular that

$$(i,j) \notin \{(1,3),(3,1),(2,4),(4,2)\} \quad \Longrightarrow \quad D_{(i,a),(j,b),(k,c)} = 0 \tag{9.114}$$

(since $|\Phi_{a_1,a_2}\rangle$ only has support on vectors $|\chi_{i,a}\rangle|\chi_{j,b}\rangle$ with $i, j \in \{(1,3),(3,1),(2,4),(4,2)\}$).

Using this fact for subsystems consisting of particles $2,3$ and $1,3$, respectively, gives

$$(j,k) \notin \{(1,3),(3,1),(2,4),(4,2)\} \implies D_{(i,a),(j,b),(k,c)} = 0 \tag{9.115}$$

$$(i,k) \notin \{(1,3),(3,1),(2,4),(4,2)\} \implies D_{(i,a),(j,b),(k,c)} = 0. \tag{9.116}$$

Putting together equations (9.114), (9.115), and (9.116), we see that $|\Gamma\rangle = 0$. This is a contradiction, so no three-particle frustration-free states exist. □

With this gadget allowing us to entangle the locations of particles, we will be able to create a pseudo-history state, in which time is encoded in the location of particles. This is the large workhorse of the construction, as it allows us to understand the multi-particle ground space by understanding the simple two-particle ground states.

9.2.2.2 Two-qubit unitary gadget

We can now use the W-gadget as a building block to encode graphs with more interesting ground-state behavior. In particular, we can use the W-gadget to force the two-particle state of a larger gadget to have entangled locations. If we then place connections in a particular manner, we can use these guarantees to force the ground state to encode a computation corresponding to a permutation of the computational basis states (such as a controlled-not operation). In particular, we will be to define a gate graph for each of the two-qubit unitaries

$$\{\mathrm{CNOT}_{12}, \mathrm{CNOT}_{21}, \mathrm{CNOT}_{12}\,(H \otimes \mathbb{I})\,, \mathrm{CNOT}_{12}\,(HT \otimes \mathbb{I})\}. \tag{9.117}$$

Here CNOT_{12} is the standard controlled-not gate with the second qubit as a target, whereas CNOT_{21} has the first qubit as target.

We define the gate graphs by exhibiting their gate diagrams. For the three cases

$$U = \mathrm{CNOT}_{12}(\tilde{U} \otimes \mathbb{I}) \tag{9.118}$$

with $\tilde{U} \in \{\mathbb{I}, H, HT\}$, we associate U with the gate diagram shown in Figure 9.5a. In Figure 9.5b we also indicate a shorthand used to represent this gate diagram. As one might expect, for the case $U = \mathrm{CNOT}_{21}$, we use the same gate diagram as for $U = \mathrm{CNOT}_{12}$; however, we use the slightly different shorthand shown in Figure 9.5c.

Roughly speaking, the two-qubit gate gadgets work as follows. There are four move-together gadgets, one for each two-qubit basis state $|00\rangle, |01\rangle, |10\rangle, |11\rangle$. These enforce the constraint that two particles must move through the graph together, while their connections to the four diagram elements labeled $1,2,3,4$ ensure that most of the frustration-free two-particle states encode two-qubit computations, while the connections between diagram elements $1,2,3,4$ and $5,6,7,8$ ensure that the remaining frustration-free two-particle states are removed from the ground space. The 24 $\mathbb{I}^{(1,1)}_{(1,0)}$ diagram elements are simply used to separate the locations of the particles when more than one are located on the gadget, but can simply be thought of as a part of the connections between the other gadgets.

To describe the frustration-free states of the gate graph depicted in Figure 9.5, first recall the definition of the states $|\chi_{j,a}\rangle$ for $j \in [4]$ from equations (9.93)–(9.96). For each of the move-together gadgets $xy \in \{00,01,10,11\}$ in Figure 9.5b, write $|\chi^{xy}_{j,a}\rangle$ for the state $|\chi_{j,a}\rangle$ with support (only) on the gadget labeled xy. Additionally, write

$$U^a = \begin{cases} U & \text{if } a = 0 \\ \overline{U} & \text{if } a = 1 \end{cases} \tag{9.119}$$

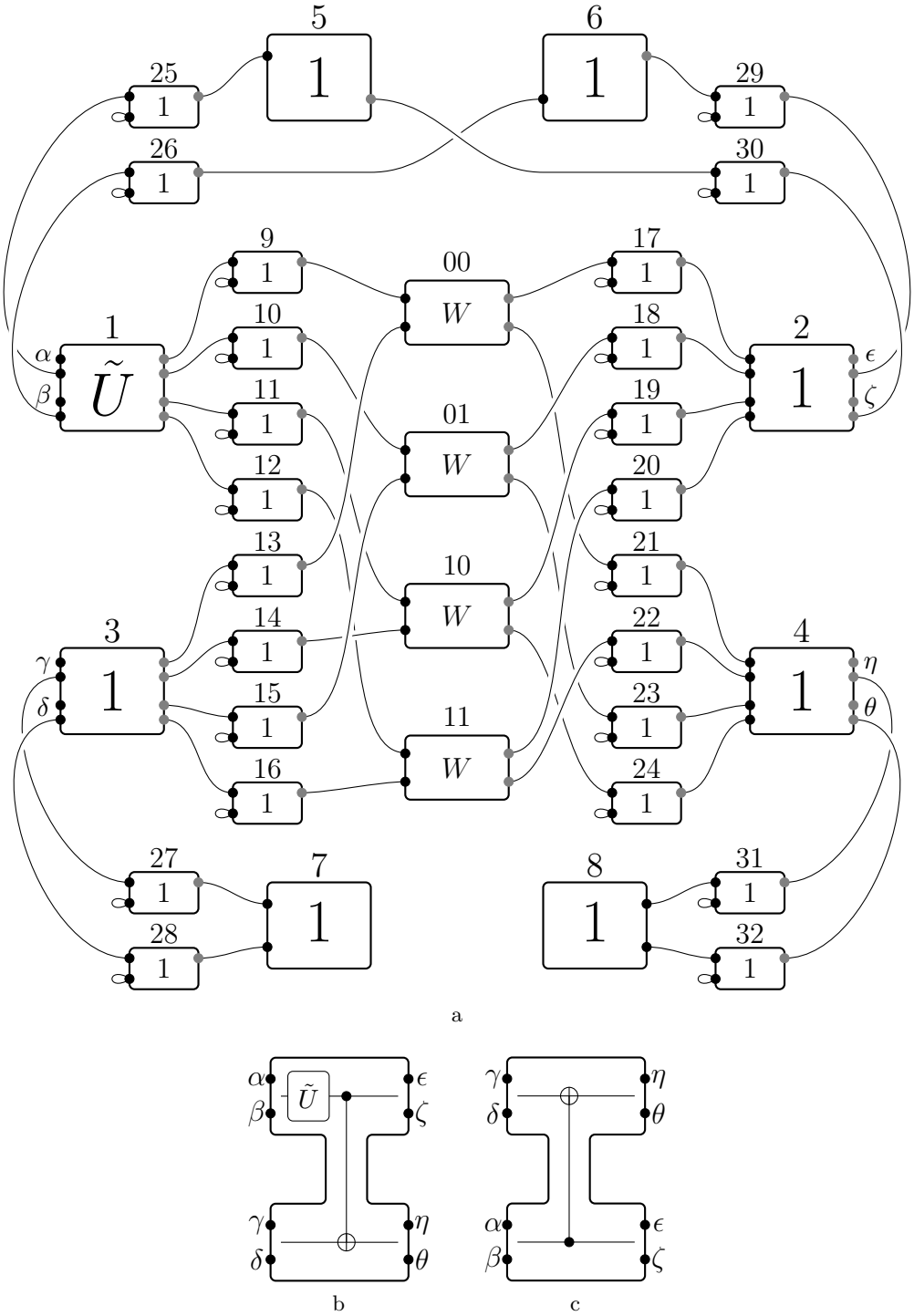

Figure 9.5: (a) Gadget for the two-qubit unitary $U = \mathrm{CNOT}_{12}(\tilde{U} \otimes \mathbb{I})$ with $\tilde{U} \in \{1, H, HT\}$. (b) A schematic encoding for $U = \mathrm{CNOT}_{12}(\tilde{U} \otimes \mathbb{I})$, where the eight labeled nodes correspond to the eight labeled nodes of (a). (c) For the $U = \mathrm{CNOT}_{21}$ gate (first qubit is the target), we use the same gate graph as in (b) with $\tilde{U} = 1$, but with a different location for the eight labeled nodes.

and similarly for $\tilde{U}$. This notation will help us to define the ground states of the resulting Hamiltonian, as the encoded computation will change depending on α.

We now show that G_U is an e_1-gate graph and solves for its frustration-free states.

Lemma 24. *Let $U = \mathrm{CNOT}_{12}(\tilde{U} \otimes \mathbb{I})$ where $\tilde{U} \in \{\mathbb{I}, H, HT\}$. The corresponding gate graph G_U is defined by its gate diagram shown in Figure 9.5a. The adjacency matrix $A(G_U)$ has ground energy e_1; a basis for the corresponding eigenspace is*

$$|\rho^{1,U}_{z,a}\rangle = \frac{1}{\sqrt{15}}\Big(|\psi^{1}_{z,a}\rangle + |\psi^{5+z}_{z,a}\rangle - |\psi^{25+z}_{z,a}\rangle + \sum_{x,y\in\mathbb{F}_2} \tilde{U}^a_{yz}\big(\sqrt{5}|\chi^{yx}_{1,a}\rangle - |\psi^{9+x+2y}_{0,a}\rangle\big)\Big) \tag{9.120}$$

$$|\rho^{2,U}_{z,a}\rangle = \frac{1}{\sqrt{15}}\Big(|\psi^{2}_{z,a}\rangle + |\psi^{6-z}_{z,a}\rangle - |\psi^{29+z}_{z,a}\rangle + \sum_{x\in\mathbb{F}_2} \big(\sqrt{5}|\chi^{zx}_{2,a}\rangle - |\psi^{17+2z+x}_{0,a}\rangle\big)\Big) \tag{9.121}$$

$$|\rho^{3,U}_{z,a}\rangle = \frac{1}{\sqrt{15}}\Big(|\psi^{3}_{z,a}\rangle + |\psi^{7}_{z,a}\rangle - |\psi^{27+z}_{z,a}\rangle + \sum_{x\in\mathbb{F}_2} \big(\sqrt{5}|\chi^{xz}_{3,a}\rangle - |\psi^{17+2z+x}_{0,a}\rangle\big)\Big) \tag{9.122}$$

$$|\rho^{4,U}_{z,a}\rangle = \frac{1}{\sqrt{15}}\Big(|\psi^{4}_{z,a}\rangle + |\psi^{8}_{z,a}\rangle - |\psi^{31+z}_{z,a}\rangle + \sum_{x\in\mathbb{F}_2} \big(\sqrt{5}|\chi^{x(z\oplus x)}_{4,a}\rangle - |\psi^{21+2z+x}_{0,a}\rangle\big)\Big) \tag{9.123}$$

where $z, a \in \mathbb{F}_2$.

Proof. As the gate graph G_U is specified by its gate diagram, shown in Figure 9.5a, the adjacency matrix of the gate graph G_U is of the form in equation (9.70). There are 14 diagram elements for each of the move-together gadgets, so there are 88 diagram elements in total. We will only need to refer to those diagram elements labeled $q \in [32]$ in Figure 9.5a (i.e., those not contained in the move-together gadgets), as we will refer to Lemma 22 for those contained in the move-together gadgets.

Write

$$A(G_U) = A(G'_U) + h_{\mathcal{E}'} \tag{9.124}$$

where G'_U is the gate graph obtained from G_U by removing all 48 edges shown in Figure 9.5a (G'_U does include the edges within each of the move-together gadgets along with the selfloops of G_U). Here $h_{\mathcal{E}'}$ is given by equation (9.73) with $\mathcal{E}'$ the set of 48 edges shown in Figure 9.5a.

If we use the results of Lemma 22, we can see that one basis for the e_1-energy ground space of $A(G'_U)$ is given by the 112 states

$$|\psi^{q}_{z,a}\rangle, \quad q \in [32],\ z, a \in \mathbb{F}_2 \tag{9.125}$$

$$|\chi^{xy}_{j,a}\rangle, \quad x, y, a \in \mathbb{F}_2,\ j \in [4], \tag{9.126}$$

where we exclude $|\psi^{q}_{1,a}\rangle$ if $q > 8$ (as these states are removed via a self-loop). It will be convenient to work with the following slightly rotated basis for this space, however, given by:

$$|\psi^{q}_{z,a}\rangle \qquad q \in [8],\ z, a \in \mathbb{F}_2 \tag{9.127}$$

$$\sum_{x\in\mathbb{F}_2} \tilde{U}^a_{xz}|\psi^{j+2x}_{0,a}\rangle \qquad a, z \in \mathbb{F}_2, j \in \{9, 10\} \tag{9.128}$$

$$|\psi^{q}_{0,a}\rangle \qquad a \in \mathbb{F}_2, 13 \le q \le 32 \tag{9.129}$$

$$\sum_{x\in\mathbb{F}_2} \tilde{U}^a_{xz}|\chi^{xy}_{1,a}\rangle \qquad y, z, a \in \mathbb{F}_2 \tag{9.130}$$

$$|\chi^{xy}_{j,a}\rangle \qquad x, y, a \in \mathbb{F}_2,\ j \in \{2, 3, 4\}. \tag{9.131}$$

In this basis, the states supported on diagram elements connected to the output of the $q = 1$ diagram element are in a superposition corresponding to the correct output of the single-qubit unitary $\tilde{U}$.

We are interested in the intersection of the ground space of $A(G'_U)$ with the nullspace of $h_{\mathcal{E}'}$, so we compute the matrix elements of $h_{\mathcal{E}'}$ in the above basis. The resulting 112×112 matrix is block diagonal with sixteen 7×7 blocks. Each block is identical, with entries

$$\frac{1}{8k}\begin{pmatrix} 3 & 1 & 1 & 1 & 0 & 0 & 0 \\ 1 & 2 & 0 & 0 & \frac{1}{\sqrt{5}} & 0 & 0 \\ 1 & 0 & 2 & 0 & 0 & \frac{1}{\sqrt{5}} & 0 \\ 1 & 0 & 0 & 2 & 0 & 0 & 1 \\ 0 & \frac{1}{\sqrt{5}} & 0 & 0 & \frac{1}{5} & 0 & 0 \\ 0 & 0 & \frac{1}{\sqrt{5}} & 0 & 0 & \frac{1}{5} & 0 \\ 0 & 0 & 0 & 1 & 0 & 0 & 1 \end{pmatrix}. \tag{9.132}$$

The seven states involved in each block are given by (in order from left to right as in the matrix above):

$$|\psi^1_{z,a}\rangle, \sum_{x\in\mathbb{F}_2} \tilde{U}^a_{xz}|\psi^{9+2x}_{0,a}\rangle, \sum_{x\in\mathbb{F}_2} \tilde{U}^a_{xz}|\psi^{10+2x}_{0,a}\rangle, |\psi^{25+z}_{0,a}\rangle, \sum_{x\in\mathbb{F}_2} \tilde{U}^a_{xz}|\chi^{x0}_{1,a}\rangle, \sum_{x\in\mathbb{F}_2} \tilde{U}^a_{xz}|\chi^{x1}_{1,a}\rangle, |\psi^{5+z}_{z,a}\rangle \tag{9.133}$$

$$|\psi^2_{z,a}\rangle, |\psi^{17+2z}_{0,a}\rangle, |\psi^{18+2z}_{0,a}\rangle, |\psi^{29+z}_{0,a}\rangle, |\chi^{z0}_{2,a}\rangle, |\chi^{z1}_{2,a}\rangle, |\psi^{6-z}_{z,a}\rangle \tag{9.134}$$

$$|\psi^3_{z,a}\rangle, |\psi^{13+2z}_{0,a}\rangle, |\psi^{14+2z}_{0,a}\rangle, |\psi^{27+z}_{0,a}\rangle, |\chi^{0z}_{3,a}\rangle, |\chi^{1z}_{3,a}\rangle, |\psi^{7}_{z,a}\rangle \tag{9.135}$$

$$|\psi^4_{z,a}\rangle, |\psi^{21+2z}_{0,a}\rangle, |\psi^{22+2z}_{0,a}\rangle, |\psi^{31+z}_{0,a}\rangle, |\chi^{0z}_{4,a}\rangle, |\chi^{1(z\oplus 1)}_{4,a}\rangle, |\psi^{8}_{z,a}\rangle. \tag{9.136}$$

The unique zero eigenvector of the matrix (9.132) is

$$\frac{1}{\sqrt{15}}\begin{pmatrix} 1 & -1 & -1 & -1 & \sqrt{5} & \sqrt{5} & 1 \end{pmatrix}^T. \tag{9.137}$$

Constructing this vector within each of the 16 blocks, we get the states described in the lemma. □

With this understanding of the ground states of $A(G_U)$, we can then give some meaning to the nodes of the graph. In particular, we view the nodes labeled $\alpha, \beta, \gamma, \delta$ in Figure 9.5 as "input" nodes and those labeled $\epsilon, \zeta, \eta, \theta$ as "output nodes". Each of the states $|\rho^{i,U}_{z,a}\rangle$ is associated with one of the nodes, depending on the values of $i \in [4]$ and $z \in \mathbb{F}_2$. For example, the states $|\rho^{1,U}_{0,0}\rangle$ and $|\rho^{1,U}_{0,1}\rangle$ are associated with input node α since they both have nonzero amplitude on vertices of the gate graph that are associated with α (and zero amplitude on vertices associated with other labeled nodes).

With the single particle states found, we now turn our attention to the two-particle states. It will turn out that the two particle eigenstates of the move-together gadget found in Lemma 23 will play a critical part in our construction.

Lemma 25. *A basis for the nullspace of $H(G_U, 2)$ is*

$$|T^{U,\pm}_{z_1,a,z_2,b}\rangle = \frac{1}{2}\Big(|\rho^{1,U}_{z_1,a}\rangle|\rho^{3,U}_{z_2,b}\rangle \pm |\rho^{3,U}_{z_2,b}\rangle|\rho^{1,U}_{z_1,a}\rangle + \sum_{x_1,x_2=0}^{1} U(a)_{x_1x_2,z_1z_2}\big(|\rho^{2,U}_{x_1,a}\rangle|\rho^{4,U}_{x_2,b}\rangle \pm |\rho^{4,U}_{x_2,b}\rangle|\rho^{2,U}_{x_1,a}\rangle\big)\Big) \tag{9.138}$$

for $z_1, z_2, a, b \in \mathbb{F}_2$ when $d_{max} > 0$, and if $d_{max} = 0$ a basis for the nullspace of $H(G_U, 2)$ when restricted to symmetric states is $|T^{U,+}_{z_1,a,z_2,b}\rangle$ for $z_1, z_2, a, b \in \mathbb{F}_2$. For any $N \geq 3$, there are no N-particle frustration-free states on G_U for any $d_{max} > 0$ and there are no N-particle symmetric frustration-free states on G_U when $d_{max} = 0$, i.e.,

$$\lambda_N^1(G_U) > 0 \quad \textit{for } N \geq 3. \tag{9.139}$$

Proof. Let us first show that the states $|T^{U,\pm}_{z_1,a,z_2,b}\rangle$ are contained within the nullspace of $H(G_U, 2)$. We we can expand these states in terms of the $|\psi^q_{z,a}\rangle$ for $q \in [32]$ and $|\chi^{xy}_{j,a}\rangle$, and see that the state $|T^{U,\pm}_{z_1,a,z_2,b}\rangle$ has no support on pairs of adjacent diagram elements, unless possibly both particles are contained in a single move-together gadget. In particular, whenever one particle is in state $|\psi^q_{z,a}\rangle$ (and thus localized to the diagram element q), the other particle is located on a diagram element separated from the first by at least one additional diagram element. The only difficult case to check is when both particles are in move-together gadgets, but the structure of the states $|T^{U,\pm}_{z_1,a,z_2,b}\rangle$ is such that either the particles are in separate move-together gadgets (and thus on states with support at a distance much larger than k), or the two particles are in a state within the span of $|\Phi^{\pm}_{a,b}\rangle$ and thus by Lemma 23 are not penalized by the interaction term. Altogether, we have that the states $|T^{U,\pm}_{z_1,a,z_2,b}\rangle$ are contained in the nullspace of the interaction Hamiltonian, and thus are frustration-free.

Now let us show that any state in the nullspace of $H(G_U, 2)$ are within the span of the states $|T^{U,\pm}_{z_1,a,z_2,b}\rangle$. Using Lemma **??**, we can write any two-particle frustration-free state as

$$|\Theta\rangle = \sum_{z,a,x,b \in \{0,1\}} \sum_{I,J \in [4]} B_{(z,a,I),(x,b,J)} |\rho^{I,U}_{z,a}\rangle |\rho^{J,U}_{x,b}\rangle, \tag{9.140}$$

with the additional constraint that

$$\langle \psi^q_{x,a}| \langle \psi^q_{z,b}|\Theta\rangle = 0 \tag{9.141}$$

for all $x, z, a, b \in \{0, 1\}$ and $q \in [88]$, and if $d_{\max} = 0$ we will use the additional constraint that

$$B_{(z,a,I),(x,b,J)} = B_{(x,b,J),(z,a,I)}. \tag{9.142}$$

To enforce equation (9.141) we consider the diagram elements $q \in [32]$ (as labeled in Figure **??**) separately from the other 56 diagram elements (those inside the move-together gadgets).

Using equation (9.141) with $q \in \{1, 2, 3, 4, 7, 8\}$ and $x, z, a, b \in \mathbb{F}_2$ gives

$$B_{(x,a,I),(z,b,I)} = 0 \quad I \in [4],\ x, z, a, b \in \mathbb{F}_2. \tag{9.143}$$

Using $q = 5$, $x = 0$, and $z = 1$ in equation (9.141) gives

$$\langle \psi^5_{0,a}| \langle \psi^5_{1,b}|\Theta\rangle = \frac{1}{15} B_{(0,a,1),(1,b,2)} = 0, \tag{9.144}$$

for $a, b \in \{0, 1\}$, while $q = 6$, $x = 0$, and $z = 1$ gives

$$\langle \psi^6_{0,a}| \langle \psi^6_{1,b}|\Theta\rangle = \frac{1}{15} B_{(0,a,2),(1,b,1)} = 0. \tag{9.145}$$

Note that we can use the same equations with $x = 1$ and $z = 0$ to see that $B_{(1,a,2),(0,b,1)} = B_{(1,a,1),(0,b,2)} = 0$ as well. If we then apply equation (9.141) with $q = 5$ or $q = 6$ and other choices for x and z, or for any or $9 \leq q \leq 32$, we find that the equation does not lead to any additional independent constraints on the state $|\Theta\rangle$.

Now consider the constraint (9.141) for diagram elements inside the move-together gadgets in Figure **??**. Let Π_{xy} be the projector onto two-particle states where both particles are located at vertices contained within the move-together gadget labeled $xy \in \{00, 01, 10, 11\}$. Using the results of Lemma 23, we see that for diagram elements inside the move-together gadgets, (9.141) is satisfied if and only if

$$\Pi_{xy}|\Theta\rangle \in \operatorname{span}\big\{|\chi^{xy}_{1,a}\rangle|\chi^{xy}_{3,b}\rangle \pm |\chi^{xy}_{3,b}\rangle|\chi^{xy}_{1,a}\rangle + |\chi^{xy}_{2,a}\rangle|\chi^{xy}_{4,b}\rangle \pm |\chi^{xy}_{4,b}\rangle|\chi^{xy}_{2,a}\rangle,\ a, b \in \{0, 1\}\big\}. \tag{9.146}$$

Since we already know

$$\Pi_{xy}|\Theta\rangle \in \operatorname{span}\big\{|\chi^{xy}_{i,a}\rangle|\chi^{xy}_{j,b}\rangle,\ i, j \in [4], a, b \in \mathbb{F}_2\big\}, \tag{9.147}$$

we get

$$\langle\chi^{xy}_{K,a}|\langle\chi^{xy}_{K,b}|\Theta\rangle = 0 \quad K \in [4] \tag{9.148}$$

$$\langle\chi^{xy}_{K,a}|\langle\chi^{xy}_{L,b}|\Theta\rangle = 0 \quad |K - L| \neq 2 \tag{9.149}$$

$$\big(\langle\chi^{xy}_{1,a}|\langle\chi^{xy}_{3,b}| - \langle\chi^{xy}_{2,a}|\langle\chi^{xy}_{4,b}|\big)|\Theta\rangle = 0 \tag{9.150}$$

$$\big(\langle\chi^{xy}_{3,a}|\langle\chi^{xy}_{1,b}| - \langle\chi^{xy}_{4,a}|\langle\chi^{xy}_{2,b}|\big)|\Theta\rangle = 0 \tag{9.151}$$

for all $a, b \in \{0, 1\}$. Note that (9.148) is automatically satisfied whenever (9.143) holds.

Applying equation (9.149) with $(K, L) = (1, 2)$ and $a, b, x, y \in \mathbb{F}_2$, we get

$$\langle\chi^{xy}_{1,a}|\langle\chi^{xy}_{2,b}|\Theta\rangle = \frac{1}{3}\sum_{z\in\mathbb{F}_2} \tilde{U}^a_{xz} B_{(z,a,1),(x,b,2)} = \frac{1}{3}\tilde{U}^a_{xx} B_{(x,a,1),(x,b,2)} = 0. \tag{9.152}$$

In the second equality we used the fact that $B_{(z,a,1),(x,b,2)}$ is zero whenever $z \neq x$ (from equations (9.142), (9.144), and (9.145)). Since $\tilde{U} \in \{1, H, HT\}$ we have $\tilde{U}^a_{xx} \neq 0$, and it follows that

$$B_{(x,a,1),(x,b,2)} = 0 \tag{9.153}$$

for all $x, a, b \in \mathbb{F}_2$, while the same argument for $(K, L) = (2, 1)$ gives $B_{(x,a,2),(x,b,1)} = 0$ for all $x, a, b \in \mathbb{F}_2$.

Applying equation (9.149) with $(K, L) = (1, 4)$ gives

$$\langle\chi^{xy}_{1,a}|\langle\chi^{xy}_{4,b}|\Theta\rangle = \frac{1}{3}\sum_{z\in\mathbb{F}_2} \tilde{U}(a)_{xz} B_{(z,a,1),(x\oplus y,b,4)} = 0 \qquad x, y, a, b \in \mathbb{F}_2. \tag{9.154}$$

By taking appropriate combinations of these equations, we have

$$\sum_{x\in\mathbb{F}_2} \tilde{U}^{a,\dagger}_{wx}\langle\chi^{x(y\oplus x)}_{1,a}|\langle\chi^{x(y\oplus x)}_{4,b}|\Theta\rangle = \frac{1}{3}B_{(w,a,1),(y,b,4)} = 0 \qquad w, y, a, b \in \mathbb{F}_2, \tag{9.155}$$

while the same argument with $(K, L) = (4, 1)$ gives $B_{(x,a,4),(z,b,1)} = 0$ for $x, z, a, b \in \mathbb{F}_2$

Applying equation (9.149) with $(K, L) \in \{(2, 3), (3, 2), (3, 4), (4, 3)\}$ gives

$$\langle\chi^{xy}_{2,a}|\langle\chi^{xy}_{3,b}|\Theta\rangle = \frac{1}{3}B_{(x,a,2),(y,b,3)} = 0 \qquad \langle\chi^{xy}_{3,a}|\langle\chi^{xy}_{2,b}|\Theta\rangle = \frac{1}{3}B_{(x,a,3),(y,b,2)} = 0 \tag{9.156}$$

$$\langle\chi^{xy}_{3,a}|\langle\chi^{xy}_{4,b}|\Theta\rangle = \frac{1}{3}B_{(x,a,3),(x\oplus y,b,4)} = 0 \qquad \langle\chi^{xy}_{4,a}|\langle\chi^{xy}_{3,b}|\Theta\rangle = \frac{1}{3}B_{(x,a,4),(x\oplus y,b,3)} = 0 \tag{9.157}$$

for all $x, y, a, b \in \mathbb{F}_2$.

Now putting together equations (9.143), (9.144), (9.145), (9.153), (9.155), (9.156), and (9.157), we get

$$B_{(x,a,I),(z,b,J)} = 0 \quad \text{for all } x,z,a,b \in \mathbb{F}_2, \text{ where } |I-J| \neq 2, \tag{9.158}$$

and thus we have

$$|\Theta\rangle = \sum_{\substack{z,c,w,d\in\mathbb{F}_2 \\ j\in[4]}} B_{(z,c,j),(w,d,j+2)} |\rho^{j,U}_{z,c}\rangle |\rho^{j+2,U}_{w,d}\rangle. \tag{9.159}$$

Now

$$\langle\chi^{xy}_{1,a}|\langle\chi^{xy}_{3,b}|\rho^{1,U}_{z,c}\rangle|\rho^{3,U}_{w,d}\rangle = \frac{1}{3}\delta_{a,c}\delta_{b,d}\tilde{U}(a)_{xz}\delta_{y,w} = \langle\chi^{xy}_{3,b}|\langle\chi^{xy}_{1,a}|\rho^{3,U}_{z,d}\rangle|\rho^{1,U}_{w,c}\rangle \tag{9.160}$$

$$\langle\chi^{xy}_{2,a}|\langle\chi^{xy}_{4,b}|\rho^{2,U}_{z,c}\rangle|\rho^{4,U}_{w,d}\rangle = \frac{1}{3}\delta_{a,c}\delta_{b,d}\delta_{x,z}\delta_{y,w\oplus x} = \langle\chi^{xy}_{4,a}|\langle\chi^{xy}_{2,b}|\rho^{4,U}_{z,c}\rangle|\rho^{2,U}_{w,d}\rangle, \tag{9.161}$$

so enforcing equation (9.150) gives

$$\sum_{z\in\mathbb{F}_2} \tilde{U}^a_{xz} B_{(z,a,1),(y,b,3)} = B_{(x,a,2),(x\oplus y,b,4)}, \tag{9.162}$$

while enforcing equation (9.151) gives

$$\sum_{z\in\mathbb{F}_2} \tilde{U}^a_{xz} B_{(y,b,3),(z,a,1)} = B_{(x\oplus y,b,4),(x,a,2)}, \tag{9.163}$$

for each $x,y,a,b \in \mathbb{F}_2$. In other words

$$B_{(z,c,2),(w,d,4)} = \sum_{x\in\mathbb{F}_2} \tilde{U}^c_{zx} B_{(x,c,1),(z\oplus w,d,3)} = \sum_{x,y\in\mathbb{F}_2} U^c_{zw,xy} B_{(x,c,1),(y,d,3)}, \tag{9.164}$$

and

$$B_{(w,d,4),(z,c,2)} = \sum_{x,y\in\mathbb{F}_2} U^c_{zw,xy} B_{(y,d,3),(x,c,1)}, \tag{9.165}$$

where we used $U^a = \mathrm{CNOT}_{12}(\tilde{U}^a \otimes 1)$. Plugging this into (9.159) gives

$$\begin{aligned}
|\Theta\rangle = \sum_{z,a,w,b\in\mathbb{F}_2} \Big[& B_{(z,a,1),(w,b,3)} |\rho^{1,U}_{z,a}\rangle|\rho^{3,U}_{w,b}\rangle + B_{(z,a,3),(w,b,1)} |\rho^{3,U}_{z,a}\rangle|\rho^{1,U}_{w,b}\rangle \\
& + \sum_{x,y\in\mathbb{F}_2} U^a_{zw,xy} B_{(x,a,1),(y,b,3)} |\rho^{2,U}_{z,a}\rangle|\rho^{4,U}_{w,b}\rangle + U^b_{wz,yx} B_{(x,a,3),(y,b,1)} |\rho^{4,U}_{z,a}\rangle|\rho^{2,U}_{w,b}\rangle \Big] \qquad (9.166) \\
= \sum_{z,a,w,b\in\mathbb{F}_2} \Big[& B_{(z,a,1),(w,b,3)} \Big(|\rho^{1,U}_{z,a}\rangle|\rho^{3,U}_{w,b}\rangle + \sum_{x,y\in\mathbb{F}_2} U^a_{xy,zw} |\rho^{2,U}_{x,a}\rangle|\rho^{4,U}_{y,b}\rangle \Big) \\
& + B_{(z,a,3),(w,b,1)} \Big(|\rho^{3,U}_{z,a}\rangle|\rho^{1,U}_{w,b}\rangle + \sum_{x,y\in\mathbb{F}_2} U^b_{yx,wz} |\rho^{4,U}_{x,a}\rangle|\rho^{2,U}_{y,b}\rangle \Big) \Big] \qquad (9.167) \\
= \sum_{z,a,w,b\in\mathbb{F}_2} & B_{(z,a,1),(w,b,3)} \big(|T^{U,+}_{z,a,w,b}\rangle + |T^{U,-}_{z,a,w,b}\rangle \big) - B_{(z,a,3),(w,b,1)} \big(|T^{U,+}_{w,b,z,a}\rangle - |T^{U,-}_{w,b,z,a}\rangle \big) \qquad (9.168)
\end{aligned}$$

This is the general solution to equations (9.140)–(9.141), so the space of two-particle frustration-free states for G_U is spanned by the 32 orthonormal states (9.138).

Note that the above analysis only uses Lemma 23, and thus if $d_{\max} = 0$ and we restrict ourselves to the symmetric states, the entire computation follows. Further, we also have that only the states $|T^{U,+}_{z,a,w,b}\rangle$ are symmetric, and thus these states span the symmetric subspace.

Finally, we show that there are no three-particle frustration-free states (for any $d_{\max}$). By Lemma **??**, this implies that there are no frustration-free states for more than two particles. Suppose (to reach a contradiction) that $|\Gamma\rangle$ is a normalized three-particle frustration-free state. Write

$$|\Gamma\rangle = \sum E_{(x,a,q),(y,b,r),(z,c,s)} |\rho^q_{x,a}\rangle |\rho^r_{y,b}\rangle |\rho^s_{z,c}\rangle \tag{9.169}$$

and note that each reduced density matrix of $|\Gamma\rangle$ on two of the three subsystems must have all of its support on two-particle frustration-free states (see the remark following Lemma **??**). As the two-particle ground space is supported on states of the form

$$|\,\rho^r_{x,a}\,\rangle |\,\rho^q_{z,b}\,\rangle \tag{9.170}$$

for $|r-q| = 2$, we have that each two-particle reduced state must also exist in this subspace. We then find that

$$\{q,r\} \notin \{\{1,3\},\{2,4\}\} \implies E_{(x,a,q),(y,b,r),(z,c,s)} = 0 \tag{9.171}$$

$$\{q,s\} \notin \{\{1,3\},\{2,4\}\} \implies E_{(x,a,q),(y,b,r),(z,c,s)} = 0 \tag{9.172}$$

$$\{r,s\} \notin \{\{1,3\},\{2,4\}\} \implies E_{(x,a,q),(y,b,r),(z,c,s)} = 0 \tag{9.173}$$

which together imply that $|\Gamma\rangle = 0$ (a contradiction). Hence no three-particle frustration-free state exists. □

The two-particle state $|\,T^{U,\pm}_{z_1,a,z_2,b}\,\rangle$ is a superposition of a term

$$\frac{1}{2}\big(|\rho^{1,U}_{z_1,a}\rangle |\rho^{3,U}_{z_2,b}\rangle \pm |\,\rho^{3,U}_{z_2,b}\,\rangle |\,\rho^{1,U}_{z_1,a}\,\rangle\big) \tag{9.174}$$

with both particles located on vertices corresponding to input nodes and a term

$$\frac{1}{2}\Big(\sum_{x_1,x_2\in\{0,1\}} U^a_{x_1x_2,z_1z_2}\big(|\rho^{2,U}_{x_1,a}\rangle |\rho^{4,U}_{x_2,b}\rangle \pm |\,\rho^{4,U}_{x_2,b}\,\rangle |\,\rho^{2,U}_{x_1,a}\,\rangle\big)\Big) \tag{9.175}$$

with both particles on vertices corresponding to output nodes. The two-qubit gate U^a is applied as the particles move from input nodes to output nodes. Note that we have essentially constructed a graph such that the ground states correspond to the history states. Assuming that we can guarantee that particles will have the correct locations, we will be able to combine these gadgets together to construct a history state.

9.2.2.3 Boundary gadget

In addition to the gadgets that will allow us to implement two-qubit gates, it will be useful to also have gadgets with similar ground states, but without the ability to move through the gadget. In particular, we will need to have gadgets that act as boundaries on where the particles can move. In practice, we will simply use a slightly modified version of the two-qubit gate gadget, but with additional self loops placed so that the gadget only has single-particle self-loops.

We will actually need two types of boundary gadgets, corresponding to whether or not we will want to force the state of a particular qubit into the zero state, such as initializing ancilla or forcing the output qubit to accept.

The most simple type of *boundary gadget* will be one without penalties. The gate diagram is nearly the same as in Figure 9.5a (with $\tilde{U} = \mathbb{I}$) by adding self-loops to eight of the labeled vertices. In particular, the adjacency matrix is given by

$$A(G_{\text{bnd}}) = A(G_{\text{CNOT}_{12}}) + h_{\mathcal{S}} \tag{9.176}$$

$$h_{\mathcal{S}} = \sum_{z\in\mathbb{F}_2} \Big(|1,z,2kz+2\rangle\langle 1,z,2kz+2| \otimes \mathbb{I}_8 \otimes \mathbb{I}_2 + |2,z,4k+2kz+2\rangle\langle 2,z,4k+2kz+2| \otimes \mathbb{I}_j \\ + |3,z,2kz+2\rangle\langle 3,z,2kz+2| \otimes \mathbb{I}_j \Big). \tag{9.177}$$

The second type of boundary gadget with penalties, is shown in Figure **??**. Again the gate diagram is obtained from Figure 9.5a by adding self-loops, but we also change the $q = 8$ element from a $\mathbb{I}^{(1,1)}_{(0,0)}$ element to a $\mathbb{I}^{(1,1)}_{(0,1)}$ diagram element. In particular, we have that its adjacency matrix is

$$A(G_{\text{bnd,pen}}) = A(G_{\text{bnd}}) - 2\sum_{j\in[8]} |8,1,6k+2,j,+\rangle\langle 8,1,6k+2,j,+| \tag{9.178}$$

Note that $A(G_{\text{bnd,pen}})$ is still a positive semidefinite matrix, as the subtracted terms correspond to changing the $q = 8$ element from a $\mathbb{I}^{(1,1)}_{(0,0)}$ element to a $\mathbb{I}^{(1,1)}_{(1,1)}$ element. This does not affect any of our previous results on the single- or two- particle eigenstates, but will allow us to have an additional node for that logical state.

For both types of boundary gadgets, the single-particle ground states (with energy e_1) are superpositions of the states $|\rho^{i,U}_{z,a}\rangle$ from Lemma 24 that are in the nullspace of $h_{\mathcal{S}}$. Note that

$$\langle \rho^{j,U}_{x,b} | h_{\mathcal{S}} | \rho^{i,U}_{z,a} \rangle = \delta_{a,b}\delta_{x,z} \left(\delta_{i,1}\delta_{j,1} + \delta_{i,2}\delta_{j,2} + \delta_{i,3}\delta_{j,3}\right) \frac{1}{15} \cdot \frac{1}{8k} \tag{9.179}$$

and thus we have that the only single-particle ground states are

$$|\rho^{\text{bnd}}_{z,a}\rangle = |\rho^{4,U}_{z,a}\rangle \tag{9.180}$$

with $z, a \in \mathbb{F}_2$. Additionally, there are no two- (or more) particle frustration-free states, because no superposition of the states (9.138) lies in the subspace

$$\text{span}\{|\rho^{4,U}_{z,a}\rangle|\rho^{4,U}_{x,b}\rangle : z,a,x,b \in \mathbb{F}_2\} \tag{9.181}$$

of states with single-particle reduced density matrices in the ground space of $A(G_{\text{bnd}})$. We summarize these results as follows.

[**TO DO:** *fix figure*]

Lemma 26. *The smallest eigenvalue of $A(G_{bnd})$ and of $A(G_{bnd,pen})$ is e_1, with corresponding eigenvectors*

$$|\rho^{bnd}_{z,a}\rangle = \frac{1}{\sqrt{15}}\Big(|\psi^4_{z,a}\rangle + |\psi^8_{z,a}\rangle - |\psi^{31+z}_{z,a}\rangle + \sum_{x\in\mathbb{F}_2} \big(\sqrt{5}|\chi^{x(z\oplus x)}_{4,a}\rangle - |\psi^{21+2z+x}_{0,a}\rangle\big)\Big). \tag{9.182}$$

For any $N \geq 2$, there are no N-particle frustration-free states on G_{bnd} or $G_{bnd,pen}$ for any $d_{max} > 0$ and there are no N-particle symmetric frustration-free states on G_{bnd} or $G_{bnd,pen}$ when $d_{max} = 0$, i.e.,

$$\lambda^1_N(G_{bnd}) \geq \lambda^1_N(G_{bnd,pen}) > 0 \quad \textit{for } N \geq 2. \tag{9.183}$$

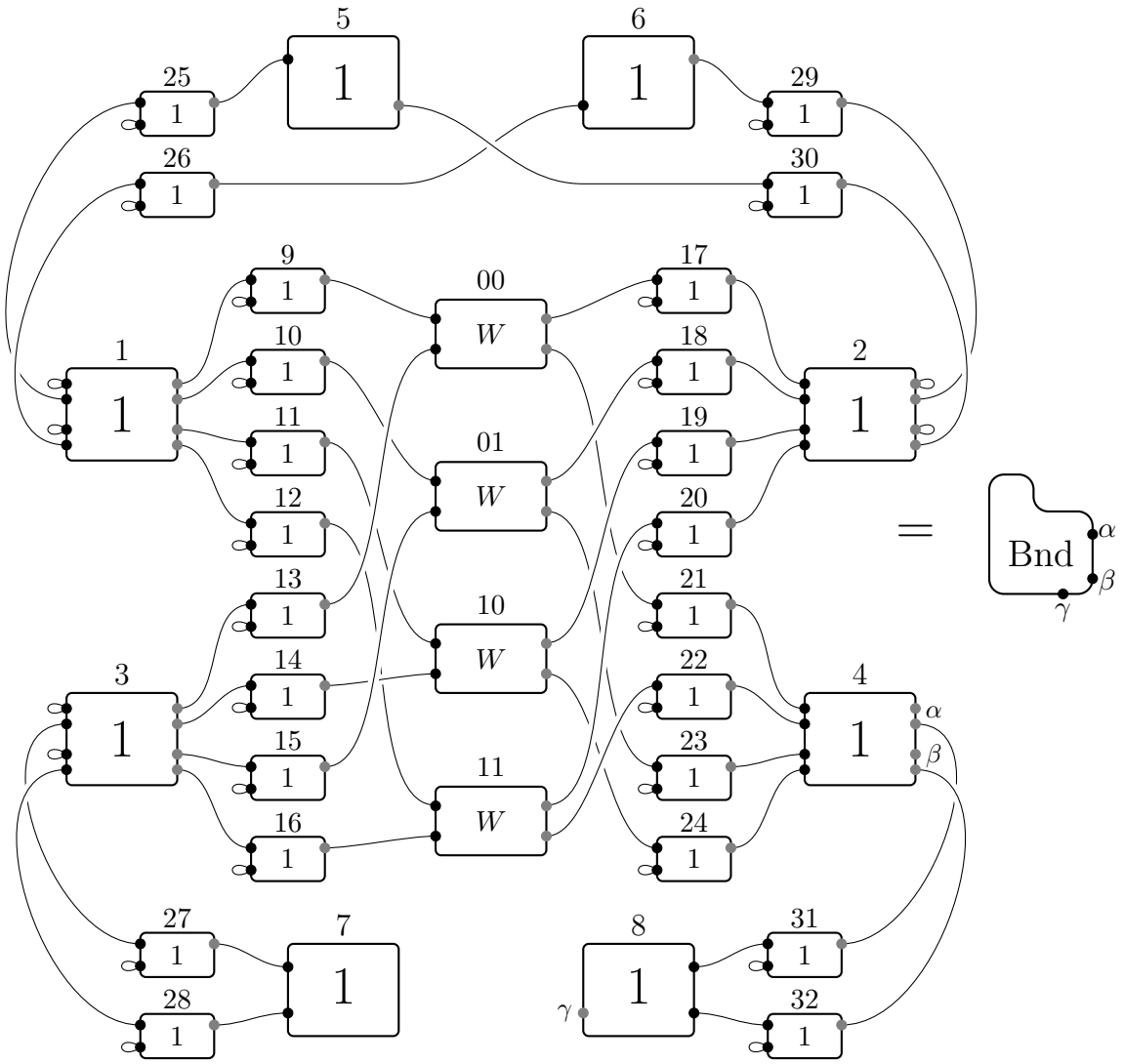

Figure 9.6: The gate diagram for the boundary gadget is obtained from Figure 9.5a by setting $\tilde{U} = 1$ and adding 6 self-loops. Note that this is actually the boundary gadget with penalty, as we include the node γ.

9.3 The occupancy constraints lemma

While the graphs defined in Section 9.2 have many useful features, such as simple single- and two-particle states and a constant energy gap, they do require that the particles are located in very specific locations. In particular, in order for the two-particle gadgets to encode a computation we require that two-particles have non-zero amplitude on the same gadget. While this is simple to achieve if the number of particles is larger than the number of gadgets, the final gate graph that we construct will have many more gate graphs than particles, which will result in the existence of many unwanted states remaining in the n-particle ground space.

To get around this problem, we will need to ensure that certain two-particle states are removed from the ground space. In particular, if we want to encode each logical qubit via a single particle, we will want to ensure that only one particle corresponds to a specific qubit. If we encode time in a spatial manner, this will require that two particles don't correspond to the same qubit at different times.

We will get around this problem via a lemma that we call the *occupancy constraints lemma*. The basic idea is that it will take in a gate graph, and a set of two-particle states that we don't want to occur, and then construct a larger graph that has related n-particle ground states but without the unwanted states.

9.3.1 Occupancy constraints

With the idea of excluding certain two-particle states from the ground space of a quantum walk on a gate graph, we will somehow need to encode these constraints. To do so, let us assume that G is a gate graph with R diagram elements (of some type). We will then define G^{occ} to be a graph with R vertices, where the vertices of G^{occ} correspond to the diagram elements of G. The edge set of G^{occ} is then defined to encode the occupancy constraints of G, namely there exists an edge between two vertices of G^{occ} if and only if we want to exclude those states from the ground-space of G where two particles are supported on the corresponding diagram elements of G. In this way, we can easily encode our requisite occupancy constraints: simply add an edge in the graph G^{occ}.

[**TO DO:** *find whatever section we defined frustration-free stuff, and reference*]

With these occupancy constraints well defined, it will also be useful to define the frustration-free ground space that also respects these constraints. In particular, remember that for a particular gate graph G, we defined the N-particle frustration-free ground space of the gate graph without edges between the diagram elements and without self-loops as

$$\mathcal{I}(G,N) = \text{span}\left\{ |\psi^{q_1}_{z_1,a_1}\rangle \cdots |\psi^{q_N}_{z_N,a_N}\rangle : \forall i,j \in [N], z_i, a_i \in \mathbb{F}_2, q_i \in [R], i \neq j \Rightarrow q_i \neq q_j \right\}. \quad (9.184)$$

In particular, this subspace guarantees that each individual particle is in the ground state of a diagram element, and further that no two particles are located on the same element. To also ensure that the particles satisfy a particular pair of occupancy constraints, we can restrict this subspace even farther. Concretely, if G is a gate graph, and if G^{occ} is a set of occupancy constraints for G, then we can define

$$\begin{aligned}\mathcal{I}(G,G^{\text{occ}},N) := \text{span}\Big\{ |\psi^{q_1}_{z_1,a_1}\rangle \cdots |\psi^{q_N}_{z_N,a_N}\rangle : \\ \forall i,j \in [N], z_i, a_i \in \mathbb{F}_2, q_i \in [R], i \neq j \Rightarrow q_i \neq q_j \text{ and } (i,j) \notin E(G^{\text{occ}})\Big\}.\end{aligned} \quad (9.185)$$

This subspace explicitly excludes those states that violate the occupancy constraints of G^{occ}, and thus will be useful for when we want to assume that the occupancy constraints are satisfied.

Now that we have a subspace that satisfy our occupancy constraints, we will want to understand how the eigenvalues change when we add in the various edges and self-loops of the original gate graph. In particular, we will define

$$H(G, G^{\text{occ}}, N) = H(G, N)\big|_{\mathcal{I}(G,G^{\text{occ}},N)} \tag{9.186}$$

to be the MPQW Hamiltonian when restricted to the subspace that satisfies the occupancy constraints. We then define $\lambda_N^1(G, G^{\text{occ}})$ for the smallest eigenvalue of this Hamiltonian. Note that if the system is exactly frustration-free, $\lambda_N^1(G, G^{\text{occ}}) = 0$.

9.3.2 Occupancy Constraints Lemma statement

Now that we can easily encode our occupancy constraints, we would like to have the technical results that our transformation allows us to perform. Specifically, while our transform might raise certain states out of the ground space, it might also drastically reduce the energy gap of the Hamiltonian as well. As our eventual goal is to show that the MPQW-ground state problem is **QMA**-complete, we need to bound this reduction in the gap.

With this in mind, we can state the explicit bounds for our lemma:

Lemma 27 (**Occupancy Constraints Lemma**). *Let G be an e_1-gate graph specified as a gate diagram with $R \geq 2$ diagram elements. Let $N \in [R]$, let G^{occ} specify a set of occupancy constraints on G, and suppose the subspace $\mathcal{I}(G, G^{occ}, N)$ is nonempty. Then there exists an efficiently computable e_1-gate graph $G^{\square}$ with at most $7R^2$ diagram elements such that*

1. *If $\lambda_N^1(G, G^{occ}) \leq a$ then $\lambda_N^1(G^{\square}) \leq \frac{a}{R}$.*
2. *If $\lambda_N^1(G, G^{occ}) \geq b$ with $b \in [0, 1]$, then $\lambda_N^1(G^{\square}) \geq \frac{\gamma_{\square} b}{R^{9+\nu}}$, where $\gamma_{\square}$ is a constant that depends only on the interaction $\mathcal{U}$, and ν is the bound on the largest degree of the interaction potential polynomials.*

In the next subsection we give the explicit transformation of the graph G to the graph $G^{\square}$. While the actual transformation itself is not particularly complicated, in order to show how the energy gap transforms we will need to define several intermediate graphs in which not all of the edges are added. Thus our proof of the occupancy constraints lemma will also be rather iterative, and will be done later in this section.

9.3.2.1 Definition of $G^{\square}$

We will now show how to construct $G^{\square}$ from G and an occupancy constraints graph G^{occ}. To ensure that the ground space has the appropriate form, the construction of $G^{\square}$ differs slightly for even and odd R is even or odd as a result of the edges in gate diagrams adding an additional sign between connected diagram elements. The following description handles both cases.

In order to ease the definition of $G^{\square}$, let us first fix notation for the gate graph G and the occupancy constraints graph G^{occ}. Write the adjacency matrix of G as (see equation (9.70))

$$A(G) = \sum_{q=1}^{R} |q\rangle\langle q| \otimes A(g_q) + h_{\mathcal{E}^G} + h_{\mathcal{S}^G} \tag{9.187}$$

where $h_{\mathcal{E}^G}$ and $h_{\mathcal{S}^G}$ are determined (through equations (9.73) and (9.72)) by the sets $\mathcal{E}^G$ and $\mathcal{S}^G$ of edges and self-loops in the gate diagram for G, and where g_q is the $256k$-vertex graph corresponding to the diagram element labeled q.

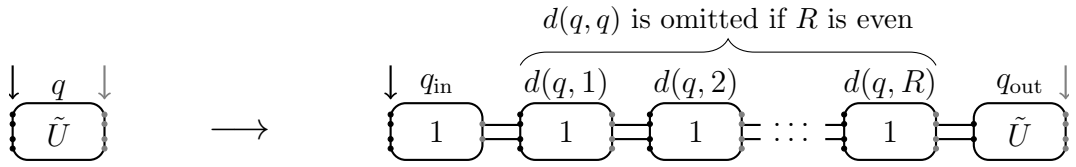

Figure 9.7: The first step in constructing the gate diagram of $G^{\square}$ from that of G is to replace each diagram element as shown. The four input nodes (black arrow) and four output nodes (grey arrow) on the left-hand side are identified with nodes on the right-hand side as shown.

1. For each diagram element $q \in [R]$ in the gate diagram for G, construct a gadget as shown in Figure 9.7, with diagram elements labeled $q_{\text{in}}, q_{\text{out}}$ and $d(q,s)$ where $s \in [R]$ and $s \neq q$ if R is even. In particular, if the diagram element labeled q is a $U^{(a,b)}_{(c,d)}$ diagram element, then q_{in} is a $\mathbb{I}^{(a,b)}_{(1,1)}$ diagram element, q_{out} is a $U^{(1,1)}_{(c,d)}$ diagram element, and each $d(q,s)$ is a $\mathbb{I}^{(2,2)}_{(2,2)}$ diagram element. Each node (q,z,t) in the gate diagram for G is mapped to a new node $\text{new}(q,z,t)$ as shown by the black and grey arrows, i.e.,

$$\text{new}(q,z,t) = \begin{cases} (q_{\text{in}}, z, t) & \text{if } (q,z,t) \text{ is an input node} \\ (q_{\text{out}}, z, t) & \text{if } (q,z,t) \text{ is an output node.} \end{cases} \tag{9.188}$$

   Edges and self-loops in the gate diagram for G are replaced by edges and self-loops between the corresponding nodes in the modified diagram.

2. For each edge $\{q_1, q_2\} \in E(G^{\text{occ}})$ in the occupancy constraints graph we add four $\mathbb{I}^{(1,1)}_{(0,0)}$ diagram elements. We refer to these diagram elements by labels $e_{ij}(q_1,q_2)$ with $i,j \in \mathbb{F}_2$. For these diagram elements the labeling function is symmetric, i.e., $e_{ij}(q_1,q_2) = e_{ji}(q_2,q_1)$ whenever $\{q_1,q_2\} \in E(G^{\text{occ}})$.

3. For each non-edge $\{q_1,q_2\} \notin E(G^{\text{occ}})$ with $q_1,q_2 \in [R]$ and $q_1 \neq q_2$ we add 8 $\mathbb{I}^{(1,1)}_{(0,0)}$ diagram elements. We refer to these diagram elements as $e_{ij}(q_1,q_2)$ and $e_{ij}(q_2,q_1)$ with $i,j \in \mathbb{F}_2$; when $\{q_1,q_2\} \notin E(G^{\text{occ}})$ the labeling function is not symmetric, i.e., $e_{ij}(q_1,q_2) \neq e_{ji}(q_2,q_1)$. If R is odd we also add $4R$ $\mathbb{I}^{(1,1)}_{(0,0)}$ diagram elements labeled $e_{ij}(q,q)$ with $i,j \in \mathbb{F}_2$ and $q \in [R]$.

4. Finally, we add edges and self-loops to the gate diagram as shown in Figure 9.8. This gives the gate diagram for $G^{\square}$.

[**TO DO:** *fix these graphs*]

The set of diagram elements in the gate graph for $G^{\square}$ is indexed by

$$L^{\square} = Q_{\text{in}} \cup D \cup E_{\text{edges}} \cup E_{\text{non-edges}} \cup Q_{\text{out}} \tag{9.189}$$

where

$$Q_{\text{in}} = \{q_{\text{in}} : q \in [R]\} \tag{9.190}$$

$$D = \{d(q,s) : q,s \in [R] \text{ and } q \neq s \text{ if } R \text{ is even}\} \tag{9.191}$$

$$E_{\text{edges}} = \{e_{ij}(q,s) : q,s \in [R], i,j \in \{0,1\}, \{q,s\} \in E(G^{\text{occ}}) \text{ and } q < s\}$$

$$E_{\text{non-edges}} = \{e_{ij}(q,s) : q,s \in [R], i,j \in \{0,1\}, \{q,s\} \notin E(G^{\text{occ}}) \text{ and } q \neq s \text{ if } R \text{ is even}\}$$

$$Q_{\text{out}} = \{q_{\text{out}} : q \in [R]\}\,. \tag{9.192}$$

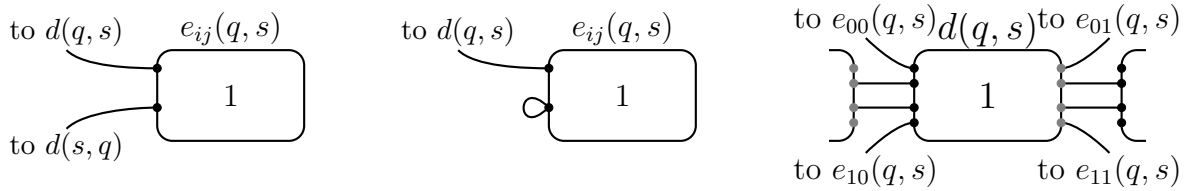

a $\{q,s\} \in E(G^{\text{occ}})$, $q < s$ b $\{q,s\} \notin E(G^{\text{occ}})$ c

Figure 9.8: Edges and self-loops added in step 4 of the construction of the gate diagram of $G^{\square}$. When $\{q,s\} \in E(G^{\text{occ}})$ with $q < s$, we add two outgoing edges to $e_{ij}(q,s)$ as shown in (a). Note that if $q > s$ and $\{q,s\} \in E(G^{\text{occ}})$ then $e_{ij}(q,s) = e_{ji}(s,q)$. When $\{q,s\} \notin E(G^{\text{occ}})$ we add a self-loop and a single outgoing edge from $e_{ij}(q,s)$ as shown in (b). Each diagram element $d(q,s)$ has eight outgoing edges (four of which are added in step 4), as shown in (c).

The total number of diagram elements in $G^{\square}$ is

$$|L^{\square}| = |Q_{\text{in}}| + |D| + |E_{\text{edges}}| + |E_{\text{non-edges}}| + |Q_{\text{out}}| \tag{9.193}$$

$$= \begin{cases} R + R^2 + 4|E(G^{\text{occ}})| + 4\left(R^2 - 2|E(G^{\text{occ}})|\right) + R & R \text{ odd} \\ R + R\,(R-1) + 4|E(G^{\text{occ}})| + 4\,(R(R-1) - 2|E(G^{\text{occ}})|) + R & R \text{ even} \end{cases} \tag{9.194}$$

$$= \begin{cases} 5R^2 + 2R - 4|E(G^{\text{occ}})| & R \text{ odd} \\ 5R^2 - 3R - 4|E(G^{\text{occ}})| & R \text{ even.} \end{cases} \tag{9.195}$$

In both cases this is upper bounded by $7R^2$ as claimed in the statement of the Lemma. Write

$$A(G^{\square}) = \sum_{l \in L^{\square}} |l\rangle\langle l| \otimes A(g_l) + h_{\mathcal{S}^{\square}} + h_{\mathcal{E}^{\square}} \tag{9.196}$$

where g_l corresponds to the diagram element labeled $l \in L^{\square}$, $\mathcal{S}^{\square}$ and $\mathcal{E}^{\square}$ are the sets of self-loops and edges in the gate diagram for $G^{\square}$.

We now focus on the input nodes of diagram elements in Q_{in} and the output nodes of the diagram elements in Q_{out}. These are the nodes indicated by the black and grey arrows in Figure 9.7. Write $\mathcal{E}^0 \subset \mathcal{E}^{\square}$ and $\mathcal{S}^0 \subset \mathcal{S}^{\square}$ for the sets of edges and self-loops that are incident on these nodes in the gate diagram for $G^{\square}$. Note that the sets $\mathcal{E}^0$ and $\mathcal{S}^0$ are in one-to-one correspondence with (respectively) the sets $\mathcal{E}^G$ and $\mathcal{S}^G$ of edges and self-loops in the gate diagram for G (by definition). The other edges and self-loops in $G^{\square}$ do not depend on the sets of edges and self-loops in G, as they are created in our effort to enforce the occupancy constraints. Writing

$$\mathcal{S}^{\triangle} = \mathcal{S}^{\square} \setminus S^0 \qquad \mathcal{E}^{\triangle} = \mathcal{E}^{\square} \setminus \mathcal{E}^0, \tag{9.197}$$

we have

$$h_{\mathcal{S}^{\square}} = h_{\mathcal{S}^0} + h_{\mathcal{S}^{\triangle}} \qquad h_{\mathcal{E}^{\square}} = h_{\mathcal{E}^0} + h_{\mathcal{E}^{\triangle}}. \tag{9.198}$$

It will be useful to define several graphs that only depend on the occupancy constraints as a stepping stone in order to understand $\lambda_N^1(G^{\square})$. In particular, we will first examine the gate graph that only has the self-loops added during the transformation from G to $G^{\square}$, namely the self-loops on nodes in $\mathcal{S}^{\triangle}$, as this graph has a particularly simple ground space, and we will label this graph $G^{\diamondsuit}$. We will then analyze the graph that arises by adding the edges of $\mathcal{E}^{\triangle}$ to $G^{\diamondsuit}$, and we will label this graph by $G^{\triangle}$. With these foundational graphs understood (and in particular understanding

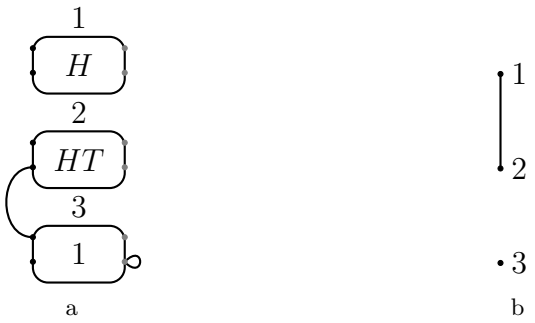

Figure 9.9: An example (a) Gate diagram for a gate graph G and (b) Occupancy constraints graph G^{occ}. In the text we describe how these two ingredients are mapped to a gate graph $G^{\square}$; the gate diagram for $G^{\square}$ is shown in Figure 9.10.

their N-particle frustration-free ground states), we will then easily understand the ground states and ground energies of $G^{\square}$ in term of the ground energies of G.

Along these lines, we will define the gate diagram for $G^{\diamondsuit}$ to be the diagram with all of the elements labeled by $L^{\square}$, and only include the self-loops in $\mathcal{S}^{\triangle}$. We then have that the adjacency matrix for $G^{\diamondsuit}$ is

$$A(G^{\diamondsuit}) = \sum_{\ell \in L^{\square}} |\,\ell\rangle\langle\,\ell| \otimes A(g_{\ell}) + h_{\mathcal{S}^{\triangle}}. \tag{9.199}$$

We can also define the gate diagram for $G^{\triangle}$ to be the same as for $G^{\diamondsuit}$, but including the edges in $\mathcal{E}^{\triangle}$. We can then define the adjacency matrix for $G^{\triangle}$ as

$$A(G^{\triangle}) = \sum_{l \in L^{\square}} |l\rangle\langle l| \otimes A(g_l) + h_{\mathcal{S}^{\triangle}} + h_{\mathcal{E}^{\triangle}}. \tag{9.200}$$

Note that $G^{\triangle} = G^{\square}$ whenever the gate diagram for G contains no edges or self-loops.

We provide an example of this construction in Figure 9.9 (which shows a gate graph and an occupancy constraints graph) and Figure 9.10 (which describes the derived gate graphs $G^{\square}$, $G^{\triangle}$, and $G^{\diamondsuit}$).

[**TO DO:** *completely fix these example graphs*]

9.3.3 The gate graph $G^{\diamondsuit}$

With the various graphs well defined, let us now find the ground states of $A(G^{\diamondsuit})$. We know from (9.199) that each component of $G^{\diamondsuit}$ is a diagram element g_l, with self-loops on some of the nodes. Using Lemma 20, we can then see that each component of $G^{\diamondsuit}$ has at most 4 orthonormal e_1-energy eigenstates, and that the minimum energy is e_1.

More concretely, for each diagram element labeled by $l \in L^{\square}$ in $A(G^{\diamondsuit})$, we can write g'_l for the graph with adjacency matrix

$$A(g'_l) = A(g_l) + |1, 2k\rangle\langle 1, 2k+2| \otimes \mathbb{I}_{16} \tag{9.201}$$

(i.e., g_l with 16 self-loops added), and note that each component of $G^{\diamondsuit}$ is either g_l or g'_l.

We can then use Lemma 20 to see that $A(g_{\ell})$ has four orthonormal e_1-energy ground states for each ℓ namely $|\overline{\psi_{z,a}}\rangle$ for $z, a \in \mathbb{F}_2$, as defined in (9.10), (9.11), using the transform of (9.56). As the states with $z = 0$ are in the nullspace of $|\,1, 2k\rangle\langle\,1, 2k|\otimes \mathbb{I}_{16}$, while the operator is strictly positive

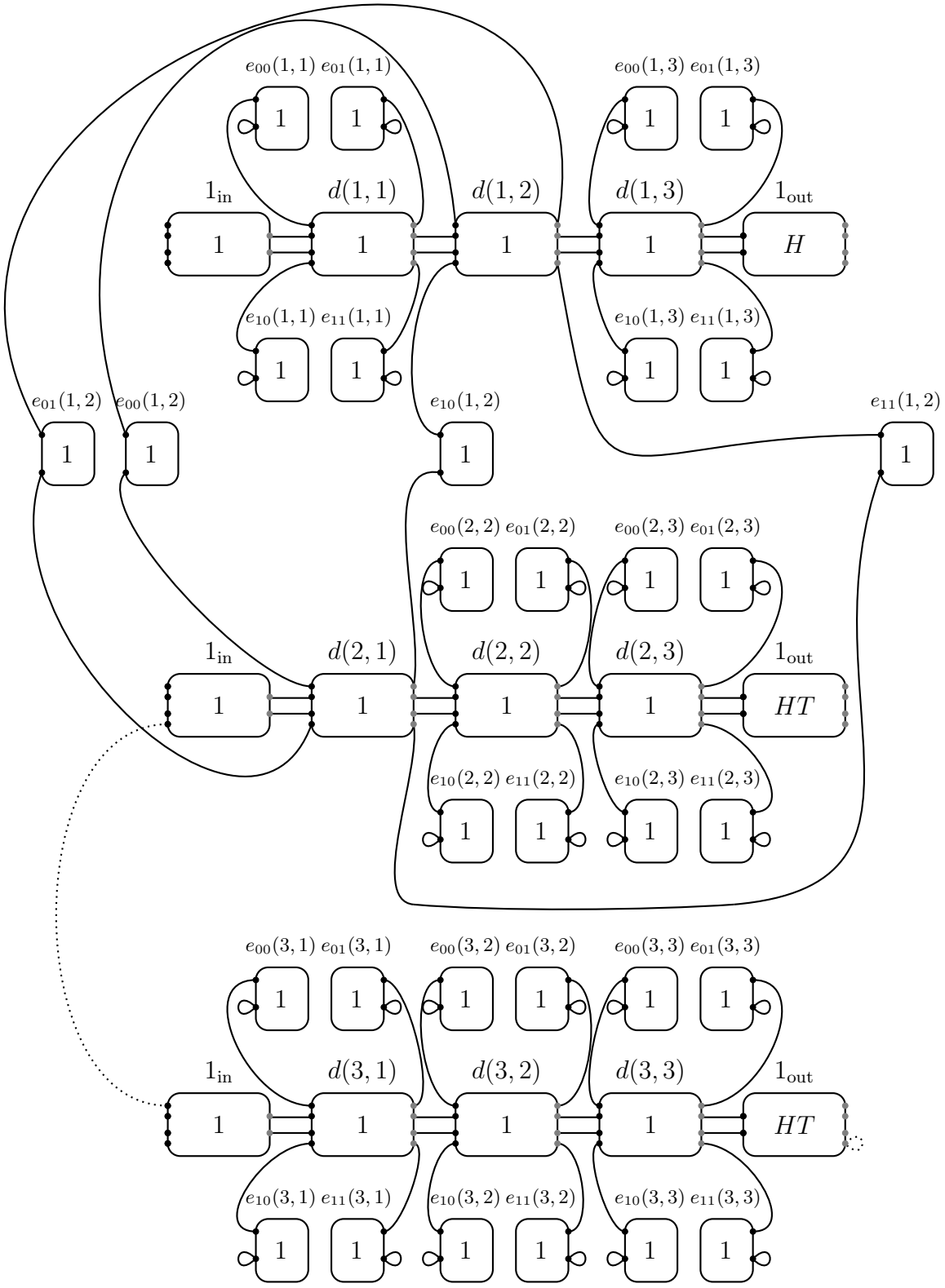

Figure 9.10: The gate diagram for $G^{\triangle}$ (only solid lines) and $G^{\square}$ (including dotted lines) derived from the example gate graph G and occupancy constraints graph G^{occ} from Figure 9.9. The gate diagram for $G^{\diamondsuit}$ is obtained from that of $G^{\triangle}$ by removing all edges (but leaving the undotted self-loops).

for the states with $z = 1$, we can see that the ground space of $A(g'_l)$ is spanned by the states $|\overline{\psi_{0,a}}\rangle$ for $a \in \mathbb{F}_2$. If we now label the states by the $l \in L^{\square}$, (i.e., $|\psi^l_{z,a}\rangle = |l\rangle|\overline{\psi_{z,a}}\rangle$), we can choose a basis $\mathcal{W}$ for the e_1-energy ground space of $A(G^{\diamondsuit})$ where each basis vector is supported on one of the components:

$$\mathcal{W} = \left\{|\psi^l_{0,a}\rangle : a \in \mathbb{F}_2,\, l \in E_{\text{non-edges}}\right\} \bigcup \left\{|\psi^l_{z,a}\rangle : z, a \in \mathbb{F}_2,\, l \in L^{\square} \setminus E_{\text{non-edges}}\right\}. \tag{9.202}$$

The eigenvalue gap of $A(G^{\diamondsuit})$ is equal to that of either $A(g_l)$ or $A(g'_l)$ for some l. Since g_l and g'_l are constant-sized $256k$-vertex graphs, there exists a constant sized gap for each; let $c_{\diamondsuit}$ be the minimum value of this gap for all possible diagram elements, both with and without the added self-loops. We then have that

$$\gamma(A(G^{\diamondsuit}) - e_1) \geq c_{\diamondsuit} \tag{9.203}$$

The ground space of $A(G^{\diamondsuit})$ has dimension

$$|\mathcal{W}| = 4\left|L^{\square}\right| - 2\left|E_{\text{non-edges}}\right| \tag{9.204}$$

$$= \begin{cases} 4\left(5R^2 + 2R - 4|E(G^{\text{occ}})|\right) - 2\left(4R^2 - 8|E(G^{\text{occ}})|\right) & R \text{ odd} \\ 4\left(5R^2 - 3R - 4|E(G^{\text{occ}})|\right) - 2\left(4R(R-1) - 8|E(G^{\text{occ}})|\right) & R \text{ even} \end{cases} \tag{9.205}$$

$$= \begin{cases} 12R^2 + 8R & R \text{ odd} \\ 12R^2 - 4R & R \text{ even.} \end{cases} \tag{9.206}$$

We now consider the N-particle Hamiltonian $H(G^{\diamondsuit}, N)$ and characterize its nullspace.

Lemma 28. *If $d_{max} > 0$ and if $|L^{\square}| \geq N$, then the nullspace of $H(G^{\diamondsuit}, N)$ is*

$$\mathcal{I}_{\diamondsuit} = \text{span}\left\{|\psi^{q_1}_{z_1,a_1}\rangle|\psi^{q_2}_{z_2,a_2}\rangle \cdots |\psi^{q_N}_{z_N,a_N}\rangle \;:\; |\psi^{q_i}_{z_i,a_i}\rangle \in \mathcal{W} \text{ and } \forall i,j \in [N], i \neq j \Rightarrow q_i \neq q_j\right\} \tag{9.207}$$

where $\mathcal{W}$ is given in equation (9.202). If $d_{max} = 0$ and if $|L^{\square}| \geq N$, then when restricted to symmetric states, then nullspace of $H(G^{\diamondsuit}, N)$ is given by

$$\mathcal{I}^{\text{Sym}}_{\diamondsuit} = \text{span}\{\text{Sym}(|\Phi\rangle) : |\Phi\rangle \in \mathcal{I}_{\diamondsuit}\}. \tag{9.208}$$

When $d_{max} > 0$ (and when restricted to symmetric states for $d_{max} = 0$), the smallest nonzero eigenvalue satisfies

$$\gamma(H(G^{\diamondsuit}, N)) > \gamma_{\diamondsuit}, \tag{9.209}$$

where $\gamma_{\diamondsuit}$ is a constant that depends only on the interaction $\mathcal{U}$.

Proof. The main tool used in this proof is our characterization of the 2-particle ground states on diagram elements from Lemma 21, namely that they don't exist. Combined with our results for interactions on disconnected graphs from Lemma 15, we essentially have the proof.

In particular, we have from Lemma 21 that in the N-particle ground space, no component of $G^{\diamondsuit}$ supports a two-particle frustration-free state (i.e., $\lambda^1_2(g_l) > 0$ for each $l \in L^{\square}$), while $\lambda^1_1(g_l) = 0$. If we assume that $L^{\square} \geq N$ and $d_{\max} > 0$, we then have from Lemma 15 that the N-particle nullspace for $G^{\diamondsuit}$ is exactly $\mathcal{I}_{\diamondsuit}$. If we restrict our attention to symmetric states, the same argument holds for all $d_{\max}$.

Additionally, we have from Lemma 15 that the smallest nonzero eigenvector of $H(G^{\diamondsuit}, N)$ is either the smallest eigenvalue of a single-particle excited state for some diagram element g_l, or else the smallest energy of a two-particle state on some diagram element g_l (where we used the fact

that adding the self-loops can only increase the energy of a state). As such, we can then bound the eigenvalue gap for the N-particle sector on $G^{\diamondsuit}$ as

$$\gamma(H(G^{\diamondsuit}, N)) \geq \min_{l \in L^{\square}} \{\min\{\lambda_2^1(g_l), \gamma(H(g_l, 1))\}\} \tag{9.210}$$

$$\geq \min_{\substack{U \in \{\mathbb{I}, H, HT\} \\ 0 \leq a,b,c,d \leq 2}} \min\{\lambda_2^1(G_U^{(a,b),(c,d)}), \gamma(H(G_U^{(a,b),(c,d)}, 1))\} = \gamma_{\diamondsuit}. \tag{9.211}$$

Note that $\gamma_{\diamondsuit}$ depends only on $d_{\max}$ (from the size of the graph g_0) and on the 2-particle energy (from the two-particle ground energy), and thus $\gamma_{\diamondsuit}$ is some constant that depends only on the interaction. □

At this point, we have a foundational graph with a constant eigenvalue gap, upon which we can add edges and see how the eigenvalue gap changes.

9.3.4 Single particles on $G^{\triangle}$

With the graph $G^{\diamondsuit}$ defined and its ground-states defined and energy gaps bounded, we now want to examine the graph with the edges that enforce the occupancy constraints. In particular, we now want to examine $G^{\triangle}$.

We begin by solving for the ground space of the adjacency matrix $A(G^{\triangle})$. From equation (9.200) we have

$$A(G^{\triangle}) = A(G^{\diamondsuit}) + h_{\mathcal{E}^{\triangle}}. \tag{9.212}$$

We already know that the e_1-energy ground space of $A(G^{\diamondsuit})$ is spanned by $\mathcal{W}$ from equation (9.202). Since $h_{\mathcal{E}^{\triangle}} \geq 0$ it follows that $A(G^{\triangle}) \geq e_1$. If we then want to find the e_1-energy groundspace of $A(G^{\triangle})$, we construct superpositions of vectors from $\mathcal{W}$ that are in the nullspace of $h_{\mathcal{E}^{\triangle}}$. To this end we consider the restriction

$$h_{\mathcal{E}^{\triangle}}\big|_{\mathrm{span}(\mathcal{W})}, \tag{9.213}$$

and we will show that it is block diagonal in the basis $\mathcal{W}$.

Recall from equation (9.73) that

$$h_{\mathcal{E}^{\triangle}} = \sum_{\{(l,z,t),(l',z',t')\} \in \mathcal{E}^{\triangle}} \left(|l,z,t\rangle + |l',z',t'\rangle\right)\left(\langle l,z,t| + \langle l',z',t'|\right) \otimes \mathbb{I}_{16}. \tag{9.214}$$

The edges $\{(l,z,t),(l',z',t')\} \in \mathcal{E}^{\triangle}$ can be read off from Figure 9.7 and Figure 9.8, where we refer back to Figure 9.2 for the labeling convention of nodes on a diagram element. The edges from Figure 9.7 are

$$\big\{(q_{\mathrm{in}}, z, (5+z)k+2), (d(q,1), z, (1+z)k+2)\big\}, \tag{9.215}$$

$$\big\{(d(q,i), z, (5+z)k+2), (d(q,i+1), z, (1+z)k+2)\big\}, \tag{9.216}$$

$$\big\{(d(q,R), z, (5+z)k+2), (q_{\mathrm{out}}, z, (1+z)k+2)\big\}, \tag{9.217}$$

with $q \in [R]$, $i \in [R-1]$ and $z \in \mathbb{F}_2$, and where $d(q,q)$ does not appear if R is even (i.e., $d(q,q-1)$ is followed by $d(q,q+1)$). The edges from Figure 9.8 take the form

$$\left\{(d(q,s), z, k(3z+4x)+2), (e_{zx}(q,s), \alpha(q,s), 2k\alpha(q,s)+2)\right\}, \tag{9.218}$$

with $q, s \in [R]$, $q \neq s$ if R is even, $z, x \in \mathbb{F}_2$, and where

$$\alpha(q,s) = \begin{cases} 1 & q > s \text{ and } \{q,s\} \in E(G^{\text{occ}}) \\ 0 & \text{otherwise.} \end{cases} \tag{9.219}$$

The set $\mathcal{E}^{\triangle}$ consists of all edges in equations (9.215)–(9.218).

It will turn out that (9.213) is block diagonal, with blocks $\mathcal{W}_{(z,a,q)} \subseteq \mathcal{W}$ of size

$$\left|\mathcal{W}_{(z,a,q)}\right| = \begin{cases} 3R+2 & R \text{ odd} \\ 3R-1 & R \text{ even} \end{cases} \tag{9.220}$$

for each for each triple (z,a,q) with $z, a \in \mathbb{F}_2$ and $q \in [R]$. Using equation (9.206) we can confirm that $|\mathcal{W}| = 4R\left|\mathcal{W}_{(z,a,q)}\right|$, so this accounts for all basis vectors in $\mathcal{W}$. The subset of basis vectors for a given block is

$$\begin{aligned} \mathcal{W}_{(z,a,q)} = &\left\{|\psi^{q_{\text{in}}}_{z,a}\rangle, |\psi^{q_{\text{out}}}_{z,a}\rangle\right\} \cup \left\{|\psi^{d(q,s)}_{z,a}\rangle \colon s \in [R],\ s \neq q \text{ if } R \text{ even}\right\} \\ &\cup \left\{|\psi^{e_{zx}(q,s)}_{\alpha(q,s),a}\rangle \colon x \in \{0,1\},\ s \in [R],\ s \neq q \text{ if } R \text{ even}\right\}. \end{aligned} \tag{9.221}$$

Using equation (9.214) and the description of $\mathcal{E}^{\triangle}$ from using the edges of equations (9.215) – (9.218), we can check by direct inspection that (9.213) only has nonzero matrix elements between basis vectors in $\mathcal{W}$ from the same block. The graph $G^{\triangle}$ was designed to expand the states $|\overline{\psi_{z,a}}\rangle$ over many diagram elements, and block structure reflects this idea.

We can now compute the matrix elements between states from the same block. For example, if R is odd there are edges $\{(q_{\text{in}}, 0, 5k), (d(q,1), 0, k+2)\}$ and $\{(q_{\text{in}}, 1, 6k+2), (d(q,1), 1, 2k)\}$ in $\mathcal{E}^{\triangle}$. Using the fact that $|\psi^{l}_{z,a}\rangle = |l\rangle|\psi_{z,a}, -\rangle$ where $|\psi_{z,a}\rangle$ is given by (9.10) and (9.11), we can then compute the relevant matrix elements:

$$\begin{aligned} &\langle \psi^{q_{\text{in}}}_{z,a} | h_{\mathcal{E}^{\triangle}} | \psi^{d(q,1)}_{z,a} \rangle \\ &\quad = \langle \psi^{q_{\text{in}}}_{z,a} | \Bigg(\sum_{x \in \mathbb{F}_2} \left(|q_{\text{in}}, x, 5(k+x)+2\rangle + |d(q,1), (1+x)k+2, 1\rangle \right) \\ &\qquad\qquad \left(\langle q_{\text{in}}, x, (5+x)k+2| + \langle d(q,1), (1+x)k+2, 1| \right) \otimes \mathbb{I} \Bigg) |\psi^{d(q,1)}_{z,a}\rangle \qquad (9.222) \\ &\quad = \sum_{x \in \mathbb{F}_2} \langle \overline{\psi_{z,a}} | \left(|x, (5+x)k+2\rangle\langle x, (1+x)k+2| \otimes \mathbb{I} \right) |\overline{\psi_{z,a}}\rangle = \frac{1}{8k}. \qquad (9.223) \end{aligned}$$

Continuing in this manner, we can compute the principal submatrix of (9.213) corresponding to the set $\mathcal{W}_{(z,a,q)}$. A diagrammatic representation of this matrix is shown in Figure 9.11a. In the figure each vertex is associated with a state in the block and the weight on a given edge is the matrix element between the two states associated with vertices joined by that edge. The diagonal matrix elements are described by the weights on the self-loops. The matrix described by Figure 9.11a is the same for each block. [**TO DO:** *fix this figure for the correct values* $1/8k$]

For each triple (z,a,q) with $z, a \in \mathbb{F}_2$ and $q \in [R]$, define

$$|\phi^{q}_{z,a}\rangle = \begin{cases} \frac{1}{\sqrt{3R+2}} \left[|\psi^{q_{\text{in}}}_{z,a}\rangle + |\psi^{q_{\text{out}}}_{z,a}\rangle + \sum_{j \in [R]} (-1)^j \left(|\psi^{d(q,j)}_{z,a}\rangle - |\psi^{e_{z0}(q,j)}_{\alpha(q,j),a}\rangle - |\psi^{e_{z1}(q,j)}_{\alpha(q,j),a}\rangle \right) \right] & R \text{ odd} \\ \frac{1}{\sqrt{3R-1}} \Bigg[|\psi^{q_{\text{in}}}_{z,a}\rangle + |\psi^{q_{\text{out}}}_{z,a}\rangle + \sum_{j<q} (-1)^j \left(|\psi^{d(q,j)}_{z,a}\rangle - |\psi^{e_{z0}(q,j)}_{\alpha(q,j),a}\rangle - |\psi^{e_{z1}(q,j)}_{\alpha(q,j),a}\rangle \right) \\ \qquad - \sum_{j<q} (-1)^j \left(|\psi^{d(q,j)}_{z,a}\rangle - |\psi^{e_{z0}(q,j)}_{\alpha(q,j),a}\rangle - |\psi^{e_{z1}(q,j)}_{\alpha(q,j),a}\rangle \right) \Bigg] & R \text{ even.} \end{cases} \tag{9.224}$$

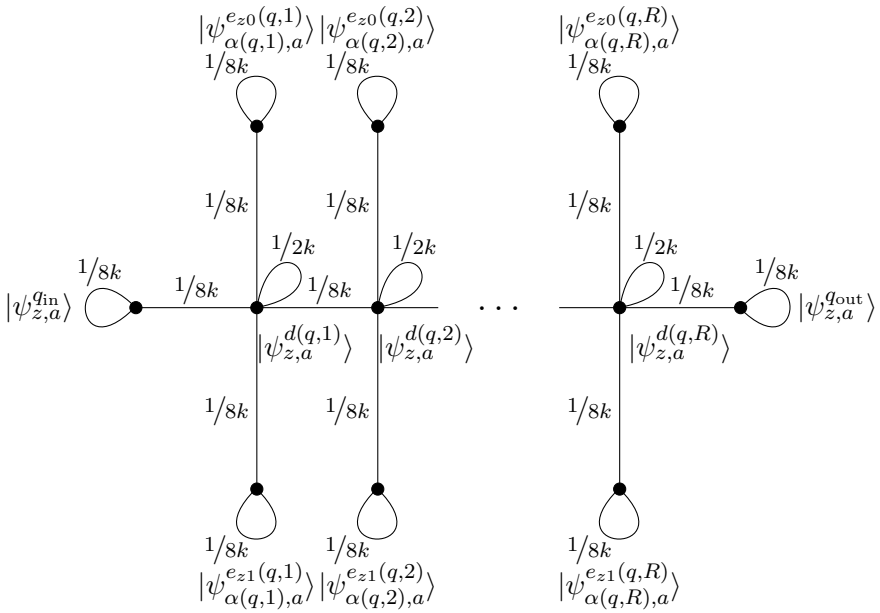

a The matrix $h^{\triangle}_{\mathcal{E}}|_{\mathrm{span}(\mathcal{W})}$ is block diagonal in the basis $\mathcal{W}$, with a block $\mathcal{W}_{(z,a,q)}$ for each $z, a \in \{0,1\}$ and $q \in \{1,\ldots,R\}$. The states involved in a given block and the matrix elements between them are depicted.

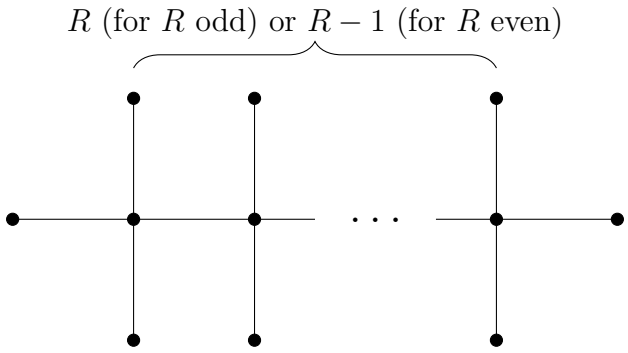

b After multiplying some of the basis vectors by -1, the matrix depicted in (a) is transformed into $1/8k$ times the Laplacian matrix of this graph.

Figure 9.11

The choice to omit $d(q,q)$ for R even ensures that $|\psi_{z,a}^{q_{\text{in}}}\rangle$ and $|\psi_{z,a}^{q_{\text{out}}}\rangle$ have the same sign in these ground states, similar to the original gate diagram this gate graph replaced. We now show that these states span the ground space of $A(G^{\triangle})$.

Lemma 29. *An orthonormal basis for the e_1-energy ground space of $A(G^{\triangle})$ is given by the states*

$$\left\{|\phi_{z,a}^{q}\rangle : z,a \in \{0,1\},\, q \in [R]\right\} \tag{9.225}$$

defined by equation (9.224). The eigenvalue gap is bounded as

$$\gamma(A(G^{\triangle}) - e_1) > \frac{c_{\triangle}}{R^2}, \tag{9.226}$$

where $c_{\triangle}$ is a constant that only depends on the interaction $\mathcal{U}$.

Proof. The e_1-energy ground space of $A(G^{\triangle})$ is equal to the nullspace of (9.213). Since this operator is block diagonal in the basis $\mathcal{W}$, we can solve for the eigenvectors in the nullspace of each block. Thus, to prove the first part of the lemma, we will analyze the $|\mathcal{W}_{(z,a,q)}| \times |\mathcal{W}_{(z,a,q)}|$ matrix described by Figure 9.11a and show that (9.224) is the unique vector in its nullspace.

We first rewrite the matrix in a slightly different basis obtained by multiplying some of the basis vectors by a phase of -1. Specifically, we use the basis

$$\left\{|\psi_{z,a}^{q_{\text{in}}}\rangle, -|\psi_{z,a}^{d(q,1)}\rangle, |\psi_{\alpha(q,1),a}^{e_{z0}(q,1)}\rangle, |\psi_{\alpha(q,1),a}^{e_{z1}(q,1)}\rangle, |\psi_{z,a}^{d(q,2)}\rangle, -|\psi_{\alpha(q,2),a}^{e_{z0}(q,2)}\rangle, -|\psi_{\alpha(q,2),a}^{e_{z1}(q,2)}\rangle, \ldots, |\psi_{z,a}^{q_{\text{out}}}\rangle\right\} \tag{9.227}$$

where the state associated with each vertex on one side of a bipartition of the graph is multiplied by -1; these are the phases appearing in equation (9.224). Changing to this basis replaces the weight $\frac{1}{8k}$ on each edge in Figure 9.11a by $-\frac{1}{8k}$ and does not change the weights on the self-loops. The resulting matrix is $\frac{1}{8k}L_0$, where L_0 is the Laplacian matrix of the graph shown in Figure 9.11b.

Now we use the fact that the Laplacian of any connected graph has smallest eigenvalue zero, with a unique eigenvector equal to the all-ones vector. [**TO DO:** *Find a citation for this claim*] . Hence for each block we get an eigenvector in the nullspace of (9.213)) given by (9.224). Ranging over all $z,a \in \mathbb{F}_2$ and $q \in [R]$ gives the claimed basis for the e_1-energy ground space of $A(G^{\triangle})$.

To prove the lower bound on the eigenvalue gap, we use the Nullspace Projection Lemma (Lemma 2) with

$$H_A = A(G^{\diamondsuit}) - e_1 \qquad H_B = h_{\mathcal{E}^{\triangle}} \tag{9.228}$$

and where $S = \text{span}(\mathcal{W})$ is the nullspace of H_A as shown in Section 9.3.3. Since the restriction of H_B to $\mathcal{S}$ is block diagonal in the basis $\mathcal{W}$, the smallest nonzero eigenvalue of (9.213) is equal to the smallest nonzero eigenvalue of one of its blocks. The matrix for each block is $\frac{1}{8k}L_0$. Thus we can lower bound the smallest nonzero eigenvalue of $H_B|_S$ using standard bounds on the smallest nonzero eigenvalue of the Laplacian L of a graph G. In particular, Theorem 4.2 of reference [29] shows that

$$\gamma(L) \geq \frac{4}{|V(G)|\,\text{diam}(G)} \geq \frac{4}{|V(G)|^2}$$

(where $\text{diam}(G)$ is the diameter of G). Since the size of the graph in Figure 9.11b is either $3R-1$ or $3R+2$, we have

$$\gamma(H_B|_S) = \frac{1}{8k}\gamma(L_0) \geq \frac{1}{8k}\frac{4}{(3R+2)^2} \geq \frac{1}{32kR^2}$$

since $R \geq 2$.

Using this bound and the fact that $\gamma(H_A) > c_\diamondsuit$ (from equation (9.203)) and $\|H_B\| = 2$ (from equation (9.75)) and plugging into Lemma 2 gives

$$\gamma(A(G^\triangle) - e_1) \geq \frac{c_\diamondsuit \cdot \frac{1}{32kR^2}}{c_\diamondsuit + 2} > \frac{c_\diamondsuit}{94kR^2} = \frac{c_\triangle}{R^2}. \tag{9.229}$$

where we used the fact that $c_\diamondsuit \leq 1$, and we define $c_\triangle = c_\diamondsuit/(96k)$. As $c_\diamondsuit$ is a constant that only depends on the interaction, so too is $c_\triangle$. □

9.3.5 The Hamiltonian $H(G^\triangle, N)$

With the previous sections results about the graph $G^\triangle$, and in particular knowing its ground states and eigenvalue gap, we can now analyze the multi-particle Hamiltonian. Namely, we can now consider the N-particle Hamiltonian $H(G^\triangle, N)$ and solve for its nullspace.

In preparation for understanding the N-particle states, it will be useful to note the following fact about the subsets $\mathcal{W}_{(z,a,q)} \subset \mathcal{W}$ defined in equation (9.221).

Definition 9. We say $\mathcal{W}_{(z_1,a_1,q_1)}$ and $\mathcal{W}_{(z_2,a_2,q_2)}$ *overlap in support* if there exist two $l_1, l_2 \in L^\square$ such that $|\psi^{l_1}_{x_1,b_1}\rangle \in \mathcal{W}_{(z_1,a_1,q_1)}$ and $|\psi^{l_2}_{x_2,b_2}\rangle \in \mathcal{W}_{(z_2,a_2,q_2)}$ for some $x_1, x_2, b_1, b_2 \in \mathbb{F}_2$, and either $l_1 = l_2$ or l_1 and l_2 are adjacent diagram elements.

Fact 2 (Key property of $\mathcal{W}_{(z,a,q)}$)**.** *Sets $\mathcal{W}_{(z_1,a_1,q_1)}$ and $\mathcal{W}_{(z_2,a_2,q_2)}$ overlap in support if and only if $q_1 = q_2$ or $\{q_1, q_2\} \in E(G^{occ})$.*

This fact can be confirmed by direct inspection of the sets $\mathcal{W}_{(z,a,q)}$. If $q_1 = q_2 = q$ the diagram element l on which they overlap can be chosen to be $l = q_{\text{in}}$; if $q_1 \neq q_2$ and $\{q_1, q_2\} \in E(G^{\text{occ}})$ then $l = e_{z_1 z_2}(q_1, q_2) = e_{z_2 z_1}(q_2, q_1)$. Conversely, if $\{q_1, q_2\} \notin E(G^{\text{occ}})$ with $q_1 \neq q_2$, then the two blocks don't have support on the same diagram elements, and in fact the diagram elements supporting the two blocks are separated by at least one additional diagram element (due to the pairwise definitions for the connections between the gate diagrams corresponding to each diagram element of G). This fact is the intuitive reason behind our construction of $G^\square$; we designed the graph $G^\triangle$ so that Fact 2 held.

We will show that the nullspace $\mathcal{I}_\triangle$ of $H(G^\triangle, N)$ is

$$\mathcal{I}_\triangle = \text{span}\left\{|\phi^{q_1}_{z_1,a_1}\rangle|\phi^{q_2}_{z_2,a_2}\rangle \ldots |\phi^{q_N}_{z_N,a_N}\rangle \colon z_i, a_i \in \mathbb{F}_2,\ q_i \in [R],\ q_i \neq q_j, \text{ and } \{q_i, q_j\} \notin E(G^{\text{occ}})\right\}, \tag{9.230}$$

for $d_{\max} > 0$, and if $d_{\max} = 0$ we will show that when restricted to symmetric states, the nullspace of $H(G^\triangle, N)$ is

$$\mathcal{I}^{\text{Sym}}_\triangle = \left\{ \text{Sym}(|\Phi\rangle) \ : \ |\Phi\rangle \in \mathcal{I}_\triangle \right\}. \tag{9.231}$$

Note that $\mathcal{I}_\triangle$ is very similar to $\mathcal{I}(G, G^{\text{occ}}, N)$ (from equation (**??**)) but with each single-particle state $|\psi^q_{z,a}\rangle \in \mathcal{Z}_N(G)$ replaced by $|\phi^q_{z,a}\rangle \in \mathcal{Z}_N(G^\triangle)$ (with the same similarity for the symmetric states).

[**TO DO:** *Change from $\mathcal{Z}$ to something else*]

Lemma 30. *The nullspace of $H(G^\triangle, N)$ is $\mathcal{I}_\triangle$ as defined in equation (9.230) for $d_{max} > 0$, or when restricted to symmetric states the nullspace of $H(G^\triangle, N)$ is $\mathcal{I}^{\text{Sym}}_\triangle$. In either case, its smallest nonzero eigenvalue is*

$$\gamma(H(G^\triangle, N)) > \frac{\gamma_\triangle}{R^7}, \tag{9.232}$$

where $\gamma_\triangle$ is a constant that only depends on $\mathcal{U}$.

In addition to Fact 2, we use the following simple fact in the proof of the Lemma.

Fact 3. *Let* $|p\rangle = c|\alpha_0\rangle + \sqrt{1-c^2}|\alpha_1\rangle$ *with* $\langle\alpha_i|\alpha_j\rangle = \delta_{ij}$ *and* $c \in [0,1]$. *Then*

$$|p\rangle\langle p| = c^2|\alpha_0\rangle\langle\alpha_0| + M \tag{9.233}$$

where $\|M\| \leq 1 - \frac{3}{4}c^4$.

To prove this Fact, one can calculate $\|M\| = \frac{1}{2}(1-c^2) + \frac{1}{2}\sqrt{1+2c^2-3c^4}$ and use the inequality $\sqrt{1+x} \leq 1 + \frac{x}{2}$ for $x \geq -1$.

Proof of Lemma 30. Using equation (9.212) and the fact that the smallest eigenvalues of $A(G^{\diamondsuit})$ and $A(G^{\triangle})$ are the same (equal to e_1, from Section 9.3.3 and Lemma 29), we can break the MPQW-Hamiltonian on $G^{\triangle}$ into three terms. Namely, we have

$$H(G^{\triangle}, N) = H(G^{\diamondsuit}, N) + \sum_{w=1}^{N} h_{\mathcal{E}^{\triangle}}^{(w)} + B, \tag{9.234}$$

where B is the change in interaction terms resulting from vertices changing distance. It is important to realize that B only adds terms to the Hamiltonian, as any vertices that were originally at a distance less than $d_{\max}$ remain at the same distance when adding the edges in $\mathcal{E}^{\triangle}$, and thus B is positive semi-definite. Recall from Lemma 28 that the nullspace of $H(G^{\diamondsuit}, N)$ is $\mathcal{I}_{\diamondsuit}$ (or $\mathcal{I}_{\diamondsuit}^{\text{Sym}}$ if we are restricting to symmetric states). We consider

$$\sum_{w=1}^{N} h_{\mathcal{E}^{\triangle}}^{(w)}\Big|_{\mathcal{I}_{\diamondsuit}}. \tag{9.235}$$

We show that its nullspace is equal to $\mathcal{I}_{\triangle}$, and we lower bound its smallest nonzero eigenvalue. Specifically, we prove

$$\gamma\left(\sum_{w=1}^{N} h_{\mathcal{E}^{\triangle}}^{(w)}\Big|_{\mathcal{I}_{\diamondsuit}}\right) > \frac{12c_{\triangle}}{(4R)^6}. \tag{9.236}$$

Additionally, we will show that B annihilates those states in $\mathcal{I}_{\triangle}$, so that $\mathcal{I}_{\triangle}$ is the nullspace of $H(G^{\triangle}, N)$ as claimed.

We will first prove equation (9.232) using this bound on the added movement terms (equation (9.236)) and the fact that B annihilates $\mathcal{I}_{\triangle}$. We apply the Nullspace Projection Lemma (Lemma 2) with H_A and H_B given by the first and second terms in equation (9.234); in this case the nullspace of H_A is $S = \mathcal{I}_{\diamondsuit}$ (from Lemma 28). Now applying Lemma 2 and using the bounds $\gamma(H_A) > \gamma_{\diamondsuit}$ (from Lemma 28), $\|H_B\| \leq N\|h_{\mathcal{E}^{\triangle}}\| = 2N \leq 2R$ (from equation (9.75) and the fact that $N \leq R$), and the bound (9.236) on $\gamma(H_B|_S)$, we find

$$\gamma(H(G^{\triangle}, N) - B) \geq \frac{\frac{12c_{\triangle}\gamma_{\diamondsuit}}{(4R)^6}}{\gamma_{\diamondsuit} + 2R} \geq \frac{16\gamma_{\diamondsuit}c_{\triangle}}{(4R)^7} = \frac{\gamma_{\triangle}}{R^7}. \tag{9.237}$$

If we now use the fact that B annihilates all states in $\mathcal{I}_{\triangle}$, we can use a variational argument to show that the same bound holds for the entire MPQW Hamiltonian (i.e., adding B to the Hamiltonian does not reduce the gap):

$$\gamma(H(G^{\triangle}, N)) \geq \frac{\gamma_{\triangle}}{R^7}. \tag{9.238}$$

With the final reductions for the proof completed, we must now establish that B annihilates all terms in $\mathcal{I}_{\triangle}$, the nullspace of (9.235) is $\mathcal{I}_{\triangle}$, and prove the lower bound (9.236). Let us first show

that each state in $\mathcal{I}_\triangle$ has no energy penalty due to new interactions arising from the addition of edges in the graph $G^\triangle$. By definition, note that the only vertices in $G^\triangle$ that have vertices at a distance closer than $d_{\max}$ either belong to the same diagram element, belong to diagram elements corresponding to $\{q_{\text{in}}, q_{\text{out}}, d(q,s)\}$ for some $q \in [R]$, or else belong to diagram elements labeled $\{d(q,s), e_{z_1,z_2}(q,s)\}$ for some $q, s \in [R]$, and $z_1, z_2 \in \mathbb{F}_2$. As such, if any state has energy penalties resulting from the added edges (i.e., is not annihilated by the operator B,), then it must have at least two particles located in two sets W_{z_1,a_1,q_1} and W_{z_2,a_2,q_2} that overlap in support. However, each state $|\Phi\rangle \in \mathcal{I}_\triangle$ is guaranteed by definition to not have any such overlap of support between its several particles, and thus $B|\Phi\rangle = 0$ as required.

To analyze (9.235) we use the fact (established in Section 9.3.4) that (9.213) is block diagonal with a block $\mathcal{W}_{(z,a,q)} \subset \mathcal{W}$ for each triple (z,a,q) with $z, a \in \mathbb{F}_2$ and $q \in [R]$, as the operator (9.235) inherits a block structure from this fact. For any basis vector

$$|\psi^{q_1}_{z_1,a_1}\rangle |\psi^{q_2}_{z_2,a_2}\rangle \dots |\psi^{q_N}_{z_N,a_N}\rangle \in \mathcal{I}_\diamondsuit, \tag{9.239}$$

we define a set of occupation numbers that correspond to the number of particles in each block. Namely, we will define

$$\mathcal{N} = \left\{ N_{(x,b,r)} \colon x, b \in \{0,1\},\, r \in [R] \right\} \tag{9.240}$$

where

$$N_{(x,b,r)} = |\{j \colon |\psi^{q_j}_{z_j,a_j}\rangle \in \mathcal{W}_{(x,b,r)}\}|. \tag{9.241}$$

Observe that (9.235) conserves the set of occupation numbers (due to the inherited block structure) and is therefore block diagonal with a block for each possible set $\mathcal{N}$.

(Note that the same definition can be made for the symmetrized states, as we only care about the number of particles in each block.)

For a given block corresponding to a set of occupation numbers $\mathcal{N}$, we write $\mathcal{I}_\diamondsuit(\mathcal{N}) \subset \mathcal{I}_\diamondsuit$ for the subspace spanned by basis vectors (9.239) in the block. We classify the blocks into three categories depending on $\mathcal{N}$.

Classification of the blocks of (9.235) according to $\mathcal{N}$

Consider the following two conditions on a set $\mathcal{N} = \{N_{(x,b,r)} \colon x, b \in \{0,1\},\, r \in [R]\}$ of occupation numbers:

(a) $N_{(x,b,r)} \in \{0,1\}$ for all $x, b \in \{0,1\}$ and $r \in [R]$. If this holds, write (y_i, c_i, s_i) for the nonzero occupation numbers (with some arbitrary ordering), i.e., $N_{(y_i,c_i,s_i)} = 1$ for $i \in [N]$.

(b) The sets $\mathcal{W}_{(y_i,c_i,s_i)}$ and $\mathcal{W}_{(y_j,c_j,s_j)}$ do not overlap on a diagram element for all distinct $i, j \in [N]$.

We say a block is of type 1 if $\mathcal{N}$ satisfies (a) and (b). We say it is of type 2 if $\mathcal{N}$ does not satisfy (a). We say it is of type 3 if $\mathcal{N}$ satisfies (a) but does not satisfy (b).

Note that every block must be of type 1, 2, or 3. We will show that each block of type 1 contains one state in the nullspace of (9.235) and, ranging over all blocks of this type, we will obtain a basis for $\mathcal{I}_\triangle$. We will also show that the smallest nonzero eigenvalue within a block of type 1 is at least $\frac{\gamma_\diamondsuit}{R^2}$. We will then show that blocks of type 2 and 3 do not contain any states in the nullspace of (9.235) and that the smallest eigenvalue within any block of type 2 or 3 is greater than $\frac{12 c_\triangle}{(4R)^6}$.

Hence, the nullspace of (9.235) is $\mathcal{I}_\triangle$ and its smallest nonzero eigenvalue is lower bounded as in equation (9.236).

Type 1

Let us first investigate those blocks of type 1. Note (from Definition 9) that requirement (b) implies $q \neq r$ whenever

$$|\psi^q_{x,b}\rangle \in \mathcal{W}_{(y_i,c_i,s_i)} \text{ and } |\psi^r_{z,a}\rangle \in \mathcal{W}_{(y_j,c_j,s_j)} \tag{9.242}$$

for distinct $i, j \in [N]$. Hence, we can remove the requirement that $q_i \neq q_j$:

$$\mathcal{I}_\diamondsuit(\mathcal{N}) = \text{span}\{|\psi^{q_1}_{z_1,a_1}\rangle|\psi^{q_2}_{z_2,a_2}\rangle \dots |\psi^{q_N}_{z_N,a_N}\rangle \colon q_i \neq q_j \text{ and } \exists \pi \in S_N, |\psi^{q_j}_{z_j,a_j}\rangle \in \mathcal{W}_{(y_{\pi(j)},c_{\pi(j)},s_{\pi(j)})}\} \tag{9.243}$$

$$= \text{span}\{|\psi^{q_1}_{z_1,a_1}\rangle|\psi^{q_2}_{z_2,a_2}\rangle \dots |\psi^{q_N}_{z_N,a_N}\rangle \colon \exists \pi \in S_N, |\psi^{q_j}_{z_j,a_j}\rangle \in \mathcal{W}_{(y_{\pi(j)},c_{\pi(j)},s_{\pi(j)})}\}. \tag{9.244}$$

From this we see that

$$\dim(\mathcal{I}_\diamondsuit(\mathcal{N})) = (N!) \prod_{j=1}^N \left|\mathcal{W}_{(y_j,c_j,s_j)}\right| = \begin{cases} (N!)\,(3R+2)^N & R \text{ odd} \\ (N!)\,(3R-1)^N & R \text{ even.} \end{cases} \tag{9.245}$$

We now solve for all the eigenstates of (9.235) within the block. (Note that if we restrict to the symmetric subspace, the symmetrization condition simply reduces the size of these subspaces by a factor of $N!$, as the only symmetric state in this subspace is given by the uniform superposition over all these states.)

As we need only understand the eigenvectors of each individual block, it will be useful to remember Lemma 29 as we have already determined all of the single-particle eigenstates. It will convenient to write an orthonormal basis of eigenvectors of the $|\mathcal{W}_{(z,a,q)}| \times |\mathcal{W}_{(z,a,q)}|$ matrix described by Figure 9.11a as

$$|\phi^q_{z,a}(u)\rangle, \quad u \in [|\mathcal{W}_{(z,a,q)}|] \tag{9.246}$$

and their ordered eigenvalues as

$$\theta_1 \leq \theta_2 \leq \ldots \leq \theta_{|\mathcal{W}_{(z,a,q)}|}. \tag{9.247}$$

From the proof of Lemma 29, the eigenvector with smallest eigenvalue $\theta_1 = 0$ is $|\phi^q_{z,a}\rangle = |\phi^q_{z,a}(1)\rangle$ and $\theta_2 \geq \frac{c_\diamondsuit}{R^2}$. For any $u_1, u_2, \ldots, u_N \in [|\mathcal{W}_{(z,a,q)}|]$, the state

$$|\phi^{s_1}_{y_1,c_1}(u_1)\rangle|\phi^{s_2}_{y_2,c_2}(u_2)\rangle \dots |\phi^{s_N}_{y_N,c_N}(u_N)\rangle \tag{9.248}$$

is an eigenvector of (9.235) with eigenvalue $\sum_{j=1}^N \theta_{u_j}$. Furthermore, states corresponding to different choices of $u_1, \ldots, u_N$ are orthogonal, and ranging over all $\dim(\mathcal{I}_\diamondsuit(\mathcal{N}))$ choices we get every eigenvector in the block. The smallest eigenvalue within the block is $N\theta_1 = 0$ and there are $N!$ vectors in the nullspace, given by

$$|\,\Phi^\pi_{\mathcal{N}}\rangle := |\phi^{s_{\pi(1)}}_{y_{\pi(1)},c_{\pi(1)}}\rangle|\phi^{s_{\pi(2)}}_{y_{\pi(2)},c_{\pi(2)}}\rangle \dots |\phi^{s_{\pi(N)}}_{y_{\pi(N)},c_{\pi(N)}}\rangle, \tag{9.249}$$

where $\pi \in S_N$, and where $|\phi^q_{z,a}\rangle = |\phi^q_{z,a}(1)\rangle$. The smallest nonzero eigenvalue of (9.235) within the block is $(N-1)\theta_1 + \theta_2 = \theta_2 \geq \frac{c_\diamondsuit}{R^2}$, as expected. If we restrict ourselves to the symmetric states, this nullspace becomes 1-dimensional, but we still have the same bounds on the eigenvalue gap.

With the knowledge that each state of the form (9.249) minimizes the energy of (9.235), we will now show that the collection of all such states span the space $\mathcal{I}_\triangle$. As the second requirement on type 1 blocks requires that the sets $\mathcal{W}_{(y_i,c_i,s_i)}$ no not pairwise overlap, we can use Fact 2 to see

that this is equivalent to the sets satisfying $s_i \neq s_j$ and $\{s_i, s_j\} \notin E(G^{\text{occ}})$ for distinct $i, j \in [N]$ (as well as arbitrary y_i and c_i). Hence the set of states (9.249) obtained from of all blocks of type 1 is

$$\begin{aligned}&\left\{|\,\Phi_{\mathcal{N}}\rangle : \mathcal{N} \text{ is a type 1 block}\right\} \\ &\quad = \Big\{|\phi^{s_1}_{y_1,c_1}\rangle|\phi^{s_2}_{y_2,c_2}\rangle \ldots |\phi^{s_N}_{y_N,c_N}\rangle : \\ &\qquad \forall i,j \in [N], y_i, c_i \in \mathbb{F}_2,\ s_i \in [R],\ i \neq j \Rightarrow s_i \neq s_j \text{ and } \{s_i, s_j\} \notin E(G^{\text{occ}})\Big\} \end{aligned} \tag{9.250}$$

which by definition spans $\mathcal{I}_\triangle$. Again, if we restrict ourselves to the symmetric subspace, we also have that these states also span $\mathcal{I}_\triangle^{\text{Sym}}$.

Type 2

Now let $\mathcal{N}$ be of type 2. We then have that there exist $x, b \in \mathbb{F}_2$ and $r \in [R]$ such that $N_{(x,b,r)} \geq 2$. We will show there are no eigenvectors in the nullspace of (9.235) within a block of this type and we lower bound the smallest eigenvalue within the block. Specifically, we show

$$\min_{|\kappa\rangle \in \mathcal{I}_\diamondsuit(\mathcal{N})} \langle\kappa| \sum_{w=1}^{N} h^{(w)}_{\mathcal{E}^\triangle} |\kappa\rangle > \frac{12 c_\triangle}{(4R)^6}. \tag{9.251}$$

First note that all $|\kappa\rangle \in \mathcal{I}_\diamondsuit$ satisfy $(A(G^\diamondsuit) - e_1)^{(w)}|\kappa\rangle = 0$ for each $w \in [N]$, which can be seen using the definition of $\mathcal{I}_\diamondsuit$ and the fact that $\mathcal{W}$ spans the nullspace of $A(G^\diamondsuit) - e_1$. We can then add these terms to equation (9.212), so that

$$\min_{|\kappa\rangle \in \mathcal{I}_\diamondsuit(\mathcal{N})} \langle\kappa| \sum_{w=1}^{N} h^{(w)}_{\mathcal{E}^\triangle} |\kappa\rangle = \min_{|\kappa\rangle \in \mathcal{I}_\diamondsuit(\mathcal{N})} \langle\kappa| \sum_{w=1}^{N} \Big(A(G^\triangle) - e_1\Big)^{(w)} |\kappa\rangle. \tag{9.252}$$

If we then examine only the ground space of this operator, we can see that

$$\begin{aligned}\sum_{w=1}^{N} \Big(A(G^\triangle) - e_1\Big)^{(w)} &\geq \gamma \left(\sum_{w=1}^{N} \Big(A(G^\triangle) - e_1\Big)^{(w)}\right) \cdot \Big(1 - \Pi^\triangle\Big) \\ &= \gamma (A(G^\triangle) - e_1) \cdot \Big(1 - \Pi^\triangle\Big) > \frac{c_\triangle}{R^2}\Big(1 - \Pi^\triangle\Big), \end{aligned} \tag{9.253}$$

where $\Pi^\triangle$ is the projector onto the nullspace of $\sum_{w=1}^{N} \left(A(G^\triangle) - e_1\right)^{(w)}$, and where in the last step we used Lemma 29. Plugging equation (9.253) into equation (9.252) gives

$$\min_{|\kappa\rangle \in \mathcal{I}_\diamondsuit(\mathcal{N})} \langle\kappa| \sum_{w=1}^{N} h^{(w)}_{\mathcal{E}^\triangle} |\kappa\rangle > \frac{c_\triangle}{R^2}\Big(1 - \max_{|\kappa\rangle \in \mathcal{I}_\diamondsuit(\mathcal{N})} \langle\kappa|\Pi^\triangle|\kappa\rangle\Big). \tag{9.254}$$

Using Lemma 29 we can write $\Pi^\triangle$ explicitly as

$$\Pi^\triangle = \sum_{(\vec{z},\vec{a},\vec{q}) \in \mathcal{Q}} \mathcal{P}_{(\vec{z},\vec{a},\vec{q})} \tag{9.255}$$

where

$$\mathcal{P}_{(\vec{z},\vec{a},\vec{q})} = |\phi^{q_1}_{z_1,a_1}\rangle\langle\phi^{q_1}_{z_1,a_1}| \otimes |\phi^{q_2}_{z_2,a_2}\rangle\langle\phi^{q_2}_{z_2,a_2}| \otimes \cdots \otimes |\phi^{q_N}_{z_N,a_N}\rangle\langle\phi^{q_N}_{z_N,a_N}| \tag{9.256}$$

$$\mathcal{Q} = \{(z_1, \ldots z_N, a_1, \ldots, a_N, q_1, \ldots, q_N) :\ z_i, a_i \in \mathbb{F}_2 \text{ and } q_i \in [R]\}. \tag{9.257}$$

Essentially, each particle is projected onto the ground state of a block, where the blocks are labeled by the elements of $\mathcal{Q}$ and there are no correlations between the particles. For each $(\vec{z},\vec{a},\vec{q}) \in \mathcal{Q}$ we also define a space

$$S_{(\vec{z},\vec{a},\vec{q})} = \text{span}(\mathcal{W}_{(z_1,a_1,q_1)}) \otimes \text{span}(\mathcal{W}_{(z_2,a_2,q_2)}) \otimes \cdots \otimes \text{span}(\mathcal{W}_{(z_N,a_N,q_N)}). \tag{9.258}$$

Note that $\mathcal{P}_{(\vec{z},\vec{a},\vec{q})}$ has all of its support in $S_{(\vec{z},\vec{a},\vec{q})}$, and that

$$S_{(\vec{z},\vec{a},\vec{q})} \perp S_{(\vec{z}',\vec{a}',\vec{q}')} \text{ for distinct } (\vec{z},\vec{a},\vec{q}),(\vec{z}',\vec{a}',\vec{q}') \in \mathcal{Q}. \tag{9.259}$$

Therefore $\mathcal{P}_{(\vec{z},\vec{a},\vec{q})}\mathcal{P}_{(\vec{z}',\vec{a}',\vec{q}')} = 0$ for distinct $(\vec{z},\vec{a},\vec{q}),(\vec{z}',\vec{a}',\vec{q}') \in \mathcal{Q}$. (Below we use similar reasoning to obtain a less obvious result.) Note that $\mathcal{P}_{(\vec{z},\vec{a},\vec{q})}$ is orthogonal to $\mathcal{I}_\diamondsuit(\mathcal{N})$ unless

$$|\{j : (z_j,a_j,q_j) = (w,u,v)\}| = N_{(w,u,v)} \text{ for all } w,u \in \{0,1\},\ v \in [R]. \tag{9.260}$$

We restrict our attention to the projectors that are not orthogonal to $\mathcal{I}_\diamondsuit(\mathcal{N})$. Letting $\mathcal{Q}(\mathcal{N}) \subset \mathcal{Q}$ be the set of $(\vec{z},\vec{a},\vec{q})$ satisfying equation (9.260), we have

$$\langle\kappa| \sum_{(\vec{z},\vec{a},\vec{q})\in\mathcal{Q}} \mathcal{P}_{(\vec{z},\vec{a},\vec{q})}|\kappa\rangle = \langle\kappa| \sum_{(\vec{z},\vec{a},\vec{q})\in\mathcal{Q}(\mathcal{N})} \mathcal{P}_{(\vec{z},\vec{a},\vec{q})}|\kappa\rangle \quad \text{for all } |\kappa\rangle \in \mathcal{I}_\diamondsuit(\mathcal{N}). \tag{9.261}$$

Since $N_{(x,b,r)} \geq 2$, note that in each term $\mathcal{P}_{(\vec{z},\vec{a},\vec{q})}$ with $(\vec{z},\vec{a},\vec{q}) \in \mathcal{Q}(\mathcal{N})$, the operator

$$|\phi^r_{x,b}\rangle\langle\phi^r_{x,b}| \otimes |\phi^r_{x,b}\rangle\langle\phi^r_{x,b}| \tag{9.262}$$

appears between two of the N registers (tensored with rank-1 projectors on the other $N-2$ registers). Using equation (9.224) we may expand $|\phi^r_{x,b}\rangle$ as a sum of states from $\mathcal{W}_{(x,b,r)}$. This gives

$$|\phi^r_{x,b}\rangle|\phi^r_{x,b}\rangle = c_0|\psi^{r_{\text{in}}}_{x,b}\rangle|\psi^{r_{\text{in}}}_{x,b}\rangle + \left(1-c_0^2\right)^{\frac{1}{2}}|\Phi^r_{x,b}\rangle \tag{9.263}$$

where c_0 is either $\frac{1}{3R+2}$ (if R is odd) or $\frac{1}{3R-1}$ (if R is even), and where $|\psi^{r_{\text{in}}}_{x,b}\rangle|\psi^{r_{\text{in}}}_{x,b}\rangle$ is orthogonal to $|\Phi^r_{x,b}\rangle$. Note that each of the states $|\phi^r_{x,b}\rangle|\phi^r_{x,b}\rangle$, $|\psi^{r_{\text{in}}}_{x,b}\rangle|\psi^{r_{\text{in}}}_{x,b}\rangle$, and $|\Phi^r_{x,b}\rangle$ lie in the space

$$\text{span}(\mathcal{W}_{(x,b,r)}) \otimes \text{span}(\mathcal{W}_{(x,b,r)}). \tag{9.264}$$

Now applying Fact 3 gives

$$|\phi^r_{x,b}\rangle\langle\phi^r_{x,b}| \otimes |\phi^r_{x,b}\rangle\langle\phi^r_{x,b}| = c_0^2|\psi^{r_{\text{in}}}_{x,b}\rangle\langle\psi^{r_{\text{in}}}_{x,b}| \otimes |\psi^{r_{\text{in}}}_{x,b}\rangle\langle\psi^{r_{\text{in}}}_{x,b}| + M^r_{x,b} \tag{9.265}$$

where $M^r_{x,b}$ is a Hermitian operator with all of its support on the space (9.264) and

$$\left\|M^r_{x,b}\right\| \leq 1 - \frac{3}{4}c_0^4 \leq 1 - \frac{3}{4}\left(\frac{1}{3R+2}\right)^4 \leq 1 - \frac{3}{4}\frac{1}{(4R)^4} \tag{9.266}$$

since $R \geq 2$. For each $(\vec{z},\vec{a},\vec{q}) \in \mathcal{Q}(\mathcal{N})$ we define $\mathcal{P}^M_{(\vec{z},\vec{a},\vec{q})}$ to be the operator obtained from $\mathcal{P}_{(\vec{z},\vec{a},\vec{q})}$ by replacing

$$|\phi^r_{x,b}\rangle\langle\phi^r_{x,b}| \otimes |\phi^r_{x,b}\rangle\langle\phi^r_{x,b}| \mapsto M^r_{x,b} \tag{9.267}$$

on two of the registers (if $N_{(x,b,r)} > 2$ there is more than one way to do this; we fix one choice for each $(\vec{z},\vec{a},\vec{q}) \in \mathcal{Q}(\mathcal{N})$). Note that $\mathcal{P}^M_{(\vec{z},\vec{a},\vec{q})}$ has all of its support in the space $S_{(\vec{z},\vec{a},\vec{q})}$. Using (9.259) gives

$$\mathcal{P}^M_{(\vec{z},\vec{a},\vec{q})}\mathcal{P}^M_{(\vec{z}',\vec{a}',\vec{q}')} = 0 \text{ for distinct } (\vec{z},\vec{a},\vec{q}),(\vec{z}',\vec{a}',\vec{q}') \in \mathcal{Q}(\mathcal{N}). \tag{9.268}$$

Using equation (9.265) and the fact that

$$\langle\kappa|\Big(|\psi^{r_{\text{in}}}_{x,b}\rangle\langle\psi^{r_{\text{in}}}_{x,b}|^{(w_1)}\Big)\Big(|\psi^{r_{\text{in}}}_{x,b}\rangle\langle\psi^{r_{\text{in}}}_{x,b}|^{(w_2)}\Big)|\kappa\rangle = 0 \quad \text{for all } |\kappa\rangle \in \mathcal{I}_\diamondsuit(\mathcal{N}) \text{ and distinct } w_1, w_2 \in [N] \tag{9.269}$$

(which can be seen from the definition of $\mathcal{I}_\diamondsuit$), we have

$$\langle\kappa|\mathcal{P}_{(\vec{z},\vec{a},\vec{q})}|\kappa\rangle = \langle\kappa|\mathcal{P}^M_{(\vec{z},\vec{a},\vec{q})}|\kappa\rangle \quad \text{for all } |\kappa\rangle \in \mathcal{I}_\diamondsuit(\mathcal{N}). \tag{9.270}$$

Hence, letting

$$\Pi^\triangle_{\mathcal{N}} = \sum_{(\vec{z},\vec{a},\vec{q})\in\mathcal{Q}(\mathcal{N})} \mathcal{P}^M_{(\vec{z},\vec{a},\vec{q})}, \tag{9.271}$$

we have $\langle\kappa|\Pi^\triangle|\kappa\rangle = \langle\kappa|\Pi^\triangle_{\mathcal{N}}|\kappa\rangle$ for all $|\kappa\rangle \in \mathcal{I}_\diamondsuit(\mathcal{N})$. To obtain a bound on the norm of $\Pi^\triangle_{\mathcal{N}}$, we use the fact that the norm of a sum of pairwise orthogonal Hermitian operators is upper bounded by the maximum norm of an operator in the sum, so

$$\big\|\Pi^\triangle_{\mathcal{N}}\big\| = \left\|\sum_{(\vec{z},\vec{a},\vec{q})\in\mathcal{Q}(\mathcal{N})} \mathcal{P}^M_{(\vec{z},\vec{a},\vec{q})}\right\| = \max_{(\vec{z},\vec{a},\vec{q})\in\mathcal{Q}(\mathcal{N})} \big\|\mathcal{P}^M_{(\vec{z},\vec{a},\vec{q})}\big\| = \big\|M^r_{x,b}\big\| \leq 1 - \frac{3}{4}\frac{1}{(4R)^4}. \tag{9.272}$$

Putting this together, we then have that

$$\max_{|\kappa\rangle\in\mathcal{I}_\diamondsuit(\mathcal{N})} \langle\kappa|\Pi^\triangle|\kappa\rangle = \max_{|\kappa\rangle\in\mathcal{I}_\diamondsuit(\mathcal{N})} \langle\kappa|\Pi^\triangle_{\mathcal{N}}|\kappa\rangle \leq \|\Pi^\triangle_{\mathcal{N}}\| \leq 1 - \frac{3}{4(4R)^4}. \tag{9.273}$$

If we then use (9.254), we have that

$$\min_{|\kappa\rangle\in\mathcal{I}_\diamondsuit(\mathcal{N})} \langle\kappa|\sum_{w=1}^N h^{(w)}_{\mathcal{E}^\triangle}|\kappa\rangle > \frac{c_\triangle}{R^2}\Big(1 - \max_{|\kappa\rangle\in\mathcal{I}_\diamondsuit(\mathcal{N})} \langle\kappa|\Pi^\triangle|\kappa\rangle\Big) \geq \frac{12c_\triangle}{(4R)^6}. \tag{9.274}$$

Type 3

Let us finally examine the case where $\mathcal{N}$ is of type 3 then $N_{(x,b,r)} \in \{0,1\}$ for all $x, b \in \mathbb{F}_2$ and $r \in [R]$, and

$$N_{(y,c,s)} = N_{(t,d,u)} = 1 \tag{9.275}$$

for some $(y,c,s) \neq (t,d,u)$ with either $u = s$ or $\{u,s\} \in E(G^{\text{occ}})$ (using property (b) and Fact 2). We show there are no eigenvectors in the nullspace of (9.235) within a block of this type and we lower bound the smallest eigenvalue within the block. We establish the same bound (9.251) as for blocks of Type 2.

The proof is very similar to that given above for blocks of Type 2. In fact, the first part of proof is identical, from equation (9.252) up to and including equation (9.261). That is to say, as in the previous case we have

$$\langle\kappa|\sum_{(\vec{z},\vec{a},\vec{q})\in\mathcal{Q}} \mathcal{P}_{(\vec{z},\vec{a},\vec{q})}|\kappa\rangle = \langle\kappa|\sum_{(\vec{z},\vec{a},\vec{q})\in\mathcal{Q}(\mathcal{N})} \mathcal{P}_{(\vec{z},\vec{a},\vec{q})}|\kappa\rangle \quad \text{for all } |\kappa\rangle \in \mathcal{I}_\diamondsuit(\mathcal{N}). \tag{9.276}$$

In this case, since $N_{(y,c,s)} = N_{(t,d,u)} = 1$, in each term $\mathcal{P}_{(\vec{z},\vec{a},\vec{q})}$ with $(\vec{z},\vec{a},\vec{q}) \in \mathcal{Q}(\mathcal{N})$, the operator

$$|\phi^s_{y,c}\rangle\langle\phi^s_{y,c}| \otimes |\phi^u_{t,d}\rangle\langle\phi^u_{t,d}| \tag{9.277}$$

appears between two of the N registers (tensored with rank 1 projectors on the other $N-2$ registers). Using equation (9.224) we may expand $|\phi^s_{y,c}\rangle$ and $|\phi^u_{t,d}\rangle$ as superpositions (with amplitudes $\pm\frac{1}{\sqrt{3R+2}}$

if R is odd or $\pm\frac{1}{\sqrt{3R-1}}$ if R is even) of the basis states from $\mathcal{W}_{(y,c,s)}$ and $\mathcal{W}_{(t,d,u)}$ respectively. Since $\mathcal{W}_{(y,c,s)}$ and $\mathcal{W}_{(t,d,u)}$ overlap on some diagram element, there exists $l \in L^{\square}$ such that $|\psi^l_{x_1,b_1}\rangle \in \mathcal{W}_{(y,c,s)}$ and $|\psi^l_{x_2,b_2}\rangle \in \mathcal{W}_{(t,d,u)}$ for some $x_1, x_2, b_1, b_2 \in \{0,1\}$. Hence

$$|\phi^s_{y,c}\rangle|\phi^u_{t,d}\rangle = c_0\left(\pm|\psi^l_{x_1,b_1}\rangle|\psi^l_{x_2,b_2}\rangle\right) + \left(1-c_0^2\right)^{\frac{1}{2}}|\Phi^{s,u}_{y,c,t,d}\rangle \tag{9.278}$$

where c_0 is either $\frac{1}{3R+2}$ (if R is odd) or $\frac{1}{3R-1}$ (if R is even). Now applying Fact 3 we get

$$|\phi^s_{y,c}\rangle\langle\phi^s_{y,c}| \otimes |\phi^u_{t,d}\rangle\langle\phi^u_{t,d}| = c_0^2|\psi^l_{x_1,b_1}\rangle\langle\psi^l_{x_1,b_1}| \otimes |\psi^l_{x_2,b_2}\rangle\langle\psi^l_{x_2,b_2}| + M^{s,u}_{y,c,t,d} \tag{9.279}$$

where $\|M^{s,u}_{y,c,t,d}\| \leq 1 - \frac{3}{4}\left(\frac{1}{4R}\right)^4$. For each $(\vec{z},\vec{a},\vec{q}) \in \mathcal{Q}(\mathcal{N})$ we define $\mathcal{P}^M_{(\vec{z},\vec{a},\vec{q})}$ to be the operator obtained from $\mathcal{P}_{(\vec{z},\vec{a},\vec{q})}$ by replacing

$$|\phi^s_{y,c}\rangle\langle\phi^s_{y,c}| \otimes |\phi^u_{t,d}\rangle\langle\phi^u_{t,d}| \mapsto M^{s,u}_{y,c,t,d} \tag{9.280}$$

on two of the registers and we let $\Pi^{\triangle}_{\mathcal{N}}$ be given by (9.271). Then, as in the previous case, $\langle\kappa|\Pi^{\triangle}|\kappa\rangle = \langle\kappa|\Pi^{\triangle}_{\mathcal{N}}|\kappa\rangle$ for all $|\kappa\rangle \in \mathcal{I}_{\diamondsuit}(\mathcal{N})$ and using the same reasoning as before, we get the bound (9.272) on $\|\Pi^{\triangle}_{\mathcal{N}}\|$. Using these two facts we get the same bound on the smallest eigenvalue within a block of type 3 as the bound we obtained for blocks of type 2:

$$\min_{|\kappa\rangle\in\mathcal{I}_{\diamondsuit}(\mathcal{N})}\langle\kappa|\sum_{w=1}^{N} h^{(w)}_{\mathcal{E}^{\triangle}}|\kappa\rangle > \frac{c_{\triangle}}{R^2}\left(1 - \max_{|\kappa\rangle\in\mathcal{I}_{\diamondsuit}(\mathcal{N})}\langle\kappa|\Pi^{\triangle}|\kappa\rangle\right) \geq \frac{12c_{\triangle}}{(4R)^6}. \qquad \square$$

9.3.6 The gate graph $G^{\square}$

With all of the intermediate graphs characterized, we now consider the gate graph $G^{\square}$ and prove Lemma 27. We first show that $G^{\square}$ is an e_1-gate graph. From equations (9.196), (9.198), and (9.200) we have

$$A(G^{\square}) = A(G^{\triangle}) + h_{\mathcal{E}^0} + h_{\mathcal{S}^0}. \tag{9.281}$$

Lemma 29 characterizes the e_1-energy ground space of $G^{\triangle}$ and gives an orthonormal basis for it. To solve for the e_1-energy ground space of $A(G^{\square})$, we solve for superpositions of the ground states of $A(G^{\triangle})$, $\{|\phi^q_{z,a}\rangle\}$, in the nullspace of $h_{\mathcal{E}^0} + h_{\mathcal{S}^0}$.

Recall the definition of the sets $\mathcal{E}^0$ and $\mathcal{S}^0$, as these are the edges and self-loops that are inherited from the graph G. From Section 9.3.2.1, each node (q,z,t) in the gate diagram for G is associated with a node $\text{new}(q,z,t)$ in the gate diagram for $G^{\square}$ as described by (9.188). This mapping is depicted in Figure 9.7 by the black and grey arrows. Applying this mapping to each pair of nodes in the edge set $\mathcal{E}^G$ and each node in the self-loop set $\mathcal{S}^G$ of the gate diagram for G, we get the sets $\mathcal{E}^0$ and $\mathcal{S}^0$. Hence, using equations (9.72) and (9.73),

$$h_{\mathcal{S}^0} = \sum_{(q,z,t)\in\mathcal{S}^G} |\text{new}(q,z,t)\rangle\langle\text{new}(q,z,t)| \otimes \mathbb{I} \tag{9.282}$$

$$h_{\mathcal{E}^0} = \sum_{\{(q,z,t),(q',z',t')\}\in\mathcal{E}^G} \left(|\text{new}(q,z,t)\rangle + |\text{new}(q',z',t')\rangle\right)\left(\langle\text{new}(q,z,t)| + \langle\text{new}(q',z',t')|\right) \otimes \mathbb{I}. \tag{9.283}$$

Using equation (9.224), we see that for all nodes (q, z, t) in the gate diagram for G and for all $j \in [8]$, $x, b, d \in \mathbb{F}_2$, and $r \in [R]$,

$$\begin{aligned}\langle \mathrm{new}(q,z,t), j, d | \phi^r_{x,b} \rangle &= \sqrt{c_0} \begin{cases} \langle q_{\mathrm{in}}, z, t, j, d | \psi^{r_{\mathrm{in}}}_{x,b} \rangle & \text{if } (q,z,t) \text{ is an input node} \\ \langle q_{\mathrm{out}}, z, t, j, d | \psi^{r_{\mathrm{out}}}_{x,b} \rangle & \text{if } (q,z,t) \text{ is an output node} \end{cases} \\ &= \sqrt{c_0} \delta_{r,q} \langle z, t, j, d | \overline{\psi_{x,b}} \rangle \end{aligned} \tag{9.284}$$

where c_0 is $\frac{1}{3R+2}$ if R is odd or $\frac{1}{3R-1}$ if R is even, and where $|\psi_{x,b}\rangle$ is defined by equations (9.10) and (9.11). The matrix element on the left-hand side of this equation is evaluated in the Hilbert space $\mathbb{C}^{|V(G^\square)|}$ where each basis vector corresponds to a vertex of the graph $G^\square$; these vertices are labeled (l, z, t, j, d) with $l \in L^\square$, $z, d \in \mathbb{F}_2$, $t \in [8k]$, and $j \in [8]$. However, from (9.284) we see that

$$\underbrace{\langle \mathrm{new}(q,z,t), j, d | \phi^r_{x,b} \rangle}_{\text{in } \mathcal{Z}_1(G^\square)} = \sqrt{c_0} \underbrace{\langle q, z, t, j, d | \psi^r_{x,b} \rangle}_{\text{in } \mathcal{Z}_1(G)} \tag{9.285}$$

where the right-hand side is evaluated in the Hilbert space $\mathbb{C}^{|V(G)|}$.

Putting together equations (9.282), (9.283), and (9.285) gives

$$\langle \phi^q_{z,a} | h_{\mathcal{E}^0} + h_{\mathcal{S}^0} | \phi^r_{x,b} \rangle = \langle \psi^q_{z,a} | h_{\mathcal{E}^G} + h_{\mathcal{S}^G} | \psi^r_{x,b} \rangle \cdot \begin{cases} \frac{1}{3R+2} & R \text{ odd} \\ \frac{1}{3R-1} & R \text{ even} \end{cases} \tag{9.286}$$

for all $z, a, x, b \in \mathbb{F}_2$ and $q, r \in [R]$.

We use equation (9.286) to relate the e_1-energy ground states of $A(G)$ to those of $A(G^\square)$. Since G is an e_1-gate graph, there is a state

$$|\Gamma\rangle = \sum_{z,a,q} \alpha_{z,a,q} |\psi^q_{z,a}\rangle \in \mathbb{C}^{|V(G)|} \tag{9.287}$$

that satisfies $A(G)|\Gamma\rangle = e_1|\Gamma\rangle$ and hence $h_{\mathcal{E}^G}|\Gamma\rangle = h_{\mathcal{S}^G}|\Gamma\rangle = 0$. Letting

$$|\Gamma'\rangle = \sum_{z,a,q} \alpha_{z,a,q} |\phi^q_{z,a}\rangle \in \mathbb{C}^{|V(G^\square)|} \tag{9.288}$$

and using equation (9.286), we see that $\langle \Gamma' | h_{\mathcal{E}^0} + h_{\mathcal{S}^0} | \Gamma' \rangle = 0$ and therefore $\langle \Gamma' | A(G^\square) | \Gamma' \rangle = e_1$. Hence $G^\square$ is an e_1-gate graph. Moreover, the linear mapping from $\mathbb{C}^{|V(G)|}$ to $\mathbb{C}^{|V(G^\square)|}$ defined by

$$|\psi^q_{z,a}\rangle \mapsto |\phi^q_{z,a}\rangle \tag{9.289}$$

maps each e_1-energy eigenstate of $A(G)$ to an e_1-energy eigenstate of $A(G^\square)$.

Now consider the N-particle Hamiltonian $H(G^\square, N)$. Using equation (9.281) and the fact that both $A(G^\square)$ and $A(G^\triangle)$ have smallest eigenvalue e_1, we have

$$H(G^\square, N) = H(G^\triangle, N) + \sum_{w=1}^{N} \left(h_{\mathcal{E}^0} + h_{\mathcal{S}^0} \right)^{(w)} \Big|_{\mathcal{Z}_N(G^\square)} + C', \tag{9.290}$$

where C corresponds to the added interactions resulting from the additional edges. Recall from Lemma 29 that the nullspace of the first term is $\mathcal{I}_\triangle$. The N-fold tensor product of the mapping (9.289) acts on basis vectors of $\mathcal{I}(G, G^{\mathrm{occ}}, N)$ as

$$|\psi^{q_1}_{z_1,a_1}\rangle |\psi^{q_2}_{z_2,a_2}\rangle \dots |\psi^{q_N}_{z_N,a_N}\rangle \mapsto |\phi^{q_1}_{z_1,a_1}\rangle |\phi^{q_2}_{z_2,a_2}\rangle \dots |\phi^{q_N}_{z_N,a_N}\rangle, \tag{9.291}$$

where $z_i, a_i \in \mathbb{F}_2$, $q_i \neq q_j$, and $\{q_i, q_j\} \notin E(G^{\text{occ}})$. Clearly this defines an invertible linear map between the two spaces $\mathcal{I}(G, G^{\text{occ}}, N)$ and $\mathcal{I}_\triangle$. Let $|\Theta\rangle \in \mathcal{I}(G, G^{\text{occ}}, N)$ and write $|\Theta'\rangle \in \mathcal{I}_\triangle$ for its image under the map (9.291). Then

$$\langle\Theta'|H(G^\square, N) - C'|\Theta'\rangle = \langle\Theta'| \sum_{w=1}^{N} \left(h_{\mathcal{E}^0} + h_{\mathcal{S}^0}\right)^{(w)} |\Theta'\rangle \tag{9.292}$$

$$= \langle\Theta| \sum_{w=1}^{N} \left(h_{\mathcal{E}^G} + h_{\mathcal{S}^G}\right)^{(w)} |\Theta\rangle \cdot \begin{cases} \frac{1}{3R+2} & R \text{ odd} \\ \frac{1}{3R-1} & R \text{ even} \end{cases} \tag{9.293}$$

where in the first equality we used the fact that $|\Theta'\rangle$ is in the nullspace $\mathcal{I}_\triangle$ of $H(G^\triangle, N)$ and in the second equality we used equation (9.286) and the fact that $\langle\phi^q_{z,a}|\phi^r_{x,b}\rangle = \langle\psi^q_{z,a}|\psi^r_{x,b}\rangle$.

We now want to understand how C' changes the ground space along with the eigenvalue gap. While the added edges will add energy to those states on $G^\square$ if and only if they add energy to the corresponding state on G that also satisfy the occupancy constraints, the fact that the states on $G^\square$ are much more spread out means that the added energy can be drastically less. In particular, an arbitrary state on G might have N-particle interactions which under our transformation would require a factor of $(3R)^{-N}$ to the energy. However, the fact that each state in $\mathcal{I}_\triangle$ and each state in $\mathcal{I}(G, G^{\text{occ}}, N)$ satisfy the occupancy constraints implies that at most a single particle ever occupies a single diagram element (and thus $C' = 0$ if $d_{\max} = 0$). Using this, we have that when restricted to those states in $\mathcal{I}_\triangle$, each term in C' affects at most two particles, and the requisite change to the energy penalty will only be $(3R)^{-2}$.

As such, let u' and v' be two vertices of $G^\square$ that can now interact but were separated by a distance more than $d_{\max}$ in $G^\triangle$. We can see that each such vertex is contained within some diagram element q_{in} or q_{out}. Further, each pair (u', v') of vertices in $G^\square$ for which interactions are added has a corresponding pair of vertices (u, v) in G for which the interactions were also added, derived by simply dropping the in/out from the label for the diagram element. Similarly, for any two vertices (u, v) in G for which the added edges cause an interaction, there exist two vertices (u', v') in $G^\square$ that also have an interaction, which can be found by adding in the in/out to the diagram element labels for u and v, depending where the edge that connects the two diagram elements is located (i.e., whether it connects to the input or output of the element). Since this is a bijection between pairs of vertices (but not individual vertices), we will have that the added interactions will be proportional between those states in $\mathcal{I}_\triangle$ and $\mathcal{I}(G, G^{\text{occ}}, N)$. We will let $V^\square \subset V(G^\square) \times V(G^\square)$ be those vertices in $G^\square$ that are now at a distance less than or equal to $d_{\max}$ that were farther apart than $d_{\max}$ in $G^\triangle$, and let $V \subset V(G) \times V(G)$ be the corresponding pairs of vertices in G.

Explicitly, note that for any pair of vertices $(u', v') \in V^\square$ that are now a distance d, and any state $|\Theta'\rangle \in \mathcal{I}(G^\triangle, N)$,

$$\langle\Theta'|\mathcal{U}_d(\hat{n}_{u'}, \hat{n}_{v'})|\Theta'\rangle = U_d^{(1,1)} \sum_{w_1 \neq w_2 \in [N]} \langle\Theta'|\left(|u'\rangle\langle u'|^{(w_1)} \otimes |v'\rangle\langle v'|^{(w_2)}\right)|\Theta'\rangle \tag{9.294}$$

$$= U_d^{(1,1)} \sum_{w_1 \neq w_2 \in [N]} \langle\Theta|\left(|u\rangle\langle u|^{(w_1)} \otimes |v\rangle\langle v|^{(w_2)}\right)|\Theta\rangle \begin{cases} \frac{1}{(3R+2)^2} & R \text{ odd} \\ \frac{1}{(3R-1)^2} & R \text{ even} \end{cases} \tag{9.295}$$

$$= \langle\Theta|\mathcal{U}_d(\hat{n}_u, \hat{n}_v)|\Theta\rangle \begin{cases} \frac{1}{(3R+2)^2} & R \text{ odd} \\ \frac{1}{(3R-1)^2} & R \text{ even.} \end{cases} \tag{9.296}$$

This uses a relation almost identical to (9.284), which can be derived in an identical manner.

With this identity in mind, we have that

$$\langle \Theta' | C' | \Theta' \rangle = \sum_{(u',v') \in \mathcal{V}^{\square}} \langle \Theta' | \mathcal{U}_{d(u',v')}(\hat{n}_{u'}, \hat{n}_{v'}) | \Theta' \rangle \tag{9.297}$$

$$= \sum_{(u,v) \in \mathcal{V}} \langle \Theta | \mathcal{U}_{d(u,v)}(\hat{n}_u, \hat{n}_v) | \Theta \rangle \begin{cases} \frac{1}{(3R+2)^2} & R \text{ odd} \\ \frac{1}{(3R-1)^2} & R \text{ even.} \end{cases} \tag{9.298}$$

$$= \langle \Theta | C | \Theta \rangle \begin{cases} \frac{1}{(3R+2)^2} & R \text{ odd} \\ \frac{1}{(3R-1)^2} & R \text{ even} \end{cases} \tag{9.299}$$

We now complete the proof of Lemma 27 using equation (9.293) and (9.299).

Case 1: $\lambda_N(G, G^{\mathbf{occ}}) \leq a$

In this case there exists a state $|\Theta\rangle \in \mathcal{I}(G, G^{\text{occ}}, N)$ satisfying

$$\langle \Theta | \sum_{w=1}^{N} (h_{\mathcal{E}^G} + h_{\mathcal{S}^G})^{(w)} + C | \Theta \rangle = a_{\text{adj}} + a_{\text{int}} \leq a, \tag{9.300}$$

From equation (9.293) we see that the state $|\Theta'\rangle \in \mathcal{I}_{\triangle}$ satisfies $\langle \Theta' | \Theta' \rangle \leq \frac{a_{\text{adj}}}{3R-1}$, and from (9.299) that it also satisfies $\langle \Theta' | C' | \Theta' \rangle \leq \frac{a_{\text{int}}}{(3R-1)^2}$.

Putting this together, (along with the fact that $|\Theta'\rangle \in \mathcal{I}_{\triangle}$ and thus is in the nullspace of $H(G^{\triangle}, N)$),

$$\langle \Theta' | H(G^{\square}, N) | \Theta' \rangle \leq \frac{a_{\text{adj}}}{3R-1} + \frac{a_{\text{int}}}{(3R-1)^2} < \frac{a_{\text{adj}}}{R} + \frac{a_{\text{int}}}{R} = \frac{a}{R}. \tag{9.301}$$

Case 2: $\lambda_N(G, G^{\mathbf{occ}}) \geq b$

In this case

$$\lambda_N(G, G^{\text{occ}}) = \min_{|\Theta\rangle \in \mathcal{I}(G, G^{\text{occ}}, N)} \langle \Theta | H(G, G^{\text{occ}}, N) | \Theta \rangle \tag{9.302}$$

$$= \min_{|\Theta\rangle \in \mathcal{I}(G, G^{\text{occ}}, N)} \langle \Theta | \sum_{w=1}^{N} (h_{\mathcal{E}^G} + h_{\mathcal{S}^G})^{(w)} | \Theta \rangle + \langle \Theta | C | \Theta \rangle \tag{9.303}$$

$$= b_{\text{adj}} + b_{\text{int}} \geq b. \tag{9.304}$$

Now applying equation (9.293) and (9.299) gives

$$\min_{|\Theta'\rangle \in \mathcal{I}_{\triangle}} \langle \Theta' | H(G^{\square}, N) | \Theta' \rangle = \min_{|\Theta'\rangle \in \mathcal{I}_{\triangle}} \langle \Theta' | \sum_{w=1}^{N} (h_{\mathcal{E}^0} + h_{\mathcal{S}^0})^{(w)} | \Theta' \rangle + \langle \Theta' | C' | \Theta' \rangle \tag{9.305}$$

$$= \frac{b_{\text{adj}}}{3R+2} + \frac{b_{\text{int}}}{(3R+2)^2} \tag{9.306}$$

$$\geq \frac{1}{(3R+2)^2} b, \tag{9.307}$$

This establishes that the nullspace of $H(G^{\square}, N)$ is empty, i.e., $\lambda_N^1(G^{\square}) > 0$, so $\lambda_N^1(G^{\square}) = \gamma(H(G^{\square}, N))$. We lower bound $\lambda_N^1(G^{\square})$ using the Nullspace Projection Lemma (Lemma 2) with

$$H_A = H(G^{\triangle}, N) \qquad H_B = \sum_{w=1}^{N} (h_{\mathcal{E}^0} + h_{\mathcal{S}^0})^{(w)} \Big|_{\mathcal{Z}_N(G^{\square})} + C' \tag{9.308}$$

and where the nullspace of H_A is $S = \mathcal{I}_\triangle$. We apply Lemma 2 and use the bounds $\gamma(H_A) > \frac{\gamma_\triangle}{R^7}$ (from Lemma 30), $\gamma(H_B|_S) \geq \frac{b}{(3R+2)^2}$ (from equation (9.307)), and

$$\|H_B\| \leq N \|h_{\mathcal{E}^0} + h_{\mathcal{S}^0}\| + \|H_{\text{int}}\| \leq 3N + d_{\mathcal{U}} N^\nu \leq d_{\mathcal{U}} R^{\nu_{\mathcal{U}}} \tag{9.309}$$

(using equations (9.75) and (9.74), the bounds on H_{int}, and the fact that $N \leq R$) to find

$$\lambda_N^1(G^\square) = \gamma(H(G^\square, N)) \tag{9.310}$$

$$\geq \frac{\gamma_\triangle b}{(3R+2)^2 R^7} \frac{1}{\frac{\gamma_\triangle}{R^7} + d_{\mathcal{U}} R^{\nu_{\mathcal{U}}}} \tag{9.311}$$

$$> \frac{\gamma_\square b}{R^{9+\nu}} \tag{9.312}$$

where $\gamma_\square$ depends only on the interaction $\mathcal{U}$, and we have our requisite bound.

9.4 Constructing the graph for a give circuit

In order to prove that bounding the ground energy of a MPQW on some graph G_X is as hard as bounding the maximal acceptance probability of a circuit $\mathcal{C}_X$, we will need to somehow relate the ground energy of G_X to the maximal acceptance probability for the circuit $\mathcal{C}_X$.

With the graphs defined in Section 9.2 and the ability to ensure that certain states are excluded from the ground space via the occupancy constraints lemma Section 9.3.1, we will be able to do this. In particular, we will show how to transform a circuit with a given form into a graph, such that the n-particle ground-energy will correspond to whether the circuit has an accepting state when certain states are excluded from the ground space.

The main idea will be to use the graph primitives of Section 9.2 to replace each gate from $\mathcal{C}_X$ with a particular gadget. By using a single particle for each qubit, and forcing each unitary to affect the first qubit, we will be able to use the location of the first particle to encode the current "time" of the occupation. Using our two-particle graph gadgets, we can then ensure that the particles move together through the entire computation (assuming that they start in the correct positions).

This construction is somewhat complicated, but we will define the graph G_X and the necessary occupancy constraints in this section. We will then prove the bound relating the acceptance probability of the circuit to the smallest eigenvalue (with the occupancy constraints) in Section 9.5.

9.4.1 Verification circuits

We take the verification circuit $\mathcal{C}_X$ that we want to simulate to be from the following universal circuit family. We will assume that $\mathcal{C}_X$ acts on $n \geq 4$ qubits and has M total gates

$$U_{\mathcal{C}_X} = U_M U_{M-1} \dots U_1, \tag{9.313}$$

where each gate U_j is a two-qubit gate acting nontrivially on the qubit labeled 1 and another qubit $s(j) \in \{2, \dots, n\}$, and is chosen from the set

$$\{\text{CNOT}_{1s(j)}, \text{CNOT}_{s(j)1}, \text{CNOT}_{1s(j)} (H \otimes \mathbb{I}), \text{CNOT}_{1s(j)} (HT \otimes \mathbb{I})\}. \tag{9.314}$$

Additionally, we will assume that no two consecutive gates (U_j and U_{j+1}) act between the same two qubits, i.e.,

$$s(j) \neq s(j+1) \qquad j \in [M-1], \tag{9.315}$$

and we assume that each qubit be involved in at least one gate.

We will think of the input state to the circuit being given to us on the qubits labeled $1, \ldots, n_{\text{in}}$, while the remaining $n - n_{\text{in}}$ qubits are each initialized to $|0\rangle$ and are used as ancilla. We will assume that the output of the circuit is contained in the state of the second qubit, as the first mediates all of the other interactions.

Note that the acceptance probability for the circuit acting on input state $|\psi_{\text{in}}\rangle \in (\mathbb{C}^2)^{\otimes n_{\text{in}}}$ is the probability that a final measurement of the output qubit in the computational basis gives the value 1:

$$\text{AP}\left(\mathcal{C}_X, |\psi_{\text{in}}\rangle\right) = \left\| |1\rangle\langle 1|^{(2)} U_{\mathcal{C}_X} |\psi_{\text{in}}\rangle |0\rangle^{\otimes n - n_{\text{in}}} \right\|^2, \tag{9.316}$$

and thus we will eventually want to ensure that the final state of qubit 2 to be 1.

We will now establish that circuits of this form are universal. We show that any quantum circuit (with $n \geq 4$ qubits) expressed using the universal gate set

$$\{\text{CNOT}, H, HT\} \tag{9.317}$$

can be efficiently rewritten in the prescribed form without increasing the number of qubits and with at most a constant factor increase in the number of gates.

First we map a circuit from the gate set (9.317) to the gate set (9.314) (without necessarily satisfying condition (9.315)). A SWAP gate between qubits 1 and k can be performed using the identity

$$\text{SWAP}_{1k} = \text{CNOT}_{1k}\text{CNOT}_{k1}\text{CNOT}_{1k}. \tag{9.318}$$

To perform a CNOT_{ik} gate between two qubits i, k (neither of which is qubit 1), we swap qubits 1 and i, apply CNOT_{1k}, and then swap back. Similarly, we can apply a single-qubit gate $U \in \{H, HT\}$ to some qubit $k \neq 1$ using the sequence of gates

$$\text{SWAP}_{1k}\text{CNOT}_{12}\left(\text{CNOT}_{12} U \otimes \mathbb{I}\right)\text{SWAP}_{1k}. \tag{9.319}$$

Applying these replacement rules, we obtain a circuit over the gate set (9.314). However, the resulting circuit will not in general satisfy equation (9.315). To enforce this condition, we insert a sequence of four gates equal to the identity, namely

$$\mathbb{I} = \text{CNOT}_{1a}\text{CNOT}_{1b}\text{CNOT}_{1a}\text{CNOT}_{1b}, \tag{9.320}$$

between any two consecutive gates U_j and U_{j+1} with $s(j) = s(j+1)$, where $a \neq b \neq s(j)$. For example,

$$\text{CNOT}_{15}\text{CNOT}_{51} \quad \longrightarrow \quad \text{CNOT}_{15}\text{CNOT}_{12}\text{CNOT}_{13}\text{CNOT}_{12}\text{CNOT}_{13}\text{CNOT}_{51}. \tag{9.321}$$

Thus we map any circuit over the gate set (9.317) into the prescribed form. Note that $n \geq 4$ is needed to ensure that any quantum circuit can be efficiently rewritten so that $s(j) \neq s(j+1)$. There do exist circuits with $n = 3$ for which our construction works, such as the example shown in Figure 9.12.

9.4.2 Gate graph for a given circuit

For any n-qubit, M-gate verification circuit $\mathcal{C}_X$ of the form described in Section 9.4.1, we associate a gate graph G_X. The gate diagram for G_X is built using the gadgets described in Section 9.2; specifically, we use M two-qubit gadgets and $2(n-1)$ boundary gadgets. Since each two-qubit gadget and each boundary gadget contains 88 diagram elements, the total number of diagram elements in G_X is $R = 88(M + 2n - 2)$.

[**TO DO:** *fix this paragraph*] We now present the construction of the gate diagram for G_X. We also describe some gate graphs obtained as intermediate steps that are used in our analysis in Section **??**. The reader may find this description easier to follow by looking ahead to Figure 9.12, which illustrates this construction for a specific 3-qubit circuit.

1. **Draw a grid** with columns labeled $j = 0, 1, \ldots, M+1$ and rows labeled $i = 1, \ldots, n$ (this grid is only used to help describe the diagram).

2. **Place gadgets in the grid to mimic the quantum circuit.** For each $j = 1, \ldots, M$, place a gadget for the two-qubit gate U_j between rows 1 and $s(j)$ in the jth column. Place boundary gadgets in rows $2, \cdots, n_{\text{in}}$ of column 0 and in rows $3, \cdots, n$ of column $M+1$. Place boundary gadgets with penalties in rows $n_{\text{in}} + 1, \cdots, n$ of column 0 and in row 2 of column $M+1$ (where this boundary gadget is upside down, so that we can penalize the 0 state). Write G_1 for the gate graph associated with the resulting diagram.

3. **Connect the nodes within each row.** First add edges connecting the nodes in rows $i = 2, \ldots, n$; call the resulting gate graph G_2. Then add edges connecting the nodes in row 1; call the resulting gate graph G_3.

4. **Add self-loops to the boundary gadgets.** In this step we add self-loops to enforce initialization of ancillas (at the beginning) and the proper output of the circuit (at the end). For each boundary gadget with penalties in column 0, add a self-loop to the unused node, giving the gate diagram for G_4. Finally, add a self-loop to the boundary gadget with penalty in row 2 and column $M+1$, giving the gate diagram for G_X.

Figure 9.12 illustrates the step-by-step construction of G_X using a simple 3-qubit circuit with four gates

$$\text{CNOT}_{12}\,(\text{CNOT}_{13} HT \otimes \mathbb{I})\,\text{CNOT}_{21}\text{CNOT}_{13}. \tag{9.322}$$

In this example, two of the qubits are input qubits (so $n_{\text{in}} = 2$), while the third qubit is an ancilla initialized to $|0\rangle$. Following the convention described in Section 9.4.1, we take qubit 2 to be the output qubit. (In this example the circuit is not meant to compute anything interesting; its only purpose is to illustrate our method of constructing a gate graph).

[**TO DO:** *fix figure!*]

We made some choices in designing this circuit-to-gate graph mapping that may seem arbitrary (e.g., we chose to place boundary gadgets in each row except the first). This is done in an attempt to balance between simplicity of description and ease of analysis, but we expect that other choices could be made to work.

9.4.2.1 Notation for G_X

We now introduce some notation that allows us to easily refer to a subset $\mathcal{L}$ of the diagram elements in the gate diagram for G_X, which will be useful for stating our occupancy constraints.

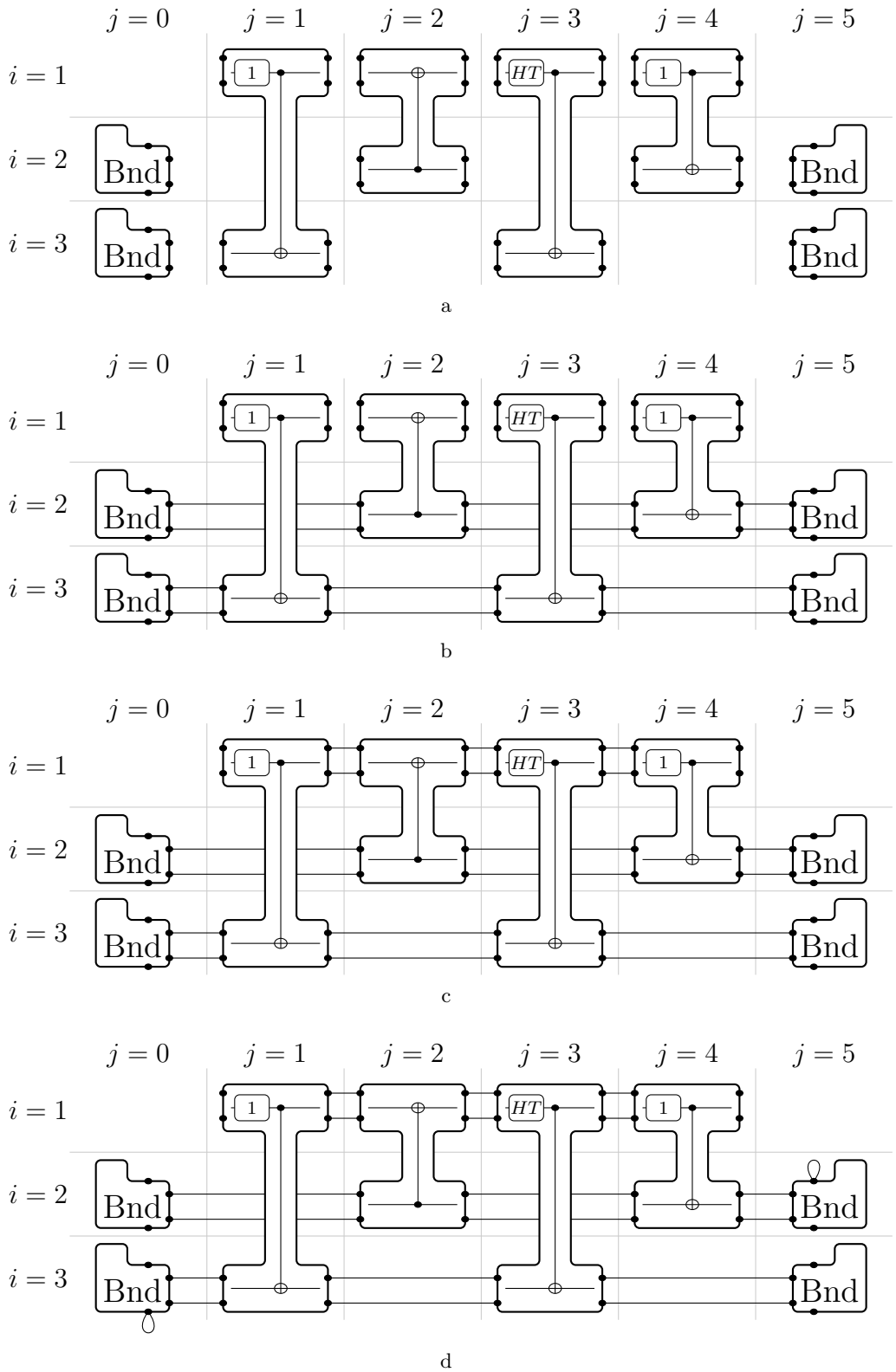

Figure 9.12: Step-by-step construction of the gate diagram for G_X for the three-qubit example circuit described in the text. (a) The gate diagram for G_1. (b) Add edges in all rows except the first to obtain the gate diagram for G_2. (c) Add edges in the first row to obtain the gate diagram for G_3. (d) Add self-loops to the boundary gadgets to obtain the gate diagram for G_X (the diagram for G_4 in this case differs from (d) by removing the self-loop in column 5; this diagram is not shown).

Recall from Section 9.2 that each two-qubit gate gadget and each boundary gadget is composed of 88 diagram elements. This can be seen by looking at Figure 9.5a and noting (from Figure 9.4) that each move-together gadget comprises 14 diagram elements.

For each of the two-qubit gate gadgets in the gate diagram for G_X, we focus our attention on the four diagram elements labeled 1–4 in Figure 9.5a. In total there are $4M$ such diagram elements in the gate diagram for G_X: in each column $j \in \{1, \ldots, M\}$ there are two in row 1 and two in row $s(j)$. When $U_j \in \{\mathrm{CNOT}_{1s(j)}, \mathrm{CNOT}_{1s(j)}\,(H \otimes \mathbb{I})\,, \mathrm{CNOT}_{1s(j)}\,(HT \otimes \mathbb{I})\}$ the diagram elements labeled $1, 2$ are in row 1 and those labeled $3, 4$ are in row $s(j)$; when $U_j = \mathrm{CNOT}_{s(j)1}$ those labeled $1, 2$ are in row $s(j)$ and those labeled $3, 4$ are in row 1. We denote these diagram elements by triples (i, j, d). Here i and j indicate (respectively) the row and column of the grid in which the diagram element is found, and d indicates whether it is the leftmost ($d = 0$) or rightmost ($d = 1$) diagram element in this row and column. We define

$$\mathcal{L}_{\mathrm{gates}} = \{(i, j, d) : i \in \{1, s(j)\},\ j \in [M],\ d \in \{0, 1\}\} \tag{9.323}$$

to be the set of all such diagram elements.

For example, in Figure 9.12 the first gate is

$$U_1 = \mathrm{CNOT}_{13}, \tag{9.324}$$

so the gadget from Figure 9.5a (with $\tilde{U} = 1$) appears between rows 1 and 3 in the first column. The diagram elements labeled $1, 2, 3, 4$ from Figure 9.5a are denoted by $(1, 1, 0), (1, 1, 1), (3, 1, 0), (3, 1, 1)$, respectively. The second gate in Figure 9.12 is $U_2 = \mathrm{CNOT}_{21}$, so the gadget from Figure 9.5a (with $\tilde{U} = 1$) appears between rows 2 and 1; in this case the diagram elements labeled $1, 2, 3, 4$ in Figure 9.5a are denoted by $(2, 2, 0), (2, 2, 1), (1, 2, 0), (1, 2, 1)$, respectively.

We also define notation for the boundary gadgets both with and without penalty in G_X. For each boundary gadget, we focus on a single diagram element, labeled 4 in Figure 9.6. For the left hand-side and right-hand side boundary gadgets, respectively, we denote these diagram elements as

$$\mathcal{L}_{\mathrm{in}} = \{(i, 0, 1) \colon i \in \{2, \ldots, n\}\} \tag{9.325}$$

$$\mathcal{L}_{\mathrm{out}} = \{(i, M + 1, 0) \colon i \in \{2, \ldots, n\}\}\,. \tag{9.326}$$

Definition 10. Let $\mathcal{L}$ be the set of diagram elements

$$\mathcal{L} = \mathcal{L}_{\mathrm{in}} \cup \mathcal{L}_{\mathrm{gates}} \cup \mathcal{L}_{\mathrm{out}} \tag{9.327}$$

where $\mathcal{L}_{\mathrm{in}}$, $\mathcal{L}_{\mathrm{gates}}$, and $\mathcal{L}_{\mathrm{out}}$ are given by equations (9.325), (9.323), and (9.326), respectively.

Finally, it is convenient to define a function F that describes horizontal movement within the rows of the gate diagram for G_X. The function F takes as input a two-qubit gate $j \in [M]$, a qubit $i \in \{2, \ldots, n\}$, and a single bit and outputs a diagram element from the set $\mathcal{L}$. If the bit is 0 then F outputs the diagram element in row i that appears in a column $0 \leq k < j$ with k maximal (i.e., the closest diagram element in row i to the left of column j):

$$F(i, j, 0) = \begin{cases} (i, k, 1) & \text{where } 1 \leq k < j \text{ is the largest } k \text{ such that } s(k) = i, \text{ if it exists} \\ (i, 0, 1) & \text{otherwise.} \end{cases} \tag{9.328}$$

On the other hand, if the bit is 1, then F outputs the diagram element in row i that appears in a column $j < k \leq M + 1$ with k minimal (i.e., the closest diagram element in row i to the right of

column j).

$$F(i,j,1) = \begin{cases} (i,k,0) & \text{where } j < k \leq M \text{ is the smallest } k \text{ such that } s(k) = j, \text{ if it exists} \\ (i, M+1, 0) & \text{otherwise.} \end{cases} \tag{9.329}$$

9.4.2.2 Occupancy constraints graph

With our explicitly defined graph G_X, we can now define an occupancy constraints graph G_X^{oc} so that the allowed multi-particle ground space on G_X encode the computation of $\mathcal{C}_X$.

We will want to encode quantum data in the locations of n particles in the graph G_X, where each particle encodes one qubit and is located in one row of the graph G_X. Since all two-qubit gates in $\mathcal{C}_X$ involve the first qubit, the location of the particle in the first row determines how far along the computation has proceeded. We design the occupancy constraints graph to ensure that low-energy states of $H(G_X, G_X^{\text{oc}}, n)$ have exactly one particle in each row (since there are n particles and n rows), and so that the particles in rows $2, \ldots, n$ are not too far behind or ahead of the particle in the first row. To avoid confusion, we emphasize that not *all* states in the subspace $\mathcal{I}(G_X, G_X^{\text{oc}}, n)$ have the desired properties—for example, there are states in this subspace with more than one particle in a given row. However, we will be able to use the Occupancy Constraints Lemma (Lemma 27) to construct a graph $G_X^{\square}$ with the correct ground space.

We now define G_X^{oc}, which is a simple graph with a vertex for each diagram element in G_X. Each edge in G_X^{oc} places a constraint on the locations of particles in G_X. The graph G_X^{oc} only has edges between diagram elements in the set $\mathcal{L}$ from Definition 10; we define the edge set $E(G_X^{\text{oc}})$ by specifying pairs of diagram elements $L_1, L_2 \in \mathcal{L}$. We also indicate (in bold) the reason for choosing the constraints, which will become clearer in Section 9.5.

1. **No two particles in the same row.** For each $i \in [n]$ we add constraints between diagram elements $(i,j,c) \in \mathcal{L}$ and $(i,k,d) \in \mathcal{L}$ in row i but in different columns, i.e.,

$$\{(i,j,c), (i,k,d)\} \in E(G_X^{\text{oc}}) \text{ whenever } j \neq k. \tag{9.330}$$

2. **Synchronization with the particle in the first row.** For each $j \in [M]$ we add constraints between row 1 and row $s(j)$:

$$\{(1,j,c), (s(j),k,d)\} \in E(G_X^{\text{oc}}) \text{ whenever } k \neq j \text{ and } (s(j),k,d) \neq F(s(j),j,c). \tag{9.331}$$

For each $j \in [M]$ we also add constraints between row 1 and rows $i \in [n] \setminus \{1, s(j)\}$:

$$\{(1,j,c), (i,k,d)\} \in E(G_X^{\text{oc}}) \text{ whenever } (i,k,d) \notin \{F(i,j,0), F(i,j,1)\}. \tag{9.332}$$

9.5 Eigenspace bounds for $H(G_X, G_X^{\text{oc}}, n)$

With our graph G_X defined for a given circuit $\mathcal{C}_X$, we will now want to relate the smallest eigenvalue of $H(G_X, G_X^{\text{oc}}, n)$ to the maximum acceptance probability of $\mathcal{C}_X$. To do this, we will investigate a sequence of Hamiltonians on graphs related to G_X (as defined in Section 9.4), namely G_1, G_2, G_3 and G_4. Each of these Hamiltonians will have a particular ground space and eigenvalue gap that is independent of the acceptance probability of $\mathcal{C}_X$, as they do not include the term in G_X that penalizes the non-accepting states.

Once we have a thorough understanding of the ground space of $H(G_4, G_X^{\text{oc}}, n)$ and the related eigenvalue gap, we will be able to relate the maximum acceptance probability of $\mathcal{C}_X$ to the smallest eigenvalue of $H(G_X, G_X^{\text{oc}}, n)$. In particular, we will prove the following theorem:

Theorem 6. *If there exists a state* $|\psi_{wit}\rangle$ *with* $\mathrm{AP}(\mathcal{C}_X, |\psi_{wit}\rangle) \geq 1 - \frac{1}{2^{|X|}}$*, then*

$$\lambda_n^1(G_X, G_X^{oc}) \leq \frac{1}{2^{|X|}}. \tag{9.333}$$

Similarly, if $\mathrm{AP}(\mathcal{C}_X, |\phi\rangle) \leq \frac{1}{3}$ *for all states* $|\phi\rangle$*, then*

$$\lambda_n^1(G_X, G_X^{oc}) \geq \frac{\mathcal{K}}{n^4 M^4}, \tag{9.334}$$

where $\mathcal{K} \in (0, 1]$ *is a constant that depends only on the interaction.*

Note that $\mathcal{K}$ is related to the eigenvalue gaps for the single-, two-, and three-particle Hamiltonians on the graph gadgets of Section 9.2.2, and this is why it depends on the particular interaction.

9.5.1 Single-particle ground-states

We begin by discussing the graphs

$$G_1, G_2, G_3, G_4, G_X \tag{9.335}$$

(as defined in Section 9.4.2; see Figure 9.12) in more detail and deriving some properties of their adjacency matrices.

The graph G_1 has a component for each of the two-qubit gates $j \in [M]$, for each of the boundary gadgets $i = 2, \ldots, n$ in column 0, and for each of the boundary gadgets $i = 2, \ldots, n$ in column $M+1$. In other words

$$G_1 = \underbrace{\left(\bigcup_{i=2}^{n_{\mathrm{in}}} G_{\mathrm{bnd}} \cup \bigcup_{i=n_{\mathrm{in}}+1}^{n_{\mathrm{in}}} G_{\mathrm{bnd,pen}} \right)}_{\text{left boundary}} \cup \underbrace{\left(\bigcup_{j=1}^{M} G_{U_j} \right)}_{\text{two-qubit gates}} \cup \underbrace{\left(G_{\mathrm{bnd,pen}} \cup \bigcup_{i=3}^{n} G_{\mathrm{bnd}} \right)}_{\text{right boundary}}. \tag{9.336}$$

We use our knowledge of the adjacency matrices of the components G_{bnd}, $G_{\mathrm{bnd,pen}}$, and G_{U_j} to understand the ground space of $A(G_1)$. Recall (from Section 9.2.2) that the smallest eigenvalue of $A(G_{U_j})$ is

$$e_1 = -1 - 3\sqrt{2} \tag{9.337}$$

(with degeneracy 16) which is also the smallest eigenvalue of $A(G_{\mathrm{bnd}})$ and $A(G_{\mathrm{bnd,pen}})$ (both with degeneracy 4). For each diagram element $L \in \mathcal{L}$ and pair of bits $z, a \in \{0, 1\}$ there is an eigenstate $|\rho_{z,a}^L\rangle$ of $A(G_1)$ with this minimal eigenvalue e_1 that has support on the diagram element L (these are the state defined in Lemma 24 and Lemma 26). In total we get sixteen eigenstates

$$|\rho_{z,a}^{(1,j,0)}\rangle, |\rho_{z,a}^{(1,j,1)}\rangle, |\rho_{z,a}^{(s(j),j,0)}\rangle, |\rho_{z,a}^{(s(j),j,1)}\rangle, \quad z, a \in \{0, 1\} \tag{9.338}$$

for each two-qubit gate $j \in [M]$, four eigenstates

$$|\rho_{z,a}^{(i,0,1)}\rangle, \quad z, a \in \{0, 1\} \tag{9.339}$$

for each boundary gadget $i \in \{2, \ldots, n\}$ in column 0, and four eigenstates

$$|\rho_{z,a}^{(i,M+1,0)}\rangle, \quad z, a \in \{0, 1\} \tag{9.340}$$

for each boundary gadget $i \in \{2, \ldots, n\}$ in column $M + 1$. The set

$$\left\{ |\rho_{z,a}^L\rangle \colon z, a \in \{0, 1\},\ L \in \mathcal{L} \right\} \tag{9.341}$$

is an orthonormal basis for the ground space of $A(G_1)$.

We write the adjacency matrices of G_2, G_3, G_4, and G_X as

$$A(G_2) = A(G_1) + h_1 \qquad A(G_4) = A(G_3) + \sum_{i=n_{\text{in}}+1}^{n} h_{\text{in},i} \tag{9.342}$$

$$A(G_3) = A(G_2) + h_2 \qquad A(G_X) = A(G_4) + h_{\text{out}}. \tag{9.343}$$

From step 3 of the construction of the gate diagram in Section 9.4.2, we see that h_1 and h_2 are both sums of terms of the form

$$\left(|q,z,t\rangle + |q',z,t'\rangle\right)\left(\langle q,z,t| + \langle q',z,t'|\right) \otimes \mathbb{I}, \tag{9.344}$$

where h_1 contains a term for each edge in rows $2,\ldots,n$ and h_2 contains a term for each of the $2(M-1)$ edges in the first row. The operators

$$h_{\text{in},i} = |(i,0,1),1,6k+2\rangle\langle(i,0,1),1,6k+2| \otimes \mathbb{I} \tag{9.345}$$

$$h_{\text{out}} = |(2,M+1,0),1,6k+2\rangle\langle(2,M+1,0),1,6k+2| \otimes \mathbb{I} \tag{9.346}$$

correspond to the self-loops added in the gate diagram in step 4 of Section 9.4.2.

We prove that G_1, G_2, G_3, G_4, and G_X are e_1-gate graphs.

Lemma 31. *The smallest eigenvalues of G_1, G_2, G_3, G_4 and G_X are*

$$\mu(G_1) = \mu(G_2) = \mu(G_3) = \mu(G_4) = \mu(G_X) = e_1. \tag{9.347}$$

Proof. We showed in the above discussion that $\mu(G_1) = e_1$. The adjacency matrices of G_2, G_3, G_4, and G_X are obtained from that of G_1 by adding positive semidefinite terms to the adjacency matrix. It therefore suffices to exhibit a groundstate $|\varrho\rangle$ of $A(G_1)$ with

$$h_1|\varrho\rangle = h_2|\varrho\rangle = h_{\text{in},i}|\varrho\rangle = h_{\text{out}}|\varrho\rangle = 0 \tag{9.348}$$

(for each $i \in \{n_{\text{in}}+1,\ldots,n\}$). There are many states $|\varrho\rangle$ satisfying these conditions; one example is

$$|\varrho\rangle = |\rho_{0,0}^{(1,1,0)}\rangle \tag{9.349}$$

which is supported on vertices where h_1, h_2, $h_{\text{in},i}$, and h_{out} have no support. □

9.5.2 Multi-particle Hamiltonian

We now outline the sequence of Hamiltonians considered in the following Sections and describe the relationships between them. As a first step, in Section **??** we exhibit a basis $\mathcal{B}_n$ for the nullspace of $H(G_1,n)$ and we prove that its smallest nonzero eigenvalue is lower bounded by a positive constant. We then discuss the restriction

$$H(G_1,G_X^{\text{oc}},n) = H(G_1,n)\big|_{\mathcal{I}(G_1,G_X^{\text{oc}},n)} \tag{9.350}$$

in Section **??**, where we prove that a subset $\mathcal{B}_{\text{legal}} \subset \mathcal{B}_n$ is a basis for the nullspace of (9.350), and that its smallest nonzero eigenvalue is also lower bounded by a positive constant.

For the remainder of the proof we use the Nullspace Projection Lemma (Lemma 2) four times, using the decompositions

$$H(G_2, G_X^{\text{oc}}, n) = H(G_1, G_X^{\text{oc}}, n) + H_1\big|_{\mathcal{I}(G_2, G_X^{\text{oc}}, n)} \tag{9.351}$$

$$H(G_3, G_X^{\text{oc}}, n) = H(G_2, G_X^{\text{oc}}, n) + H_2\big|_{\mathcal{I}(G_3, G_X^{\text{oc}}, n)} \tag{9.352}$$

$$H(G_4, G_X^{\text{oc}}, n) = H(G_3, G_X^{\text{oc}}, n) + \sum_{i=n_{\text{in}}+1}^{n} H_{\text{in},i}\big|_{\mathcal{I}(G_4, G_X^{\text{oc}}, n)} \tag{9.353}$$

$$H(G_X, G_X^{\text{oc}}, n) = H(G_4, G_X^{\text{oc}}, n) + H_{\text{out}}\big|_{\mathcal{I}(G_X, G_X^{\text{oc}}, n)} \tag{9.354}$$

where

$$H_1 = \sum_{w=1}^{n} h_1^{(w)} \qquad H_{\text{in},i} = \sum_{w=1}^{n} h_{\text{in},i}^{(w)} \qquad H_2 = \sum_{w=1}^{n} h_2^{(w)} \qquad H_{\text{out}} = \sum_{w=1}^{n} h_{\text{out}}^{(w)}$$

are all positive semidefinite, with $h_1, h_2, h_{\text{in},i}, h_{\text{out}}$ as defined in Section 9.5.1. Note that in writing equations (9.351), (9.352), (9.353), and (9.354), we have used the fact (from Lemma 31) that the adjacency matrices of the graphs we consider all have the same smallest eigenvalue e_1. Also note that

$$\mathcal{I}\left(G_i, G_X^{\text{oc}}, n\right) = \mathcal{I}\left(G_X, G_X^{\text{oc}}, n\right) \tag{9.355}$$

for $i \in [4]$ since the gate diagrams for each of the graphs G_1, G_2, G_3, G_4 and G_X have the same set of diagram elements.

Note that it looks like we forgot to include terms corresponding to the interactions resulting from the additional edges added going from G_1 to G_2 and from G_2 to G_3. However, these terms only occur between vertices in diagram elements that have been connected by the added edges, and all such pairs of diagram elements are connected in the occupancy constraints graph G_X^{oc}. As such, for all states $|\Phi\rangle \in \mathcal{I}(G_X, G_X^{\text{oc}}, n)$, these additional terms are zero, and we can exclude them from our analysis.

Let S_k be the nullspace of $H(G_k, G_X^{\text{oc}}, n)$ for $k = 1, 2, 3, 4$. Since these positive semidefinite Hamiltonians are related by adding positive semidefinite terms, their nullspaces satisfy

$$S_4 \subseteq S_3 \subseteq S_2 \subseteq S_1 \subseteq \mathcal{I}\left(G_X, G_X^{\text{oc}}, n\right). \tag{9.356}$$

We solve for $S_1 = \text{span}(\mathcal{B}_{\text{legal}})$ in Section **??** and we characterize the spaces S_2, S_3, and S_4 in Section **??** in the course of applying our strategy.

For example, to use the Nullspace Projection Lemma to lower bound the smallest nonzero eigenvalue of $H(G_2, G_X^{\text{oc}}, n)$, we consider the restriction

$$\left(H_1\big|_{\mathcal{I}(G_2, G_X^{\text{oc}}, n)}\right)\Big|_{S_1} = H_1\big|_{S_1}. \tag{9.357}$$

We also solve for S_2, which is equal to the nullspace of (9.357). To obtain the corresponding lower bounds on the smallest nonzero eigenvalues of $H(G_k, G_X^{\text{oc}}, n)$ for $k = 2, 3, 4$ and $H(G_X, G_X^{\text{oc}}, n)$, we consider restrictions

$$H_2\big|_{S_2}, \quad \sum_{i=n_{\text{in}}+1}^{n} H_{\text{in},i}\big|_{S_3}, \quad \text{and} \quad H_{\text{out}}\big|_{S_4}. \tag{9.358}$$

Analyzing these restrictions involves extensive computation of matrix elements, which is the point of this section. We first define a useful subspace and basis for these interactions, which is related to the allowed positions of the particles, but then we explicitly calculate these matrix elements. Once we have the matrix elements, we can then find the ground states for each of the Hamiltonians, and use the Nullspace Projection Lemma (Lemma 2) to calculate the various eigenvalue gaps.

9.5.3 Configurations

In this Section we use Lemma 15 to solve for the nullspace of $H(G_1, n)$, i.e., the n-particle frustration-free states on G_1. Lemma 15 describes how frustration-free states for G_1 are built out of frustration-free states for its components.

To see how this works, consider the example from Figure 9.12a. In this example, with $n = 3$, we construct a basis for the nullspace of $H(G_1, 3)$ by considering two types of eigenstates. First, there are frustration-free states

$$|\rho^{L_1}_{z_1,a_1}\rangle|\rho^{L_2}_{z_2,a_2}\rangle|\rho^{L_3}_{z_3,a_3}\rangle \tag{9.359}$$

where $L_k = (i_k, j_k, d_k) \in \mathcal{L}$ belong to different components of G_1. That is to say, $j_w \neq j_t$ unless $j_w = j_t \in \{0, 5\}$, in which case $i_w \neq i_t$ (in this case the particles are located either at the left or right boundary, in different rows of G_1). There are also frustration-free states where two of the three particles are located in the same two-qubit gadget $J \in [M]$ and one of the particles is located in a diagram element L_1 from a different component of the graph. These states have the form

$$|T^{J}_{z_1,a_1,z_2,a_2}\rangle|\rho^{L_1}_{z_3,a_3}\rangle \tag{9.360}$$

where

$$|T^{J}_{z_1,a_1,z_2,a_2}\rangle = \frac{1}{\sqrt{2}}|\rho^{(1,J,0)}_{z_1,a_1}\rangle|\rho^{(s(J),J,0)}_{z_2,a_2}\rangle + \frac{1}{\sqrt{2}}\sum_{x_1,x_2\in\{0,1\}} U_J(a_1)_{x_1x_2,z_1z_2}|\rho^{(1,J,1)}_{x_1,a_1}\rangle|\rho^{(s(J),J,1)}_{x_2,a_2}\rangle \tag{9.361}$$

and $L_1 = (i, j, k) \in \mathcal{L}$ satisfies $j \neq J$ (where we assume that the first particle is located in the first row). Each of the states (9.359) and (9.360) is specified by 6 "data" bits $z_1, z_2, z_3, a_1, a_2, a_3 \in \{0, 1\}$ and a "configuration" indicating where each of the particles are located in the graph. The configuration is specified either by three diagram elements $L_1, L_2, L_3 \in \mathcal{L}$ from different components of G_1 or by a two-qubit gate $J \in [M]$ with two integers $a \neq b \in [3]$ along with a diagram element $L_c \in \mathcal{L}$ from a different component of the graph. (Note that these configurations include the locations of each particle, but if we are looking at $d_{\max} = 0$ and the symmetrized states we only need to know the three diagram elements and not include the ordering of them as well.)

We now define the notion of a configuration for general n. Informally, we can think of an n-particle configuration as a way of placing n particles in the graph G_1 subject to the following restrictions. We first place each of the n particles in a component of the graph, with the restriction that no boundary gadget may contain more than one particle and no two-qubit gadget may contain more than two particles. For each particle on its own in a component (i.e., in a component with no other particles), we assign one of the diagram elements $L \in \mathcal{L}$ associated to that component. We therefore specify a configuration by a set of two-qubit gadgets $J_1, \ldots, J_Y$ that contain two particles, along with a set of diagram elements $L_k \in \mathcal{L}$ that give the locations of the remaining $n - 2Y$ particles, along with the permutation $\pi \in S_n$ that tells us where each particle gets placed. We choose to order the Js and the Ls so that each configuration is specified by a unique tuple $(J_1, \ldots, J_Y, L_1, \ldots, L_{n-2Y}, \pi)$. For concreteness, we use the lexicographic order on diagram elements in the set $\mathcal{L}$: $L_A = (i_A, j_A, d_A)$ and $L_B = (i_B, j_B, d_B)$ satisfy $L_A < L_B$ iff either $i_A < i_B$, or $i_A = i_B$ and $j_A < j_B$, or $(i_A, j_A) = (i_B, j_B)$ and $d_A < d_B$. We also have that the two particles in each J_i are given by $(\pi(2i - 1), \pi(2i))$, while the particle on L_i is given by $\pi(2Y + i)$.

Definition 11 (Configuration). An n-particle configuration on the gate graph G_1 is a tuple

$$(J_1, \ldots, J_Y, L_1, \ldots, L_{n-2Y}, \pi) \tag{9.362}$$

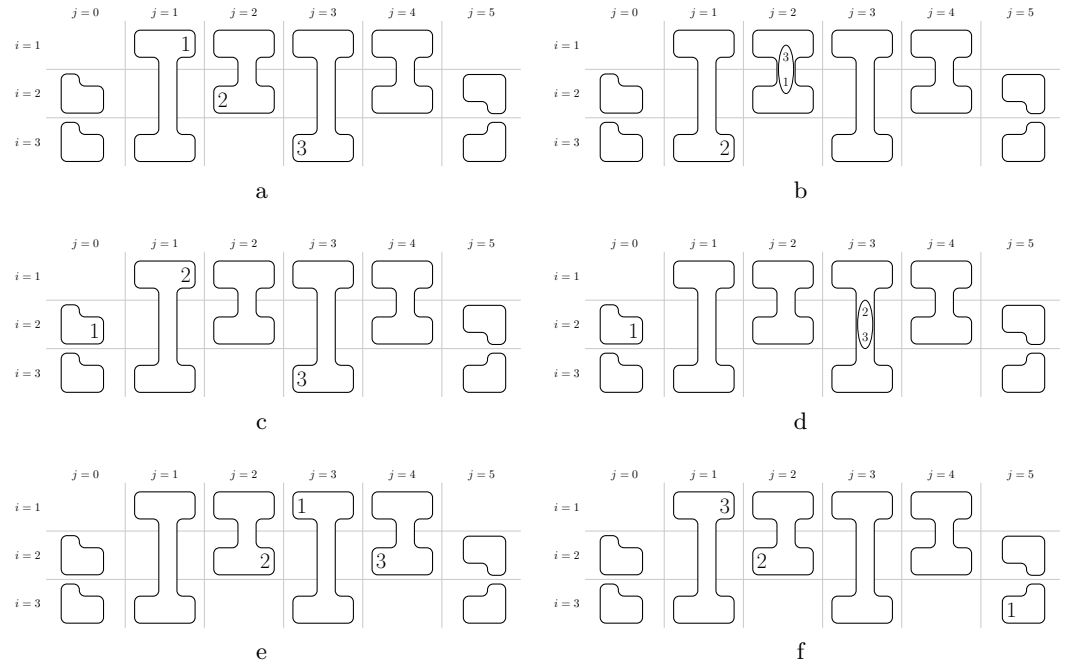

Figure 9.13: Diagrammatic depictions of configurations for the example where G_1 is the gate graph from Figure 9.12a. The Figures show the locations of each of the three particles in the gate graph. The number in the figure indicates a single-particle state corresponding to that particle and the two numbers within an ellipse corresponds to a two-particle state, with the top particle corresponding to the first particle. (a) $((1,1,1),(2,2,0),(3,3,0),123)$. (b) $(2,(3,1,1),312)$. (c) $((1,1,1),(2,0,1),(3,3,0),213)$. (d) $(3,(2,0,1),231)$. (e) $((1,3,0),(2,2,1),(2,4,0),123)$. (f) $((1,1,1),(2,2,0),(3,5,0),321)$.

with $Y \in \{0, \ldots, \lfloor \frac{n}{2} \rfloor\}$, ordered integers

$$1 \leq J_1 < J_2 < \cdots < J_Y \leq M, \tag{9.363}$$

lexicographically ordered diagram elements

$$L_1 < L_2 < \cdots < L_{n-2Y}, \qquad L_k = (i_k, j_k, d_k) \in \mathcal{L}, \tag{9.364}$$

and a permutation

$$\pi \in S_n. \tag{9.365}$$

We further require that each L_k is from a different component of G_1, i.e.,

$$j_w = j_t \quad \Longrightarrow \quad j_w \in \{0, M+1\} \text{ and } i_w \neq i_t, \tag{9.366}$$

and we require that $j_u \neq J_v$ for all $u \in [n-2Y]$ and $v \in [Y]$.

In Figure 9.13 we give some examples of configurations (for the example from Figure 9.12a with $n = 3$) and we introduce a diagrammatic notation for them.

For any configuration and n-bit strings $\vec{z}$ and $\vec{a}$, there is a state in the nullspace of $H(G_1, n)$, given by

$$V_\pi |T^{J_1}_{z_1,a_1,z_2,a_2}\rangle \ldots |T^{J_Y}_{z_{2Y-1},a_{2Y-1},z_{2Y},a_{2Y}}\rangle |\rho^{L_1}_{z_{2Y+1},a_{2Y+1}}\rangle \ldots |\rho^{L_{n-2Y}}_{z_n,a_n}\rangle, \tag{9.367}$$

where V_π permutes the particles according to the permutation π, so that they are in the location given by the configuration. The ordering in the definition of a configuration ensures that each distinct choice of configuration and n-bit strings $\vec{z}, \vec{a}$ gives a different state.

Definition 12. Let $\mathcal{B}_n$ be the set of all states of the form (9.367), where $(J_1, \ldots, J_Y, L_1, \ldots, L_{n-2Y}, \pi)$ is a configuration and $\vec{z}, \vec{a} \in \{0,1\}^n$ if $d_{\max} > 0$, and let $\mathcal{B}_n$ be the corresponding symmetric subspace if $d_{\max} = 0$.

Note that from this point on, the proofs assume that $d_{\max} > 0$, and in particular that each of the particles are distinguishable and have a fixed location. The proofs all rely on the various lemmas corresponding to the multi-particle ground states of the gadgets from Section 9.2.2, which form most $d_{\max}$ does not require the symmetric subspace. However, it will turn out that all of our results are independent of the particular $\pi \in S_n$ used in the configuration, and thus the same results hold if we originally assumed that the states in $\mathcal{B}_n$ consisted of the uniform superposition of configuration states that only differ in the permutation. As these states span the symmetric subspace of $\mathcal{B}_n$ (due to the occupancy constraints), everything works the same for interactions with $d_{\max} = 0$.

Lemma 32. *The set $\mathcal{B}_n$ is an orthonormal basis for the nullspace of $H(G_1, n)$. Furthermore,*

$$\gamma(H(G_1, n)) \geq \mathcal{K}_0 \tag{9.368}$$

where $\mathcal{K}_0 \in (0, 1]$ is a constant that only depends on the interaction.

Proof. Each component of G_1 is either a two-qubit gadget or a boundary gadget (see equation (9.336)). The single-particle states of $A(G_1)$ with energy e_1 are the states $|\rho^L_{z,a}\rangle$ for $L \in \mathcal{L}$ and $z, a \in \{0,1\}$, as discussed in Section 9.5.1. Each of these states has support on only one component of G_1. In addition, G_1 has two two-particle frustration-free states for each two-qubit gadget $J \in [M]$ and bits z, a, x, b, namely $|T^J_{z,a,x,b}\rangle$ for each particle acting as the control. Furthermore, no

component of G_1 has any three- (or more) particle frustration-free states. Using these facts and applying Lemma 15, we see that $\mathcal{B}_n$ spans the nullspace of $H(G_1, n)$.

Lemma 15 also expresses each eigenvalue of $H(G_1, n)$ as a sum of eigenvalues for its components. We use this fact to obtain the desired lower bound on the smallest nonzero eigenvalue. Our analysis proceeds on a case-by-case basis, depending on the occupation numbers for each component of G_1 (the values $N_1, \ldots, N_k$ in Lemma 15).

First consider any set of occupation numbers where some two-qubit gate gadget $J \in [M]$ contains 3 or more particles. By Lemma **??** and Lemma 15, any such eigenvalue is at least $\lambda_3^1(G_{U_J})$, which is a positive constant by Lemma 24. Next consider a case where some boundary gadget contains more than one particle. The corresponding eigenvalues are similarly lower bounded by $\lambda_2^1(G_{\text{bnd}})$, which is also a positive constant by Lemma 26. Finally, consider a set of occupation numbers where each two-qubit gadget contains at most two particles and each boundary gadget contains at most one particle. The smallest eigenvalue with such a set of occupation numbers is zero. The smallest nonzero eigenvalue is either

$$\gamma(H(G_{U_J}, 1)),\ \gamma(H(G_{U_J}, 2)) \text{ for some } J \in [M], \text{ or } \gamma(H(G_{\text{bnd}}, 1)). \tag{9.369}$$

However, these quantities are at least some positive constant since $H(G_{U_J}, 1)$, $H(G_{U_J}, 2)$, and $H(G_{\text{bnd}}, 1)$ are nonzero constant-sized positive semidefinite matrices.

Now combining the lower bounds discussed above and using the fact that, for each $J \in [M]$, the two-qubit gate U_J is chosen from a fixed finite gate set (given in (9.314)), we see that $\gamma(H(G_1, n))$ is lower bounded by the positive constant

$$\min\{\lambda_3^1(G_U), \lambda_2^1(G_{\text{bnd,pen}}), \gamma(H(G_U, 1)), \gamma(H(G_U, 2)), \gamma(H(G_{\text{bnd,pen}}, 1)) : U \in (9.314)\}. \tag{9.370}$$

The condition $\mathcal{K}_0 \leq 1$ can be ensured by setting $\mathcal{K}_0$ to be the minimum of 1 and (9.370). □

Note that the constant $\mathcal{K}_0$ can in principle be computed using (9.370): each quantity on the right-hand side can be evaluated by diagonalizing a specific finite-dimensional matrix.

9.5.3.1 Legal configurations

In this section we define a subset of the n-particle configurations that we call legal configurations, and we prove that the subset of the basis vectors in $\mathcal{B}_n$ that have legal configurations spans the nullspace of $H(G_1, G_X^{\text{oc}}, n)$.

We begin by specifying the set of legal configurations. Every legal configuration

$$(J_1, \ldots, J_Y, L_1, \ldots, L_{n-2Y}, \pi) \tag{9.371}$$

has $Y \in \{0, 1\}$. The legal configurations with $Y = 0$ are

$$((1, j, d_1), F(2, j, d_2), F(3, j, d_3), \ldots, F(n, j, d_n), \pi) \tag{9.372}$$

where $j \in [M]$ and where $\vec{d} = (d_1, \ldots, d_n)$ satisfies $d_i \in \{0, 1\}$ and $d_1 = d_{s(j)}$. (Recall that the function F, defined in equations (9.328) and (9.329), describes horizontal movement of particles.) The legal configurations with $Y = 1$ are

$$(j, F(2, j, d_2), \ldots, F(s(j) - 1, j, d_{s(j)-1}), F(s(j) + 1, j, d_{s(j)+1}), \ldots, F(n, j, d_n), \pi) \tag{9.373}$$

where $j \in \{1, \ldots, M\}$ and $d_i \in \{0, 1\}$ for $i \in [n] \setminus \{1, s(j)\}$. Although the values d_1 and $d_{s(j)}$ are not used in equation (9.373), we choose to set them to

$$d_1 = d_{s(j)} = 2 \tag{9.374}$$

for any legal configuration with $Y = 1$. In this way we identify the set of legal configurations with the set of triples $j, \vec{d}, \pi$ with $j \in [M]$,

$$\vec{d} = (d_1, d_2, d_3, \ldots, d_n) \tag{9.375}$$

and $\pi \in S_n$, satisfying

$$d_1 = d_{s(j)} \in \{0, 1, 2\} \quad \text{and} \quad d_i \in \{0, 1\} \text{ for } i \notin \{1, s(j)\}. \tag{9.376}$$

The legal configuration is given by equation (9.372) if $d_1 = d_{s(j)} \in \{0, 1\}$ and equation (9.373) if $d_1 = d_{s(j)} = 2$. Note that the permutation does not effect whether a given configuration is legal or not; this makes sense as whether a given configuration violates the occupancy constraints does not depend on the particular location of each particle, only on the locations of all particles.

The examples in Figures 9.13a, (b), and (c) show legal configurations whereas the examples in Figures 9.13d, (e), and (f) are illegal. The legal examples correspond to $j = 1$, $\vec{d} = (1, 1, 1)$, $\pi = 123$; $j = 2$, $\vec{d} = (2, 2, 0)$, $\pi = 312$; and $j = 1$, $\vec{d} = (1, 0, 1)$, $\pi = 213$, respectively. We now explain why the other examples are illegal. Looking at (9.373), we see that the configuration $(3, (2, 0, 1), 231)$ depicted in Figure 9.13d is illegal since $F(2, 3, 0) = (2, 2, 1) \neq (2, 0, 1)$ and $F(2, 3, 1) = (2, 4, 0) \neq (2, 0, 1)$. The configuration in Figure 9.13e is illegal since there are two particles in the same row. Looking at equation (9.372), we see that the configuration $((1, 1, 1), (2, 2, 0), (3, 5, 0), 321)$ in Figure 9.13f is illegal since $(3, 5, 0) \notin \{F(3, 1, 0), F(3, 1, 1)\} = \{(3, 0, 1), (3, 3, 0)\}$.

With this intuition behind legal and illegal configurations, it will be useful to have some conditions for a particular configuration to be illegal. As such, we will us the following lemma.

Lemma 33. *For any illegal configuration*

$$(J_1, \ldots, J_Y, L_1, \ldots, L_{n-2Y}, \pi) \tag{9.377}$$

there exist diagram elements $\{Q_1, Q_2\} \in E(G_X^{occ})$ *satisfying at least one of the following conditions:*

(i) $Q_1 = (1, J_k, 0)$ *and* $Q_2 = (1, J_l, 0)$ *for some* $k, l \in [Y]$.

(ii) $Y \in \{0, 1\}$, $Q_1 = L_s$, *and* $Q_2 = L_t$ *for some* $s, t \in [n - 2Y]$.

(iii) $Y = 1$ *and* $Q_1 = (i, J_1, d)$ *and* $Q_2 = L_t$ *for some* $i \in \{1, s(J_1)\}$, $t \in [n - 2]$ *and* $d \in \{0, 1\}$.

Proof. We prove the contrapositive: we suppose the configuration (9.377) violates each of the conditions (i), (ii), and (iii) for all $\{Q_1, Q_2\} \in E(G_X^{occ})$ and show it is a legal configuration.

From part (1) of the definition of the occupancy constraints graph in Section 9.4.2.2, we see that

$$\{(1, j, 0), (1, k, 0)\} \in E(G_X^{occ}) \tag{9.378}$$

for all $j, k \in [M]$ with $j \neq k$. If the configuration (9.377) has $Y \geq 2$, then we may choose $Q_1 = (1, J_1, 0)$ and $Q_2 = (1, J_2, 0)$ so that $\{Q_1, Q_2\} \in E(G_X^{occ})$ and condition (i) is satisfied (note $J_1 \neq J_2$ follows from the definition of a configuration). Since by assumption, (9.377) violates condition (i) for all $\{Q_1, Q_2\} \in E(G_X^{occ})$, this implies that $Y \in \{0, 1\}$. We consider the cases $Y = 0$ and $Y = 1$ separately.

First suppose $Y = 0$, so (9.377) is equal to

$$(L_1, \ldots, L_n, \pi). \tag{9.379}$$

Since (ii) is violated, $\{L_s, L_t\} \notin E(G_X^{occ})$ for all $s, t \in [n]$. Using part (1) of the definition of G_X^{occ} and the definition of a configuration, this implies that each diagram element is in a different row,

i.e., $L_i = (i, j_i, c_i)$ for each $i \in [n]$. From part (2) of the definition of G_X^{occ}, we see in particular that $\{L_1, L_t\} \notin E(G_X^{\text{occ}})$ for each $t \in \{2, \ldots, n\}$ implies

$$L_{s(j_1)} = (s(j_1), j_1, c_1) \quad \text{and} \quad L_i = F(i, j_1, d_i) \tag{9.380}$$

for $i \in [n] \setminus \{1, s(j_1)\}$ and bits $d_2, \ldots, d_n \in \{0, 1\}$, i.e., the configuration is legal.

Now suppose $Y = 1$, so (9.377) is

$$(J_1, L_1, \ldots, L_{n-2}, \pi). \tag{9.381}$$

Since (ii) is violated, each L_i for $i \in [n-2]$ is from a different row. Since (iii) is violated, none of these diagram elements are in rows 1 or $s(J_1)$. Now applying part (2) of the definition of G_X^{occ}, we see that the configuration is legal:

$$(J_1, L_1, \ldots, L_{n-2}, \pi) \tag{9.382}$$

$$= (J_1, F(2, J_1, d_2), \ldots, F(s(J_1) - 1, J_1, d_{s(J_1)-1}), F(s(J_1) + 1, J_1, d_{s(J_1)+1}), \ldots, F(n, J_1, d_n), \pi) \tag{9.383}$$

where $d_i \in \{0, 1\}$ for $i \in [n] \setminus \{1, s(J_1)\}$. □

9.5.4 Legal configuration basis

With our legal and illegal configurations defined, we will want to translate this back into an understanding of the ground space for the relevant graphs, by identifying the subset of basis vectors $\mathcal{B}_{\text{legal}} \subset \mathcal{B}_n$ that have legal configurations. We write each such basis vector as

$$|j, \vec{d}, \vec{z}, \vec{a}, \pi\rangle = \begin{cases} V_\pi \left(|\rho_{z_1,a_1}^{(1,j,d_1)}\rangle \bigotimes_{i=2}^{n} |\rho_{z_i,a_i}^{F(i,j,d_i)}\rangle \right) & d_1 = d_{s(j)} \in \{0, 1\} \\ V_\pi \left(|T_{z_1,a_1,z_{s(j)},a_{s(j)}}^{j}\rangle \bigotimes_{\substack{i=2 \\ i \neq s(j)}}^{n} |\rho_{z_i,a_i}^{F(i,j,d_i)}\rangle \right) & d_1 = d_{s(j)} = 2 \end{cases} \tag{9.384}$$

where $j, \vec{d}, \pi$ specifies the legal configuration and $\vec{z}$,$\vec{a} \in \{0, 1\}^n$. (Note that the bits in $\vec{z}$ and $\vec{a}$ are ordered slightly differently than in equation (9.367); here the labeling reflects the indices of the encoded qubits). Additionally, we have that V_π places the particular particles into the correct locations.

Definition 13. Let

$$\mathcal{B}_{\text{legal}} = \big\{ |j, \vec{d}, \vec{z}, \vec{a}, \pi\rangle : j \in [M],\ d_1 = d_{s(j)} \in \{0, 1, 2\},\ d_i \in \{0, 1\} \text{ for } i \notin \{1, s(j)\}, \\ \vec{z}, \vec{a} \in \{0, 1\}^n, \pi \in S_n \big\} \tag{9.385}$$

and $\mathcal{B}_{\text{illegal}} = \mathcal{B}_n \setminus \mathcal{B}_{\text{illegal}}$.

The basis $\mathcal{B}_n = \mathcal{B}_{\text{legal}} \cup \mathcal{B}_{\text{illegal}}$ is convenient when considering the restriction to the subspace $\mathcal{I}(G_1, G_X^{\text{oc}}, n)$. Letting Π_0 be the projector onto $\mathcal{I}(G_1, G_X^{\text{oc}}, n)$, the following Lemma shows that the restriction

$$\Pi_0 \big|_{\text{span}(\mathcal{B}_n)} \tag{9.386}$$

is diagonal in the basis $\mathcal{B}_n$. The Lemma also bounds the diagonal entries for the illegal states.

Lemma 34. *Let Π_0 be the projector onto $\mathcal{I}(G_1, G_X^{oc}, n)$. For any $|j, \vec{d}, \vec{z}, \vec{a}, \pi\rangle \in \mathcal{B}_{legal}$, we have*

$$\Pi_0 |j, \vec{d}, \vec{z}, \vec{a}, \pi\rangle = |j, \vec{d}, \vec{z}, \vec{a}, \pi\rangle. \tag{9.387}$$

Furthermore, for any two distinct basis vectors $|\phi\rangle, |\psi\rangle \in \mathcal{B}_{illegal}$, we have

$$\langle\phi|\Pi_0|\phi\rangle \leq \frac{899}{900} \tag{9.388}$$

$$\langle\phi|\Pi_0|\psi\rangle = 0. \tag{9.389}$$

Proof. We begin with equation (9.387). Recall from (9.185) that

$$\mathcal{I}(G_1, G_X^{\text{occ}}, n) = \text{span}\{|\psi^{q_1}_{z_1,a_1}\rangle|\psi^{q_2}_{z_2,a_2}\rangle \dots |\psi^{q_n}_{z_n,a_n}\rangle \colon z_i, a_i \in \mathbb{F}_2,\ q_i \neq q_j, \text{ and } \{q_i, q_j\} \notin E(G_X^{\text{occ}})\} \tag{9.390}$$

which can alternatively be characterized as the subspace of

$$\mathcal{I}(G_1, n) = \text{span}\{|\psi^{q_1}_{z_1,a_1}\rangle|\psi^{q_2}_{z_2,a_2}\rangle \dots |\psi^{q_n}_{z_n,a_n}\rangle \colon z_i, a_i \in \mathbb{F}_2,\ q_i \neq q_j\} \tag{9.391}$$

consisting of zero eigenvectors of each of the operators

$$V_\pi |\psi^q_{s,t}\rangle\langle\psi^q_{s,t}| \otimes |\psi^r_{u,v}\rangle\langle\psi^r_{u,v}| \otimes \mathbb{I}^{\otimes n-2} V_\pi^\dagger, \qquad \{q, r\} \in E(G_X^{\text{occ}}), \quad s, t, u, v \in \mathbb{F}_2, \qquad \pi \in S_n. \tag{9.392}$$

Now using equation (9.384) and the fact that

$$\langle\psi^{\tilde{L}}_{x,b}|\rho^L_{z,a}\rangle = \frac{1}{\sqrt{15}}\delta_{\tilde{L},L}\delta_{x,z}\delta_{a,b} = \frac{1}{\sqrt{15}}\langle\rho^{\tilde{L}}_{x,b}|\rho^L_{z,a}\rangle \tag{9.393}$$

for all $x, z, a, b \in \mathbb{F}_2$ and $\tilde{L}, L \in \mathcal{L}$ (from Lemma 24 and Lemma 26), we get

$$\langle j, \vec{d}, \vec{z}, \vec{a}, \pi| V_\sigma \left(|\psi^q_{s,t}\rangle\langle\psi^q_{s,t}| \otimes |\psi^r_{u,v}\rangle\langle\psi^r_{u,v}| \otimes \mathbb{I}^{\otimes n-2}\right) V_\sigma^\dagger |j, \vec{d}, \vec{z}, \vec{a}, \pi\rangle \tag{9.394}$$

$$= \frac{1}{225}\langle j, \vec{d}, \vec{z}, \vec{a}, \sigma^{-1}\pi| \left(|\rho^q_{s,t}\rangle\langle\rho^q_{s,t}| \otimes |\rho^r_{u,v}\rangle\langle\rho^r_{u,v}| \otimes \mathbb{I}^{\otimes n-2}\right) |j, \vec{d}, \vec{z}, \vec{a}, \sigma^{-1}\pi\rangle \tag{9.395}$$

$$= 0 \quad \text{if } \{q, r\} \in E(G_X^{\text{occ}}). \tag{9.396}$$

In the last line we used equations (9.361) and (9.384) and the definition of the occupancy constraints graph G_X^{occ} from Section 9.4.2.2. Hence each legal state $|j, \vec{d}, \vec{z}, \vec{a}, \pi\rangle \in \mathcal{I}(G_1, n)$ is a zero eigenvector of each of the operators (9.392), so $|j, \vec{d}, \vec{z}, \vec{a}, \pi\rangle \in \mathcal{I}(G_1, G_X^{\text{occ}}, n)$. This gives equation (9.387).

Now we prove equation (9.388). For each illegal configuration we associate two diagram elements Q_1 and Q_2 with $(Q_1, Q_2) \in E(G_X^{\text{occ}})$ as in Lemma 33 (if there is more than one such pair we fix a specific choice). Likewise for each basis vector $|\phi\rangle \in \mathcal{B}_{\text{illegal}}$ we associate the two diagram elements Q_1 and Q_2 corresponding to its (illegal) configuration. Let P_ϕ be the projector onto the space

$$\text{span}\{V_\pi V_{(1,q_1)(2,q_2)} |\psi^{Q_1}_{z_1,a_1}\rangle|\psi^{Q_2}_{z_2,a_2}\rangle|\psi^{q_3}_{z_3,a_3}\rangle \dots |\psi^{q_n}_{z_n,a_n}\rangle \colon z_i, a_i \in \{0, 1\},\ q_i \notin \{Q_1, Q_2\}\} \tag{9.397}$$

where (exactly) one particle is located at Q_1 and (exactly) one particle is located at Q_2, where $\pi \in S_n$ is the permutation in the state $|\phi\rangle$, and where the unitary $V_{(1,q_1)(2,q_2)}$ permutes the underlying particles, so that the two states supported in diagram element Q_1 and Q_2 get moved to the same particle as in the vector $|\phi\rangle$. We show that

$$\langle\phi|P_\phi|\phi\rangle \geq \frac{1}{900}. \tag{9.398}$$

Note that $\Pi_0 P_\phi = 0$ since Π_0 projects onto a subspace for which no two (or more) particles are simultaneously located at Q_1 and Q_2. Therefore

$$\langle\phi|\Pi_0|\phi\rangle + \langle\phi|P_\phi|\phi\rangle \leq 1, \tag{9.399}$$

and applying (9.398) gives (9.387). Equation (9.398) can be shown by considering cases (i), (ii), and (iii) from Lemma 33. It is convenient to define

$$\Pi_{Q_1} = \sum_{x,y\in\{0,1\}} |\psi^{Q_1}_{x,y}\rangle\langle\psi^{Q_1}_{x,y}| \qquad\qquad \Pi_{Q_2} = \sum_{x,y\in\{0,1\}} |\psi^{Q_2}_{x,y}\rangle\langle\psi^{Q_2}_{x,y}|. \tag{9.400}$$

In case (i) we have $Q_1 = (1, J_k, 0)$ and $Q_2 = (1, J_l, 0)$ for some $k, l \in [Y]$. Here we consider the case $k = 1, l = 2$ without loss of generality. Then

$$P_\phi|\phi\rangle = P_\phi V_\pi\big((|T^{J_1}_{z_1,a_1,z_2,a_2}\rangle|T^{J_2}_{z_3,a_3,z_4,a_4}\rangle\dots|T^{J_Y}_{z_{2Y-1},a_{2Y-1},z_{2Y},a_{2Y}}\rangle|\rho^{L_1}_{z_{2Y+1},a_{2Y+1}}\rangle\dots|\rho^{L_{n-2Y}}_{z_n,a_n}\rangle)\big) \tag{9.401}$$

$$= V_\pi\big((\Pi_{Q_1}\otimes\mathbb{I})|T^{J_1}_{z_1,a_1,z_2,a_2}\rangle(\Pi_{Q_2}\otimes\mathbb{I})|T^{J_2}_{z_3,a_3,z_4,a_4}\rangle\dots|T^{J_Y}_{z_{2Y-1},a_{2Y-1},z_{2Y},a_{2Y}}\rangle \otimes|\rho^{L_1}_{z_{2Y+1},a_{2Y+1}}\rangle\dots|\rho^{L_{n-2Y}}_{z_n,a_n}\rangle\big) \tag{9.402}$$

for some configuration and some $\vec{z}, \vec{a}$. From this, we then have that

$$\langle\phi|P_\phi|\phi\rangle = \langle T^{J_1}_{z_1,a_1,z_2,a_2}|\,(\Pi_{Q_1}\otimes\mathbb{I})\,|T^{J_1}_{z_1,a_1,z_2,a_2}\rangle\cdot\langle T^{J_2}_{z_3,a_3,z_4,a_4}|\,(\Pi_{Q_2}\otimes\mathbb{I})\,|T^{J_2}_{z_3,a_3,z_4,a_4}\rangle \tag{9.403}$$

$$= \left(\frac{1}{2}\langle\rho^{(1,J_1,0)}_{z_1,a_1}|\langle\rho^{(s(J_1),J_1,0)}_{z_2,a_2}|\Pi_{Q_1}\otimes\mathbb{I}|\rho^{(1,J_1,0)}_{z_1,a_1}\rangle|\rho^{(s(J_1),J_1,0)}_{z_2,a_2}\rangle\right)^2 \tag{9.404}$$

$$= \left(\frac{1}{30}\right)^2 = \frac{1}{900}. \tag{9.405}$$

where in the second line we used the fact that both terms in the product are equal and in the third line we used equation (9.393).

In case (ii) we have $Y \in \{0, 1\}$ and $Q_1 = L_s$, $Q_2 = L_t$ for some $s, t \in [n - 2Y]$. By a similar argument as in (9.402),

$$\langle\phi|P_\phi|\phi\rangle = \langle\rho^{L_s}_{z_s a_s}|\Pi_{Q_1}|\rho^{L_s}_{z_s,a_s}\rangle\cdot\langle\rho^{L_t}_{z_t a_t}|\Pi_{Q_2}|\rho^{L_t}_{z_t,a_t}\rangle = \frac{1}{15}\cdot\frac{1}{15} = \frac{1}{225}. \tag{9.406}$$

In case (iii) we have $Y = 1$, $Q_1 = (i, J_1, d)$, and $Q_2 = L_t$ for some $i \in \{1, s(J_1)\}$, $t \in [n - 2]$, and $d \in \{0, 1\}$. If $i = 1$ then, again by a similar reasoning as in (9.402),

$$\langle\phi|P_\phi|\phi\rangle = \langle T^{J_1}_{z_1,a_1,z_2,a_2}|\Pi_{Q_1}\otimes\mathbb{I}|T^{J_1}_{z_1,a_1,z_2,a_2}\rangle\cdot\langle\rho^{L_t}_{z_{2Y+t}a_{2Y+t}}|\Pi_{Q_2}|\rho^{L_t}_{z_{2Y+t}a_{2Y+t}}\rangle \tag{9.407}$$

$$= \frac{1}{30}\cdot\frac{1}{15} = \frac{1}{450}. \tag{9.408}$$

If $i = s(J_1)$ then $\Pi_{Q_1}\otimes\mathbb{I}$ should be replaced with $\mathbb{I}\otimes\Pi_{Q_1}$ in (9.407) but the lower bound in (9.408) is the same.

From equations (9.405), (9.406), and (9.408), we see that equation (9.398) holds in cases (i), (ii), and (iii), respectively, thereby establishing (9.388).

Finally, we prove equation (9.389), showing that $\Pi_0|_{\mathrm{span}(\mathcal{B}_n)}$ is diagonal in the basis $\mathcal{B}_n$. Let

$$|\phi\rangle = V_\pi(|T^{J_1}_{z_1,a_1,z_2,a_2}\rangle\dots|T^{J_Y}_{z_{2Y-1},a_{2Y}-1,z_{2Y},a_{2Y}}\rangle|\rho^{L_1}_{z_{2Y+1},a_{2Y+1}}\rangle\dots|\rho^{L_{n-2Y}}_{z_n,a_n}\rangle) \tag{9.409}$$

$$|\psi\rangle = V_\sigma(|T^{\tilde{J}_1}_{x_1,b_1,x_2,b_2}\rangle\dots|T^{\tilde{J}_K}_{x_{2K-1},b_{2K}-1,x_{2K},b_{2K}}\rangle|\rho^{\tilde{L}_1}_{x_{2K+1},b_{2K+1}}\rangle\dots|\rho^{\tilde{L}_{n-2K}}_{x_n,b_n}\rangle) \tag{9.410}$$

be distinct vectors from $\mathcal{B}_n$ (note it is possible that $K = 0$ or $Y = 0$ or both).

Note that $\Pi_0 V_\sigma = V_\sigma \Pi_0$, since a configuration's legality does not depend on which particles occupy a given location. As such, we have that

$$\langle \psi | \Pi_0 | \phi \rangle = \langle \psi | V_\sigma \Pi_0 V_\sigma^\dagger V_\pi \Pi_0 V_\pi^\dagger | \phi \rangle. \tag{9.411}$$

Note that the particles in $V_\pi^\dagger | \phi \rangle$ and $V_\sigma^\dagger | \psi \rangle$ all follow the lexicographic ordering of the underlying configuration, and thus the support of the particles has the same ordering. If $\pi \neq \sigma$, then we have that $V_\sigma^\dagger V_\pi \neq \mathbb{I}$ and the operation changes the order of the particles away from the lexicographic ordering. Hence, if $\pi \neq \sigma$, we have that

$$| \psi \rangle \Pi_0 | \phi \rangle = 0 \tag{9.412}$$

as expected.

Now let us assume that $\pi = \sigma = ()$, and expand each of the $|T\rangle$ states using equation (9.361), which we can also write as

$$|T^J_{z,a,y,b}\rangle = \frac{1}{\sqrt{2}} \sum_{c=0}^{1} U_J(a)^c |\rho^{(1,J,c)}_{z,a}\rangle |\rho^{(s(J),J,c)}_{y,b}\rangle \tag{9.413}$$

where we use the shorthand

$$U_J(a) |\rho^{(1,J,1)}_{z,a}\rangle |\rho^{(s(J),J,1)}_{y,b}\rangle = \sum_{x_1,x_2 \in \mathbb{F}_2} U_J(a)_{x_1 x_2, zy} |\rho^{(1,J,1)}_{x_1,a}\rangle |\rho^{(s(J),J,1)}_{x_2,b}\rangle. \tag{9.414}$$

For the state $|\phi\rangle$, this gives the expansion

$$|\phi\rangle = \left(\frac{1}{\sqrt{2}}\right)^Y \sum_{c_1,\ldots,c_Y \in \mathbb{F}_2} |O^{(J_1,\ldots,J_Y,L_1,\ldots,L_{n-2Y}),(c_1,\ldots,c_Y)}_{\vec{z},\vec{a}}\rangle \tag{9.415}$$

where

$$\begin{aligned} &|O^{(J_1,\ldots,J_Y,L_1,\ldots,L_{n-2Y}),(c_1,\ldots,c_Y)}_{\vec{z},\vec{a}}\rangle \\ &\quad = \left(\bigotimes_{i=1}^{Y} U_{J_i}(a_{2i-1})^{c_i} |\rho^{(1,J_i,c_i)}_{z_{2i-1},a_{2i-1}}\rangle |\rho^{(s(J_i),J_i,c_i)}_{z_{2i},a_{2i}}\rangle \right) |\rho^{L_1}_{z_{2Y+1},a_{2Y+1}}\rangle \ldots |\rho^{L_{n-2Y}}_{z_n,a_n}\rangle. \end{aligned} \tag{9.416}$$

Define the projector

$$P^1_{\mathcal{L}} = \sum_{z,a \in \mathbb{F}_2} \sum_{L \in \mathcal{L}} |\psi^L_{z,a}\rangle\langle\psi^L_{z,a}| \tag{9.417}$$

which has support only on diagram elements contained in $\mathcal{L}$, and let $P^0_{\mathcal{L}} = \mathbb{I} - P^1_{\mathcal{L}}$. Note that for each $L \in \mathcal{L}$ and $z, a \in \{0, 1\}$, we can write

$$|\rho^L_{z,a}\rangle = P^1_{\mathcal{L}} |\rho^L_{z,a}\rangle + P^0_{\mathcal{L}} |\rho^L_{z,a}\rangle \tag{9.418}$$

where (from equation (9.393))

$$P^1_{\mathcal{L}} |\rho^L_{z,a}\rangle = \frac{1}{\sqrt{15}} |\psi^L_{z,a}\rangle. \tag{9.419}$$

Since the states $|\rho^L_{z,a}\rangle$ are orthonormal, and similarly for the states $|\psi^L_{z,a}\rangle$, we get

$$\langle \rho^{\tilde{L}}_{x,b} | P^\alpha_{\mathcal{L}} | \rho^L_{z,a} \rangle = \begin{cases} \frac{1}{15} \delta_{z,x} \delta_{a,b} \delta_{L,\tilde{L}} & \alpha = 1 \\ \frac{14}{15} \delta_{z,x} \delta_{a,b} \delta_{L,\tilde{L}} & \alpha = 0. \end{cases} \tag{9.420}$$

Inserting n copies of the identity $P_{\mathcal{L}}^1 + P_{\mathcal{L}}^0 = 1$ gives

$$|\phi\rangle = \left(\frac{1}{\sqrt{2}}\right)^Y \sum_{c_1,\ldots,c_Y \in \mathbb{F}_2} \sum_{\alpha_1,\ldots,\alpha_n \in \mathbb{F}_2} P_{\mathcal{L}}^{\alpha_1} \otimes \cdots \otimes P_{\mathcal{L}}^{\alpha_n} |O_{\vec{z},\vec{a}}^{(J_1,\ldots,J_Y,L_1,\ldots,L_{n-2Y}),(c_1,\ldots,c_Y)}\rangle \tag{9.421}$$

Likewise for $|\psi\rangle$ we get

$$|\psi\rangle = \left(\frac{1}{\sqrt{2}}\right)^K \sum_{e_1,\ldots,e_K \in \mathbb{F}_2} \sum_{\beta_1,\ldots,\beta_n \in \mathbb{F}_2} (P_{\mathcal{L}}^{\beta_1} \otimes \cdots \otimes P_{\mathcal{L}}^{\beta_n} |O_{\vec{x},\vec{b}}^{(\tilde{J}_1,\ldots,\tilde{J}_K,\tilde{L}_1,\ldots,\tilde{L}_{n-2K}),(e_1,\ldots,e_K)}\rangle. \tag{9.422}$$

Using equations (9.393), (9.416), and (9.414), we see that the states

$$|O_{\vec{z},\vec{a}}^{(J_1,\ldots,J_Y,L_1,\ldots,L_{n-2Y}),(c_1,\ldots,c_Y)}\rangle \qquad \text{and} \qquad |O_{\vec{x},\vec{b}}^{(\tilde{J}_1,\ldots,\tilde{J}_K,\tilde{L}_1,\ldots,\tilde{L}_{n-2K}),(e_1,\ldots,e_K)}\rangle \tag{9.423}$$

are orthogonal for any choice of bit strings $c_1,\ldots,c_Y$ and $e_1,\ldots,e_K$, since $|\phi\rangle \neq |\psi\rangle$ implies that

$$((J_1,\ldots,J_Y,L_1,\ldots,L_{n-2Y}),\vec{z},\vec{a},\pi) \neq ((\tilde{J}_1,\ldots,\tilde{J}_K,\tilde{L}_1,\ldots,\tilde{L}_{n-2K}),\vec{x},\vec{b},\sigma), \tag{9.424}$$

and we assume $\pi = \sigma$. Using equation (9.420), we have

$$\begin{aligned}
&\langle O_{\vec{x},\vec{b}}^{(\tilde{J}_1,\ldots,\tilde{J}_K,\tilde{L}_1,\ldots,\tilde{L}_{n-2K}),(e_1,\ldots,e_K)} | P_{\mathcal{L}}^{\alpha_1} \otimes \cdots \otimes P_{\mathcal{L}}^{\alpha_n} | O_{\vec{z},\vec{a}}^{(J_1,\ldots,J_Y,L_1,\ldots,L_{n-2Y}),(c_1,\ldots,c_Y)}\rangle \\
&\quad = \left(\frac{1}{15}\right)^{\sum_{i=1}^n \alpha_i} \left(\frac{14}{15}\right)^{n-\sum_{i=1}^n \alpha_i} \langle O_{\vec{x},\vec{b}}^{(\tilde{J}_1,\ldots,\tilde{J}_K,\tilde{L}_1,\ldots,\tilde{L}_{n-2K}),(e_1,\ldots,e_K)} | O_{\vec{z},\vec{a}}^{(J_1,\ldots,J_Y,L_1,\ldots,L_{n-2Y}),(c_1,\ldots,c_Y)}\rangle,
\end{aligned} \tag{9.425}$$

so the states

$$P_{\mathcal{L}}^{\alpha_1} \otimes \cdots \otimes P_{\mathcal{L}}^{\alpha_n} |O_{\vec{z},\vec{a}}^{(J_1,\ldots,J_Y,L_1,\ldots,L_{n-2Y}),(c_1,\ldots,c_Y)}\rangle \tag{9.426}$$

and

$$P_{\mathcal{L}}^{\beta_1} \otimes \cdots \otimes P_{\mathcal{L}}^{\beta_n} |O_{\vec{x},\vec{b}}^{(\tilde{J}_1,\ldots,\tilde{J}_K,\tilde{L}_1,\ldots,\tilde{L}_{n-2K}),(e_1,\ldots,e_K)}\rangle \tag{9.427}$$

are orthogonal for each choice of bit strings $\alpha_1,\ldots,\alpha_n$, $\beta_1,\ldots,\beta_n$, $c_1,\ldots,c_Y$, and $e_1,\ldots,e_K$.

To complete the proof, we show that

$$\Pi_0 |\phi\rangle \tag{9.428}$$

is a superposition of a *subset* of the states in the sum (9.421) and hence is orthogonal to $|\psi\rangle$. To see this, first note that $|\phi\rangle \in \mathcal{I}(G_1, n)$ since it is in the nullspace of $H(G_1, n)$ (by Lemma 32) and G_1 is an e_1-gate graph (by Lemma 31). Now comparing $\mathcal{I}(G_1, n)$ and $\mathcal{I}(G_1, G_X^{\text{occ}}, n)$, we see that

$$\Pi_0 |\Gamma\rangle = \Pi_0^{\text{occ}} |\Gamma\rangle \text{ for all } |\Gamma\rangle \in \mathcal{I}(G_1, n) \tag{9.429}$$

where Π_0^{occ} projects onto the space

$$\text{span}\{|\psi_{z_1,a_1}^{q_1}\rangle |\psi_{z_2,a_2}^{q_2}\rangle \ldots |\psi_{z_n,a_n}^{q_n}\rangle \colon z_i, a_i \in \mathbb{F}_2, q_i \in [R], \{q_i, q_j\} \notin E(G_X^{\text{occ}})\}. \tag{9.430}$$

In particular, $\Pi_0 |\phi\rangle = \Pi_0^{\text{occ}} |\phi\rangle$. We claim that this quantity is a superposition of a subset of the states in the sum (9.421).

The diagram elements $q_1,\ldots,q_n$ appearing in (9.430) range over the set of all R diagram elements in the gate graph G_1; however, recall that $E(G_X^{\text{occ}})$ only contains edges between diagram

elements in the subset $\mathcal{L}$ of these diagram elements. Since the $P_{\mathcal{L}}^{\alpha}$ either project onto this set of diagram elements or onto the complement, each state

$$P_{\mathcal{L}}^{\alpha_1} \otimes \cdots \otimes P_{\mathcal{L}}^{\alpha_n} |O_{\vec{z},\vec{a}}^{(J_1,\ldots,J_Y,L_1,\ldots,L_{n-2Y}),(c_1,\ldots,c_Y)}\rangle \tag{9.431}$$

is an eigenvector of Π_0^{occ}. Hence $\Pi_0|\phi\rangle$ is a superposition of the terms in (9.421) that are $+1$ eigenvectors of Π_0^{occ} (as the 0 eigenvectors are annihilated). It follows that $\langle\psi|\Pi_0|\phi\rangle = 0$ since we established above that each such term is orthogonal to $|\psi\rangle$. □

With this characterization of the legal projections, we can characterize the nullspace of $H(G_1, G_X^{\text{oc}}, n)$ and bound its smallest nonzero eigenvalue.

Lemma 35. *The nullspace S_1 of $H(G_1, G_X^{oc}, n)$ is spanned by the orthonormal basis $\mathcal{B}_{legal}$. Its smallest nonzero eigenvalue is*

$$\gamma(H(G_1, G_X^{oc}, n)) \geq \frac{\mathcal{K}_0}{900} \tag{9.432}$$

where $\mathcal{K}_0 \in (0, 1]$ is the absolute constant from Lemma 32.

Proof. Recall that

$$H(G_1, G_X^{\text{oc}}, n) = H(G_1, n)|_{\mathcal{I}(G_1, G_X^{\text{oc}}, n)}. \tag{9.433}$$

Its nullspace is the space of states $|\kappa\rangle$ satisfying

$$\Pi_0|\kappa\rangle = |\kappa\rangle \quad \text{and} \quad H(G_1, n)|\kappa\rangle = 0 \tag{9.434}$$

(recall that Π_0 is the projector onto $\mathcal{I}(G_1, G_X^{\text{oc}}, n)$, the states satisfying the occupancy constraints). Since $\mathcal{B}_n$ is a basis for the nullspace of $H(G_1, n)$, to solve for the nullspace of $H(G_1, G_X^{\text{oc}}, n)$ we consider the restriction (9.386) and solve for the eigenspace with eigenvalue 1. This calculation is simple because (9.386) is diagonal in the basis $\mathcal{B}_n$, according to Lemma 34. We see immediately from the Lemma that $\mathcal{B}_{\text{legal}}$ spans the nullspace of $H(G_1, G_X^{\text{oc}}, n)$; we now show that Lemma 34 also implies the lower bound (9.432). Note that

$$\gamma(H(G_1, G_X^{\text{oc}}, n)) = \gamma(\Pi_0 H(G_1, n)\Pi_0). \tag{9.435}$$

Let Π_{legal} and Π_{illegal} project onto the spaces spanned by $\mathcal{B}_{\text{legal}}$ and $\mathcal{B}_{\text{illegal}}$ respectively, so $\Pi_{\text{legal}} + \Pi_{\text{illegal}}$ projects onto the nullspace of $H(G_1, n)$. The operator inequality

$$H(G_1, n) \geq \gamma(H(G_1, n)) \cdot (1 - \Pi_{\text{legal}} - \Pi_{\text{illegal}}) \tag{9.436}$$

implies

$$\Pi_0 H(G_1, n)\Pi_0 \geq \gamma(H(G_1, n)) \cdot \Pi_0(1 - \Pi_{\text{legal}} - \Pi_{\text{illegal}})\Pi_0. \tag{9.437}$$

Since the operators on both sides of this inequality are positive semidefinite and have the same nullspace, their smallest nonzero eigenvalues are bounded as

$$\gamma(\Pi_0 H(G_1, n)\Pi_0) \geq \gamma(H(G_1, n)) \cdot \gamma(\Pi_0(1 - \Pi_{\text{legal}} - \Pi_{\text{illegal}})\Pi_0). \tag{9.438}$$

Hence

$$\gamma(H(G_1, G_X^{\text{oc}}, n)) = \gamma(\Pi_0 H(G_1, n)\Pi_0) \geq \mathcal{K}_0 \cdot \gamma(\Pi_0(1 - \Pi_{\text{legal}} - \Pi_{\text{illegal}})\Pi_0) \tag{9.439}$$

where we used Lemma 32. From equations (9.388) and (9.389) we see that

$$\Pi_0|g\rangle = |g\rangle \quad \text{and} \quad \Pi_{\text{illegal}}|f\rangle = |f\rangle \qquad \Longrightarrow \qquad \langle f|g\rangle\langle g|f\rangle \leq \frac{899}{900}. \tag{9.440}$$

The nullspace of

$$\Pi_0 \left(1 - \Pi_{\text{legal}} - \Pi_{\text{illegal}}\right) \Pi_0 \tag{9.441}$$

is spanned by

$$\mathcal{B}_{\text{legal}} \cup \{|\tau\rangle \colon \Pi_0 |\tau\rangle = 0\} \,. \tag{9.442}$$

To see this, note that (9.441) commutes with Π_0, and the space of $+1$ eigenvectors of Π_0 that are annihilated by (9.441) is spanned by $\mathcal{B}_{\text{legal}}$ (by Lemma 34). Any eigenvector $|g_1\rangle$ corresponding to the smallest nonzero eigenvalue of this operator therefore satisfies $\Pi_0|g_1\rangle = |g_1\rangle$ and $\Pi_{\text{legal}}|g_1\rangle = 0$, so

$$\gamma(\Pi_0(1 - \Pi_{\text{legal}} - \Pi_{\text{illegal}})\Pi_0) = 1 - \langle g_1|\Pi_{\text{illegal}}|g_1\rangle \geq \frac{1}{900} \tag{9.443}$$

using equation (9.440). Plugging this into equation (9.439) gives the lower bound (9.432). □

This is then the expected bound for our most simple graphs.

9.5.5 Legal configuration matrix elements

Now that we have a decent understanding of the legal configurations, it will be useful to start understanding how the added edges change the ground space. In particular, we will now consider

$$H_1|_{S_1}, H_2|_{S_1}, H_{\text{in},i}|_{S_1}, H_{\text{out}}|_{S_1} \tag{9.444}$$

where these operators are defined in Section 9.5.2 and

$$S_1 = \text{span}(\mathcal{B}_{\text{legal}}) \tag{9.445}$$

is the nullspace of $H(G_1, G_X^{\text{oc}}, n)$.

We specify the operators (9.444) by their matrix elements in an orthonormal basis for S_1. Although the basis $\mathcal{B}_{\text{legal}}$ was convenient in Section 9.5.3.1, here we use a different basis in which the matrix elements of H_1 and H_2 are simpler. We define

$$|j, \vec{d}, \text{In}(\vec{z}), \vec{a}, \pi\rangle = \sum_{\vec{x}\in\{0,1\}^n} \left(\langle \vec{x}|\bar{U}_{j,d_1}(a_1)|\vec{z}\rangle\right)|j, \vec{d}, \vec{x}, \vec{a}, \pi\rangle \tag{9.446}$$

where

$$\bar{U}_{j,d_1}(a_1) = \begin{cases} U_{j-1}(a_1)U_{j-2}(a_1)\ldots U_1(a_1) & \text{if } d_1 \in \{0,2\} \\ U_j(a_1)U_{j-1}(a_1)\ldots U_1(a_1) & \text{if } d_1 = 1. \end{cases} \tag{9.447}$$

In each of these states the quantum data (represented by the $\vec{x}$ register on the right-hand side) encodes the computation in which the unitary $\bar{U}_{j,d_1}(a_1)$ is applied to the initial n-qubit state $|\vec{z}\rangle$ (the notation $\text{In}(\vec{z})$ indicates that $\vec{z}$ is the input). The vector $\vec{a}$ is only relevant insofar as its first bit a_1 determines whether or not each two-qubit unitary is complex conjugated; the other bits of $\vec{a}$ go along for the ride (and this is why we want each unitary to interact with the first qubit). Letting $\vec{z}, \vec{a} \in \{0,1\}^n$, $j \in [M]$, and

$$\vec{d} = (d_1, \ldots, d_n) \quad \text{with} \quad d_1 = d_{s(j)} \in \{0,1,2\} \quad \text{and} \quad d_i \in \{0,1\},\ i \notin \{1, s(j)\}, \tag{9.448}$$

we see that the states (9.446) form an orthonormal basis for S_1.

Note that from this point, we will not make a special point to include the

9.5.5.1 Matrix elements of H_1

Roughly speaking, the nonzero off-diagonal matrix elements of the operator H_1 in the basis (9.446) occur between states $|j, \vec{d}, \mathrm{In}(\vec{z}), \vec{a}, \pi\rangle$ and $|j, \vec{c}, \mathrm{In}(\vec{z}), \vec{a}, \pi\rangle$ where the legal configurations $j, \vec{d}$ and $j, \vec{c}$ are related by horizontal motion of a particle in one of the rows $i \in \{2, \dots, n\}$.

Matrix elements of H_1

$$\langle k, \vec{c}, \mathrm{In}(\vec{x}), \vec{b}, \sigma | H_1 | j, \vec{d}, \mathrm{In}(\vec{z}), \vec{a}, \pi\rangle$$
$$= \frac{\delta_{\pi,\sigma}\delta_{k,j}\delta_{\vec{a},\vec{b}}\delta_{\vec{z},\vec{x}}}{240} \cdot \begin{cases} n-1 & \vec{c} = \vec{d} \\ \prod_{\substack{r=1 \\ r\neq i}}^{n} \delta_{d_r,c_r} & d_i \neq c_i \text{ for some } i \in [n] \setminus \{1, s(j)\} \\ \frac{1}{\sqrt{2}} \prod_{\substack{r=2 \\ r\neq s(j)}}^{n} \delta_{d_r,c_r} & (c_1, d_1) \in \{(2,0),(0,2),(1,2),(2,1)\} \\ 0 & \text{otherwise.} \end{cases} \tag{9.449}$$

We begin by computing the matrix elements of

$$H_1 = \sum_{w=1}^{n} h_1^{(w)} \tag{9.450}$$

in the basis $\mathcal{B}_{\text{legal}}$; then we use them to compute the matrix elements of H_1 in the basis (9.446).

Note that since H_1 is symmetric under permutations of the n registers,

$$H_1 |j, \vec{d}, \vec{z}, \vec{a}, \pi\rangle = \begin{cases} V_\pi\left(H_1 |\rho_{z_1,a_1}^{(1,j,d_1)}\rangle \bigotimes_{i=2}^{n} |\rho_{z_i,a_i}^{F(i,j,d_i)}\rangle \right) & d_1 = d_{s(j)} \in \{0,1\} \\ V_\pi\left(H_1 |T_{z_1,a_1,z_{s(j)},a_{s(j)}}^{j}\rangle \bigotimes_{\substack{i=2 \\ i\neq s(j)}}^{n} |\rho_{z_i,a_i}^{F(i,j,d_i)}\rangle \right) & d_1 = d_{s(j)} = 2, \end{cases} \tag{9.451}$$

and since H_1 does not interchange the particle locations,

$$\langle k, \vec{c}, \vec{x}, \vec{b}, \sigma | H_1 | j, \vec{d}, \vec{z}, \vec{a}, \pi\rangle = \delta_{\pi,\sigma} \langle k, \vec{c}, \vec{x}, \vec{b}, () | H_1 | j, \vec{d}, \vec{z}, \vec{a}, ()\rangle. \tag{9.452}$$

Additionally, recall that

$$|T_{z_1,a_1,z_{s(j)},a_{s(j)}}^{j}\rangle = \frac{1}{\sqrt{2}} |\rho_{z_1,a_1}^{(1,j,0)}\rangle |\rho_{z_{s(j)},a_{s(j)}}^{(s(j),j,0)}\rangle + \frac{1}{\sqrt{2}} \sum_{x_1,x_2\in\{0,1\}} U_j(a_1)_{x_1x_2,z_1z_{s(j)}} |\rho_{x_1,a_1}^{(1,j,1)}\rangle |\rho_{x_2,a_{s(j)}}^{(s(j),j,1)}\rangle. \tag{9.453}$$

To compute $\langle k, \vec{c}, \vec{x}, \vec{b}, ()|H_1|j, \vec{d}, \vec{z}, \vec{a}, ()\rangle$, we first evaluate the matrix elements of h_1 between single-particle states of the form

$$|\rho_{z,a}^{(1,j,d)}\rangle,\ |\rho_{z,a}^{(s(j),j,d)}\rangle,\ |\rho_{z,a}^{F(i,j,d)}\rangle \tag{9.454}$$

(for $j \in [M]$, $i \in \{2, \dots, n\}$, $z, a \in \mathbb{F}_2$, and $d \in \{0,1\}$) that appear in equation (9.451). To evaluate these matrix elements, we use the fact that h_1 is of the form (9.73), where $\mathcal{E}$ is the set of edges in rows $2, \dots, n$ that are added to the gate diagram in step 3 of Section 9.4.2.

We have

$$\langle \rho_{x,b}^{F(i,j,0)} | h_1 | \rho_{z,a}^{F(i,j,0)} \rangle = \frac{1}{15} \langle \psi_{x,b}^{F(i,j,0)} | h_1 | \psi_{z,a}^{F(i,j,0)} \rangle = \frac{1}{240} \delta_{x,z} \delta_{a,b} \tag{9.455}$$

$$\langle \rho_{x,b}^{F(i,j,1)} | h_1 | \rho_{z,a}^{F(i,j,1)} \rangle = \frac{1}{240} \delta_{x,z} \delta_{a,b} \tag{9.456}$$

for all $i \in \{2, \ldots, n\}$, $j \in [M]$, and $x, z, a, b \in \mathbb{F}_2$. Similarly,

$$\langle \rho_{x,b}^{F(i,j,0)} | h_1 | \rho_{z,a}^{F(i,j,1)} \rangle = \langle \rho_{x,b}^{F(i,j,1)} | h_1 | \rho_{z,a}^{F(i,j,0)} \rangle = \frac{1}{240} \delta_{x,z} \delta_{a,b} \tag{9.457}$$

for all $i \in [n] \setminus \{1, s(j)\}$, $j \in [M]$, and $z, x, a, b \in \mathbb{F}_2$. Furthermore,

$$h_1 | \rho_{z,a}^{(1,j,d)} \rangle = 0 \tag{9.458}$$

for all $j \in [M]$, $z, a \in \mathbb{F}_2$, and $d \in \{0, 1\}$, and

$$\langle \rho_{x,b}^{F(s(j),j,c)} | h_1 | \rho_{z,a}^{(s(j),j,d)} \rangle = \frac{1}{240} \delta_{x,z} \delta_{a,b} \delta_{c,d} \tag{9.459}$$

$$\langle \rho_{x,b}^{(s(j),j,c)} | h_1 | \rho_{z,a}^{(s(j),j,d)} \rangle = \frac{1}{240} \delta_{x,z} \delta_{a,b} \delta_{c,d} \tag{9.460}$$

for all $j \in [M]$, $z, x, a, b \in \mathbb{F}_2$, and $c, d \in \{0, 1\}$.

Using equations (9.455), (9.456), (9.458), and (9.460), we compute the diagonal matrix elements of H_1:

$$\begin{aligned} &\langle j, \vec{d}, \vec{z}, \vec{a}, () | H_1 | j, \vec{d}, \vec{z}, \vec{a}, () \rangle \\ &\quad = \begin{cases} \sum_{i=2}^{n} \langle \rho_{z_i,a_i}^{F(i,j,d_i)} | h_1 | \rho_{z_i,a_i}^{F(i,j,d_i)} \rangle & d_1 \in \{0,1\} \\ \langle T_{z_1,a_1,z_{s(j)},a_{s(j)}}^{j} | \mathbb{I} \otimes h_1 | T_{z_1,a_1,z_{s(j)},a_{s(j)}}^{j} \rangle + \sum\limits_{\substack{i=2 \\ i \neq s(j)}}^{n} \langle \rho_{z_i,a_i}^{F(i,j,d_i)} | h_1 | \rho_{z_i,a_i}^{F(i,j,d_i)} \rangle & d_1 = 2. \end{cases} \qquad (9.461) \\ &\quad = \frac{n-1}{240} \qquad (9.462) \end{aligned}$$

where in the last line we used equation (9.453) and the fact that $U_j(a_1)$ is unitary. We use equations (9.457) and (9.459) to compute the nonzero off-diagonal matrix elements of H_1 between states in $\mathcal{B}_{\text{legal}}$. We get

$$\begin{aligned} &\langle k, \vec{c}, \vec{x}, \vec{b}, \pi | H_1 | j, \vec{d}, \vec{z}, \vec{a}, \sigma \rangle \\ &\quad = \frac{\delta_{\pi,\sigma} \delta_{j,k} \delta_{\vec{a},\vec{b}}}{240} \cdot \begin{cases} \delta_{\vec{x},\vec{z}} (n-1) & \vec{c} = \vec{d} \\ \delta_{\vec{x},\vec{z}} \prod\limits_{\substack{r=1 \\ r \neq i}}^{n} \delta_{c_r,d_r} & c_i \neq d_i \text{ for some } i \in [n] \setminus \{1, s(j)\} \\ \frac{1}{\sqrt{2}} \delta_{\vec{x},\vec{z}} \prod\limits_{\substack{r=2 \\ r \neq s(j)}}^{n} \delta_{c_r,d_r} & (c_1, d_1) \in \{(2,0), (0,2)\} \\ \frac{1}{\sqrt{2}} U_j(a_1)^*_{z_1 z_{s(j)}, x_1 x_{s(j)}} \prod\limits_{\substack{r=2 \\ r \neq s(j)}}^{n} \delta_{c_r,d_r} \delta_{x_r,z_r} & (c_1, d_1) = (2,1) \\ \frac{1}{\sqrt{2}} U_j(a_1)_{x_1 x_{s(j)}, z_1 z_{s(j)}} \prod\limits_{\substack{r=2 \\ r \neq s(j)}}^{n} \delta_{c_r,d_r} \delta_{x_r,z_r} & (c_1, d_1) = (1,2) \\ 0 & \text{otherwise.} \end{cases} \qquad (9.463) \end{aligned}$$

For the second case we used equation (9.457), for the third case we used equation (9.459) to get

$$\langle T^j_{x_1,b_1,x_{s(j)},b_{s(j)}} | \mathbb{I} \otimes h_1 | \rho^{(1,j,0)}_{z_1,a_1} \rangle | \rho^{F(s(j),j,0)}_{z_{s(j)}a_{s(j)}} \rangle = \delta_{x_1,z_1}\delta_{b_1,a_1}\delta_{x_{s(j)},z_{s(j)}}\delta_{b_{s(j)},a_{s(j)}}\frac{1}{240\sqrt{2}}, \tag{9.464}$$

and for the fourth and fifth cases we used equation (9.459) to get

$$\langle T^j_{x_1,b_1,x_{s(j)},b_{s(j)}} | \mathbb{I} \otimes h_1 | \rho^{(1,j,1)}_{z_1,a_1} \rangle | \rho^{F(s(j),j,1)}_{z_{s(j)}a_{s(j)}} \rangle = \delta_{b_1,a_1}\delta_{b_{s(j)},a_{s(j)}}\frac{1}{240\sqrt{2}} U_j(a_1)^*_{z_1 z_{s(j)},x_1 x_{s(j)}}. \tag{9.465}$$

In the remaining case, $(c_1, d_1) \in \{(1,0),(0,1)\}$ and the matrix element is 0.

We now compute the matrix elements of H_1 in the basis (9.446). We have

$$\begin{aligned}&\langle j, \vec{c}, \mathrm{In}(\vec{x}), \vec{a}, \sigma | H_1 | j, \vec{d}, \mathrm{In}(\vec{z}), \vec{a}, \pi \rangle \\ &\quad = \sum_{\vec{x}', \vec{z}' \in \{0,1\}^n} \langle j, \vec{c}, \vec{x}', \vec{a}, \sigma | H_1 | j, \vec{d}, \vec{z}', \vec{a}, \pi \rangle \langle \vec{x} | \bar{U}_{j,d_1}(a_1)^\dagger | \vec{x}' \rangle \langle \vec{z}' | \bar{U}_{j,d_1}(a_1) | \vec{z} \rangle.\end{aligned} \tag{9.466}$$

Using this with (9.463) gives

$$\begin{aligned}&\langle k, \vec{c}, \mathrm{In}(\vec{x}), \vec{b}, \sigma | H_1 | j, \vec{d}, \mathrm{In}(\vec{z}), \vec{a}, \pi \rangle \\ &\quad = \frac{\delta_{\pi,\sigma}\delta_{j,k}\delta_{\vec{a},\vec{b}}\delta_{\vec{x},\vec{z}}}{240} \cdot \begin{cases} n-1 & \vec{c} = \vec{d} \\ \prod_{\substack{r=1 \\ r \neq i}}^{n} \delta_{c_r,d_r} & c_i \neq d_i \text{ for some } i \in [n] \setminus \{1, s(j)\} \\ \frac{1}{\sqrt{2}} \prod_{\substack{r=2 \\ r \neq s(j)}}^{n} \delta_{c_r,d_r} & (c_1,d_1) \in \{(2,0),(0,2),(2,1),(1,2)\} \\ 0 & \text{otherwise} \end{cases}\end{aligned} \tag{9.467}$$

as claimed in equation (9.449). Note that in the basis $\mathcal{B}_{\text{legal}}$, H_1 has nonzero matrix elements between states with different values of $\vec{z}$; the basis (9.446) is convenient because H_1 only connects basis states with the same value of $\vec{z}$.

From this expression we see that $H_1|_{S_1}$ is block diagonal in the basis (9.446), with a block for each $\vec{z}, \vec{a} \in \mathbb{F}_2^n$, $\pi \in S_n$, and $j \in [M]$. Moreover, the submatrix for each block is the same.

9.5.5.2 Matrix elements of H_2

Next, we present the matrix elements of H_2.

Matrix elements of H_2

$$\begin{aligned}&\langle k, \vec{c}, \mathrm{In}(\vec{x}), \vec{b}, \pi | H_2 | j, \vec{d}, \mathrm{In}(\vec{z}), \vec{a}, \sigma \rangle \\ &\quad = \Big[f_{\text{diag}}(\vec{d}, j)\delta_{j,k}\delta_{\vec{a},\vec{b}}\delta_{\vec{z},\vec{x}}\delta_{\vec{c},\vec{d}} + \big(f_{\text{off-diag}}(\vec{c}, \vec{d}, j) \cdot \delta_{k,j-1} + f_{\text{off-diag}}(\vec{d}, \vec{c}, k) \cdot \delta_{k-1,j} \big) \delta_{\vec{a},\vec{b}}\delta_{\vec{z},\vec{x}} \Big] \delta_{\pi,\sigma}\end{aligned} \tag{9.468}$$

where

$$f_{\text{diag}}(\vec{d}, j) = \begin{cases} 0 & d_1 = 0 \text{ and } j = 1, \text{ or } d_1 = 1 \text{ and } j = M \\ \frac{1}{480} & d_1 = 2 \text{ and } j \in \{1, M\} \\ \frac{1}{240} & \text{otherwise} \end{cases} \tag{9.469}$$

and

$$f_{\text{off-diag}}(\vec{c},\vec{d},j) = \left(\prod_{\substack{r=2\\ r\notin\{s(j-1),s(j)\}}}^{n} \delta_{d_r,c_r}\right) \cdot \begin{cases} \frac{1}{240\sqrt{2}} & (c_1, c_{s(j)}, d_1, d_{s(j-1)}) \in \{(2,0,0,0),(1,1,2,1)\} \\ \frac{1}{240} & (c_1, c_{s(j)}, d_1, d_{s(j-1)}) = (1,0,0,1) \\ \frac{1}{480} & (c_1, c_{s(j)}, d_1, d_{s(j-1)}) = (2,1,2,0) \\ 0 & \text{otherwise.} \end{cases} \tag{9.470}$$

Recall that

$$H_2 = \sum_{w=1}^{n} h_2^{(w)} \tag{9.471}$$

and note, just as in (9.451), that because H_2 is permutation invariant,

$$H_2|j,\vec{d},\vec{z},\vec{a},\pi\rangle = \begin{cases} V_\pi\left(H_2|\rho_{z_1,a_1}^{(1,j,d_1)}\rangle \bigotimes_{i=2}^{n}|\rho_{z_i,a_i}^{F(i,j,d_i)}\rangle\right) & d_1 = d_{s(j)} \in \{0,1\} \\ V_\pi\left(H_2|T^{j}_{z_1,a_1,z_{s(j)},a_{s(j)}}\rangle \bigotimes_{\substack{i=2\\ i\neq s(j)}}^{n}|\rho_{z_i,a_i}^{F(i,j,d_i)}\rangle\right) & d_1 = d_{s(j)} = 2, \end{cases} \tag{9.472}$$

and thus, H_2 is block diagonal for each $\pi \in S_n$, and is equal in each block. Also recall that h_2 is of the form (9.73), where $\mathcal{E}$ is the set of edges in row 1 that are added in step 3 of Section 9.4.2.

To compute $\langle k,\vec{c},\vec{x},\vec{b},()|H_2|j,\vec{d},\vec{z},\vec{a},()\rangle$ we first evaluate the matrix elements of h_2 between the relevant single-particle states $|\rho_{z,a}^{L}\rangle$ with $L \in \mathcal{L}$ and $z,a \in \mathbb{F}_2$. The only such matrix elements that are nonzero are

$$\langle\rho_{x,b}^{(1,j,0)}|h_2|\rho_{z,a}^{(1,j,0)}\rangle = \begin{cases} 0 & j=1 \\ \frac{1}{240}\delta_{z,x}\delta_{a,b} & j\in\{2,\dots,M\} \end{cases} \tag{9.473}$$

$$\langle\rho_{x,b}^{(1,j,1)}|h_2|\rho_{z,a}^{(1,j,1)}\rangle = \begin{cases} \frac{1}{240}\delta_{z,x}\delta_{a,b} & j\in\{1,\dots,M-1\} \\ 0 & j=M \end{cases} \tag{9.474}$$

for $z,a,x,b \in \mathbb{F}_2$ and

$$\langle\rho_{x,b}^{(1,j-1,1)}|h_2|\rho_{z,a}^{(1,j,0)}\rangle = \langle\rho_{z,a}^{(1,j,0)}|h_2|\rho_{x,b}^{(1,j-1,1)}\rangle = \frac{1}{240}\delta_{z,x}\delta_{a,b} \tag{9.475}$$

for $j \in \{2,\dots,M\}$ and $z,x,a,b \in \mathbb{F}_2$.

Using equations (9.472) and (9.474), we compute the diagonal matrix elements of H_2 in the basis $\mathcal{B}_{\text{legal}}$:

$$\langle j,\vec{d},\vec{z},\vec{a},()|H_2|j,\vec{d},\vec{z},\vec{a},()\rangle = \begin{cases} 0 & d_1 = 0 \text{ and } j=1, \text{ or } d_1=1 \text{ and } j=M \\ \frac{1}{480} & d_1 = 2 \text{ and } j\in\{1,M\} \\ \frac{1}{240} & \text{otherwise.} \end{cases} \tag{9.476}$$

Using equations (9.472) and (9.475), we compute the nonzero off-diagonal matrix elements, which are all of the form

$$\langle j-1,\vec{c},\vec{x},\vec{a},()|H_2|j,\vec{d},\vec{z},\vec{a},()\rangle = \left(\langle j,\vec{d},\vec{z},\vec{a},()|H_2|j-1,\vec{c},\vec{x},\vec{a},()\rangle\right)^* \tag{9.477}$$

for $j \in \{2, \dots, M\}$, $\vec{x}, \vec{z}, \vec{a} \in \mathbb{F}_2^n$, and

$$\vec{d} = (d_1, \dots, d_n) \quad \text{with} \quad d_1 = d_{s(j)} \in \{0,1,2\} \quad \text{and} \quad d_i \in \{0,1\} \text{ for all } i \notin \{1, s(j)\}. \tag{9.478}$$

We get

$$\begin{aligned}
&\langle j-1, \vec{c}, \vec{x}, \vec{a}, ()|H_2|j, \vec{d}, \vec{z}, \vec{a}, ()\rangle \\
&= \prod_{\substack{r=2 \\ r \notin \{s(j), s(j-1)\}}}^{n} \delta_{d_r, c_r} \begin{cases} \frac{1}{240}\delta_{\vec{x},\vec{z}} & (c_1, c_{s(j)}, d_1, d_{s(j-1)}) = (1,0,0,1) \\ \frac{U_{j-1}(a_1)^*_{z_1 z_{s(j-1)}, x_1 x_{s(j-1)}}}{240\sqrt{2}} \prod_{\substack{r=2 \\ r \neq s(j-1)}}^{n} \delta_{x_r, z_r} & (c_1, c_{s(j)}, d_1, d_{s(j-1)}) = (2,0,0,0) \\ \frac{U_{j-1}(a_1)^*_{z_1 z_{s(j-1)}, x_1 x_{s(j-1)}}}{480} \prod_{\substack{r=2 \\ r \neq s(j-1)}}^{n} \delta_{x_r, z_r} & (c_1, c_{s(j)}, d_1, d_{s(j-1)}) = (2,1,2,0) \\ \frac{1}{240\sqrt{2}}\delta_{\vec{x},\vec{z}} & (c_1, c_{s(j)}, d_1, d_{s(j-1)}) = (1,1,2,1). \end{cases}
\end{aligned} \tag{9.479}$$

Now we compute the diagonal matrix elements of H_2 in the basis (9.446) using equations (9.466) and (9.476):

$$\langle j, \vec{d}, \mathrm{In}(\vec{z}), \vec{a}, \pi|H_2|j, \vec{d}, \mathrm{In}(\vec{z}), \vec{a}, \sigma\rangle = \delta_{\pi,\sigma} \cdot \begin{cases} 0 & d_1 = 0 \text{ and } j = 1, \text{ or } d_1 = 1 \text{ and } j = M \\ \frac{1}{480} & d_1 = 2 \text{ and } j \in \{1, M\} \\ \frac{1}{240} & \text{otherwise.} \end{cases} \tag{9.480}$$

The nonzero off-diagonal matrix elements are (using equations (9.466) and (9.479))

$$\begin{aligned}
&\langle j-1, \vec{c}, \mathrm{In}(\vec{x}), b, \vec{\pi}|H_2|j, \vec{d}, \mathrm{In}(\vec{z}), \vec{a}, \sigma\rangle = \langle j, \vec{d}, \mathrm{In}(\vec{z}), \vec{a}, \sigma|H_2|j-1, \vec{c}, \mathrm{In}(\vec{x}), \vec{b}, \pi\rangle \\
&= \delta_{\pi,\sigma}\delta_{\vec{x},\vec{z}}\delta_{\vec{a},\vec{b}} \left(\prod_{\substack{r=2 \\ r \notin \{s(j), s(j-1)\}}}^{n} \delta_{d_r, c_r} \right) \cdot \begin{cases} \frac{1}{64} & (c_1, c_{s(j)}, d_1, d_{s(j-1)}) = (1,0,0,1) \\ \frac{1}{64\sqrt{2}} & (c_1, c_{s(j)}, d_1, d_{s(j-1)}) = (2,0,0,0) \\ \frac{1}{128} & (c_1, c_{s(j)}, d_1, d_{s(j-1)}) = (2,1,2,0) \\ \frac{1}{64\sqrt{2}} & (c_1, c_{s(j)}, d_1, d_{s(j-1)}) = (1,1,2,1). \end{cases}
\end{aligned} \tag{9.481}$$

Combining equations (9.480) and (9.481) gives the result claimed in equations (9.468), (9.469), and (9.470).

This shows that $H_2|_{S_1}$ is block diagonal in the basis (9.446), with a block for each $\vec{z}, \vec{a} \in \mathbb{F}_2^n$ and $\pi \in S_n$. Also note that (in contrast with H_1) H_2 connects states with different values of j.

9.5.5.3 Matrix elements of $H_{\mathrm{in},i}$

We next present the matrix elements of $H_{\mathrm{in},i}$ (for $i \in \{n_{\mathrm{in}} + 1, \dots, n\}$)

Matrix elements of $H_{\mathrm{in},i}$

For each ancilla qubit $i \in \{n_{\mathrm{in}} + 1, \dots, n\}$, define $j_{\min,i} = \min\{j \in [M] \colon s(j) = i\}$ to be the index of the first gate in the circuit that involves this qubit (recall from Section **??** that we consider circuits where each ancilla qubit is involved in at least one gate). The operator $H_{\mathrm{in},i}$

is diagonal in the basis (9.446), with entries

$$\langle j, \vec{d}, \mathrm{In}(\vec{z}), \vec{a}, \pi | H_{\mathrm{in},i} | j, \vec{d}, \mathrm{In}(\vec{z}), \vec{a}, \pi \rangle = \begin{cases} \frac{1}{240} & j \leq j_{\min,i},\ z_i = 1, \text{ and } d_i = 0 \\ 0 & \text{otherwise.} \end{cases} \tag{9.482}$$

We now consider

$$H_{\mathrm{in},i} = \sum_{w=1}^{n} h_{\mathrm{in},i}^{(w)} \tag{9.483}$$

where i is from the set of indices of the ancilla qubits, i.e., $i \in \{n_{\mathrm{in}} + 1, \ldots, n\}$. Using equation (9.346) we get

$$\langle \rho_{x,b}^{L_2} | h_{\mathrm{in},i} | \rho_{z,a}^{L_1} \rangle = \frac{1}{15} \langle \psi_{x,b}^{L_2} | h_{\mathrm{in},i} | \psi_{z,a}^{L_1} \rangle = \frac{1}{240} \delta_{x,1} \delta_{z,1} \delta_{a,b} \delta_{L_1,(i,0,1)} \delta_{L_2,(i,0,1)} \tag{9.484}$$

for $L_1, L_2 \in \mathcal{L}$ and $a, b, x, z \in \mathbb{F}_2$. If we also use the fact that H_{in} commutes with all permutations of the particles, we have that $H_{\mathrm{in},i}$ is diagonal in the basis $\mathcal{B}_{\mathrm{legal}}$ with entries

$$\langle j, \vec{d}, \vec{z}, \vec{a}, \pi | H_{\mathrm{in},i} | j, \vec{d}, \vec{z}, \vec{a}, \pi \rangle = \begin{cases} \frac{1}{240} & d_i = 0,\ z_i = 1, \text{ and } F(i,j,0) = (i,0,1) \\ 0 & \text{otherwise.} \end{cases} \tag{9.485}$$

Note that $F(i,j,0) = (i,0,1)$ if and only if none of the gates $U_1, U_2, \ldots, U_{j-1}$ acts on the ith qubit, i.e.,

$$j \leq j_{\min,i} \tag{9.486}$$

where

$$j_{\min,i} = \min\{j \in [M] : \ s(j) = i\}. \tag{9.487}$$

Now using this fact and equations (9.466) and (9.485), we get the following expression for the nonzero matrix elements of $H_{\mathrm{in},i}$ in the basis (9.446):

$$\langle j, \vec{d}, \mathrm{In}(\vec{x}), \vec{a}, \pi | H_{\mathrm{in},i} | j, \vec{d}, \mathrm{In}(\vec{z}), \vec{a}, \pi \rangle \tag{9.488}$$

$$= \sum_{\vec{w}, \vec{y} \in \{0,1\}^n} \langle \vec{x} | \bar{U}_{j,d_1}^{\dagger}(a_1) | \vec{w} \rangle \langle \vec{y} | \bar{U}_{j,d_1}(a_1) | \vec{z} \rangle \langle j, \vec{d}, \vec{w}, \vec{a}, \pi | H_{\mathrm{in},i} | j, \vec{d}, \vec{y}, \vec{a}, \pi \rangle \tag{9.489}$$

$$= \begin{cases} \sum_{\vec{y} \in \{0,1\}^n} \langle \vec{x} | \bar{U}_{j,d_1}^{\dagger}(a_1) | \vec{y} \rangle \langle \vec{y} | \bar{U}_{j,d_1}(a_1) | \vec{z} \rangle \frac{1}{240} \delta_{y_i,1} & j \leq j_{\min,i} \text{ and } d_i = 0 \\ 0 & \text{otherwise} \end{cases} \tag{9.490}$$

$$= \begin{cases} \langle \vec{x} | \bar{U}_{j,d_1}^{\dagger}(a_1) | 1 \rangle \langle 1 |_i \bar{U}_{j,d_1}(a_1) | \vec{z} \rangle \frac{1}{240} & j \leq j_{\min,i} \text{ and } d_i = 0 \\ 0 & \text{otherwise} \end{cases} \tag{9.491}$$

$$= \begin{cases} \langle \vec{x} | U_1^{\dagger}(a_1) \ldots U_{j-1}^{\dagger}(a_1) | 1 \rangle \langle 1 |_i U_{j-1}(a_1) \ldots U_1(a_1) | \vec{z} \rangle \frac{1}{240} & (j < j_{\min,i}, d_i = 0, \text{ and } d_1 \in \{0,2\}) \\ & \text{or } (j = j_{\min,i} \text{ and } d_i = 0) \\ \langle \vec{x} | U_1^{\dagger}(a_1) \ldots U_j^{\dagger}(a_1) | 1 \rangle \langle 1 |_i U_j(a_1) \ldots U_1(a_1) | \vec{z} \rangle \frac{1}{240} & j < j_{\min,i}, d_i = 0, \text{ and } d_1 = 1 \\ 0 & \text{otherwise.} \end{cases} \tag{9.492}$$

In the last line we use the fact that $d_1 = d_i$ when $j = j_{\min,i}$ (since $s(j_{\min,i}) = i$). Since $[U_J(a_1), |1\rangle\langle 1|_i] = 0$ for $J < j_{\min,i}$, we have

$$\langle j, \vec{d}, \mathrm{In}(\vec{x}), \vec{a}, \pi | H_{\mathrm{in},i} | j, \vec{d}, \mathrm{In}(\vec{z}), \vec{a}, \pi \rangle = \begin{cases} \frac{1}{240} \langle \vec{x}| \left(|1\rangle\langle 1|_i \right) |\vec{z}\rangle & j \leq j_{\min,i} \text{ and } d_i = 0 \\ 0 & \text{otherwise} \end{cases} \tag{9.493}$$

$$= \begin{cases} \frac{1}{240} \delta_{\vec{x},\vec{z}} \delta_{x_i,1} & j \leq j_{\min,i} \text{ and } d_i = 0 \\ 0 & \text{otherwise} \end{cases} \tag{9.494}$$

(with all other matrix elements equal to zero), which confirms the result stated in equation (9.482).

9.5.5.4 Matrix elements of H_{out}

We finally present the matrix elements for H_{out}:

Matrix elements of H_{out}

Let $j_{\max} = \max\{j \in [M] \colon s(j) = 2\}$ be the index of the last gate $U_{j_{\max}}$ in the circuit that acts between qubits 1 and 2 (the output qubit). Then

$$\begin{aligned} &\langle k, \vec{c}, \mathrm{In}(\vec{x}), \vec{b}, \sigma | H_{\mathrm{out}} | j, \vec{d}, \mathrm{In}(\vec{z}), \vec{a}, \pi \rangle \\ &\quad = \delta_{\pi,\sigma} \delta_{j,k} \delta_{\vec{c},\vec{d}} \delta_{\vec{a},\vec{b}} \begin{cases} \langle \vec{x}| U^\dagger_{\mathcal{C}_X}(a_1) |0\rangle\langle 0|_2 U_{\mathcal{C}_X}(a_1) |\vec{z}\rangle \frac{1}{240} & j \geq j_{\max} \text{ and } d_2 = 1 \\ 0 & \text{otherwise.} \end{cases} \end{aligned} \tag{9.495}$$

Finally, consider

$$H_{\mathrm{out}} = \sum_{w=1}^{n} h^{(w)}_{\mathrm{out}} \tag{9.496}$$

where (from equation (9.346))

$$\langle \rho^{L_2}_{x,b} | h_{\mathrm{out}} | \rho^{L_1}_{z,a} \rangle = \frac{1}{240} \delta_{a,b} \delta_{x,0} \delta_{z,0} \delta_{L_1,(2,M+1,0)} \delta_{L_2,(2,M+1,0)} \tag{9.497}$$

for $L_1, L_2 \in \mathcal{L}$ and $z, a, x, b \in \mathbb{F}_2$. From this and the fact that H_{out} commutes with all permutations of the underlying particles, we see that H_{out} is diagonal in the basis $\mathcal{B}_{\mathrm{legal}}$, with entries

$$\langle j, \vec{d}, \vec{z}, \vec{a}, \pi | H_{\mathrm{out}} | j, \vec{d}, \vec{z}, \vec{a}, \pi \rangle = \begin{cases} \frac{1}{240} & d_2 = 1,\ F(2, j, 1) = (2, M+1, 0) \text{ and } z_2 = 0 \\ 0 & \text{otherwise.} \end{cases} \tag{9.498}$$

Note that $F(2, j, 1) = (2, M+1, 0)$ if and only if $j \geq j_{\max}$, where

$$j_{\max} = \max\{j \in [M] : \ s(j) = 2\}. \tag{9.499}$$

Using this fact we compute the nonzero matrix elements of H_{out} in the basis (9.446):

$$\begin{aligned}
&\langle j, \vec{d}, \text{In}(\vec{x}), \vec{a}, \pi | H_{\text{out}} | j, \vec{d}, \text{In}(\vec{z}), \vec{a}\pi \rangle \\
&= \sum_{\vec{w},\vec{y}\in\{0,1\}^n} \langle \vec{x}|\bar{U}^\dagger_{j,d_1}(a_1)|\vec{w}\rangle\langle \vec{y}|\bar{U}_{j,d_1}(a_1)|\vec{z}\rangle \langle j, \vec{d}, \vec{w}, \vec{a}, \pi | H_{\text{out}} | j, \vec{d}, \vec{y}, \vec{a}, \pi\rangle && (9.500)\\
&= \begin{cases} \langle \vec{x}|\bar{U}^\dagger_{j,d_1}(a_1)|0\rangle\langle 0|_2 \bar{U}_{j,d_1}(a_1)|\vec{z}\rangle \frac{1}{240} & j \geq j_{\max} \text{ and } d_2 = 1 \\ 0 & \text{otherwise} \end{cases} && (9.501)\\
&= \begin{cases} \langle \vec{x}|U_1^\dagger(a_1)\dots U_j^\dagger(a_1)|0\rangle\langle 0|_2 U_j(a_1)\dots U_1(a_1)|\vec{z}\rangle \frac{1}{240} & j \geq j_{\max} \text{ and } d_1 = d_2 = 1 \\ \langle \vec{x}|U_1^\dagger(a_1)\dots U_{j-1}^\dagger(a_1)|0\rangle\langle 0|_2 U_{j-1}(a_1)\dots U_1(a_1)|\vec{z}\rangle \frac{1}{240} & j > j_{\max}, d_2 = 1, \text{ and } d_1 \in \{0,2\} \\ 0 & \text{otherwise} \end{cases} && (9.502)\\
&= \begin{cases} \langle \vec{x}|U_1^\dagger(a_1)\dots U_M^\dagger(a_1)|0\rangle\langle 0|_2 U_M(a_1)\dots U_1(a_1)|\vec{z}\rangle \frac{1}{240} & j \geq j_{\max} \text{ and } d_2 = 1 \\ 0 & \text{otherwise} \end{cases} && (9.503)\\
&= \begin{cases} \langle \vec{x}|U_{\mathcal{C}_X}^\dagger(a_1)|0\rangle\langle 0|_2 U_{\mathcal{C}_X}(a_1)|\vec{z}\rangle \frac{1}{240} & j \geq j_{\max} \text{ and } d_2 = 1 \\ 0 & \text{otherwise.} \end{cases} && (9.504)
\end{aligned}$$

In going from the second to the third equality we use the fact that $j = j_{\max}$ implies $d_1 = d_2$ (since $s(j_{\max}) = 2$). In the next-to-last line we use the fact that $[U_J(a_1), |0\rangle\langle 0|_2] = 0$ for $J > j_{\max}$. This confirms the result stated in equation (9.495).

9.5.6 Frustration-Free states

Now that we have a thourough understanding of the various matrix elements between legal configurations, it will be useful to actually compute the eigenvalue gaps for these different Hamiltonians. We will do so by looking at hypercubes, and connecting them in a particular manner. Since most of the non-zero matrix elements are from some small set of values, our problem reduces to these graph problems, which then become tractable.

This section actually proves the various bounds on the different ground spaces, and we proceed by finding the ground space of $H(G_i, G_x^{\text{oc}}, n)$ iteratively, and bounding the eigenvalue gap for each G_i.

9.5.6.1 Ground space of $H(G_2, G_X^{\text{oc}}, n)$

We first want to bound the n particle ground space on G_2, so let us define the $(n-2)$-dimensional hypercubes

$$\mathcal{D}_k^j = \left\{(d_1, \dots, d_n) \colon d_1 = d_{s(j)} = k,\ d_i \in \{0,1\} \text{ for } i \in [n] \setminus \{1, s(j)\}\right\} \tag{9.505}$$

for $j \in \{1, \dots, M\}$ and $k \in \{0,1,2\}$, and the superpositions

$$|\text{Cube}_k(j, \vec{z}, \vec{a}, \pi)\rangle = \frac{1}{\sqrt{2^{n-2}}} \sum_{\vec{d}\in\mathcal{D}_k^j} (-1)^{\sum_{i=1}^n d_i} |j, \vec{d}, \text{In}(\vec{z}), \vec{a}, \pi\rangle \tag{9.506}$$

for $k \in \{0,1,2\}$, $j \in [M]$, $\vec{z}, \vec{a} \in \mathbb{F}_2^n$ and $\pi \in S_n$. For each $j \in [M]$, $\vec{z}, \vec{a} \in \mathbb{F}_2^n$ and $\pi \in S_n$, let

$$|C(j, \vec{z}, \vec{a}, \pi)\rangle = \frac{1}{2}|\text{Cube}_0(j, \vec{z}, \vec{a}, \pi)\rangle + \frac{1}{2}|\text{Cube}_1(j, \vec{z}, \vec{a}, \pi)\rangle - \frac{1}{\sqrt{2}}|\text{Cube}_2(j, \vec{z}, \vec{a}, \pi)\rangle. \tag{9.507}$$

We prove

Lemma 36. *The Hamiltonian $H(G_2, G_X^{oc}, n)$ has nullspace S_2 spanned by the states*

$$|C(j, \vec{z}, \vec{a}, \pi)\rangle \tag{9.508}$$

for $j \in [M]$, $\vec{z}, \vec{a} \in \mathbb{F}_2^n$ and $\pi \in S_n$. Its smallest nonzero eigenvalue is

$$\gamma(H(G_2, G_X^{oc}, n)) \geq \frac{\mathcal{K}_0}{35000n} \tag{9.509}$$

where $\mathcal{K}_0 \in (0, 1]$ is the absolute constant from Lemma 32.

Proof. Recall from the previous section that $H_1|_{S_1}$ is block diagonal in the basis (9.446), with a block for each $j \in [M]$, $\vec{z}, \vec{a} \in \mathbb{F}_2^n$, and $\pi \in S_n$. That is to say, $\langle k, \vec{c}, \mathrm{In}(\vec{x}), \vec{b}, \sigma | H_1 | j, \vec{d}, \mathrm{In}(\vec{z}), \vec{a}, \pi \rangle$ is zero unless $\vec{a} = \vec{b}$, $k = j$, $\vec{z} = \vec{x}$, and $\pi = \sigma$. Equation (9.449) gives the nonzero matrix elements within a given block, which we use to compute the frustration-free ground states of $H_1|_{S_1}$.

Looking at equation (9.449), we see that the matrix for each block can be written as a sum of n commuting matrices: $\frac{n-1}{240}$ times the identity matrix (case 1 in equation (9.449)), $n-2$ terms that each flip a single bit $i \notin \{1, s(j)\}$ of $\vec{d}$ (case 2), and a term that changes the value of the "special" components $d_1 = d_{s(j)} \in \{0, 1, 2\}$ (case 3). Thus

$$\begin{aligned}
&\langle j, \vec{c}, \mathrm{In}(\vec{z}), \vec{a}, \pi | H_1 | j, \vec{d}, \mathrm{In}(\vec{z}), \vec{a}, \pi \rangle \\
&\quad = \langle j, \vec{c}, \mathrm{In}(\vec{z}), \vec{a}, \pi | \left[\frac{1}{240}(n-1) + \frac{1}{240} \sum_{i \in [n] \setminus \{1, s(j)\}} H_{\mathrm{flip},i} + \frac{1}{240} H_{\mathrm{special},j} \right] | j, \vec{d}, \mathrm{In}(\vec{z}), \vec{a}, \pi \rangle
\end{aligned} \tag{9.510}$$

where

$$\langle j, \vec{c}, \mathrm{In}(\vec{z}), \vec{a}, \pi | H_{\mathrm{flip},i} | j, \vec{d}, \mathrm{In}(\vec{z}), \vec{a}, \pi \rangle = \delta_{c_i, d_i \oplus 1} \prod_{r \in [n] \setminus \{i\}} \delta_{c_r, d_r} \tag{9.511}$$

and

$$\langle j, \vec{c}, \mathrm{In}(\vec{z}), \vec{a}, \pi | H_{\mathrm{special},j} | j, \vec{d}, \mathrm{In}(\vec{z}), \vec{a}, \pi \rangle = \begin{cases} \frac{1}{\sqrt{2}} & (c_1, d_1) \in \{(2,0), (0,2), (1,2), (2,1)\} \\ & \text{and } d_r = c_r \text{ for } r \in [n] \setminus \{1, s(j)\} \\ 0 & \text{otherwise.} \end{cases} \tag{9.512}$$

Note that these n matrices are mutually commuting, each eigenvalue of $H_{\mathrm{flip},i}$ is ± 1, and each eigenvalue of $H_{\mathrm{special},j}$ is equal to one of the eigenvalues of the matrix

$$\frac{1}{\sqrt{2}} \begin{pmatrix} 0 & 0 & 1 \\ 0 & 0 & 1 \\ 1 & 1 & 0 \end{pmatrix}, \tag{9.513}$$

which are $\{-1, 0, 1\}$. Thus we see that the eigenvalues of $H_1|_{S_1}$ within a given block for some $j \in [M]$

$$\frac{1}{240} \left(n - 1 + \sum_{i \notin \{1, s(j)\}} y_i + w \right) \tag{9.514}$$

where $y_i \in \pm 1$ for each $i \in [n] \setminus \{1, s(j)\}$ and $w \in \{-1, 0, 1\}$. In particular, the smallest eigenvalue within the block is zero (corresponding to $y_i = w = -1$).

The corresponding eigenspace is spanned by the simultaneous -1 eigenvectors of each $H_{\text{flip},i}$ for $i \in [n] \setminus \{1, s(j)\}$ and $H_{\text{special},j}$. The space of simultaneous -1 eigenvectors of $H_{\text{flip},i}$ for $i \in [n] \setminus \{1, s(j)\}$ within the block is spanned by $\{|\text{Cube}_0(j, \vec{z}, \vec{a}, \pi)\rangle, |\text{Cube}_1(j, \vec{z}, \vec{a}, \pi)\rangle, |\text{Cube}_2(j, \vec{z}, \vec{a}, \pi)\rangle\}$. The state $|C(j, \vec{z}, \vec{a}, \pi)\rangle$ is the unique superposition of these states that is a -1 eigenvector of $H_{\text{special},j}$. Hence, for each block we obtain a unique state $|C(j, \vec{z}, \vec{a}, \pi)\rangle$ in the space S_2. Ranging over all blocks $j \in [M]$, $\vec{z}, \vec{a} \in \mathbb{F}_2^n$, and $\pi \in S_n$, we get the basis described in the Lemma.

The smallest nonzero eigenvalue within each block is $\frac{1}{240}$ (corresponding to $y_i = -1$ and $w = 0$ in equation (9.514)), so

$$\gamma(H_1|_{S_1}) = \frac{1}{240}. \tag{9.515}$$

To get the stated lower bound, we use Lemma 2 with $H(G_2, G_X^{\text{oc}}, n) = H_A + H_B$ where

$$H_A = H(G_1, G_X^{\text{oc}}, n) \qquad H_B = H_1|_{\mathcal{I}(G_2, G_X^{\text{oc}}, n)} \tag{9.516}$$

(as in equation (9.351)), along with the bounds

$$\gamma(H_A) \geq \frac{\mathcal{K}_0}{900} \qquad \gamma(H_B|_{S_1}) = \gamma(H_1|_{S_1}) = \frac{1}{240} \qquad \|H_B\| \leq \|H_1\| \leq n \|h_1\| = 2n \tag{9.517}$$

from Lemma 35, equations (9.357) and (9.515), and the fact that $\|h_1\| = 2$ from (9.75). This gives

$$\gamma(H(G_2, G_X^{\text{oc}}, n)) \geq \frac{\mathcal{K}_0}{240\mathcal{K}_0 + 2n \cdot 240 \cdot 900} \geq \frac{\mathcal{K}_0}{500000n} \tag{9.518}$$

where we used the facts that $\mathcal{K}_0 \leq 1$ and $n \geq 1$. □

9.5.6.2 Ground states of $H(G_3, G_X^{\text{oc}}, n)$

Now that we have the ground states of $H(G_2, G_X^{\text{oc}}, n)$, along with the corresponding eigenvalue gap, we will want to investigate G_3. As the states $|C(j, \vec{z}, \vec{a}, \pi)\rangle$ can be viewed as a kind of analog to the states $|\psi\rangle|t\rangle + U_{t+1}|\psi\rangle|t+1\rangle$, we will want to show that the ground states of $H(G_2, G_X^{\text{oc}}, n)$ are similar to the history states.

In particular, for each $\vec{z}, \vec{a} \in \mathbb{F}_2^n$ and each $\pi \in S_n$ define the uniform superposition

$$|\mathcal{H}(\vec{z}, \vec{a}, \pi)\rangle = \frac{1}{\sqrt{M}} \sum_{j=1}^{M} |C(j, \vec{z}, \vec{a}, \pi)\rangle. \tag{9.519}$$

that encodes (somewhat elaborately) the history of the computation that consists of applying either $U_{\mathcal{C}_X}$ or $U_{\mathcal{C}_X}^*$ to the state $|\vec{z}\rangle$. The first bit of $\vec{a}$ determines whether the circuit $\mathcal{C}_X$ or its complex conjugate is applied.

Lemma 37. *The Hamiltonian $H(G_3, G_X^{oc}, n)$ has nullspace S_3 spanned by the states*

$$|\mathcal{H}(\vec{z}, \vec{a}, \pi)\rangle \tag{9.520}$$

for $\vec{z}, \vec{a} \in \mathbb{F}_2^n$. Its smallest nonzero eigenvalue is

$$\gamma(H(G_3, G_X^{oc}, n)) \geq \frac{\mathcal{K}_0}{10^8 n^2 M^2} \tag{9.521}$$

where $\mathcal{K}_0 \in (0, 1]$ is the absolute constant from Lemma 32.

Proof. Recall that

$$H(G_3, G_X^{\text{oc}}, n) = H(G_2, G_X^{\text{oc}}, n) + H_2|_{\mathcal{I}(G_3, G_X^{\text{oc}}, n)} \tag{9.522}$$

with both terms on the right-hand side positive semidefinite (as there are no additional interactions when restricted to $\mathcal{I}(G_3, G_X^{\text{oc}}, n)$). To solve for the nullspace of $H(G_3, G_X^{\text{oc}}, n)$, it suffices to restrict our attention to the space

$$S_2 = \text{span}\{|C(j, \vec{z}, \vec{a}, \pi)\rangle : j \in [M],\ \vec{z}, \vec{a} \in \mathbb{F}_2^n, \pi \in S_n\} \tag{9.523}$$

of states in the nullspace of $H(G_2, G_X^{\text{oc}}, n)$. We begin by computing the matrix elements of H_2 in the basis for S_2 given above. We use equations (9.468) and (9.507) to compute the diagonal matrix elements:

$$\begin{aligned}
&\langle C\left(j, \vec{z}, \vec{a}, \pi\right) |H_2| C\left(j, \vec{z}, \vec{a}, \pi\right)\rangle \\
&\quad = \frac{1}{4}\langle \text{Cube}_0(j, \vec{z}, \vec{a}, \pi)|H_2|\text{Cube}_0(j, \vec{z}, \vec{a}, \pi)\rangle + \frac{1}{4}\langle \text{Cube}_1(j, \vec{z}, \vec{a}, \pi)\rangle|H_2|\text{Cube}_1(j, \vec{z}, \vec{a}, \pi)\rangle \\
&\qquad + \frac{1}{2}\langle \text{Cube}_2(j, \vec{z}, \vec{a}, \pi)|H_2|\text{Cube}_2(j, \vec{z}, \vec{a}, \pi)\rangle \qquad (9.524) \\
&\quad = \begin{cases} 0 + \frac{1}{960} + \frac{1}{960} & j = 1 \\ \frac{1}{960} + \frac{1}{960} + \frac{1}{480} & j \in \{2, \ldots, M-1\} \\ \frac{1}{960} + 0 + \frac{1}{960} & j = M \end{cases} \qquad (9.525) \\
&\quad = \begin{cases} \frac{1}{480} & j \in \{1, M\} \\ \frac{1}{240} & j \in \{2, \ldots, M-1\}. \end{cases} \qquad (9.526)
\end{aligned}$$

In the second line we used equation (9.469). Looking at equation (9.468), we see that the only nonzero off-diagonal matrix elements of H_2 in this basis are of the form

$$\langle C(j-1, \vec{z}, \vec{a}, \pi)|H_2|C(j, \vec{z}, \vec{a}, \pi)\rangle = \left(\langle C(j, \vec{z}, \vec{a}, \pi)|H_2|C(j-1, \vec{z}, \vec{a}, \pi)\rangle\right)^* \tag{9.527}$$

for $j \in \{2, \ldots, M\}$, $\vec{z}, \vec{a} \in \mathbb{F}_2^n$, and $\pi \in S_n$. To compute these matrix elements we first use equation (9.470) to evaluate

$$\langle \text{Cube}_w(j-1, \vec{z}, \vec{a}, \pi)|H_2|\text{Cube}_v(j, \vec{z}, \vec{a}, \pi)\rangle \tag{9.528}$$

for $v, w \in \{0, 1, 2\}$, $j \in \{2, \ldots, M\}$ and $\pi \in S_n$. For example, using the second case of equation (9.470), we get

$$\begin{aligned}
&\langle \text{Cube}_1\left(j-1, \vec{z}, \vec{a}, \pi\right)|H_2|\text{Cube}_0\left(j, \vec{z}, \vec{a}, \pi\right)\rangle \\
&\quad = \frac{1}{2^{n-2}} \sum_{\vec{d} \in \mathcal{D}_0^j} \sum_{\vec{c} \in \mathcal{D}_1^{j-1}} (-1)^{\sum_{i \in [n]}(c_i + d_i)} \langle j-1, \vec{c}, \text{In}(\vec{z}), \vec{a}, \pi|H_2|j, \vec{d}, \text{In}(\vec{z}), \vec{a}, \pi\rangle \qquad (9.529) \\
&\quad = \frac{1}{2^{n-2}} \sum_{\vec{d} \in \mathcal{D}_0^j : d_{s(j-1)} = 1} (-1) \cdot \frac{1}{240} = -\frac{1}{480}. \qquad (9.530)
\end{aligned}$$

To go from the first to the second line we used the fact that, for each $\vec{d} \in \mathcal{D}_0^j$ with $d_{s(j-1)} = 1$, there is one $\vec{c} \in \mathcal{D}_1^{j-1}$ for which $\langle j-1, \vec{c}, \text{In}(\vec{z}), \vec{a}, \pi|H_2|j, \vec{d}, \text{In}(\vec{z}), \vec{a}, \pi\rangle = \frac{1}{240}$ (with all other such matrix elements equal to zero). This $\vec{c}$ satisfies $c_1 = c_{s(j-1)} = 1$ and $c_{s(j)} = 0$, with all other bits equal to those of $\vec{d}$, so

$$(-1)^{\sum_{i=1}^n (c_i + d_i)} = (-1)^{c_1 + c_{s(j)} + c_{s(j-1)} + d_1 + d_{s(j)} + d_{s(j-1)}} = -1 \tag{9.531}$$

for each nonzero term in the sum.

We perform a similar calculation using cases 1, 3, and 4 in equation (9.470) to obtain

$$\langle \mathrm{Cube}_w(j-1,\vec{z},\vec{a},\pi)|H_2|\mathrm{Cube}_v(j,\vec{z},\vec{a},\pi)\rangle = \begin{cases} -\frac{1}{480} & (w,v)=(1,0) \\ \frac{1}{480\sqrt{2}} & (w,v)\in\{(2,0),(1,2)\} \\ -\frac{1}{960} & (w,v)=(2,2) \\ 0 & \text{otherwise.} \end{cases} \tag{9.532}$$

Hence

$$\begin{aligned} \langle C\left(j-1,\vec{z},\vec{a},\pi\right)|H_2|C\left(j,\vec{z},\vec{a},\pi\right) &= \frac{1}{4}\langle \mathrm{Cube}_1\left(j-1,\vec{z},\vec{a},\pi\right)|H_2|\mathrm{Cube}_0\left(j,\vec{z},\vec{a},\pi\right)\rangle \\ &\quad - \frac{1}{2\sqrt{2}}\langle \mathrm{Cube}_2\left(j-1,\vec{z},\vec{a},\pi\right)|H_2|\mathrm{Cube}_0\left(j,\vec{z},\vec{a},\pi\right)\rangle \\ &\quad + \frac{1}{2}\langle \mathrm{Cube}_2\left(j-1,\vec{z},\vec{a},\pi\right)|H_2|\mathrm{Cube}_2\left(j,\vec{z},\vec{a},\pi\right)\rangle \\ &\quad - \frac{1}{2\sqrt{2}}\langle \mathrm{Cube}_1\left(j-1,\vec{z},\vec{a},\pi\right)|H_2|\mathrm{Cube}_2\left(j,\vec{z},\vec{a},\pi\right)\rangle \qquad (9.533) \\ &= -\frac{1}{480}. \qquad (9.534) \end{aligned}$$

Combining this with equation (9.526), we see that $H_2|_{S_2}$ is block diagonal in the basis (9.523), with a block for each pair of n-bit strings $\vec{z},\vec{a}\in\mathbb{F}_2^n$ and each $\pi\in S_n$. Each of the $2^{2n}n!$ blocks is equal to the $M\times M$ matrix

$$\frac{1}{480}\begin{pmatrix} 1 & -1 & 0 & 0 & \cdots & 0 \\ -1 & 2 & -1 & 0 & \cdots & 0 \\ 0 & -1 & 2 & -1 & \ddots & \vdots \\ 0 & 0 & -1 & \ddots & \ddots & 0 \\ \vdots & \vdots & \ddots & \ddots & 2 & -1 \\ 0 & 0 & \cdots & 0 & -1 & 1 \end{pmatrix}. \tag{9.535}$$

This matrix is just $\frac{1}{128}$ times the Laplacian of a path of length M, whose spectrum is well known. In particular, it has a unique eigenvector with eigenvalue zero (the all-ones vector) and its eigenvalue gap is $2(1-\cos(\frac{\pi}{M}))\geq\frac{4}{M^2}$. Thus for each of the $2^{2n}n!$ blocks there is an eigenvector of $H_2|_{S_2}$ with eigenvalue 0, equal to the uniform superposition $|\mathcal{H}(\vec{z},\vec{a},\pi)\rangle$ over the M states in the block. Furthermore, the smallest nonzero eigenvalue within each block is at least $\frac{1}{120M^2}$. Hence

$$\gamma(H_2|_{S_2})\geq\frac{1}{120M^2}. \tag{9.536}$$

To get the stated lower bound on $\gamma(H(G_3,G_X^{\mathrm{oc}},n))$, we apply Lemma 2 with

$$H_A = H(G_2,G_X^{\mathrm{oc}},n) \qquad H_B = H_2|_{\mathcal{I}(G_3,G_X^{\mathrm{oc}},n)} \tag{9.537}$$

and

$$\gamma(H_A)\geq\frac{\mathcal{K}_0}{500000n} \qquad \gamma(H_B|_{S_2})=\gamma(H_2|_{S_2})\geq\frac{1}{120M^2} \qquad \|H_B\|\leq\|H_2\|\leq n\|h_2\|=2n \tag{9.538}$$

from Lemma 36, equation (9.536), and the fact that $\|h_2\|=2$ from (9.75). This gives

$$\begin{aligned} \gamma(H(G_3,G_X^{\mathrm{oc}},n)) &\geq \frac{\mathcal{K}_0}{120M^2\mathcal{K}_0+2n(500000n)(120M^2)} \qquad (9.539) \\ &\geq \frac{\mathcal{K}_0}{120M^2n^2(500001)} \geq \frac{\mathcal{K}_0}{10^8M^2n^2}. \end{aligned}$$

□

At this point, we essentially have that the ground space of $H(G_3, G_X^{\text{oc}}, n)$ corresponds to the history states of the usual circuit-to-Hamiltonian mappings.

9.5.6.3 The ground space of $H(G_4, G_X^{\text{oc}}, n)$

With our "history" states spanning the ground space of $H(G_3, G_X^{\text{oc}}, n)$, we will want to impose the initial boundary conditions so that the ancilla of the history states are guaranteed to be in the states $|0\rangle$. This corresponds to the state G_4, and we thus prove the following lemma about the ground states on this graph:

Lemma 38. *The nullspace S_4 of $H(G_4, G_X^{oc}, n)$ is spanned by the states*

$$|\mathcal{H}(\vec{z}, \vec{a}, \pi)\rangle \quad \textit{where} \quad \vec{z} = z_1 z_2 \dots z_{n_{in}} \underbrace{00\dots0}_{n-n_{in}} \tag{9.540}$$

for $\vec{a} \in \mathbb{F}_2^n$ and $z_1, \dots, z_{n_{in}} \in \mathbb{F}_2$. Its smallest nonzero eigenvalue satisfies

$$\gamma(H(G_4, G_X^{oc}, n)) \geq \frac{\mathcal{K}_0}{10^{11} M^3 n^3} \tag{9.541}$$

where $\mathcal{K}_0 \in (0, 1]$ is the absolute constant from Lemma 32.

Proof. Using equation (9.482), we find

$$\begin{aligned}\langle C(k, \vec{x}, \vec{b}, \sigma)|H_{\text{in},i}|C(j, \vec{z}, \vec{a}, \pi)\rangle = \delta_{\pi,\sigma}\delta_{k,j}\delta_{\vec{x},\vec{z}}\delta_{\vec{a},\vec{b}}\Big(&\frac{1}{4}\langle \text{Cube}_0(j, \vec{z}, \vec{a}, \pi)|H_{\text{in},i}|\text{Cube}_0(j, \vec{z}, \vec{a}, \pi)\rangle \\ &+ \frac{1}{4}\langle \text{Cube}_1(j, \vec{z}, \vec{a}, \pi)|H_{\text{in},i}|\text{Cube}_1(j, \vec{z}, \vec{a}, \pi)\rangle \\ &+ \frac{1}{2}\langle \text{Cube}_2(j, \vec{z}, \vec{a}, \pi)|H_{\text{in},i}|\text{Cube}_2(j, \vec{z}, \vec{a}, \pi)\rangle\Big) \qquad (9.542)\end{aligned}$$

$$= \frac{\delta_{\pi,\sigma}\delta_{k,j}\delta_{\vec{x},\vec{z}}\delta_{\vec{a},\vec{b}}\delta_{z_i,1}}{240}\begin{cases}\frac{1}{4}\cdot\frac{1}{2} + \frac{1}{4}\cdot\frac{1}{2} + \frac{1}{2}\cdot\frac{1}{2} & j < j_{\min,i} \\ \frac{1}{4} + 0 + 0 & j = j_{\min,i} \\ 0 + 0 + 0 & j > j_{\min,i}\end{cases} \tag{9.543}$$

for each $i \in \{n_{\text{in}} + 1, \dots, n\}$. Hence

$$\langle \mathcal{H}(\vec{x}, \vec{b}, \sigma)| \sum_{i=n_{\text{in}}+1}^{n} H_{\text{in},i}|\mathcal{H}(\vec{z}, \vec{a}, \pi)\rangle = \frac{1}{M}\delta_{\pi,\sigma}\delta_{\vec{x},\vec{z}}\delta_{\vec{a},\vec{b}} \sum_{i=n_{\text{in}}+1}^{n} \frac{1}{240}\left(\frac{j_{\min,i} - 1}{2} + \frac{1}{4}\right)\delta_{z_i,1}. \tag{9.544}$$

Therefore

$$\sum_{i=n_{\text{in}}+1}^{n} H_{\text{in},i}\big|_{S_3} \tag{9.545}$$

is diagonal in the basis $\{|\mathcal{H}(\vec{z}, \vec{a}, \pi)\rangle : \vec{z}, \vec{a} \in \mathbb{F}_2^n, \pi \in S_n\}$. The zero eigenvectors are given by equation (9.540), and the smallest nonzero eigenvalue is

$$\gamma\left(\sum_{i=n_{\text{in}}+1}^{n} H_{\text{in},i}\big|_{S_3}\right) \geq \frac{1}{960M} \tag{9.546}$$

since $j_{\min,i} \geq 1$. To get the stated lower bound we now apply Lemma 2 with

$$H_A = H(G_3, G_X^{\text{oc}}, n) \qquad H_B = \sum_{i=n_{\text{in}}+1}^{n} H_{\text{in},i}\big|_{\mathcal{I}(G_4, G_X^{\text{oc}}, n)} \tag{9.547}$$

and

$$\gamma(H_A) \geq \frac{\mathcal{K}_0}{10^8 M^2 n^2} \qquad \gamma(H_B|_{S_3}) \geq \frac{1}{960M} \qquad \|H_B\| \leq n \left\| \sum_{i=n_{\text{in}}+1}^{n} h_{\text{in},i} \right\| = n \tag{9.548}$$

where we used Lemma 37, equation (9.546), and the fact that $\left\|\sum_{i=n_{\text{in}}+1}^{n} h_{\text{in},i}\right\| = 1$ (from equation (9.74). This gives

$$\begin{aligned} \gamma\left(H(G_4, G_X^{\text{oc}}, n)\right) &\geq \frac{\mathcal{K}_0}{960M\mathcal{K}_0 + n(960M)(10^8 n^2 M^2)} \qquad (9.549) \\ &\geq \frac{\mathcal{K}_0}{10^{11} M^3 n^3}. \end{aligned}$$

□

9.5.7 Proof of Theorem 6

At this point, we have our "history" states corresponding to the circuit $\mathcal{C}_X$, we are guaranteed that the ancilla are initialize to the correct value, and all we need to do is penalize those states that the circuit does not accept.

In particular, we can now prove Theorem 6. Using equation (9.495) we get

$$\begin{aligned} &\langle C(k, \vec{x}, \vec{b}, \sigma)|H_{\text{out}}|C(j, \vec{z}, \vec{a}, \pi)\rangle \\ &\quad = \delta_{\pi,\sigma}\delta_{k,j}\delta_{\vec{a},\vec{b}}\Bigg(\frac{1}{4}\langle \text{Cube}_0(j, \vec{x}, \vec{a}, \pi)|H_{\text{out}}|\,\text{Cube}_0(j, \vec{z}, \vec{a}, \pi)\rangle \\ &\qquad + \frac{1}{4}\langle \text{Cube}_1(j, \vec{x}, \vec{a}, \pi)|H_{\text{out}}|\,\text{Cube}_1(j, \vec{z}, \vec{a}, \pi)\rangle \qquad (9.550) \\ &\qquad + \frac{1}{2}\langle \text{Cube}_2(j, \vec{x}, \vec{a}, \pi)|H_{\text{out}}|\,\text{Cube}_2(j, \vec{z}, \vec{a}, \pi)\rangle\Bigg) \qquad (9.551) \\ &\quad = \frac{\delta_{\pi,\sigma}\delta_{k,j}\delta_{\vec{a},\vec{b}}}{240}\langle \vec{x}|U_{\mathcal{C}_X}^{\dagger}(a_1)\left(|0\rangle\langle 0|_2\right)U_{\mathcal{C}_X}(a_1)|\vec{z}\rangle \begin{cases} \frac{1}{4}\cdot\frac{1}{2} + \frac{1}{4}\cdot\frac{1}{2} + \frac{1}{2}\cdot\frac{1}{2} & j > j_{\max} \\ 0 + \frac{1}{4} + 0 & j = j_{\max} \\ 0 + 0 + 0 & j < j_{\max} \end{cases} \qquad (9.552) \end{aligned}$$

and thus

$$\langle \mathcal{H}(\vec{x}, \vec{b}, \sigma)|H_{\text{out}}|\mathcal{H}(\vec{z}, \vec{a}, \pi)\rangle = \frac{\delta_{\pi,\sigma}\delta_{\vec{a},\vec{b}}}{480M}(M - j_{\max} + \tfrac{1}{2})\langle \vec{x}|U_{\mathcal{C}}^{\dagger}(a_1)\left(|0\rangle\langle 0|_2\right)U_{\mathcal{C}}(a_1)|\vec{z}\rangle. \tag{9.553}$$

For any n_{in}-qubit state $|\phi\rangle$, define

$$|\widehat{\mathcal{H}}(\phi, \vec{a}, \pi)\rangle = \sum_{\vec{z}\in\{0,1\}^n} \left(\langle \vec{z}|\phi\rangle|0\rangle^{\otimes n - n_{\text{in}}}\right)|\mathcal{H}(\vec{z}, \vec{a}, \pi)\rangle. \tag{9.554}$$

Note (from Lemma 38) that $|\widehat{\mathcal{H}}(\phi, \vec{a}, \pi)\rangle$ is in the nullspace of $H(G_4, G_X^{\text{occ}}, n)$.

9.5.7.1 Accepting circuit

Let us suppose there exists an n_{in}-qubit state $|\psi_{\text{wit}}\rangle$ such that $\text{AP}(\mathcal{C}_X, |\psi_{\text{wit}}\rangle) \geq 1 - \frac{1}{2^{|X|}}$, i.e.,

$$\langle\psi_{\text{wit}}|\langle 0|^{n-n_{\text{in}}} U_{\mathcal{C}_X}^\dagger |0\rangle\langle 0|_2 U_{\mathcal{C}_X} |\psi_{\text{wit}}\rangle|0\rangle^{n-n_{\text{in}}} \leq \frac{1}{2^{|X|}}. \tag{9.555}$$

Then (letting $\vec{0}$ denote the all-zeros vector)

$$\begin{aligned}
&\langle\widehat{\mathcal{H}}(\psi_{\text{wit}}, \vec{0}, \pi)|H(G_X, G_X^{\text{occ}}, n)|\widehat{\mathcal{H}}(\psi_{\text{wit}}, \vec{0}, \pi)\rangle \\
&\quad = \langle\widehat{\mathcal{H}}(\psi_{\text{wit}}, \vec{0}, \pi)|H(G_4, G_X^{\text{occ}}, n) + H_{\text{out}}|\widehat{\mathcal{H}}(\psi_{\text{wit}}, \vec{0}, \pi)\rangle && (9.556)\\
&\quad = \langle\widehat{\mathcal{H}}(\psi_{\text{wit}}, \vec{0}, \pi)|H_{\text{out}}|\widehat{\mathcal{H}}(\psi_{\text{wit}}, \vec{0}, \pi)\rangle && (9.557)\\
&\quad = \frac{1}{480M}(M - j_{\max} + \tfrac{1}{2})\langle\psi_{\text{wit}}|\langle 0|^{n-n_{\text{in}}} U_{\mathcal{C}_X}^\dagger |0\rangle\langle 0|_2 U_{\mathcal{C}_X} |\psi_{\text{wit}}\rangle|0\rangle^{n-n_{\text{in}}} && (9.558)\\
&\quad \leq \frac{1}{2^{|X|}} && (9.559)
\end{aligned}$$

(using equations (9.553) and (9.554) to go from the second to the third line, and equation (9.555) in the last line). Hence $\lambda_n^1(G_X, G_X^{\text{occ}}) \leq \frac{1}{2^{|X|}}$, establishing equation (9.333).

9.5.7.2 Rejecting circuit

Now suppose $\text{AP}(\mathcal{C}_X, |\phi\rangle) \leq \frac{1}{3}$ for all normalized n_{in}-qubit states $|\phi\rangle$, i.e.,

$$\langle\phi|\langle 0|^{n-n_{\text{in}}} U_{\mathcal{C}_X}^\dagger |0\rangle\langle 0|_2 U_{\mathcal{C}_X} |\phi\rangle|0\rangle^{n-n_{\text{in}}} \geq \frac{2}{3} \quad \text{for all normalized } |\phi\rangle \in (\mathbb{C}^2)^{\otimes n_{\text{in}}}. \tag{9.560}$$

Complex-conjugating this equation gives

$$\langle\phi|^*\langle 0|^{n-n_{\text{in}}} U_{\mathcal{C}_X}^{\dagger *} |0\rangle\langle 0|_2 U_{\mathcal{C}_X}^* |\phi\rangle^*|0\rangle^{n-n_{\text{in}}} \geq \frac{2}{3} \quad \text{for all normalized } |\phi\rangle \in (\mathbb{C}^2)^{\otimes n_{\text{in}}}, \tag{9.561}$$

or equivalently (replacing $|\phi\rangle$ with its complex conjugate),

$$\langle\phi|\langle 0|^{n-n_{\text{in}}} U_{\mathcal{C}_X}^{\dagger *} |0\rangle\langle 0|_2 U_{\mathcal{C}_X}^* |\phi\rangle|0\rangle^{n-n_{\text{in}}} \geq \frac{2}{3} \quad \text{for all normalized } |\phi\rangle \in (\mathbb{C}^2)^{\otimes n_{\text{in}}}. \tag{9.562}$$

Recall that S_4 is the nullspace of $H(G_4, G_X^{\text{occ}}, n)$ and consider the restriction

$$H_{\text{out}}\big|_{S_4}. \tag{9.563}$$

We now show that the smallest eigenvalue of (9.563) is strictly positive. This implies that the nullspace of $H(G_X, G_X^{\text{occ}}, n)$ is empty, which can be seen from (9.354) since both terms in this equation are positive semidefinite and S_4 is the nullspace of the first term. We then use Lemma 2 to lower bound the smallest eigenvalue $\lambda_n^1(G_X, G_X^{\text{occ}})$ of $H(G_X, G_X^{\text{occ}}, n)$.

By Lemma 38, the states

$$|\widehat{\mathcal{H}}(\vec{z}, \vec{a}, \pi)\rangle = |\mathcal{H}(z_1 z_2 \dots z_{n_{\text{in}}} \underbrace{00\dots0}_{n-n_{\text{in}}}, \vec{a}, \pi)\rangle, \quad \vec{a} \in \mathbb{F}_2^n,\ \vec{z} \in \mathbb{F}_2^{n_{\text{in}}} \tag{9.564}$$

are a basis for S_4 and in this basis H_{out} is block diagonal with a block for each $\vec{a} \in \mathbb{F}_2^n$ and $\pi \in S_n$, as can be seen using equation (9.553). From equation (9.554) we can see that any normalized state

that lives in the block corresponding to some fixed $\vec{a} \in \mathbb{F}_2^n$ and $\pi \in S_n$ can be written as $|\widehat{\mathcal{H}}(\phi, \vec{a}, \pi)\rangle$ for some normalized n_{in}-qubit state $|\phi\rangle$. The smallest eigenvalue of $H_{\text{out}}|_{S_4}$ is therefore

$$\langle \widehat{\mathcal{H}}(\theta, \vec{\alpha}, \pi)|H_{\text{out}}|\widehat{\mathcal{H}}(\theta, \vec{\alpha}, \pi)\rangle \tag{9.565}$$

for some normalized n_{in}-qubit state $|\theta\rangle$, some $\vec{\alpha} \in \mathbb{F}_2^n$ and some $\pi \in S_n$. Now

$$\langle \widehat{\mathcal{H}}(\theta, \vec{\alpha}, \pi)|H_{\text{out}}|\widehat{\mathcal{H}}(\theta, \vec{\alpha}, \pi)\rangle = \frac{1}{480M}(M - j_{\max} + \tfrac{1}{2})\langle\theta|\langle 0|^{n-n_{\text{in}}} U^\dagger_{\mathcal{C}_X}(\alpha_1)|0\rangle\langle 0|_2 U_{\mathcal{C}_X}(\alpha_1)|\theta\rangle|0\rangle^{n-n_{\text{in}}} \tag{9.566}$$

$$\geq \frac{1}{960M} \cdot \frac{2}{3} \tag{9.567}$$

using equation (9.560) if $\alpha_1 = 0$ and equation (9.562) if $\alpha_1 = 1$. Since (9.567) is a lower bound on the smallest eigenvalue within each block, the nullspace of $H_{\text{out}}|_{S_4}$ is empty and

$$\gamma(H_{\text{out}}|_{S_4}) \geq \frac{1}{1440M}. \tag{9.568}$$

As noted above, the fact that this matrix has strictly positive eigenvalues implies that so does $H(G_X, G_X^{\text{occ}}, n)$, i.e.,

$$\lambda_n^1(G_X, G_X^{\text{occ}}) = \gamma(H(G_X, G_X^{\text{occ}}, n)). \tag{9.569}$$

To lower bound this quantity we apply Lemma 2 with

$$H_A = H(G_4, G_X^{\text{occ}}, n) \qquad H_B = H_{\text{out}}\big|_{\mathcal{I}(G_X, G_X^{\text{occ}}, n)} \tag{9.570}$$

and we use the bound (9.568) as well as

$$\gamma(H_A) \geq \frac{\mathcal{K}_0}{10^{11} n^3 M^3} \tag{9.571}$$

(from Lemma 38) and $\|H_B\| \leq \|H_{\text{out}}\| \leq n\,\|h_{\text{out}}\| = n$ (using equation (9.346)). Applying the Lemma gives

$$\lambda_n^1(G_X, G_X^{\text{occ}}) = \gamma(H(G_X, G_X^{\text{occ}}, n)) \tag{9.572}$$

$$\geq \frac{\mathcal{K}_0}{1440M\mathcal{K}_0 + n(10^{11} n^3 M^3)(1440M)} \tag{9.573}$$

$$\geq \frac{\mathcal{K}_0}{2 \times 10^{14} n^4 M^4}. \tag{9.574}$$

Now choosing $\mathcal{K}$ (the constant in the statement of Theorem 6) to be equal to $\frac{\mathcal{K}_0}{2\times 10^{14}}$ (recall $\mathcal{K}_0 \in (0, 1]$ is the absolute constant from Lemma 32) proves equation (9.334). This completes the proof of Theorem 6.

9.6 Proof of QMA-hardness

Now that we have

9.7 Discussion and open problems

While these results generalized the problem of the Bose-Hubbard model to arbitrary interactions between bosons, it leaves open the related question of fermions. I would expect that our proof would naturally extend to fermions as well, but the extensions where too extensive to finish in time for this thesis.

Making the eventual graph regular.

Remove the restriction to fixed particle number. Currently, this corresponds to

Chapter 10

Conclusions

Many-body systems have, in general, been found to be extremely difficult to understand.

10.1 Open Problems

While we have shown several interesting results, many interesting avenues remain open for investigation.

References

[1] Dorit Aharonov and Amnon Ta-Shma, *Adiabatic Quantum State Generation and Statistical Zero Knowledge*, Proceedings of the Thirty-fifth Annual ACM Symposium on Theory of Computing, STOC '03, pp. 20–29, ACM, 2003, arXiv:quant-ph/0301023.

[2] Andris Ambainis, *Quantum walk algorithm for element distinctness*, SIAM Journal on Computing **37** (2007), no. 1, 210–239, quant-ph/0311001, Preliminary version in FOCS 2004.

[3] Sanjeev Arora and Boaz Barak, *Computational Complexity: A Modern Approach*, Cambridge University Press, 2009.

[4] Dominic W. Berry, Graeme Ahokas, Richard Cleve, and Barry C. Sanders, *Efficient Quantum Algorithms for Simulating Sparse Hamiltonians*, "Communications in Mathematical Physics **270** (2007), no. 2, 359–371, arXiv:quant-ph/0508139.

[5] Dominic W. Berry and Andrew M. Childs, *Black-box Hamiltonian simulation and unitary implementation*, Quantum Information & Computation **12** (2012), no. 1-2, 29–62, arXiv:0910.4157.

[6] Dominic W Berry, Andrew M Childs, Richard Cleve, Robin Kothari, and Rolando D. Somma, *Exponential improvement in precision for simulating sparse Hamiltonians*, Proceedings of the 46th Annual ACM Symposium on Theory of Computing, pp. 283–292, ACM, 2014, arXiv:1312.1414.

[7] Dominic W. Berry, Andrew M. Childs, Richard Cleve, Robin Kothari, and Rolando D. Somma, *Simulating Hamiltonian dynamics with a truncated Taylor series*, Physical review letters **114** (2015), no. 9, 090502, arXiv:1412.4687.

[8] Dominic W. Berry, Andrew M. Childs, and Robin Kothari, *Hamiltonian simulation with nearly optimal dependence on all parameters*, Foundations of Computer Science (FOCS), 2015 IEEE 56th Annual Symposium on, pp. 792–809, IEEE, 2015, arXiv:1501.01715.

[9] Benjamin A. Blumer, Michael S. Underwood, and David L. Feder, *Single-qubit unitary gates by graph scattering*, Physical Review A **84** (2011), no. 6, 062302, arXiv:1111.5032.

[10] Yaron Bromberg, Yoav Lahini, Roberto Morandotti, and Yaron Silberberg, *Quantum and classical correlations in waveguide lattices*, Physical Review Letters **102** (2009), 253904.

[11] Andrew M. Childs, *Universal computation by quantum walk*, Physical Review Letters **102** (2009), no. 18, 180501, arXiv:0806.1972.

[12] Andrew M. Childs, *On the relationship between continuous- and discrete-time quantum walk*, Communications in Mathematical Physics **294** (2010), 581–603, arXiv:0810.0312.

[13] Andrew M. Childs, Richard Cleve, Enrico Deotto, Edward Farhi, Sam Gutmann, and Daniel A. Spielman, *Exponential algorithmic speedup by quantum walk*, Proceedings of the 35th ACM Symposium on Theory of Computing, pp. 59–68, 2003, quant-ph/0209131.

[14] Andrew M. Childs and David Gosset, *Levinson's theorem for graphs II*, Journal of Mathematical Physics **53** (2012), no. 10, 102207, arXiv:1203.6557.

[15] Andrew M. Childs, David Gosset, Daniel Nagaj, Mouktik Raha, and Zak Webb, *Momentum switches*, Quantum Information and Computation **15** (2015), 601–621, arXiv:1406.4510.

[16] Andrew M. Childs, David Gosset, and Zak Webb, *Universal computation by multiparticle quantum walk*, Science **339** (2013), no. 6121, 791–794, arXiv:1205.3782.

[17] ———, *The Bose-Hubbard model is QMA-complete*, Proceedings of the 41st International Colloquium on Automata, Languages, and Programming, pp. 308–319, 2014, arXiv:1311.3297.

[18] Andrew M. Childs and DJ Strouse, *Levinson's theorem for graphs*, Journal of Mathematical Physics **52** (2011), no. 8, 082102, arXiv:1103.5077.

[19] John D. Cook, *Upper and lower bounds for the normal distribution function*, 2009.

[20] Binh Do, Michael L. Stohler, Sunder Balasubramanian, Daniel S. Elliott, Christopher Eash, Ephraim Fischbach, Michael A. Fischbach, Arthur Mills, and Benjamin Zwickl, *Experimental realization of a quantum quincunx by use of linear optical elements*, Journal of the Optical Society of America B **22** (2005), no. 2, 499–504.

[21] Edward Farhi, Jeffrey Goldstone, and Sam Gutmann, *A quantum algorithm for the Hamiltonian NAND tree*, Theory of Computing **4** (2008), no. 1, 169–190, quant-ph/0702144.

[22] Richard Feynmann, *Simulating Physics with Computers*, International Journal of Theoretical Physics **21** (1982), 467–488.

[23] ———, *Quantum Mechanical Computers*, Optics News **11** (1985), 11–20.

[24] David J. Griffiths, *Introduction to Quantum Mechanics*, 2nd ed., Pearson, 2005.

[25] Michał Karski, Leonid Förster, Jai-Min Choi, Andreas Steffen, Wolfgang Alt, Dieter Meschede, and Artur Widera, *Quantum walk in position space with single optically trapped atoms*, Science **325** (2009), no. 5937, 174–177, arXiv:0907.1565.

[26] Seth Lloyd, *Universal Quantum Simulators*, Science **273** (1996), no. 5278, 1073–1078, http://science.sciencemag.org/content/273/5278/1073.full.pdf.

[27] Neil B. Lovett, Sally Cooper, Matthew Everitt, Matthew Trevers, and Viv Kendon, *Universal quantum computation using the discrete-time quantum walk*, Phys. Rev. A **81** (2010), 042330, arXiv:0910.1024.

[28] JH McCabe, *A continued fraction expansion, with a truncation error estimate, for dawson?s integral*, Mathematics of Computation **28** (1974), no. 127, 811–816.

[29] Bojan Mohar, *Eigenvalues, diameter, and mean distance in graphs*, Graphs Combin. **7** (1991), 53–64.

[30] Hagai B. Perets, Yoav Lahini, Francesca Pozzi, Marc Sorel, Roberto Morandotti, and Yaron Silberberg, *Realization of quantum walks with negligible decoherence in waveguide lattices*, Physical Review Letters **100** (2008), no. 17, 170506, arXiv:0707.0741.

[31] Alberto Peruzzo, Mirko Lobino, Jonathan C. F. Matthews, Nobuyuki Matsuda, Alberto Politi, Konstantinos Poulios, Xiao-Qi Zhou, Yoav Lahini, Nur Ismail, Kerstin Wörhoff, Yaron Bromberg, Yaron Silberberg, Mark G. Thompson, and Jeremy L. O'Brien, *Quantum walks of correlated particles*, Science **329** (2010), no. 5998, 1500–1503, arXiv:1006.4764.

[32] David Poulin, Angie Qarry, Rolando Somma, and Frank Verstraete, *Quantum simulation of time-dependent Hamiltonians and the convenient illusion of Hilbert space*, Physical review letters **106** (2011), no. 17, 170501, arXiv:1102.1360.

[33] Michael Saks and Avi Wigderson, *Probabilistic boolean decision trees and the complexity of evaluating game trees*, Foundations of Computer Science, 1986., 27th Annual Symposium on, pp. 29–38, IEEE, 1986.

[34] Jun John Sakurai, *Modern Quantum Mechanics*, Addison-Wesley, 1994.

[35] Linda Sansoni, Fabio Sciarrino, Giuseppe Vallone, Paolo Mataloni, Andrea Crespi, Roberta Ramponi, and Roberto Osellame, *Two-particle bosonic-fermionic quantum walk via integrated photonics*, Physical Review Letters **108** (2012), 010502.

[36] Miklos Santha, *On the monte carlo boolean decision tree complexity of read-once formulae*, Random Structures & Algorithms **6** (1995), no. 1, 75–87.

[37] Michael Sipser, *Introduction to the Theory of Computation*, 2 ed., Thomas Course Technology, 2006.

[38] Elias M. Stein and Rami Shakarchi, *Complex Analysis*, Princeton University Press, 2003.

[39] John Watrous, *Quantum computational complexity*, Encyclopedia of Complexity and System Science, Springer, 2009, arXiv:0804.3401.

[40] Nathan Wiebe, Dominic W. Berry, Peter Høyer, and Barry C Sanders, *Simulating quantum dynamics on a quantum computer*, Journal of Physics A: Mathematical and Theoretical **44** (2011), no. 44, 445308, arXiv:1011.3489.